High-Resolution Laser and Far-Infrared Fourier Transform Synchrotron-Based Spectroscopy of Selected Molecules

by

Hanif Zarringhalam

Master of Science, University of Guilan, 2008

A Dissertation Submitted in Partial Fulfillment
of the Requirements for the Degree of

Doctor of Philosophy

in the Graduate Academic Unit of Physics

Supervisors: D. W. Tokaryk, Ph.D., Physics
A. G. Adam, Ph.D., Chemistry

Examining Board: I. Mastikhin, Ph.D., Physics
W. Ward, Ph.D., Physics
J. Neville, Ph.D., Chemistry

External Examiner: W. S. Hopkins, Ph.D., Chemistry, University of Waterloo

This dissertation is accepted by the
Dean of Graduate Studies

THE UNIVERSITY OF NEW BRUNSWICK

February, 2022

©Hanif Zarringhalam, 2022

ABSTRACT

In the first part of this thesis, three ruthenium-bearing diatomic molecules have been studied in the visible region of the electromagnetic spectrum. Ruthenium monofluoride, ruthenium monochloride and ruthenium monoxide molecules were created in a molecular beam apparatus. The high-and low-resolution spectra of these small molecules were taken with the laser-induced fluorescence technique. The dispersed fluorescence technique was used to determine the vibrational frequencies of the RuF, RuCl and RuO molecules. The results of the high-resolution analysis of the spectra revealed extensive isotopic structures of the three molecules. Spin-orbit and hyperfine interactions in the ruthenium monofluoride molecule were observed and analyzed. Hyperfine structure in the ruthenium monoxide molecule was also detected and studied.

In the second part of the thesis, three medium-sized ring molecules, catechol, furan and pyrrole, belonging to the C_{2v} point group, have been studied in the infrared region. Vibrational bands of pyrrole and furan were collected between 800-900 cm^{-1} at the Canadian Light Source with an FTIR technique. Observed vibrational bands of pyrrole and furan in that region were studied. A nearby level that had A_2 symmetry which could not be accessed from the ground states had perturbed the fully overlapped bands of these molecules. Also, progress has been made in obtaining the first high-resolution rotationally resolved vibrational band of catechol at the Canadian Light Source.

DEDICATION

With Love: To my family

ACKNOWLEDGEMENTS

I would like to acknowledge my supervisors Dr. Dennis Tokaryk and Dr. Allan Adam for their support, guidance and encouragement during the course of my PhD studies. They provided me with the opportunity to expand my research and explore a broader area of molecular spectroscopy by visiting the Canadian Light Source (CLS). Dr. Tokaryk is a sincere scientist, brilliant researcher and a great teacher who generously allocates lots of his time sharing his knowledge and experience with his students. I learned a lot from him discussing different aspects of quantum mechanics and molecular spectroscopy. We had lots of fruitful online meetings even when I was away from UNB, and during the pandemic. Dr. Adam made me familiar with conducting experiments in the Laser Lab and creating cold molecules in the beginning of my studies. He was never hesitant to advise me and answer my questions. I remember calling him once when running some experiments, and he answered while siting on a dentist chair! I would like to thank Dr. Colin Linton for discussing different aspects of molecular spectroscopy with me and his sense of humor that would make my life easier. I would like to thank Joyce Macgregor for her expert laser assistance and teaching me how to work with different kinds of lasers with her calm and patient manner. I would also like to thank Dr. Brant Billinghurst and Dr. Jainbo Zao for their assistance in data collection during my visit to the Canadian Light Source (CLS). I would like to thank the committee members for reading my dissertation and their valuable comments. I would also like to acknowledge the financial supports from NSERC and UNB that made this research possible. Last but not least, I

would like to thank my wonderful wife, Pegah, for her unconditional love, support and encouragements during my studies.

Table of Contents

ABSTRACT ii
DEDICATION iii
ACKNOWLEDGMENTS iv
Table of Contents vi
List of Tables xi
List of Figures xiv
Chapter 1 Introduction 1
Chapter 2 Theory 6
2.1 Symmetric and asymmetric top molecules 6
2.1.1 Quantum rigid rotors: symmetric and asymmetric tops 7
2.1.2 Classical treatment of rotation of a rigid body 9
2.1.3 Laboratory-fixed and molecular-fixed coordinate systems 11
2.1.4 Angular momentum algebra 18
2.1.5 The symmetric top and its rotational energy level structure 19
2.1.6 Energy levels of asymmetric top molecules in the rigid rotor approximation 21
2.2 Vibrational energy of polyatomic molecules 30
2.2.1 Anharmonic effects 36
2.2.2 Centrifugal distortion 36
2.3 Coriolis interactions 37
2.3.1 Coriolis interactions in polyatomic molecules 39
2.4 Transition between rotation-vibration levels of polyatomic molecules 41
2.4.1 Selection rules 42
2.4.2 Vibrational selection rules 44
2.5 Molecular symmetry 46
2.6 Electronic structure of diatomics 49
2.6.1 Quantum many body systems 50
2.6.2 Born-Oppenheimer approximation 50
2.6.3 Total energy 52
2.6.4 The molecular energy 56
2.7 Angular momenta and labelling electronic states in diatomic molecules 57

2.8 Rotational structure of diatomic molecules 58
2.8.1 Combination differences 60
2.8.2 Band heads 61
2.9 Interactions between different angular momenta 62
2.9.1 Spin-orbit interactions 64
2.9.2 Hyperfine interactions 66
2.10 Selection rules for diatomic molecules 69
Chapter 3 Experimental 72
3.1 The molecular beam source 72
3.1.1 Gas board 75
3.2 Data acquisition and lasers 77
3.2.1 Boxcar integrator and photon counter 77
3.2.2 Delay generator and optimization 78
3.2.3 Experimental set up for the low-resolution survey 79
3.2.4 Dispersed fluorescence technique 80
3.2.5 Experimental set up for the high-resolution survey 82
3.2.5.1 Tuneable lasers 82
3.2.5.1.1 Dye lasers 82
3.2.5.1.2 Titanium sapphire laser 86
3.2.6 Data Calibration 86
3.2.7 Loomis-Wood Plots 89
3.2.8 Pgopher and data fitting 91
Chapter 4 Ruthenium monofluoride: observation, results and analysis 94
4.1 Introduction 94
4.2 Previous studies of RuF 98
4.3 Experimental conditions for production of RuF 100
4.4 Low-resolution survey 100
4.4.1 Three transitions in the green region 101
4.4.2 A transition in the blue region 102
4.4.3 A transition in the infrared region 103
4.5 Dispersed fluorescence analysis 104
4.6 High-resolution analysis 106

4.6.1 The [18.2] $^4\Gamma_{5.5} \rightarrow X^4\Phi_{4.5}$ transition 107
4.6.2 Hyperfine analysis and fitting results 114
4.6.3 The [18.2] $^4\Gamma_{4.5} \rightarrow X^4\Phi_{3.5}$ transition: higher-lying spin-orbit components 121
4.6.4 The 1-1 vibration of the [18.3] $^4\Gamma_{4.5} \rightarrow X^4\Phi_{4.5}$ transition 130
4.6.5 The [22.1] $^4\Delta_{3.5} \rightarrow X^4\Phi_{4.5}$ transition 137
4.6.6 The [13.1] $^4\Delta_{3.5} \rightarrow X^4\Phi_{4.5}$ transition 149
4.7 Multiple state fitting 157
4.8 Calculating the equilibrium bond length 160
4.9 Summary 162
Chapter 5 Ruthenium monochloride: observation, results and analysis 165
5.1 Introduction 165
5.2 Experimental conditions for production of RuCl 166
5.3 Low-resolution survey 166
5.4 Dispersed fluorescence analysis 169
5.5 High-resolution analysis 173
5.5.1 Hot and cold spectra 175
5.5.2 The $^4\Phi_{4.5} \rightarrow X\,^4\Phi_{4.5}$ electronic transition of RuCl near ~ 569 nm 178
5.5.3 The $^4\Gamma_{5.5} \rightarrow X^4\Phi_{4.5}$ electronic transition of RuCl near ~ 508 nm 178
5.5.4 Analysis and discussion 179
5.6 Concluding remarks 188
Chapter 6 Ruthenium monoxide: the 1-0 band of the [18.1] $4 \rightarrow X^5\Delta_4$ transition 191
6.1 Observation of a band of RuO 191
6.2 Dispersed fluorescence 194
6.3 High-resolution data: further confirmation that ~530 nm band is from the RuO molecule 196
6.4 Discussion 204
6.5 Analysis 205
6.6 Hyperfine analysis 207
6.7 Isotopic analysis 211
6.8 Comparison of the ground state parameters of RuO, RuF and RuCl 214
6.9 Concluding remarks 215

Chapter 7 Introduction to the ring molecules (catechol, pyrrole, furan), and experimental techniques at the CLS 217
7.1 Far-infrared spectroscopy at the Canadian light source 217
7.2 Introduction to the ring molecules 217
7.2.1 Pyrrole and furan 218
7.2.2 Catechol and 1,4 benzenedithiol 219
7.3 Experimental methods 223
7.3.1 Synchrotron 223
7.3.2 Synchrotron radiation 220
7.3.3 Infrared Fourier transform spectroscopy 230
Chapter 8 Far-infrared synchrotron-based spectroscopy of catechol 237
8.1 Low-resolution infrared spectrum of catechol 237
8.2 Experimental conditions at the CLS 240
8.2.1 First phase of the experiment 240
8.2.2 The second phase of the experiment 242
8.3 Concluding remarks 244
Chapter 9 Far infrared synchrotron-based spectroscopy of pyrrole 247
9.1 Modes of vibrations of pyrrole 247
9.2 Possible transitions and interactions 248
9.3 Asymmetric top Hamiltonian 252
9.4 The correlation diagram of pyrrole 254
9.5 The spectral assignment process 255
9.6 Data analysis and results 255
9.6.1 The ν_{13} state of pyrrole 256
9.6.2 The ν_9 and ν_{24} states of pyrrole 263
9.6.3 Molecular constants for three states of pyrrole 272
9.7 Inertial defect of analysed states of pyrrole 274
9.8 Conclusion 275
Chapter 10 Far-infrared synchrotron-based spectroscopy of furan 278
10.1 Modes of vibrations of furan 278
10.2 Possible transitions and interactions 279
10.3 The ν_8 and ν_{21}states of furan 281

10.3.1 Analysis of the ν_8 and ν_{21}states of furan 282
10.3.2 Results of the fitting for the ν_8 state of furan 285
10.4 The asymmetric parameter diagram of furan 289
10.5 Conclusion 290
Chapter 11 Conclusions 292
Appendix A Observed and calculated frequencies (cm^{-1}) of the ^{102}RuF, ^{104}RuF, ^{100}RuF and ^{96}RuF isotopologues extracted from the multiple state fitting for the 0-0 band of the [18.2] $^4\Gamma_{5.5} \rightarrow X^4\Phi_{4.5}$, [22.1] $^4\Delta_{3.5} \rightarrow X^4\Phi_{4.5}$ and [13.1] $^4\Delta_{3.5} \rightarrow X^4\Phi_{4.5}$ transitions. 296
Appendix B Observed and calculated frequencies (cm^{-1}) of the ^{101}RuF, ^{99}RuF and ^{98}RuF isotopologues extracted from the fit for the [22.1] $^4\Delta_{3.5} \rightarrow X^4\Phi_{4.5}$ transition. 322
Appendix C Observed and calculated frequencies (cm^{-1}) of the ^{102}RuF, ^{104}RuF and ^{100}RuF isotopologues extracted from the fit for the [18.2] $^4\Gamma_{4.5} \rightarrow X^4\Phi_{3.5}$ transition 329
Appendix D Observed and calculated frequencies (cm^{-1}) of the ^{102}RuF, ^{104}RuF and ^{100}RuF isotopologues extracted from fit for the 1-1 vibration band of the [18.2] $^4\Gamma_{5.5} \rightarrow X^4\Phi_{4.5}$ transition 335
Appendix E Observed and calculated frequencies (cm^{-1}) of the $^{102}Ru^{35}Cl$, $^{104}Ru^{35}Cl$ and $^{100}Ru^{35}Cl$ isotopologues extracted from the multiple state fitting for the [17.5] $^4\Phi_{4.5} \rightarrow X^4\Phi_{4.5}$ and [19.6] $^4\Gamma_{5.5} \rightarrow X^4\Phi_{4.5}$ transitions 341
Appendix F Observed and calculated frequencies (cm^{-1}) of the $^{102}Ru^{37}Cl$ isotopologue extracted from the multiple state fitting for the [17.5] $^4\Phi_{4.5} \rightarrow X^4\Phi_{4.5}$ and [19.6] $^4\Gamma_{5.5} \rightarrow X^4\Phi_{4.5}$ transitions 351
Appendix G Observed and calculated frequencies (cm^{-1}) for the ^{102}RuO, ^{104}RuO, ^{100}RuO, ^{99}RuO and ^{101}RuO isotopologues of 1-0 band of the [18.1] $4 \rightarrow X^5\Delta_4$ transition 354
Appendix H Observed and calculated frequencies (cm^{-1}) for the ν_{13} state of pyrrole 363
Appendix I Observed and calculated frequencies (cm^{-1}) for the ν_9 state of pyrrole 407
Appendix J Observed and calculated frequencies (cm^{-1}) for the ν_{24} state of pyrrole 427
Appendix K Observed and calculated frequencies (cm^{-1}) for the ν_8 state of furan 447
Appendix L Assigned observed frequencies (cm^{-1}) for the ν_{21} state of furan 457
CV

List of Tables

Table 2.1 Expressions for the reduced energies 28
Table 2.2 C_{2v} character table 47
Table 4.1 Stable isotopes of ruthenium, their natural abundance and nuclear spin 107
Table 4.2 Rotational numbering and combination difference analysis for the upper state of the [18.2] $^4\Gamma_{5.5} \rightarrow X^4\Phi_{4.5}$ transition of ^{102}RuF 110
Table 4.3 Rotational numbering and combination difference analysis for the lower state of the [18.2] $^4\Gamma_{5.5} \rightarrow X^4\Phi_{4.5}$ transition of ^{102}RuF 111
Table 4.4 Molecular constants for the states involved in the [18.2] $^4\Gamma_{5.5} \rightarrow X^4\Phi_{4.5}$ transition of ^{102}RuF 119
Table 4.5 Molecular constants for the states involved in the [18.2] $^4\Gamma_{5.5} \rightarrow X^4\Phi_{4.5}$ transition of ^{104}RuF 120
Table 4.6 Molecular constants for the states involved in the [18.2] $^4\Gamma_{5.5} \rightarrow X^4\Phi_{4.5}$ transition of ^{100}RuF 120
Table 4.7 Molecular constants for the states involved in the [18.2] $^4\Gamma_{5.5} \rightarrow X^4\Phi_{4.5}$ transition of ^{96}RuF 121
Table 4.8 Rotational numbering and analysis for the upper state of the [18.2] $^4\Gamma_{4.5} \rightarrow X^4\Phi_{3.5}$ transition of ^{102}RuF 125
Table 4.9 Rotational numbering and analysis for the lower state of the [18.2] $^4\Gamma_{4.5} \rightarrow X^4\Phi_{3.5}$ transition of ^{102}RuF 126
Table 4.10 Molecular constants for states involved in the [18.2] $^4\Gamma_{4.5} \rightarrow X^4\Phi_{3.5}$ transition of ^{102}RuF 127
Table 4.11 Molecular constants for states involved in the [18.2] $^4\Gamma_{4.5} \rightarrow X^4\Phi_{3.5}$ transition of ^{104}RuF 127
Table 4.12 Molecular constants for states involved in the [18.2] $^4\Gamma_{4.5} \rightarrow X^4\Phi_{3.5}$ transition of ^{100}RuF 128
Table 4.13 Rotational numbering and analysis for the upper state of the 1-1 vibration band of the [18.2] $^4\Gamma_{5.5} \rightarrow X^4\Phi_{4.5}$ transition of ^{102}RuF 133
Table 4.14 Rotational numbering and analysis for the lower state of the 1-1 vibration band of the [18.2] $^4\Gamma_{5.5} \rightarrow X^4\Phi_{4.5}$ transition of ^{102}RuF 134

Table 4.15 Molecular constants for states involved in the 1-1 vibration band of the [18.2] $^4\Gamma_{5.5} \rightarrow X^4\Phi_{4.5}$ transition of ^{102}RuF 135
Table 4.16 Molecular constants for states involved in the 1-1 vibration band of the [18.2] $^4\Gamma_{5.5} \rightarrow X^4\Phi_{4.5}$ transition of ^{104}RuF 135
Table 4.17 Molecular constants for states involved in the 1-1 vibration band of the [18.2] $^4\Gamma_{5.5} \rightarrow X^4\Phi_{4.5}$ transition of ^{100}RuF 136
Table 4.18 Rotational numbering and analysis for the upper state of the [22.1] $^4\Delta_{3.5} \rightarrow X^4\Phi_{4.5}$ transition of ^{102}RuF 140
Table 4.19 19 Rotational numbering and analysis for the lower state of the [22.1] $^4\Delta_{3.5} \rightarrow X^4\Phi_{4.5}$ transition of ^{102}RuF 141
Table 4.20 Molecular constants for states involved in the [22.1] $^4\Delta_{3.5} \rightarrow X^4\Phi_{4.5}$ transition of ^{102}RuF 144
Table 4.21 Molecular constants for states involved in the [22.1] $^4\Delta_{3.5} \rightarrow X^4\Phi_{4.5}$ transition of ^{104}RuF 145
Table 4.22 Molecular constants for states involved in the [22.1] $^4\Delta_{3.5} \rightarrow X^4\Phi_{4.5}$ transition of ^{101}RuF 145
Table 4.23 Molecular constants for states involved in the [22.1] $^4\Delta_{3.5} \rightarrow X^4\Phi_{4.5}$ transition of ^{99}Ru 146
Table 4.24 Molecular constants for states involved in the [22.1] $^4\Delta_{3.5} \rightarrow X^4\Phi_{4.5}$ transition of ^{100}RuF 146
Table 4.25 Molecular constants for states involved in the [22.1] $^4\Delta_{3.5} \rightarrow X^4\Phi_{4.5}$ transition of ^{96}RuF 147
Table 4.26 Molecular constants for states involved in the [22.1] $^4\Delta_{3.5} \rightarrow X^4\Phi_{4.5}$ transition of ^{98}RuF 147
Table 4.27 Rotational numbering and analysis for the upper state of [13.1] $^4\Delta_{3.5} \rightarrow X^4\Phi_{4.5}$ transition of ^{102}RuF 153
Table 4.28 Rotational numbering and analysis for the lower state of the [13.1] $^4\Delta_{3.5} \rightarrow X^4\Phi_{4.5}$ transition of ^{102}RuF 154
Table 4.29 Molecular constants for states involved in the [13.1] $^4\Delta_{3.5} \rightarrow X^4\Phi_{4.5}$ transition of ^{102}RuF 155
Table 4.30 Molecular constants for states involved in the [13.1] $^4\Delta_{3.5} \rightarrow X^4\Phi_{4.5}$

transition of ^{104}RuF 155
Table 4.31 Molecular constants for states involved in the [13.1] $^4\Delta_{3.5} \rightarrow X^4\Phi_{4.5}$ transition of ^{100}RuF 156
Table 4.32 Molecular constants for states involved in the [13.1] $^4\Delta_{3.5} \rightarrow X^4\Phi_{4.5}$ transition of ^{96}RuF 156
Table 4.33 Molecular constants for ^{102}RuF, ^{104}RuF, ^{100}RuF and ^{96}RuF as extracted from multiple state fitting 158
Table 4.34 Equilibrium molecular constants for ^{102}RuF, ^{104}RuF and ^{100}RuF 161
Table 4.35 Comparison of the isotopic ratios and the reduced mass 161
Table 5.1 Laser wavelength and first vibration of DFs 172
Table 5.2 Molecular constants for $^{102}Ru^{35}Cl$, $^{104}Ru^{35}Cl$ and $^{100}Ru^{35}Cl$ 183
Table 5.3 Comparison of the isotopic ratios and the reduced mass for the $^{102}Ru^{35}Cl$, $^{104}Ru^{35}Cl$ and $^{100}Ru^{35}Cl$ isotopologues 184
Table 5.4 Molecular constants for $^{102}Ru^{37}Cl$ 187
Table 5.5 Comparison of the isotopic ratios and the reduced mass for the $^{102}Ru^{35}Cl$, and $^{102}Ru^{37}Cl$ isotopologues 188
Table 6.1 Positions of the peaks observed in the DF spectrum of the 1-0 band of the [18.1] $4 \rightarrow X^5\Delta_4$ transition of RuO 195
Table 6.2 Rotational numbering and combination difference analysis for the upper state of the 1-0 band of the [18.1] $4 \rightarrow X^5\Delta_4$ transition of ^{102}RuO 198
Table 6.3 Rotational numbering and combination difference analysis for the lower state of the 1-0 band of the [18.1] $4 \rightarrow X^5\Delta_4$ transition of ^{102}RuO 199
Table 6.4 Molecular constants for ^{102}RuO, ^{104}RuO, ^{100}RuO, ^{99}RuO and ^{101}RuO 206
Table 6.5 Comparison of the ratios of reduced masses as obtained from nuclear data and spectral analysis 207
Table 6.6 The results of the calculation of T_e for different isotopologues of RuO 212
Table 6.7 Ground state parameters of RuO, RuF and RuCl 214
Table 9.1 C_{2v} character table when a is chosen as $\hat{C}_2$ symmetry axis 249
Table 9.2 Multiplication table of A_1, A_2, B_1 and B_2 symmetries 249
Table 9.3 Molecular constants (in cm^{-1}) for four states of pyrrole 273
Table 9.4 Inertial defects of four analysed states of pyrrole 274

Table 10.1 Molecular constants (in cm^{-1}) for the ν_8 state of furan 288

List of Figures

Figure 1.1 Energy level diagram of two different electronic states of a molecule.....2
Figure 2.1 Five types of quantum rigid rotators based on the relation between their moment of inertia: 1) linear 2) spherical top 3) oblate symmetric top 4) prolate symmetric top and 5) asymmetric top 7
Figure 2.2 Euler angles between two coordinate systems 12
Figure 2.3 A spinning symmetric top in the gravitational force field 15
Figure 2.4 The restricted motion of a symmetric top 18
Figure 2.5 The block diagonal infinite Hamiltonian matrix for a given *J*.....23
Figure 2.6 The correlation energy level diagram of furan molecule for J=0, 1, 2 and 3 rotational levels labeled as J_{KaKc} and with $\kappa = 0.923$ identified as a vertical dotted line 30
Figure 2.7 The trajectory of a moving particle in a rotating frame 38
Figure 2.8 Excitation of the bending mode during antisymmetric stretch 38
Figure 2.9 Different angular momenta in a diatomic molecule.....58
Figure 2.10 Rotational level structure of a diatomic molecule 59
Figure 2.11 Lower-state (left) and upper-state (right) state combination differences.....61
Figure 2.12 The diagram summarizes interactions between different angular momenta..63
Figure 2.13 Orbiting motion of a charged particle 65
Figure 2.14 Splittings of two $^5\Delta$ state into five spin-orbit components with the band origin identified as a vertical dotted line 66
Figure 3.1 Schematic experimental set-up of the laser ablation molecular beam apparatus.....74
Figure 3.2 Schematic of the laser ablation source 75
Figure 3.3 Typical schematic set-up of the gas board 76
Figure 3.4 Laser dye performance when pumped with a Nd:YAG Laser at 355nm and 532 nm 80
Figure 3.5 Dispersed fluorescence diagram showing the vibrational levels of the

ground and low-lying excited states 81
Figure 3.6 Schematic diagram of the cavity of a ring laser 84
Figure 3.7 A schematic of a Fabry-Perot etalon 85
Figure 3.8 An example of the four traces recorded to calibrate the molecular spectrum: a) coarse etalon trace b) fine etalon trace c) I_2 LIF trace, and d) molecular LIF trace 89
Figure 3.9 Loomis-Wood plot of selected series in the P branch of the 0-0 band of the [18.2] $^4\Gamma_{5.5} \rightarrow X^4\Phi_{4.5}$ of the RuF molecule 90
Figure 4.1 Olefin metathesis 94
Figure 4.2 Different types of olefin metathesis reactions: ring opening metathesis polymerization (ROMP), ring opening metathesis (ROM), ring closing metathesis (RCM) and ethenolysis cross metathesis (CM) 95
Figure 4.3 The reaction mechanism of olefin metathesis 96
Figure 4.4 Chemical structures of different Grubbs' catalysts, tricyclohexylphosphine is abbreviated as PCy_3 ($P(C_6H_{11})$) 96
Figure 4.5 Chemical structure of imidazolium-trans-tetrachloro(dimethylsulfoxide)-imidazoleruthenium(III) (NAMI-A) 97
Figure 4.6 Different dissociations of NAMI-A based on pH 98
Figure 4.7 A portion of the low resolution survey of the RuF molecule in the visible region 101
Figure 4.8 Low-resolution spectra of three transitions in the green region 102
Figure 4.9 Low-resolution spectrum of a transition in the blue region 103
Figure 4.10 Low-resolution spectrum of a transition in the infrared region 104
Figure 4.11 Dispersed fluorescence spectra of RuF originating from the [22.1] 3.5, [18.2] 5.5 and [13.1] 3.5 excited electronic states. Decays to spin-orbit (SO) components and excited states (ES) are also shown. 106
Figure 4.12 Overview of the high-resolution spectrum of the [18.2] $^4\Gamma_{5.5} \rightarrow X^4\Phi_{4.5}$ transition of RuF 108
Figure 4.13 Loomis-Wood plot of selected series in the P branch of the [18.2] $^4\Gamma_{5.5} \rightarrow X^4\Phi_{4.5}$ band of RuF molecule 109
Figure 4.14 Isotopic and hyperfine structures of two R transitions in the [18.2] $^4\Gamma_{5.5}$

→ $X^4\Phi_{4.5}$ transition of RuF 113
Figure 4.15 Energy level diagram of the 0-0 band of the [18.2] $^4\Gamma_{5.5} \rightarrow X^4\Phi_{4.5}$ transition 114
Figure 4.16 Three possible transitions from the corresponding hyperfine splittings of two rotational levels J″=4.5 and J′=5.5 in the R branch 116
Figure 4.17 A portion of the R branch, R (4.5), 0-0 band of the [18.2] $^4\Gamma_{5.5} \rightarrow X^4\Phi_{4.5}$ transition of ^{102}RuF; the upper trace is the experimental spectrum and the lower trace is the calculated. Three transitions of the ^{102}RuF molecule with the corresponding F values for the upper and lower states which were used to measure the hyperfine parameter are shown 117
Figure 4.18 An overview of the spectrum of the weak feature of RuF observed beside the 0-0 band of the [18.2] $^4\Gamma_{5.5} \rightarrow X^4\Phi_{4.5}$ transition 122
Figure 4.19 Isotopic and hyperfine structures of RuF including an expanded view of the first two R lines of the weaker band 123
Figure 4.20 Diagram of the 0-0 band of the [18.2] $^4\Gamma_{5.5} \rightarrow X^4\Phi_{4.5}$ and spin-orbit transitions 129
Figure 4.21 High-resolution spectrum of the 1-1 vibration of the [18.2] $^4\Gamma_{4.5} \rightarrow X^4\Phi_{4.5}$ transition of RuF 130
Figure 4.22 Expanded view of the high-resolution spectrum of the 1-1 vibration of the [18.2] $^4\Gamma_{4.5} \rightarrow X^4\Phi_{4.5}$ transition of RuF 131
Figure 4.23 Loomis-Wood plot of series in the R branch of the 1-1 vibration band of the [18.2] $^4\Gamma_{4.5} \rightarrow X^4\Phi_{4.5}$ transition of RuF molecule 132
Figure 4.24 An overview of the high resolution spectrum of the [22.1] $^4\Delta_{3.5} \rightarrow X^4\Phi_{4.5}$ transition 137
Figure 4.25 Expanded view of the high-resolution spectrum of the [22.1] $^4\Delta_{3.5} \rightarrow X^4\Phi_{4.5}$ transition 138
Figure 4.26 Loomis-Wood plot of series in the P branch of the [22.1] $^4\Delta_{3.5} \rightarrow X^4\Phi_{4.5}$ band of RuF molecule 139
Figure 4.27 The variation of the rotational parameter B′ versus J(J+1) 142
Figure 4.28 The variation of the rotational parameter B″ versus J(J+1) 143
Figure 4.29 Assignment of features in the dispersed fluorescence spectrum taken from

the [22.1] $^4\Delta_{3.5} \rightarrow X^4\Phi_{4.5}$ band 149
Figure 4.30 High-resolution spectrum of the [13.1] $^4\Delta_{3.5} \rightarrow X^4\Phi_{4.5}$ transition 150
Figure 4.31 Expanded view of the high-resolution spectrum of the [13.1] $^4\Delta_{3.5} \rightarrow X^4\Phi_{4.5}$ band 151
Figure 4.32 Loomis-Wood plot of series in the P branch of [13.1] $^4\Delta_{3.5} \rightarrow X^4\Phi_{4.5}$ band of the RuF molecule 152
Figure 4.33 The difference between observed and calculated line positions in terms of the observation number for ^{102}RuF. The green, blue and red colors correspond to the transitions from the ground state to [18.3] $^4\Gamma_{5.5}$, [22.1] $^4\Delta_{3.5}$ and [13.1] $^4\Delta_{3.5}$ states respectively 159
Figure 4.34 Energy level diagram of five observed transitions in the blue, green and infrared regions 163
Figure 5.1 Ru-based complexes are used in the ring closing metathesis reaction of a diene in water 165
Figure 5.2 Low-resolution survey of RuCl 167
Figure 5.3 Low-resolution spectrum of a RuCl transition in the green region 168
Figure 5.4 Low-resolution spectrum of a RuCl transition in the yellow region 169
Figure 5.5 The dispersed fluorescence of the observed transitions in the low-resolution spectra. Vibrations form series that are indicated with dotted vertical lines 171
Figure 5.6 The RuCl band near ~569 nm expanded to show isotopic structure 174
Figure 5.7 A portion of the RuCl spectrum taken near ~569 nm with helium as the carrier gas 176
Figure 5.8 A portion of the RuCl spectrum near ~569 nm taken with argon as the carrier gas 177
Figure 5.9 High-resolution spectrum of a $^4\Gamma_{5.5} \rightarrow X^4\Phi_{4.5}$ transition of RuCl near 508 nm 179
Figure 5.10 The upper and lower traces are the experimental and calculated spectra respectively for the $^4\Phi_{4.5} \rightarrow X^4\Phi_{4.5}$ transition of $^{102}Ru^{35}Cl$. Simulations are done at 50 K 181
Figure 5.11 The upper and lower traces are the experimental and calculated spectra respectively for the $^4\Gamma_{5.5} \rightarrow X^4\Phi_{4.5}$ transition of $^{102}Ru^{35}Cl$. Simulations are done

at 50 K 182
Figure 5.12 The upper and lower traces are the experimental and calculated spectra respectively for $X^4\Phi_{4.5} \rightarrow {}^4\Phi_{4.5}$ transition of $^{102}Ru^{37}Cl$. Simulations are done at 50 K. 185
Figure 5.13 The upper and lower traces are the experimental and calculated spectra respectively for the $X^4\Phi_{4.5} \rightarrow {}^4\Gamma_{5.5}$ transition of $^{102}Ru^{37}Cl$. Simulations are done at 50 K 186
Figure 5.14 Energy level diagram of the two band systems observed in experiments on RuCl, with transitions observed between levels indicated..... 189
Figure 6.1 Three possible transitions in the green region for the [18.2] $^4\Gamma_{5.5} \rightarrow X\ ^4\Phi_{4.5}$ system of RuF needed to measure the lower and upper state vibrational frequencies with high precision 192
Figure 6.2 The 1-0 band of the [18.1] $4 \rightarrow X^5\Delta_4$ transition of RuO taken in a low-resolution survey scan 193
Figure 6.3 The low-resolution spectra of the 1-1 and 0-0 bands of the [18.2] $^4\Gamma_{5.5} \rightarrow X^4\Phi_{4.5}$ and [18.2] $^4\Gamma_{4.5} \rightarrow X\ ^4\Phi_{3.5}$ transitions of RuF 193
Figure 6.4 Dispersed fluorescence spectrum of the 1-0 band of the [18.1] $4 \rightarrow X^5\Delta_4$ transition of RuO 195
Figure 6.5 Loomis-Wood plot of selected series of the ^{102}RuO molecule 197
Figure 6.6 A portion of P branch for the 1-0 band of the [18.1] $4 \rightarrow X^5\Delta_4$ transition of ^{102}RuO. The first line of the P branch starts with J=5, i.e., P(5). Unassigned lines in the Figure are due to other isotopologues of RuO..... 200
Figure 6.7 A portion of the R branch for the 1-0 band of the [18.1] $4 \rightarrow X^5\Delta_4$ transition of ^{102}RuO. The first line of the R branch is R(4), and the first lines of P and Q branches are P(5) and Q(4) (not shown in picture), indicating that this band has $\Omega' = \Omega'' = 4$. Unassigned lines in the Figure are due to other isotopologues of RuO 201
Figure 6.8 The dependence of the angular momentum for the P, Q and R transitions versus wavenumber for the 1-0 band of the [18.1] $4 \rightarrow X^5\Delta_4$ transition of ^{102}RuO 202
Figure 6.9 The high-resolution spectrum of the R region with isotopic structure and the band heads of different isotopologues of RuO 203
Figure 6.10 The upper trace is the band head region for the ^{101}RuO isotopologue for

the 1-0 band of the [18.1] $4 \rightarrow X^5\Delta_4$ transition and the lower trace is the simulated spectrum. There are four nearly coincident R-clusters close to one another, the assignments are for R(9) and R(10).....208
Figure 6.11 RuO molecular orbital energy level diagram taken from reference 2.....209
Figure 6.12 The graph of reduced band origins versus the scaling parameter for ^{102}RuO, ^{104}RuO and ^{100}RuO isotopologues 213
Figure 7.1 Molecular structure of benzene.....221
Figure 7.2 The molecules 1,4 benzenedithiol (left) and 1,2-dihydroxybenzene (catechol) (right) are illustrated.....221
Figure 7.3 A single organic molecule that is connected to two electrodes 222
Figure 7.4 An overview of the synchrotron facility at the University of Saskatchewan 224
Figure 7.5 Schematic diagram of different parts of the synchrotron.....224
Figure 7.6 An overview of the synchrotron facility 225
Figure 7.7 An electron in circular motion with velocity $\vec{v}$ and acceleration $\dot{\vec{v}}$ 227
Figure 7.8 Angular distribution for $\beta = 0.1$ (left) and 0.6 (right). The electron acceleration is directed to the right in both Figures 228
Figure 7.9 Synchrotron radiation intensity versus ξ, the radiated frequency normalized to ω_c. 229
Figure 7.10 A setup for a Michelson interferometer used in Fourier transform spectroscopy 231
Figure 7.11 The interferogram and the spectra are both a Fourier transform of one another 232
Figure 7.12 The Bruker IFS125HR Fourier transform infrared spectrometer attached to the Far-Infrared beamline at the Canadian Light Source is pictured.....233
Figure 8.1 Schematic structure of catechol molecule.....237
Figure 8.2 A low-resolution infrared survey spectrum of catechol.....237
Figure 8.3 The top trace is the simulated band of catechol at ~ 970 cm^{-1} and the bottom trace is an expanded view of a portion in the R region of the band. Simulation details are given in the text.....239
Figure 8.4 The result of the first high-resolution survey spectrum taken between 400-

1200 cm^{-1} 241
Figure 8.5 An expanded view of the first high-resolution band observed at 970 cm^{-1} is shown.....242
Figure 8.6 A picture of the sample wrapped in an aluminum foil (left) is shown and a picture of 30 cm White cell is also shown (right) 243
Figure 8.7 The result of the second high-resolution survey scan between 500-1200 cm^{-1} 244
Figure 9.1 Schematic structure of the pyrrole molecule.....247
Figure 9.2 Vibrational levels of pyrrole grouped based on their symmetries. Selected allowed transitions are shown as solid lines and symmetry-forbidden transitions are given with dashed lines with a superimposed "X" 248
Figure 9.3 The ν_9 and ν_{24} vibrational modes of pyrrole 251
Figure 9.4 The correlation diagram of pyrrole for J=0, 1, 2 and 3 rotational levels labeled as J_{KaKc} with $\kappa = 0.9438$ identified as a vertical dotted line 254
Figure 9.5 Absorption spectrum of the c-type ν_{13} fundamental of pyrrole.....256
Figure 9.6 A Loomis-Wood plot of the P branch of the ν_9 vibrational mode of pyrrole.....257
Figure 9.7 The expanded view of the high-resolution spectrum of pyrrole between 814-816 cm^{-1} with the corresponding simulated spectrum at the bottom 258
Figure 9.8 The P(20) cluster of the ν_{13} band of pyrrole: the quantum numbers of each transition are given as (J′, $K_{a'}$, $K_{c'}$)-(J″, $K_{a''}$, $K_{c''}$). For most features only the $J=K_a+K_c-1$ member of a degenerate pair is labeled 259
Figure 9.9 A portion of the Q branch of the ν_{13} band. The upper trace is the experimental spectrum and the lower trace is the calculated spectrum.....260
Figure 9.10 Simulated rotational structure of the ν_{13} band with selected K_a values excluding the Q branch.....261
Figure 9.11 The difference between observed and calculated transitions shown as circles with the root mean square error of the fit for the ν_{13} band of pyrrole. 262
Figure 9.12 The ring puckering mode, ν_{13}, of pyrrole 263
Figure 9.13 Two overlapping vibrational bands of pyrrole, ν_{24} and ν_9, at ~ 864 and 881 cm^{-1} 264

Figure 9.14 A Loomis-Wood plot of the P branch of the *a*-type ν_9 vibrational mode of pyrrole.....265
Figure 9.15 A portion of the rotational structure of a cluster in the P branch of the ν_9 band of pyrrole: the quantum numbers of each transitions are given as (J', $K_{a'}$, $K_{c'}$)-(J'', $K_{a''}$, $K_{c''}$). For most features only the $J=K_a+K_c-1$ member of a degenerate pair is labeled 266
Figure 9.16 The upper and lower traces are the experimental and simulated spectra of the ν_9 band of pyrrole.....267
Figure 9.17 The difference between observed and calculated transitions shown as circles with root mean square error of the fit for the ν_9 band of pyrrole.....268
Figure 9.18 Loomis-Wood plot of the P branch of the *b*-type ν_{24} vibrational mode of pyrrole 269
Figure 9.19 A portion of the rotational structure of a cluster in the P branch of the *b*-type ν_{24} band of pyrrole: the quantum numbers of each transitions are given as (J', $K_{a'}$, $K_{c'}$)-(J'', $K_{a''}$, $K_{c''}$).....270
Figure 9.20 The upper and lower traces shown are the experimental and simulated spectra of the ν_{24} band of pyrrole 271
Figure 9.21 The difference between observed and calculated transitions shown as circles with the root mean square error of the fit for the ν_{24} band of pyrrole.....272
Figure 10.1 Schematic structure of the furan molecule.....278
Figure 10.2 A vibrational energy level diagram of furan is shown where the levels are grouped by their symmetries. Selected allowed transitions are depicted as solid lines and symmetry forbidden transitions are drawn as dashed lines with a superimposed "X" 279
Figure 10.3 Two overlapping vibrational bands of furan, ν_8 and ν_{21}, at ~ 870 and 873 cm^{-1} 281
Figure 10.4 A Loomis-Wood plot of a portion of the P branch region of the *a*-type ν_8 band of furan is shown 282
Figure 10.5 A Loomis-Wood plot of a portion of the R branch region of the *a*-type ν_8 band of furan is shown 283
Figure 10.6 A Loomis-Wood plot of a portion of the P branch region of the *b*-type ν_{21}

band of furan is shown 284
Figure 10.7 A Loomis-Wood plot of a portion of the R branch of the *b*-type ν_{21} band of furan is shown 285
Figure 10.8 The upper and lower traces are the experimental and simulated spectra of the *a*-and *b*-type vibrational bands of furan, ν_8 and ν_{21}, at ~ 870 and ~ 873 cm^{-1} 286
Figure 10.9 The difference between observed and calculated transitions shown as circles with the root mean square error of the fit for the ν_8 band of furan 289

Chapter 1

Introduction

Light-matter interaction holds a pivotal role in spectroscopy. We can study matter by subjecting it to electromagnetic radiation as a probe and observing its response. In the present study, selected molecules in the gas phase are studied using various kinds of lasers and synchrotron radiation as the electromagnetic radiation. In spectroscopy we deal with transitions between different states. Upon absorbing photons of the correct energy from the external field, molecules undergo a transition from a lower energy state to a higher energy state. After a short time, the higher quantum state can decay possibly by emitting a photon which can be detected as fluorescence. The analysis of the fluorescence or the absorption presents invaluable information about physical and chemical properties of the molecules. Figure 1.1 shows a schematic energy level diagram of two different electronic states of a molecule. In each electronic state, there are vibrational levels labeled by v corresponding to increasing vibrational energy of the molecule. Within each vibration, there are rotational levels (J) associated with increased rotational energy of the molecule. Figure 1.1 shows the three types of transitions designated by the arrows that can occur in molecules if they are excited. These transitions happen in different regions of the electromagnetic spectrum, defining three types of molecular spectroscopy. The arrows A correspond to transitions in the ultra violet (UV) and visible (Vis) regions of the electromagnetic spectrum. The energy of UV/Vis radiation can excite a transition between two electronic states hence the name electronic spectroscopy. During an

electronic excitation, vibrational and rotational transitions can also occur. Therefore, the corresponding electronic spectra contains rotational lines within each vibration hence the name rovibronic transition. At the University of New Brunswick this type of spectroscopy for collecting the laser-induced fluorescence spectra of metal bearing diatomic molecules in the visible region has a long tradition.

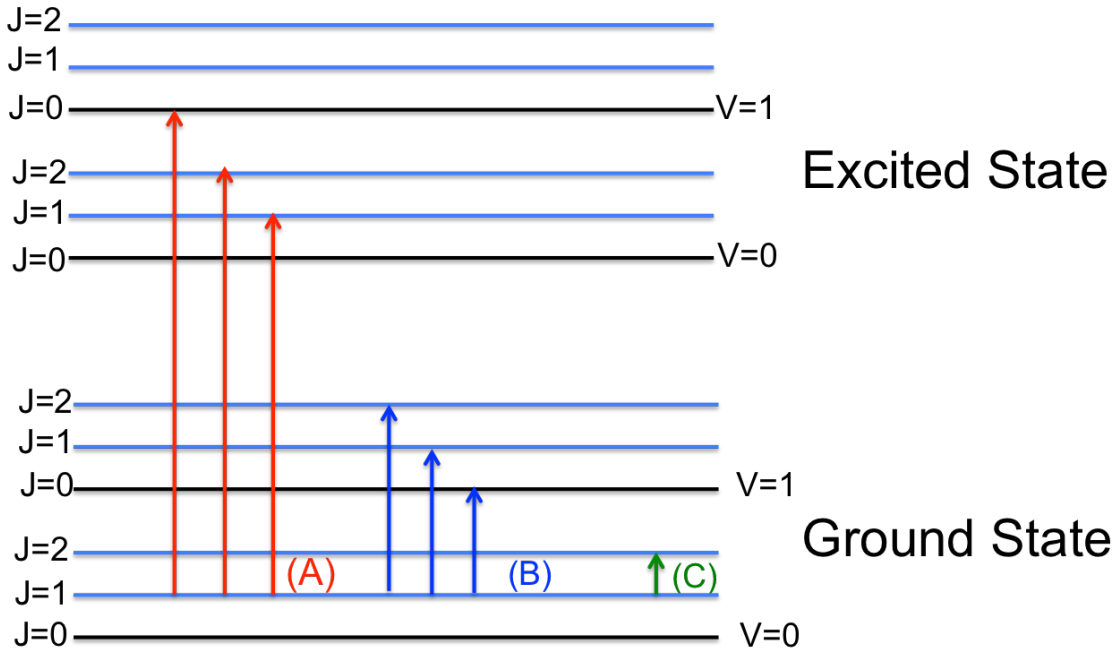

Figure 1.1 Energy level diagram of two different electronic states of a molecule.

In the arrows B, which lie in the infrared, both the vibrational and rotational transitions occur within the same electronic state. Therefore, rotation-vibration or rovibrational spectra can be collected in this region. The absorption rovibrational spectra of some ring molecules in the far infrared spectral region were collected at the Canadian Light Source using synchrotron radiation. The C arrow indicates a transition between rotational levels which are the lowest in energy. Its energy change is in the microwave region and hence

microwave spectroscopy can be used to obtain the spectra related to the pure rotational transitions.

The laser spectroscopy lab at the University of New Brunswick specializes in studies of metal containing diatomic molecules. These molecules are often open *d* shell species with short lifetimes. Lasers are used for both probing and making these free radicals. Diatomic molecules are the simplest molecular systems and hence can be thought of as building blocks of larger molecules. Therefore understanding how the metal is attached to the ligand in these systems can also elucidate how larger systems work in general. From a theoretical perspective, these experiments can also provide a base measurement for comparing the results to those of *ab initio* electronic structure calculations. The measurements can lay the foundations to refine the theory, explain new phenomena, and interpret the experimental findings. The three ruthenium-bearing diatomic molecules, i.e., RuF, RuCl and RuO, that I have studied are all examples of an open *d* shell electronic structure. In these systems, the ruthenium atom with $4d^7\ 5s^1$ shell structure makes bonds with two halogens, fluorine and chlorine, and also oxygen. Furthermore, the nuclear spin of fluorine, chlorine and some ruthenium atoms is non-zero. The nuclear spin and electron moments can interact in the ruthenium monofluoride, ruthenium monochloride and ruthenium monoxide molecules. Therefore it is possible that hyperfine structure may be observed in these molecules. Further information about the electronic structure these molecules may be obtained.

Apart from diatomic molecules, another aspect of this thesis involved studying medium-sized molecules, the spectra of which were taken at the Canadian Light Source (CLS). As we move from diatomic to polyatomic molecules by adding more atoms, the degrees of freedom and hence the number of vibrations increase. In some spectral regions the vibrations may overlap producing entangled spectra. Also, the moments of inertia of heavier molecules are larger than those of diatomic molecules, which decreases the separation of spectral lines and makes their spectrum more congested. Therefore, the spectra of polyatomic systems are generally more complex than diatomic molecules. In this study, a highly collimated beam of synchrotron radiation in the far infrared region, coupled with a Fourier transform spectrometer based on a Michelson interferometer was used to obtain the rovibrational spectra of a class of ring molecules. Catechol was the first molecule that I studied at the CLS. This molecule has been rotationally analysed; literature suggests that it has a suitable vapour pressure for measuring absorption using synchrotron radiation. Also, it has less congested spectra when compared with 1,4 benzenedithiol, a molecule suitable to form the building block of future electronics known as "molecular electronics". These molecules are structurally similar; they are planar and posses a hexagonal benzene ring with two OH (S) fragments. Apart from these systems, two five membered planar ring molecules, furan and pyrrole were also studied. All the above-mentioned ring molecules belong to the C_{2v} point group. The structural resemblance of the molecules makes their interpretations similar.

The remainder of the thesis is outlined as follows:

In Chapter Two, a brief introduction to the theory of diatomic and polyatomic molecules required to interpret the spectra is presented. Chapter Three provides a description of the experimental technique used to produce the diatomic molecules and obtain their spectra. In Chapter Four of the thesis, the observation and analysis of ruthenium monofluoride is presented. Chapter Five describes the production of ruthenium monochloride and the analysis of several of its spectra. The observation and analysis of ruthenium monoxide spectra are given in Chapter Six. Chapter Seven provides an introduction to the ring molecules that were studied (catechol, pyrrole, furan), and gives a general description of the experimental technique used at the CLS. Chapter Eight describes the progress toward obtaining the far infrared spectra of catechol. Chapter Nine provides the analysis of some rovibrational bands of pyrrole. In Chapter Ten, the analysis of the analogous rotation-vibration spectra of furan is discussed. Chapter Eleven summarizes the results obtained and presents an outlook for future projects.

Chapter 2

Theory

In this chapter I discuss the theoretical framework and models associated with the quantum mechanical description of molecules, focusing on their rotation and vibration. The Hamiltonian will be developed for both symmetric-and asymmetric-top molecules. The rotation and vibration of diatomic molecules will be described as a special case of a symmetric top, and the electronic excitation of diatomic molecules will be factored in. The interplay between angular momenta (spin-orbit effects, hyperfine interactions, etc.) and vibration-rotation interactions (Coriolis coupling, centrifugal effects, etc.) will also be introduced. Finally the mechanism by which electromagnetic radiation induces transitions between energy states of molecules will be discussed, since this topic is central to the spectroscopy described in the remainder of the thesis.

2.1 Symmetric and asymmetric top molecules

In this section a brief introduction to rotation and vibration of polyatomic molecules within the framework of the rigid rotor and harmonic oscillator models is presented.

2.1.1 Quantum rigid rotors: symmetric and asymmetric tops

Within the rigid rotor approximation, the bond lengths and hence the distances between the atoms in the molecules are considered to be fixed. In order to find the rotational energy level structure of molecules, we can model them as quantum rigid rotors. Therefore, the kinetic energy operator of the Hamiltonian can be formed and the rotational energy level structures can be obtained. The description of rotational motion of a molecule can be simplified the most using its principal axes of inertia. To do so, we label the axes of the principal reference frame with a, b and c and denote the moment of inertia with respect to these axes as I_a (smallest), I_b and I_c (largest). Then, as shown in Figure 2.1, we can group all the molecules based on these values to five types [1]:

1) Linear molecules where one of the moments of inertia is zero and the two others are the same, i.e., $I_a=0$ and $I_b=I_c$.

2) Spherical top molecules where all of the moments of inertia are the same, i.e., $I_a=I_b=I_c$.

3) Oblate symmetric top molecules where two of the moments of inertia are the same but smaller than the third one, i.e., $I_a = I_b< I_c$.

4) Prolate symmetric top molecules where two of the moments of inertia are the same but larger than the first one, i.e., $I_a < I_b= I_c$.

5) Asymmetric top molecules where all of the moments of inertia are unequal, i.e., $I_a < I_b<I_c$.

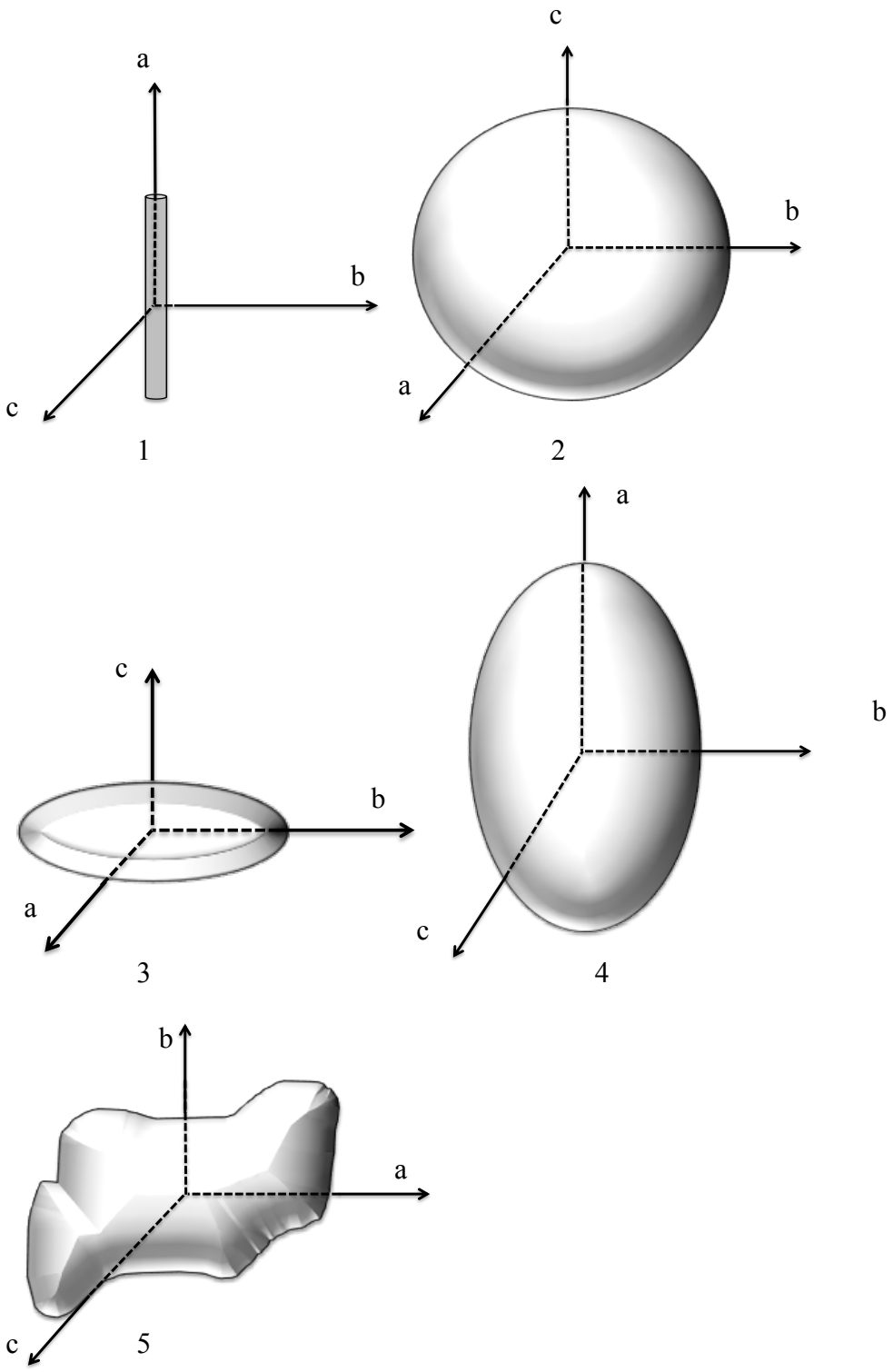

Figure 2.1 Five types of quantum rigid rotators based on the relation between their moments of inertia: 1) linear 2) spherical top 3) oblate symmetric top 4) prolate symmetric top and 5) asymmetric top.

2.1.2 Classical treatment of rotation of a rigid body

In classical mechanics the rotation of a rigid body is described by angular quantities such as the angular momentum $\vec{J}$, the moment of inertia I, and the rotational energy T_{rot} [2]. Consider a rigid body in space with position (x, y, z) rotating around an arbitrary axis with the angular velocity $\vec{\omega}$ whose components along the x, y and z axes are denoted by (ω_x, ω_y, ω_z) respectively. The rotational energy of the rotor is given by

$$T_{rot} = \frac{1}{2}\vec{\omega}.\vec{\vec{I}}.\vec{\omega} \tag{2.01}$$

where $\vec{\vec{I}}$ is inertia tensor and is described by [2, 3]

$$\vec{\vec{I}} = \begin{pmatrix} I_{xx} & I_{xy} & I_{xz} \\ I_{yx} & I_{yy} & I_{yz} \\ I_{zx} & I_{zy} & I_{zz} \end{pmatrix}. \tag{2.02}$$

The diagonal matrix elements, which represent the moments of inertia about x, y and z axes are given by

$$\begin{aligned} I_{xx} &= \sum_i m_i(y_i^2 + z_i^2) \\ I_{yy} &= \sum_i m_i(x_i^2 + z_i^2) \\ I_{zz} &= \sum_i m_i(x_i^2 + y_i^2) \end{aligned} \tag{2.03}$$

and the off-diagonal elements known as the products of inertia are defined as

$$\begin{aligned} I_{xy} &= -\sum_i m_i x_i y_i \\ I_{xz} &= -\sum_i m_i x_i z_i \\ I_{yz} &= -\sum_i m_i y_i z_i \end{aligned} \tag{2.04}$$

Note that the summations are over all the representative particles i at coordinates x_i, y_i and z_i with their corresponding mass m_i and $I_{xy} = I_{yx}, I_{xz} = I_{zx}$, and $I_{yz} = I_{zy}$. The rotational energy of the rotor can be rewritten as

$$T_{rot} = \frac{1}{2}\begin{pmatrix} \omega_x & \omega_y & \omega_z \end{pmatrix}\begin{pmatrix} I_{xx} & I_{xy} & I_{xz} \\ I_{yx} & I_{yy} & I_{yz} \\ I_{zx} & I_{zy} & I_{zz} \end{pmatrix}\begin{pmatrix} \omega_x \\ \omega_y \\ \omega_z \end{pmatrix} \tag{2.05}$$

$$= \frac{1}{2}(I_{xx}\omega_x^2 + I_{yy}\omega_y^2 + I_{zz}\omega_z^2 + I_{xy}\omega_x\omega_y + I_{yz}\omega_y\omega_z + I_{xz}\omega_x\omega_z)$$

In the principal axes reference frame only the diagonal elements of moment of inertia remain. Hence the rotational energy takes the following form:

$$T_{rot} = \frac{1}{2}(I_x\omega_x^2 + I_y\omega_y^2 + I_z\omega_z^2) \tag{2.06}$$

where I_x, I_y and I_z are the moments of inertia about the principal axes system.

The angular momentum $\vec{J}$ and the angular velocity $\vec{\omega}$ are related to each other with the following relation

$$\vec{J} = \vec{\vec{I}}.\vec{\omega} \tag{2.07}$$

so the rotational energy can be expressed as

$$T_{rot} = \frac{1}{2}\vec{J}.\vec{\omega}$$

$$= \frac{1}{2}\vec{J}.\vec{\vec{I}}^{-1}.\vec{J} \tag{2.08}$$

$$= \frac{1}{2}\left(\frac{J_x^2}{I_x} + \frac{J_y^2}{I_y} + \frac{J_z^2}{I_z}\right)$$

According to the conservation of energy and the conservation of angular momentum in the absence of external torques the rotational energy and the angular momentum are conserved therefore

$$(\frac{J_x^2}{I_x}+\frac{J_y^2}{I_y}+\frac{J_z^2}{I_z})=Const \text{ and } J_x^2+J_y^2+J_z^2=Const.$$

The above are the equations of an ellipsoid and a sphere, respectively, in the angular momentum space.

2.1.3 Laboratory-fixed and molecular-fixed coordinate systems

When describing the motion of a body, a non-inertial reference frame is often convenient to use and sometimes essential. In non-inertial reference frames fictitious forces that are due to the acceleration of the reference frame appear. These forces do not exist in inertial frames and do not stem from the interactions with other particles but merely from the acceleration of the reference frame. A molecular reference frame, which is rotating when viewed from the laboratory frame, is non-inertial. Even with this complication, the vibrational motion of a molecule is easier to describe in the body-fixed frame. Hence, the laboratory frame is used to describe the rotation and the molecular frame is used to describe the internal motion of the molecule. The calculated quantities can also be transformed from one reference frame to another.

Two sets of axes systems, i.e., space fixed (X, Y, Z) and molecular fixed (x, y, z) are introduced in this section [4].

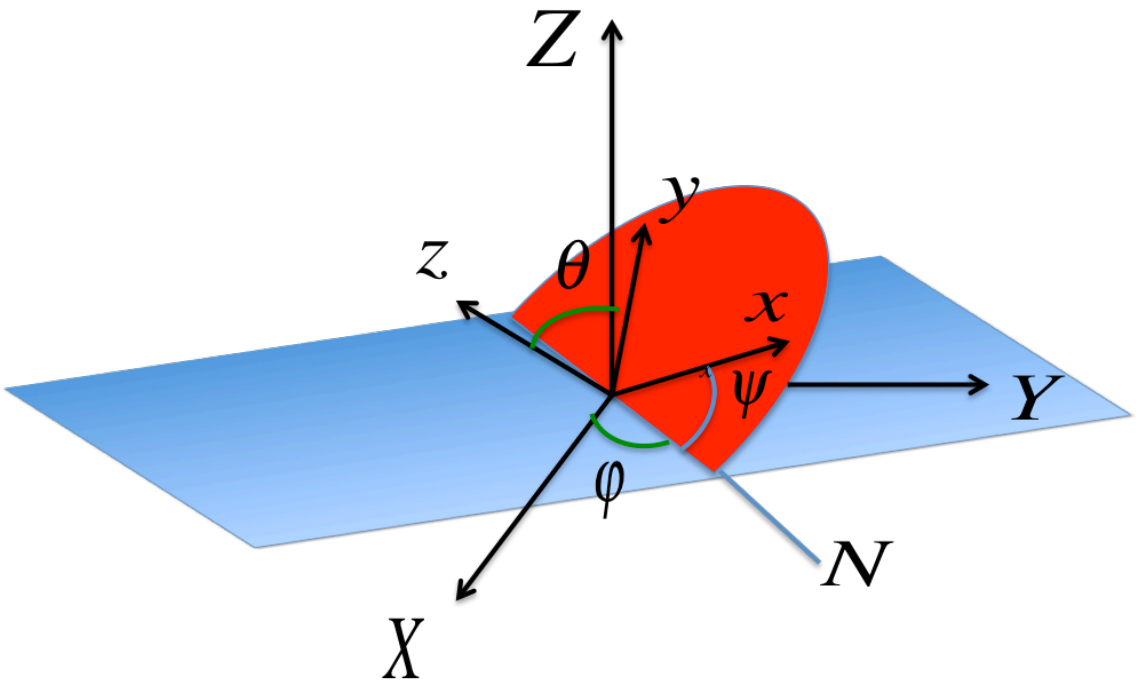

Figure 2.2 Euler angles between two coordinate systems.

The orientation of a rigid body in space can be characterized by three angles (θ, φ, ψ) which are referred to as "Euler angles" (see Figure 2.2). (θ, φ) are the usual polar and azimuthal angles in spherical coordinates and ψ describes the internal rotation of the body. By applying three successive rotations as described below the molecular axis system can be obtained from the laboratory fixed reference frame.

1. Rotation about the Z-axis through angle φ. This rotation which leaves the Z-axis unchanged, is characterized by the following 3x3 matrix:

$$S_1 = \begin{pmatrix} \cos\varphi & -\sin\varphi & 0 \\ \sin\varphi & \cos\varphi & 0 \\ 0 & 0 & 1 \end{pmatrix} \tag{2.09}$$

As a result of this rotation, we define a new axis N in the x-y plane with an angle φ from the X axis as shown in Figure 2.2.

2. Space rotation of the new reference frame about the new axis (N) through angle θ. This rotation is characterized by the following 3x3 matrix:

$$S_2 = \begin{pmatrix} 1 & 0 & 0 \\ 0 & \cos\theta & -\sin\theta \\ 0 & \sin\theta & \cos\theta \end{pmatrix} \tag{2.10}$$

This rotation defines a new axis z with an angle θ from the Z-axis.

3. Space rotation of the new reference frame about the new axis (z) through angle ψ. This operation is described by the following 3x3 matrix:

$$S_3 = \begin{pmatrix} \cos\psi & -\sin\psi & 0 \\ \sin\psi & \cos\psi & 0 \\ 0 & 0 & 1 \end{pmatrix} \tag{2.11}$$

and establishes the x, y, z axes as shown.

Now the total rotation matrix (S) that matches the laboratory reference frame (X, Y, Z) to the molecular reference frame (x, y, z) is generated by the product of the three aforementioned matrices, i.e.,

$$S = S_1 S_2 S_3 \tag{2.12}$$

$$S = \begin{pmatrix} \cos\psi\cos\varphi - \sin\psi\cos\theta\sin\varphi & -\cos\psi\sin\varphi - \sin\psi\cos\theta\cos\varphi & \sin\psi\sin\theta \\ \cos\varphi\sin\psi + \cos\psi\cos\theta\sin\varphi & \cos\psi\cos\theta\cos\varphi - \sin\psi\sin\varphi & -\cos\psi\sin\theta \\ \sin\theta\sin\varphi & \sin\theta\cos\varphi & \cos\theta \end{pmatrix}$$

Any vector, such as the position of a particle $\vec{r}$ or angular momentum of the molecule $\vec{J}$, can now be transformed from the space fixed system (J_X, J_Y, J_Z) to the molecular frame (J_x, J_y, J_z) using the transformation matrix S through the following relation.

$$J_i = S_{ij} J_j \tag{2.13}$$

where i=x, y, z, j=X, Y, Z and S_{ij} are the related S matrix elements.

Now that the relation between the quantities in the rotating and fixed reference frames has been established, we can describe the motion of a rotator in the two systems. Consider a symmetric top that is rotating about its symmetry axis with angular velocity of $\vec{\omega}$ in the gravitational field as shown in Figure 2.3. The centre of gravity of the top is on the symmetry axis and represented by G. The Euler (θ, φ, ψ) angles specify the orientation of the top with respect to the space fixed (X, Y, Z) axis.

The Euler's equations of motion for describing the motion of a rigid rotator can be written as

$$\left(\frac{d\vec{L}}{dt}\right)_s = \left(\frac{d\vec{L}}{dt}\right)_b + \vec{\omega} \times \vec{L} \tag{2.14}$$

where the subscripts s and b denote that time derivatives are with respect to space fixed and body fixed axes respectively and $(\frac{d\vec{L}}{dt})_s$ is the torque $\vec{\tau}$ acting on the top. Hence, dropping the subscript b the equation 2.14 takes the following form:

$$\vec{\tau} = \frac{d\vec{L}}{dt} + \vec{\omega} \times \vec{L} \tag{2.15}$$

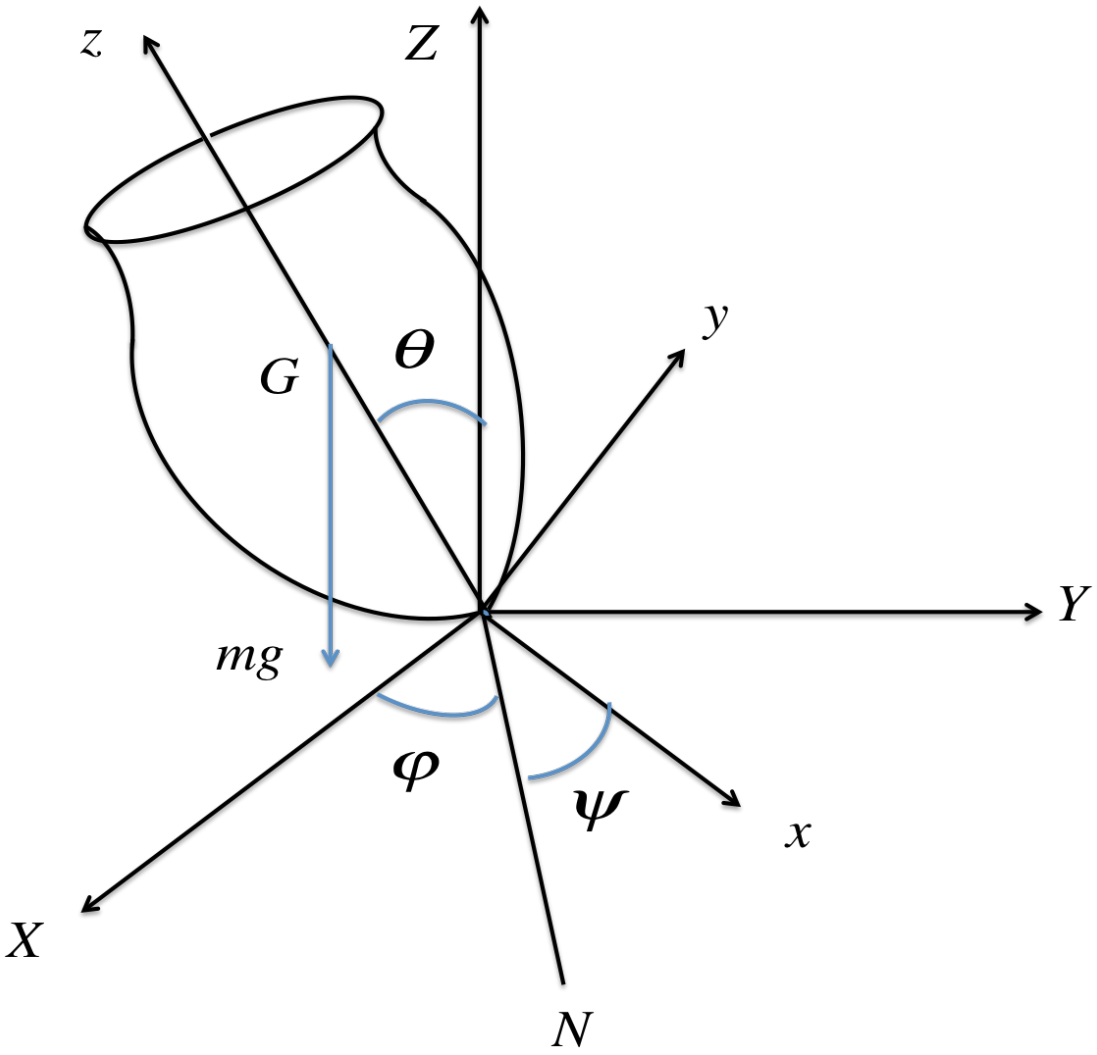

Figure 2.3 A spinning symmetric top in the gravitational force field.

whose ith component can be written as [5]

$$\tau_i = \frac{dL_i}{dt} + \varepsilon_{ijk}\omega_j L_k . \tag{2.16}$$

Since $L_i = I_i\omega_i$ the above equation takes the following compact form

$$\tau_i = I_i \frac{d\omega_i}{dt} + \varepsilon_{ijk}\omega_j\omega_k I_k \tag{2.17}$$

Note that the summation is only over the repetitive index of the second term on the right and ε_{ijk} is the Levi-Civita symbol. Therefore, the expanded form of the Euler's equation of motion can be written as

$$\tau_x = I_x\dot{\omega}_x - \omega_y\omega_z(I_y - I_z) \tag{2.18}$$

$$\tau_y = I_y\dot{\omega}_y - \omega_z\omega_x(I_z - I_x)$$

$$\tau_z = I_z\dot{\omega}_z - \omega_x\omega_y(I_x - I_y)$$

For the special case of the torque-free motion, we can multiply equations 2.18 by $I_x\omega_x$, $I_y\omega_y$ and $I_z\omega_z$. After rearranging we have

$$I_x^2\dot{\omega}_x\omega_x - I_x\omega_x\omega_y\omega_z(I_y - I_z) = 0$$

$$I_y^2\dot{\omega}_y\omega_y - I_y\omega_x\omega_y\omega_z(I_z - I_x) = 0 \tag{2.19}$$

$$I_z^2\dot{\omega}_z\omega_z - I_z\omega_x\omega_y\omega_z(I_x - I_y) = 0.$$

Adding the above equations gives

$$I_x^2\dot{\omega}_x\omega_x + I_y^2\dot{\omega}_y\omega_y + I_y^2\dot{\omega}_y\omega_y = 0 \tag{2.20}$$

and hence

$$\frac{1}{2}\frac{d}{dt}(I_x^2\omega_x^2 + I_y^2\omega_y^2 + I_z^2\omega_z^2) = 0\,. \tag{2.21}$$

Therefore, $\frac{d}{dt}(L^2) = 0$ and we have

$$L_x^2 + L_y^2 + L_z^2 = L^2 = \text{constant}. \tag{2.22}$$

This result implies that when there is no torque the square of the total angular momentum in the body-fixed frame is constant. With the same analogy, for the case of a torque free motion if we multiply the equation by ω_x, ω_y and ω_z we get

$$E_{rot} = \frac{1}{2}(I_x\omega_x^2 + I_y\omega_y^2 + I_z\omega_z^2) = \frac{1}{2}(\frac{L_x^2}{I_x} + \frac{L_y^2}{I_y} + \frac{L_z^2}{I_z}) = \text{constant} \tag{2.23}$$

which implies that the rotational energy in the torque free motion is constant.

In the case of the symmetric top I_x=I_y and from equation 2.18 we have:

$$\frac{dL_z}{dt} = 0 \text{ and } L_z = \text{constant}. \tag{2.24}$$

Therefore, L_z is constant of motion.

In the space-fixed frame $\vec{L} = L_X\hat{i} + L_Y\hat{j} + L_Z\hat{k}$ and if the torque $\vec{\tau} = \tau_X\hat{i} + \tau_Y\hat{j} + \tau_Z\hat{k}$ is applied to the top then we know that $\vec{\tau} = \frac{d\vec{L}}{dt}$. If $\vec{\tau} = 0$ then $\vec{L} = \text{constant}$ and hence

$$L_X^2 + L_Y^2 + L_Z^2 = L^2 = \text{constant}. \tag{2.25}$$

Therefore, in both of the molecular- and spaced-fixed reference frames we have $L^2 = \text{constant}$. Now the components of $\vec{L}$ must simultaneously satisfy equations 2.22 and 2.23 which are for a sphere and an ellipsoid. Therefore, for a symmetric top, $\vec{L}$ sweeps a circle around the ellipsoid [6]. This motion is shown in blue in Figure 2.4.

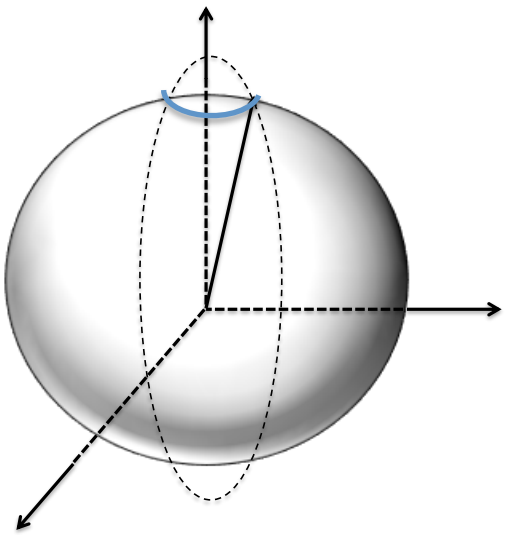

Figure 2.4 The restricted motion of a symmetric top.

On the other hand, in an asymmetric top rotator $I_x \neq I_y \neq I_z$ and therefore, its rotational motion is different from symmetric tops.

2.1.4 Angular momentum algebra

In quantum mechanics, angular momentum is an operator and its arithmetic obeys certain rules. For instance, in quantum mechanics the relation J_xJ_y-J_yJ_x is not equal to zero as is the case in classical mechanics. In the previous section, we presented a scheme to relate the components of angular momentum as observed in the laboratory to the components of a set of axes attached to the molecule. The commutation relations between the components relative to the angular momentum in the molecular frame obey $[J_x, J_y] = -i\hbar J_z$ while in the space fixed axes $[J_X, J_Y] = i\hbar J_Z$ holds true [1, 6, 7]. It is evident that all the components of J in the molecular-fixed frame commute with those

measured in the laboratory frame. This is because these axes systems are essentially independent. Note that J^2 commutes with all components of angular momentum in both systems. Therefore, J^2, J_z and J_Z operators have simultaneous eigenfunctions.

2.1.5 The symmetric top and its rotational energy level structure

In previous sections we obtained the rotational energy of a classical rigid rotator (see equation 2.23). In quantum mechanics the rotational Hamiltonian of a rigid rotator can analogously be written as $H = B_\alpha J_\alpha^2$ with $\alpha = a$, b and c which were described in section 2.1.1. This equation contains the products of the B_α called the rotational constants and the squares of corresponding angular momentums J_α^2. The rotational constants can be expressed as $B_a = A = \frac{1}{2I_a}$, $B_b = B = \frac{1}{2I_b}$ and $B_c = C = \frac{1}{2I_c}$. Therefore, we will have $H = \frac{J_a^2}{2I_a} + \frac{J_b^2}{2I_b} + \frac{J_c^2}{2I_c}$. For simplicity it can be rewritten as

$$H = AJ_a^2 + BJ_b^2 + CJ_c^2 \qquad (2.26)$$

For a prolate symmetric top molecule, since B=C, and $J_b^2 + J_c^2 = J^2 - J_a^2$ then the Hamiltonian can be written as $H = BJ^2 + (A - B)J_z^2$. Note that we have chosen that $z = a$ in a prolate symmetric top molecule for this discussion. Therefore, the rotational Hamiltonian only consists of J^2, J_z and hence commutes with J^2, J_z and J_Z. Therefore they possess common eignfunctions which are represented by $|JKM\rangle$. The eigenvalues are given by the following relations [1, 6, 7, 8]:

$$
\begin{aligned}
H\left|JKM\right\rangle &= E\left|JKM\right\rangle \\
J^2\left|JKM\right\rangle &= J(J+1)\hbar^2\left|JKM\right\rangle \\
J_Z\left|JKM\right\rangle &= M\hbar\left|JKM\right\rangle \\
J_z\left|JKM\right\rangle &= K\hbar\left|JKM\right\rangle
\end{aligned}
\tag{2.27}
$$

where E, $J(J+1)\hbar^2$, $M\hbar$ and $K\hbar$ represent the eigenvalues of H, J^2, J_Z and J_z associated with the $\left|JKM\right\rangle$ eignfunctions with

J=0, 1, 2,…;

M=-J, 1-J,…,J-1, J;

K=-J, 1-J,…, J-1, J .

K can be interpreted as the projection of the angular momentum along the molecular z-axis.

The corresponding energy levels for prolate tops can be obtained by applying the associated Hamiltonian to the eignfunction;

$$
\begin{aligned}
H\left|JKM\right\rangle &= (BJ^2 + (A-B)J_z^2)\left|JKM\right\rangle \\
&= BJ^2\left|JKM\right\rangle + (A-B)J_z^2\left|JKM\right\rangle
\end{aligned}
\tag{2.28}
$$

$$E(J,K) = BJ(J+1) + (A-B)K^2$$

Similarly the energy level expression for oblate tops can be derived as follows [1, 5]:

$$E(J,K) = BJ(J+1) + (C-B)K^2 \tag{2.29}$$

Since (A-B)>0 and (C-B)<0 for a given J, the energy increases with K for prolate molecules while it decreases for oblate molecules. It is also evident that the states with $\pm K$ are degenerate hence a twofold degeneracy is observed for each rotational level.

2.1.6 Energy levels of asymmetric top molecules in the rigid rotor approximation

As mentioned in section 2.1.3 for the case of an asymmetric top none of the principal moments of inertia are equal. Therefore, the rotational Hamiltonian cannot be arranged in such a way that consists of J^2, J_z as was the case for symmetric top (see Figure 2.2 for the classical analogue). There is no axis in the molecule about which the rotation is conserved [6, 7]. Therefore, it is customary to use the symmetric top basis to find the matrix elements of an asymmetric top. To construct the matrix representation of the rotational Hamiltonian, a ladder operator, $J^{\pm}$, is used where:

$$J^{\pm} = J_a \pm iJ_b . \tag{2.30}$$

Hence the asymmetric top Hamiltonian can be rearranged as follows [1, 6, 7]:

$$H = \left(\frac{A+B}{2}\right)J^2 + \left(C - \frac{A+B}{2}\right)J_c^2 + \left(\frac{A-B}{4}\right)\left((J^+)^2 + (J^-)^2\right) \tag{2.31}$$

then the matrix elements of the Hamiltonian can be calculated using 2.27 and the following relation

$$J^{\pm}\left|JKM\right\rangle = \hbar\left[J(J+1)-K(K\mp 1)\right]^{1/2}\left|J(K\mp 1)M\right\rangle \qquad (2.32)$$

Therefore, in the symmetric top basis the matrix elements of the operators involved in the Hamiltonian take the following form:

$$\left\langle JKM\left|J^2\right|JKM\right\rangle = \hbar^2 J(J+1)$$

$$\left\langle JKM\left|J_z^2\right|JKM\right\rangle = \hbar^2 K^2 \qquad (2.33)$$

$$\left\langle JK\mp 2M\left|J^{\pm}\right|JKM\right\rangle = \hbar^2\{[(J\mp K)(J\mp K+1)(J\mp K-1)(J\pm K+1)]\}^{1/2}$$

Since K=-J,…, J the Hamiltonian matrix dimension is (2J+1)x(2J+1) for a given M. Figure 2.5 shows how the infinite Hamiltonian matrix including all values of K is factorized into blocks of common J [6]. Note that the overall matrix is diagonal in J.

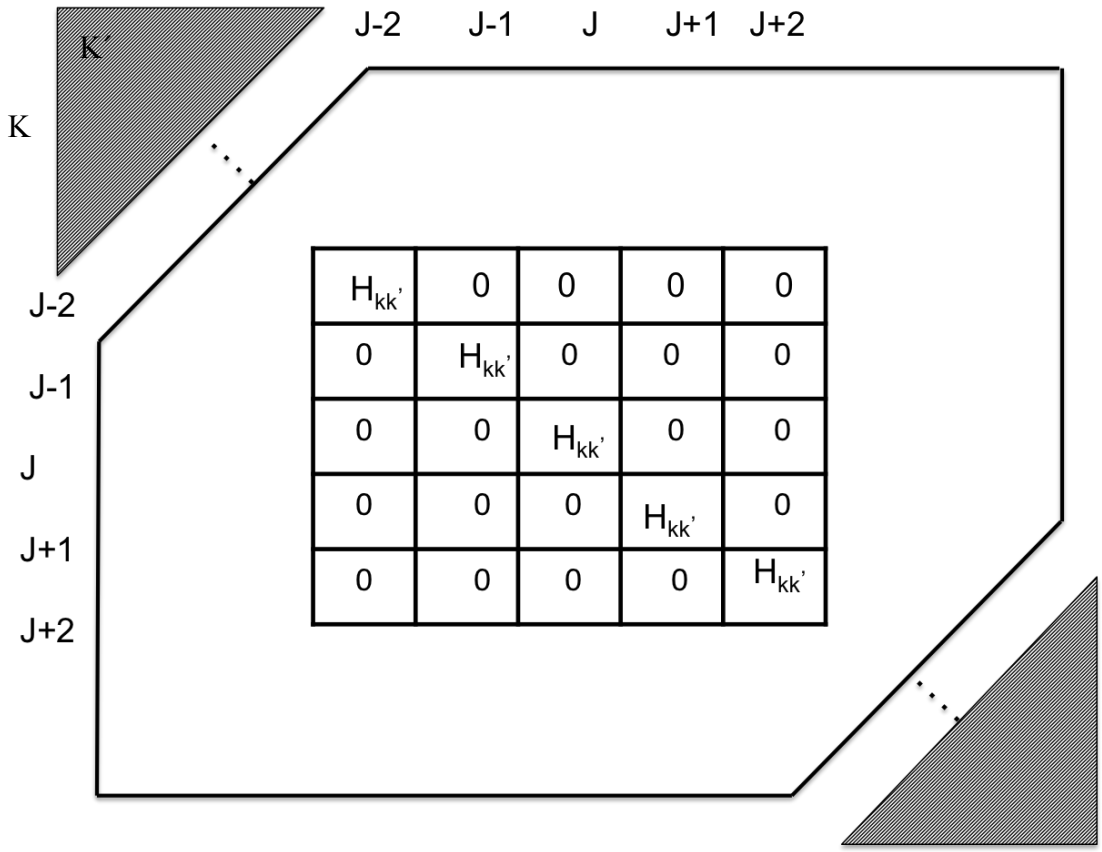

Figure 2.5 The block diagonal infinite Hamiltonian matrix for a given *J*.

For instance for J=1, we can consider a 3x3 matrix of the full Hamilton with:

$|J=1,K=0\rangle$, $|J=1,K=-1\rangle$, and $|J=1,K=1\rangle$ as the basis functions

$$H = \begin{array}{c} \\ \langle 1,1| \\ \langle 1,0| \\ \langle 1,-1| \end{array} \begin{array}{c} \begin{array}{ccc} |1,1\rangle & |1,0\rangle & |1,-1\rangle \end{array} \\ \begin{pmatrix} C+\frac{A+B}{2} & 0 & \frac{A-B}{2} \\ 0 & A+B & 0 \\ \frac{A-B}{2} & 0 & C+\frac{A+B}{2} \end{pmatrix} \end{array} \tag{2.34}$$

Although the diagonalization of the above tridiagonal matrix can be simply done by solving a secular equation of $|H-EI|$=0 to find the energies, another approach is adapted for the reason that will be clear shortly. The Hamiltonian matrix can be readily diagonalized using a Wang transformation [6, 7]

$$U_J H U_J \tag{2.35}$$

where U for J=1 is given by

$$U = \frac{1}{\sqrt{2}} \begin{pmatrix} -1 & 0 & 1 \\ 0 & \sqrt{2} & 0 \\ 1 & 0 & 1 \end{pmatrix} \tag{2.36}$$

Therefore we will have,

$$\frac{1}{2}\begin{pmatrix} -1 & 0 & 1 \\ 0 & \sqrt{2} & 0 \\ 1 & 0 & 1 \end{pmatrix}\begin{pmatrix} C+\frac{A+B}{2} & 0 & \frac{A-B}{2} \\ 0 & A+B & 0 \\ \frac{A-B}{2} & 0 & C+\frac{A+B}{2} \end{pmatrix}\begin{pmatrix} -1 & 0 & 1 \\ 0 & \sqrt{2} & 0 \\ 1 & 0 & 1 \end{pmatrix}$$

$$=\begin{pmatrix} B+C & 0 & 0 \\ 0 & A+B & 0 \\ 0 & 0 & A+C \end{pmatrix}$$

Therefore, eigenvalues are found to be: B+C, A+B and A+C.

In principle, the problem of finding the eigenvalues of asymmetric top Hamiltonian can be obtained by solving the secular equation. However, further simplification is possible by considering the symmetry of the Hamiltonian. Further examination of the Hamiltonian matrix 2.34 reveals its symmetry in both diagonals. We have the degeneracy $E_{KK}= E_{-K-K}$ and $E_{K,K+2}=E_{K+2,K}=E_{-K,-K-2}=E_{-K-2,-K}$ in $\pm K$.

So, in general if we take the tridiagonal matrix in a symmetric basis and apply the Wang transformation (see equation 2.35) we get a matrix diagonalized in two blocks. Even and odd K can be partitioned. Then the Hamiltonian matrix can be factorized into four tridiagonal submatrices such that

$$H(K)=UHU=E^{+}(K)+E^{-}(K)+O^{+}(K)+O^{-}(K) \qquad (2.37)$$

where E and O refer to even and odd K and the plus and minus signs indicate if $\alpha=0$ or 1 in a new basis function proposed by Wang [6]

$$\frac{1}{\sqrt{2}}[|J+K\rangle+(-1)^{\alpha}|J-K\rangle \qquad (2.38)$$

For instance, for J=9 the tridiagonal four submatrices take the following form as a result of applying 2.35.

$$E^{+}(K)=\begin{pmatrix} E_{0,0} & \sqrt{2}E_{0,2} & 0 & 0 & 0 \\ \sqrt{2}E_{0,2} & E_{2,2} & E_{2,4} & 0 & 0 \\ 0 & E_{2,4} & E_{4,4} & E_{4,6} & 0 \\ 0 & 0 & E_{4,6} & E_{6,6} & E_{6,8} \\ 0 & 0 & 0 & E_{6,8} & E_{8,8} \end{pmatrix} \tag{2.39}$$

$$E^{-}(K)=\begin{pmatrix} E_{2,2} & E_{2,4} & 0 & 0 \\ E_{2,4} & E_{4,4} & E_{4,6} & 0 \\ 0 & E_{4,6} & E_{6,6} & E_{6,8} \\ 0 & 0 & E_{6,8} & E_{8,8} \end{pmatrix}$$

$$O^{+}(K)=\begin{pmatrix} E_{1,1}+E_{-1,1} & E_{1,3} & 0 & 0 & 0 \\ E_{1,3} & E_{3,3} & E_{3,5} & 0 & 0 \\ 0 & E_{3,5} & E_{5,5} & E_{5,7} & 0 \\ 0 & 0 & E_{5,7} & E_{7,7} & E_{7,9} \\ 0 & 0 & 0 & E_{7,9} & E_{9,9} \end{pmatrix}$$

$$O^{-}(K)=\begin{pmatrix} E_{1,1}-E_{-1,1} & E_{1,3} & 0 & 0 & 0 \\ E_{1,3} & E_{3,3} & E_{3,5} & 0 & 0 \\ 0 & E_{3,5} & E_{5,5} & E_{5,7} & 0 \\ 0 & 0 & E_{5,7} & E_{7,7} & E_{7,9} \\ 0 & 0 & 0 & E_{7,9} & E_{9,9} \end{pmatrix}$$

The dimensions of these submatrices are either (J+1)/2 or (J-1)/2 which can be independently diagonalized.

The above-mentioned method lays the foundation for the general numerical procedures that are being employed for calculation of the eigenvalues of the asymmetric top molecule.

To conclude this section, we present a correlation diagram that connects the energy levels of the prolate and oblate symmetric tops to the asymmetric top. If we have arbitrary values of A, B and C for an asymmetric molecule then we can define a parameter $\kappa = \frac{2B - A - C}{A - C}$ [1, 7]. This parameter indicates the degree of asymmetry of a molecule. The energy levels can be characterized in terms of κ. For the case of an oblate symmetric top, $\kappa = 1$ and for a prolate symmetric top, $\kappa = -1$. For asymmetric top molecules if this value is closer to the oblate or the prolate case, then the molecule is called near oblate or near prolate.

To plot the correlation energy level diagram, we can use the algebraic expressions that have been obtained up to J=30 for the rotational energy levels of an asymmetric rotor [9]. This algebraic expression for a specific level can be represented by [6, 9]:

$$E(J\kappa) = \frac{1}{2}(A + C)J(J + 1) + \frac{1}{2}(A - C)E_{J\tau}(\kappa) \qquad (2.40)$$

where $E_{J\tau}(\kappa)$ are the reduced energies (a part of eigenvalues related to the 2.31 Hamiltonian) with $\tau = K_a - K_c$ and given in table 2.1 [6, 9]. K_a and K_c are the projections of the total angular momentum along *a* and *c* axes for the prolate and oblate molecules respectively. Note that J_{KaKc} is used to label the rotational states of asymmetric top molecules.

Table 2.1 Expressions for the reduced energies.

J_{KaKc}	τ	$E_{J\tau}(\kappa)$
0_{00}	0	0
1_{10}	-1	$\kappa+1$
1_{11}	0	0
1_{01}	+1	$\kappa-1$
2_{20}	-2	$2(\kappa+\sqrt{\kappa^2+3})$
2_{21}	-1	$\kappa+3$
2_{11}	0	4κ
2_{12}	1	$\kappa-3$
2_{02}	2	$2(\kappa-\sqrt{\kappa^2+3})$
3_{30}	-3	$5\kappa+3+2\sqrt{4\kappa^2-6\kappa+6}$
3_{31}	-2	$2(\kappa+\sqrt{\kappa^2+15})$
3_{21}	-1	$5\kappa-3+2\sqrt{4\kappa^2+6\kappa+6}$
3_{22}	0	4κ
3_{12}	1	$5\kappa+3-2\sqrt{4\kappa^2-6\kappa+6}$
3_{13}	2	$2(\kappa-\sqrt{\kappa^2+15})$
3_{03}	3	$5\kappa-3-2\sqrt{4\kappa^2+6\kappa+6}$

For instance for an asymmetric top molecule (furan) with A=0.315 cm^{-1}, B=0.308 cm^{-1} and C=0.155 cm^{-1}, $\kappa = 0.923$, which shows that the molecule is closer to an oblate symmetric top than to a prolate symmetric top.

The correlation energy level diagram for furan molecule is shown in Figure 2.6. This Figure shows the relation of the asymmetric rotor energy levels between two limiting cases of symmetric tops, i.e., prolate and oblate. A vertical dotted line at $\kappa = 0.923$ which corresponds to the measure of its asymmetry is also shown in the picture. Note that the levels with the same K_c are no longer degenerate as the symmetry of the molecules is broken, i.e., around $\kappa = 0.923$.

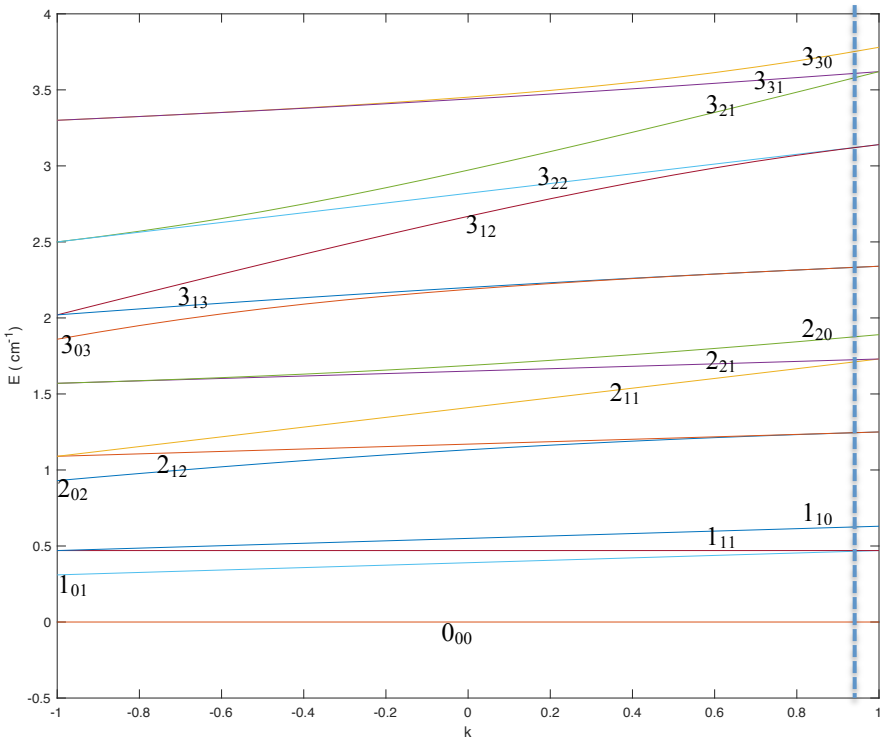

Figure 2.6 The correlation energy level diagram of furan molecule for J=0, 1, 2 and 3 rotational levels labeled as J_{KaKc} and with $\kappa = 0.923$ identified as a vertical dotted line.

Finding the analytical solutions for the asymmetric top Hamiltonian can be extended to other low *J* cases. However, the full Hamiltonian of an asymmetric top cannot be solved analytically and must be solved numerically. Further discussion of the asymmetric top Hamiltonian used in the thesis can be found in chapter 9.

2.2 Vibrational energy of polyatomic molecules

The classical kinetic energy for a system of N atoms is given by

$$T = \frac{1}{2}\sum_{i=1}^{N} m_i V_i^2 \tag{2.41}$$

where m_N is the mass of each nucleus and V_N is its associated speed. The above expression can be reformulated using the following mass-weighted Cartesian displacement coordinates [1]:

$$\begin{aligned}
q_1 &= (m_1)^{\frac{1}{2}}(x_1 - x_{1e}) \\
q_2 &= (m_1)^{\frac{1}{2}}(y_1 - y_{1e}) \\
q_3 &= (m_1)^{\frac{1}{2}}(z_1 - z_{1e}) \\
q_4 &= (m_2)^{\frac{1}{2}}(x_2 - x_{2e}) \\
&\cdot \\
&\cdot \\
&\cdot \\
q_{3N} &= (m_N)^{\frac{1}{2}}(z_N - z_{Ne})
\end{aligned} \tag{2.42}$$

where q_i describes the displacement of the nuclear coordinates from the equilibrium position denoted by the subscript. Hence the kinetic energy can be rewritten as:

$$T = \frac{1}{2}\sum_{i=1}^{3N} \dot{q}_i^2 \tag{2.43}$$

The potential energy of this system can be expanded as a Taylor series around the nuclear equilibrium positions

$$V = V(q_i = 0) + \sum_i \left.\frac{\partial V}{\partial q_i}\right|_{q_i=0} q_i + \frac{1}{2}\sum_i\sum_j \left.\frac{\partial^2 V}{\partial q_i \partial q_j}\right|_{q_i=0,\, qj=0} q_i q_j +$$

$$\frac{1}{3!}\sum_i\sum_j \left.\frac{\partial^3 V}{\partial q_i \partial q_j \partial q_k}\right|_{q_i=0,\, qj=0,\, q_k=0} q_i q_j q_k + \ldots \tag{2.44}$$

We choose the potential energy to be zero at the equilibrium position. At the minimum of the potential $\sum_i \left.\frac{\partial V}{\partial q_i}\right|_{q_i=0}$ is also zero. Within the harmonic approximation, the higher orders of the expansion which are greater than two can be neglected. The force constants f_{ij}, are the second derivative of the potential energy and are defined as

$$f_{ij} = \left.\frac{\partial^2 V}{\partial q_i \partial q_j}\right|_{q_i=0} \tag{2.45}$$

Hence the potential energy can be rewritten as

$$V = \frac{1}{2}\sum_{i,j} f_{ij} q_i q_j \tag{2.46}$$

Therefore, the Lagrangian of the system can be formed as

$$L = T(\dot{q}_i) - V(q_i) = \frac{1}{2}\sum_{i=1}^{3N} \dot{q}_i^2 - \frac{1}{2}\sum_{i,j} f_{ij} q_i q_j \,. \tag{2.47}$$

Substituting the above Lagrangian into the Lagrangian equation

$$\frac{d}{dt}\left(\frac{\partial L}{\partial \dot{q}_i}\right)_{q_i} - \left(\frac{\partial L}{\partial q_i}\right)_{\dot{q}_i} = 0 \tag{2.48}$$

the equation of motion can be derived as

$$\ddot{q}_i + \sum_j f_{ij} q_j = 0 \quad i = 1,...,3N \tag{2.49}$$

which forms a set of 3N coupled second order differential equations. This can be solved by considering a solution in form of

$$q_i = A_i \cos(\omega t + \theta) \tag{2.50}$$

which gives the following result when substituted in (2.49)

$$-\omega^2 A_i + \sum_j f_{ij} A_j = 0 \,. \tag{2.51}$$

In above equation, ω is the vibrational frequency associated with the vibrational motion of the nucleus from the equilibrium position. To find the answer to the 3N equations written in compact form, the determinant of the coefficient matrix must be equal to zero, therefore:

$$\begin{vmatrix} f_{11}-\omega^2 & f_{12} & \cdots & f_{1,3N} \\ f_{21} & f_{22}-\omega^2 & \cdots & \vdots \\ \vdots & & & \vdots \\ \vdots & & & \vdots \\ \vdots & & & \\ f_{3N,1} & \cdots & & f_{3N,3N}-\omega^2 \end{vmatrix} = 0 \tag{2.52}$$

Expanding the above 3N by 3N determinant leads to an equation of the order of 3N in terms of ω^2, hence there will be 3N solutions to it. These eigenvalues describe the frequencies associated with each degree of freedom. For linear and nonlinear molecules there will be 3N-5 and 3N-6 eigenvalues when degrees of freedom associated with translational and rotational motion are subtracted. These frequencies are zero because there is no restoring force related to translational and rotational motion of the molecules.

There is a normal mode Q_K related to each of the eigenvalues. By using the following linear transformation, the normal modes can be related to the nuclear coordinates q_j [1, 10]

$$Q_k = \sum_j l_{kj} q_j \,. \tag{2.53}$$

where l_{kj} are elements of an orthogonal matrix L where $L^T L=1$. Note that there is a double sum in equation 2.46 which is quadratic with cross products. By using the l_{kj} as a change of variables equation 2.46 transforms to a singe sum of squares. The kinetic and potential energies of the system can be reformulated as follows using the normal modes

$$T = \frac{1}{2}\sum_i \dot{Q}_i^2$$

(2.54)

$$V = \frac{1}{2}\sum_i \omega_i^2 Q_i^2 \ .$$

Also, the generalized momenta P_i associated with normal modes Q_i can be written as

$P_i = \left(\frac{\partial L}{\partial \dot{Q}_i}\right)_{Q_i} = \dot{Q}_i$ where L is Lagrangian of the system, i.e., $L(Q_i, \dot{Q}_i) = T(\dot{Q}_i) - V(Q_i)$.

Now the classical Hamiltonian takes the following form

$$H = \frac{1}{2}\sum_i P_i^2 + \frac{1}{2}\sum_i \omega_i^2 Q_i^2 \qquad (2.55)$$

By using the quantum mechanical operator for momentum P_i

$$P_i = -i\hbar\frac{\partial}{\partial Q_i} \qquad (2.56)$$

the quantum mechanical Hamiltonian can be formed as

$$H = -\frac{\hbar^2}{2}\sum_i \frac{\partial^2}{\partial Q_i^2} + \frac{1}{2}\sum_i \omega_i^2 Q_i^2 \ . \qquad (2.57)$$

Then the total Hamiltonian can be written as sum of independent harmonic oscillators:

$$H = \sum_i H_i \qquad (2.58)$$

The wave function in the Schrödinger equation

$$H\psi = E\psi \tag{2.59}$$

can also be established using the product of the wave functions of the individual harmonic oscillators

$$\psi = \psi_1(Q_1)\psi_2(Q_2)..\psi_{3N-6}(Q_{3N-6}) = \prod_{i=1}^{3N-6}\psi_i(Q_i). \tag{2.60}$$

Replacing the quantum mechanical Hamiltonian described by (2.57) in the wave equation gives

$$-\frac{\hbar^2}{2}\frac{\partial^2\psi_i(Q_i)}{\partial Q_i^2} + \frac{1}{2}\omega_i^2 Q_i^2\psi_i(Q_i) = E_i\psi_i(Q_i) \tag{2.61}$$

where $\psi_i(Q_i) = N_{vi}H_{vi}(\xi_i)e^{-\frac{\xi_i^2}{2}}$ are the vibrational wave functions, N_{vi} are the normalization factors and $H_{vi}(\xi_i)$ are the Hermite polynomials with $\xi_i = Q_i\left(\frac{\omega_i}{\hbar}\right)^{\frac{1}{2}}$.

The eigenvalues are found to be

$$E_i = \hbar\omega_i(v_i + \frac{1}{2}) \tag{2.62}$$

where v_i is the vibrational quantum number associated with mode i with 0,1,2,.. values. The total vibrational energy is the summation of all individual oscillators

$$E = \sum_i E_i \tag{2.63}$$

Therefore, for a nonlinear molecule

$$E = \hbar\omega_1(v_1 + \frac{1}{2}) + ... + \hbar\omega_{3N-6}(v_{3N-6} + \frac{1}{2}) \tag{2.64}$$

which can be rewritten as

$$E = \sum_i \hbar\omega_i(v_i + \frac{1}{2}). \tag{2.65}$$

Since the degrees of freedom determine the upper limit of the summations in the above equations, for the case of a linear molecule 3N-6 is replaced by 3N-5.

2.2.1 Anharmonic effects

In the harmonic approximation the cubic, quadratic and other higher order terms have not been taken into account in the potential energy expression which lead to the (2.62) expression for the vibrational energy levels. However, these terms can be considered as perturbations and can be added to the Hamiltonian as perturbing potentials. Using the perturbation theory the following modified expression can be obtained [1, 10]

$$E = \sum_i \hbar\omega_i (v_i + \frac{1}{2}) + \sum_{i,j} \hbar x_{i,j} (v_i + \frac{1}{2})(v_j + \frac{1}{2}) + \hbar G_0 \qquad (2.66)$$

where $x_{i,j}$ are anharmonicity coupling coefficients and G_0 is a constant that appears partly due to anharmonicity and partly due to vibration-rotation coupling.

This provides a more realistic picture of a molecular system, "a rotating anharmonic oscillator".

2.2.2 Centrifugal distortion

Molecules are not rigid; this is a useful assumption for simplifying the problem and the interpretation of rotational spectra. In accelerated frames, such as the molecular reference frame, fictitious forces are present. Consequently, the bonds between atoms experience additional forces leading to bond distortion. Hence, the geometry of the molecule is

changed which affects its moments and products of inertia. As the molecule goes to higher rotational excitation, it rotates faster and the bonds lengths become longer [10]. This can cause bond breaking at the dissociation limit. Therefore, corrections to our ideal Hamiltonian need to be made by adding some additional terms to compensate for nonrigidity of the molecule. For instance, in the case of a symmetric rotor the Hamiltonian takes the following form when centrifugal distortion constants are taken into account [1, 6, 11].

$$E(J,K) = BJ(J+1) - D_J[J(J+1)]^2 + (A-B)K^2 - D_k K^2 - D_{JK} J(J+1)K^2 . \qquad (2.67)$$

In the above equation, D_J and D_K are centrifugal distortion corrections for rotations about the *a* and *b* axes respectively and D_{JK} splits the transitions into J+1 components. For the case of an asymmetric rotor quartic and sextic distortion constants are also included in the Hamiltonian as done by Watson et al. [4, 7] (see section 9.2).

2.3 Coriolis interactions

As with the centrifugal distortion corrections, the Coriolis force is fictional. This fictitious force is only present in the rotating reference frame attached to the molecule and not in the fixed laboratory frame. From a classical point of view, a particle of mass m and velocity $\vec{V}$ experiences the Coriolis force of $\vec{F} = 2m(\vec{V} \times \vec{\omega})$ in a frame rotating with angular velocity $\vec{\omega}$. As shown in Figure 2.7, if the system is rotating clockwise then the direction of angular velocity will be normal to the plane and the particle deviates to the left while moving radially.

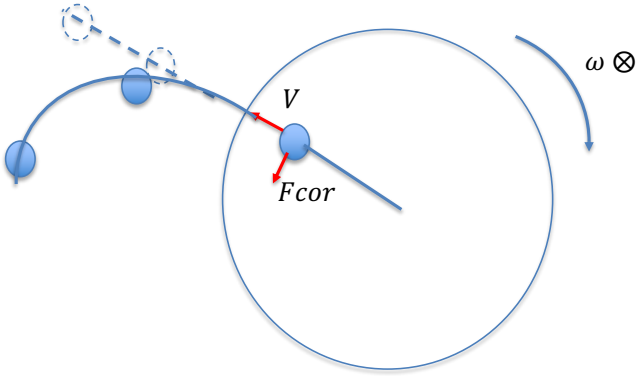

Figure 2.7 The trajectory of a moving particle in a rotating frame.

Now we can consider how the Coriolis force is exerted on particles in a triatomic linear molecule during its antisymmetric vibration. As shown in Figure 2.8 the rotating molecule experiences a Coriolis force which bends the molecule while the bonds are stretching or shortening. Therefore, a bending mode is excited [12].

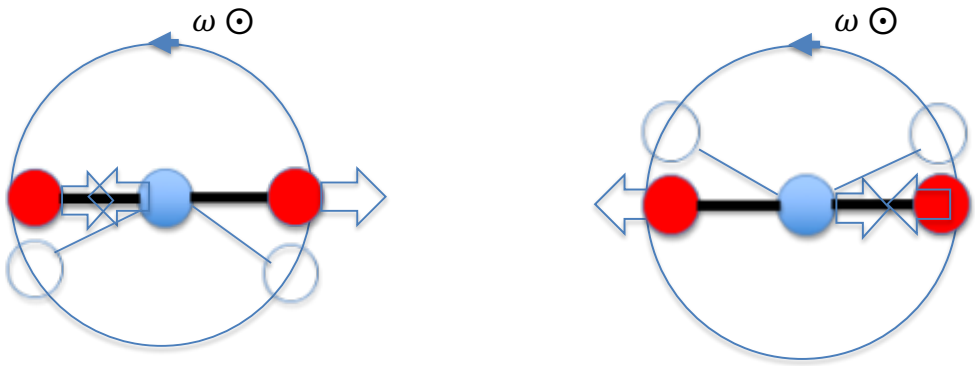

Figure 2.8 Excitation of the bending mode during antisymmetric stretch.

From the quantum point of view, to address the Coriolis interactions in polyatomic molecules the starting point is to define a proper Hamiltonian to model the system. This will be explained in the next section.

2.3.1 Coriolis interactions in polyatomic molecules

If we neglect the anharmonicity in the vibrational potential, the following Hamiltonian can provide a model for describing Coriolis interactions in polyatomic molecules [6, 13, 14, 15].

$$H = \frac{(J_x - \pi_x)^2}{2I_x} + \frac{(J_y - \pi_y)^2}{2I_y} + \frac{(J_z - \pi_z)^2}{2I_z} + \frac{1}{2}\sum_{i=1}^{3N-6}(P_i^2 + \omega_i^2 Q_i^2) \tag{2.68}$$

where π_x ,π_y and π_z are the components of vibrational angular momenta that are described by

$$\pi_\alpha = \sum_{i=1}^{3N-6}\sum_{j>1}^{3N-6}\xi_{ij}^{\alpha}(Q_i P_j - P_i Q_j) \tag{2.69}$$

where $\alpha = x, y, z$ and ξ_{ij}^{α} are Coriolis coupling constants.

The Hamiltonian can be decomposed into three different terms.

$$H = H_r + H_v + H_{rv}$$

$$H_r = \frac{J_x^2}{2I_x} + \frac{J_y^2}{2I_y} + \frac{J_z^2}{2I_z}$$

$$H_v = \frac{1}{2}\sum_{i=1}^{3N-6}(P_i^2 + \omega_i^2 Q_i^2) \tag{2.70}$$

$$H_{rv} = -\frac{J_x \pi_x}{I_x} - \frac{J_y \pi_y}{I_y} - \frac{J_z \pi_z}{I_z} + \frac{\pi_x^{\,2}}{2I_x} + \frac{\pi_y^{\,2}}{2I_y} + \frac{\pi_z^{\,2}}{2I_z}$$

where H_r is the rigid rotor Hamiltonian, H_v is the pure vibrational part and H_{rv} is the Coriolis coupling. For a case where $\pi_x = \pi_y = 0$ the rotational part of the (2.68) Hamiltonian takes the following form

$$H_r + H_{rv} = \frac{J_x^{\,2}}{2I_x} + \frac{J_y^{\,2}}{2I_y} + \frac{(J_z - \pi_z)^2}{2I_z}$$

$$= \frac{J_x^{\,2}}{2I_x} + \frac{J_y^{\,2}}{2I_y} + \frac{J_z^{\,2}}{2I_z} - \frac{J_z\pi_z}{I_z} + \frac{\pi_z^2}{2I_z} \quad . \tag{2.71}$$

If we neglect the last term in the above equation, which is purely vibrational, and does not change by rotation, the Hamiltonian becomes

$$H_r + H_{rv} = \frac{J_x^{\,2}}{2I_x} + \frac{J_y^{\,2}}{2I_y} + \frac{J_z^{\,2}}{2I_z} - \frac{J_z\pi_z}{I_z} \quad . \tag{2.72}$$

For the case of prolate and oblate symmetric tops we can rewrite the Hamiltonian as

$$H_r + H_{rv} = BJ^2 + (A - B)J_z^2 - \frac{J_z\pi_z}{I_a} \tag{2.73}$$

and

$$H_r + H_{rv} = BJ^2 + (C - B)J_z^2 - \frac{J_z\pi_z}{I_c} \tag{2.74}$$

respectively.

The effect of applying the π_z operator on the vibrational part of the wave function can be represented by

$$\pi_z \left| v \right\rangle = \xi l\hbar \left| v \right\rangle \tag{2.75}$$

where ξ is the Coriolis coupling constant ($\left|\xi\right| \le 1$), $l\hbar$ is the projection of vibrational angular momentum along the z axis with

$l = -v, ..., v$

and v being the vibrational quantum number. Now the energies for prolate and oblate symmetric tops can be calculated from the expectation value of $\left\langle v; r \left| H_r + H_{rv} \right| v; r \right\rangle$.

The term energies can therefore be calculated from

$$\langle v;r|H_r + H_{rv}|v;r\rangle = \langle v|\langle r|H_r + H_{rv}|r\rangle|v\rangle = \langle r|H_r|r\rangle + \langle rv|H_{rv}|rv\rangle \tag{2.76}$$

For the case of a prolate symmetric top substituting (2.73) into (2.76) gives

$$E = BJ(J+1) + (A-B)K^2 - 2\xi lKA \tag{2.77}$$

and for the oblate symmetric top substituting (2.74) into (2.76) provides

$$E = BJ(J+1) + (C-B)K^2 - 2\xi lKC. \tag{2.78}$$

This obviously shows that rotational term energies are shifted due to the Coriolis coupling.

2.4 Transition between rotation-vibration levels of polyatomic molecules

Consider an arbitrary molecule with a permanent dipole moment of $\vec{\mu}$. This moment can be resolved along the principal axes a, b and c of the molecule which are denoted by μ_a, μ_b and μ_c. If the molecule is initially at ground state Φ_g and is excited to the final state of Φ_e by interacting with an electromagnetic field, then the transition moment integral can be given by

$$\langle \mu \rangle = \langle \Phi_e | \mu | \Phi_g \rangle = \langle \Phi_e | \mu_a | \Phi_g \rangle + \langle \Phi_e | \mu_b | \Phi_g \rangle + \langle \Phi_e | \mu_c | \Phi_g \rangle \tag{2.79}$$

If the above equation evaluates to zero we call the transition “forbidden”. Nonzero components of a dipole moment contribute to three types of transitions:

1) If the molecule has a dipole moment component along the *a* axis and the other components are zero then an *a* type transition can occur.
2) If the molecule has a dipole moment component along the *b* axis and the other components are zero then a *b* type transition can occur.
3) If the molecule has a dipole moment component along the *c* axis and the other components are zero then a *c* type transition can occur.

2.4.1 Selection rules

For a particular type of transition to occur, the molecules must have specific properties. When a transition happens between two states, the difference in quantum numbers associated with each state should satisfy specific relations known as "selection rules" [1, 12].

Consider a molecule in the initial state denoted by $|\varepsilon v J M_J\rangle$ where ε and v represent the electronic and vibrational parts of the wavefunction and $|JM_J\rangle$ is the rotational part. The electric dipole moment of the molecule can be expressed as $\vec{\mu} = \mu_x \hat{i} + \mu_y \hat{j} + \mu_z \hat{k}$ and if we suppose $\mu_x = \mu_y = \mu_z = \mu_\circ$ then

$$\vec{\mu} = \mu_\circ(\sin\theta\cos\varphi\hat{i} + \sin\theta\sin\varphi\hat{j} + \cos\theta\hat{k}) \ . \qquad (2.80)$$

The pure rotational selection rules can be established by evaluating the $\langle \varepsilon v J' M_J' | \vec{\mu} | \varepsilon v J'' M_J'' \rangle$ matrix elements. According to the Born-Openhiemer approximation the overall wavefunction of the molecules can be separated and

represented by $|\varepsilon\rangle|v\rangle|JM_J\rangle$. Then the transition moment matrix elements can be written as

$$\begin{aligned}
&\langle \varepsilon v J'M_J'|\vec{\mu}|\varepsilon v J''M_J''\rangle \\
&= \langle \varepsilon|\langle J'M_J'|\vec{\mu}|\varepsilon\rangle\langle v|v\rangle|J''M_J''\rangle \\
&= \langle J'M_J'|\langle \varepsilon|\vec{\mu}|\varepsilon\rangle|J''M_J''\rangle \\
&= \langle J'M_J'|\vec{\mu}_\varepsilon|J''M_J''\rangle
\end{aligned} \tag{2.81}$$

where the $\langle \varepsilon|\vec{\mu}|\varepsilon\rangle = \vec{\mu}_\varepsilon$ is the dipole moment of the molecule when it is in the electronic state ε. In order to find the selection rules for pure rotational transitions, the matrix elements of (2.81) are only non-zero for specific values of $J''M''$ and $J'M'$. This provides us with the selection rules for pure rotational transitions as observed in the microwave region.

$$\langle J'M_J'|\vec{\mu}_\varepsilon|J''M_J''\rangle = \int_0^{\pi}\int_0^{2\pi} y^*_{J'M'}(\theta,\varphi)\vec{\mu}_\varepsilon y_{J''M_J''}(\theta,\varphi)\sin\theta d\theta d\varphi \tag{2.82}$$

where $y_{JM(\theta,\varphi)}$ are the spherical harmonics and $y_{JM(\theta,\varphi)} \propto e^{iM\varphi}\Theta_{JM}(\theta)$. The electric dipole moment can also be expressed in terms of spherical harmonics as well, i.e., $\vec{\mu}_\varepsilon \propto y_{1,M}$ (see equation 2.80) where $M = 0,\pm 1$. Therefore, the selection rules can then be determined to be $\Delta M = 0,\pm 1$ and $\Delta J = \pm 1$. Note that if the molecule has no electric dipole moment, i.e., $\mu_\varepsilon = 0$, then pure rotation transitions cannot happen.

2.4.2 Vibrational selection rules

Within a given electronic state ε, the selection rules for a vibrational transition can be deduced from $\langle \varepsilon v' | \vec{\mu} | \varepsilon v'' \rangle$ where $|v''\rangle$ and $|v'\rangle$ are the initial and final vibrational states respectively. For a case of a nonlinear polyatomic molecule with 3N-6 modes of vibration these states can be represented by $|v''\rangle = |v_1''...v_k''...v_{3N-6}''\rangle$ and $\langle v'| = \langle v_1'...v_k'...v_{3N-6}'|$. Within the Born-Openhiemer approximation the matrix elements of the permanent dipole moment can be obtained from $\vec{\mu}_{v''v'} = \langle v' | \vec{\mu} | v'' \rangle$ where $\vec{\mu}$ corresponds to the dipole moment of the molecule in the electronic state ε. The dipole moment in polyatomic molecules is dependent on all nuclear coordinates. It can change with changes in bond angles as well as bond lengths. We can express the dipole moment of a polyatomic molecule in terms of its normal coordinate Q_i and it can be expanded using the Taylor series around the equilibrium Q_{ie} as [1, 12]:

$$\vec{\mu} = \sum_{i=1}^{3N-6} \vec{\mu}_{ei} + \sum_{i=1}^{3N-1} \left(\frac{d\vec{\mu}}{dQ_i} \right)_{Q_{ie}} (Q_i - Q_{ie}) + \sum_{i,j=1}^{3N-6} \frac{1}{2} \left(\frac{\partial^2 \vec{\mu}}{\partial Q_i \partial Q_j} \right)_{Q_{ie} Q_{je}} (Q_i - Q_{ie})(Q_j - Q_{je}) + ... \quad (2.83)$$

where $\vec{\mu}_{ei}$ describes the dipole moment at the equilibrium for the ith mode of vibration. Therefore, the transition matrix elements become

$$\left\langle v_1'...v_k'...v_{3N-6}' \middle| \vec{\mu} \middle| v_1''...v_k''...v_{3N-6}'' \right\rangle = \sum_{i=1}^{3N-6} \left\langle v_1'...v_k'...v_{3N-6}' \middle| \vec{\mu}_{ie} \middle| v_1''...v_k''...v_{3N-6}'' \right\rangle +$$

$$\sum_{i=1}^{3N-1} \left(\frac{d\vec{\mu}}{dQ_i} \right)_{Q_{ei}} \left\langle v_1'...v_k'...v_{3N-6}' \middle| Q_i \middle| v_1''...v_k''...v_{3N-6}'' \right\rangle + \tag{2.84}$$

$$\sum_{i,j=1}^{3N-6} \frac{1}{2} \left(\frac{\partial^2 \vec{\mu}}{\partial Q_i \partial Q_j} \right)_{Q_{ie}Q_{je}} \left\langle v_1'...v_k'...v_{3N-6}' \middle| (Q_i - Q_{ie})(Q_j - Q_{je}) \middle| v_1''...v_k''...v_{3N-6}'' \right\rangle ...$$

Now in the above equation since the vibrational states are orthogonal, i.e., $\sum_{i=1}^{3N-6} \vec{\mu}_{ie} \left\langle v_1'...v_k'...v_{3N-6}' \middle| v_1''...v_k''...v_{3N-6}'' \right\rangle = \sum_{i=1}^{3N-6} \vec{\mu}_{ie} \prod_{k}^{3N-6} \delta_{v_k' v_k''}$ the first term disappears and hence we will have

$$\left\langle v_1'...v_k'...v_{3N-6}' \middle| \vec{\mu} \middle| v_1''...v_k''...v_{3N-6}'' \right\rangle = \sum_{i=1}^{3N-1} \left(\frac{d\vec{\mu}}{dQ_i} \right)_{Q_{ei}} \left\langle v_1'...v_k'...v_{3N-6}' \middle| Q_i \middle| v_1''...v_k''...v_{3N-6}'' \right\rangle +$$

$$\sum_{i,j=1}^{3N-6} \frac{1}{2} \left(\frac{\partial^2 \vec{\mu}}{\partial Q_i \partial Q_j} \right)_{Q_{ie}Q_{je}} \left\langle v_1'...v_k'...v_{3N-6}' \middle| (Q_i - Q_{ie})(Q_j - Q_{je}) \middle| v_1''...v_k''...v_{3N-6}'' \right\rangle ... \tag{2.85}$$

Therefore, if the dipole moment of the molecule changes with extension, there will be a vibrational transition and hence a vibrational spectrum. If quadratic and higher terms in 2.85 are ignored for small displacements only the first term remains and

$$\left\langle v_1'...v_k'...v_{3N-6}' \middle| \vec{\mu} \middle| v_1''...v_k''...v_{3N-6}'' \right\rangle = \sum_{i=1}^{3N-6} \left(\frac{d\vec{\mu}}{dQ_i} \right)_{Q_{ei}} \left\langle v_1'...v_k'...v_{3N-6}' \middle| Q_i \middle| v_1''...v_k''...v_{3N-6}'' \right\rangle. \tag{2.86}$$

We can write Q_i in terms raising and lowering operators, $Q_i \propto v_i^+ + v_i$, where their operations are defined as $v_i^+ \left| v_1...v_i...v_{3N-6} \right\rangle = \sqrt{v_i + 1} \left| v_1...v_{i+1}...v_{3N-6} \right\rangle$ and $v_i \left| v_1...v_i...v_{3N-6} \right\rangle = \sqrt{v_i} \left| v_1...v_{i-1}...v_{3N-6} \right\rangle$ and can be substituted in 2.28. Therefore, within the harmonic approximation this becomes:

$$\left\langle v_1'...v_k'...v_{3N-6}' \middle| \vec{\mu} \middle| v_1''...v_k''...v_{3N-6}'' \right\rangle \propto \sum_{k=1}^{3N-6} \left[\sqrt{v_k'' + 1} \delta_{v_k' v_k'' + 1} + \sqrt{v_k'} \delta_{v_k' v_k'' - 1} \right]. \tag{2.87}$$

Note that, if we only consider one mode of excitation of k, i.e., $\langle 0...v'_k...0|$ the vibrational transition for a harmonic oscillator can be written as:

$$\Delta v_k = \pm 1. \tag{2.88}$$

If anharmonicity is taken into account transitions corresponding to $\Delta v_k = \pm 2, \pm 3, ...$ are also allowed.

2.5 Molecular symmetry

When a symmetry operation is applied to a molecule, it leaves the molecule indistinguishable from its original structure. The symmetry operation is done with respect to a reference such as a point, line or a plane called the symmetry element. A point group is a collection of all symmetry elements that keeps a point invariant in the molecule. Symmetry operations are classified into several types such as rotation and reflection.

A large number of molecules can be classified into certain groups based on their symmetry. The symmetry of different molecular states can also be characterized. This is very helpful determining whether or not a transition is allowed. All polyatomic molecules studied in this thesis belong to the C_{2V} symmetry point group. Hence, a brief description to understand the corresponding character table (see table 2.2) is presented here.

Table 2.2 C_{2v} character table.

C_{2v}	$\hat{E}$	$\hat{C}_2$	$\hat{\sigma}_v(xz)$	$\hat{\sigma}_v(yz)$	linear functions, rotations
A_1	1	1	1	1	z
A_2	1	1	-1	-1	R_z
B_1	1	-1	1	-1	x , R_y
B_2	1	-1	-1	1	y , R_x

The symmetry operations can be understood if one considers the effect of applying these operators on coordinates of atoms in molecules.

The identity operation denoted by $\hat{E}$ leaves all atoms in their initial positions. For instance if the position of a nucleus in the molecule is represented by (x, y, z), after applying the identity operation it remains at the same point. This is shown by $\hat{E}\begin{pmatrix} x \\ y \\ z \end{pmatrix} = \begin{pmatrix} x \\ y \\ z \end{pmatrix}$.

The rotation operation denoted by $\hat{C}_2$ rotates the atoms by 180° around the z axis. Therefore, we can write $\hat{C}_2\begin{pmatrix} x \\ y \\ z \end{pmatrix} = \begin{pmatrix} -x \\ -y \\ z \end{pmatrix}$.

The reflection operation with respect to xz and yz planes is denoted by $\hat{\sigma}_v(xz)$ and $\hat{\sigma}_v(yz)$ respectively. Their operation can be represented by $\hat{\sigma}_v(xz)\begin{pmatrix} x \\ y \\ z \end{pmatrix} = \begin{pmatrix} x \\ -y \\ z \end{pmatrix}$ and $\hat{\sigma}_v(yz)\begin{pmatrix} x \\ y \\ z \end{pmatrix} = \begin{pmatrix} -x \\ y \\ z \end{pmatrix}$.

Therefore, the symmetry operations for the C_{2v} point group can be represented by four 3 by 3 matrices [16]. They are called the total representation of the C_{2v} point group and can be written as:

$$\hat{E} = \begin{pmatrix} 1 & 0 & 0 \\ 0 & 1 & 0 \\ 0 & 0 & 1 \end{pmatrix}, \qquad \hat{C}_2 = \begin{pmatrix} -1 & 0 & 0 \\ 0 & -1 & 0 \\ 0 & 0 & 1 \end{pmatrix}, \qquad \hat{\sigma}_v(xz) = \begin{pmatrix} 1 & 0 & 0 \\ 0 & -1 & 0 \\ 0 & 0 & 1 \end{pmatrix} \quad \text{and}$$

$$\hat{\sigma}_v(yz) = \begin{pmatrix} -1 & 0 & 0 \\ 0 & 1 & 0 \\ 0 & 0 & 1 \end{pmatrix}.$$

Note that all the four matrices are block diagonal, which can be reduced to one dimension. If we take the z coordinate for instance, only the last row of the total representation is needed to produce the first row of the C_{2v} character table (see table 2.2). The same procedure can be applied to other coordinates to generate the irreducible representations. For the rotations along x, y and z-axes, the irreducible representations denoted in the character table can be understood as well. For example, if we consider R_x we can see that the identity does not change the rotation direction and hence the number 1 is written in the corresponding place. The same holds true if one applies $\hat{\sigma}_v(yz)$. However, by applying $\hat{\sigma}_v(xz)$ the rotation direction is not conserved and the -1 is

assigned to it as such a 180º rotation about z-axis does not preserve the rotation direction around x (see the last row of character table). The same analogy can be applied to produce the irreducible representation for rotation around z and y axes which are shown by R_z and R_y respectively. The squares and binary operations such as y^2 and xy, etc. can be worked out readily by the multiplication of individual elements.

The symbols A and B are used to emphasize if the character is 1 (A, symmetric) or -1 (B, antisymmetric) under $\hat{C}_2$ rotation. The subscripts 1 and 2 indicate if the related quantity changes sign upon applying $\hat{\sigma}_v(xz)$ or not, respectively.

This information is useful when calculating the integrals encountered in the transition dipole moment. For instance, if we look at the expectation value of the dipole moment $\langle \vec{\mu} \rangle \propto \langle \phi_g | r | \phi_e \rangle$ we can determine whether a transition is allowed or forbidden. This is non-zero if the representation is totally symmetric. Suppose the ground state and the upper state wavefuntions are both characterized as A_1. Then only the component related to z remains because the product $A_1 \otimes A_1 \otimes A_1 \sim A_1$ is totally symmetric and hence the integral is non-zero.

2.6 Electronic structure of diatomics

Since some of the experiments performed in this thesis involve electronic transitions in diatomic molecules, a brief introduction to the theory of their electronic structure starting from the quantum many body system Hamiltonian is presented here.

2.6.1 Quantum many body systems

Consider a many-body system such as a molecule that consists of n electrons and z nuclei. The non-relativistic Hamiltonian for such a system consisting of point charges is described as follows [17]:

$$H = -\frac{\hbar^2}{2}\sum_r \frac{1}{m_r}\nabla_r^2 - \frac{\hbar^2}{2m_e}\sum_p \nabla_p^2 + \sum_{r,s}\frac{e^2 Z_r Z_s}{\left|\vec{r}_r - \vec{r}_s\right|} - \sum_{r,p}\frac{e^2 Z_r}{\left|\vec{r}_r - \vec{r}_p\right|} + \sum_{p,q}\frac{e^2}{\left|\vec{r}_p - \vec{r}_q\right|} \qquad (2.89)$$

where the first and second terms are kinetic energy operators for nuclei and electrons with mass m_r and m_e respectively. The third term is the Coulomb interaction between nuclei r and s with Z_r and Z_s protons and distance $r_{rs} = \left|\vec{r}_r - \vec{r}_s\right|$ between them. The fourth term is the Coulomb interaction between nucleus r at $\vec{r}_r$ and the electron p at $\vec{r}_p$ and the last term describes the repulsive potential between the electrons p and q at $\vec{r}_p$ and $\vec{r}_q$ respectively. There is no exact solution for the above Hamiltonian even for the simplest molecular system. Approximations need to be considered to solve the Schrödinger equation and find the eigenvalues and wave functions of the system.

2.6.2 Born-Oppenheimer approximation

The molecular wave function can be represented by $\psi(q_i, q_\alpha)$ where q_i and q_α denote the electronic and nuclear coordinates respectively. The Schrödinger equation can be constructed as [18]

$$H\psi(q_i,q_\alpha) = E\psi(q_i,q_\alpha) \tag{2.90}$$

We know that the mass of the nuclei is much larger than that of the electrons. We can imagine that the nuclei are kept fixed at their sites. Therefore, we can set the related kinetic energy operator of the nuclei to zero and the equation 2.89 Hamiltonian takes the following form

$$H = -\frac{\hbar^2}{2m_e}\sum_p \nabla_p^2 - \sum_{r,p}\frac{e^2 Z_r}{|\vec{r}_r - \vec{r}_p|} + \sum_{p,q}\frac{e^2}{|\vec{r}_p - \vec{r}_q|} + \sum_{r,s}\frac{e^2 Z_r Z_s}{|\vec{r}_r - \vec{r}_s|} \ . \tag{2.91}$$

The first three terms in the above equation are purely electronic H_{el}, and the last term is the nuclear repulsion potential V_{NN}. Note that our assumption that nuclei do not move defines a fixed set of nuclei positions. And, V_{NN} is the external potential associated with the given configuration of nuclei in which the electrons are moving. Therefore, we can claim that the electronic motion can be treated separately from the nuclear motion. As a consequence of the Born-Oppenheimer approximation the molecular wave function can be written as

$$\psi(q_i,q_\alpha) = \psi_{el}(q_i,q_\alpha)\psi_N(q_\alpha) \tag{2.92}$$

where $\psi_{el}(q_i,q_\alpha)$ is the electronic wave function which depends on nuclear coordinates parametrically and $\psi_N(q_\alpha)$ is the nuclear wave function. Hence the electronic Schrödinger equation can be written as

$$(H_{el} + V_{NN})\psi_{el} = U\psi_{el} \tag{2.93}$$

where the purely electronic Hamiltonian is

$$H_{el} = -\frac{\hbar^2}{2m_e}\sum_p \nabla_p^2 - \sum_{r,p}\frac{e^2 Z_r}{|\vec{r}_r - \vec{r}_p|} + \sum_{p,q}\frac{e^2}{|\vec{r}_p - \vec{r}_q|} \tag{2.94}$$

and U is the electronic energy that also encompasses the nuclear repulsion.

Note that in equation 2.93, V_{NN} is just a constant, which does not change the wave function and only shifts the eigenvalues. So we are left with a purely electronic Hamiltonian, which gives a purely electronic energy that parametrically depends on nuclear coordinates. Therefore, we can write $H_{el}\psi_{el} = E_{el}\psi_{el}$ and $U = E_{el} + V_{NN}$ with E_{el} being the pure electronic energy.

We know that there is an infinite number of electronic states with associated electronic energies and wave functions for a given nuclear configuration. However, there is also an infinite set of nuclear configurations. Consequently, as the nuclei change their configuration, the electrons respond by changing their wave function and their electronic energy. This defines different electronic states that have energies with parametric dependence on nuclear positions.

Now that we solved the electronic part of the Schrödinger equation, the nuclear part can be constructed to find the total energy of the molecule [10, 18]. The nuclear wave function describes the rotation and vibration motions of the molecule.

2.6.3 Total energy

Now that the electronic energies have been obtained, they can be used in the Schrödinger equation for the nuclear part to find the total energy E. This energy includes the electronic, vibrational, rotational and translational energies. The governing Schrödinger equation for the nuclear part is

$$H_N \psi_N = E \psi_N \tag{2.95}$$

where

$$H_N = -\frac{\hbar^2}{2} \sum_r \frac{\nabla_r^2}{m_r} + U \tag{2.96}$$

For the case of a diatomic molecule it takes the following form

$$(-\frac{\hbar^2}{2} \sum_r \frac{\nabla_r^2}{m_r} - \frac{\hbar^2}{2} \sum_s \frac{\nabla_s^2}{m_s} + U) \psi_N = E \psi_N \tag{2.97}$$

Note that within a given electronic state U is a function of the distance between two nuclei [10, 18]. The nuclear wave function ψ_N can be broken into two segments, i.e., the translational $\psi_{N,trans}$ and internal $\psi_{N,\text{int}}$ parts with their related energies:

$$\psi_N = \psi_{N,trans} \psi_{N,\text{int}} \tag{2.98}$$

$$E = E_{trans} + E_{\text{int}}$$

The two-particle Hamiltonian (see equation 2.97) can be reduced to one particle and the corresponding Schrödinger equation can be written as

$$(-\frac{\hbar^2}{2\mu} \nabla^2 + U) \psi_{N,\text{int}} = E_{\text{int}} \psi_{N,\text{int}} \tag{2.99}$$

where $\mu = \frac{m_r m_s}{m_r + m_s}$ is the reduced mass of the two nuclei. As mentioned, E_{int} is the total energy of the diatomic system that consists of electrons and nuclei without the translational part.

Equation 2.99 is a central force problem and the wave function can be written as

$$\psi_{N,\text{int}} = F(R) y_{JM}(\theta, \varphi) \tag{2.100}$$

where J=0, 1, 2, 3…and M=-J, -J+1,… , J-1, J.

The radial part of the equation 2.99 is obtained by solving the following differential equation [10, 18]

$$-\frac{\hbar^2}{2\mu}[F''(R)+\frac{2}{R}F'(R)]+\frac{J(J+1)\hbar^2}{2\mu R^2}F(R)+U(R)F(R)=EF(R) \quad (2.101)$$

which can be further simplified by the following variables

$$G(R)=RF(R) \quad (2.102)$$

to give

$$-\frac{\hbar^2}{2\mu}G''(R)+[\frac{J(J+1)\hbar^2}{2\mu R^2}+U(R)]G(R)=E_{\text{int}}G(R) \quad (2.103)$$

This is a one dimensional Schrödinger equation with $\frac{J(J+1)\hbar^2}{2\mu R^2}+U(R)$ as an effective potential. The potential $U(R)$ can be Taylor-expanded around the equilibrium internuclear distance R_e:

$$U(R)=U(R_e)+U'(R_e)(R-R_e)+\frac{1}{2}U''(R_e)(R-R_e)^2+... \quad (2.104)$$

which can be further approximated as

$$U(R)\approx U(R_e)+\frac{1}{2}U''(R_e)(R-R_e)^2 \quad (2.105)$$

since $U'(R_e)=0$ at the minimum of the potential. Introducing the equilibrium force constant K_e we find

$$U(R)\approx U(R_e)+\frac{1}{2}K_e(R-R_e)^2 \quad (2.106)$$

and with the change of variable $X=R-R_e$ we find

$$U(R)\approx U(R_e)+\frac{1}{2}K_eX^2 \quad (2.107)$$

If this is substituted in 2.103 we have

$$-\frac{\hbar^2}{2\mu}G''(R)+[U(R_e)+\frac{1}{2}K_eX^2+\frac{J(J+1)\hbar^2}{2\mu(X+R_e)^2}]G(R)=E_{\text{int}}G(R) \tag{2.108}$$

Then $\frac{1}{(X+R_e)^2}$ can be Taylor-expanded

$$\frac{1}{(X+R_e)^2}=\frac{1}{R_e^2(1+X/R_e)^2}=\frac{1}{R_e^2}(1-2\frac{X}{R_e}+3\frac{X^2}{R_e^2}-...)\approx\frac{1}{R_e^2} \tag{2.109}$$

Therefore the equation 2.108 becomes

$$-\frac{\hbar^2}{2\mu}G''(R)+\frac{1}{2}K_eX^2G(R)=(E_{\text{int}}-U(R_e)-\frac{J(J+1)\hbar^2}{2\mu R_e^{\,2}})G(R) \tag{2.110}$$

which resembles the one dimensional harmonic oscillator whose eigenvalues $(E_{\text{int}}-U(R_e)-\frac{J(J+1)\hbar^2}{2\mu R_e^{\,2}})$ are equal to $(v+\frac{1}{2})\hbar\omega_e$. Therefore,

$$E_{\text{int}}=U(R_e)+(v+\frac{1}{2})\hbar\omega_e+\frac{J(J+1)\hbar^2}{2\mu R_e^{\,2}}\ . \tag{2.111}$$

To improve the accuracy, the neglected terms in (2.104) and (2.109) can be included using time independent perturbation theory. Therefore, the expressions for vibration–rotation interaction, the centrifugal distortion and anharmonicity can be found

$$\begin{aligned}E\approx{}&U(R_e)+(v+\frac{1}{2})\hbar\omega_e+hB_eJ(J+1)-(v+\frac{1}{2})^2\hbar\omega_e\chi_e\\&-(v+\frac{1}{2})h\alpha_eJ(J+1)-hD_eJ^2(J+1)^2\end{aligned} \tag{2.112}$$

where ω_e, B_e, χ_e, α_e and D_e are vibrational, rotational, anharmonicity, vibration-rotation and centrifugal constants respectively [1, 7]. The accurate energy for a diatom can be expressed by a general expansion in terms of $(v+\frac{1}{2})$ and $J(J+1)$ as:

$$E = U(R_e) + \sum_{l,m} Y_{l,m} (v + \frac{1}{2})^l J^m (J+1)^m \qquad (2.113)$$

where Y_{lm} are called the Dunham coefficients. If we compare equations 2.112 and 2.113, we see that $Y_{10} = \hbar\omega_e$, $Y_{01} = hB_e$, $Y_{20} = \hbar\omega_e\chi_e$, $Y_{11} = h\alpha_e$ and $Y_{02} = -hD_e$.

2.6.4 The molecular energy

As discussed, the total energy of an electronic state of a diatomic molecule is obtained approximately by adding the translational (E_{tr}), rotational (E_{rot}), vibrational (E_{vib}) and electronic (E_{elec}) energies, i.e., $E=E_{tr}+E_{rot}+E_{vib}+E_{elec}=E_{tr}+E_{int}$.

Therefore, the Hamiltonian operator can be decomposed into electronic, vibrational and rotational parts. Other interactions such as spin-orbit, hyperfine, centrifugal distortion, etc. can also be included in the Hamiltonian. Therefore, the total expression for the Hamiltonian can be of the following form

$$H=H_{elec}+H_{vib}+H_{rot}+H_{cd}+H_{so}+H_{hf}+H_{cor}. \qquad (2.114)$$

where the energy of electronic and vibrational parts can be denoted as T_0. The additional parts will be described in the next sections.

2.7 Angular momenta and labeling electronic states in diatomic molecules

There are four types of magnetic angular momenta in a molecule: the electron orbital angular momentum, electron spin angular momentum, nuclear spin angular momentum and end-over-end rotation of the molecule which are represented by L, S, I and R operators / vectors respectively. The electronic angular momentum can be written as a summation of the angular momenta of individual electrons. So if we represent the individual orbital angular momentum of electron i with $\vec{l}_i$ then we have $\vec{L} = \sum_i \vec{l}_i$. Note that since there is no center of symmetry in diatomic molecules $\vec{L}$ is not conserved. However, there is symmetry around the internuclear axis which means that the z component of L is conserved and we will have a good quantum number. The spin angular momentum is the summation of all electron spins of the system represented by $\vec{S} = \sum_i \vec{s}_i$ where $\vec{s}_i$ is the spin of the ith electron. The rotational angular momentum can be written as $\vec{R} = \sum_i \vec{r}_i$ where $\vec{r}_i$ is the rotational angular momentum of nucleus i around the center of mass. The total angular momentum $\vec{J}$ of the molecule (neglecting the nuclear spin) is the addition of all angular momenta, i.e., $\vec{J} = \vec{L} + \vec{S} + \vec{R}$. The projection of orbital angular momentum along the internuclear axis is represented by Λ (see Figure 2.9) and is used for labeling electronic states. In analogy to the atomic orbitals of s, p, d,…for *l*= 0, 1, 2,… these states with $|\Lambda| = 0,\ 1,\ 2,\ 3,\ 4\ldots$ are called Σ, Π, Δ, Φ, Γ,... states respectively [19]. The projection of spin angular momenta along the internuclear axis is

represented by Σ with quantum number values of -S, -S+1,…, S giving 2S+1 components. As shown in Figure 2.9 the addition of the two projections is equal to $\Omega = |\Lambda + \Sigma|$. Now the electronic state can be labeled by ${}^{2S+1}\Lambda_{\Omega}$. For instance, consider a state with $\Lambda = 3$ and S=1.5 which is characterized by the ${}^{4}\Phi_{\Omega}$ symbol. Since we have $\Lambda = 3,\ 2S+1 = 4 \Rightarrow S = 1.5$ there are four Ω values associated with this state namely $\Omega = 1.5, 2.5, 3.5, 4.5$. Hence the four components of the electronic state are characterized by ${}^{4}\Phi_{1.5}, {}^{4}\Phi_{2.5}, {}^{4}\Phi_{3.5}, {}^{4}\Phi_{4.5}$.

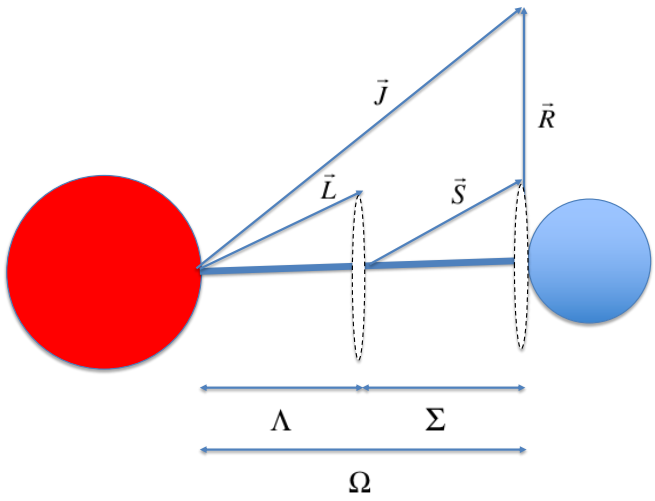

Figure 2.9 Different angular momenta in a diatomic molecule.

2.8 Rotational structure of diatomic molecules

Figure 2.10 shows a diagram of a typical rotational level structure of a diatomic molecule. The angular quantum number J for each rotational level for the lower and upper states are denoted by J″ and J′ respectively with their corresponding values. The

change in the angular momentum during each transition should follow one of the following selection rules:

$$1.\ \Delta J = -1$$

$$2.\ \Delta J = 0 \qquad (2.115)$$

$$3.\ \Delta J = 1\,.$$

Accordingly, the possible transitions can be classified in three groups (see Figure 2.10). The transitions for which $\Delta J = -1$ form a branch that is called P. Those with no change in the angular momentum are named the Q branch. Finally, if the angular momentum is increased by one, the related branch is called R.

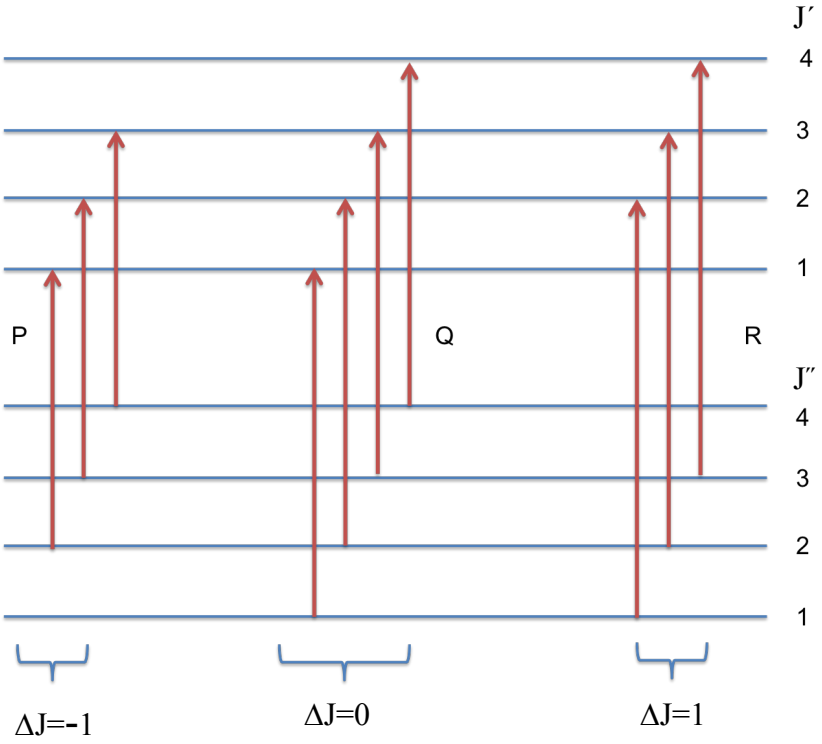

Figure 2.10 Branches in an electronic transition of a diatomic molecule.

Therefore, the related spectra can be divided into three segments called P, Q and R branches.

2.8.1 Combination differences

If two transitions share a common upper or lower level (see Figure 2.11), the difference in their energies can be used to extract an approximate rotational constant B for the related states. This is known as the method of combination differences which serves as a powerful technique for analysis of a spectrum. In section 2.6.3, the rotational energy associated with each level was obtained to be $\sim BJ\,(J+1)$. Therefore, for instance we can calculate the energy difference between one pair of R and P transitions as follows:

$$R(J)-P(J)=B'[(J+1)(J+2)-(J-1)J] =4B'(J+1/2). \quad (2.116)$$

This eliminates the information for the lower state and we can find the rotational constant B′ for the upper state, hence the name upper state combination differences. Similarly, the lower state combination differences can be found from the following relation

$$R(J-1)-P(J+1)=4B''(J+1/2) \quad (2.117)$$

This gives the lower state constant B''.

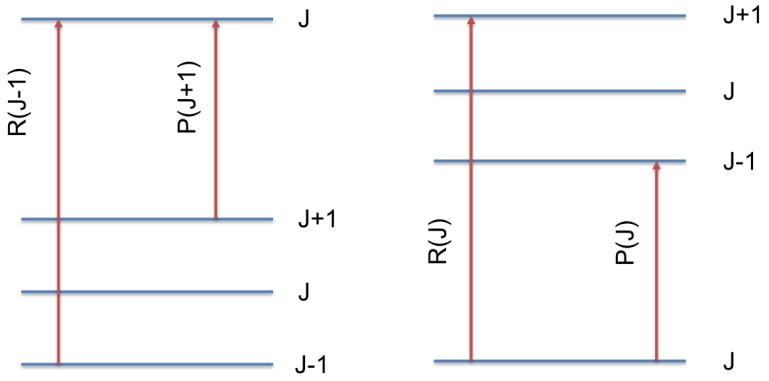

Figure 2.11 Lower-state (left) and upper-state (right) state combination differences.

2.8.2 Band heads

Band heads can appear in some spectra in the P, Q and R regions based on the relative values of the rotational constant B in the upper and lower states [2, 20, 21]. If $B'' < B'$, the P branch will form a head. An R head occurs when $B'' > B'$. If $B'' = B'$, all the rotational lines in the Q branch will collapse to a single wavenumber.

For example, if the head happens in the R branch, the rotational lines shift toward larger wavenumbers with increasing *J* while the spacing between them is decreasing. This trend continues until they reach a specific rotational quantum number, *J**. At *J** the R branch then forms a head, and the wavenumber of the rotational lines decreases with increasing

angular momentum. The head position J^* occurs at a point where $\frac{dv(R)}{dJ} = 0$ where $v(R)$ is the wavenumber of each transition for the R branch and is given by

$$v(R) = v_0 + (B' - B'')J(J+1) - 2B'(J+1) \quad (2.118)$$

in the rigid rotor approximation. In the above formula B'' and B' are the rotational constants for the lower and upper states and υ_0 is the band origin. Then the rotational number J^*, can also be calculated beforehand from the following expression;

$$J^* = \frac{3B' - B''}{2(B'' - B')} \quad (2.119)$$

Also, the head-origin spacing can be obtained from the following expression,

$$v_{head} - v_o = \frac{(B' + B'')^2}{4(B'' - B')} \quad (2.120)$$

This information may help the assignment process of the band.

2.9 Interactions between different angular momenta

Figure 2.12 shows possible pairwise interactions between different angular momenta that can occur in molecules in the absence of external fields [22]. In order to model the energy level structure of the molecules, a suitable effective Hamiltonian needs to be constructed. The effective Hamiltonian may contain any of the six pairwise interactions between electronic spin $\vec{S}$, electronic orbital $\vec{L}$, nuclear spin $\vec{I}$ and rotational $\vec{R}$ angular momenta. The corresponding terms for the interactions are $\vec{S}.\vec{L}$, $\vec{S}.\vec{I}$, $\vec{L}.\vec{I}$, $\vec{S}.\vec{R}$, $\vec{L}.\vec{R}$ and $\vec{I}.\vec{R}$. The related terms that are important in this thesis will be discussed.

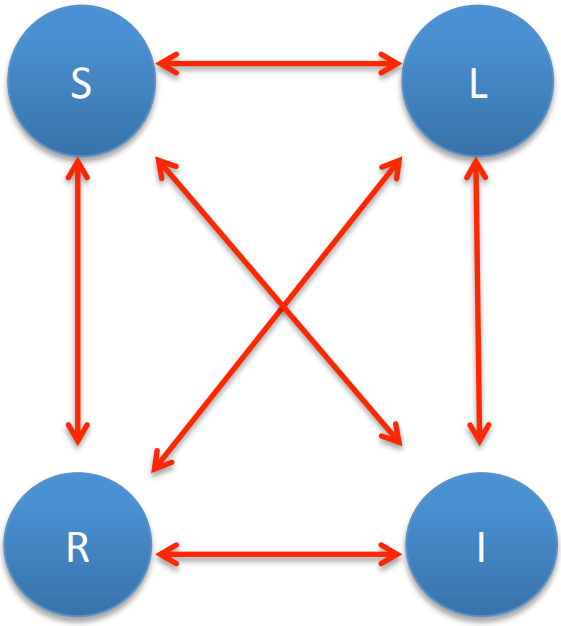

Figure 2.12 The diagram summarizes interactions between different angular momenta.

The rotational Hamiltonian can be expressed as

$$H = BR^2 \tag{2.121}$$

where $\vec{R} = \vec{J} - \vec{L} - \vec{S}$.

Therefore, the Hamiltonian can be rewritten as:

$$H = B(\vec{J} - \vec{L} - \vec{S})^2 \tag{2.122}$$

This can be expanded as:

$$H = B(J^2 + L^2 + S^2 - 2\vec{J}.\vec{L} - 2\vec{J}.\vec{S} + 2\vec{L}.\vec{S}) \tag{2.123}$$

Using the ladder operators defined as:

$$\begin{aligned} J_{\pm} &= J_x \pm iJ_y \\ L_{\pm} &= L_x \pm iL_y \\ S_{\pm} &= S_x \pm iS_y \end{aligned} \tag{2.124}$$

equation 2.123 can be further expanded to obtain:

$$H = B(J^2 + (L_x^2 + L_y^2 + L_z^2) + S^2 - 2J_zL_z - 2J_zS_z + 2L_zS_z - (J_+S_- + J_-S_+) \\ -(J_+L_- + J_-L_+) + (L_+S_- + L_-S_+)) \quad (2.125)$$

A simpler approach to expressing the rotational Hamiltonian is the use of the *N* operator instead of *R* where it is defined as $N = J - S$. Therefore, the rotational Hamiltonian can be stated as:

$$H = BN^2 = B(J-S)^2 = B(J^2 + S^2 - 2J.S) = B(J^2 + S^2 - 2J_zS_z - J_+S_- - J_-S_+) \quad (2.126)$$

Subtracting equations 2.125 from 2.126 gives

$$BR^2 - BN^2 = B(L_x^2 + L_y^2 + L_z^2) - 2BJ_zL_z - 2BL_zS_z - (J_+L_- + J_-L_+) + (L_+S_- + L_-S_+) \quad (2.127)$$

As we will see in chapter 6, the R^2 form of the Hamiltonian is useful when we are dealing with isotopic analysis. It allows separating the terms related to the rotation from the electronic part of the Hamiltonian more neatly. We can then obtain the pure electronic term energy which is isotopically independent and the term B (L_x^2+L_y^2) which depends on isotope. Therefore, if we have a set of isotopologues the term B (L_x^2+L_y^2) is experimentally determinable, when normally it cannot be separated from the effective term energy.

2.9.1 Spin-orbit interactions

From a classical standpoint, the orbiting motion of a charged particle produces a current and hence a magnetic field (see Figure 2.13). The charged particle can be viewed as a magnetic dipole moment. For the case of an electron carrying spin with an associated dipole, the two magnetic moments can interact with each other and we will have spin-

orbit interaction. The spin-orbit Hamiltonian is defined as $H_{so} = A\vec{L}.\vec{S}$ where A is the spin-orbit coupling constant. With the aid of ladder operators it can be expanded to

$$H_{so} = AL_zS_z + A(L_+S_- + L_-S_+)/2 \qquad (2.128)$$

The values of diagonal elements due to the first term are equal to

$$A\Lambda\Sigma. \qquad (2.129)$$

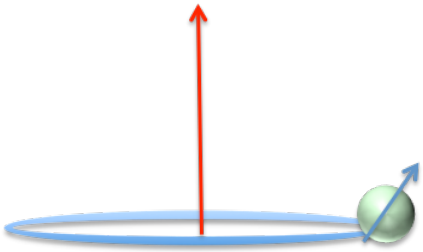

Figure 2.13 Orbiting motion of a charged particle.

For example, consider two electronic states of $^5\Delta$. The spin multiplicity of these states is 5 and therefore $S = 2$. The spin-orbit interactions separate these electronic states to 5 components. Since $\Lambda = 2$, and $\Sigma = -2,...,2$ according to equation 2.129 the energy associated with each of these components is $-4A$, $-2A$, 0, $2A$ and $4A$. Therefore, as shown if Figure 2.14 these components are all $2A$ apart from one another. Note that the red dotted vertical line between the middle of the spin-orbit levels of the lower and upper states can be considered as the band origin.

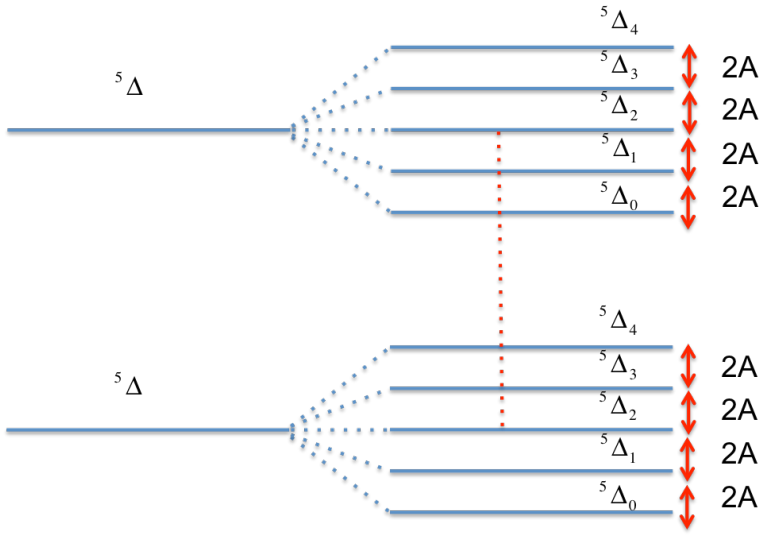

Figure 2.14 Splittings of two $^5\Delta$ states into five spin-orbit components with the band origin identified as a vertical dotted line.

In equation 2.129 if the spin-orbit constant is positive then the highest Ω value in the spin-orbit component lies the highest, which is an example of a regular case. If the spin-orbit constant is negative we will have an inverted case in which the spin-orbit component with the lowest value of Ω lies the highest. The inverted case happens when the related orbital in the electronic configuration is more than half filled.

2.9.2 Hyperfine interactions

Hyperfine interactions refer to the interactions between nuclear moments and the fields generated by electrons. These interactions could be either electric such as the interaction of the nuclear quadrupole moment with the electric field gradients of the electrons or

magnetic like the interaction of the dipole moment of the nucleus and the electron. In what follows we will consider magnetic hyperfine interactions.

Classically the energy of interaction between a dipole moment in an external magnetic field is given by $\vec{\mu}.\vec{B}$. This energy is proportional to $\vec{I}.\vec{J}$ for the case of a nucleus of spin I interacting with electrons with total angular momentum $\vec{J}$. The interaction energy between an electron with orbital angular momentum $\vec{l}$ with a nucleus of spin I is given by [23]

$$H_{ll} = \frac{2\mu_0\mu_I}{Ir^3}\vec{I}.\vec{l} \qquad (2.103)$$

where r is the distance between the electron and nucleus, μ_0 is Bohr magneton and μ_I is the nuclear magnetic moment. In a molecule, ℓ and r are not constant so to write the above equation in this case taking an average value of these quantities is beneficial. The average value for the total orbital angular moment $\vec{L}$ is given by $\hat{k}\Lambda$ where $\hat{k}$ is the unit vector along the internuclear axis and Λ is the projection of $\vec{L}$ on it. If there are n electrons contributing to the interaction, one can sum up the average to account for all electrons [23]. Therefore the orbital part of hyperfine interaction is given by

$$H_{lL} = \frac{2\mu_0\mu_I}{Ir^3}\sum_n (\frac{1}{r^3})_{av}\Lambda_n \vec{I}.\vec{k} \qquad (2.131)$$

where the summation is over all electrons and Λ_n is the average of the projection of nth electron orbital angular moment.

The other interaction is between the spin of the nucleus and the electron. From classical

electrodynamics, the classical interaction energy between two dipoles at distance r is given by the following formula:

$$W = \frac{\vec{\mu}_1 . \vec{\mu}_2}{r^3} - \frac{3(\vec{\mu}_1 . \vec{r})(\vec{\mu}_2 . \vec{r})}{r^5} \tag{2.132}$$

Substituting $\vec{\mu}_l = \frac{\mu_I}{I}\vec{I}$ for the moment of the nucleus and $\vec{\mu}_2 = -2\mu_0 \vec{S}$ for the spin of electron the above expression transforms to

$$(H_{IS})_1 = \frac{-2\mu_0 \mu}{I}\left[\frac{\vec{I}.\vec{S}}{r^3} - \frac{3(\vec{I}.\vec{r})(\vec{S}.\vec{r})}{r^5}\right] \tag{2.133}$$

For s electrons that have nonzero probability density at the nucleus, the interaction energy is given by

$$(H_{IS})_2 = \frac{16\pi}{3}\frac{\mu_0 \mu_I}{I}\psi^2(0)\vec{I}.\vec{S} \tag{2.134}$$

This term is called the Fermi contact term.

Frosch and Foley [24] studied and formulated the hyperfine interactions in diatomic molecules. They extracted the hyperfine interactions for diatomic molecules by applying the Dirac equation. The magnetic hyperfine Hamiltonian is written as:

$$H = aL_z S_z + b\vec{I}.\vec{S} + cI_z S_z \tag{2.135}$$

where

$$a = 2g_I \mu_0 \mu_N \left\langle \frac{1}{r^3} \right\rangle$$

$$b = 2g_I \mu_0 \mu_N \left\langle \frac{2}{3}\frac{\delta(r)}{r^2} - \frac{3\cos^2\theta - 1}{2r^3} \right\rangle \tag{2.136}$$

$$c = 2g_I\mu_0\mu_N\left\langle\frac{3\cos^2\theta-1}{r^3}\right\rangle$$

In the above expressions g_I is the nuclear *g* factor, μ_0 and μ_N are the Bohr and nuclear magnetons respectively. The distance between the interacting nucleus and electron is designated by *r* and θ is the angle between $\vec{r}$ and the internuclear axis. For *s* electrons which have a spherically distributed electron cloud, the $\langle 3\cos^2\theta-1\rangle$ is zero and hence the interaction of electron and nuclear spin is given by first part of the term *b*.

2.10 Selection rules for diatomic molecules

In the case of diatomic molecules the electronic transitions follow the selection rules that include not only the rotation but electronic properties such as Λ, S and Σ. A summary of the electronic selection rules is as follows:

$$\Delta\Lambda = 0,\pm1$$

$$\Delta S = 0$$

$$\Delta\Sigma = 0 \qquad (2.137)$$

$$\Delta J = 0,\pm1$$

More details about electronic transitions and selection rules can be found in reference [1].

References

1. P. F. Bernath, Spectra of Atoms and Molecules, New York: Oxford University Press Inc., 1995.

2. W. Demtroder, Molecular Physics. Theoretical Principles and Experimental Methods: Wiley-VCH Verlag GmbH& Co.KGaA, Weinheim., 2005.

3. G. R. Fowles, G. L. Cassiday, Analytical Mechanics, 7th ed., Brooks/Cole, 2005.

4. S. Hassani, Mathematical Methods for the Students of Physics and Related Fields, Springer, 2009.

5. H. Goldstein, C. P. Poole, J. Safko, Classical Mechanics, 3rd ed., Addison-Wesley, 2002.

6. W. Gordy, R. L. Cook, Microwave Molecular Spectra, 2nd ed., Toronto: John Wiley & Sons, Inc, 1984.

7. H. W. Kroto, Molecular Rotation Spectra, Dover 1992.

8. P. R. Bunker, P. Jensen, Molecular Symmetry and Spectroscopy 2nd ed., NRC Research Press, Canada 2006.

9. G. W. King, R. M. Hainer, P. C. Cross, J. Chem. Phys. **11**, 27 (1943).

10. I. N. Levine, Molecular spectroscopy, Wiley, New York, 1975.

11. J. M. Hollas, Modern Spectroscopy, 4th ed., Wiley, UK, 2004.

12. P. W. Atkins, R. S. Friedman, Molecular Quantum Mechanics, 5th ed., Oxford University Press, 2005.

13. C. C. Martens, J. Chem. Phys, **94**, 5 (1991).

14. I. M. Mills, Pure Appl. Chem. **11**, 325 (1966).

15. J. K. Watson, Mol. Phys. **15**, 479 (1968).

16. F. A. Cotton, Chemical applications of group theory, 3rd ed., John Wiley & Sons, 1990.

17. A. Szabo, N. S. Ostlund, Modern Quantum Chemistry, 1st ed., McGraw-Hill, 1989.

18. I. N. Levine, Quantum Chemistry, 6th ed., Pearson Prentice Hall, 2009.

19. G. Herzberg, Molecular Spectra and Molecular Structure, I. Spectra of Diatomic Molecules, D. Van Nostrand Company, Inc, 1950.

20. W. G. Richards, P. R. Scott, Structure and Spectra of Molecules, 1985.

21. H. Haken, H. C. Wolf, Molecular Physics and Elements of Quantum Chemistry: Introduction to Experiments and Theory, 2nd ed., Springer, 2004.

22. J.M. Brown, A. Carrington, Rotational Spectroscopy of Diatomic Molecules Cambridge University Press, 2003.

23. C. H. Townes, A. L. Schawlow, Microwave Spectroscopy, Dover, 1975.

24. R. A. Frosch, H. M Foley, Phys. Rev. **8**, 1337 (1952).

Chapter 3

Experimental

In the laser spectroscopy lab at the University of New Brunswick (UNB), generally diatomic metal bearing molecules are made and the ultimate goal is to obtain the high-resolution rotationally resolved spectra of these species in the gas phase. In what follows in this chapter, a brief account of the experimental technique used to obtain the spectra of two transition metal halides, ruthenium monofluoride (RuF) and ruthenium monochloride (RuCl) and one transition metal oxide, ruthenium monoxide (RuO) is presented in general. The specific experimental conditions and parameters used for each experiment will be given in the related results chapters for these molecules.

3.1 The molecular beam source

The RuF, RuCl and RuO molecules were produced in a laser / ablation molecular beam apparatus [1, 2], an overall schematic diagram of which is given in Figure 3.1. In order to make RuF, RuCl and RuO molecules, a cylindrical rod of ruthenium metal is ablated by using the third harmonic of a pulsed UV (Lumonics HY400 Nd:YAG (neodymium-doped yttrium aluminum garnet $Nd:Y_3Al_5O_{12}$)) laser as illustrated in Figure 3.2. About 5 mJ energy from the UV (ablation) laser is deposited on the surface of the metal rod which vaporizes the ruthenium atoms from the surface of the rod. To ensure that the rod is ablated uniformly, it is continuously rotated and translated by a motorized micrometer preventing any undesired non-uniformities or holes being created on the rod's surface,

which would make the rod ineffective for the experiment. A reactant and a carrier gas are also required for making the molecules. A carrier gas is an inert gas which does not participate in the reaction. Its function is to push and propel the reactant gas to react with the ruthenium atoms and further to create a supersonic expansion when the resulting molecules move into the vacuum system. In this thesis both helium and argon gases were used as carrier gases. The vaporized ruthenium atoms are then entrained in a mixture of He or Ar with SF_6 or BCl_3 as the reactant gases in a reaction chamber to make the RuF and RuCl molecules respectively. As a result of the collisions of the reactant gases with the Ru atoms, the RuF and RuCl molecules are produced in the reaction chamber. It should be noted that the system of making the molecules is kept under vacuum which is provided by a 13-inch-diameter Balzers diffusion pump backed by an Alcatel 2063 mechanical pump to keep the pressure of the system to ~$5x10^{-6}$ Torr (see Figure 3.2). As the gas starts flowing into the chamber, the pressure increases to ~$5x10^{-5}$ Torr. When molecules are made in the reaction chamber, they are expanded through a ~1 mm orifice about 5 mm after the metal rod from a region of high pressure to low pressure. Thermodynamically, this expansion produces a cold molecular beam. The low vacuum pressure helps to minimize one of the sources of line broadening, i.e., pressure broadening. This broadening is due to collisions between molecules that perturbs their energy levels. Another source of line broadening, Doppler broadening, was also minimized by directing the molecular beam to travel perpendicular [3, 4] to the probe laser beam which is delivered by either a pulsed or continuous wave laser. Molecular excitation is observed by laser-induced fluorescence (LIF), which is passed through a small monochromator (1/4 m Jarrel-Ash) and is detected by a photomultiplier tube which

converts the fluorescence to an electrical signal. This electrical current is amplified by a current amplifier and sent to a boxcar integrator for averaging. The signal can be viewed on an oscilloscope and optimized by proper adjustment of the timing between different events, i.e., opening the pulsed valve, firing the ablation and probe lasers and also modifying gas concentration, and the power of ablation laser. The output of the boxcar and laser wavelength are recorded on the computer. The details of the probe lasers and the electronics devices will be given in the next sections.

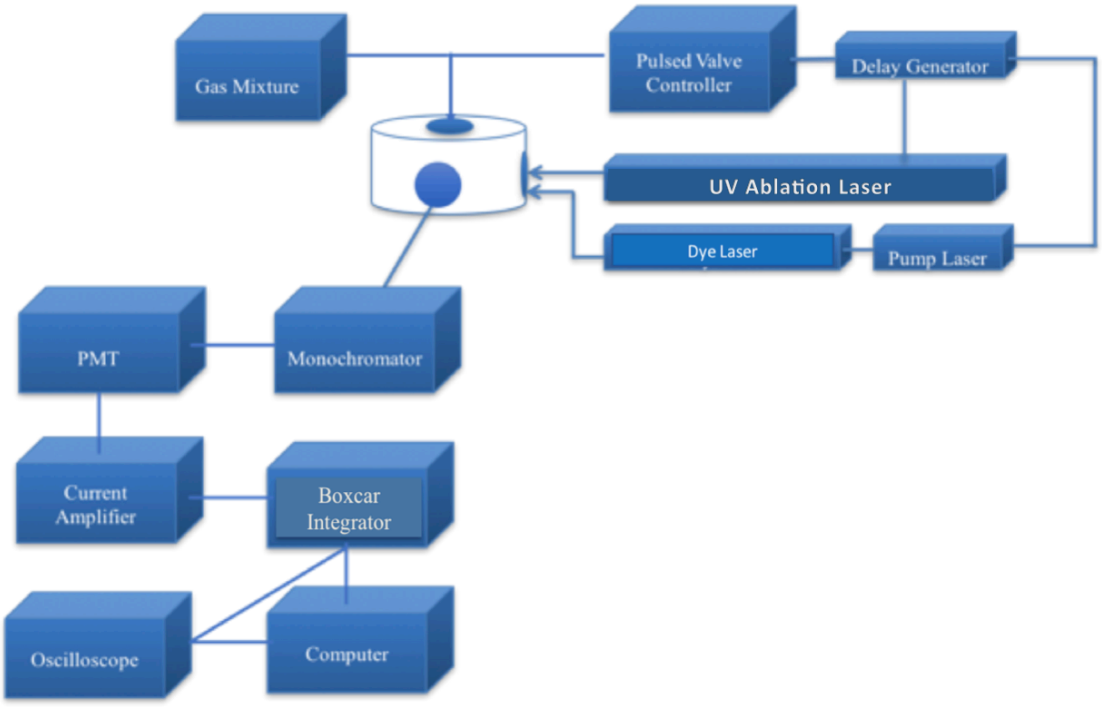

Figure 3.1 Schematic experimental set-up of the laser ablation molecular beam apparatus.

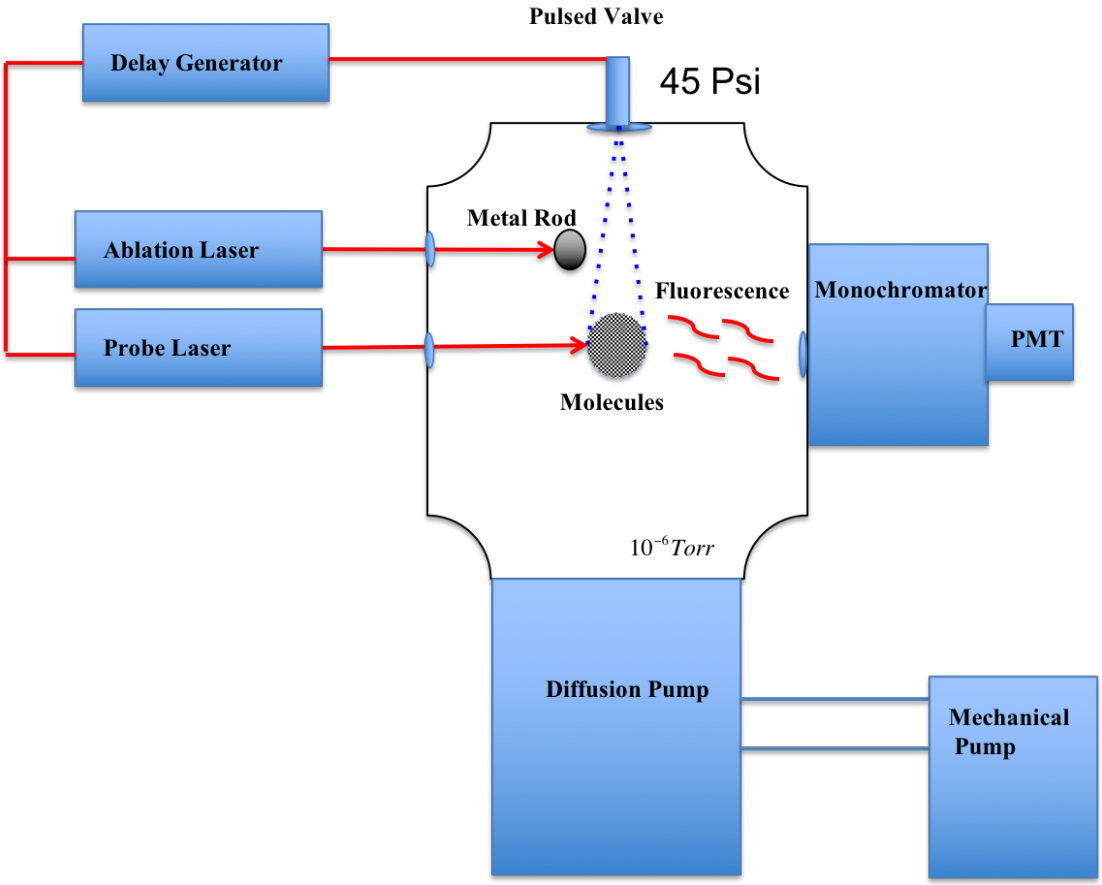

Figure 3.2 Schematic of the laser ablation source.

3.1.1 Gas board

A schematic diagram of the gas board used to make the molecules is shown in Figure 3.3. In order to make the molecules, first the gas board and all of the connections are completely evacuated by a small rotary pump. Then the reactant gas is admitted to the manifold, and kept in the container shown as “Mixture”. A low-pressure gauge is used to measure the pressure of the reactant gas.

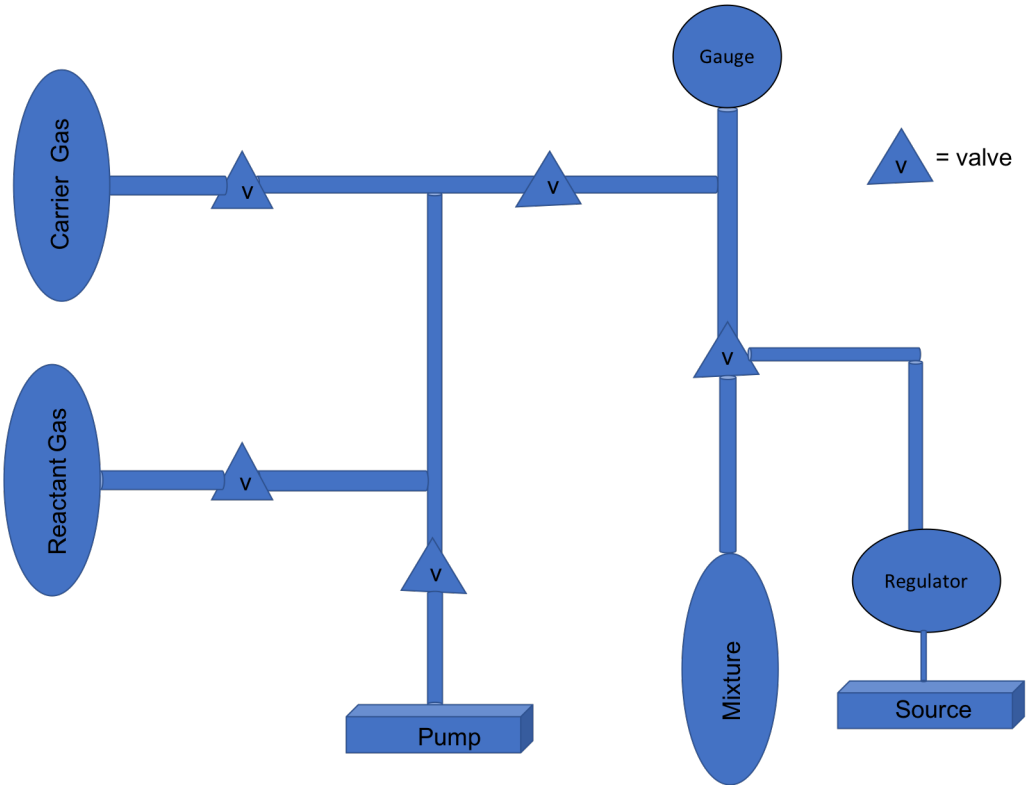

Figure 3.3 Typical schematic set-up of the gas board.

A high-pressure gauge (not shown in the picture for simplicity) is used to add carrier gas (He or Ar) to the reactant gas to reach the pressure of 150 psi. After a few minutes the gases are mixed and the "Mixture" is ready for admittance to the source through a regulator with an optimal pressure of ~ 40 psi. This pressure is suitable [5, 6] for populating higher J rotational lines. When scanning the low J lines, the pressure was closely monitored and increased if necessary to ensure that the sufficient amounts of colder molecules are generated.

3.2 Data acquisition and lasers

In this section a description of the lasers and the electronics used for collecting the laser-induced fluorescence from low and high resolution scans is presented.

3.2.1 Boxcar integrator and photon counter

The boxcar integrator is used to average the signal in a short time "gate". The results of numerous time gates are added together to generate an averaged output. Choosing the narrow time gate allows a signal to be collected when it is present and rejecting the noise at other times. This is useful in typical pulsed laser experiments where the duration of the repetitive signal is short and in the order of 10 ns. In the pulsed experiments, all molecules excite in a short time interval and fluoresce all at the same time. So, there will be lots of fluorescence all at once and the boxcar does not count individual photons. In high-resolution experiments a photon counter where individual photons are counted was used instead of the boxcar integrator. In the continuous wave (CW) laser experiments the excitation of the molecules occurs in a much larger time window, i.e., 20-30 μs, compared to the pulsed laser system and individual photons can be counted because there are not many of them to count. Hence, the laser-induced fluorescence can be directly input into the photon counter after detection by the PMT and amplification (see Figure 3.1). Using the photon counter therefore presents a couple of advantages over using the boxcar integrator. First, the photon counter averages the signal while the laser is fixed to a single wavelength. The boxcar integrator on the other hand, averages over the previous

points that may arise from a small spread of wavelengths. The photon counter improves the quality of the signal since more photons are collected over the given time interval while the frequency of the laser is fixed. This also helps eliminate any distortions of the line shape. Secondly, the amount of the noise measured is considerably reduced because undesired photomultiplier signals below a threshold can be filtered out with a discriminator.

3.2.2 Delay generator and optimization

In the low-resolution survey scans, in order to get a good strong signal, the timing of the different events needed to be adjusted. A delay generator (Stanford Research Systems Inc. Model DG535) (see Figure 3.1) was used to control the timing between opening the pulsed valve and firing the ablation and probe lasers. A typical timing sequence of these events is given by the following list:

1. A=T_0
2. B=A+500 μs
3. C=B+100 μs

If the pulsed valve is opened at A=T_0, the ablation laser will start at B=A+500 μs and the probe laser starts at C=B+100 μs. These timings, the optics guiding the beams through the chamber, the concentration of the gas mixture and proper use of slits in the monochromator were adjusted in order to get the best signal-to-noise ratio. The resulting signal can be monitored on the oscilloscope so that any changes to the above mentioned parameters can be viewed instantaneously.

3.2.3 Experimental set up for the low-resolution survey

The experiments were always started with low-resolution survey scans for two reasons. First, the scan rate is fast and second, the frequencies of the transitions, later to be used in taking high-resolution data, can be determined approximately. In the low-resolution survey scans three different types of lasers were used. A UV laser, Lumonics HY400 Nd:YAG laser, was used to ablate the ruthenium atoms from the surface of the metal rod. This pulsed laser generates UV light at 355 nm with the repetition and duration of 10 Hz and 10 ns respectively. A dye laser, Lumonics HD500 pulsed dye, pumped by a Lumonics YM600 Nd:YAG, was used as a means of probing the molecules. The active medium of this laser, the dye, is a soluble colored organic compound dissolved in methanol. Several dyes were used in order to cover the electromagnetic spectrum from 420 to 760 nm. Figure 3.4 [7] shows the names of the dyes that were used, their efficiency, the spectral range that they are useful, and the maximum wavelength of their lasing region.

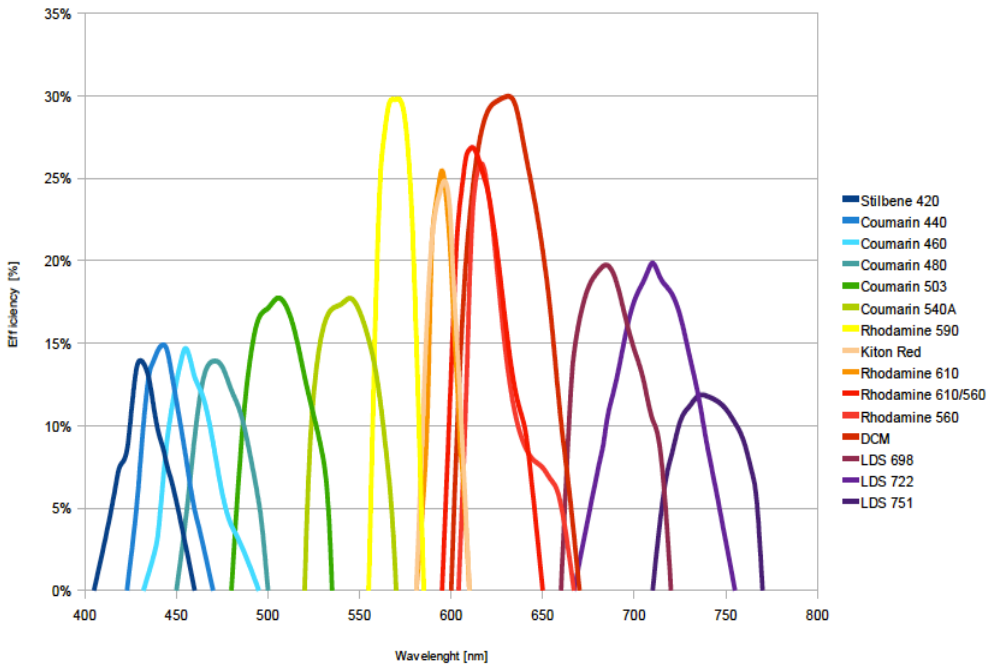

Figure 3.4 Laser dye performance when pumped with a Nd:YAG Laser at 355nm and 532nm [7].

3.2.4 Dispersed fluorescence technique

Dispersed fluorescence is a low-resolution technique applied to measure the vibrational frequencies of the molecules. As the vibrational frequencies of the molecules are characteristic of each molecule, determination of the vibrational frequency may be used to confirm that a particular molecule was observed. In this method, the probe laser is tuned to a resonance frequency of the molecule and the monochromator is scanned. The molecules are excited from the ground state to an excited state upon absorbing the photons whose energies match the energy gap between the two states and a transition occurs. The molecules decay back from the excited state to some low-lying excited states or the ground state. This fluorescence is dispersed in the monochromator. The resulting

dispersed fluorescence spectrum provides the required information to measure the vibrational spacing of molecules in the ground or low-lying states. An energy level diagram showing the absorption and fluorescence decay is shown in Figure 3.5.

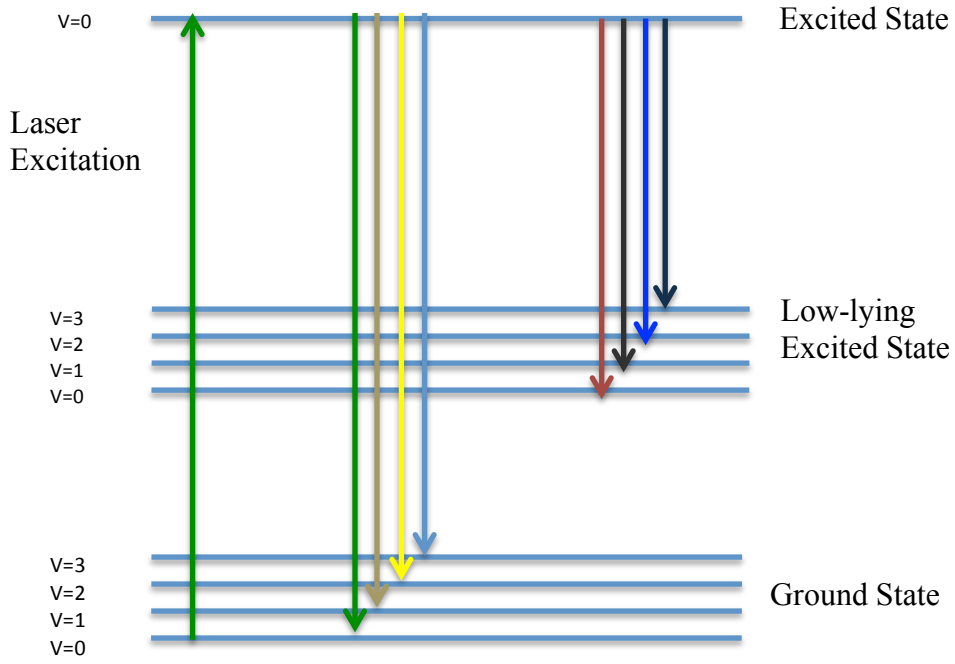

Figure 3.5 Dispersed fluorescence diagram showing the vibrational levels of the ground and low-lying excited states.

Note that to reduce the background noise and scattered light different slits were used at the entrance and exit of the monochromator. This helped to minimize the unwanted signals, reduce the bandwidth and increase the resolution.

3.2.5 Experimental set up for the high-resolution survey

In the high-resolution scans, the transitions observed in the low-resolution surveys are probed in greater detail, i.e., with a resolution of about 200 MHz. The probe lasers in our high-resolution scans were a ring dye laser and a titanium-sapphire laser. These lasers were pumped by an argon ion laser and a diode-pumped solid state Nd:YAG laser respectively.

3.2.5.1 Tuneable lasers

In this thesis two kinds of tunable lasers were used in the experiments: dye lasers and a titanium-sapphire laser.

3.2.5.1.1 Dye lasers

As mentioned dyes are complex conjugated molecules formed by a chain of hydrocarbons. In dye lasers, the active medium is a dye dissolved in a proper solvent like methanol or ethylene glycol and hence forming a solution. The performance and tunability of the dyes are shown in Figure 3.4.

The cavity of the ring laser is shown in Figure 3.6. Within the cavity, the laser beam passes through several optical elements arranged in a ring. In a ring resonator, travelling waves of the laser can still propagate in opposite directions and standing waves can form.

This can prevent sufficient laser emission and higher output powers [3]. An optical diode (a combination of two polarizers and a magneto-optic device [8]) guides the light in only one direction around the ring and consequently standing waves are not formed in the cavity. As can be seen in Figure 3.6, the fluorescence from the active medium is trapped within the cavity of the ring laser. After the proper alignment of the mirrors, the laser is said to be lasing in broadband. When the laser is lasing broadband several modes coexist in the cavity. The laser is coarsely tuned using a birefringent filter to ~1 cm^{-1}. Single mode selection is done by the thick and thin etalons with a linewidth narrowed down to $3.34x10^{-5}$ cm^{-1}. Finally, in order to scan the single mode in the cavity as selected by the etalons a Brewster plate needs to be rotated which changes the optical cavity length of the laser and therefore the output frequency. The optics inside the cavity need to be properly aligned according to the user manual [9] in order to have the laser working.

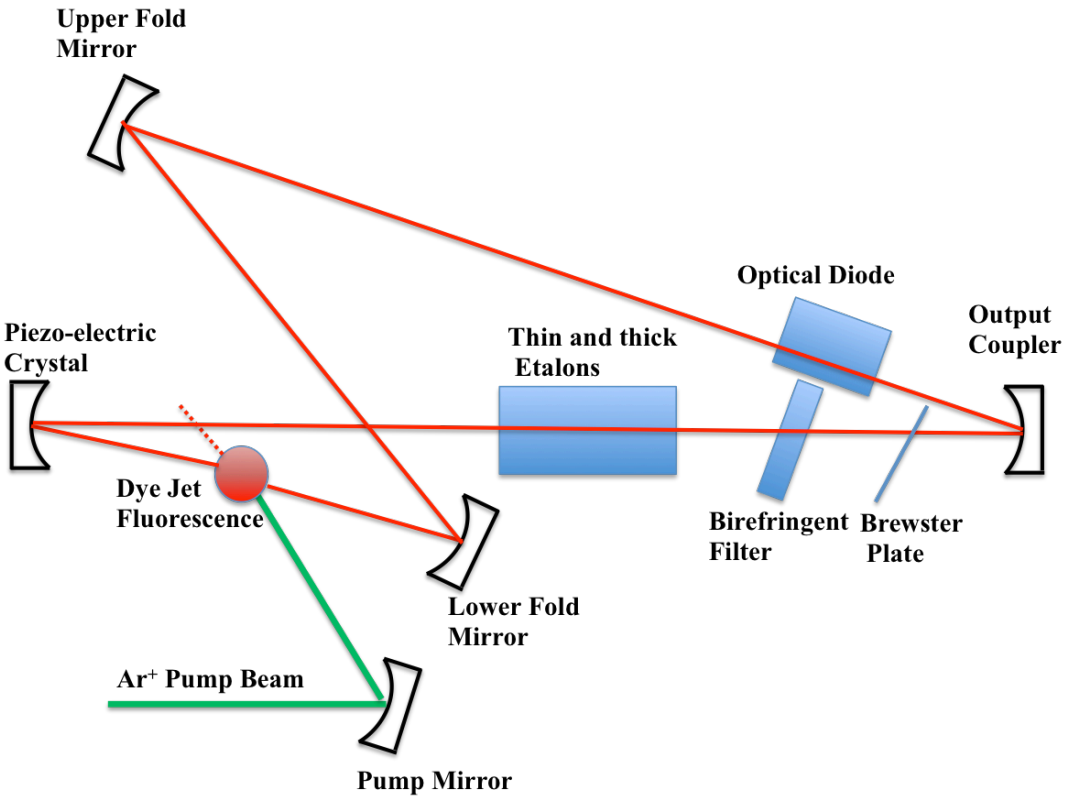

Figure 3.6 Schematic diagram of the cavity of a ring laser.

Since etalons are critical to the operation of the ring laser a brief review of their operation is given. An etalon (see Figure 3.7) is a classic device that has long been used in high-resolution spectroscopy and interferometry. It is made of two highly reflective parallel mirrors, which form a cavity. The light beam enters the first mirror and multiple reflections occur between the two mirrors. The fringes formed by the interference pattern from multiple beams are much sharper than those formed by only two beams and hence they have higher resolving power, which makes them useful in spectroscopy.

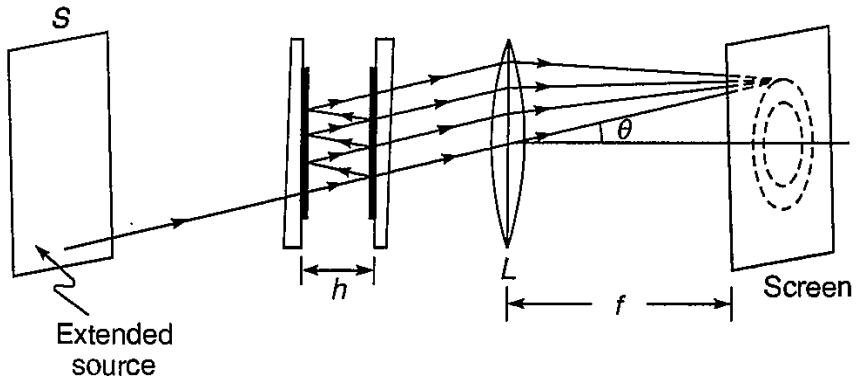

Figure 3.7 A schematic of a Fabry-Perot etalon [10].

From classical optics, the transmissivity (T) and reflectivity (R) of a typical Fabry-Perot etalon are given by [10]:

$$T = \frac{1}{1 + F\,Sin^2\frac{\delta}{2}}$$

$$R = \frac{F\,Sin^2\frac{\delta}{2}}{1 + F\,Sin^2\frac{\delta}{2}}$$

where F is the coefficient of Finesse defined by $F = \frac{4R}{(1-R)^2}$ and δ is the phase difference between two adjacent beams. F determines the width of the transmission peaks. The transmission resonances occur at c/2h apart where c is the speed of light and h is the distance between the two mirrors separated by air. The distance between two transmission peaks (fringes) defines the free spectral range of the etalon.

3.2.5.1.2 Titanium-sapphire laser

The titanium-sapphire laser is also a ring laser the schematic of which is depicted in Figure 3.6 except a titanium-sapphire crystal replaces the dye jet and they have very similar operation. The sapphire, Al_2O_3, crystal is doped with TiO_3 to create the active medium of the laser. An argon ion or a frequency-doubled YAG laser can be used to pump the continuous wave (CW) Ti:sapphire laser. The lasing wavelength range of a typical Ti:Al_2O_3 crystal is around 700-1020 nm .

3.2.6 Data Calibration

As shown in Figure 3.8, in the high-resolution data scans four traces were simultaneously recorded. The first trace is a coarse etalon (1200 MHz) trace, which is used to ensure that the laser does not have a mode hop (a jump in laser frequency). This etalon is evacuated to the pressure of 20 mTorr by a vacuum pump. The second trace is a fine etalon trace, which has a free spectral range of 150 MHz, that is used for calibration purposes explained below. It should be mentioned that both etalons were kept at the temperature of 30°C with electronically controlled heat tapes around them which would make the etalons thermally stable. Thermal stability of the etalons prevents drifting of the fringes over a time which would compromise their use in calibration. The third trace is either the iodine or uranium spectrum recorded to give accurate frequency measurements. Finally, the fourth trace is the uncalibrated laser-induced fluorescence signal of the molecule.

A calibrated frequency needs to be assigned to the molecular spectra. Igor Pro software was used for this purpose. First, the data were smoothed and occasional mode hops at the end of the scan were trimmed.

Calibration is done by matching the laser-induced fluorescence spectra recorded from either the I_2 cell or U hollow cathode lamp to previously published spectra [11, 12]. These sources have well-known spectra especially the iodine molecule which has rich and dense molecular transitions. During the high-resolution experiments, one of these two calibration sources were chosen based on whether there were calibration transitions in the region of interest. To obtain spectra of these sources in the lab, a small portion of the probe laser was directed either into an I_2 cell from which laser-induced fluorescence was collected or a small portion of the probe laser was sent into a U hollow cathode lamp where optogalvanic detection was used to get the uranium spectrum [12].

As shown in Figure 3.8, in each scan four traces are simultaneously recorded versus voltage in the horizontal axis. This refers to the applied voltage to the Brewster plate used to change the cavity length and hence the wavelength of laser. During a typical scan, about ~0.8 cm^{-1} is swept and about 1000 data points are collected. Therefore, the separation between two adjacent data points is expected to be ~0.0008 cm^{-1}. However, due to a nonlinear response of the laser wavenumber to the applied voltage the value is not constant and hence the scan is nonlinear in data points. Therefore, the laser frequency needs to be calibrated. To do so, the fine etalon with a FSR of 150 MHz is used. This etalon serves as a frequency comb that has fringes (transmission peaks) which are

~0.005 cm^{-1} apart. It is used to interpolate the points in the I_2 or U calibration trace. The iodine or uranium calibration trace was then mapped to its corresponding wavenumber given in a reference atlas [11, 12]. Finally, a plot of calibrated molecular spectra versus wavenumber was produced. The above process was repeated for each scan and finally all the files were concatenated to make a plot of the whole molecular spectrum versus wavenumber. Molecular transitions of RuF, RuCl and RuO were then tabulated for further data analysis - see chapters 4, 5 and 6.

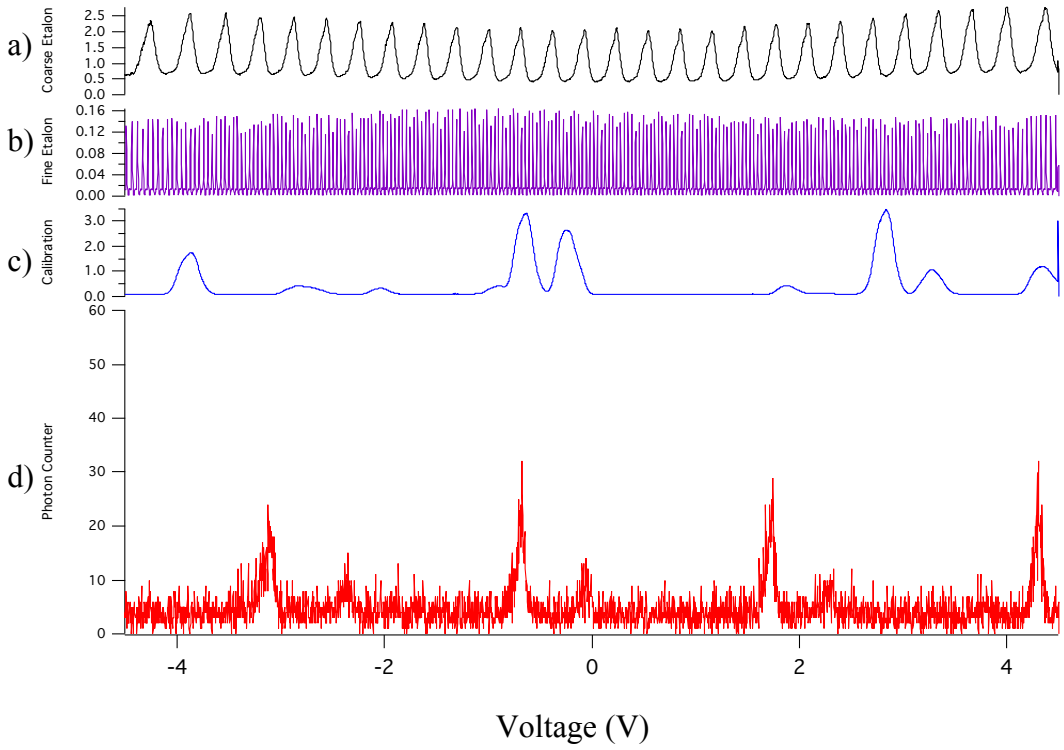

Figure 3.8 An example of the four traces recorded to calibrate the molecular spectrum: a) coarse etalon trace b) fine etalon trace c) I_2 LIF trace, and d) molecular LIF trace.

3.2.7 Loomis-Wood Plots

In 1928 Loomis and Wood developed a procedure to extract line lists for each branch given in the spectrum [13]. Conceptually, the method is to cut the spectrum into pieces and stack them on top of one another. This is a mapping from one dimension to two dimensions. In this method, the line list is mapped to a two-dimensional space [14] so that the rotational branches look like straight lines. In the spectrum, the one-dimensional line list is represented by three parameters, i.e., line index, line frequency and line intensity. First, the running index m is assigned to each rotational line in the spectrum.

Note that for an R(J) line, m=J+1, and for P(J), m=-J. Then, the line list is fitted to a polynomial function V(m). Finally, the index m is plotted against the frequency difference V_{obs}-V(m) called the residual with a certain width (see Figure 3.9). The rotational lines of each branch that lie in the same residual bandwidth, form series. The series for each rotational branch can also be color coded for ease of pattern recognition.

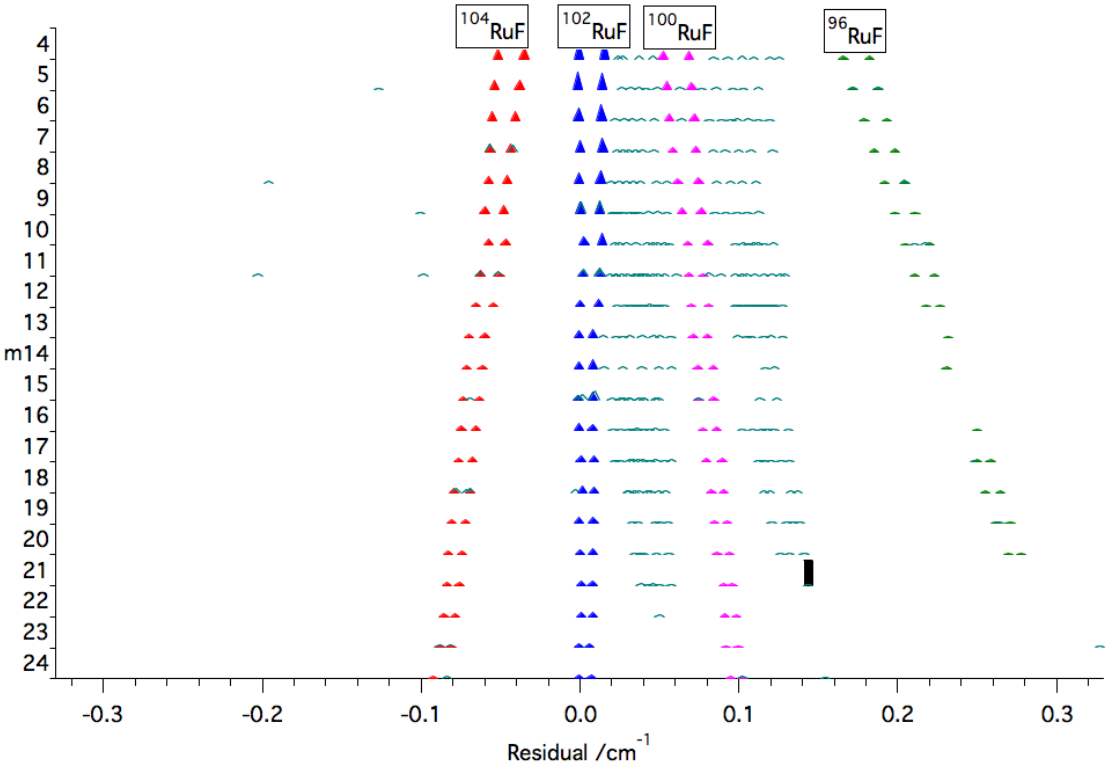

Figure 3.9 Loomis-Wood plot of selected series in the P branch of the green band of the RuF molecule.

3.2.8 Pgopher and data fitting

Pgopher [15, 16] software was used for analysis of the calibrated data. This program simulates the rotational, vibrational and electronic spectra of molecules. The user needs to upload the experimental spectra into the program and must also provide some initial guesses for molecular constants such as the rotational constants, centrifugal distortion constants, the symmetries for both the ground and excited states, and also the band origin. The Hamiltonian matrix for a given J is constructed for both the lower and upper states, diagonalized and the eigenvalues are used to generate the calculated line positions. These are then fitted to the experimental transitions by using least squares fitting methods. The initial inputs are updated and adjusted to obtain the best fit. At the end of each fit, the average error is given by the root mean square (rms) of the observed and calculated transitions [15]

$$\sigma_{rms} = \sqrt{\frac{\sum_{j=1}^{n} (Obs_j - Calc_j)^2}{n}}$$

Comprehensive documentation and details of the program is available online [16] including an explanation on how to use the program.

References

1. R. E. Smalley, L. Wharton, D. H. Levy Acc. Chem. Res. **10**, 139 (1977).

2. B. Simard, S. A. Mitchell, M. R. Humphries, P. A. Hackett, J. Mol. Spec. **129**, 186 (1988).

3. W. Demtröder, Laser Spectroscopy Basic principles, Volume 1, 4th ed., Springer, 2008.

4. W. Demtröder, Laser Spectroscopy Experimental Techniques, Volume 2, 4th ed., Springer, 2008.

5. A. D. Granger, Laser Induced Fluorescence Spectroscopy of Iridium Monofluoride, Iridium Monophosphide, Iridium Monohydride, and Iridium Monodeuteride, PhD Thesis, UNB, 2011.

6. S. W. Hopkins, High Resolution Laser Spectroscopy of Titanium Monobromide, Hafnium Monouoride and Strontium Monomethoxide, PhD Thesis, UNB, 2006.

7. http://www.exciton.com/Radiant%20Dye%20Curves%20NarrowScan%20for %20 Exciton.pdf

8. P. W. Milonni, J. H. Eberly, Laser Physics, John Wiley & Sons, 2010.

9. Coherent Autoscan Operator's Manual, USA, Coherent Inc., USA (1991).

10. A. Ghatak, OPTICS, 4th ed, McGraw Hill, 2009.

11. S. Gerkstenkorn, L. Luc, Atlas du Spectre d'Absoption de la Molecule d'Iode, Laboratoire Aimé-Cotton, CNRSII, Orsay, 1978.

12. A. B. Palmer, R. A, Keller, R. Engleman, An Atlas of Uranium Emission Intensities in a Hollow Cathode Discharge, University of California at Los Alamos, LA-8251-MS Informal Report UC-34a (1980)

13. F. W. Loomis, R. W. Wood, Phys. Rev. **32**, 223 (1928).

14. H. Lefebvre-Brion, R. W. Field, The Spectra and Dynamics of Diatomic Molecules, Elsevier Inc, 2004.

15. C. M. Western, J. Quant. Spectrosc. Radiat. Transfer **186,** 221 (2017).

16. C. M. Western, Pgopher, a program for simulating rotational, vibrational and electronic spectra, http://pgopher.chm.bris.ac.uk.

Chapter 4

Ruthenium monofluoride: observation, results and analysis

4.1 Introduction

The 4d transition metals are the basis for many useful catalytic materials. Ruthenium in particular has attracted interest in this regard. Ruthenium-bearing complexes have a significant role in catalyzing different classes of chemical reactions such as olefin (alkene) metathesis [1] and in the reactions that underlie Grubb's catalyst [2]. Olefin metathesis is an organic reaction in which carbon-carbon double bonds are redistributed (see Figure 4.1).

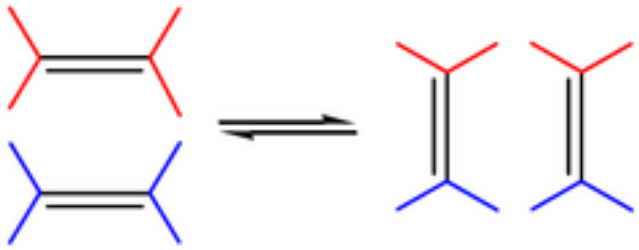

Figure 4.1 Olefin metathesis [1].

Olefin metathesis is industrially important and includes different classes such as ring opening, ring closing and ethenolysis (see Figure 4.2).

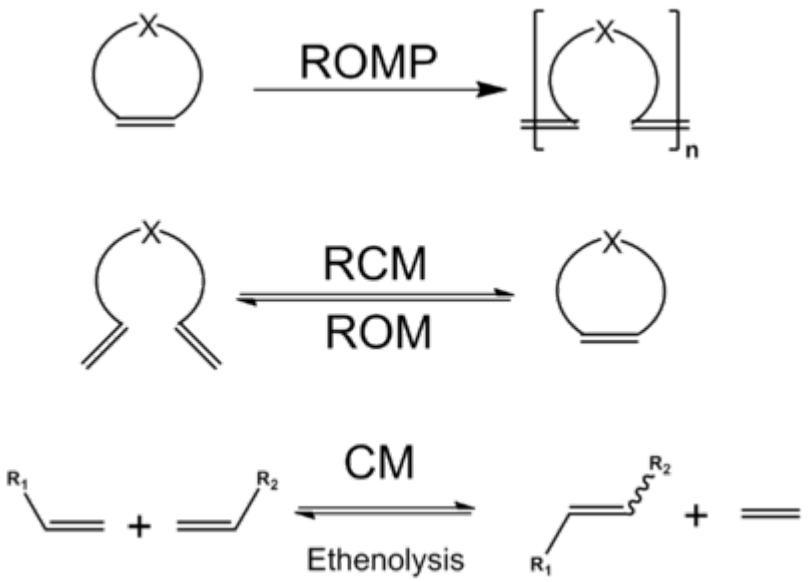

Figure 4.2 Different types of olefin metathesis reactions: ring opening metathesis polymerization (ROMP), ring opening metathesis (ROM), ring closing metathesis (RCM) and ethenolysis cross metathesis (CM) [1].

The result of adding a transition metal represented by M to the olefin metathesis process is shown in Fig. 4.3. As a result of the electron rearrangement, a four-membered ring is produced. Interactions of the d orbitals of the transition metal lower the activation energy for the electron redistribution and hence the process can occur rapidly. Without the introduction of the transition metal, the reaction is symmetry forbidden and has a high activation energy.

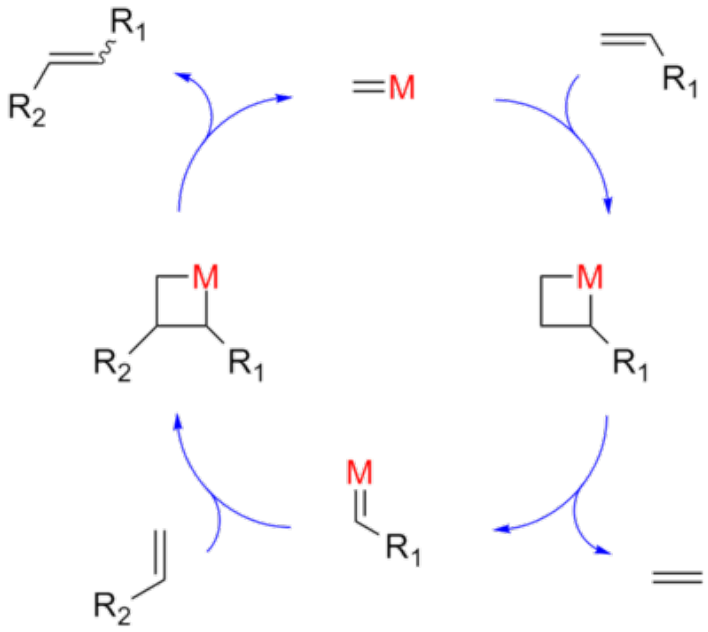

Figure 4.3 The reaction mechanism of olefin metathesis [1].

Transition metal-bearing diatom units are also present in Grubb's catalyst (see Figure 4.4), an important innovative complex containing a chlorinated ruthenium carbene ($RuCl_2CHPh$).

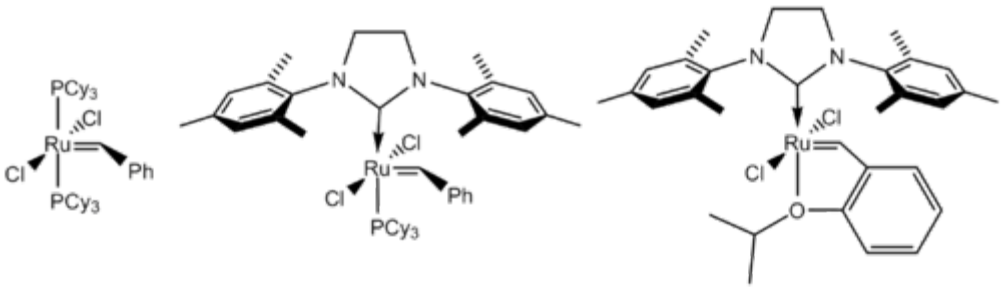

Figure 4.4 Chemical structures of different Grubbs' catalysts, tricyclohexylphosphine is abbreviated as PCy_3 ($P(C_6H_{11})$) [1].

In 2005, the Nobel Prize in chemistry was awarded to Yves Chauvin, Robert H. Grubbs and Richard R. Schrock for their contributions to elucidating the metathesis reaction mechanism and discovering Grubbs (Ru based) and Schrock (Mo, W and Re based) catalysts [3].

Apart from their catalytic nature, ruthenium-containing molecules have attracted considerable interest due to their potential applications in the pharmaceutical industry [4, 5]. They can be used as potential anticancer agents; for instance, NAMI-A, is a ruthenium based anti-cancer drug. The chemical structure of NAMI-A is shown in Figure 4.5. In a tissue, cancerous cells generally have lower pH than normal ones. NAMI-A is activated upon entering cancerous cells while it remains inactive for normal cells (see Figure 4.6). This is due to the fact that the cancerous cells growth rate is much higher than the normal cell. This creates a medium with a low level of oxygen concentration. Therefore, a reducing environment is established within the cancerous cells. Since Ru (II) compounds are more reactive than Ru (III), they are in an active form within the cancerous cells.

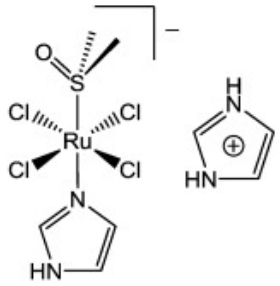

Figure 4.5 Chemical structure of imidazolium-trans-tetrachloro(dimethylsulfoxide)-imidazoleruthenium(III) (NAMI-A) [5].

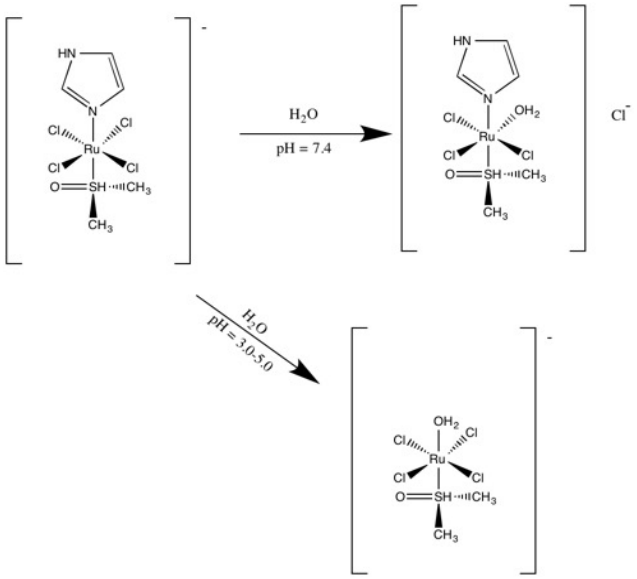

Figure 4.6 Different dissociations of NAMI-A based on pH [4].

In all of the above-mentioned complexes, ruthenium is attached to a ligand and has a significant role. Therefore, understanding the Ru-halide bond of these complexes has the potential to further elucidate their catalytic features as well as their potential pharmaceutical applications. Apart from the pure scientific merits, this explains part of the motivation behind studying ruthenium-containing molecules such as RuF, RuCl and RuO which are investigated in this thesis.

4.2 Previous studies of RuF

Ruthenium has 44 electrons and its electronic configuration is [Kr] $4d^7\ 5s^1$. Fluorine on the other hand has 9 electrons with the electronic configuration of [He] $2s^2\ 2p^5$. Under suitable conditions, the 5s electron of ruthenium can transfer to the 2p orbital of fluorine and two ions, i.e., Ru^+ and F^- can form. These ions, just like positive and negative

charges, attract each other and hence an ionic bond is formed between the two atoms to make a transition metal diatom, i.e., RuF with 53 electrons.

Ruthenium monofluoride was first theoretically studied by P. E. Siegbahn [6]. The electronic ground state of the molecule was predicted to be $^4\Phi_i$ with a bond length of 2.05 Å and a rotational constant of B=0.251 cm^{-1}. Steimle et al. [7] found the first spectrum of RuF. They observed the 0-0 band of a $^4\Gamma_{5.5} \rightarrow X^4\Phi_{4.5}$ transition in the green region at ~ 18254.8 cm^{-1} and rotationally analyzed it. They also took a low-resolution spectrum of a band in the infrared region. They were able to extract the permanent dipole moment of the molecule and information about the fluorine hyperfine interaction.

In the present work, ruthenium monofluoride is created in the molecular beam apparatus described in Chapter 3. In a low-resolution survey of RuF from 400 to 770 nm, five bands were detected in the blue, green and infrared regions of the electromagnetic spectrum. These bands were then recorded at high resolution, and were rotationally analyzed. The study resulted in the observation of a new electronic state of RuF, and in a more complete understanding of the states and transitions involved in the 540 nm bands previously reported by Steimle et al. Bond lengths, vibrational frequencies, isotopic structure, spin-orbit interactions and hyperfine splitting were all extracted from the analysis, and will be described in detail in subsequent sections of this chapter.

4.3 Experimental conditions for production of RuF

In Chapter 3 the experimental technique and apparatus needed to obtain the spectra of RuF were described. Specific experimental conditions and parameters used to make the molecule and obtain the spectra of RuF in low and high-resolution surveys are given in this section. The 3rd harmonic of a pulsed Nd:YAG laser at 355 nm was used to ablate a ruthenium rod, producing a vapor of Ru atoms. Typically, about ~ 10 mJ of ultraviolet radiation was needed in the experiments. A precursor, SF_6, at a pressure of 3 psi in the presence of 98% helium as a carrier was used to react with the Ru atoms in a reaction chamber to form the RuF molecules.

4.4 Low-resolution survey

A portion of the low-resolution survey of the RuF molecule is shown in Figure 4.7.

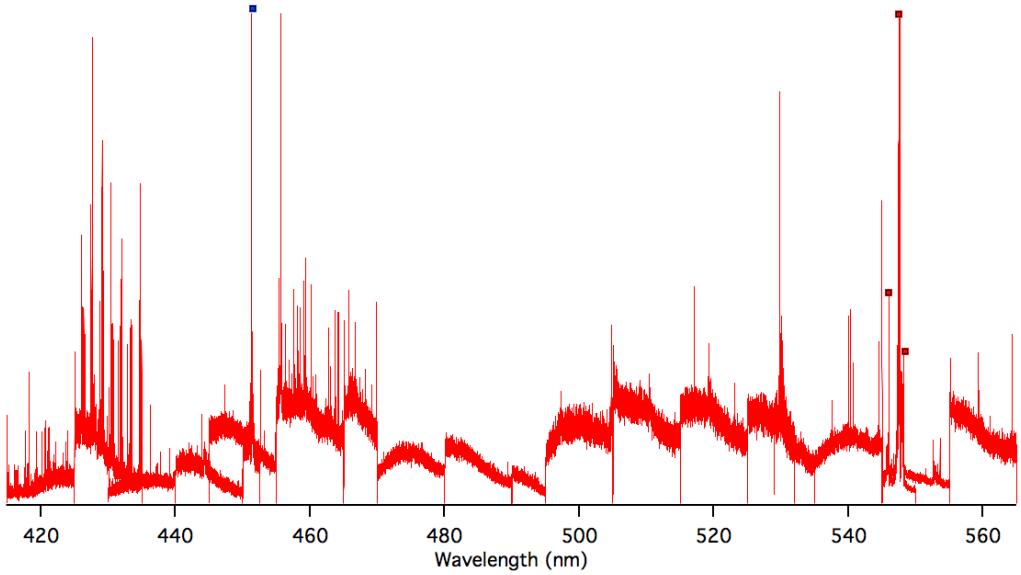

Figure 4.7 A portion of the low resolution survey of the RuF molecule in the visible region.

Five bands were detected from 420 to 760 nm for this molecule. Four of these bands are visible in Figure 4.7 and are marked with blue and red squares. As a result of the cold temperature due to supersonic expansion in the molecular jet, almost all of the molecules were in the lowest-lying levels of the ground electronic state. Hence, the observed transitions originate from the ground state. These include the first excited vibrational level v=1, and the lowest-lying excited spin-orbit component of the ground state, $^4\mathbf{\Phi}_{3.5}$.

4.4.1 Three transitions in the green region

Figure 4.8 shows a portion of a low-resolution scan in the vicinity of 550 nm, expanded

so that its coarse rotational structure can be seen. Three bands are found between 18220 and 18340 cm^{-1}. On the left there is a small band with a head near 18240 cm^{-1} directly beside the strong one. On the right there is a small feature which resembles the strong band in the middle. The three bands have weak P but strong R branches which can be indicative of a transition in which $\Delta\Omega=1$. Further analysis of these bands require more resolution which will be dealt with in the subsequent sections.

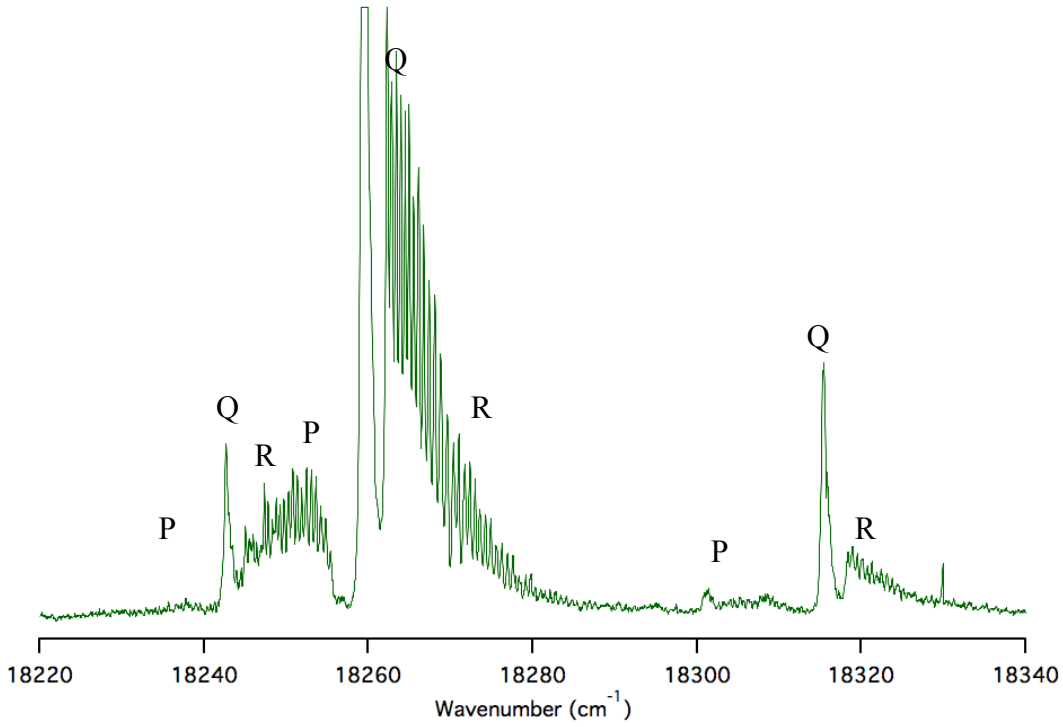

Figure 4.8 Low-resolution spectra of three transitions in the green region.

4.4.2 A transition in the blue region

Figure 4.9 shows the coarse rotational structure of a band in the blue region. As opposed

to the green transition, this band has a strong P branch but a weak R branch. This indicates a different character than the green transition and might be associated with a $\Delta\Omega$=-1 transition.

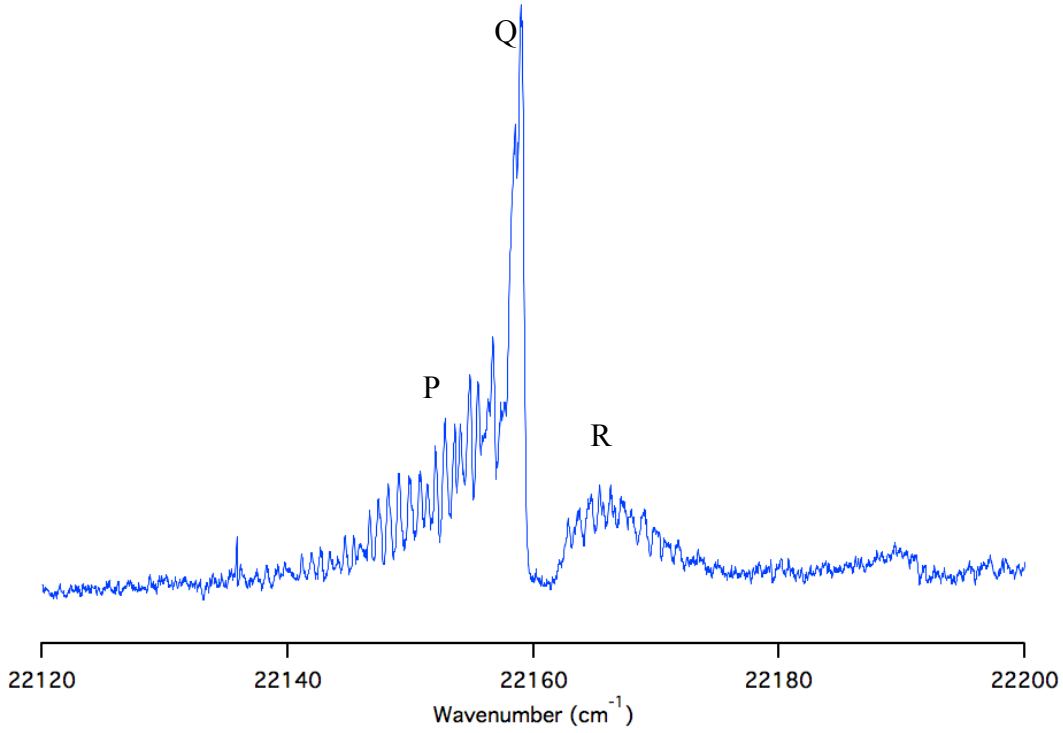

Figure 4.9 Low-resolution spectrum of a transition in the blue region.

4.4.3 A transition in the infrared region

Figure 4.10 shows a transition in the near-IR region. It has a coarse rotational structure that resembles the blue transition, with a strong P branch and a weak R branch. As with the blue band, this might suggest a $\Delta\Omega$=-1 transition.

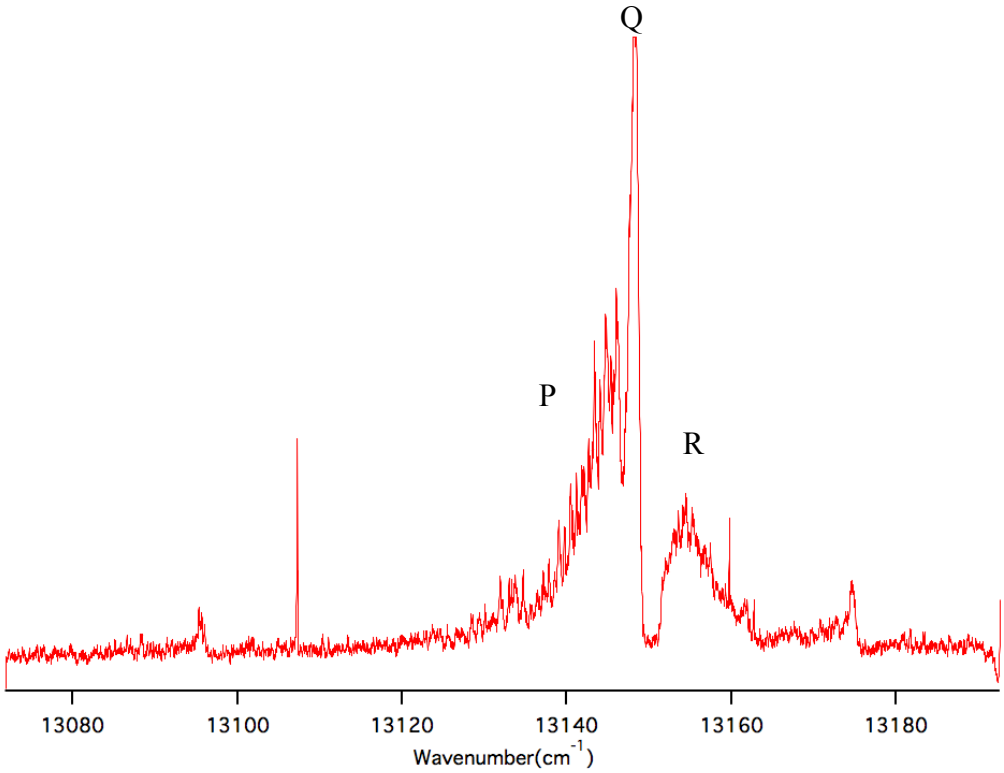

Figure 4.10 Low-resolution spectrum of a transition in the infrared region.

Detailed analysis of all transitions will be presented in the high-resolution section.

4.5 Dispersed fluorescence analysis

As described in Chapter 3, by tuning the laser to the resonance frequency of the molecules and dispersing the resulting fluorescence using a monochromator it is possible to extract the vibrational frequencies of the ground and low-lying excited states. This information facilitates the identification of the species that gives rise to the band pumped by the laser. In metal-bearing diatoms, the vibrational frequencies largely depend on the

ligands to which the metals are attached. At the spectroscopy lab in UNB some transition metal fluoride bearing molecules such as IrF [8], CoF [9], RhF [10] were previously studied, and their ground state vibrations had frequencies of 620, 663 and 575 cm^{-1} respectively. In [11], the ground state vibrational frequency of FeF which is isovalent with RuF was predicted to be 585 cm^{-1}. Hence, the vibrational frequency of ruthenium monofluoride should lie approximately in the above-mentioned range. The dispersed fluorescence analysis and fitting to equation 2.50 described in Chapter 2 results in a ground state vibrational frequency of ~ 550(10) cm^{-1} for RuF. This is in good agreement with the result measured in reference [7], i.e., 534(15) cm^{-1} for this molecule. The vibrational frequency is similar to those of RhF and FeF, so we expect some similarities in their bond strengths, which are clearly lower than those of IrF and CoF. Figure 4.11 shows samples of dispersed fluorescence from the strong infrared, green and blue bands pictured in Figures 4.8-4.10. There is a peak around ~ 550 cm^{-1} in the three dispersed fluorescence spectra which we assign to the first vibration in the ground state. The second vibration appears in the infrared DF around ~ 1100 cm^{-1}. There is also an indication of the presence of low-lying excited states (ES) at ~ 1792 and ~ 2933 cm^{-1} in the blue and green DFs respectively. In the blue DF there are extra features at ~ 1001 cm^{-1} and ~ 1994 cm^{-1} which I will later argue can be assigned as transitions to the next two excited spin-orbit (SO) components of the ground state.

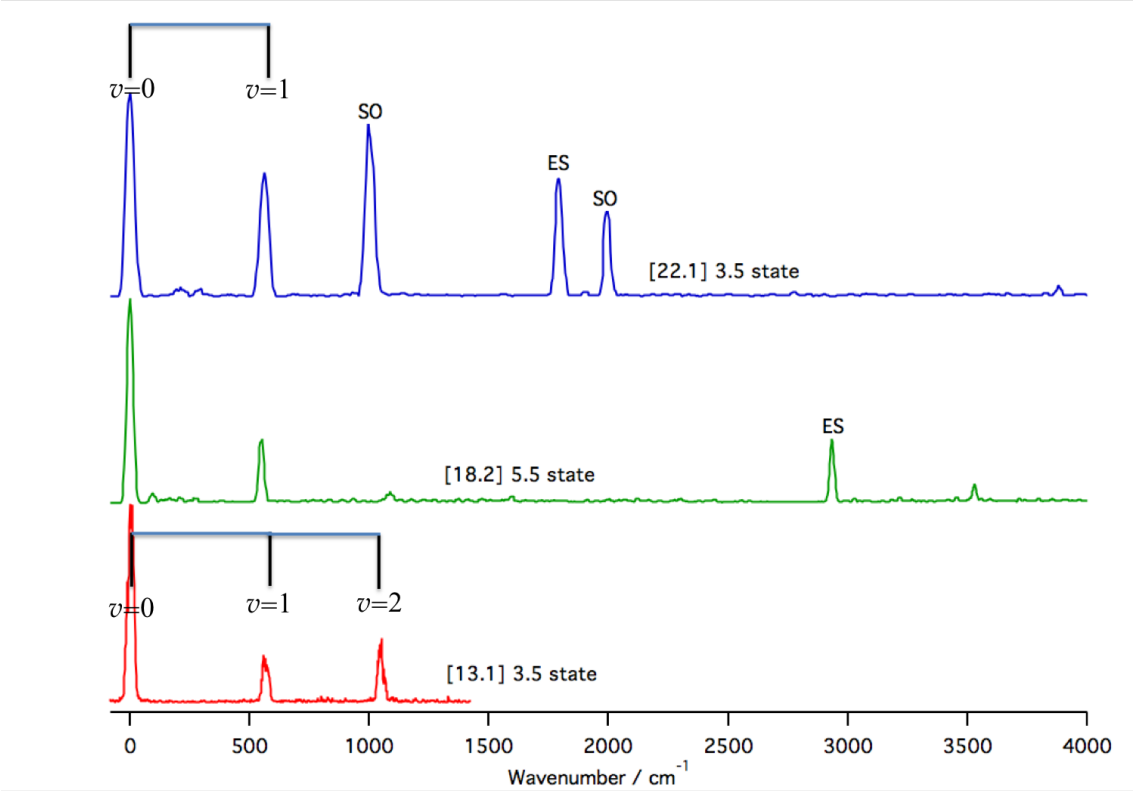

Figure 4.11 Dispersed fluorescence spectra of RuF originating from the [22.1] 3.5, [18.2] 5.5 and [13.1] 3.5 excited electronic states. Decays to spin-orbit (SO) components and excited states (ES) are also shown.

4.6 High-resolution analysis

In this section, the transitions observed in the low-resolution section will be described in detail. Equipped with higher resolution, rotational and isotopic structures of RuF are available for study. As shown in Table 4.1 ruthenium has seven stable isotopes. They have different natural abundances and only two of them have non-zero nuclear spin, i.e., I=5/2. On the other hand fluorine has only one stable isotope and it has a nuclear spin of

I=1/2. Hence, hyperfine effects can be observed in the spectra, and some hyperfine splitting is resolvable with the ~ 200 MHz resolution available in our experiments.

Table 4.1 Stable isotopes of ruthenium, their natural abundance and nuclear spin [12].

Ruthenium Isotopes	^{96}Ru	^{98}Ru	^{99}Ru	^{100}Ru	^{101}Ru	^{102}Ru	^{104}Ru
Natural Abundance (%)	5.54	1.87	12.76	12.60	17.06	31.55	18.62
Nuclear Spin	0	0	5/2	0	5/2	0	0

4.6.1 The [18.2] $^4\Gamma_{5.5} \rightarrow X^4\Phi_{4.5}$ transition

Figure 4.12 shows our high-resolution spectrum of the [18.2] $^4\Gamma_{5.5} \rightarrow X^4\Phi_{4.5}$ transition similar to the one reported by Steimle et al. [7]. Ab initio calculations by Siegbahn et al. [6] predicted an inverted $X^4\Phi_i$ ground state for the molecule which usually happens when the subshell is more than half filled**.** In the inverted case, the level with the highest value of Ω lies lowest. Also, the strong R and weak P branches can serve as a clue that $\Delta\Omega=1$ and hence, knowing the lower state is $^4\Phi$ from the theory, the upper state is $^4\Gamma$.

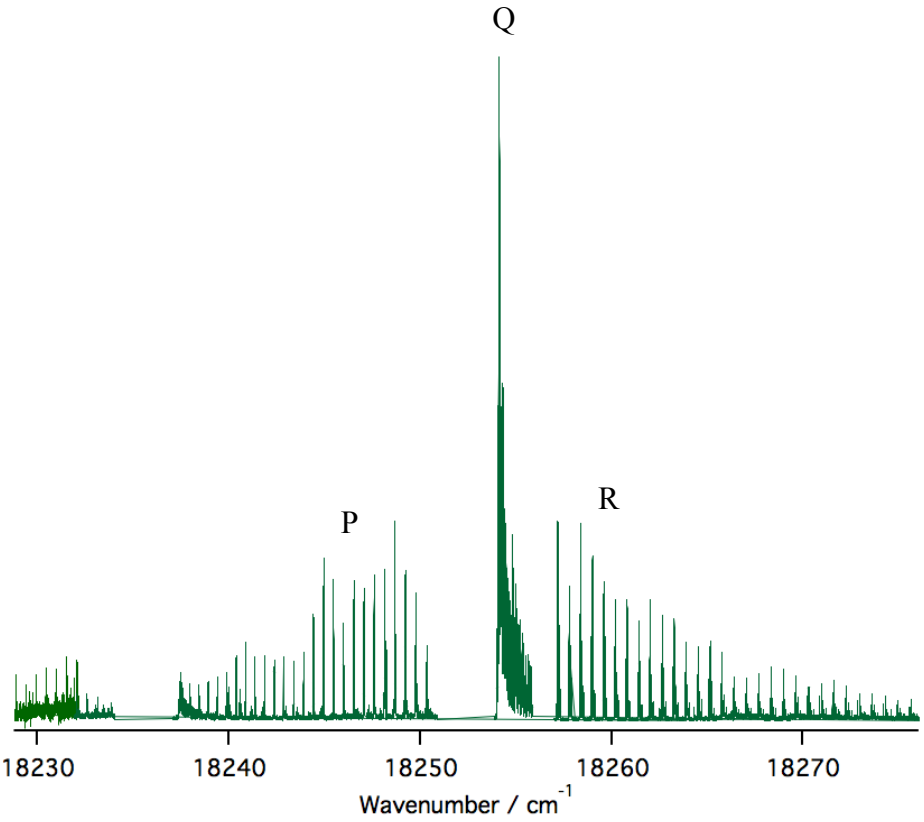

Figure 4.12 Overview of the high-resolution spectrum of the [18.2] $^4\Gamma_{5.5} \rightarrow X^4\Phi_{4.5}$ transition of RuF.

A part of the P branch in the Loomis-Wood plot of the green band is shown in Figure 4.13. The pattern shows the isotopic structure of the ^{102}RuF, ^{104}RuF, ^{100}RuF and ^{96}RuF isotopologues which are grouped in a series of doublets caused by ^{19}F hyperfine splittings. The frequencies of the rotational lines for the ^{102}RuF isotopologue analysis generated from this plot are given in Tables 4.2 and 4.3 for further processing. Note that only one hyperfine component is listed for each rotational line in order to calculate the combination differences.

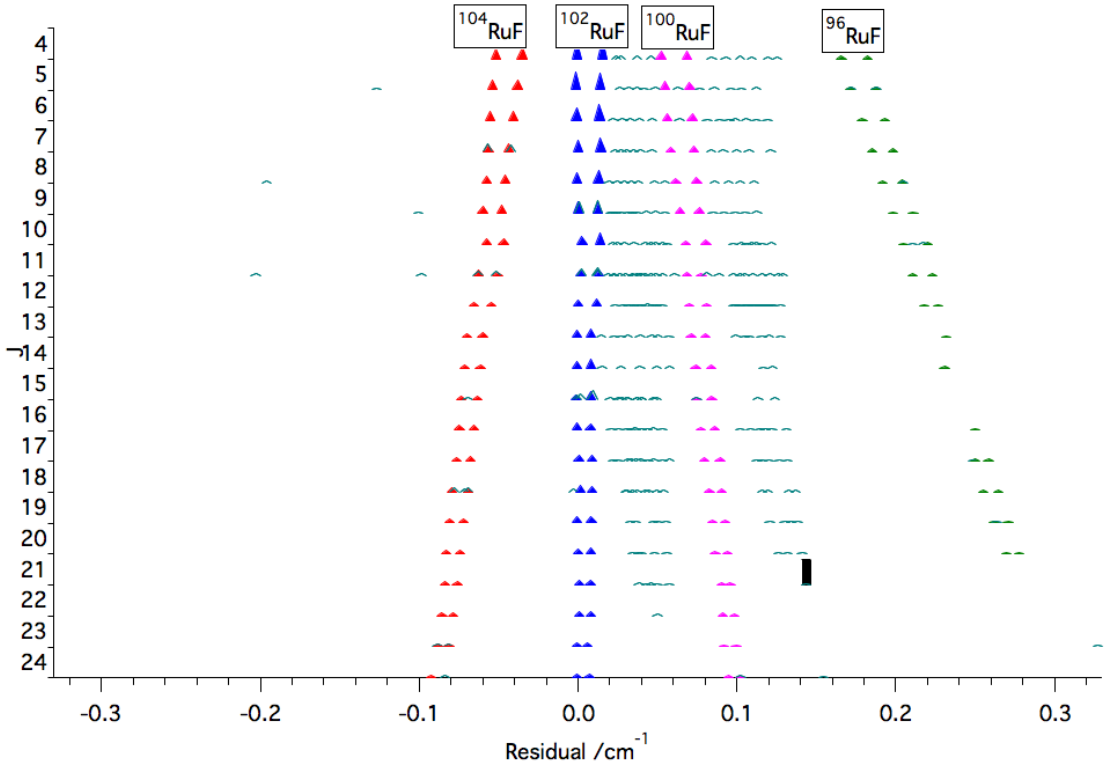

Figure 4.13 Loomis-Wood plot of selected series in the P branch of the [18.2] $^4\Gamma_{5.5} \rightarrow X^4\Phi_{4.5}$ band of RuF molecule.

The results of rotational numbering and combination difference analysis for the upper and lower states can be seen in Tables 4.2 and 4.3. The rotational numbering and the frequencies of the P and R branches are in agreement with the ones given in [7].

Table 4.2 Rotational numbering and combination difference analysis for the upper state of the [18.2] $^4\Gamma_{5.5} \rightarrow X^4\Phi_{4.5}$ transition of ^{102}RuF.

J	P(J) / cm^{-1}	P(J) /cm^{-1} [7]	R(J) / cm^{-1}	R(J) / cm^{-1} [7]	$\Delta F'(J)$ / cm^{-1}	B' / cm^{-1}
4.5			18257.1794	18257.187		
5.5			18257.7759	18257.7876		
6.5	18250.3019	18250.3095	18258.3742	18258.3832	8.0723	0.288296
7.5	18249.7513	18249.7571	18258.9752	18258.9822	9.2239	0.288246
8.5	18249.2045	18249.2098	18259.5790	18259.5846	10.3745	0.288180
9.5	18248.6606		18260.1876	18260.1919	11.5270	0.288175
10.5	18248.1166		18260.7968	18260.7981	12.6802	0.288186
11.5	18247.5788		18261.4090	18261.4129	13.8302	0.288129
12.5	18247.0409		18262.0232	18262.024	14.9823	0.288121
13.5	18246.5091		18262.6406	18262.6445	16.1315	0.288062
14.5	18245.9762		18263.2619	18263.2648	17.2857	0.288095
15.5	18245.4516		18263.8871	18263.8864	18.4355	0.288054

Table 4.3 Rotational numbering and combination difference analysis for the lower state of the [18.2] $^4\Gamma_{5.5} \rightarrow X^4\Phi_{4.5}$ transition of ^{102}RuF.

J	P(J) / cm^{-1}	R(J) / cm^{-1}	$\Delta F''(J)$ / cm^{-1}	B'' / cm^{-1}
4.5		18257.1794		
5.5		18257.7759	6.8775	0.286562
6.5	18250.3019	18258.3742	8.0246	0.286592
7.5	18249.7513	18258.9752	9.1697	0.286553
8.5	18249.2045	18259.5790	10.3146	0.286516
9.5	18248.6606	18260.1876	11.4624	0.286560
10.5	18248.1166	18260.7968	12.6088	0.286563
11.5	18247.5788	18261.4090	13.7559	0.2865812
12.5	18247.0409	18262.0232	14.8999	0.2865365
13.5	18246.5091	18262.6406	16.0470	0.2865535
14.5	18245.9762		17.1890	0.2864833
15.5	18245.4516			

As mentioned, the ruthenium atom has seven stable isotopes (see Table 4.1). Hence, seven isotopic molecular spectra should be observable given sufficient resolution. However, as shown in Figure 4.14 there are more rotational lines than can be accounted for with the Ru isotopes alone. The ruthenium isotopes with even mass number have zero nuclear spin and only the two odd ones posses a nuclear spin of 5/2. Fluorine, on the other hand has a nucleus with nuclear spin I=1/2. Figure 4.14 shows a portion of the R branch of the 0-0 band of the [18.2] $^4\Gamma_{5.5} \rightarrow X^4\Phi_{4.5}$ transition. Each rotational line is split into 2I+1 components due to hyperfine interactions. Therefore, each rotational line related to the ruthenium atom with zero nuclear spin is doubled due to fluorine spin. The other rotational lines related to the ruthenium atom with spin 5/2 should split in to 12 rotational lines due to the combined hyperfine effect of two atoms with nonzero nuclear spin. However, the hyperfine pattern is too dense to be resolved in our apparatus.

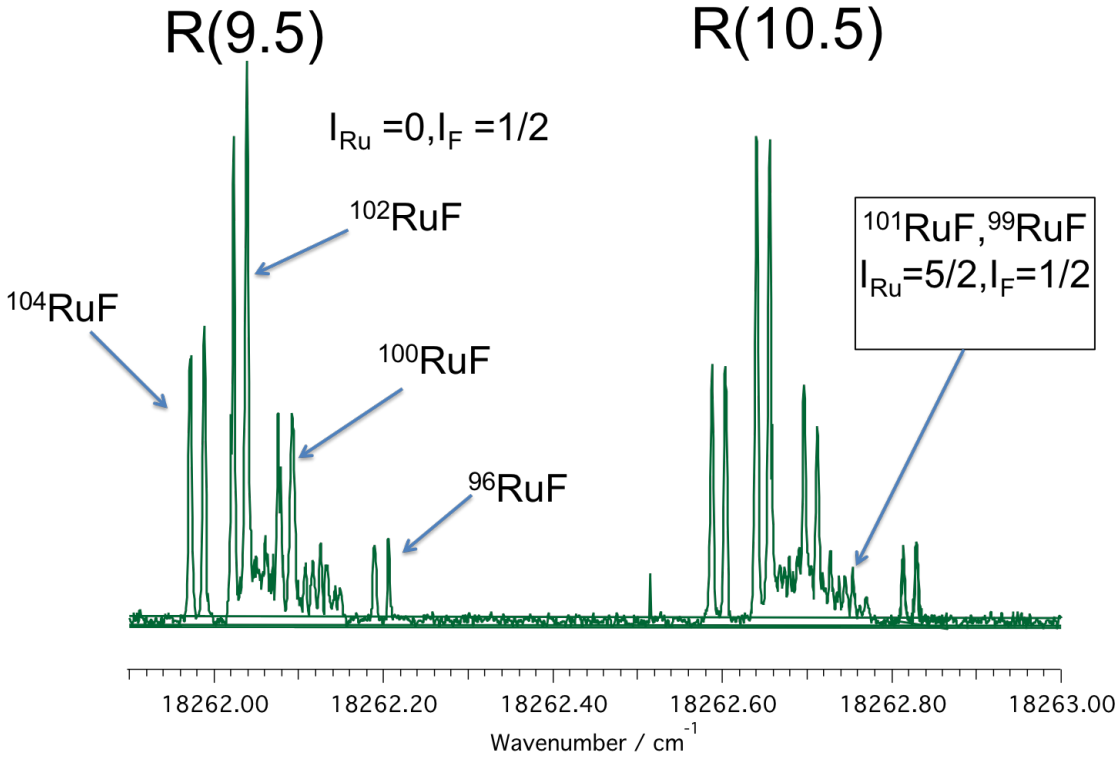

Figure 4.14 Isotopic and hyperfine structures of two R transitions in the [18.2] $^4\Gamma_{5.5} \rightarrow X^4\Phi_{4.5}$ transition of RuF.

Another interesting feature in the spectrum is the large gap between the first R and P lines. As shown in Figure 4.15, the first R line starts from J″=4.5 and the first P line starts from J″=6.5 resulting in a gap of ~ B″ [(6.5)(7.5)-(5.5)(4.5)]=24 B″ between them. Therefore, starting at relatively high rotational numbers produces a large gap. We will later see that in the other bands of the green system there is also a large gap between the R and P branches.

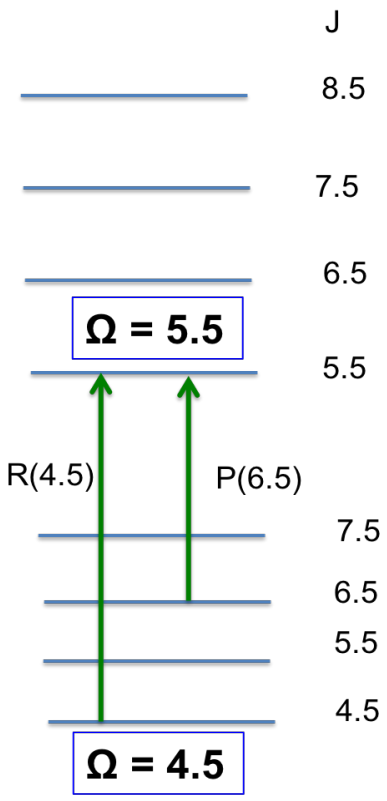

Figure 4.15 Energy level diagram of the 0-0 band of the [18.2] $^4\Gamma_{5.5} \rightarrow X^4\Phi_{4.5}$ transition, indicating the transitions due to the first lines in the R and P branches.

4.6.2 Hyperfine analysis and fitting results

As was shown in Figure 4.14, the magnetic hyperfine splitting due to the nuclear spin of fluorine is quite evident in the spectra for the isotopologues. Therefore, the procedure of calculating estimated values of the hyperfine parameters for both the ground and excited states that can be used as initial inputs in the fitting routine will be presented.

As discussed in Chapter 2, the hyperfine Hamiltonian is given by equation 2.135. This equation can be rearranged in terms of the hyperfine parameter h that can be described by the linear combination of Frosch and Foley parameters,

$$h = a\Lambda + (b + c)\Sigma \tag{4.1}$$

where the projection of electronic and spin angular momenta along the internuclear axis gives Λ and Σ respectively.

The hyperfine energy can be expressed by

$$W(F) = \frac{h\Omega[F(F+1)-J(J+1)-I(I+1)]}{2J(J+1)} \tag{4.2}$$

For a level with angular momentum F-1 it takes the following form:

$$W(F-1) = \frac{h\Omega[(F-1)F-J(J+1)-I(I+1)]}{2J(J+1)} \tag{4.3}$$

The difference gives:

$$\Delta W = W(F) - W(F-1) = \frac{h\Omega F}{J(J+1)} \tag{4.4}$$

Hence,

$$h = \frac{\Delta W J(J+1)}{\Omega F} \tag{4.5}$$

The above formula can be used to calculate an estimate for the ground and excited state hyperfine parameters.

Figure 4.16 shows the hyperfine splitting of two rotational levels of the ground and excited states with the corresponding quantum numbers. Three allowed transitions between the rotational sublevels are also depicted in the picture. These transitions are adequate to measure the hyperfine splittings of the upper and lower states

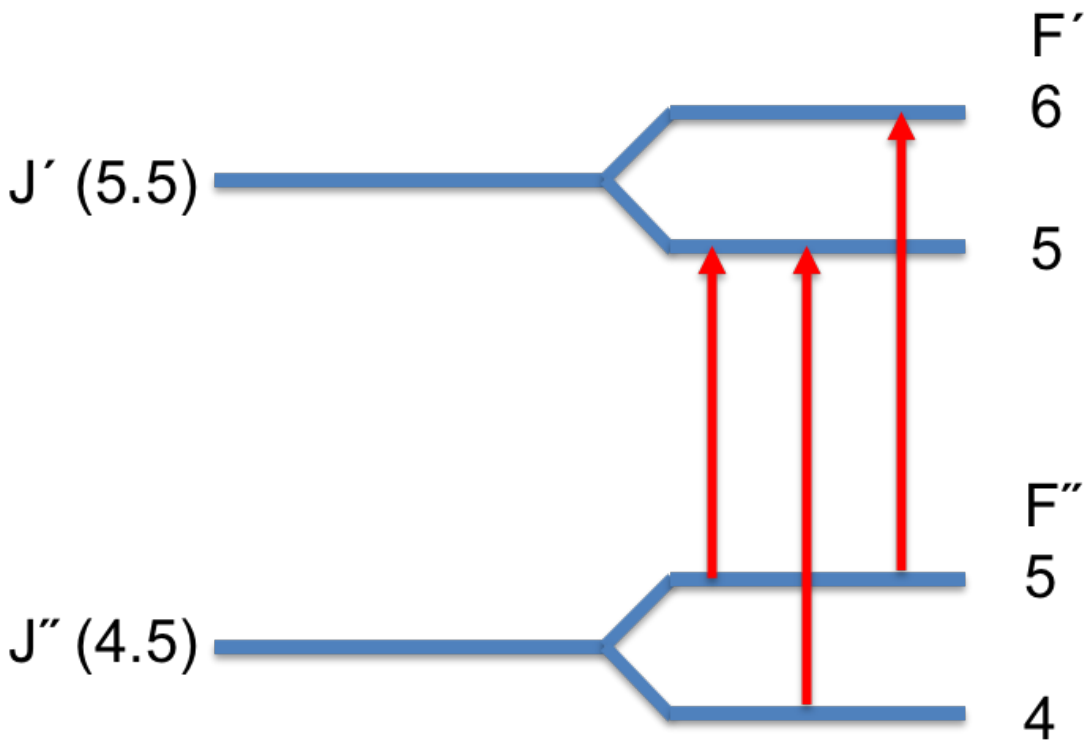

Figure 4.16 Three possible transitions from the corresponding hyperfine splittings of two rotational levels J″=4.5 and J´=5.5 in the R branch.

Figure 4.17 shows the experimental and calculated spectrum of a portion of the R branch, R (4.5), of the 0-0 band of the [18.2] $^{4}\Gamma_{5.5} \rightarrow X^{4}\Phi_{4.5}$transition for ^{102}RuF.

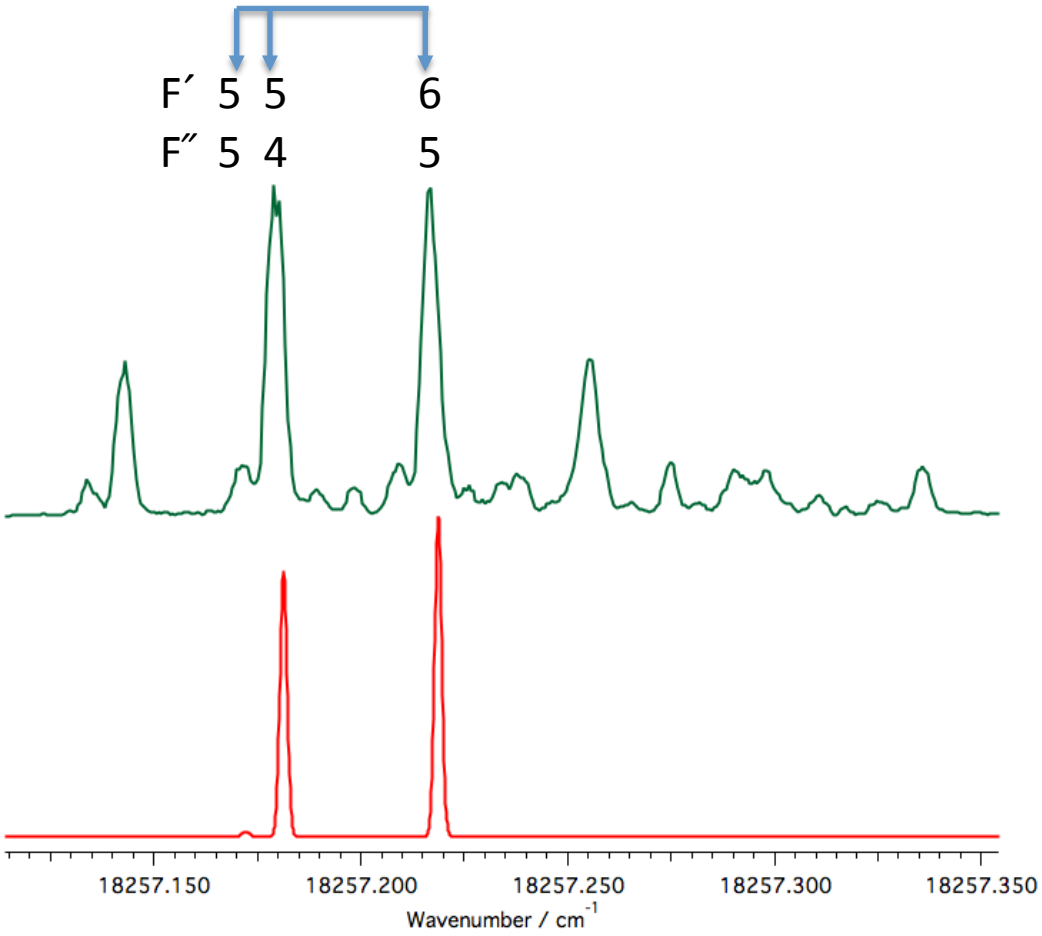

Figure 4.17 A portion of the R branch, R (4.5), 0-0 band of the [18.2] $^4\Gamma_{5.5} \rightarrow X^4\Phi_{4.5}$ transition of ^{102}RuF; the upper trace is the experimental spectrum and the lower trace is the calculated. Three transitions of the ^{102}RuF molecule with the corresponding F values for the upper and lower states which were used to measure the hyperfine parameter are shown.

The $F'' = 4 \rightarrow F' = 5$ and $F'' = 5 \rightarrow F' = 5$ transitions are measured to be 18257.1786 and 18257.1711 cm^{-1} respectively. The difference between transitions, 0.0075 cm^{-1}, gives the hyperfine energy gap of the lower state (see Figure 4.16).

Therefore, an estimate for the ground state hyperfine parameter can be readily achieved from equation 4.5.

$$h'' = \frac{0.0075 \times 4.5 \times 5.5}{4.5 \times 5} = 0.00825\ cm^{-1} = 247.32\ MHz$$

To obtain the value of *a* for the ground state, *b* and *c* can be set to zero. Since the ground state is $X^4\Phi_{4.5}$, $\Lambda = 3$ and hence $a'' = 0.0027\ \text{cm}^{-1}$. This value can then be used as the initial estimate in the fitting program. Also, the hyperfine parameter for the excited state can be readily calculated; as the $F'' = 5 \rightarrow F' = 6$ transition occurs at 18257.2166 cm^{-1} and the upper state hyperfine splitting (see Figure 4.16) is measured to be 0.0455 cm^{-1} then

$$h' = \frac{0.0455 \times 5.5 \times 6.5}{5.5 \times 6} = 0.04929\ cm^{-1} = 1477.67\ MHz$$

The upper state is $^4\Gamma_{5.5}$, $\Lambda = 4$ and hence $a' = 0.01232\ cm^{-1}$ if *b* and *c* are set to zero. The above procedure can be used for the other isotopologues and the initial values for the hyperfine parameter can be calculated. Note that in all of the fits, first the values of *a* are extracted for the lower and upper states and then multiplied by the corresponding Λ values to report the hyperfine parameters h'' and h'.

Tables 4.4, 4.5, 4.6 and 4.7 summarize the result of fitting of the green band for the ^{102}RuF, ^{104}RuF, ^{100}RuF and ^{96}RuF isotopologues with rms values of 0.0015, 0.0014, 0.0013 and 0.0021 cm^{-1} respectively. This was done using the R^2 form of the Hamiltonian (see section 2.9) [13]. The lower and upper states were fitted as Φ and Γ states respectively. The molecular constants B and D, the hyperfine parameter *a* and the band origin T are extracted from the fit. These parameters were adequate to model the

rotational and hyperfine structures of the molecule. The average of standard deviation of the fit for the four isotopologues is ~ 0.0015 cm^{-1}. This value compares favorably with our experimental precision of 0.001 cm^{-1}. The results of the present work are compared and are in good agreement with the available values in literature [7]. Note that in all the tables the number in parentheses represents one standard deviation in the particular parameter that is reported in the present study.

Table 4.4 Molecular constants for the states involved in the [18.2] $^4\Gamma_{5.5} \rightarrow X^4\Phi_{4.5}$ transition of ^{102}RuF.

Parameters	$X^4\Phi_{4.5}$	$[18.2]^4\Gamma_{5.5}$
B / cm^{-1}	0.28661381(617) *0.2866(6)*[1]	0.28814146(600) *0.2881(8)*[1]
D / 10^{-7} cm^{-1}	2.9116(445)	2.4493(425)
T / cm^{-1}		18256.90420(22) *18256.910(12)*[1]
h / 10^{-3} cm^{-1}	9.99(84) *9.30(66)*[1]	50.40(72) *48.43(2.00)*[1]

[1] Taken from reference [7].

Table 4.5 Molecular constants for the states involved in the [18.2] $^4\Gamma_{5.5} \rightarrow X^4\Phi_{4.5}$ transition of ^{104}RuF.

Parameters	$X^4\Phi_{4.5}$	$[18.2]^4\Gamma_{5.5}$
B / cm^{-1}	0.28574840(609) *0.2858(6)* [1]	0.28726893(593) *0.2873(8)* [1]
D / 10^{-7} cm^{-1}	2.8901(436)	2.4171(415)
T / cm^{-1}		18256.86911(23) *18256.875(6)* [1]
h / 10^{-3} cm^{-1}	11.52(96)	51.76(80)

Table 4.6 Molecular constants for the states involved in the [18.2] $^4\Gamma_{5.5} \rightarrow X^4\Phi_{4.5}$ transition of ^{100}RuF.

Parameters	$X^4\Phi_{4.5}$	$[18.2]^4\Gamma_{5.5}$
B / cm^{-1}	0.2875111(119) *0.2874(2)* [1]	0.2890431(116)
D / 10^{-7} cm^{-1}	3.51(24)	2.76(24)
T / cm^{-1}		18256.94129(34) *18256.947(12)* [1]
h / 10^{-3} cm^{-1}	10.56(120)	50.32(100)

Table 4.7 Molecular constants for the states involved in the [18.2] $^4\Gamma_{5.5} \rightarrow X^4\Phi_{4.5}$ transition of ^{96}RuF.

Parameters	$X^4\Phi_{4.5}$	$[18.2]^4\Gamma_{5.5}$
B / cm^{-1}	0.2890167(224)	0.2906510(212)
D / 10^{-6} cm^{-1}	1.7687(350)	1.6367(316)
T / cm^{-1}		18257.01819(39)
h / 10^{-3} cm^{-1}	9.12(195)	45.96(172)

4.6.3 The [18.2] $^4\Gamma_{4.5} \rightarrow X^4\Phi_{3.5}$ transition: higher-lying spin-orbit components

As was shown in Figure 4.8, there is a small feature beside the 0-0 band of the [18.2] $^4\Gamma_{5.5} \rightarrow X^4\Phi_{4.5}$ transition. As can be seen from the high-resolution spectrum of Figure 4.18 this band is slightly lower in wavenumber compared to the 0-0 band of the [18.2] $^4\Gamma_{5.5} \rightarrow X^4\Phi_{4.5}$ transition band but resembles it closely. It has strong R and weak P branches as does the 0-0 band of the [18.2] $^4\Gamma_{5.5} \rightarrow X^4\Phi_{4.5}$ transition. There is also a gap between the Q branch and the first P lines of the two spectra.

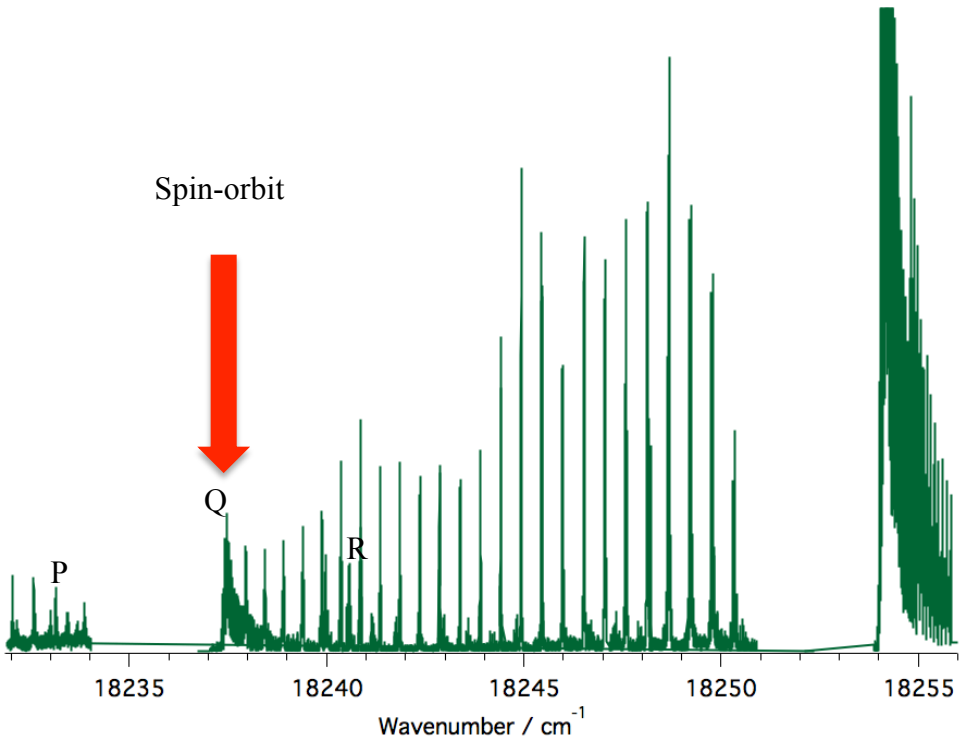

Figure 4.18 An overview of the spectrum of the weak feature of RuF observed beside the 0-0 band of the [18.2] $^4\Gamma_{5.5} \rightarrow X^4\Phi_{4.5}$ transition.

Figure 4.19 shows an expanded view of the above spectrum. In the bottom panel a portion of the two bands is depicted between 18237-18242 cm^{-1} and in the upper panel the 18239.8-18240.8 cm^{-1} spectral region is more expanded. As can be seen, the small band appears as a regular series of weaker lines interspersed between lines of the stronger spectrum. The isotopic structure of ruthenium and hyperfine splitting due to the nuclear spin of fluorine are quite evident and are similar to those of the main band.

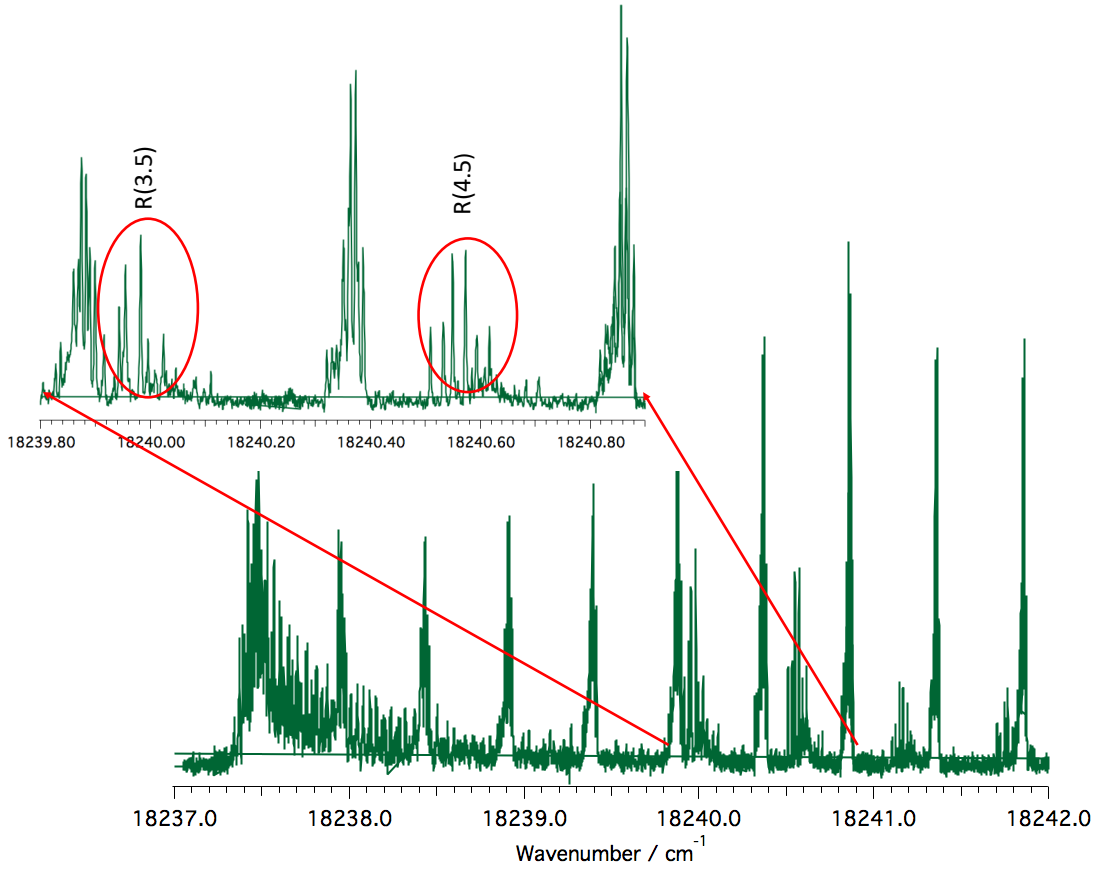

Figure 4.19 Isotopic and hyperfine structures of RuF including an expanded view of the first two R lines of the weaker band.

To obtain the rotational numbering of the weaker band, two consecutive lower state combination differences between R and Q branches were divided.

$$\frac{Q(J+1)-R(J)}{Q(J)-R(J-1)}=\frac{B''[(J+1)(J+2)-J(J+1)]}{B''[J(J+1)-J(J-1)]}=\frac{J^2+2J+J+2-J^2-J}{J^2+J-J^2+J} \qquad 4.6$$

The result of this division is equal to a (J+1)/J ratio. Knowing J should be half integer the procedure showed that the first R line starts from J″=3.5 and since its projection along the internuclear axis cannot be bigger, then Ω″=3.5. For the upper state the first J′ is equal to

4.5 so the new band is almost certainly the $^4\Gamma_{4.5} \rightarrow X^4\Phi_{3.5}$ transition, arising from the spin-orbit components second lowest in energy of this electronic transition.

Tables 4.8 and 4.9 provide the combination differences for one hyperfine component of the ground and upper states. The initial B values used as inputs for fitting and simulating the spectrum calculated from the combination differences were ~ 0.2885 and 0.2867 cm^{-1} for the upper and lower states respectively.

Table 4.8 Rotational numbering and analysis for the upper state of the [18.2] $^{4}\Gamma_{4.5} \rightarrow X^{4}\Phi_{3.5}$ transition of ^{102}RuF.

J	P(J) / cm^{-1}	R(J) / cm^{-1}	$\Delta F'(J)$ / cm^{-1}	B' / cm^{-1}
4.5		18240.5733		
5.5		18241.1679		
6.5	18233.6698	18241.7670	8.0972	0.289185
7.5	18233.1217	18242.3709	9.2492	0.289038
8.5	18232.5741	18242.9812	10.4071	0.289086
9.5	18232.0319	18243.5921	11.5602	0.289005
10.5	18231.5120	18244.2053	12.6933	0.288484
11.5	18230.9648	18244.8258	13.8610	0.288770
12.5	18230.4347	18245.4455	15.0108	0.288670
13.5	18229.9083	18246.0698	16.1615	0.288598
14.5	18229.3857	18246.7015	17.3158	0.288596
15.5	18228.8628	18247.3347	18.4719	0.288623

Table 4.9 Rotational numbering and analysis for the lower state of the [18.2] $^4\Gamma_{4.5} \rightarrow X^4\Phi_{3.5}$ transition of ^{102}RuF.

J	P(J) / cm^{-1}	R(J) / cm^{-1}	$\Delta F''$ / cm^{-1}	B'' / cm^{-1}
4.5		18240.5733		
5.5		18241.1679	6.9035	0.287645
6.5	18233.6698	18241.7670	8.0462	0.287364
7.5	18233.1217	18242.3709	9.1929	0.287278
8.5	18232.5741	18242.9812	10.3390	0.287195
9.5	18232.0319	18243.5921	11.4692	0.286730
10.5	18231.5120	18244.2053	12.6273	0.286984
11.5	18230.9648	18244.8258	13.7706	0.286887
12.5	18230.4347	18245.4455	14.9175	0.286875
13.5	18229.9083	18246.0698	16.0598	0.286783
14.5	18229.3857		17.2070	0.286783
15.5	18228.8628			

The band was fitted in Pgopher using an R^2 Hamiltonian [13]. In Tables 4.10, 4.11 and 4.12 the molecular constants and the hyperfine parameter are extracted for the ^{102}RuF, ^{104}RuF and ^{100}RuF isotopologues. The overall standard deviation of the fitting of the experimental data to the Hamiltonian are in the order of ~ 0.0016, 0.0017 and 0.0013 cm^{-1} for the ^{102}RuF, ^{104}RuF, ^{100}RuF isotopologues respectively which is consistent with the experimental uncertainty.

As can be seen from Tables 4.10, 4.11 and 4.12 in comparison, the fitted rotational parameter B for the lower and upper states and hyperfine parameter are similar to those of the main band.

Table 4.10 Molecular constants for states involved in the [18.2] $^4\Gamma_{4.5} \rightarrow X^4\Phi_{3.5}$ transition of ^{102}RuF.

Parameters	$X^4\Phi_{3.5}$	[18.2] $^4\Gamma_{4.5}$
B / cm^{-1}	0.2866701(80)	0.2884963(73)
T / cm^{-1}		18239.66719(27)
h / 10^{-3} cm^{-1}	22.02(96)	48.76(80)

Table 4.11 Molecular constants for states involved in the [18.2] $^4\Gamma_{4.5} \rightarrow X^4\Phi_{3.5}$ transition of ^{104}RuF.

Parameters	$X^4\Phi_{3.5}$	[18.2] $^4\Gamma_{4.5}$
B / cm^{-1}	0.2850573(83)	0.2869372(75)
T / cm^{-1}		18239.63234(30)
h / 10^{-3} cm^{-1}	16.98(192)	46.16(160)

Table 4.12 Molecular constants for states involved in the [18.2] $^4\Gamma_{4.5} \rightarrow X^4\Phi_{3.5}$ transition of ^{100}RuF.

Parameters	$X^4\Phi_{3.5}$	[18.2] $^4\Gamma_{4.5}$
B / cm^{-1}	0.2867923(64)	0.2887382(57)
T / cm^{-1}		18239.70743(23)
h / 10^{-3} cm^{-1}	10.26(147)	40.72(124)

Figure 4.20 shows the 0-0 band of the [18.2] $^4\Gamma_{5.5} \rightarrow X^4\Phi_{4.5}$ and its relation to the spin-orbit feature identified and analyzed in this section.

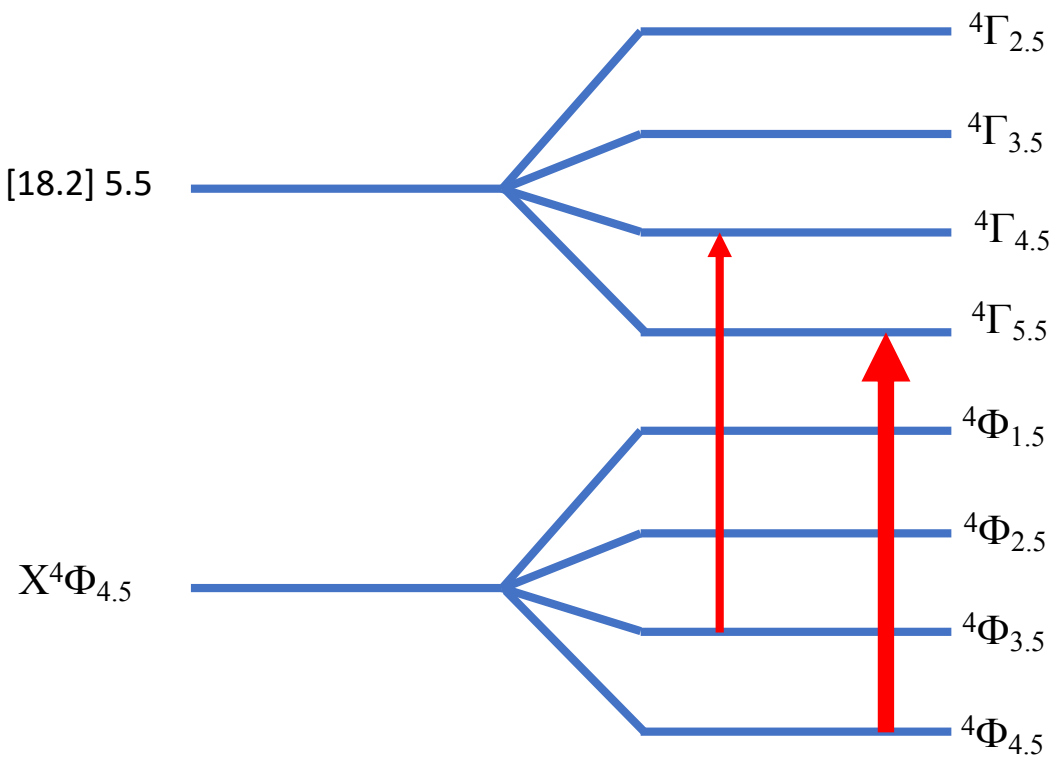

Figure 4.20 Diagram of the 0-0 band of the [18.2] $^4\Gamma_{5.5} \rightarrow X^4\Phi_{4.5}$ and spin-orbit transitions.

It should be noted the value of spin-orbit splitting in the ground state was measured to be ~1000 cm^{-1} from the DF and therefore, $H_{so} \sim A\Lambda\Sigma \sim 1000\ cm^{-1}$. Since the ground state is $^4\Phi_{4.5}$, the spin-orbit constant is determined to be $A'' \sim 1000/3\ cm^{-1}$ for this state. Then the splitting for the upper state $^4\Gamma_{5.5}$ is found to be ~ 983 cm^{-1} and the spin-orbit constant is found to be $A' \sim 983/4\ cm^{-1}$.

4.6.4 The 1-1 vibration of the [18.2] $^4\Gamma_{5.5} \rightarrow X^4\Phi_{4.5}$ transition

Figure 4.21 shows the high-resolution spectra of a second weak feature at a slightly higher wavenumber than the main band. This weak feature, which is ~ 60 cm^{-1} higher in energy than the 0-0 band of the [18.2] $^4\Gamma_{5.5} \rightarrow X^4\Phi_{4.5}$ transition of RuF, is at ~ 18131.2 cm^{-1}. This is about the right position to be the 1-1 vibration of the green system if a slightly higher vibrational frequency (i.e., ~ 606 cm^{-1}) than the lower state is assumed for the upper state. Later in the section, further evidence that the band is indeed the 1-1 vibration of the green system will be discussed.

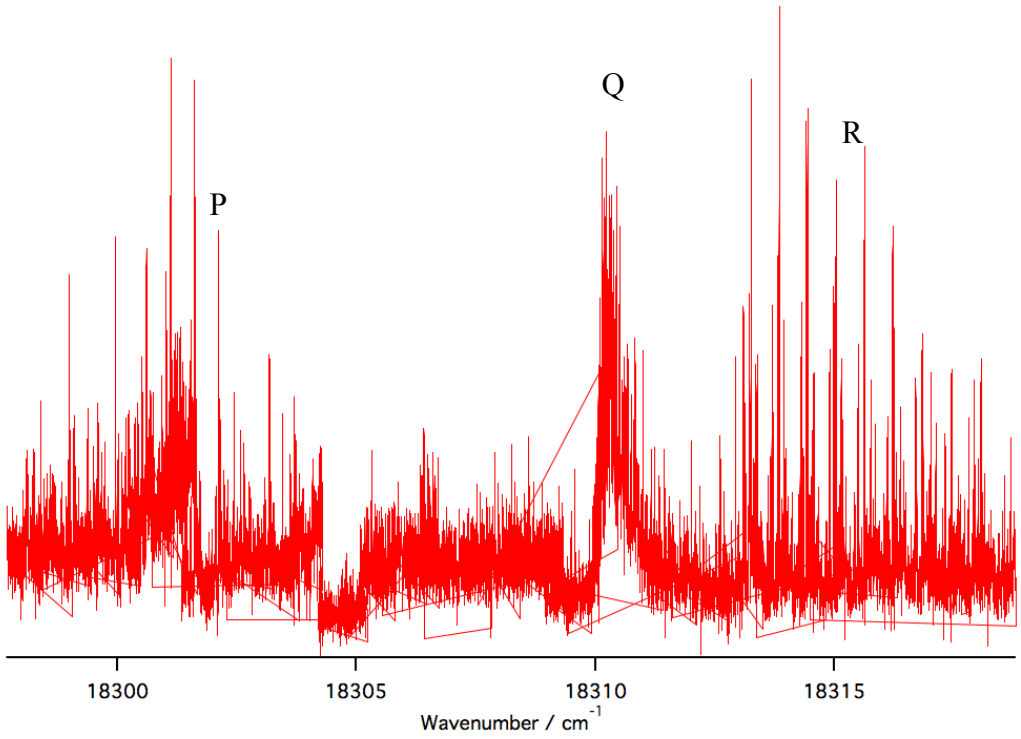

Figure 4.21 High-resolution spectrum of the 1-1 vibration of the [18.2] $^4\Gamma_{5.5} \rightarrow X^4\Phi_{4.5}$ transition of RuF.

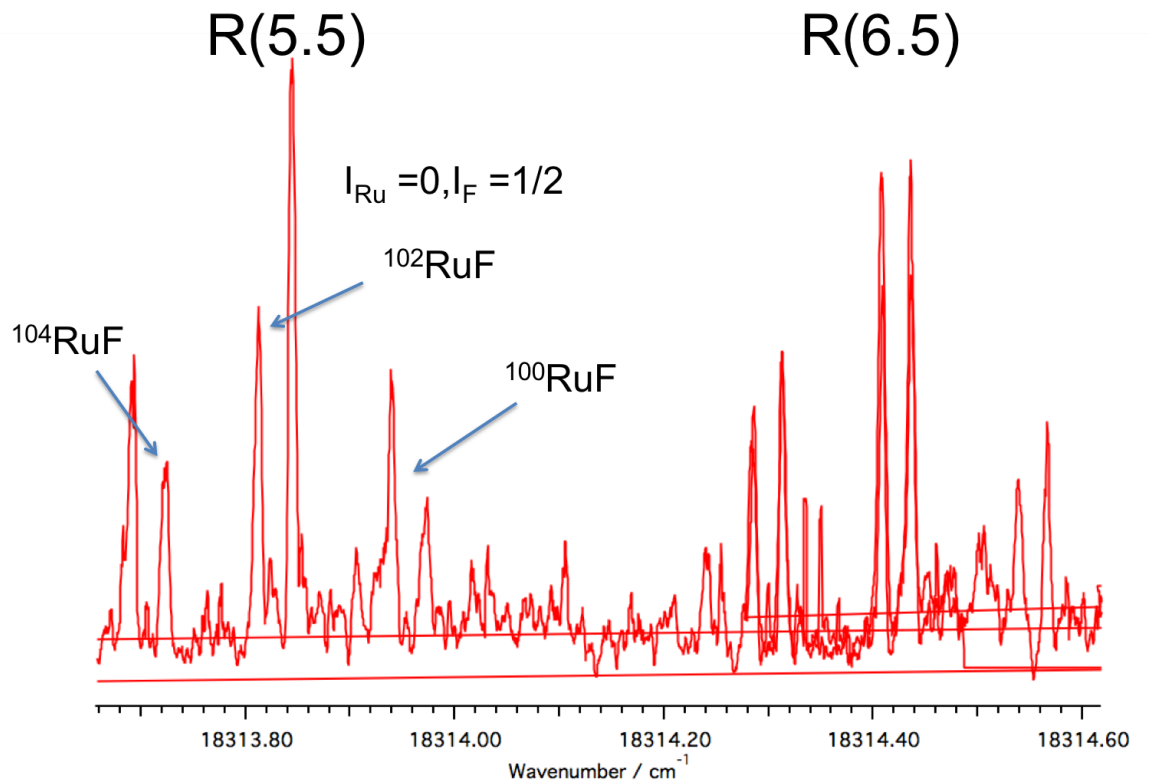

Figure 4.22 Expanded view of the high-resolution spectrum of the 1-1 vibration of the [18.2] $^4\Gamma_{5.5} \rightarrow X^4\Phi_{4.5}$ transition of RuF.

In Figure 4.22 a portion of the R region of the high-resolution spectrum of the 1-1 vibration is expanded which encompass two consecutive J clusters. In the expanded view of the band, both the isotopic structure and the hyperfine splitting due to the fluorine nuclear spin I=1/2 for ^{102}RuF, ^{104}RuF and ^{100}RuF isotopologues are evident.

A portion of the R branch in the Loomis-Wood plot of the band is depicted in Figure 4.23. The isotopic structure for the ^{102}RuF, ^{104}RuF and ^{100}RuF isotopologues can be seen in the plot. The doublet pattern observed is similar to that seen in Figure 4.13 for the 0-0 band and is due to the hyperfine splitting of the isotopologues. Note that as we go toward

higher J numbers, the hyperfine splitting becomes smaller. The line lists to be used in rotational analysis are extracted from this plot.

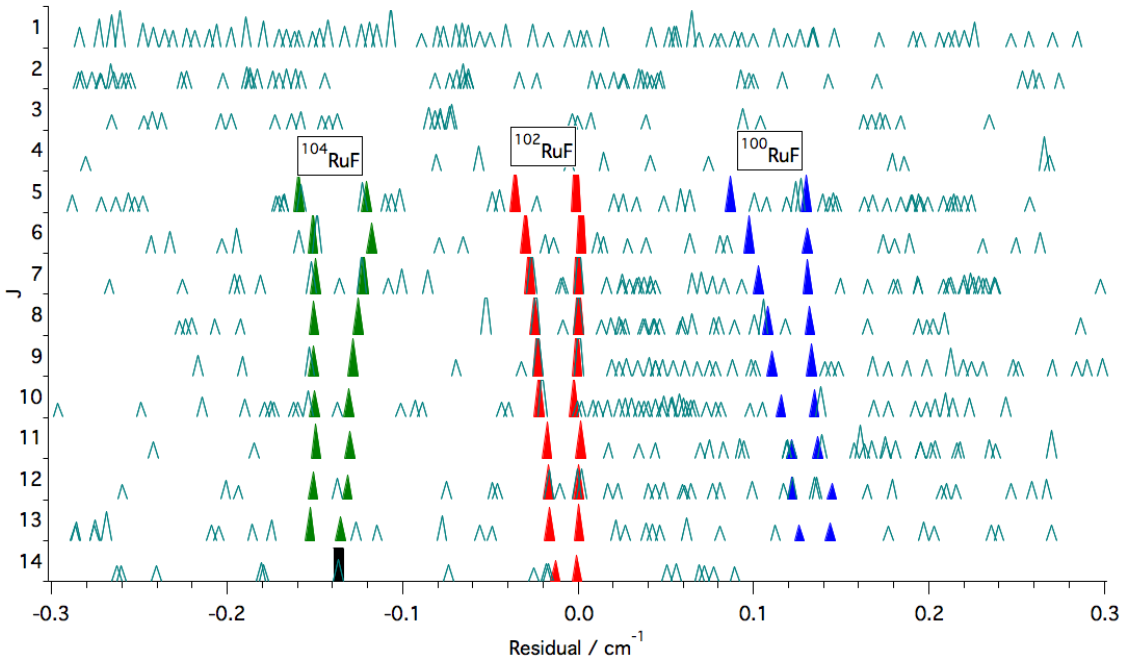

Figure 4.23 Loomis-Wood plot of series in the R branch of the 1-1 vibration band of the [18.2] $^4\Gamma_{5.5} \rightarrow X^4\Phi_{4.5}$ transition of RuF molecule.

Tables 4.13 and 4.14 illustrate the combination differences for the upper and lower states. The consistent B values for the states confirms the correct rotational numbering. The rotational numbering of the band shows that the first R and P lines start from J″=4.5 and J″=6.5 and hence Ω″=4.5. For the upper state the first J′ is equal to 5.5 and Ω′=5.5. This is consistent with the assignment of this band with the 1-1 transition of the $^4\Gamma_{5.5} \rightarrow X^4\Phi_{4.5}$ system of RuF. The obtained B constants are used as initial input for fitting and simulating the spectrum.

Table 4.13 Rotational numbering and analysis for the upper state of the 1-1 vibration band of [18.2] $^4\Gamma_{5.5} \rightarrow X^4\Phi_{4.5}$ transition of ^{102}RuF.

J	P(J) / cm^{-1}	R(J) / cm^{-1}	$\Delta F'(J)$ / cm^{-1}	B' / cm^{-1}
4.5		18313.2517		
5.5		18313.8441		
6.5	18306.4302	18314.4354	8.0052	0.285900
7.5	18305.8788	18315.0329	9.1541	0.286065
8.5	18305.3325	18315.6328	10.3003	0.286120
9.5	18304.7943	18316.2358	11.4415	0.286037
10.5	18304.2602	18316.8479	12.5878	0.286085
11.5	18303.7268	18317.4584	13.7316	0.286076
12.5	18303.1975	18318.0736	14.8762	0.286080
13.5	18302.6744	18318.6909		

Table 4.14 Rotational numbering and analysis for the lower state of the 1-1 vibration band of [18.2] $^4\Gamma_{5.5} \rightarrow X^4\Phi_{4.5}$ transition of ^{102}RuF.

J	P(J) / cm^{-1}	R(J) / cm^{-1}	$\Delta F''(J)$ / cm^{-1}	B'' / cm^{-1}
4.5		18313.2517		
5.5		18313.8441	6.8215	0.284229
6.5	18306.4302	18314.4354	7.9653	0.284475
7.5	18305.8788	18315.0329	9.1029	0.284465
8.5	18305.3325	18315.6328	10.2386	0.284405
9.5	18304.7943	18316.2358	11.3726	0.284315
10.5	18304.2602	18316.8479	12.509	0.284295
11.5	18303.7268	18317.4584	13.6504	0.284383
12.5	18303.1975		14.784	0.284307
13.5	18302.6744			

The band was modeled using an R^2 Hamiltonian as implemented in Pgopher. Tables 4.15, 4.16, 4.17 illustrate the result of the fit of the 1-1 vibration. The rms values from the fit for ^{102}RuF, ^{104}RuF and ^{100}RuF are 0.0014, 0.0016 and 0.0016 cm^{-1} respectively.

Table 4.15 Molecular constants for states involved in the 1-1 vibration band of the [18.2] $^{4}\Gamma_{5.5} \rightarrow X^{4}\Phi_{4.5}$ transition of ^{102}RuF.

Parameters	$X^{4}\Phi_{4.5}$	$[18.2]^{4}\Gamma_{5.5}$
B / cm^{-1}	0.2844142(123)	0.2861673(141)
D / 10^{-7} cm^{-1}	3.112(281)	2.876(344)
T / cm^{-1}		18312.93908(27)
h / 10^{-3} cm^{-1}	8.58(87)	48.24(72)

Table 4.16 Molecular constants for states involved in the 1-1 vibration band of the [18.2] $^{4}\Gamma_{5.5} \rightarrow X^{4}\Phi_{4.5}$ transition of ^{104}RuF.

Parameters	$X^{4}\Phi_{4.5}$	$[18.2]^{4}\Gamma_{5.5}$
B / cm^{-1}	0.2836439(243)	0.2854218(266)
D / 10^{-7} cm^{-1}	5.952(751)	7.318(936)
T / cm^{-1}		18312.81876(44)
h / 10^{-3} cm^{-1}	6.18(120)	46.96(104)

Table 4.17 Molecular constants for states involved in the 1-1 vibration band of the [18.2] $^4\Gamma_{5.5} \rightarrow X^4\Phi_{4.5}$ transition of ^{100}RuF.

Parameters	$X^4\Phi_{4.5}$	$[18.2]^4\Gamma_{5.5}$
B / cm^{-1}	0.2853236(222)	0.2870725(221)
D / 10^{-7} cm^{-1}	3.236(799)	2.462(943)
T / cm^{-1}		18313.06459(42)
h / 10^{-3} cm^{-1}	13.62(144)	54.8(120)

In comparison with the 0-0 band of the [18.2] $^4\Gamma_{5.5} \rightarrow X^4\Phi_{4.5}$ transition, as expected the value of B is lower in each state. This confirms the indication of a vibrational excitation. As with the [18.2] $^4\Gamma_{4.5} \rightarrow X^4\Phi_{3.5}$ and the [18.2] $^4\Gamma_{5.5} \rightarrow X^4\Phi_{4.5}$ bands, there is also a large gap between the P and Q branches where there are no lines.

4.6.5 The [22.1] $^4\Delta_{3.5} \rightarrow X^4\Phi_{4.5}$ transition

Figure 4.24 shows the high-resolution spectrum of the blue transition near 22160 cm^{-1}. Rotational analysis of this band confirms that it is a $^4\Delta_{3.5} \rightarrow X^4\Phi_{4.5}$ excitation.

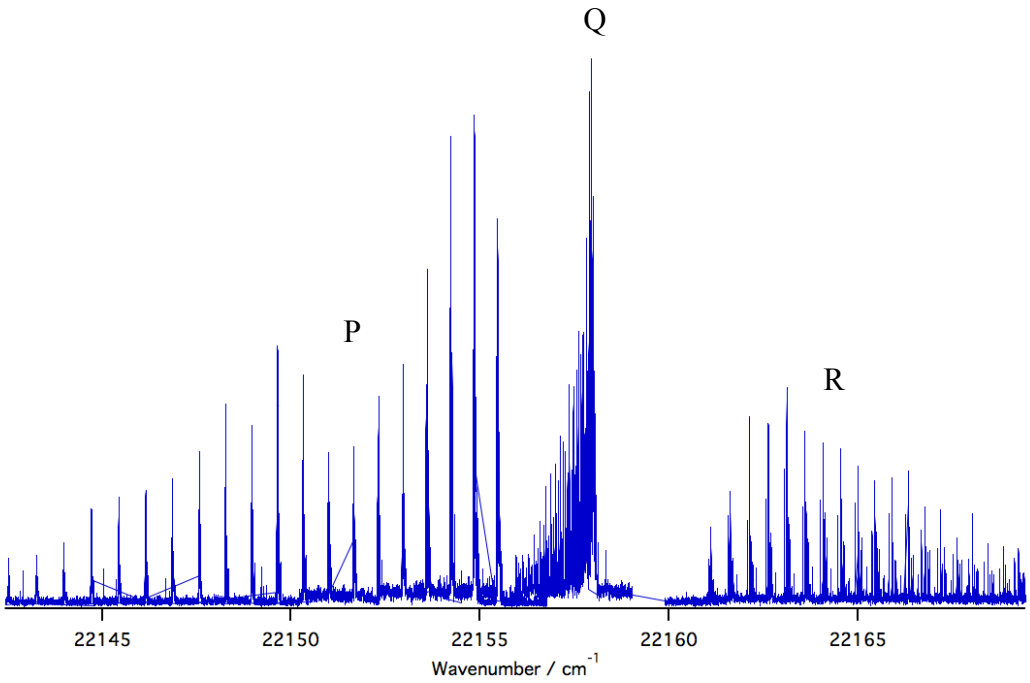

Figure 4.24 An overview of the high-resolution spectrum of the [22.1] $^4\Delta_{3.5} \rightarrow X^4\Phi_{4.5}$ transition.

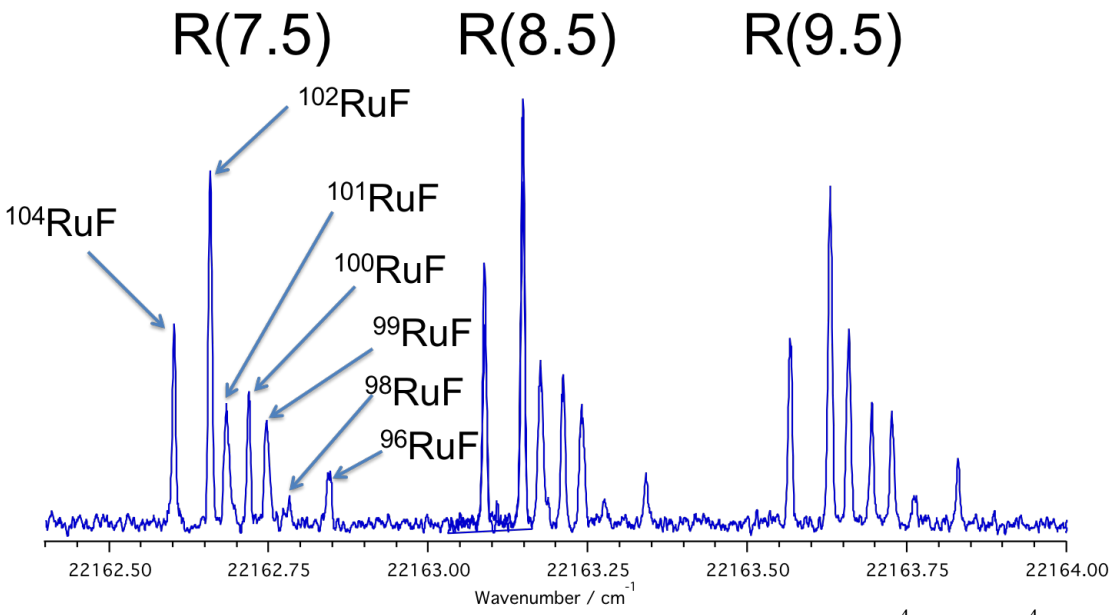

Figure 4.25 Expanded view of the high-resolution spectrum of the [22.1] $^4\Delta_{3.5} \rightarrow X^4\Phi_{4.5}$ transition.

The expanded view of the high-resolution spectrum of the blue band (see Figure 4.25) shows clear isotopic structure. They belong to the different isotopologues of RuF, i.e., the ^{102}RuF, ^{104}RuF, ^{100}RuF, ^{101}RuF, ^{99}RuF, ^{98}RuF and ^{96}RuF. Interestingly, no hyperfine pattern due to fluorine nuclear spin can be observed nor any unresolved splitting due to I=5/2 for ^{101}RuF and ^{99}RuF.

As shown in the Loomis-Wood plot (see Figure 4.26) the ^{102}RuF, ^{104}RuF, ^{100}RuF, ^{101}RuF, ^{99}RuF, ^{98}RuF and ^{96}RuF isotopologues in the blue spectrum are color coded in series and the line lists were extracted for use in the rotational analysis.

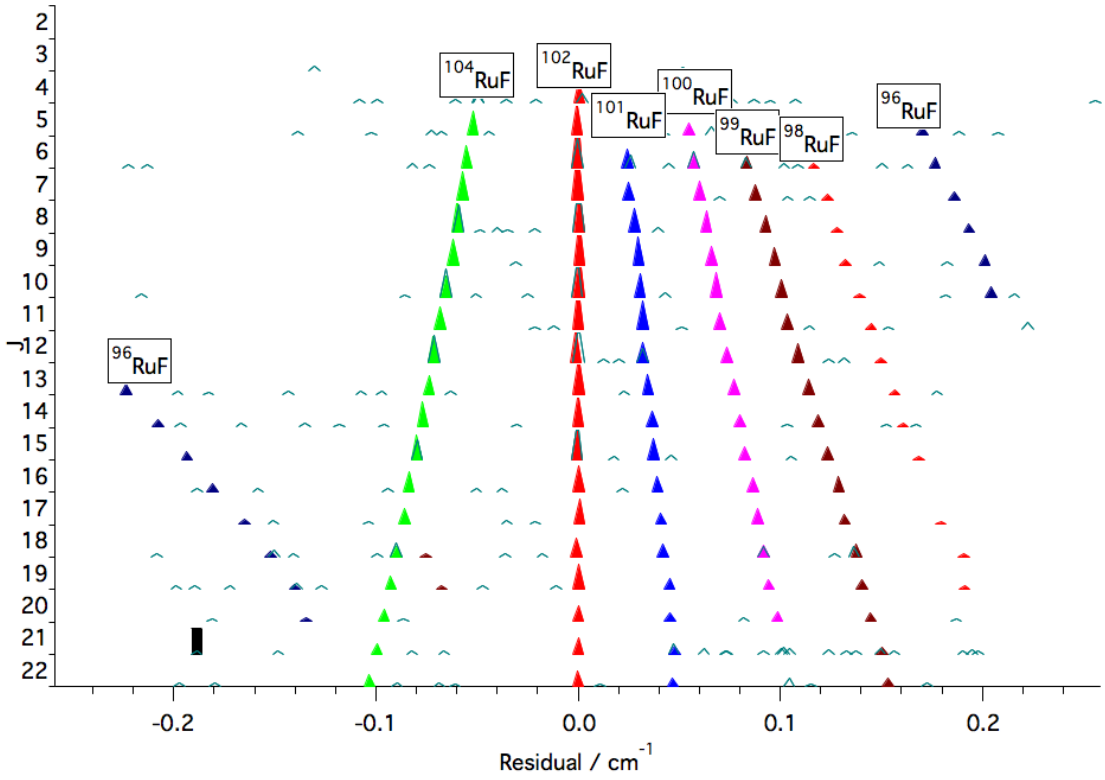

Figure 4.26 Loomis-Wood plot of series in the P branch of the [22.1] $^4\Delta_{3.5} \rightarrow X^4\Phi_{4.5}$ band of RuF molecule.

The line lists for both the P and R branches are extracted from the Loomis-Wood plots. Tables 4.18 and 4.19 illustrate the rotational numbering and analysis of the most abundant isotopolouge of the blue band. The rotational assignment shows the first J values for the lower and upper states that are J″=4.5 and J′=3.5. Therefore, $\Omega'' = 4.5$ and $\Omega' = 3.5$ and the spectrum is assigned as the $^4\Delta_{3.5} \rightarrow X^4\Phi_{4.5}$ transition. The obtained B constants for the upper and lower states that are used as initial input for fitting and simulating the spectrum are ~0.2822 and 0.2866 cm^{-1}.

Table 4.18 Rotational numbering and analysis for the upper state of the [22.1] $^{4}\Delta_{3.5} \rightarrow X^{4}\Phi_{4.5}$ transition of ^{102}RuF.

J	P(J) / cm^{-1}	R(J) / cm^{-1}	$\Delta F'(J)$ / cm^{-1}	B′ / cm^{-1}
4.5	22155.4720	22161.1193	5.6473	0.28236
5.5	22154.8558	22161.6327	6.7769	0.28237
6.5	22154.2340	22162.1385	7.9045	0.282302
7.5	22153.6035	22162.6359	9.0324	0.282261
8.5	22152.9644	22163.1261	10.1617	0.282268
9.5	22152.3179	22163.6072	11.2893	0.282233
10.5	22151.6631	22164.0805	12.4174	0.282213
11.5	22150.9990	22164.5462	13.5472	0.282234
12.5	22150.3240	22165.0039	14.6800	0.282306
13.5	22149.6449	22165.4575	15.8126	0.282366
14.5	22148.9606	22165.9027	16.9421	0.282367
15.5	22148.2685	22166.3411	18.0726	0.282383
16.5	22147.5696	22166.7750	19.2054	0.282432
17.5	22146.8642	22167.2024	20.3382	0.282475
18.5	22146.1542	22167.6226	21.4684	0.282479
19.5	22145.4368	22168.0400	22.6032	0.282540
20.5	22144.7158	22168.4510	23.7352	0.282562
21.5	22143.9901	22168.8576	24.8675	0.282585
22.5	22143.2597	22169.2595	25.9998	0.282606

Table 4.19 Rotational numbering and analysis for the lower state of the [22.1] $^4\Delta_{3.5} \rightarrow X^4\Phi_{4.5}$ transition of ^{102}RuF.

J	P(J) / cm^{-1}	R(J) / cm^{-1}	$\Delta F''(J)$ / cm^{-1}	B'' / cm^{-1}
4.5	22155.4720	22161.1193		
5.5	22154.8558	22161.6327	6.8853	0.286886
6.5	22154.2340	22162.1385	8.0291	0.286755
7.5	22153.6035	22162.6359	9.1740	0.286689
8.5	22152.9644	22163.1261	10.3180	0.286611
9.5	22152.3179	22163.6072	11.4630	0.286575
10.5	22151.6631	22164.0805	12.6082	0.286550
11.5	22150.9990	22164.5462	13.7565	0.286594
12.5	22150.3240	22165.0039	14.9013	0.286563
13.5	22149.6449	22165.4575	16.0433	0.286488
14.5	22148.9606	22165.9027	17.1890	0.286483
15.5	22148.2685	22166.3411	18.3331	0.286454
16.5	22147.5696	22166.7750	19.4769	0.286424
17.5	22146.8642	22167.2024	20.6209	0.286400
18.5	22146.1542	22167.6226	21.7657	0.286390
19.5	22145.4368	22168.0400	22.9068	0.286334
20.5	22144.7158	22168.4510	24.0499	0.286308
21.5	22143.9901	22168.8576	25.1913	0.286264
22.5	22143.2597	22169.2595		

In Figures 4.27 and 4.28, the B value for the upper and lower states are plotted against J(J+1). For the ground state, as expected, the rotational constant B is decreasing with increasing J due to centrifugal distortion. However, for the excited state the rotational constant B rises with increasing J. This is likely an indication that there is a weak interaction between the [22.1] $^4\Delta_{3.5}$ state and a nearby perturbing state.

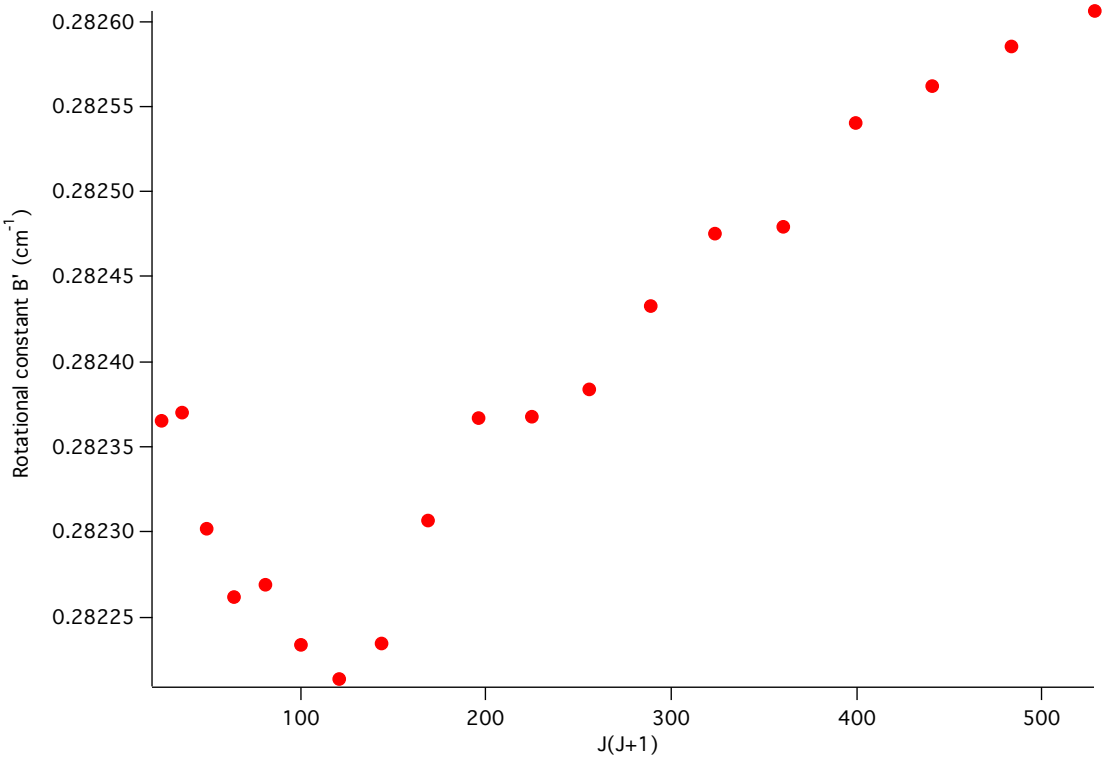

Figure 4.27 The variation of the rotational parameter B´ versus J(J+1).

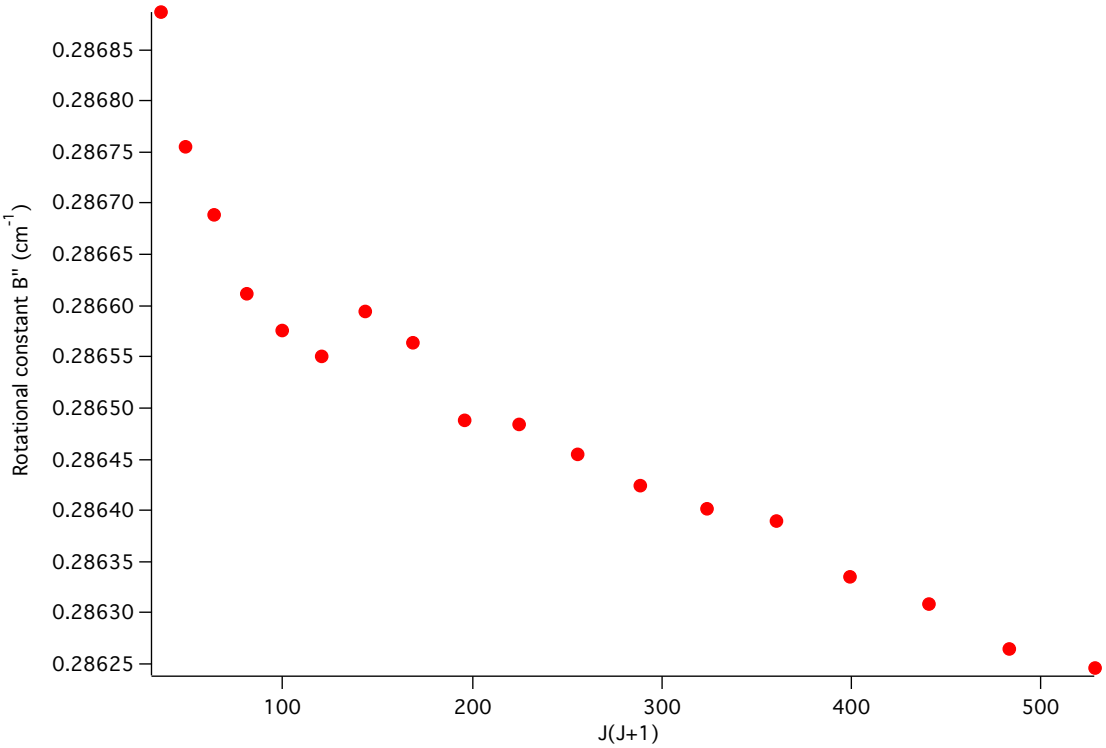

Figure 4.28 The variation of the rotational parameter B″ versus J(J+1).

Tables 4.20, 4.21, 4.22, 4.23, 4.24, 4.25 and 4.26 give the results of fitting for the ^{102}RuF, ^{104}RuF, ^{101}RuF, ^{99}RuF, ^{100}RuF and ^{96}RuF and ^{98}RuF isotopologues. The molecular constants B and D for each state and also the band origin are extracted from the fit. The centrifugal constant is negative for the excited states. This can be the result of an interaction with a nearby state close to the [22.2] 3.5 state which weakly perturbs the excited state. The hyperfine splitting is not observed in this band. This can be attributed to having nearly the same splittings for the upper and lower states. As observed in the green system, we know that the ground state has a hyperfine component. In order to extract the upper state hyperfine splitting, in the fitting procedure the values of the ground state hyperfine parameters were fixed to an average value (10.05 cm^{-1}) of those

that were previously determined from the fit to 0-0 band. The same average value was used for the ^{101}RuF and ^{99}RuF and ^{98}RuF isotopologues even though they were not fit previously for the 0-0 band.

Table 4.20 Molecular constants for states involved in the [22.1] $^4\Delta_{3.5} \rightarrow X^4\Phi_{4.5}$ transition of ^{102}RuF.

Parameters	$X^4\Phi_{4.5}$	[22.1] $^4\Delta_{3.5}$
B / cm^{-1}	0.28669326(876)	0.28219201(890)
D / 10^{-7} cm^{-1}	4.67(12)	-4.15(12)
T / cm^{-1}		22155.78047(26)
h / 10^{-3} cm^{-1}	10.05(fixed)	12.46(62)

Table 4.21 Molecular constants for states involved in the [22.1] $^4\Delta_{3.5} \rightarrow X^4\Phi_{4.5}$ transition of ^{104}RuF.

Parameters	$X^4\Phi_{4.5}$	[22.1] $^4\Delta_{3.5}$
B / cm^{-1}	0.28582575(909)	0.28127268(919)
D / 10^{-7} cm^{-1}	4.56(13)	-4.44(13)
T / cm^{-1}		22155.74830(27)
h / 10^{-3} cm^{-1}	10.05(fixed)	12.46(64)

Table 4.22 Molecular constants for states involved in the [22.1] $^4\Delta_{3.5} \rightarrow X^4\Phi_{4.5}$ transition of ^{101}RuF.

Parameters	$X^4\Phi_{4.5}$	[22.1] $^4\Delta_{3.5}$
B / cm^{-1}	0.28710236(880)	0.28262711(894)
D / 10^{-7} cm^{-1}	3.77(12)	-4.85(12)
T / cm^{-1}		22155.79334(26)
h / 10^{-3} cm^{-1}	10.05(fixed)	12.18(62)

Table 4.23 Molecular constants for states involved in the [22.1] $^4\Delta_{3.5} \rightarrow X^4\Phi_{4.5}$ transition of ^{99}RuF.

Parameters	$X^4\Phi_{4.5}$	[22.1] $^4\Delta_{3.5}$
B / cm^{-1}	0.28803055(828)	0.28360439(863)
D / 10^{-7} cm^{-1}	3.77(12)	-4.65(11)
T / cm^{-1}		22155.82951(25)
h / 10^{-3} cm^{-1}	10.05(fixed)	12.40(68)

Table 4.24 Molecular constants for states involved in the [22.1] $^4\Delta_{3.5} \rightarrow X^4\Phi_{4.5}$ transition of ^{100}RuF.

Parameters	$X^4\Phi_{4.5}$	[22.1] $^4\Delta_{3.5}$
B / cm^{-1}	0.28804989(842)	0.28361463(851)
D / 10^{-7} cm^{-1}	4.39(12)	-4.17(12)
T / cm^{-1}		22155.83004(25)
h / 10^{-3} cm^{-1}	10.05(fixed)	12.38(60)

Table 4.25 Molecular constants for states involved in the [22.1] $^4\Delta_{3.5} \rightarrow X^4\Phi_{4.5}$ transition of ^{96}RuF.

Parameters	$X^4\Phi_{4.5}$	[22.1] $^4\Delta_{3.5}$
B / cm^{-1}	0.28957759(984)	0.2852152(103)
D / 10^{-7} cm^{-1}	6.75(15)	-1.37(16)
T / cm^{-1}		0.2852152(103)
h / 10^{-3} cm^{-1}	10.05(fixed)	12.48(66)

Table 4.26 Molecular constants for states involved in the [22.1] $^4\Delta_{3.5} \rightarrow X^4\Phi_{4.5}$ transition of ^{98}RuF.

Parameters	$X^4\Phi_{4.5}$	[22.1] $^4\Delta_{3.5}$
B / cm^{-1}	0.2885316(111)	0.2841194(117)
D / 10^{-7} cm^{-1}	4.46(16)	-4.01(18)
T / cm^{-1}		22155.85023(34)
h / 10^{-3} cm^{-1}	10.05(fixed)	12.48(76)

The centrifugal distortion constant indicates the change in the bond length of the molecules as it is rotating. A negative D value may be interpreted as shrinking of the

bond length when the molecule is in rotation which is physically unrealistic. Therefore, a negative D value indicates a small amount of perturbation in the system and the model Hamiltonian used for fitting the upper state is not perfectly accurate. The centrifugal distortion constant becomes negative to compensate for the perturbations.

Figure 4.29 presents some of the results of the high-resolution analysis of the blue and green bands combined with the result of the DF analysis of the blue band. As can be seen, transitions to the spin-orbit components are allowed to occur in the [22.1] $^4\Delta_{3.5} \rightarrow X^4\Phi_{4.5}$ band but do not appear in the DF of the [18.2] $^4\Gamma_{5.5} \rightarrow X^4\Phi_{4.5}$ band. This can be explained based on selection rules. Since the upper states of the [18.2] $^4\Gamma_{5.5} \rightarrow X^4\Phi_{4.5}$ and [22.1] $^4\Delta_{3.5} \rightarrow X^4\Phi_{4.5}$ transitions are $^4\Gamma_{5.5}$ and $^4\Delta_{3.5}$ respectively and the lower state of the spin-orbit component is $^4\Phi_{3.5}$, $\Delta\Omega$=2 and 0 for these transitions. Therefore, the spin-orbit component can only be accessed from the decay out of the $^4\Delta_{3.5}$ state. Note that the third spin-orbit component is $^4\Phi_{2.5}$ and can also be accessed from the $^4\Delta_{3.5}$ state since $\Delta\Omega$= 1 between these states. Therefore, the $^4\Delta_{3.5}$ state provides an ample amount of information about the spin-orbit structure of the $^4\Phi$ state and the value of spin-orbit spacing is extracted to be ~1000 cm^{-1} for the lower state.

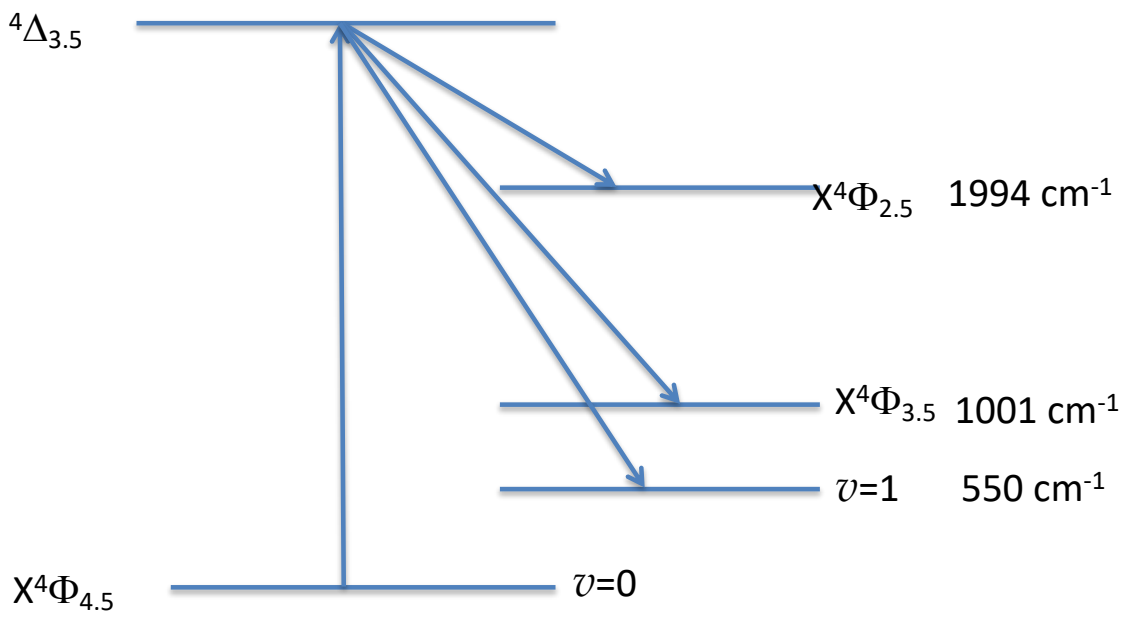

Figure 4.29 Assignment of features in the dispersed fluorescence spectrum taken from the [22.1] $^4\Delta_{3.5} \rightarrow X^4\Phi_{4.5}$ band.

Note that the accuracy in measuring the spin-orbit intervals is determined by the accuracy of the related DFs which is about ~ 10 cm^{-1}.

4.6.6 The [13.1] $^4\Delta_{3.5} \rightarrow X^4\Phi_{4.5}$ transition

Figure 4.30 shows the high-resolution spectra of the infrared transition. The result of the rotational analysis of this band confirms the assignment of a $^4\Delta_{3.5} \rightarrow X^4\Phi_{4.5}$ transition.

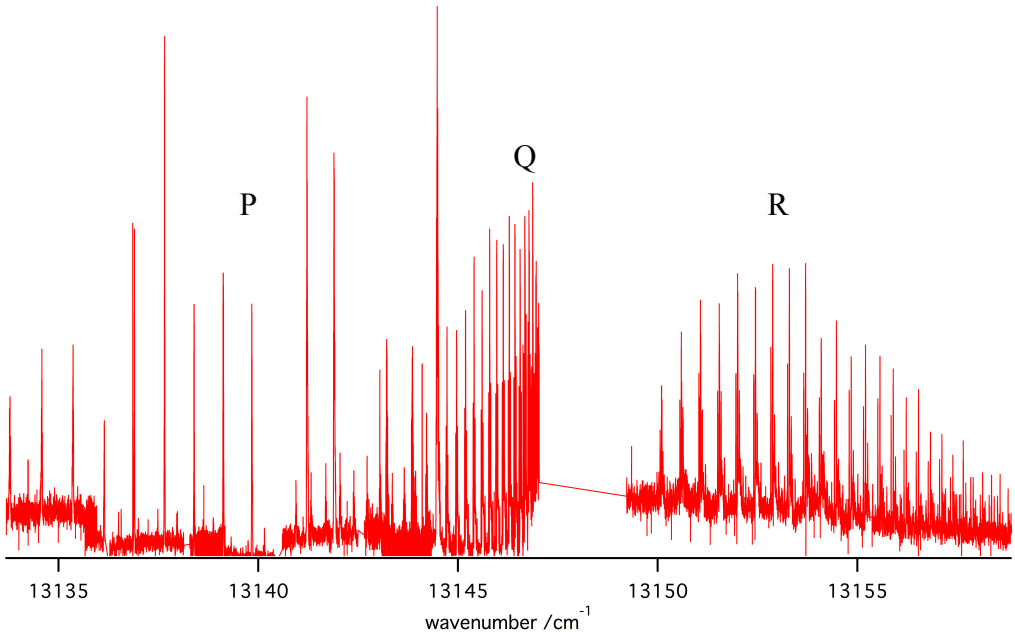

Figure 4.30 High-resolution spectrum of the [13.1] $^4\Delta_{3.5} \rightarrow X^4\Phi_{4.5}$ transition.

Two consecutive J lines of the infrared band are selected in the R region and expanded as shown in Figure 4.31. The isotopic structure of the infrared band can be seen in the expanded view of the high-resolution spectrum. The ^{102}RuF, ^{104}RuF, ^{100}RuF and ^{96}RuF isotopologues can be seen. Hyperfine splitting is also evident in the isotopologues. This splitting is due to the nuclear spin I=1/2 of fluorine.

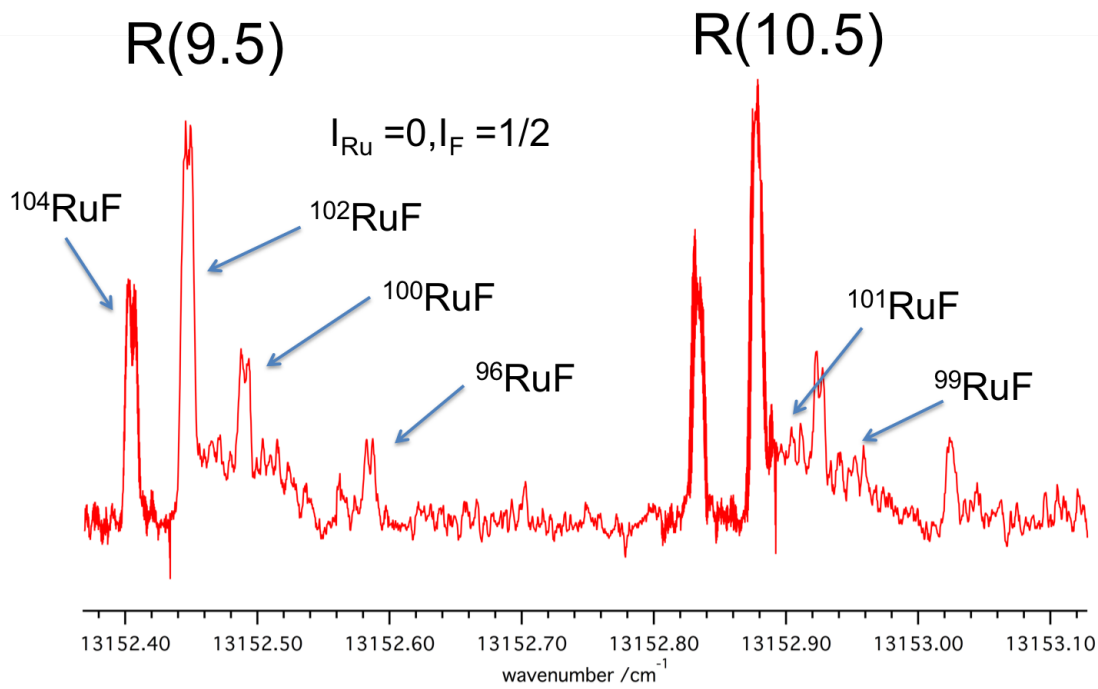

Figure 4.31 Expanded view of the high-resolution spectrum of the [13.1] $^4\Delta_{3.5} \rightarrow X^4\Phi_{4.5}$ band.

Figure 4.32 shows a portion of the P branch in the Loomis-Wood plot of the infrared band. The isotopic structure for the ^{102}RuF, ^{104}RuF, ^{100}RuF and ^{96}RuF isotopologues are shown in series in the picture. As can be seen from the Loomis-Wood plot, beside each of the series there is a similar pattern. This represents the hyperfine splitting of each isotopologue.

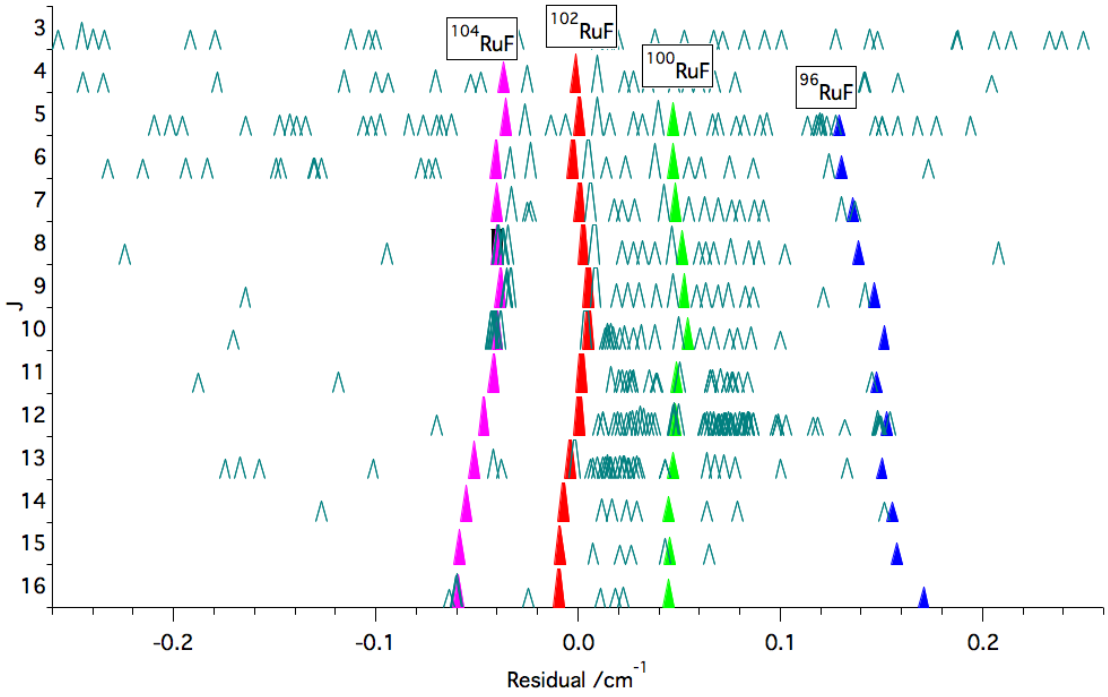

Figure 4.32 Loomis-Wood plot of series in the P branch of the [13.1] $^4\Delta_{3.5} \rightarrow X^4\Phi_{4.5}$ band of the RuF molecule.

The line lists extracted from the plot for the P and R branches of the ^{102}RuF isotopolouge are presented in Tables 4.27 and 4.28 for rotational analysis. The preliminary rotational constants for the upper and lower states are calculated to be ~ 0.2744 and ~ 0.2866 cm^{-1} respectively from the combination differences.

Table 4.27 Rotational numbering and analysis for the upper state of the [13.1] $^4\Delta_{3.5} \rightarrow X^4\Phi_{4.5}$ transition of ^{102}RuF.

J	P(J) / cm^{-1}	R(J) / cm^{-1}	$\Delta F'(J)$ / cm^{-1}	B' / cm^{-1}
4.5	13144.4798	13150.0952	5.6155	0.280773
5.5	13143.8486	13150.5904	6.7418	0.280906
6.5	13143.2140	13151.0682	7.8542	0.280506
7.5	13142.5651	13151.5404	8.9753	0.280477
8.5	13141.8952	13151.9988	10.1037	0.280656
9.5	13141.2176	13152.4458	11.2282	0.280706
10.5	13140.5304	13152.8781	12.3476	0.280628
11.5	13139.8380	13153.2951	13.4571	0.280357
12.5	13139.1189	13153.7019	14.5830	0.280441
13.5	13138.3954	13154.0930	15.6976	0.280314
14.5	13137.6548	13154.4734	16.8186	0.280309
15.5	13136.9161	13154.8430	17.9269	0.280107
16.5	13136.1570	13155.2019	19.0449	0.280071
17.5	13135.3637	13155.5625	20.1988	0.280539

Table 4.28 Rotational numbering and analysis for the lower state of the [13.1] $^4\Delta_{3.5} \rightarrow X^4\Phi_{4.5}$ transition of ^{102}RuF.

J	P(J) / cm^{-1}	R(J) / cm^{-1}	$\Delta F''$ (J) / cm^{-1}	B'' / cm^{-1}
4.5	13144.4798	13150.0952		
5.5	13143.8486	13150.5904	6.8812	0.286717
6.5	13143.2140	13151.0682	8.0252	0.286616
7.5	13142.5651	13151.5404	9.1730	0.286655
8.5	13141.8952	13151.9988	10.3229	0.286746
9.5	13141.2176	13152.4458	11.4684	0.286710
10.5	13140.5304	13152.8781	12.6078	0.286541
11.5	13139.8380	13153.2951	13.7591	0.286648
12.5	13139.1189	13153.7019	14.8997	0.286533
13.5	13138.3954	13154.0930	16.0471	0.286554
14.5	13137.6548	13154.4734	17.1769	0.286282
15.5	13136.9161	13154.8430		

The molecular constants for the ^{102}RuF, ^{104}RuF, ^{100}RuF and ^{96}RuF isotopologues of the infrared band extracted from the fit are presented in Tables 4.29, 4.30, 4.31 and 4.32 for the ground and excited states.

Table 4.29 Molecular constants for states involved in the [13.1] $^4\Delta_{3.5} \rightarrow X^4\Phi_{4.5}$ transition of ^{102}RuF.

Parameters	**$X^4\Phi_{4.5}$**	**[13.1] $^4\Delta_{3.5}$**
B / cm^{-1}	0.2866580(167)	0.2805620(163)
D / 10^{-7} cm^{-1}	2.349(361)	2.233(317)
T / cm^{-1}		13144.80149(31)
h / 10^{-3} cm^{-1}	9.54(84)	21.54(112)

Table 4.30 Molecular constants for states involved in the [13.1] $^4\Delta_{3.5} \rightarrow X^4\Phi_{4.5}$ transition of ^{104}RuF.

Parameters	**$X^4\Phi_{4.5}$**	**[13.1] $^4\Delta_{3.5}$**
B / cm^{-1}	0.2859125(352)	0.2798398(382)
D / 10^{-6} cm^{-1}	1.024(163)	1.016(168)
T / cm^{-1}		13144.78244(65)
h / 10^{-3} cm^{-1}	9.45(135)	24.84(178)

Table 4.31 Molecular constants for states involved in the [13.1] $^4\Delta_{3.5} \rightarrow X^4\Phi_{4.5}$ transition of ^{100}RuF.

Parameters	**$X^4\Phi_{4.5}$**	**[13.1] $^4\Delta_{3.5}$**
B / cm^{-1}	0.2875303(472)	0.2814190(524)
D / 10^{-7} cm^{-1}	5.80(210)	5.79(218)
T / cm^{-1}		13144.82421(94)
h / 10^{-3} cm^{-1}	12.54(147)	26.2(20)

Table 4.32 Molecular constants for states involved in the [13.1] $^4\Delta_{3.5} \rightarrow X^4\Phi_{4.5}$ transition of ^{96}RuF.

Parameters	**$X^4\Phi_{4.5}$**	**[13.1] $^4\Delta_{3.5}$**
B / cm^{-1}	0.289658(106)	0.283552(127)
D / 10^{-6} cm^{-1}	1.402(372)	1.446(400)
T / cm^{-1}		13144.8615(28)
h / 10^{-3} cm^{-1}	11.94(159)	24.2(22)

4.7 Multiple state fitting

Three bands in the blue, green and infrared regions of the electromagnetic spectrum were fitted together since they share a common lower state. In Table 4.33 the result of the multiple state fitting with the corresponding average are presented for the blue, green and IR bands of four isotopologues, i.e., ^{102}RuF, ^{104}RuF, ^{100}RuF and ^{96}RuF. The rms values of the multiple state fitting for ^{102}RuF, ^{104}RuF, ^{100}RuF and ^{96}RuF are 0.0018, 0.0018, 0.0017 and 0.0030 cm^{-1} respectively. The vibrational and excited spin-orbit bands are fitted separately as they do not have a common state with the other transitions.

Table 4.33 Molecular constants for ^{102}RuF, ^{104}RuF, ^{100}RuF and ^{96}RuF as extracted from multiple state fitting.

State		T / cm^{-1}	B / cm^{-1}	D / 10^{-7} cm^{-1}	h / 10^{-3} cm^{-1}
$X^4\Phi_{4.5}$	^{102}RuF		0.28662231(536)	3.0594(486)	9.36(63)
	^{104}RuF		0.28574262(545)	2.9140(443)	9.54(84)
	^{100}RuF		0.28753255(830)	4.00(13)	11.85(99)
	^{96}RuF		0.2893607(205)	3.330(390)	13.53(147)
[18.2] $^4\Gamma_{5.5}$	^{102}RuF	18256.90436(26)	0.28814856(519)	2.5803(454)	50.04(68)
	^{104}RuF	18256.86899(27)	0.28726286(533)	2.4359(420)	50.40(80)
	^{100}RuF	18256.94165(41)	0.2890607(97)	3.17(20)	51.32(104)
	^{96}RuF	18257.02357(51)	0.2909011(199)	2.789(357)	54.72(152)
[22.1] $^4\Delta_{3.5}$	^{102}RuF	22155.78047(36)	0.2821269(64)	-5.584(79)	11.56(114)
	^{104}RuF	22155.74835(36)	0.2811953(65)	-5.920(77)	11.82(134)
	^{100}RuF	22155.81469(37)	0.28308050(848)	-4.61(13)	14.14(146)
	^{96}RuF	22155.88670(70)	0.2849900(229)	-5.104(479)	16.4(24)
[13.1] $^4\Delta_{3.5}$	^{102}RuF	13144.80133(31)	0.2805307(55)	2.852(48)	20.66(106)
	^{104}RuF	13144.78444(49)	0.2796533(82)	2.75(17)	25.00(134)
	^{100}RuF	13144.82414(53)	0.281413(10)	3.84(20)	25.56(140)
	^{96}RuF	13144.8694(14)	0.2831912(275)	2.89(55)	25.8(28)

Figure 4.33 shows the root mean square error calculated from Pgopher for the most abundant isotopologue, i.e., ^{102}RuF. The low root mean square error shows the good quality of the fit.

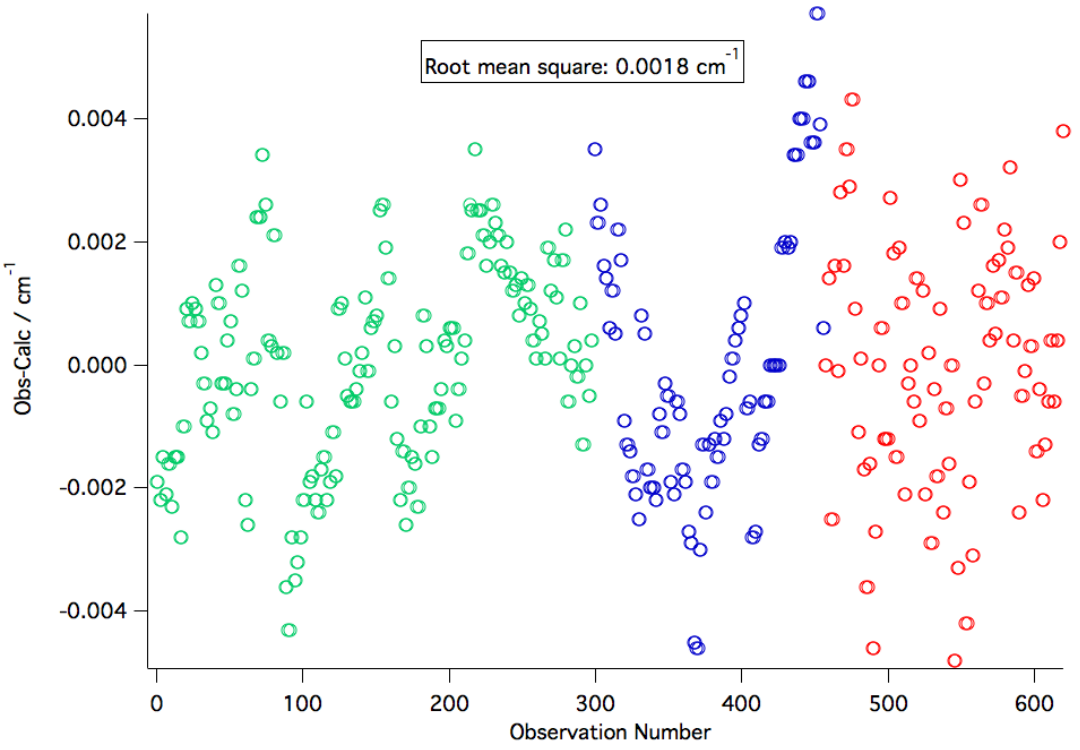

Figure 4.33 The difference between observed and calculated line positions in terms of the observation number for ^{102}RuF. The green, blue and red colors correspond to the transitions from the ground state to [18.3] $^4\Gamma_{5.5}$, [22.1] $^4\Delta_{3.5}$ and [13.1] $^4\Delta_{3.5}$ states respectively.

4.8 Calculating the equilibrium bond length

Since the 0-0 and 1-1 vibrations were observed in the green system, the equilibrium molecular constants of the three isotopologues can be calculated for the ground and excited states. The rotational constant B of each vibrational level within different electronic states can be fitted to the following formula to obtain the equilibrium molecular constants.

$$B_v = B_e - \alpha_e(v + \tfrac{1}{2}) \qquad 4.7$$

In the above formula B_v is the rotational constant of a given vibrational level, B_e is the equilibrium rotational constant and α_e is the equilibrium vibration-rotation coupling constant. If B_e is known, then the equilibrium bond length (r_e) can also be calculated from the following relation

$$r_e = \sqrt{\frac{h}{8\pi^2 c\mu B_e}} \qquad 4.8$$

where h is the Planck's constant and c and μ are the speed of light and reduced mass of the isotopologues respectively. The equilibrium molecular constants including the equilibrium rotational constant, bond length and rotation vibration coupling are presented in Table 4.34 for ground and excited states of ^{102}RuF, ^{104}RuF and ^{100}RuF. The value of the equilibrium bond length is r_e=1.9128 Å ^{102}RuF. This is to within 7% agreement with the result of theory r_e =2.05 Å [6] and in good agreement with other experimental work in which 1.916 and 1.911 Å [7] were reported for r_0 for the lower and upper states respectively.

Table 4.34 Equilibrium molecular constants for ^{102}RuF, ^{104}RuF and ^{100}RuF.

State	Isotopologues	B_e / cm^{-1}	α_e/ cm^{-1}	r_e / A$^\circ$
$X^4\Phi_{4.5}$	^{102}RuF	0.28772637	0.00220811	1.91287
	^{104}RuF	0.28679198	0.00209872	1.91598
	^{100}RuF	0.28863703	0.00220895	1.90985
[18.2] $^4\Gamma_{5.5}$	^{102}RuF	0.28913919	0.00198126	1.90819
	^{104}RuF	0.28818339	0.00184106	1.91135
	^{100}RuF	0.29005480	0.0019882	1.90517

Table 4.35 Comparison of the isotopic ratios and the reduced mass.

State	B_{e102}/B_{e104}	B_{e100}/B_{e104}	B_{e100}/B_{e102}
$X^4\Phi_{4.5}$	1.003258	1.006433	1.003165
[18.2] $^4\Gamma_{5.5}$	1.003316	1.006493	1.003166
μ^*/μ	1.003035	1.006190	1.003145

* indicates the heavier isotope.

In Table 4.35 the ratios of B_e values for the $X^4\Phi_{4.5}$ and [18.2] $^4\Gamma_{5.5}$ states of three isotopologues are compared with the ratios of the corresponding reduced mass. The ratios are in good agreement for both states which indicates that the molecules are isotopically consistent.

4.9 Summary

In summary, the ruthenium monofluoride molecule was made in a molecular beam apparatus in the gas phase and the laser-induced fluorescence spectra were recorded at both low and high-resolution. Five transitions (see Figure 4.34) in the blue, green and infrared regions of the electromagnetic spectrum have been observed and rotationally analyzed. The result of rotational analysis confirms the lower state as the $X^4\Phi_{4.5}$ state. The upper states are assigned as [18.2] $^4\Gamma_{5.5}$ for the green and [13.1] $^4\Delta_{3.5}$ and [22.1] $^4\Delta_{3.5}$ for the infrared and blue bands respectively. The spin-orbit component recorded at 18239.66719 cm^{-1} is assigned as a $^4\Gamma_{4.5} \rightarrow X^4\Phi_{3.5}$ transition. Molecular constants were determined from the multiple state fit for the ^{102}RuF, ^{104}RuF, ^{100}RuF and ^{96}RuF isotopologues. Individual fits were used to obtain the molecular parameters for the ^{101}RuF, ^{99}RuF and ^{98}RuF isotopologues. From the results of the DF analysis of the [22.1] $^4\Delta_{3.5} \rightarrow X^4\Phi_{4.5}$ transition combined with the high-resolution analysis, the values of the spin-orbit separation are obtained as ~ 1000 and ~ 983 cm^{-1} for the upper and lower states of the green band respectively. The value of the ground state vibrational frequency of the RuF molecule is determined to be ~550 cm^{-1} from the fit. The upper state vibrational frequency of ~ 606 cm^{-1} for the green band is also obtained. The ground and excited state rotational constants, vibration-rotation coupling constants and the bond lengths were all calculated at equilibrium for the ^{102}RuF, ^{104}RuF and ^{100}RuF isotopologues in the [18.2] $^4\Gamma_{4.5} \rightarrow X^4\Phi_{3.5}$ system.

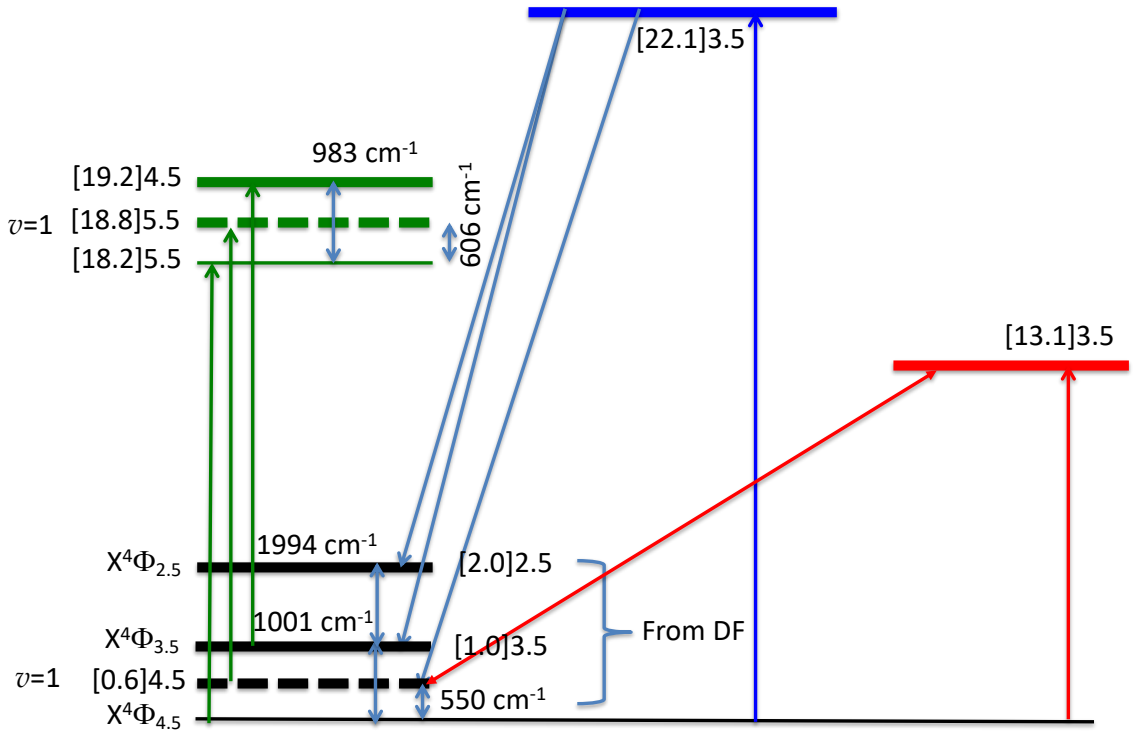

Figure 4.34 Energy level diagram of five observed transitions in the blue, green and infrared regions.

References

1. http://en.wikipedia.org/wiki/Olefin_metathesis.

2. https://en.wikipedia.org/wiki/Grubbs'_catalyst.

3. "The Nobel Prize in Chemistry 2005" (Press release). Nobelprize.org. 5 October 2005.

4. https://en.wikipedia.org/wiki/Ruthenium_anti-cancer_drugs.

5. https://en.wikipedia.org/wiki/NAMI-A.

6. P. E. Siegbahn, Theor. Chim. Acta. **86**, 219 (1993).

7. T. C. Steimle, W. Virgo, T. Ma, J. Chem. Phys. **124**, 024309 (2006).

8. A. G. Adam, A. D. Granger, L. E. Downie, D. W. Tokaryk, C. Linton, Can. J. Phys. **87**, 557 (2009).

9. A. G. Adam, L.P. Fraser, W.D. Hamilton, M. C. Steeves, Chem. Phys. Lett. **230**, 82 (1994).

10. R. Li, R. H. Jenson, W. J. Balfour, S. A. Shepard, A. G. Adam, J. Chem. Phys. **121**, 2591 (2004).

11. C. W. Bauschlicher, Chem. Phys. **211**, 163 (1996).

https://www.webelements.com.

12. C. M. Western, J. Quant. Spectrosc. Radiat. **186**, 221 (2017).

Chapter 5

Ruthenium monochloride: observation, results and analysis

5.1 Introduction

Ruthenium is used in platinum and palladium alloys to harden them and to make wear-resistant electrical contacts [1]. In the thin film industry, ruthenium can also be used as a substrate due to its promising properties for the use in microchips, and as a giant magnetoresistive read element for hard disk drives [2]. As discussed in chapter four, Ru-based compounds are also extensively used as catalysts and some cases of Ru-halide bonds were described. In Figure 5.1 another example of this is illustrated with an ammonium salt attached to a diene. The presence of the Ru-Cl bond can also be seen. This catalyst is used in the ring-closing metathesis reaction of the diene in water.

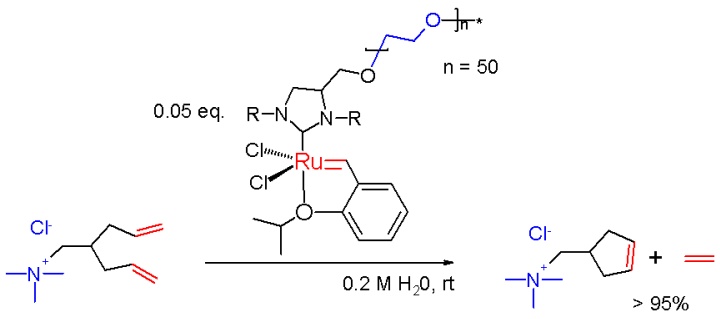

Figure 5.1 Ru-based complexes are used in the ring closing metathesis reaction of a diene in water [2].

5.2 Experimental conditions for production of RuCl

Ruthenium monochloride was made in a laser ablation molecular beam source that was described in chapter 3. For making the molecule, at first CCl_4 was used as a precursor in the presence of the He carrier gas to react with the laser ablated Ru atoms. Several promising bands were observed, however, after analysis of the dispersed fluorescence from the transitions in the low-resolution surveys, only the production of ruthenium monocarbide was confirmed. The precursor was switched to BCl_3 (boron trichloride) which led to successful production of ruthenium monochloride. The concentration of the gas mixture prepared in the reservoir on the gas board was 3% BCl_3 in the presence of He as carrier gas at a pressure of 150 psi which was delivered to the molecular jet apparatus at 40 psi.

5.3 Low-resolution survey

Figure 5.2 shows the result of the low-resolution survey of ruthenium monochloride, from 420 to 750 nm. Two transitions that are observed at ~ 508 and 569 nm were suspected to arise from RuCl and were strong enough to attempt collection at high-resolution. Apart from these two bands which are marked with green and yellow squares (see Figure 5.2), there are several peaks in the low-resolution spectra of RuCl that are marked with black dots. These bands are studied through dispersed fluorescence analysis in the next section. The bands at ~ 680 and 720 nm are likely due to an impurity since their DFs do not match the DFs (see Figure 5.5) of the other bands.

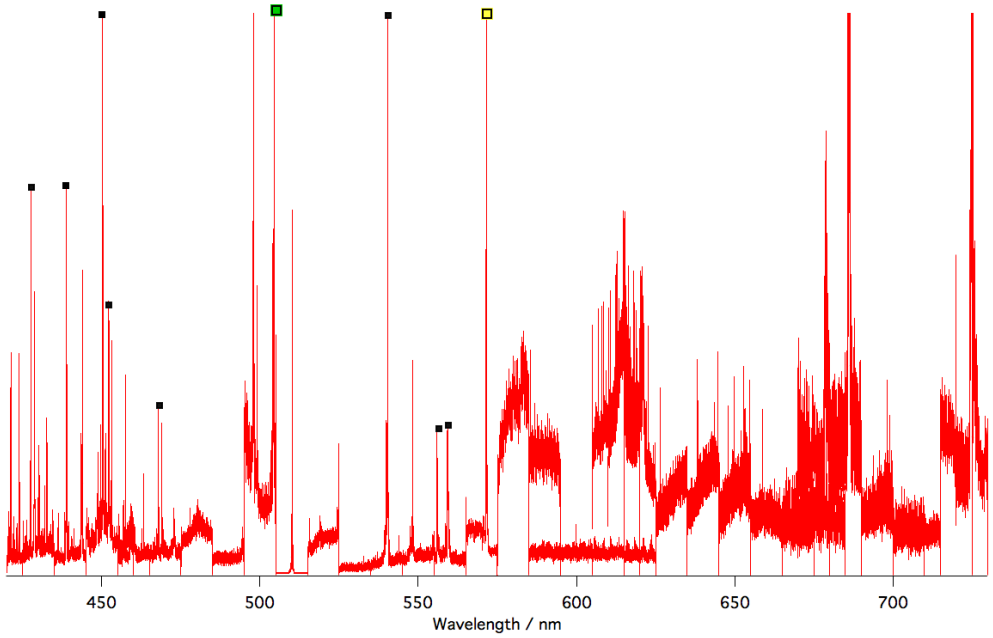

Figure 5.2 Low-resolution survey of RuCl.

Figure 5.3 shows an expanded view of the low-resolution band at ~ 508 nm. The band has a weak P and a strong R branch that suggests a transition in which $\Delta\Omega=1$. Higher resolution is required for the analysis of this band. The results will be presented in subsequent sections. There is also a small feature at ~ 508 nm in Figure 5.3 which might be a vibration that corresponds to an excitation from the $v=1$ level of the ground electronic state rather than $v=0$.

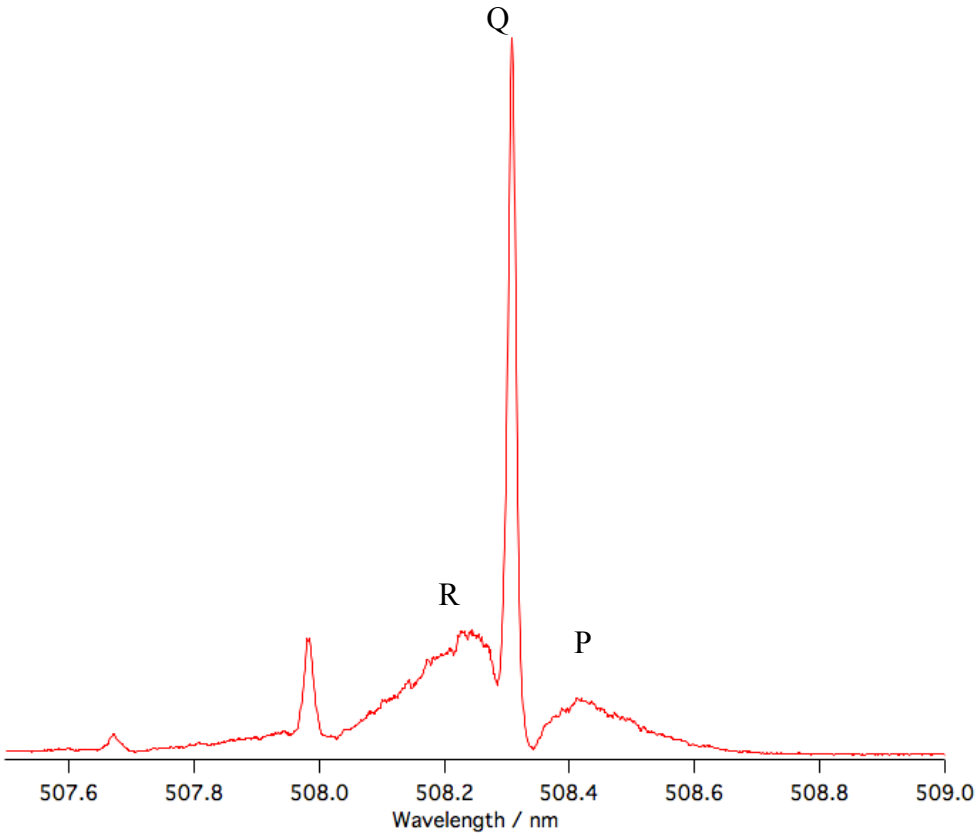

Figure 5.3 Low-resolution spectrum of a RuCl transition in the green region.

Figure 5.4 shows a band in the yellow region near ~ 570 nm. In the low-resolution survey of this band the R branch looks more intense than the P branch. However, as we will see the high-resolution analysis indicates that the transition is associated with $\Delta\Omega=0$.

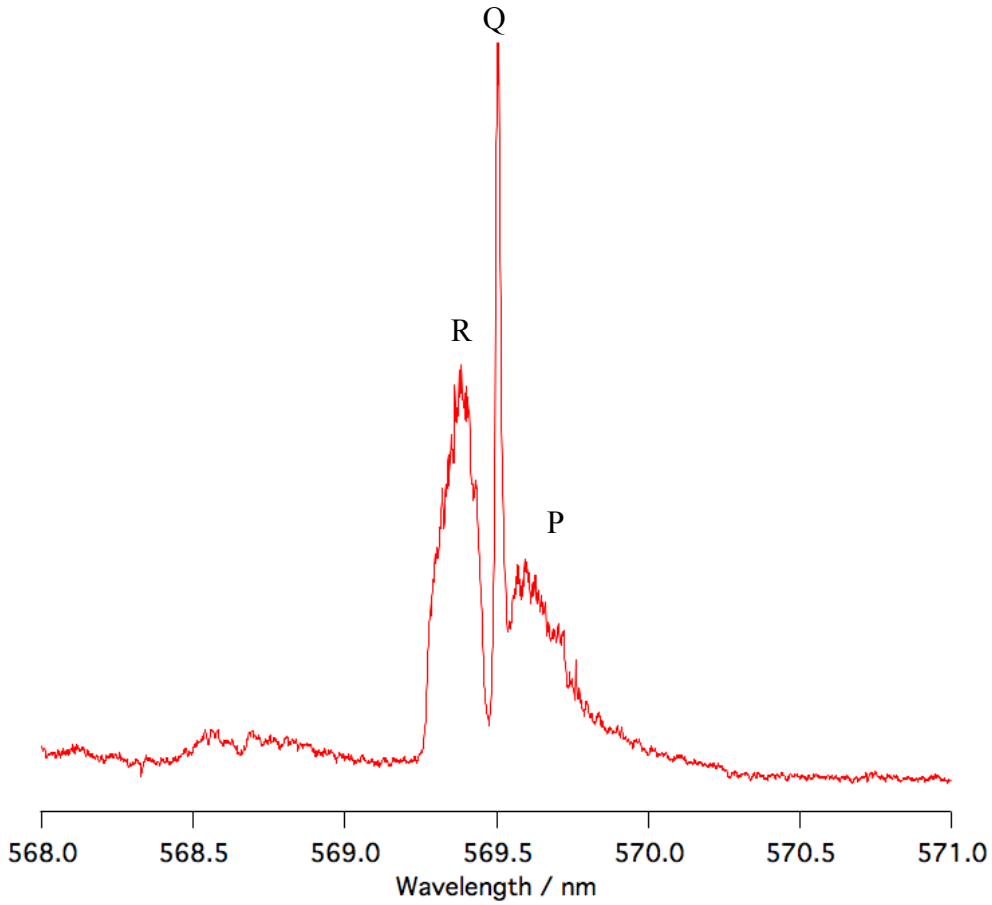

Figure 5.4 Low-resolution spectrum of a RuCl transition in the yellow region.

5.4 Dispersed fluorescence analysis

As this is the first observation of the RuCl molecule no experimental data about the vibrational frequencies are available in the literature. The one theoretical paper on RuCl only includes a predicted ground state and ground state bond length. Generally, the vibrational frequencies of metal-bearing diatoms are largely dependent on the ligands to which the metal is attached. Therefore, knowledge of the vibrational frequencies of other transition-metal chloride-bearing molecules can serve as a guide to interpreting the experimental DF results. Figure 5.5 shows the dispersed fluorescence spectra taken from

the bands observed in the low-resolution survey that are most likely RuCl (see Figure 5.2). Some of the DFs of the RuCl molecule have a very complex structure which makes their interpretation difficult.

The value for the first vibrational frequency is ~ 352 cm^{-1}. This number is in good agreement with the ~ 378 cm^{-1} [3] and ~ 405cm^{-1} [4] ground state vibrational frequencies of HfCl and FeCl respectively. Therefore, the value of ~ 352 cm^{-1} is reasonable for the difference between the v =0 and v =1 levels of the lower state. There is also a peak at ~ 260 cm^{-1} which may indicate a low-lying electronic state. The low-lying excited state around ~ 260 cm^{-1} is present in several of the spectra.

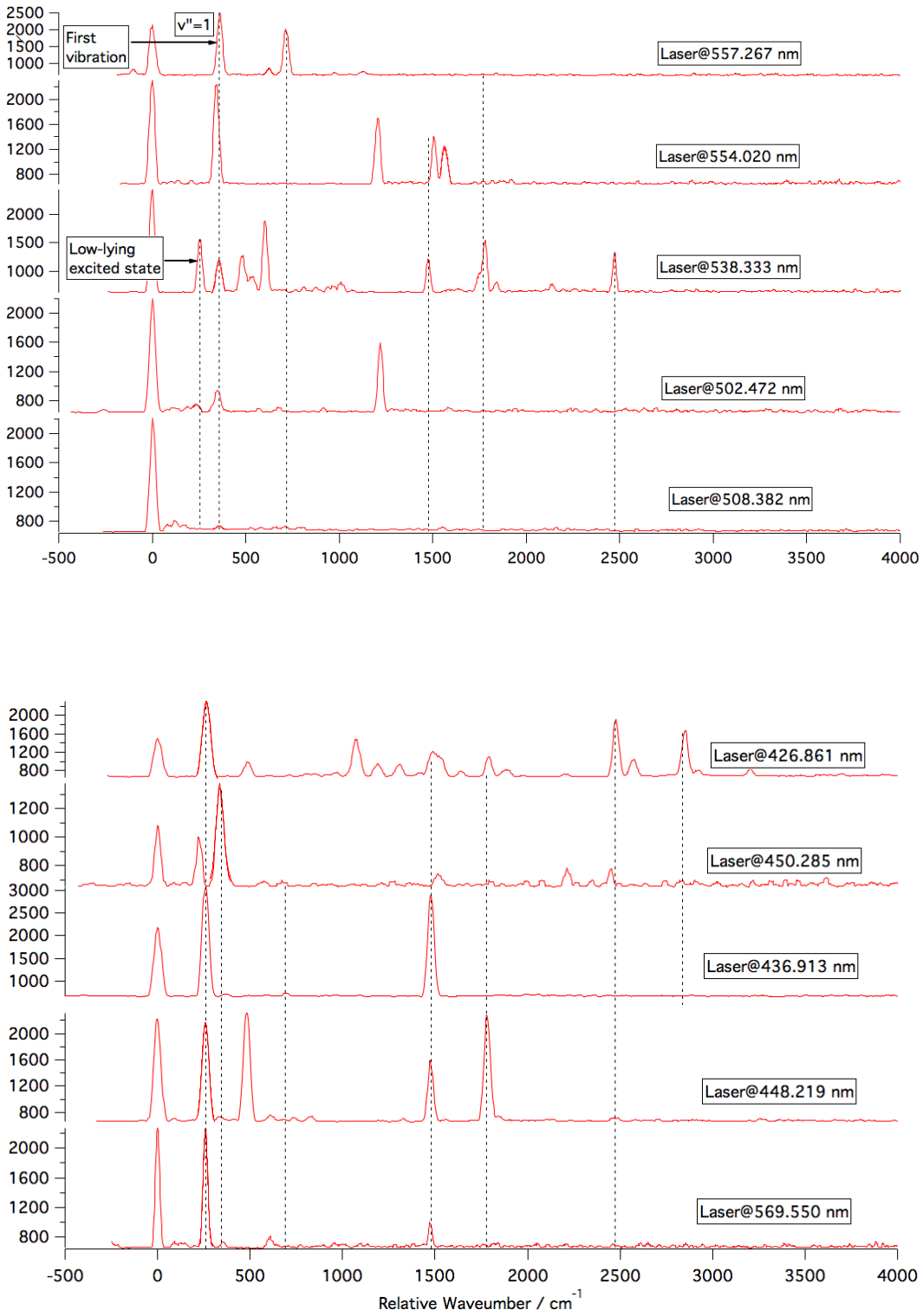

Figure 5.5 The dispersed fluorescence of the observed transitions in the low-resolution spectra of RuCl. Identified series are indicated with dotted vertical lines.

As can be seen from Figure 5.5, the first vibrational frequency peaks line up at around ~ 352 cm^{-1}. Some other frequencies consistently appear in the DFs and are shown with the dotted vertical lines. They may correspond to other low-lying excited states. The laser wavelengths and individual observations that were used to extract the v''=1 value are given in Table 5.1. The fluctuations of these numbers are about ~ 30 cm^{-1}. However, they are consistent enough to be assigned as the first vibration of RuCl. The corresponding average result of the aforementioned DF data, $\Delta G_{1/2}$, is 352±3 cm^{-1}.

Table 5.1 Laser wavelength and first vibration of DFs.

Laser wavelength (nm)	Observed v''=1 (cm^{-1})
557.267	360.927
554.020	342.599
538.333	356.953
502.472	347.958
508.382	357.423
569.550	353.533
448.219	337.083
450.285	336.801
436.913	368.404

5.5 High-resolution analysis

Chlorine has two stable isotopes, ^{35}Cl and ^{37}Cl. Ruthenium on the other hand has seven stable isotopes. Therefore, in principle fourteen molecules could be identifiable given high-resolution spectra of the molecule. As can be seen in Figure 5.6, two clusters are readily observed in the Q branch. After zooming into the P region, a repetitive pattern of the two clusters is clearly distinguished. These repeating clusters are attributed to ^{35}Cl and ^{37}Cl. The rotational and isotopic structures are quite evident in the spectra.

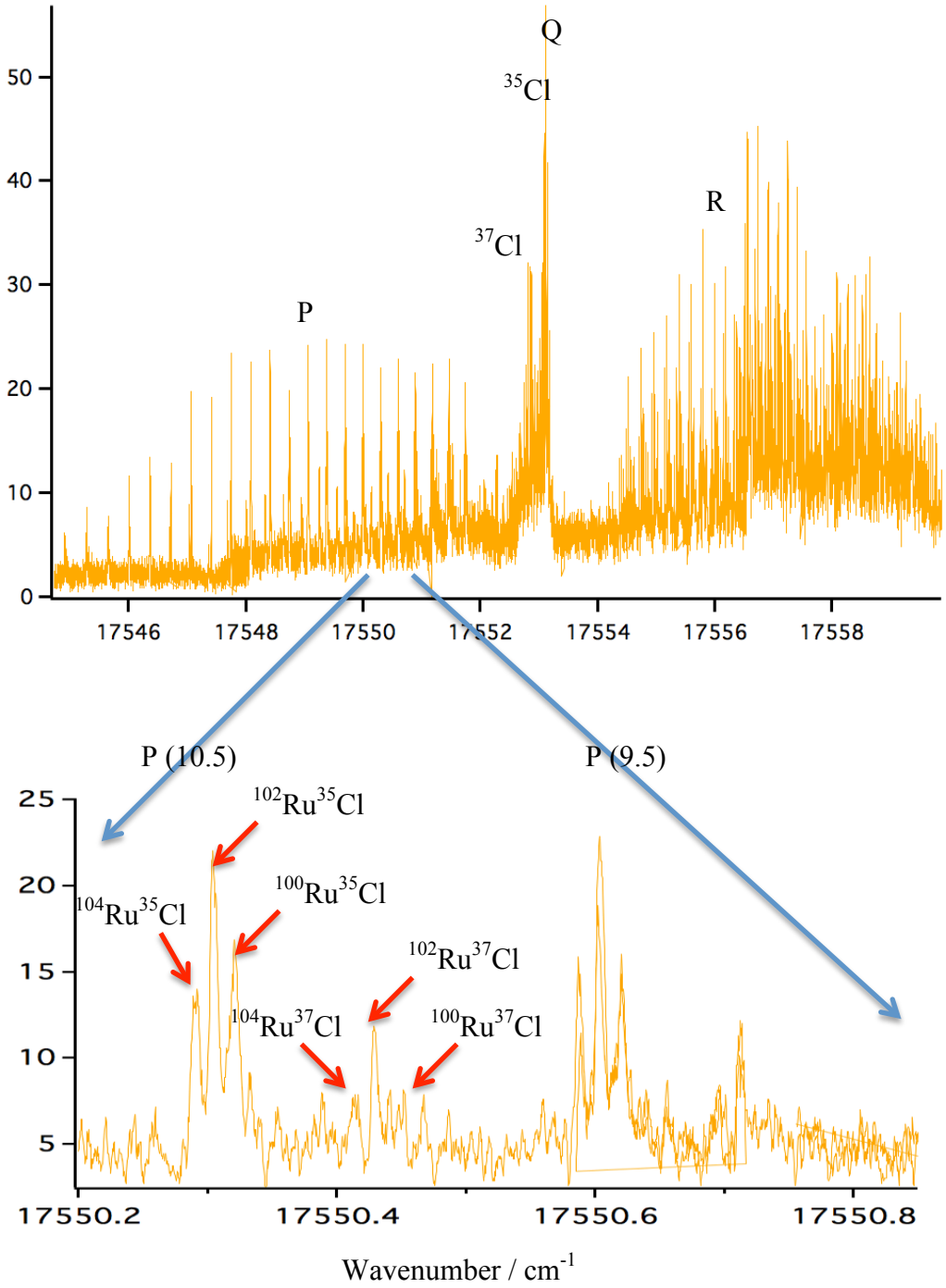

Figure 5.6 The RuCl band near ~569 nm expanded to show isotopic structure.

5.5.1 Hot and cold spectra

A useful technique to produce a colder molecular beam is to switch the carrier gas from helium to argon. The argon atom has a larger radius than the helium atom. This means when using argon as a carrier gas the number of collisions increases which slows down the rotations of the molecules and results in a colder molecular beam. As a result, higher rotational levels are less populated whereas lower rotational levels are more populated. Hence, lower J lines are more intense than higher J transitions, and higher J levels disappear from the spectrum. In general this technique assists in assignment of regions in the spectrum which are congested. A comparison of a hot and cold spectrum is illustrated in Figures 5.7 and 5.8.

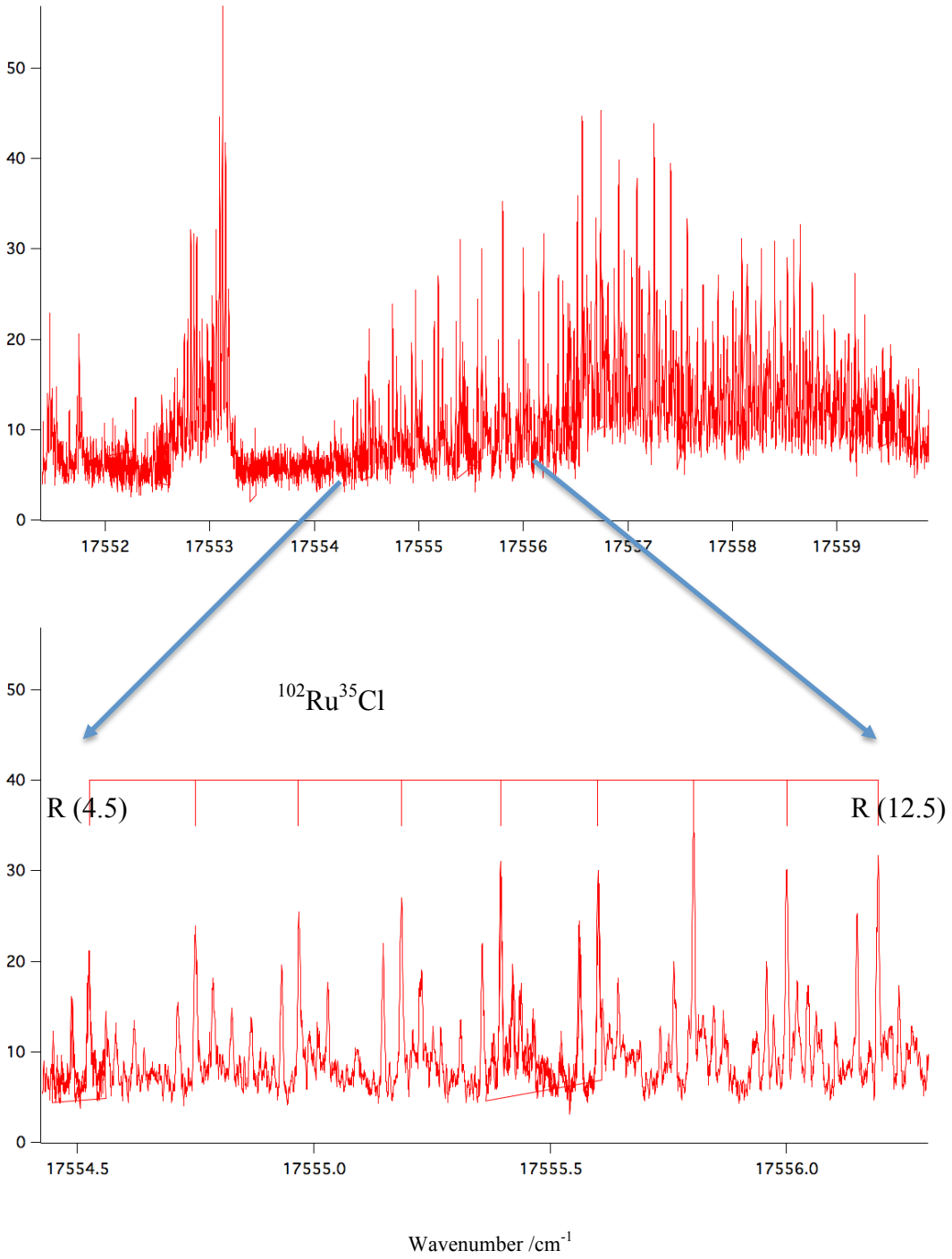

Figure 5.7 A portion of the RuCl spectrum taken near ~ 569 nm with helium as the carrier gas.

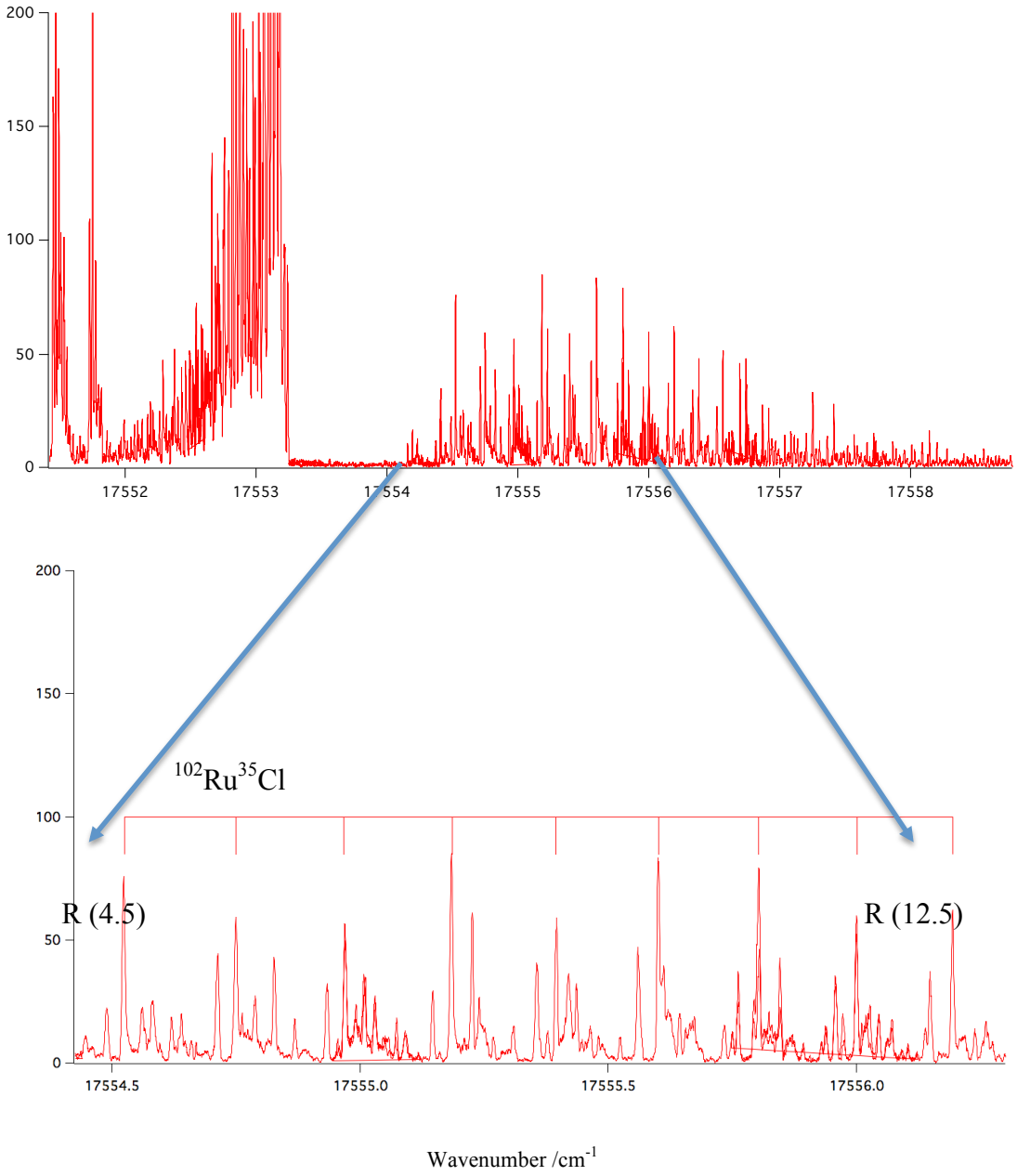

Figure 5.8 A portion of the RuCl spectrum near ~ 569 nm taken with argon as the carrier gas.

In the early stages of the data processing, the colder spectrum was used. However, the hot spectrum is sufficiently resolved such that it can be used for further analysis.

5.5.2 The $^4\Phi_{4.5} \rightarrow X\,^4\Phi_{4.5}$ electronic transition of RuCl near ~ 569 nm

Figure 5.6 shows the high-resolution spectrum of the transition observed near ~ 569 nm. The first lines of the branches were identified to be P(5.5) and R(4.5). This suggests that the levels involved in this transition have Ω=4.5 for both the lower and upper states. The ground state of the molecule was theoretically predicted as $^4\Phi$ [5]. Although the R and P branches may not look of the same intensity, high-resolution analysis confirms that $\Delta\Lambda$=0 and hence, knowing the lower state is $^4\Phi$ from the theory, the upper state would also be $^4\Phi$. Therefore, the electronic transition has been assigned as $^4\Phi_{4.5} \rightarrow X^4\Phi_{4.5}$. The assignments of this band were done using the techniques described in chapter 4. The transition data were fit to an R^2 Hamiltonian (see section 2.9) using Pgopher [6], and were later used in a combined fit of the 508 and 569 nm bands. The band origin, rotational constant and centrifugal distortion constant were adequate to model the rotational structure of the molecule and are presented in Table 5.2.

5.5.3 The $^4\Gamma_{5.5} \rightarrow X^4\Phi_{4.5}$ electronic transition of RuCl near ~ 508 nm

Figure 5.9 shows the high-resolution spectrum of the 508 nm transition of RuCl. The strong R and weak P branches suggest that $\Delta\Lambda$=1 and hence, knowing the lower state is $^4\Phi$ from the theory [5], the upper state is assigned as $^4\Gamma$. This is in agreement with the result of the rotational numbering and analysis; the first lines of the P and R branches are P(6.5) and R(4.5) which indicate that Ω''=4.5 and Ω'=5.5 for the lower and upper states

respectively. The transitions were first fitted to a R^2 Hamiltonian in Pgopher [6], then were included in a global fit with the $^4\Phi_{4.5} \rightarrow X\,^4\Phi_{4.5}$ band observed near ~ 569 nm since both bands shared the same ground state. (See Table 5.2 for molecular constants)

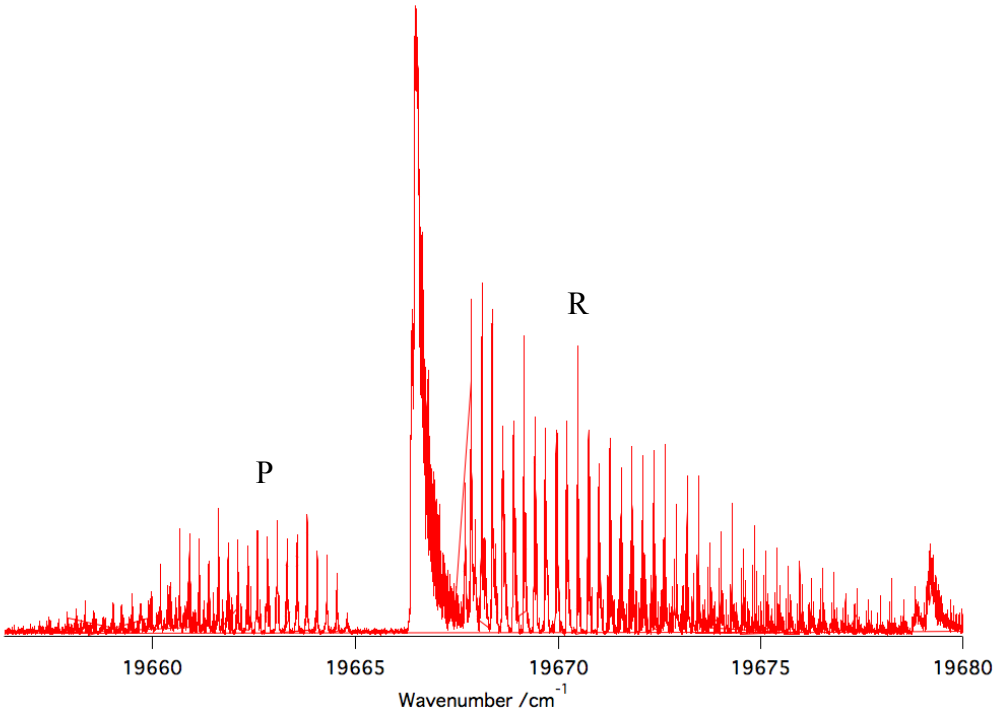

Figure 5.9 High-resolution spectrum of a $^4\Gamma_{5.5} \rightarrow X^4\Phi_{4.5}$ transition of RuCl near 508 nm.

5.5.4 Analysis and discussion

Figures 5.10 and 5.11 show the experimental and simulated spectra for the [17.5] $^4\Phi_{4.5} \rightarrow X\,^4\Phi_{4.5}$ and the [19.6] $^4\Gamma_{5.5} \rightarrow X^4\Phi_{4.5}$ electronic transitions respectively. In both Figures the upper trace is the experimental spectrum and the lower trace is the calculated spectrum at 50 K (typical of cold molecular spectra in our jet apparatus) using the fitted constants. The simulation was done for the most abundant isotopologue of ruthenium monochloride, i.e., $^{102}Ru^{35}Cl$. Spectra of each of the isotopologues were fitted

individually first, and then were included in a multistate fitting employing the R^2 Hamiltonian using Pgopher [6]. Table 5.3 shows the result of the global fit for the $^{102}Ru^{35}Cl$,$^{104}Ru^{35}Cl$ and $^{100}Ru^{35}Cl$ isotopologues. The molecular constants are given for the ground $X^4\Phi_{4.5}$ and excited $^4\Phi_{4.5}$ and $^4\Gamma_{5.5}$ states of the isotopologues. The B value, centrifugal distortion constant and band origin of the molecules are extracted from the fits for the molecules. These three constants were sufficient to give a good fit with the overall standard deviation of 0.0013, 0.0012 and 0.0018 cm^{-1} for the $^{102}Ru^{35}Cl$,$^{104}Ru^{35}Cl$ and $^{100}Ru^{35}Cl$ isotopologues respectively. The ground state B value of the molecule is ~ 0.1270 cm^{-1}. Therefore, the measured bond length for $^{102}Ru^{35}Cl$ is 2.29 Å which can be compared with the calculated equilibrium bond length of 2.49 Å [4]. The agreement is within 8%. This is consistent with the results of the experimental (1.90 Å) and theoretical (2.05 Å [4]) values obtained for the equilibrium bond length of the RuF molecule where the agreement was ~ 7% (see section 4.6.2). Therefore, the theoretical work generally predicts higher values for the bond lengths than the experimental results. For the excited $^4\Phi_{4.5}$ state the B value decreases for all of the isotopologues if compared to the ground state values. This means there is an increase in the bond length when the molecule is excited to that state, whereas, for the $^4\Gamma_{5.5}$ state the B value increases for all isotopologues. This indicates a decrease in the bond length when the molecule is excited to the $^4\Gamma_{5.5}$ state. The B values of the three states are all isotopically consistent, i.e., the larger the reduced mass of the molecule the lower the B value. The centrifugal distortion constant, D, is also reported for the three states. The values of D decrease in both of the excited states compared to the ground state values. The band origin is also given for the excited states. As discussed, the rotational and centrifugal distortion constants for each

molecule are slightly different from each other. The mass difference between different isotopologues forces the vibrational and rotational constants to vary slightly. This causes the band origin of the isotopologues to vary. As can be seen from the Table 5.2 the band origins of the excited states shifts toward the lower wavenumbers as the mass increases.

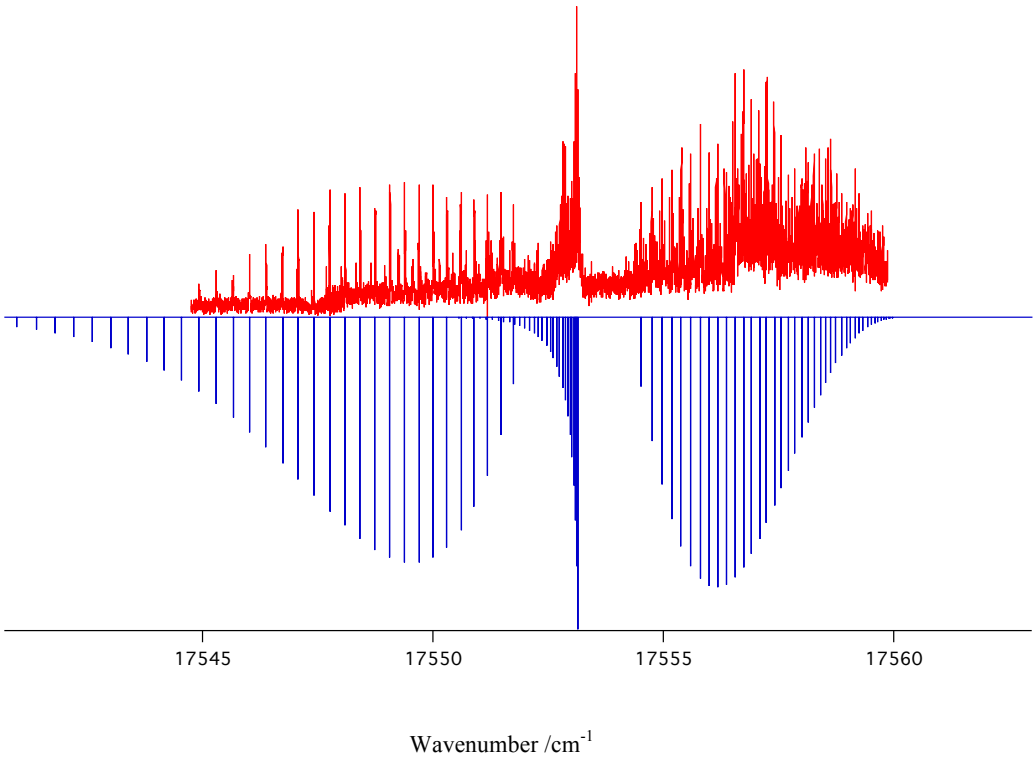

Figure 5.10 The upper and lower traces are the experimental and calculated spectra respectively for the [17.5] $^4\Phi_{4.5} \rightarrow X^4\Phi_{4.5}$ transition of $^{102}Ru^{35}Cl$. Simulations are done at 50 K.

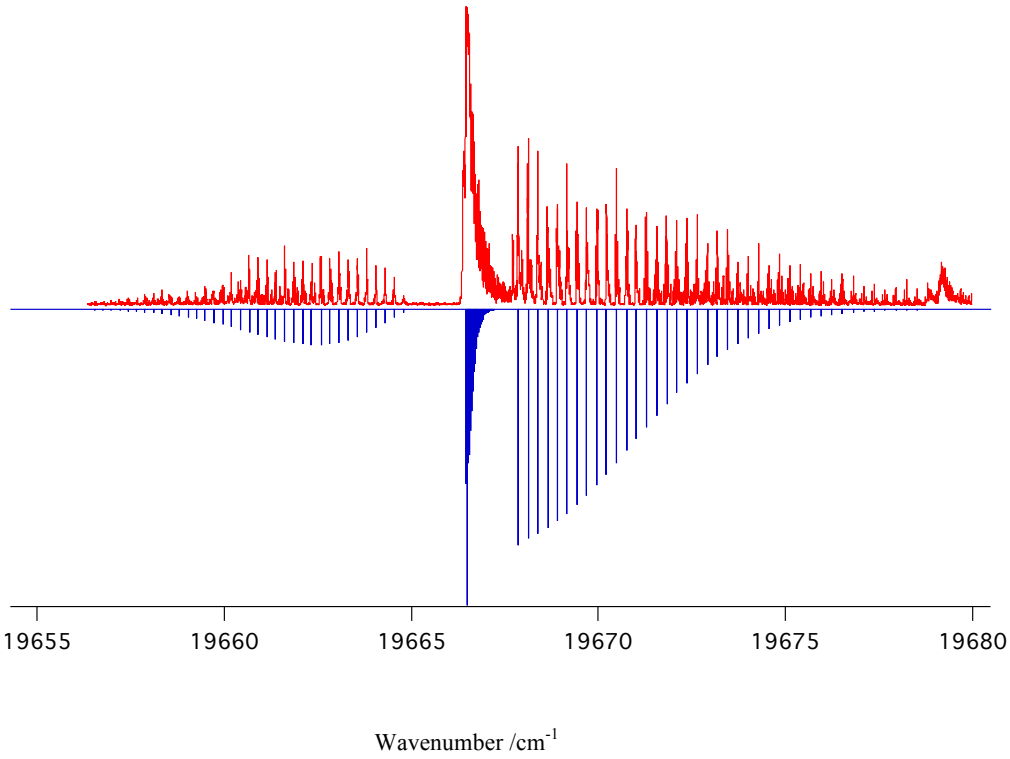

Figure 5.11 The upper and lower traces are the experimental and calculated spectra respectively for the [19.6] $^{4}\Gamma_{5.5}\rightarrow X^{4}\Phi_{4.5}$ transition of $^{102}Ru^{35}Cl$. Simulations are done at 50 K.

Table 5.2 Molecular constants for $^{102}Ru^{35}Cl$, $^{104}Ru^{35}Cl$ and $^{100}Ru^{35}Cl$.

State	Isotopologues	T / cm^{-1}	B / cm^{-1}	D / 10^{-8} cm^{-1}
$X^4\Phi_{4.5}$	$^{102}Ru^{35}Cl$		0.12726010(726)	6.666(754)
	$^{104}Ru^{35}Cl$		0.12662965(914)	6.38(133)
	$^{100}Ru^{35}Cl$		0.12792979(668)	8.605(539)
[17.5] $^4\Phi_{4.5}$	$^{102}Ru^{35}Cl$	17553.16462(28)	0.12495274(718)	4.84(72)
	$^{104}Ru^{35}Cl$	17553.13661(35)	0.12433561(900)	5.3(12)
	$^{100}Ru^{35}Cl$	17553.19557(46)	0.1255832(50)	0
[19.6] $^4\Gamma_{5.5}$	$^{102}Ru^{35}Cl$	19667.72641(29)	0.12763853(687)	6.547(682)
	$^{104}Ru^{35}Cl$	19667.71831(35)	0.12700271(838)	6.17(119)
	$^{100}Ru^{35}Cl$	19667.73922(34)	0.12830686(644)	8.173(502)

The values of rms error of the multiple state fitting for $^{102}Ru^{35}Cl$, $^{104}Ru^{35}Cl$ and $^{100}Ru^{35}Cl$ are 0.0013, 0.0012 and 0.0018 cm^{-1} respectively. Note that the number in parentheses represents one standard deviation in the particular parameter.

In Table 5.3 the ratios of the B values for the ground and excited states of different isotopologues are compared with the ratios of the corresponding reduced mass. As can be seen, the ratios are in good agreement and hence the molecules are isotopically consistent. Note that the spectra of the $^{101}RuCl$, $^{99}RuCl$, $^{98}RuCl$ and $^{96}RuCl$ isotopologues were too weak to be analyzed.

Table 5.3 Comparison of the isotopic ratios and the reduced mass for the $^{102}Ru^{35}Cl$, $^{104}Ru^{35}Cl$ and $^{100}Ru^{35}Cl$ isotopologues.

State	B_{102}/B_{104}	B_{100}/B_{104}	B_{100}/B_{102}
$X^4\Phi_{4.5}$	1.0049	1.0102	1.0052
[17.5] $^4\Phi_{4.5}$	1.0049	1.0100	1.0050
[19.6] $^4\Gamma_{5.5}$	1.0050	1.0102	1.0052
μ^*/μ	1.0049	1.0100	1.0051

* indicates the heavier isotope.

As mentioned above chlorine has two stable isotopes, i.e., ^{35}Cl and ^{37}Cl making it possible to determine the bonding between both of the chlorines and Ru atoms. The $Ru^{35}Cl$ isotopologues were described before. The high-resolution spectra of the two electronic transitions show some extra features (see Figure 5.6) such as a double cluster in the Q branch or the repeating patterns throughout the main band. These features show the presence of ^{37}Cl isotopes in the spectra. As the abundance of ^{37}Cl is ~ 0.3 that of ^{35}Cl, the intensities of the observed transitions are much weaker accordingly. Figures 5.12 and 5.13 show the experimental and simulated spectra for the [17.5] $^4\Phi_{4.5}\rightarrow X^4\Phi_{4.5}$ and [19.6] $^4\Gamma_{5.5}\rightarrow X^4\Phi_{4.5}$ electronic transitions respectively for the $^{102}Ru^{37}Cl$ molecule. The molecular constants for $^{102}Ru^{37}Cl$ that are extracted from the global fit are given in Table 5.4. As with the $Ru^{35}Cl$ isotopologues, the B value for the $^4\Phi_{4.5}$ excited state is smaller than the ground state whereas it is larger for the $^4\Gamma_{5.5}$ excited state. Hence, the bond length increases and decreases with respect to the ground state as the molecule is excited to the $^4\Phi_{4.5}$ and $^4\Gamma_{5.5}$ states respectively. This trend was also observed for the $Ru^{35}Cl$

isotopologues. The B values for the three states of $^{102}Ru^{37}Cl$ are smaller than the corresponding values of $^{102}Ru^{35}Cl$ which is consistent with the trend observed before. The band origins shifts about ~ 0.28 and 0.12 cm^{-1} to the lower wavenumbers for the $^4\Phi_{4.5}$ and $^4\Gamma_{5.5}$ states of $^{102}Ru^{37}Cl$ compared to those of the corresponding states of $^{102}Ru^{35}Cl$. This is also consistent with the band origin shifts observed in the $Ru^{35}Cl$ isotopologue that move toward the lower wavenumbers as the isotopic mass increases. The centrifugal distortion constants for $^{102}Ru^{37}Cl$ are larger by a factor of ~ 10 than the values reported for $^{102}Ru^{35}Cl$ for the three states.

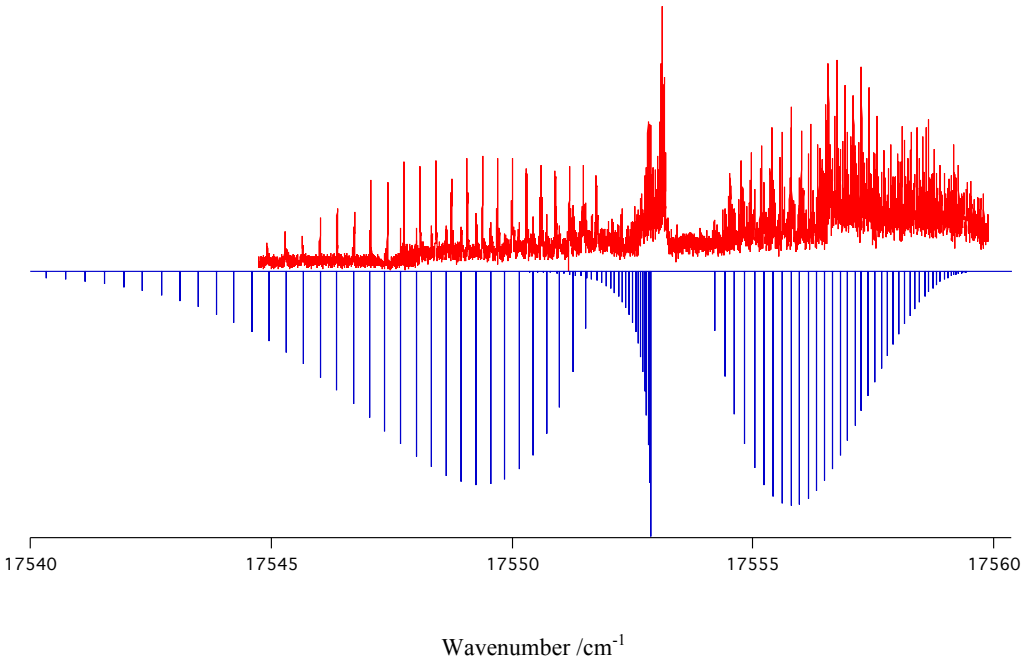

Figure 5.12 The upper and lower traces are the experimental and calculated spectra respectively for [17.5] $^4\Phi_{4.5} \rightarrow X\ ^4\Phi_{4.5}$ transition of $^{102}Ru^{37}Cl$. Simulations are done at 50 K.

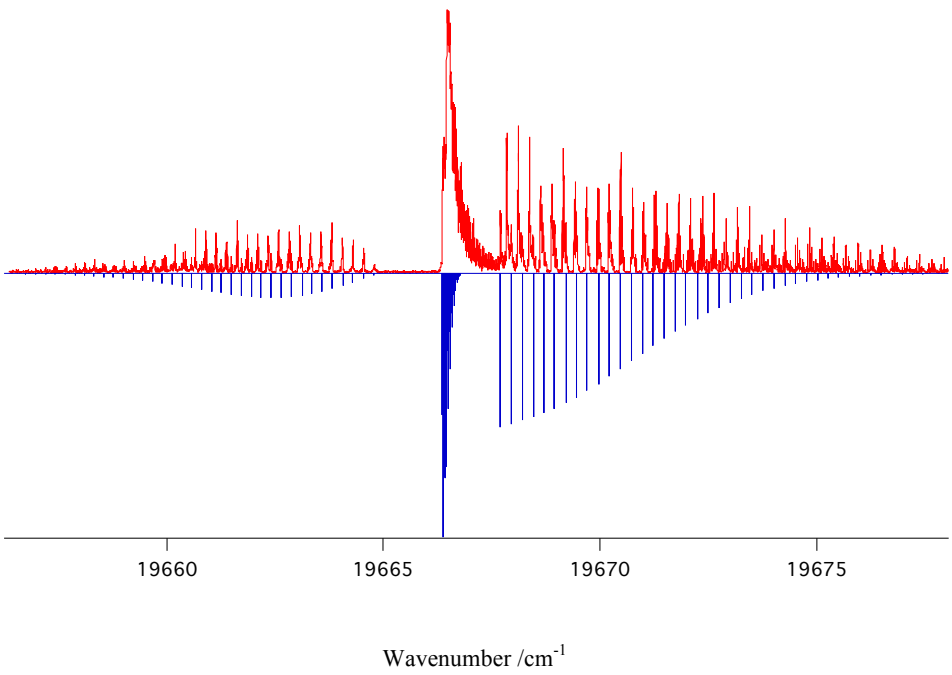

Figure 5.13 The upper and lower traces are the experimental and calculated spectra respectively for the [19.6] $^{4}\Gamma_{5.5} \rightarrow X^{4}\Phi_{4.5}$ transition of $^{102}Ru^{37}Cl$. Simulations are done at 50 K.

Table 5.4 Molecular constants for $^{102}Ru^{37}Cl$.

State	T / cm^{-1}	B / cm^{-1}	D / 10^{-7} cm^{-1}
$X^4\Phi_{4.5}$		0.1223147(183)	7.155(309)
[17.5] $^4\Phi_{4.5}$	17552.88918(61)	0.1200810(221)	7.91(41)
[19.6] $^4\Gamma_{5.5}$	19667.58673(56)	0.1225831(177)	5.457(277)

The value of rms error of the multiple state fitting is 0.0019 cm^{-1} for $^{102}Ru^{37}Cl$.

The spectra of other isotopologues corresponding to ^{37}Cl such as $^{104}Ru^{37}Cl$ and $^{100}Ru^{37}Cl$ were congested and weak. This prevented a sufficient number of transitions to be assigned and hence these isotopologues were not analyzed.

In Table 5.5 the ratios of B values for the ground and excited states of $^{102}Ru^{35}Cl$ and $^{102}Ru^{37}Cl$ are compared with the ratios of the corresponding reduced mass. As can be seen, the ratios are in good agreement.

Table 5.5 Comparison of the isotopic ratios and the reduced mass for the $^{102}Ru^{35}Cl$ and $^{102}Ru^{37}Cl$ isotopologues.

State	$^{35}B_{102}/^{37}B_{102}$	$^{37}\mu/^{35}\mu$
$X^4\Phi_{4.5}$	1.0404	1.0419
$[17.5]\ ^4\Phi_{4.5}$	1.0405	1.0419
$[19.6]\ ^4\Gamma_{5.5}$	1.0412	1.0419

5.6 Concluding remarks

The result of the low-resolution survey for RuCl shows several transitions of which two were chosen for high-resolution experiments. The ground state vibrational frequency of the molecule is determined to be ~ 352 cm^{-1} from the DF experiments. Figure 5.14 presents the summary of the transitions that were analyzed to extract the data. A low-lying electronic state is also observed at ~ 260 cm^{-1}. The results of high-resolution analysis of two transitions in the green and yellow regions, confirms that the ground state of the molecule is $X^4\Phi_{4.5}$. The results for the different isotopologues of RuCl observed are all isotopically consistent which confirms that the assignments are correct. Unlike the related molecule, RuF, no hyperfine structure due to the chlorine atoms were observed. This is due to the fact that the magnetic moment of chlorine is smaller than that of fluorine. The first observation of RuCl molecule occurred during this work. The large set

of spectroscopic data presented here provides valuable information for future reference from both the theoretical and experimental standpoints.

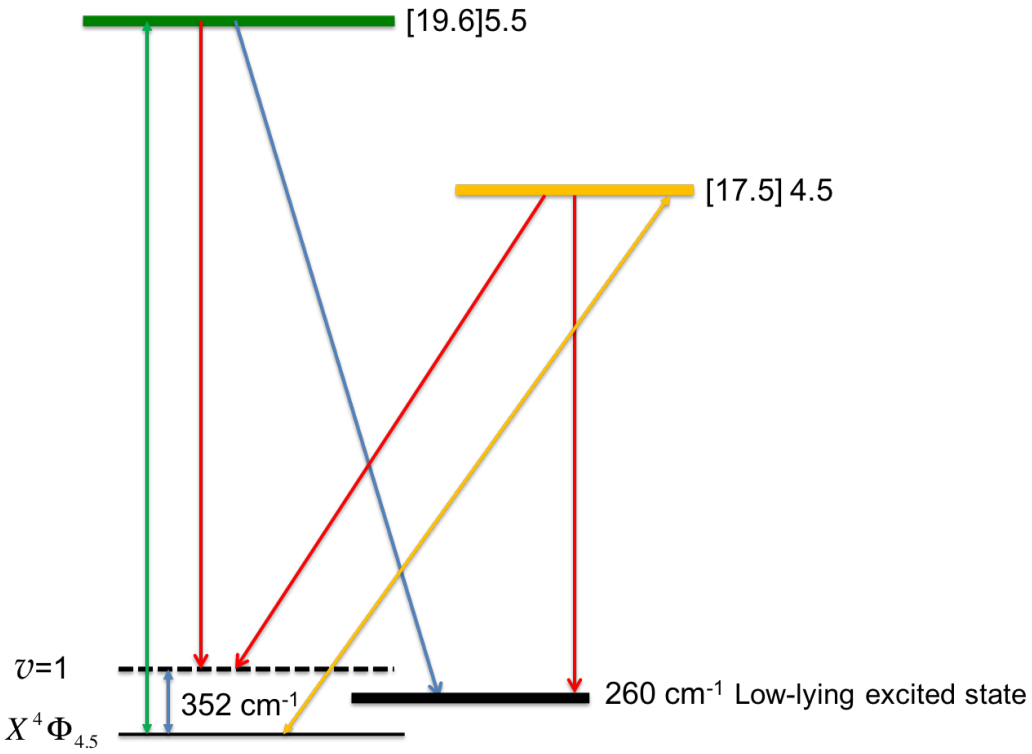

Figure 5.14 Energy level diagram of the two band systems observed in experiments on RuCl, with transitions observed between the levels indicated.

References

1. P. C. Hydes, Platinum Metals Rev. **24**, 2 (1980).

2. J. -M. Oh, B. -K. Lee, H. -K. Park, J. -W. Lim, Mater. Trans. **53**, 1680 (2012).

2. https://en.wikipedia.org/wiki/Grubbs%27_catalyst.

3. R. S. Ram, A.G. Adam, A. Tsouli, J. Lievin, P. F. Bernath, J. Mol. Spectrosc. **202**, 116 (2000).

4. J. Lei, P. J. Dagdigian, J. Chem. Phys. **12**, 23 (2000).

5. P. E. Siegbahn, Theor. Chim. Acta. **86**, 219 (1993).

6. C. M. Western, J. Quant. Spectrosc. Radiat. **186**, 221 (2017).

Chapter 6

Ruthenium monoxide: the 1-0 band of the [18.1] 4→ $X^5\Delta_4$ transition

6.1 Observation of a band of RuO

In chapter 4 the results and analysis of the RuF molecule were presented. During the low-resolution scans of the RuF molecule a band was observed at ~ 530 nm. This is about the correct position for the 1-0 band of the [18.2] $^4\Gamma_{5.5} \rightarrow X\ ^4\Phi_{4.5}$ system of RuF in the green region. This is so because the band origin for the 0-0 transition of RuF is at ~ 18256 cm^{-1} and the upper state vibrational frequency was measured to be ~ 606 cm^{-1}. Therefore the expectation was to find the 1-0 vibration of RuF around 18256+606=18862 cm^1 or ~ 530 nm. The spectrum was taken at high resolution, in order to obtain a very precise measurement of the vibrational frequency of the [18.2] $^4\Gamma_{5.5}$ state (see Figure 6.1). However, after analyzing the spectrum, lower-state combination differences in the new band did not match those of RuF. Figure 6.2 shows the low-resolution band that was detected during the survey for RuF. A coarse rotational structure of the band can be observed. Also, as shown in Figures 6.2 and 6.3, its shape is not similar to that of the 0-0 and 1-1 bands of the [18.2] $^4\Gamma_{5.5} \rightarrow X\ ^4\Phi_{4.5}$ transition of RuF. Therefore, the possibility that another molecule was responsible for the spectrum was raised. The chemicals which were present during making RuF in the molecular jet were ruthenium (Ru), sulphur hexafluoride (SF_6) and helium (He), along with small amounts of atmospheric contaminants (principally O_2 and N_2). Oxidation on the surface of the ruthenium rod

could also occur. Thus, molecules like RuS and RuO could also be produced in the jet, and could give rise to the new spectrum.

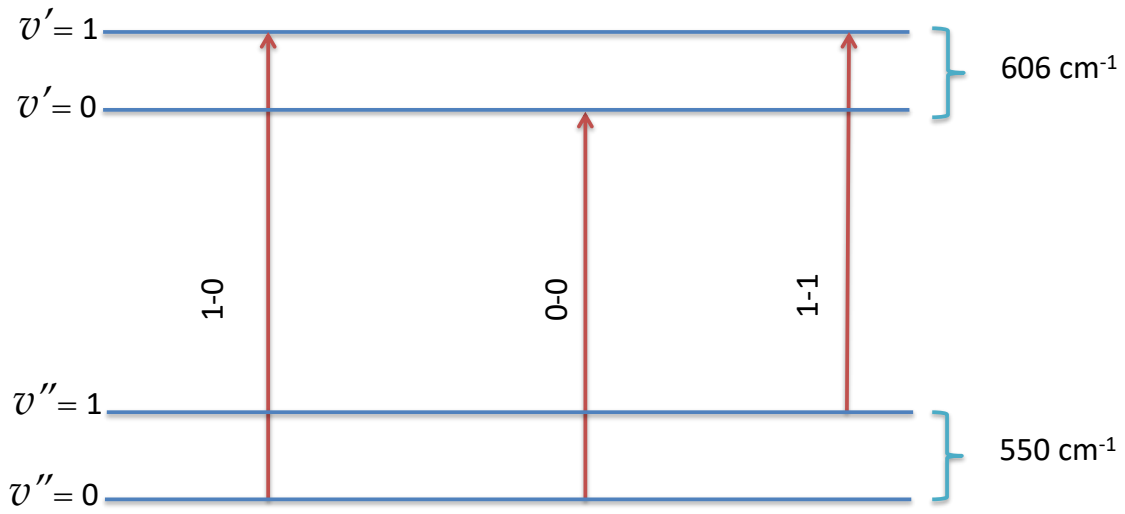

Figure 6.1 Three possible transitions in the green region for the [18.2] $^4\Gamma_{5.5} \rightarrow X\ ^4\Phi_{4.5}$ system of RuF needed to measure the lower and upper state vibrational frequencies with high precision.

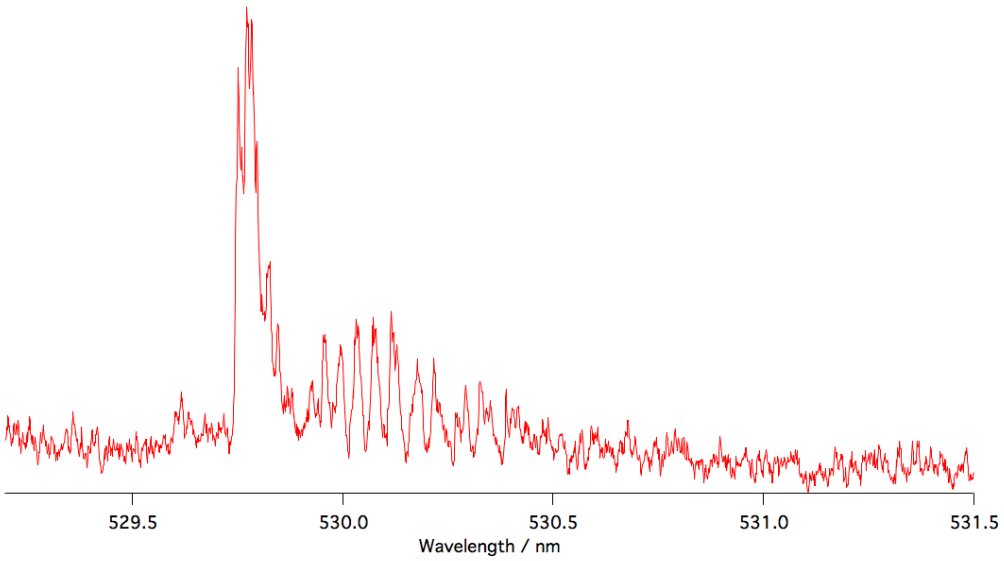

Figure 6.2 The 1-0 band of the [18.1] 4 $\rightarrow$ $X^5\Delta_4$ transition of RuO taken in a low-resolution survey scan.

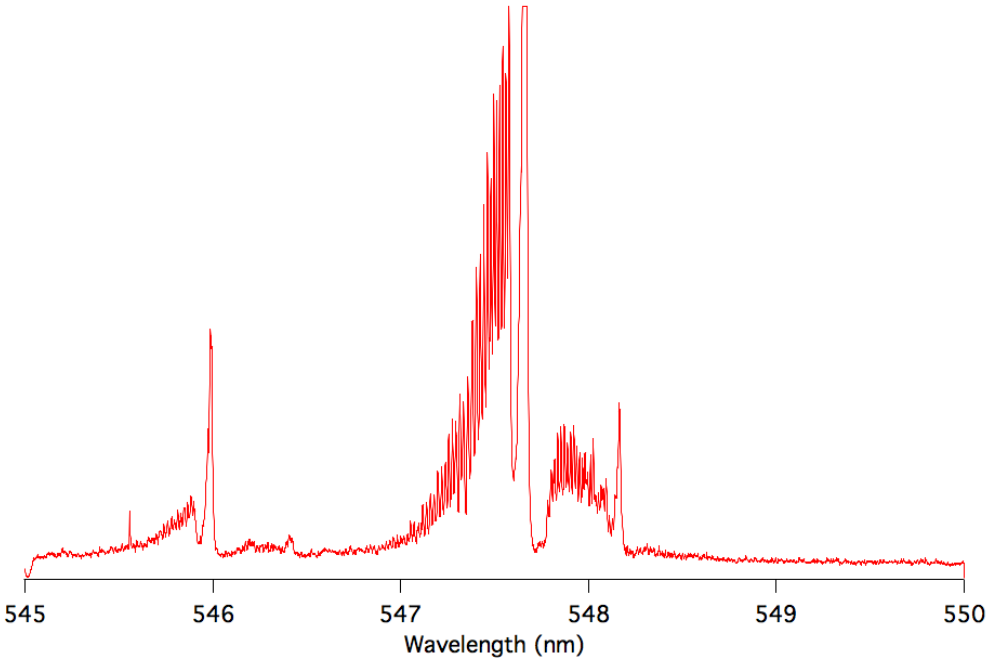

Figure 6.3 The low-resolution spectra of the 1-1 and 0-0 bands of the [18.2] $^4\Gamma_{5.5} \rightarrow X\ ^4\Phi_{4.5}$ and [18.2] $^4\Gamma_{4.5} \rightarrow X\ ^4\Phi_{3.5}$ transitions of RuF.

No work has been done on the RuS molecule yet; however, the literature [1,2] showed that there is a band of RuO at 530 nm. The high-resolution data were sufficient to identify the molecule as RuO. The dispersed fluorescence spectrum of the band was also taken, as further evidence confirming the production of ruthenium monoxide.

6.2 Dispersed fluorescence

Table 6.1 shows the position of peaks observed in the dispersed fluorescence spectrum taken at ~ 530 nm (see Figure 6.4). As was seen in chapter four (see section 4.4), the ground state vibrational frequency for the RuF molecule was measured to be ~ 550 cm^{-1} which is not present in the DF spectrum. However, two progressions can be observed from the peaks immediately. The first progression is from the peaks A, B, D and F which are ~ 850 cm^{-1} apart. This is more consistent with an assignment of the band to RuO than to RuF, since the ground state vibrational frequency of RuO was measured to be ~859 cm^{-1} [2]. The second progression is due to the peaks C and E which are ~ 1100 cm^{-1} apart. This progression is likely due to a low-lying excited state of RuO which happens to be above the first vibration of the ground state.

Table 6.1 Positions of the peaks observed in the DF spectrum of the 1-0 band of the [18.1] 4 → $X^5\Delta_4$ transition of RuO.

Index letter of the peaks in the DF	Positions of the peaks in the DF /cm^{-1}
A	0
B	858
C	1110
D	1700
E	2206
F	2532

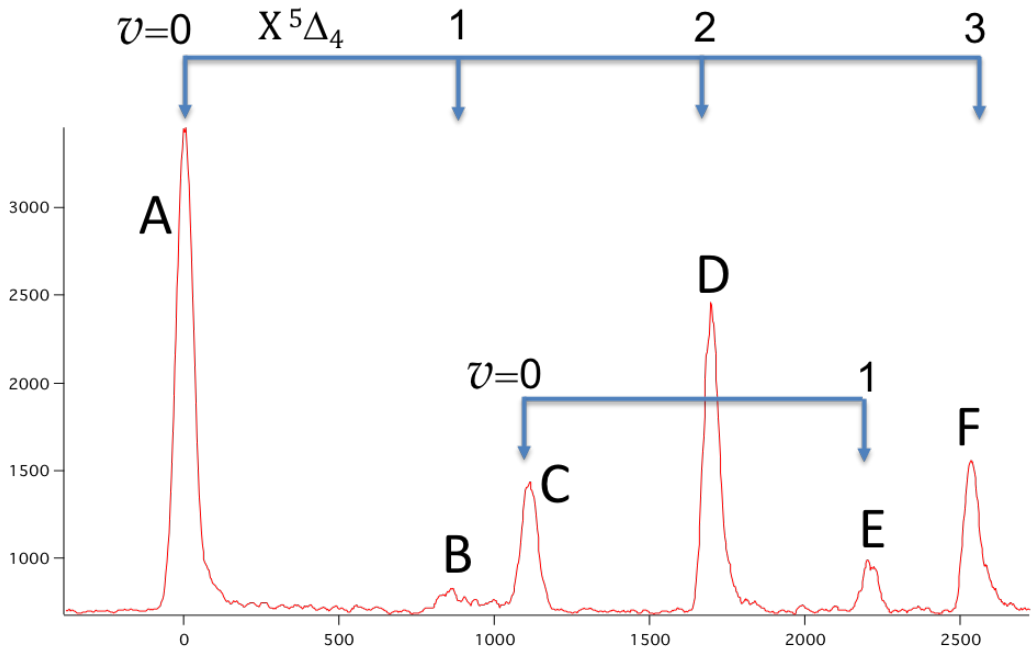

Figure 6.4 Dispersed fluorescence spectrum of the 1-0 band of the [18.1] 4 → $X^5\Delta_4$ transition of RuO.

6.3 High-resolution data: further confirmation that the ~530 nm band is from the RuO molecule

Table 6.2 shows the result of preliminary rotational numbering and combination difference analysis for the upper state of the 1-0 band of the [18.1] 4 $\rightarrow X^5\Delta_4$ transition of the ^{102}RuO molecule. This was done before the band's carrier was definitively identified. As can be seen, the rotational constants for the lower and upper states are different than those of RuF. Also, note that the rotational quantum numbers are not half-integer as was the case for RuF. This is because the ruthenium atom has 44 electrons and oxygen has eight electrons resulting in a total even number of 52. The values of the rotational constants are similar to those reported previously for the RuO molecule [1, 2]. Therefore, the band can be conclusively assigned to RuO. A Loomis-Wood plot of the band for the most abundant isotopologue of ruthenium monoxide, ^{102}RuO, is shown in Figure 6.5. Line lists required to perform the rotational analysis were extracted from the Loomis-Wood plot and are given in Tables 6.2 and 6.3.

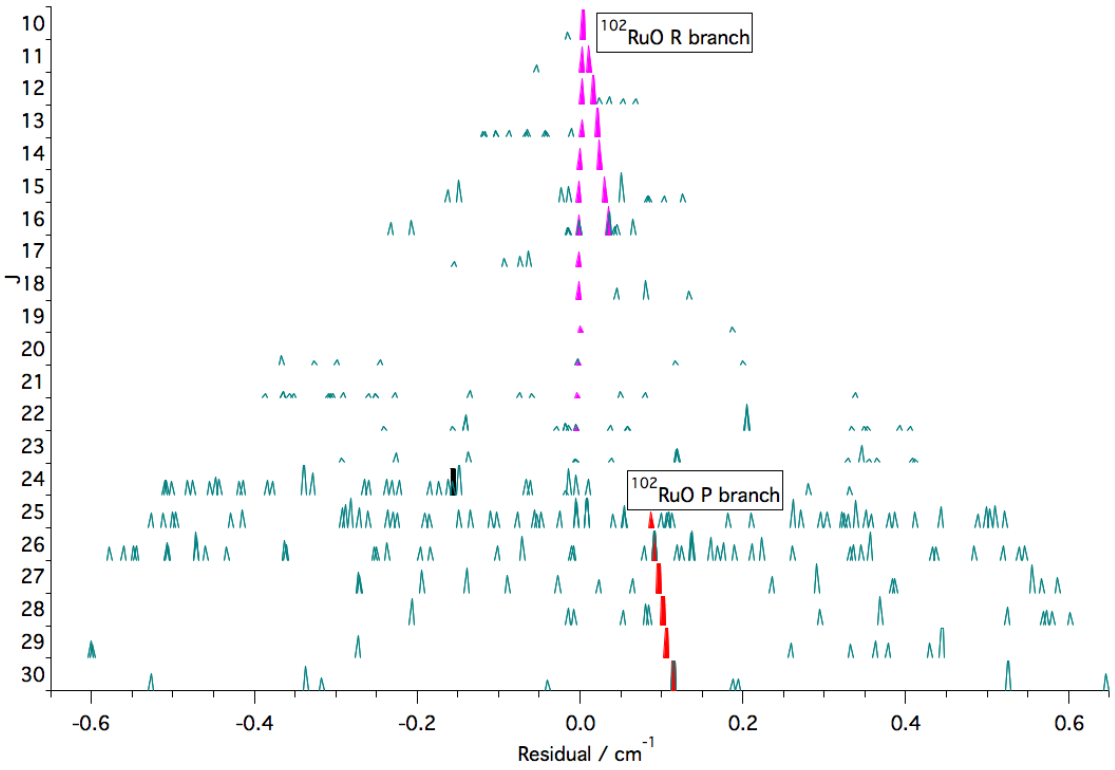

Figure 6.5 A Loomis-Wood plot of selected series of the ^{102}RuO molecule.

Tables 6.2 and 6.3 illustrate the combination differences for the upper and ground states. The consistent B values for the states show that the rotational assignments are correct. From the combination differences, the B constants were calculated to be ~ 0.3779 and 0.4124 cm^{-1} for the upper and lower states respectively. These values were then considered as initial input for fitting and simulating the spectrum.

Table 6.2 Rotational numbering and combination difference analysis for the upper state of the 1-0 band of the [18.1] $4 \rightarrow X^5\Delta_4$ transition of ^{102}RuO.

J	P(J) / cm^{-1}	R(J) / cm^{-1}	$\Delta F_2'$ / cm^{-1}	B′ / cm^{-1}
4		18874.2364		
5	18866.33353	18874.64856	8.31503	0.377955
6	18865.16365	18874.9896	9.82595	0.377921
7	18863.92493	18875.26572	11.34079	0.378026
8	18862.61601	18875.47038	12.85437	0.378069
9	18861.24265	18875.60588	14.36323	0.377979
10	18859.79744	18875.67055	15.87311	0.377931
11	18858.28443	18875.67055	17.38612	0.377959
12	18856.69903	18875.59716	18.89813	0.377962

Table 6.3 Rotational numbering and combination difference analysis for the lower state of the 1-0 band of the [18.1] 4 $\rightarrow X^5\Delta_4$ transition of ^{102}RuO.

J	P(J) / cm^{-1}	R(J) / cm^{-1}	$\Delta F_2''$ / cm^{-1}	B″ / cm^{-1}
4		18874.2364		
5	18866.33353	18874.64856	9.07275	0.412397
6	18865.16365	18874.9896	10.72363	0.412447
7	18863.92493	18875.26572	12.37359	0.412452
8	18862.61601	18875.47038	14.02307	0.412443
9	18861.24265	18875.60588	15.67294	0.412445
10	18859.79744	18875.67055	17.32145	0.412415
11	18858.28443	18875.67055	18.97152	0.412424
12	18856.69903	18875.59716		

The rotational analysis of the high-resolution data is consistent with J=4 in both the upper and lower states. Therefore, $\Omega'=\Omega''=4$ is in agreement with the assignment of $X^5\Delta_4$ in references [2] and [3]. Also, inspecting the high-resolution spectrum shows that the P and R branches are approximately of the same intensity suggesting a $\Delta\Omega=0$ transition and hence an upper state can be $^5\Delta_4$. In Figures 6.6 and 6.7 a portion of the P and R branch with the rotational numbering for ^{102}RuO is depicted.

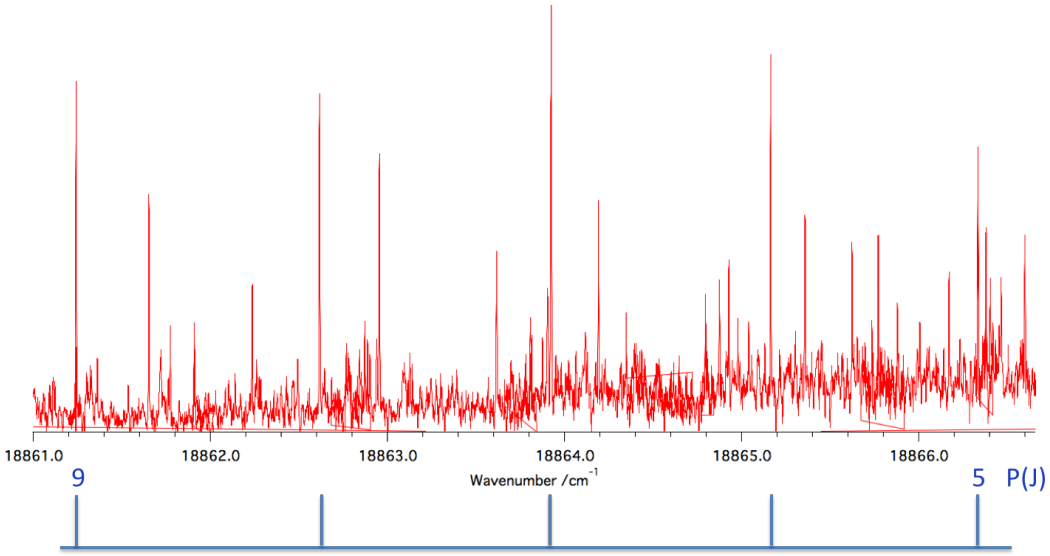

Figure 6.6 A portion of P branch for the 1-0 band of the [18.1] 4 → $X^5\Delta_4$ transition of ^{102}RuO. The first line of the P branch starts with J=5, i.e., P(5). For clarity, only the assigned lines of ^{102}RuO isotopologue are shown in the figure.

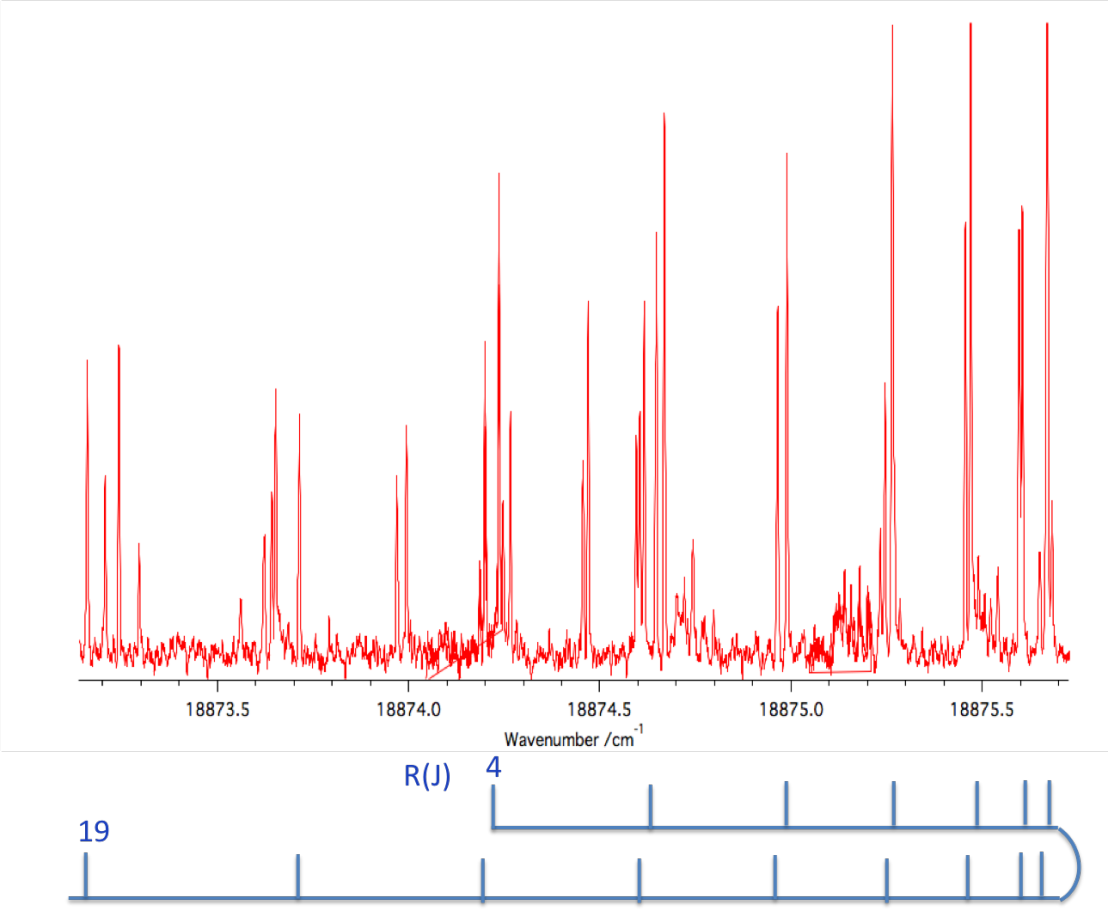

Figure 6.7 A portion of the R branch for the 1-0 band of the [18.1] $4 \rightarrow X^5\Delta_4$ transition of ^{102}RuO. The first line of the R branch is R(4), and the first lines of the P and Q branches are P(5) and Q(4) (not shown in picture), indicating that this band has $\Omega' = \Omega'' = 4$. For clarity, only the assigned lines of ^{102}RuO isotopologue are shown in the figure.

As can be seen in Figure 6.7, at first the lines in the R branch shift toward larger wavenumbers with increasing J while the spacing between them is decreasing. This trend continues until they reach a specific rotational quantum number J^*. At J^*=10 the R branch forms a band head, and the wavenumber of the rotational lines decreases with increasing

angular momentum. Knowing the quantum number at which the band forms a head is beneficial to its assignment.

In Figure 6.8 the rotational structure of the electronic transition for the P, Q and R branches of the [18.1] 4 → $X^5\Delta_4$ transition of ^{102}RuO is shown. This plot a representation of experimental data that shows the trends observed in different branches. Figure 6.8 is an example of a Fortrat diagram [4], and clearly illustrates the Fortrat parabola in the R branch indicating the formation of a "band head" in the branch.

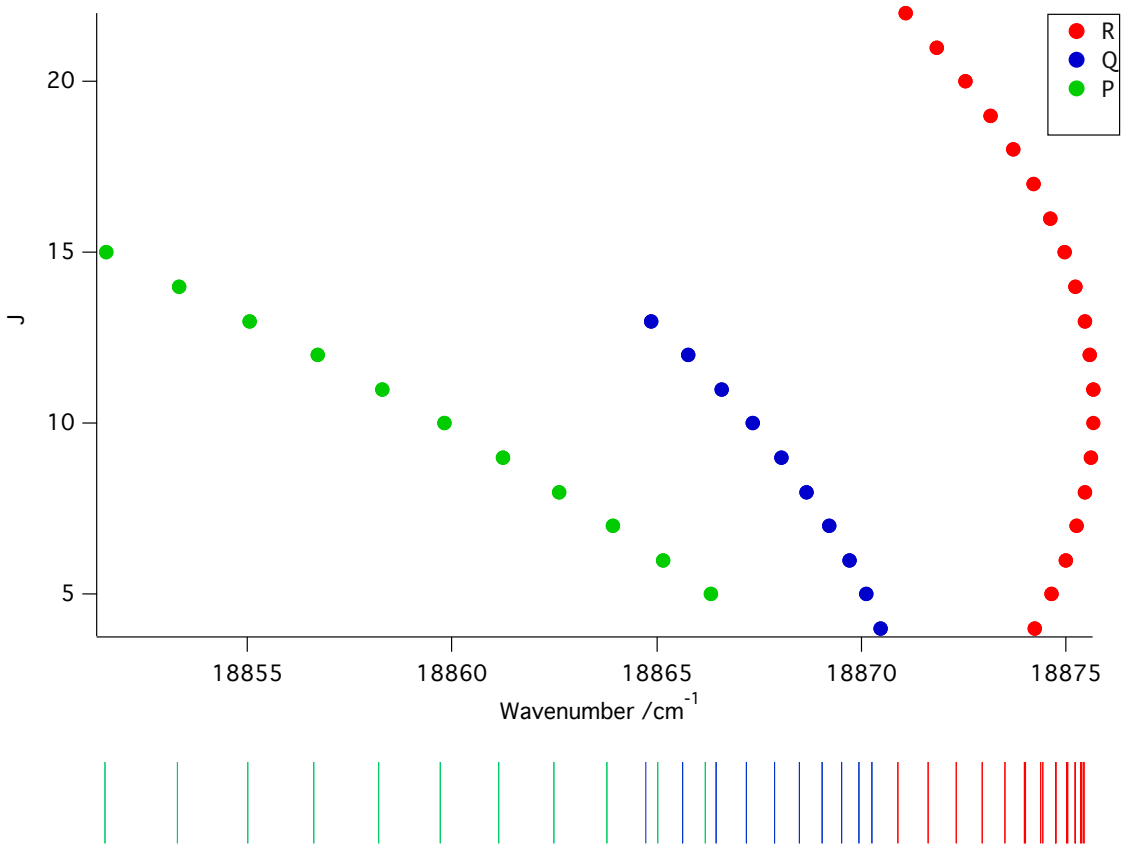

Figure 6.8 The Fortrat diagram for the 1-0 band of the [18.1] 4 → $X^5\Delta_4$ transition of ^{102}RuO.

Figure 6.9 shows the high-resolution spectrum of the R region with isotopic structure and the band heads for five isotopologues of RuO, i.e., ^{104}RuO, ^{102}RuO, ^{101}RuO, ^{100}RuO and ^{99}RuO that were identified from the assignments. Note that the ^{99}RuO and ^{101}RuO lines show clear hyperfine structure. This hyperfine structure is further depicted in Figure 6.10 and will be discussed in the next section.

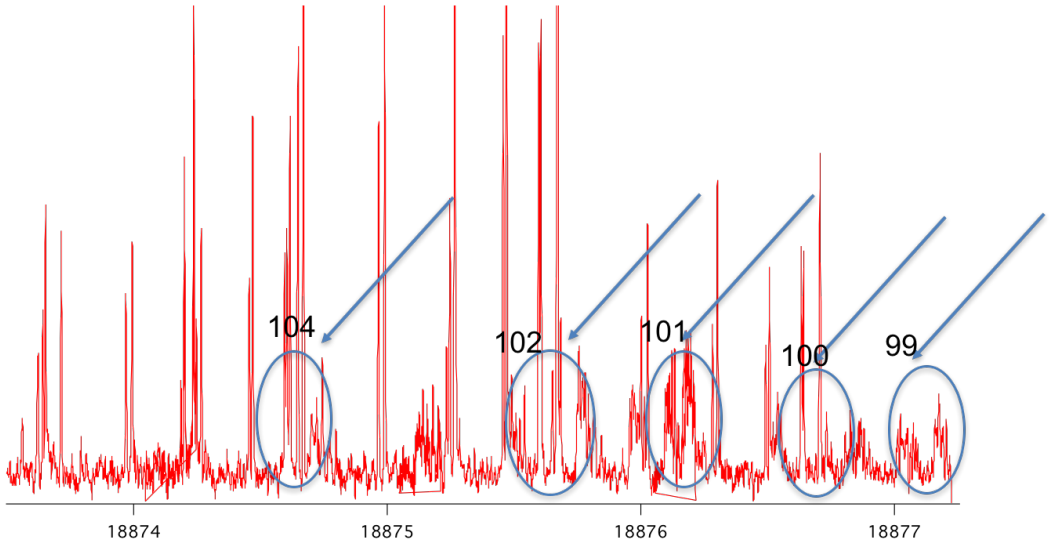

Figure 6.9 The high-resolution spectrum of the R region with isotopic structure and the band heads of different isotopologues of RuO.

6.4 Discussion

The band studied in the present work is the 1-0 vibration of the [18.1] 4–$X^5\Delta_4$ system, the levels of which were deduced by Wang et al. [2] as these authors did not observe the 1-0 band directly. This transition was also seen by Scullman and Thelin [1]. Neither of the previous experiments resolved the isotopic structure.

There was a discrepancy about the symmetry of the ground state of RuO in the literature. In reference [3] the emission spectrum of the RuO molecule was studied and the ground state of the molecule was found to be $^3\Sigma^+$. Also, the bond length was measured to be 1.70Å. In reference [5] the ground state of RuO was predicted to be $^5\Delta$. In reference [2] RuO was made in a laser ablation molecular source by reacting laser ablated Ru atoms with N_2O entrained at 6% in Ar at the total pressure of 6 atm. The apparatus used for the experiment was similar to the one at UNB (described in chapter 3) and four band systems were observed in the 545 nm to 640 nm spectral range. The ground state of RuO was determined to be $X^5\Delta_4$ and nine vibrational bands belonging to the [18.1] 4–$X^5\Delta_4$, [16.0] 5–$X^5\Delta_4$, [18.1] 3–$X^5\Delta_3$, and [15.8] 4–$X^5\Delta_3$ systems were detected. The equilibrium bond length was measured to be 1.714Å. As a result, the ground state was determined to be $^5\Delta_4$ as theoretically predicted [5]. Note that extensive isotopic and also hyperfine structure of this molecule were uncovered during the present study of this molecule. This will be discussed further below.

6.5 Analysis

As can be seen from the dispersed fluorescence spectrum (see Figure 6.4), two vibrational progressions can be identified. The ground state vibrational frequency occurs at ~865 cm^{-1} which is in good agreement with the value reported in reference [2]. Further progression of this vibration can be observed at ~ 1700 and 2532 cm^{-1}. Another peak can also be observed at ~ 1110 cm^{-1} in the DF spectra. This indicates the presence of a low-lying electronic with the vibrational frequency of ~ (2206-1110) = 1096 cm^{-1}.

Pgopher [10] was used to fit the experimental data to an R^2 Hamiltonian (see section 2.9). The T, B and D that were chosen were adequate to simulate the rotational energy level structure of the molecule. The hyperfine structure associated with ^{101}RuO isotopologue will be discussed the next section. The result of the fits to the high-resolution data is given in Table 6.4. The molecular constants for the ground and excited states are given for five isotopologues of RuO namely: ^{102}RuO, ^{104}RuO, ^{100}RuO, ^{99}RuO and ^{101}RuO. ^{98}RuO was too weak to be analyzed and the data for ^{96}RuO was incomplete since the R branch was not covered during the scans. As can be seen from the results presented in Table 6.5, the rotational constants for each molecule are slightly different from that of the other. This is due to the difference in the reduced mass between different isotopologues which causes the rotational constants to vary slightly. This results in a different rotational energy pattern and also band origin for the isotopologues.

Table 6.4 Molecular constants for ^{102}RuO, ^{104}RuO, ^{100}RuO, ^{99}RuO and ^{101}RuO.

State	Isotopologues	T / cm^{-1}	B / cm^{-1}	D / 10^{-7} cm^{-1}	*a* / 10^{-3} cm^{-1}
$X^5\Delta_4$	^{102}RuO		0.4125213(217)	6.047(704)	
	^{104}RuO		0.4113404(218)	2.059(714)	
	^{100}RuO		0.4136356(191)	4.550(570)	
	^{99}RuO		0.4143051(184)	1.630(284)	
	^{101}RuO		0.4130660(600)	0	-15.28(41)
[18.1] 4	^{102}RuO	18870.66450(24)	0.3780573(199)	5.710(582)	
	^{104}RuO	18869.67888(30)	0.3769632(199)	2.042(588)	
	^{100}RuO	18871.68716(28)	0.3790822(173)	4.647(468)	
	^{99}RuO	18872.19858(34)	0.3796895(170)	1.223(252)	
	^{101}RuO	18871.17406(15)	0.3785518(58)	0	-4.04(41)

The rms error for the fits for the ^{102}RuO, ^{104}RuO, ^{100}RuO,^{99}RuO and ^{101}RuO molecules is 0.0011, 0.0012, 0.0011, 0.0017 and 0.0014 cm^{-1} respectively. The number in parentheses represents standard deviation in the particular parameter.

Table 6.5 shows the ratios of the rotational constants for the ground and excited states and the ratios of the corresponding reduced masses of isotopologues. The results are all isotopically consistent. This serves as a confirmation of the correct assignments of each isotopologue. The values of the spin-orbit parameter A were set to -1000 cm^{-1} [2] for both

the upper and lower states in the fit to get the correct band origin. This is due to the way Pgopher [10] calculates the band origin, i.e., the energy gap between the middle of the spin-orbit levels for the lower and upper states (see Figure 2.14). If different values of A were used for calculating the energies of the lowest spin-orbit levels of the lower and upper electronic states a different value for the band origin would be calculated by Pgopher.

Table 6.5 Comparison of the ratios of reduced masses as obtained from nuclear data and spectral analysis.

State	B_{102}/B_{104}	B_{100}/B_{104}	B_{100}/B_{102}	B_{99}/B_{101}
$^5\Delta_4$	1.0028	1.0055	1.0027	1.0029
[18.1] 4	1.0029	1.0056	1.0027	1.0030
$^1\mu^*/\mu$	1.0026	1.0053	1.0027	1.0027

[1] * indicates the heavier isotope

6.6 Hyperfine analysis

In the high-resolution spectrum, the 99 and 101 isotopologues of RuO exhibit hyperfine structure. In the R region, a head is formed in which rotational lines lie close to each other. Since both odd ruthenium isotopes have a nuclear spin of 5/2 and ^{16}O has a nuclear spin of 0, each rotational line is split into 6 components. Figure 6.10 shows the experimental and simulated spectra of the band head region of ^{101}RuO at ~ 18876.2 cm^{-1}. There are two pairs of rotational lines of ^{101}RuO from ~ 18876.10 to 18876.22 cm^{-1}.

R(10) and R(11) lie from ~ 18876.16 to 18876.22 cm^{-1} and R(9) and R(12) lie from ~ 18876.10 to 18876.15 cm^{-1}. Note that this is a very congested region in the spectrum. Resolving all the hyperfine lines requires more resolution. However, the fit to the hyperfine data is robust and the molecular constants for ^{101}RuO are given in Table 6.4 where the quality of the fit can be assessed by the rms error of 0.0014 cm^{-1}.

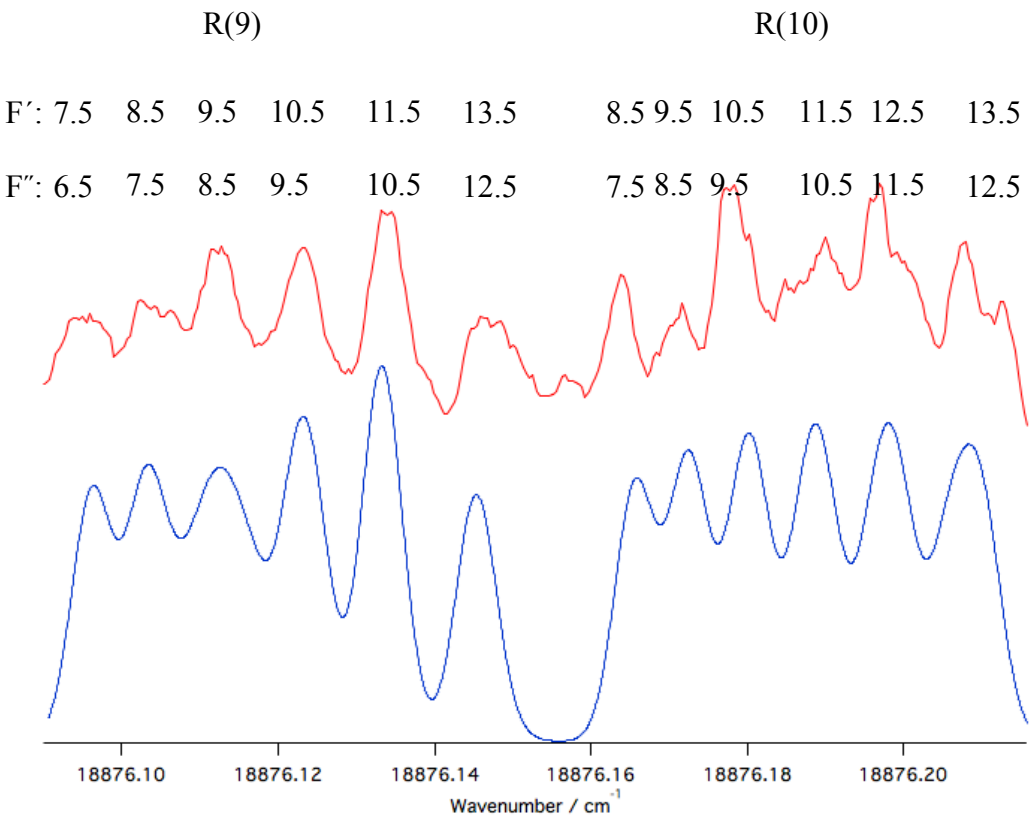

Figure 6.10 The upper trace is the band head region for the ^{101}RuO isotopologue for the 1-0 band of the [18.1] 4 → $X^5\Delta_4$ transition and the lower trace is the simulated spectrum. There are four nearly coincident R-clusters close to one another; the assignments are for R(9) and R(10).

The Frosh and Foley parameters [6] discussed in chapter two are calculated for both the ground and excited states to describe the hyperfine interactions within the RuO molecule. Morton and Preston [7] calculated the atomic parameters for several elements in the periodic table. The $< r^{-3} >$ and $\psi(0)^2$ values for ruthenium are calculated to be 6.145 a.u^{-3} and 6.085 respectively. For ^{101}Ru: I=5/2, μ=-0.7188μ_N, g_N=-0.2876μ_N, and for ^{99}Ru: I=5/2, μ=-0.6413μ_N, g_N=-0.2564μ_N [8]. Since the hyperfine structure is better resolved in ^{101}RuO compared to ^{99}RuO, only the values associated with ^{101}Ru will be used in the equations below for analysis. In Figure 6.11 the molecular orbital energy level diagram of RuO is depicted [2].

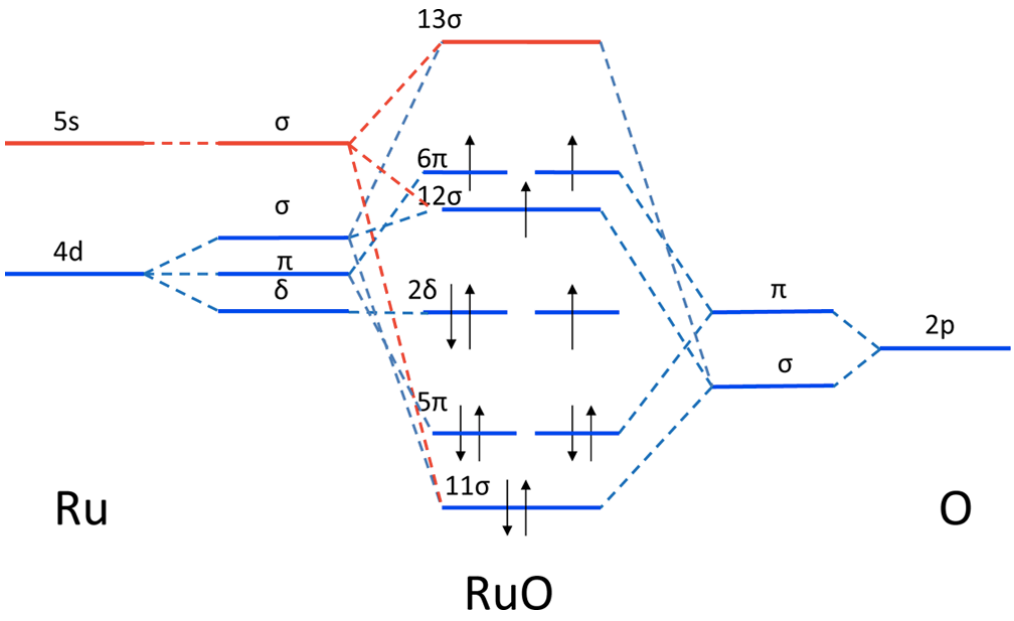

Figure 6.11 RuO molecular orbital energy level diagram taken from reference 2.

As proposed by N. Wang et al. [2], the ground and excited states of RuO arise from the $\delta^3\sigma^1\pi^2$ electronic configuration. For the $X^5\Delta_4$ state, the hyperfine parameter (see equation

4.1) $h = 2a + 2(b + \frac{2}{3}c)$ and the *a*, *b* and *c* constants in the hyperfine parameter *h* can be calculated from equations 2.119. These equations can be rewritten as

$$a = 95.412 g_N \frac{1}{\Lambda} \langle \Lambda | \sum_i \frac{l_{z_i}}{r_i^3} | \Lambda \rangle \tag{6.1}$$

$$b = 799.328 g_N \frac{1}{\Sigma} \langle \Lambda\Sigma | \sum_i s_{z_i} \delta_i(r) | \Lambda\Sigma \rangle \tag{6.2}$$

$$c = 143.119 g_N \frac{1}{\Sigma} \langle \Lambda\Sigma | \sum_i s_{z_i} \frac{(3\cos^2\theta - 1)}{r_i^3} | \Lambda\Sigma \rangle \tag{6.3}$$

For the ^{101}Ru isotope *a* and *b* are calculated to be *a*=-0.00562 and *b*=-0.0116 cm^{-1}. The $\langle 3\cos^2\theta - 1 \rangle$ term in the *c* constant for $4d\sigma, 4d\pi, 4d\delta$ and $5s\sigma$ electrons is calculated to be 4/7, 2/7, -4/7 and 0 respectively. Then the calculated values for *c* are -0.0012 and 0 for $4d\sigma$ and $5s\sigma$ respectively. If we assume that the RuO 12σ orbital is primarily due to the Ru $4d\sigma$ electron then *h*= -0.0129 cm^{-1}. However, if it is mostly due to Ru $5s\sigma$ then *h*=-0.0346 cm^{-1}. For the fitting purposes the hyperfine parameter *h* can be converted to an effective *a* constant, i.e., $h \equiv a\Lambda$, which will have the values of -0.0173 cm^{-1} and -0.00643 cm^{-1} for 5*s* and 4*d* electrons. From the fit, the effective *a* value was determined to be -0.01528 and -0.00404 cm^{-1} for the ground and excited states respectively. The agreement with calculation is promising. This indicates that the σ orbital in the ground and excited states is mostly 5*s* and 4*d* respectively.

6.7 Isotopic analysis

The energy gap between the two minima of two potential curves of different electronic states is represented by T_e. This quantity can be calculated if the rotational Hamiltonian is expressed in terms of R^2 (see chapter 2). A scaling parameter for the isotopologues can be defined as the square of the ratio of the reduced mass of the ^{102}RuO molecule to that of the other isotopologues, i.e., $\rho_i = \sqrt{\frac{\mu_{102}}{\mu_i}}$ [9]. We can rewrite equations 2.65 and 2.105 for equilibrium by substituting $\rho_i\omega_e$, $\rho_i^2\omega_e\chi_e$ and $\rho_i^2 B_e$ for ω, $\omega_e\chi_e$ and B respectively to obtain expressions for the vibration and rotation energy of isotopic molecules [9]. Then in terms of these parameters the rovibronic energy can be written as

$$E_i = T_e + [\rho_i\omega_e(v+\frac{1}{2}) - \rho_i{}^2\omega_e\chi_e(v+\frac{1}{2})^2] + \rho_i{}^2 B_e \langle \varepsilon vr | R^2 | \varepsilon vr \rangle \qquad (6.4)$$

where T_e is the pure electronic energy and $|\varepsilon vr\rangle$ represents the electronic, vibrational and rotational eigenstate. The matrix elements of the last term can be expanded as [11]

$$\langle \varepsilon vr | R^2 | \varepsilon vr \rangle = J(J+1) + \Lambda^2 + S(S+1) - 2\Omega\Sigma - 2\Omega\Lambda + 2\Lambda\Sigma + \langle L_x^2 + L_y^2 \rangle \ . \qquad (6.6)$$

Then, for the 1-0 band of the [18.1] $4 \rightarrow X^5\Delta_4$ transition we find

$$T_{1-0} = T_e' + \frac{1}{2}[\rho_i(3\omega_e' - \omega_e'')] - \frac{1}{4}[\rho_i^2(9\omega_e'\chi_e' - \omega_e''\chi_e'')] + \rho_i^2[B_e'\langle L_x^2 + L_y^2\rangle' - B_e''\langle L_x^2 + L_y^2\rangle'']$$

(6.7)

which can be rearranged as

$$T_{1-0} - \frac{1}{2}[\rho_i(3\omega_e' - \omega_e'')] + \frac{1}{4}[\rho_i^2(9\omega_e'\chi_e' - \omega_e''\chi_e'')] = T_e' + \rho_i^2[B_e'\langle L_x^2 + L_y^2\rangle' - B_e''\langle L_x^2 + L_y^2\rangle'']$$

(6.8)

If the left hand side of the above equation is denoted by T_e then a "reduced band origin" is found to be

$$T_e = T_{1-0} - \frac{1}{2}[\rho_i(3\omega'_e - \omega''_e)] + \frac{1}{4}[\rho_i^2(9\omega'_e\chi'_e - \omega''_e\chi''_e)] \qquad (6.9)$$

The values for T_e can now be calculated from the above relation. For calculating T_e, the values of $\omega''_e = 866.64$, $\omega'_e = 794.08$, $\omega''_e\chi''_e = 5.41$, and $\omega'_e\chi'_e = 4.45$ cm^{-1} taken from the literature [1, 2] were used. The results of the reduced mass, the scaling parameter, the band origins T_{1-0} and T_e for the different isotopologues are summarized in Table 6.6.

Table 6.6 The results of the calculation of T_e for different isotopologues of RuO.

Isotopologue	μ	ρ	T_{1-0} / cm^{-1}	T_e / cm^{-1}
104	13.86423305	0.998692487	18869.67888	18121.50708
102	13.82800143	1	18870.66450	18121.52450
101	13.80945365	1.000671336	18871.17406	18121.53700
100	13.79053674	1.001357426	18871.68716	18121.54203
99	13.77134988	1.002054752	18872.19858	18121.53711

The results in Table 6.7 clearly show that T_e is nearly independent of isotopologue while T_{1-0} depends on the isotopologue involved. The values for T_e are almost identical, i.e., the deviation is $\sim 0.04 cm^{-1}$. This confirms that all the information extracted for the molecule including rotational constants, vibrational frequencies for the upper and lower states,

vibrational assignments of the band, and also the band origin for the different isotopologues are correct. In Figure 6.12 the reduced band origins are plotted against ρ_i^2 where the index i corresponds to the isotopologues in which the ruthenium atom has no nuclear spin, i.e., ^{102}RuO, ^{104}RuO and ^{100}RuO. As can be seen, the resulting graph is linear.

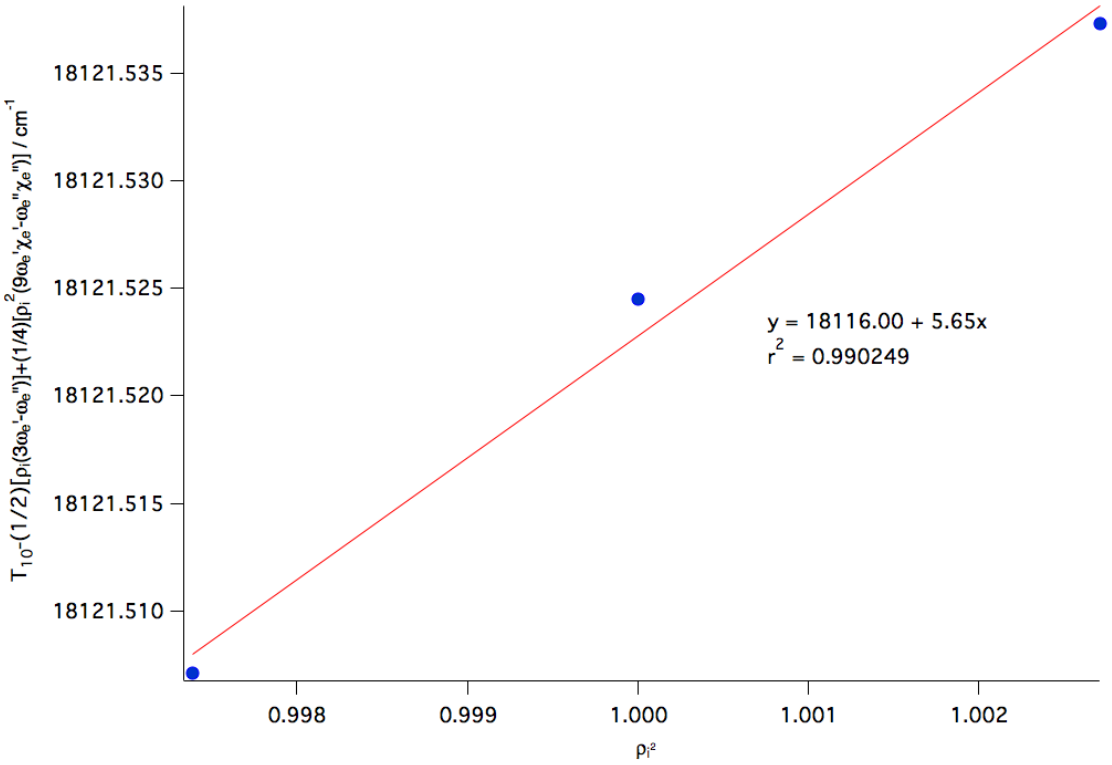

Figure 6.12 The graph of reduced band origins versus the scaling parameter for ^{102}RuO, ^{104}RuO and ^{100}RuO isotopologues.

The intercept and the slope of the graph are 18116.00(56) and 5.65(56) cm^{-1} respectively (see equation 6.8). The intercept represents the pure electronic energy and the slope is

proportional to the difference of the expectation value of the $L_x^2 + L_y^2$ operator for the upper and lower states, i.e., $B'\left\langle L_x^2 + L_y^2 \right\rangle' - B''\left\langle L_x^2 + L_y^2 \right\rangle''$.

6.8 Comparison of the ground state parameters of RuO, RuF and RuCl

Table 6.7 presents a comparison of the rotational constants, bond lengths, vibrational frequencies and the force constants of the RuO, RuF and RuCl molecules in their ground states. These are based on the results from chapters 4, 5 and 6 of the thesis. Generally, when moving from left to right and from top to bottom in the periodic table of the elements, in similar diatomic molecules such RuO, RuF and RuCl there is an increase in the bond distances. Therefore, bond strengths should decrease. This is due to the fact that the bond distances increase with mass and hence the vibrational frequency and force constant should decrease. This trend is observed in Table 6.7.

Table 6.7 Ground state parameters of RuO, RuF and RuCl.

Parameters	B (cm^{-1})	r (A)	ω_e (cm^{-1})	K (N/m)
RuO	0.412	1.71	859	600
RuF	0.286	1.91	550	285
RuCl	0.122	2.25	352	186

6.9 Concluding remarks

The work described in this chapter presents the first observation of different isotopologues of RuO in the 1-0 band of the [18.1] $4 \rightarrow X^5\Delta_4$ transition of RuO. Two progressions from the ground and a low-lying excited states can also be observed from the DF. The results of the dispersed fluorescence analysis shows the vibrational frequency of the ground state is ~ 865 cm^{-1} which is consistent with the previous measurements. There is an indication of the presence of a low-lying electronic state at ~ 1110 cm^{-1} which has a vibrational frequency of ~ 1096 cm^{-1}. The results of the rotational analysis confirms the lower electronic state as $^5\Delta_4$. The average B values for the ground and excited states are ~ 0.4129 and ~ 0.3784 cm^{-1} respectively. The results reported in reference [2] are in agreement with the more accurate values of the present work. Some hyperfine structure due to the nuclear spins of ^{101}Ru and ^{99}Ru were also observed for the first time in the spectra and were analyzed. The effective *a* values determined from the fit for the ground and excited states of RuO are in agreement with the those obtained from the calculations. This confirms that the σ orbital in the ground and excited states is mostly 5*s* and 4*d* respectively. The pure electronic energy and the differences of the expectation values of the $L^2_x+L^2_y$ operator for the upper and lower states were also calculated.

References

1. R. Scullman, B. Thelin, J. Mol. Spec. **56**, 64 (1975).

2. N. Wang, Y. W. Ng, A. S.-C. Cheung, J. Phys. Chem. A **117**, 13279 (2013).

3. V. Raziunas, J. Macur, S. Katz, J. Chem. Phys. **43**, 1010 (1965).

4. P. F. Bernath, Spectra of Atoms and Molecules, New York: Oxford University Press Inc., 1995.

5. Krauss, J. Stevens, Chem. Phys. **82**, 5584 (1985).

6. R. A. Frosch, H. M. Foley, Phys. Rev. **88**, 1 (1952).

7. J. R. Morton, K. F. Preston, J. Mag. Res. **30**, 577 (1978).

8. J.M. Brown, A. Carrington, Rotational Spectroscopy of Diatomic Molecules, Cambridge University Press, 2003.

9. G. Herzberg, Molecular Spectra and Molecular Structure, I. Spectra of Diatomic Molecules, D. Van Nostrand Company, Inc, 1950.

10. C. M. Western, J. Quant. Spectrosc. Radiat. Transfer **186**, 221 (2017).

11. C. M. Western, Pgopher, a program for simulating rotational, vibrational and electronic spectra, http://pgopher.chm.bris.ac.uk.

Chapter 7

Introduction to the ring molecules (catechol, pyrrole, furan), and experimental techniques at the CLS

7.1 Far-infrared spectroscopy at the Canadian Light Source

In addition to the laser-based experiments done at UNB, I also performed experiments at the Canadian Light Source synchrotron in Saskatoon, Sask., and analyzed some data previously taken there. These experiments allowed me to explore far-infrared spectra, in contrast to those done on ruthenium-bearing molecules in the visible region. The far-infrared rotation-vibration spectra were of polyatomic molecules and therefore required different approaches to the analysis than I had employed for the transition metal diatomics described previously. In this chapter, I will describe the molecules that I studied and the way that experiments were conducted at the CLS. Specific analyses of the molecules will be given in subsequent chapters.

7.2 Introduction to the ring molecules

In this section of the thesis an introduction to the three ring molecules, i.e., pyrrole, furan and catechol that are studied is given. The potential application of these systems and the motivation for selecting these molecules are also discussed.

7.2.1 Pyrrole and furan

Pyrrole and furan with chemical formulas of C_4H_5N and C_4H_4O respectively are two planar five-membered ring molecules. The structures of pyrrole and furan have been depicted in Figures 9.1 and 10.1. These molecules have been extensively studied both experimentally and from first principles [1, 2, 3, 4]. These molecules have dense spectra but with the advent of modern high-resolution techniques their rotational structure is resolvable.

The interest in these molecules is partly due to their possible detection in the interstellar medium [5]. Therefore, investigating them in the laboratory in turn helps broaden the related astrophysical studies. They have also some applications in the pharmaceuticals industry [6, 7]. Furan can also be produced from natural processes such as forest fires [8]. Therefore, detecting it in air may provide information about natural forest fires that might have happened in the environment.

Five-membered ring molecules can also be considered as a prototype for studying larger systems. These systems, such as isoindole, isobenzofuran and furothienopyrrole, can be made by fusing two or more heterocyclic compounds. Therefore, the principles and the method of analysis used to study these molecules can be applied to the larger molecular systems.

Furthermore, far-infrared synchrotron light is useful in collecting the spectra of medium size molecules such as pyrrole, furan and catechol. Collecting the spectra of these molecules with conventional sources such as lamps would take a very long time. To take high-resolution spectra we need to use a small aperture. If we use lamps we need to reduce the aperture size which greatly reduces the available light. However, synchrotron naturally produces a highly collimated bright beam of light that can pass through narrow apertures without significant loss to achieve high resolution.

7.2.2 Catechol and 1,4 benzenedithiol

Two other ring molecules that I wanted to study in this thesis were 1,4 benzenedithiol, $C_6H_4(SH)_2$, and 1,2-dihydroxybenzene, $C_6H_4(OH)_2$, also known as catechol. To construct the molecular structure of these systems we start by considering a benzene ring the structure of which is shown in Figure 7.1. As shown in Figure 7.2 if we take the benzene ring as the basis and substitute two neighboring H atoms with two OH groups then the 1,2-dihydroxybenzene molecular system is constructed. Again, if we take the benzene ring and this time substitute the two H atoms with SH groups at opposite sides 1,4 benzenedithiol is made (see Figure 7.2).

The catechol molecule was chosen to be studied prior to 1,4 benzenedithiol for two reasons. First, literature suggests that it has higher vapor pressure at room temperature [9, 10] compared to 1,4 benzenedithiol. Hence, it is easier to study on the far-infrared beamline. Second, its moments of inertia are smaller than those of 1,4 benzenedithiol.

This means that at the end we will be dealing with less congested spectra and therefore the rotational analysis will be more straightforward.

The interest to study thiolated (sulfur bearing) ring molecules stems from the fact that these systems have the potential to form the building blocks of future electronics also known as “molecular electronics”.

Molecular electronics is an emerging branch of solid state physics and chemistry that could revolutionize conventional silicon based electronic devices. Figure 7.3 shows how a single molecule is suspended between two electrodes to make such devices. The sulfur-bearing ring molecules like 1,4 benzenedithiol, 1,4 benzenedimethanethiol, 4,4 terphenyl dithiol (TPDT), etc. [11, 12, 13] are potential candidates to be used in molecule based electronics. If the two electrodes are made of silver or gold, the sulfur atoms will make strong contact with them, since in thiol-terminated moieties the sulfur atoms bind strongly to noble metals such as silver or gold [13].

Understanding the vibrational and structural properties of thiolated ring molecules such as 1,4 benzenedithiol may elucidate how single molecule devices work. There exist a family of molecules of thiolated ring molecules like 1,4 benzenedithiol that can be considered as potential candidates for future far-infrared projects. Therefore, a successful experiment on catechol can shed light on how to obtain the rotationally resolved spectra of 1,4 benzenedithiol in the future.

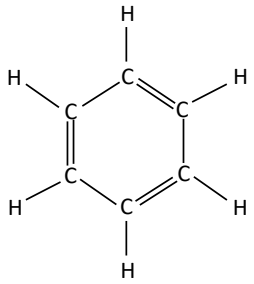

Figure 7.1 Molecular structure of benzene.

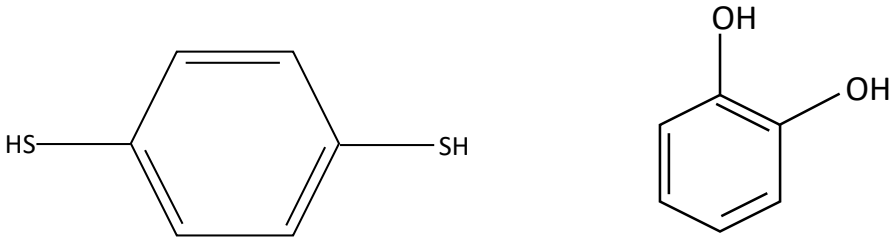

Figure 7.2 The molecules 1,4 benzenedithiol (left) and 1,2-dihydroxybenzene (catechol) (right) are illustrated.

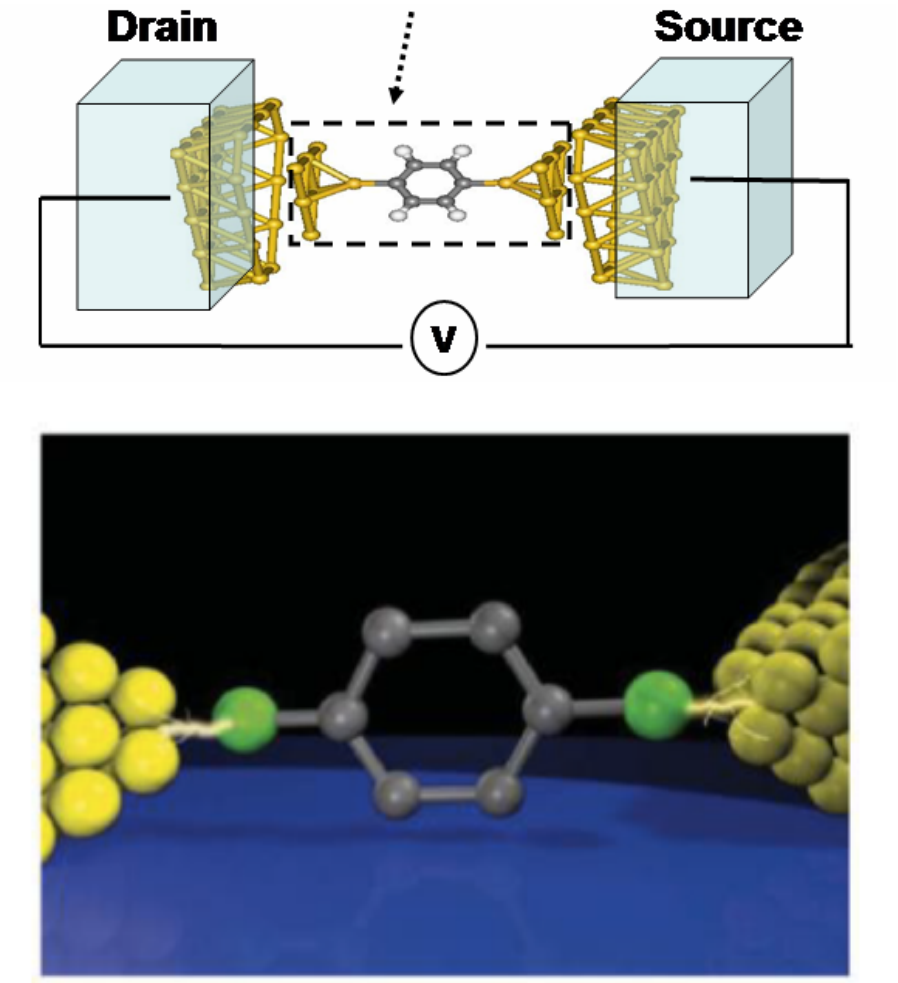

Figure 7.3 A single organic molecule that is connected to two electrodes [14, 15].

7.3 Experimental methods

Synchrotron radiation at the Canadian Light Source (CLS) was used to take the high-resolution spectra of the ring molecules. In analogy to the molecular-beam laser spectroscopy technique discussed in chapter 3, the probe laser beam is replaced by synchrotron radiation, the cold molecular beam produced in the apparatus is replaced by molecules in an absorption cell and the detection and data acquisition system is replaced by a Fourier transform spectrometer. A brief introduction of the method is presented below.

7.3.1 Synchrotron

The Canadian Light Source (CLS) is a third-generation synchrotron facility located at the University of Saskatchewan in Saskatoon, an overview of which is shown in Figure 7.4 [16].

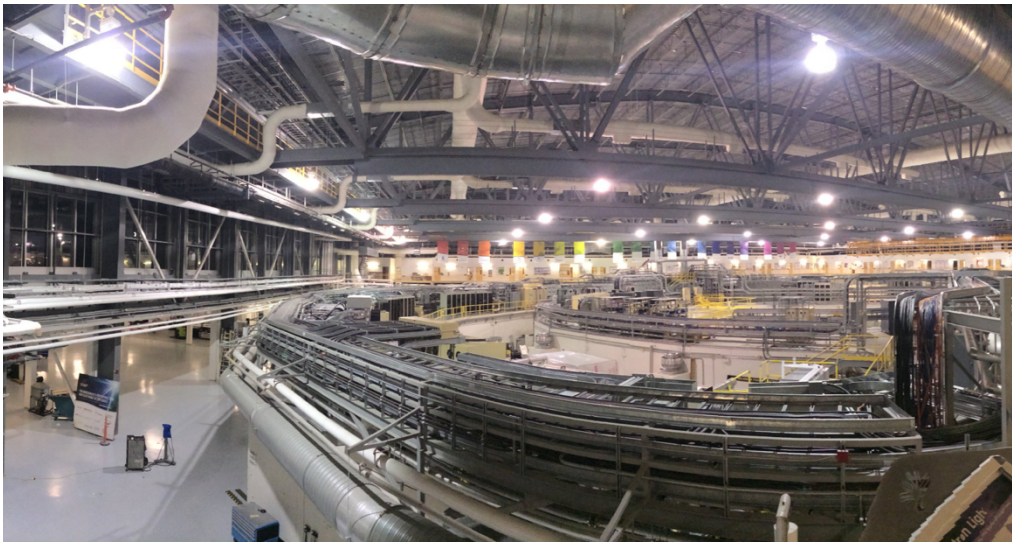

Figure 7.4 An overview of the synchrotron facility at the University Of Saskatchewan.

Figure 7.5 shows a schematic sequential diagram of different parts of the synchrotron.



Figure 7.5 Schematic diagram of different parts of the synchrotron.

In synchrotrons, electrons are created through thermionic emission in an electron gun. They are accelerated by a linear accelerator (LINAC) and reach speeds near that of light (see Figure 7.6). They enter the booster ring where they are further accelerated and get a boost in energy. The electrons now moving at 99.999998 % of the speed of light are injected into the storage ring where they circulate and produce synchrotron radiation whenever they are accelerated by bending magnets in the ring.

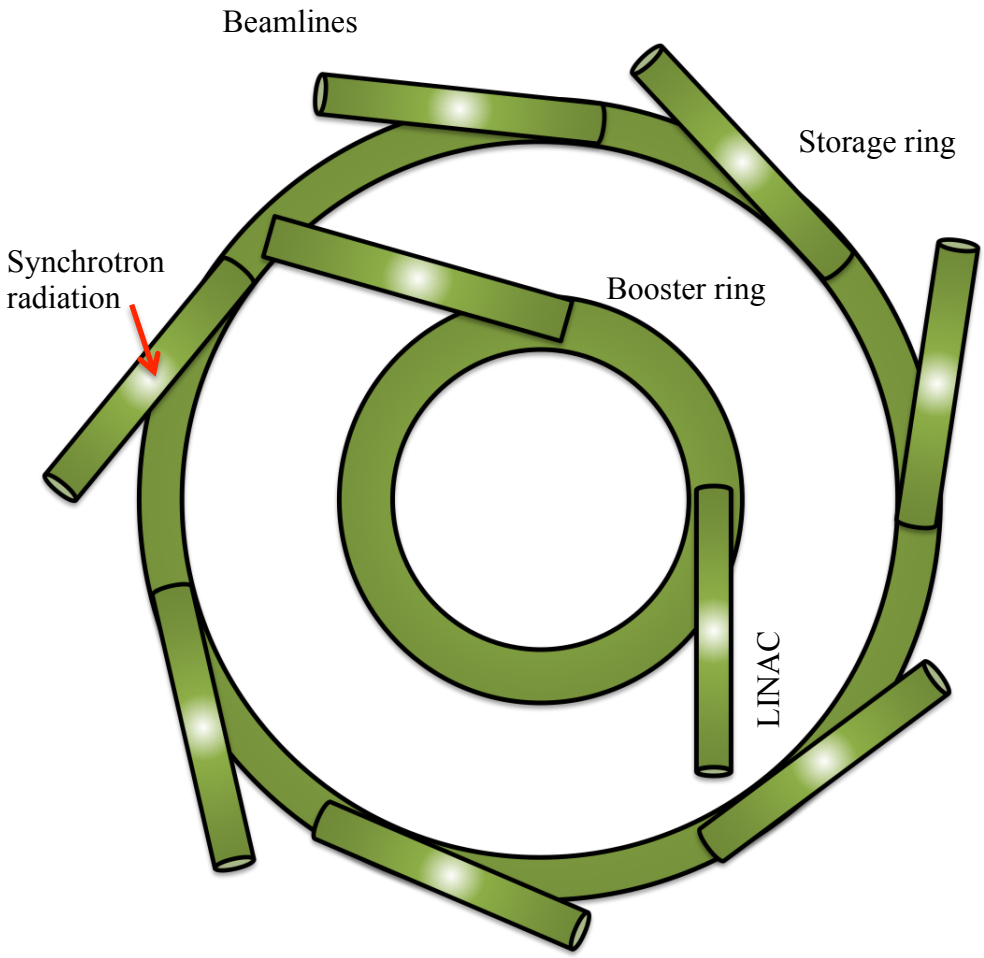

Figure 7.6 An overview of the synchrotron facility.

The basic principle of all accelerators is the interaction of the charged particles with static or dynamic electromagnetic fields [17].

According to classical theory of electromagnetism, accelerated charged particles radiate. If a particle with charge q and velocity $\vec{v}$ enters a region with electric and magnetic fields of $\vec{E}$ and $\vec{B}$, a Lorentz force $\vec{F} = q\vec{v} \times \vec{B} + q\vec{E}$ is exerted on the particle. The electric and magnetic fields can accelerate and deflect the charged particles.

To keep the electrons in circular orbit, bending magnets are used to deflect the electrons. Apart from the bending magnets, two types of insertion devices are placed around the straight sections of the storage ring, “wigglers” and “undulators” (weak wiggler). These are periodic magnetic arrays and generate broad and narrow spectral bands of synchrotron radiation, respectively.

7.3.2 Synchrotron radiation

Imagine an electron travelling in a circular path with curvature *R*, velocity $\vec{v}$ and the related acceleration $\dot{\vec{v}}$ at a specific point in time (see Figure 7.7).

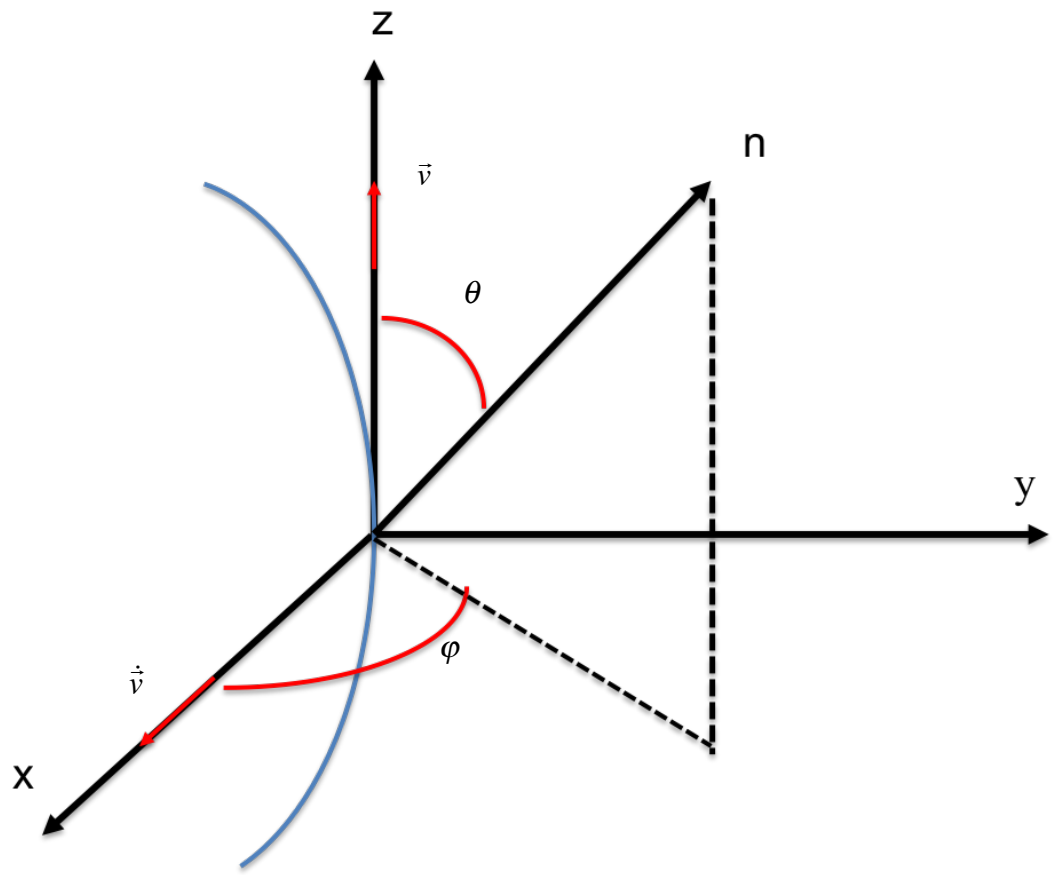

Figure 7.7 An electron in circular motion with velocity $\vec{v}$ and acceleration $\dot{\vec{v}}$.

The radiation emitted by this electron is given by [18]

$$\frac{dP}{d\Omega} = \frac{e^2}{4\pi c} \frac{\left| \hat{n} \times \{(\hat{n} - \vec{\beta}) \times \dot{\vec{\beta}}\} \right|^2}{(1 - \hat{n}.\vec{\beta})^5} \tag{7.1}$$

where $\hat{n} = \sin\theta\cos\phi\hat{i} + \sin\theta\sin\phi\hat{j} + \cos\theta\hat{k}$ and $\vec{\beta} = \frac{\vec{v}}{c}$.

By inserting $\hat{n}$ and $\vec{\beta}$ the equation transforms to [18]

$$\frac{dP}{d\Omega} = \frac{e^2\dot{v}^2}{4\pi c^3} \frac{1}{(1 - \beta\cos\theta)^3} [1 - \frac{\sin^2\theta\cos^2\phi}{\gamma^2(1 - \beta\cos\theta)^2}] \tag{7.2}$$

where $\gamma = \frac{1}{\sqrt{1-\beta^2}}$.

In synchrotrons electrons typically travel with speeds near that of light. If we plot the equation (7.2) for different values of β we will have a better sense of angular distribution of radiation at high speeds [19].

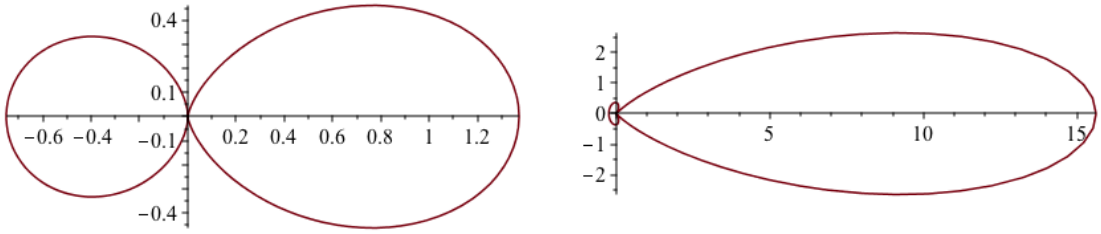

Figure 7.8 Angular distribution for $\beta = 0.1$ (left) and 0.6 (right). The electron acceleration is directed to the right in both Figures.

We see that at high speeds the radiation is tipping forward so as we increase the velocity to near that of light we will generate the synchrotron radiation.

The spectral distribution of synchrotron radiation in units of $\frac{e^2}{c}\gamma$ is given by [18]

$$I(\omega) = 2\sqrt{3}\frac{e^2}{c}\gamma\frac{\omega}{\omega_c}\int_{2\frac{\omega}{\omega_c}}^{\infty} K_{\frac{5}{3}}(x)dx \tag{7.3}$$

where e, c and $K_{\frac{5}{3}}(x)$ are the charge of electron, speed of light and a modified Bessel function and ω and $\omega_c = \frac{3\gamma^3 c}{2R}$ are the fundamental and critical frequency (beyond which there is negligible radiation). We have plotted equation 7.3 in Figure 7.9 which shows the synchrotron radiation spectrum plotted against $\xi = \frac{\omega}{\omega_c}$.

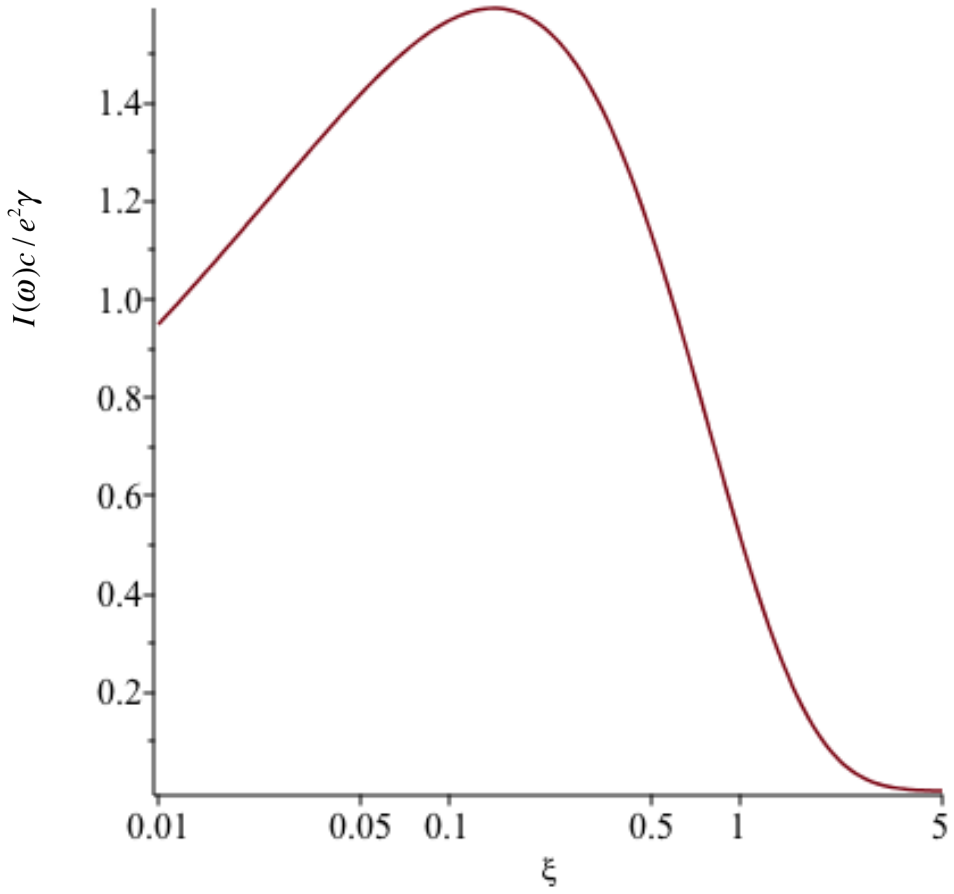

Figure 7.9 Synchrotron radiation intensity versus ξ, the radiated frequency normalized to ω_c.

The graph indicates the broad range of frequencies from infrared to X-rays, accessible with a synchrotron. The peak occurs at fundamental frequency ω where $\omega = 0.2858\omega_c$ and typically corresponds to the X-ray photons [19].

7.3.3 Infrared Fourier transform spectroscopy

Figure 7.10 shows a Michelson interferometer for Fourier transform spectroscopy. In this instrument, a light beam enters through a small aperture and then strikes a beam splitter, which divides it into two beams of roughly equal intensity. One of the beams strikes a mirror that is fixed in position while the other travels to a mirror that can move back and forth. The two light beams reflected from the moving and fixed mirrors travel different optical path lengths. They arrive at the detector where they can interfere. An interferogram is produced due to the constructive and destructive interference between them as the moving mirror is scanned.

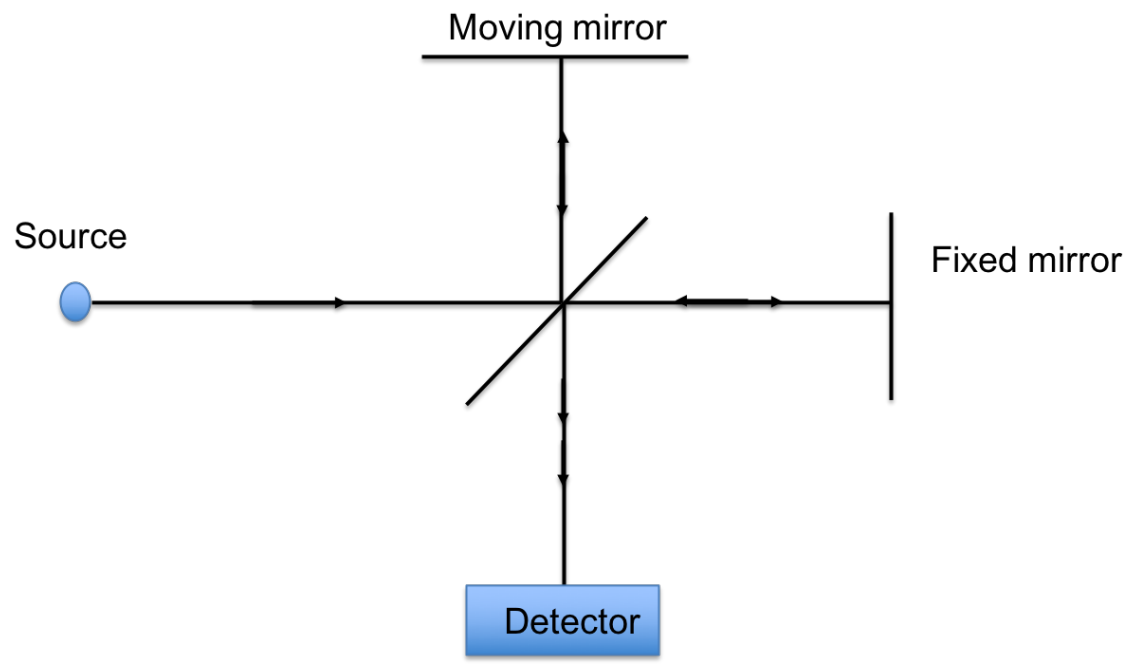

Figure 7.10 A setup for a Michelson interferometer used in Fourier-transform spectroscopy.

If we denote the spectral distribution of the light rays by $G(k)$, then the intensity is given by [19, 20]

$$I(x) = \frac{1}{\sqrt{2\pi}} \int_0^\infty G(k)\cos(kx)dk$$

where x is the path difference of the rays of light reaching the detector. The spectral distribution can be written as:

$$G(k) = \frac{1}{\sqrt{2\pi}} \int_0^\infty I(x)\cos(kx)dx \qquad (7.5)$$

Note that $I(x)$ and $G(k)$ form a Fourier transform pair where $I(x)$ is a function of distance x in units of cm and $G(k)$ is a function of wave number k in units of radians per distance. $I(x)$ is proportional to the intensity of the interferogram in W/m^2 and $G(k)$ is proportional to the spectral density of the transformed spectrum in $(W/m^2)/cm^{-1}$.

Figure 7.11 shows how the spectrum can be generated from the interferogram and vice versa using the above equations.

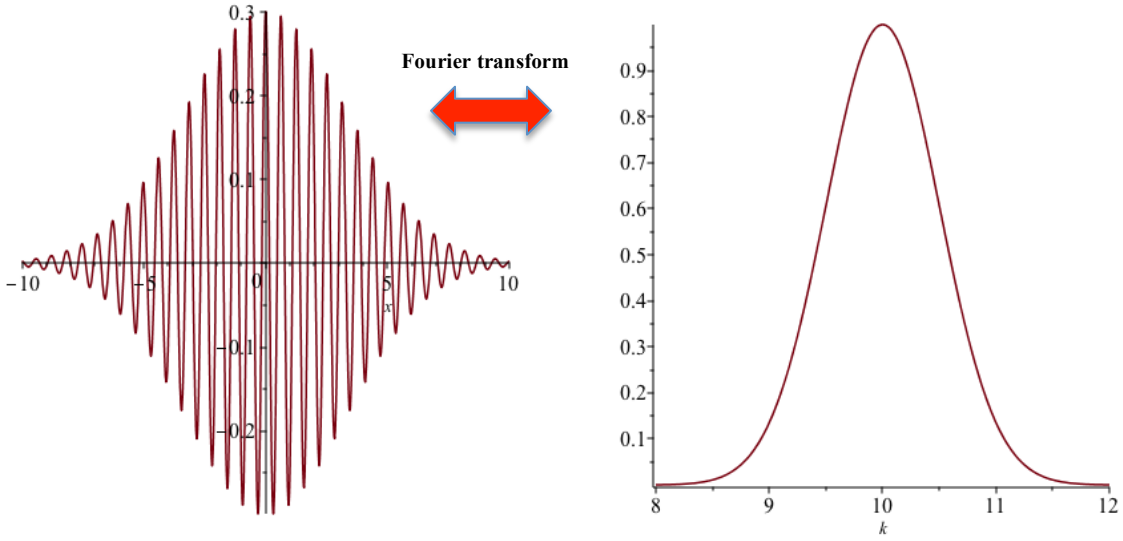

Figure 7.11 The interferogram and the spectra are both a Fourier transform of one another.

The resolution of the spectrum is inversely proportional to the maximum of the optical path length difference between the two mirrors of the instrument, as well as the angular spread of the beam.

In the Bruker IFS125HR Fourier transform infrared spectrometer attached to the Far-Infrared beamline at the Canadian Light Source (see Figure 7.12) the maximum of the optical path length difference is 10.4 m which produces a resolution of 0.00096 cm^{-1}. A potassium bromide (KBr) beam splitter is used in the instrument to cover the 400-4800 cm^{-1} spectral range.

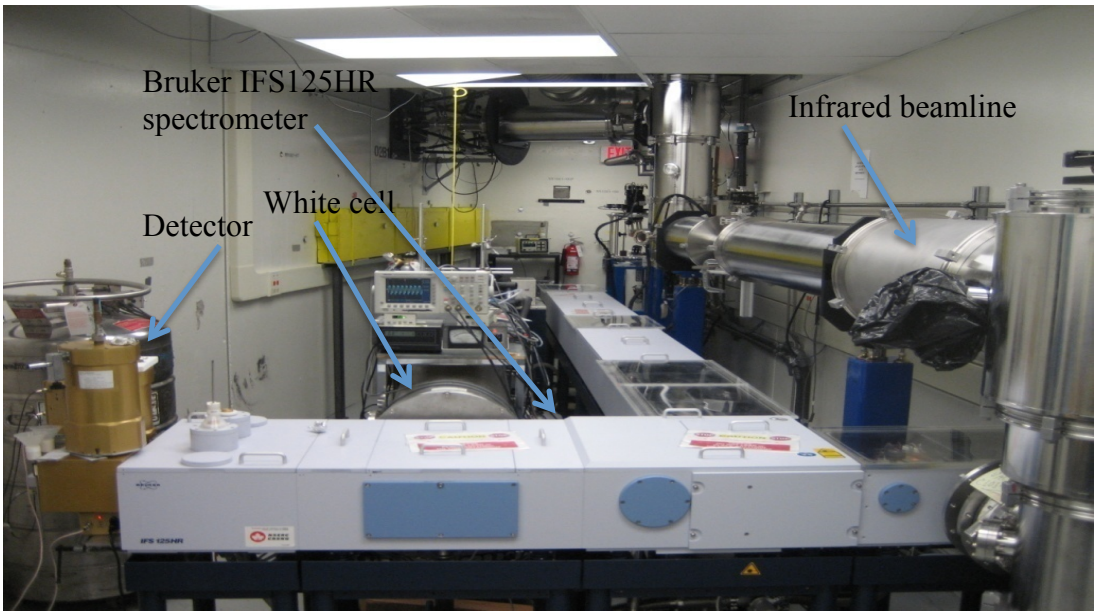

Figure 7.12 The Bruker IFS125HR Fourier transform infrared spectrometer attached to the Far-Infrared beamline at the Canadian Light Source is pictured. Different parts of the instrument are also identified in the picture.

To detect low levels of gas concentration, long pathlengths are required. Therefore, a large gas cell to contain the gas is needed. To reduce the length of the cell, we can employ a "White cell" [21] outfitted with mirrors at both ends to reflect the light back and forth multiple times. At the CLS a 2-meter long White Cell capable of 36 passes to make a 72 meter pathlength is used to accept the directed light from the interferometer.

The infrared light that is not absorbed by the sample is focused on a detector. The purpose of a detector is to convert the incoming infrared light into an electrical signal. Two detectors were used in the experiments. One was a nitrogen-cooled narrow-band mercury cadmium telluride (MCT) detector to cover the 750-10000 cm^{-1} region and the

other was a helium-cooled copper-doped germanium (Cu:Ge) detector to cover the 330-1900 cm^{-1} spectral range.

Several hundred interferograms are taken over a desired spectral region. Then all the scans are averaged and Fourier transformed using the OPUS software provided by Bruker [22]. Before the injection of the gas sample into the cell, it was evacuated and background scans were taken, averaged and Fourier transformed as well. The resultant absorption (A) is calculated using the following relation;

$A=\log(I/I_0)$

where I and I_0 are the intensity of the sample and the background spectra respectively. The experiment can be done at different temperatures and pressures that can be optimized to get a higher signal to noise ratio and better spectra.

References

1. A. Mellouki, J. Vander Auwera, M. Herman, J. Mol. Spectrosc. **193**, 195 (1999).

2. A. Mellouki, J. Lievin, M. Herman, J. Chem. Phys. **271**, 239 (2001).

3. D. W. Tokaryk, J. Van Wijngaarden, Can. J. Phys. **87**, 443 (2009).

4. S. Y. Lee, B. H. Boo, J. Phys. Chem. **100**, 15073 (1996).

5. M. L. Kutner, D. E. Machnik, K. D. Tucker, R. L. Dickman, Astrophys. J. **242**, 541, 1980.

6. G. Carrulo, S. Mazzotta, F. Giordano, F. Aiello, J. Chem. **2021**, 2021.

7. T. Graening, F. Thrun, Comprehensive Heterocyclic Chemistry III, Elsevier, 2008.

8. S. C. Moldoveanu, Pyrolysis of Organic Molecules, 2^{ed} ed., Elsevier, 2019.

9. https://pubchem.ncbi.nlm.nih.gov/compound/Catechol#section=Vapor-Density

10. https://www.lookchem.com/1-4-Benzenedithiol/

11. M. Reed, C. Zhou, C. Muller, T. Burgin, J. Tour, Science **278**, 252 (1997).

12. E. Leary et al., J. Phys. Chem. C **122**, 3211 (2018).

13. S. Piccinin, A. Selloni, S. Scandolo, R. Car, G. Scoles, J. Chem. Phys. **119**, 6729 (2003).

14. https://arxiv.org/pdf/cond-mat/0410539.pdf

15. M. Tsutsui, M. Taniguchi, Sensors **12**(6), 7259 (2012).

16. http://www.lightsource.ca

17. H. Wiedemann, Particle Accelerator Physics, 4th ed., Springer, 2015.

18. J.D. Jackson, Classical Electrodynamics, 3th ed., John Wiley & Sons, 1999.

19. F. Y. Wang, Physics with Maple, 2006.

20. G. R. Fowles, Introduction to Modern Optics, 2ed ed., 1989.

21. B. C. Smith, Fundamentals of Fourier Transform Infrared Spectroscopy, 2ed ed., 2011.

22. https://www.bruker.com

Chapter 8

Far-infrared synchrotron-based spectroscopy of catechol

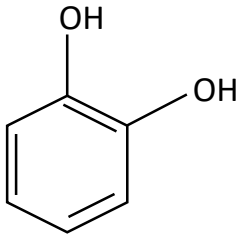

Figure 8.1 Schematic structure of the catechol molecule.

8.1 Low-resolution infrared spectrum of catechol

In Figure 8.1 the structure of the catechol molecule is depicted. The result of a low-resolution infrared survey of this molecule given in Figure 8.2 [1]. As can be seen there are several strong vibrational bands between 500 to 1500 cm^{-1}.

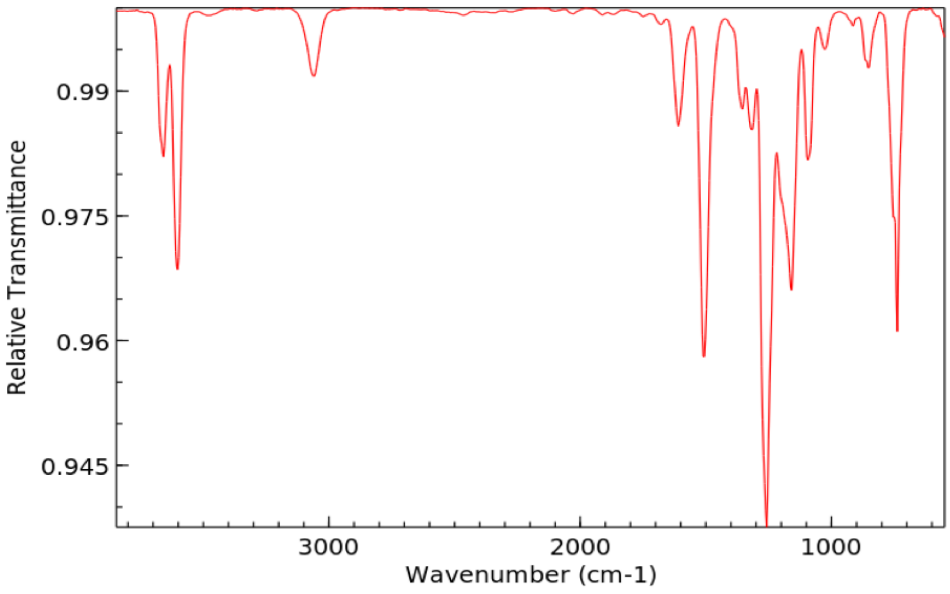

Figure 8.2 A low-resolution infrared survey spectrum of catechol [1].

The molecular rotational constants of catechol were extracted from microwave measurements [2]. They are A=0.11299, B=0.07492 and C=0.045063 cm^{-1} with small centrifugal distortion constants. Although the molecular constants are small and the resulting spectrum may be congested, the spectrum is good enough to be resolved under the CLS conditions. Figure 8.3 shows the simulated band of catechol with the above constants and a band origin at ~ 970 cm^{-1}. In the lower panel an expanded view of a portion in the R region of the band is depicted which shows the spectral lines are resolvable. Simulations were done with Pgopher [3] at room temperature. The details of the Hamiltonian used are provided in chapter 9. The linewidth of 0.001 cm^{-1} was used because that is the instrumental resolution. Note that the Doppler linewidth of catechol can be calculated from $\Delta\nu = 7.1\times10^{-7}\nu_0\sqrt{\frac{T}{M}}$ where $\nu_0 \sim 970$ cm^{-1}, T=300 K and M is the mass of catechol $C_6H_6O_2$ which is 110 amu. Substituting the values gives $\Delta\nu$ =0.0011 cm^{-1} which is nearly the same as the instrumental linewidth. Therefore, looking at the spectral range given in Figure 8.3 with high-resolution seems promising.

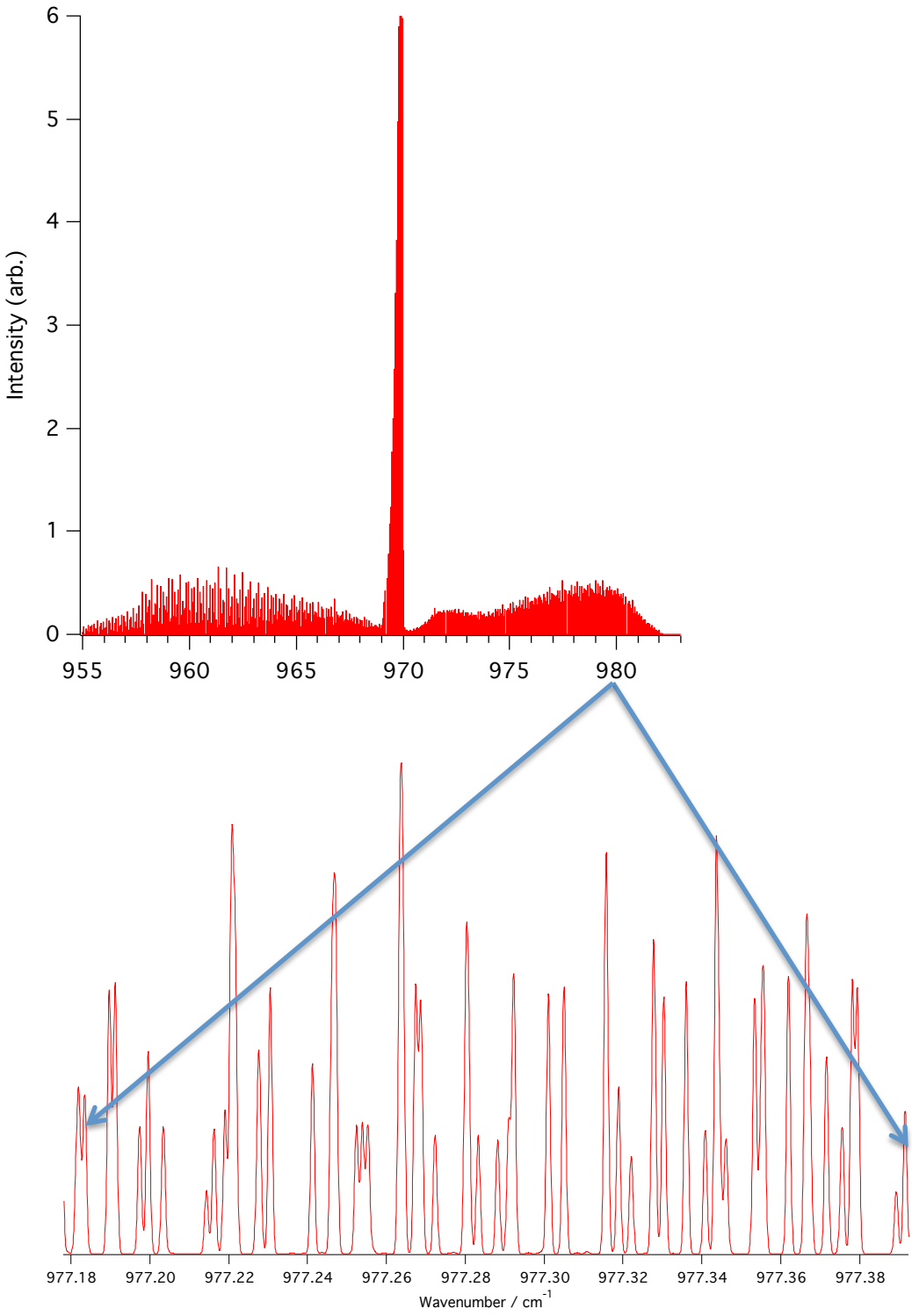

Figure 8.3 The top trace is the simulated band of catechol at ~ 970 cm^{-1} and the bottom trace is an expanded view of a portion in the R region of the band. Simulation details are given in the text.

8.2 Experimental conditions at the CLS

The commercially available solid form of catechol was purchased from Aldrich Company [4] and shipped to the CLS to perform the experiments.

8.2.1 First phase of the experiment

In the wet lab at the CLS, the common protective procedures such as wearing a lab coat, nitrile gloves and goggles were taken. In the fume hood/glovebox a small amount of catechol powder was put in a sealable Pyrex sample container. The container was sealed and taken to the far-infrared beamline and attached through a Teflon valve to the 2 m long White cell. Using a vacuum manifold the White cell was evacuated and by opening a Teflon valve the vapor was admitted into the White cell from the sample container.

Before the injection of the sample into the cell, the background scans of the empty 2 m long White cell were taken. The White cell path length was set to highest sensitivity (72 m), completely pumped out and 240 background scans were taken. Then, the sample container was connected to the cell and 1,2-dihydroxybenzene (catechol), was admitted to the White cell.

While literature [5] suggests that the vapor pressure of the catechol is 5 mTorr at 103° C and 10 mTorr at 118° C, after being stabilized, it took a long time for the pressure of the sample to reach around 14 mTorr. This vapor pressure is greater than the expected and

might be due to the presence of impurities or incorrect information. Despite this pressure, 600 interferograms were taken. The experiment was done at 60° C. Note that heating the sample helps getting the molecule into the cell however since the White cell was cold the molecules could adhere to the wall of the cell. However, usually the long path length used helped getting a spectrum even with low pressure.

Figure 8.4 shows the first attempt to take the high-resolution Fourier transform spectrum of 1,2-dihydroxybenzene. The result of a survey between 400 - 1000 cm^{-1} shows several vibrational bands. Water lines, a CO_2 band at ~670 cm^{-1} and an unknown vibration at ~970 cm^{-1} can be observed in the picture.

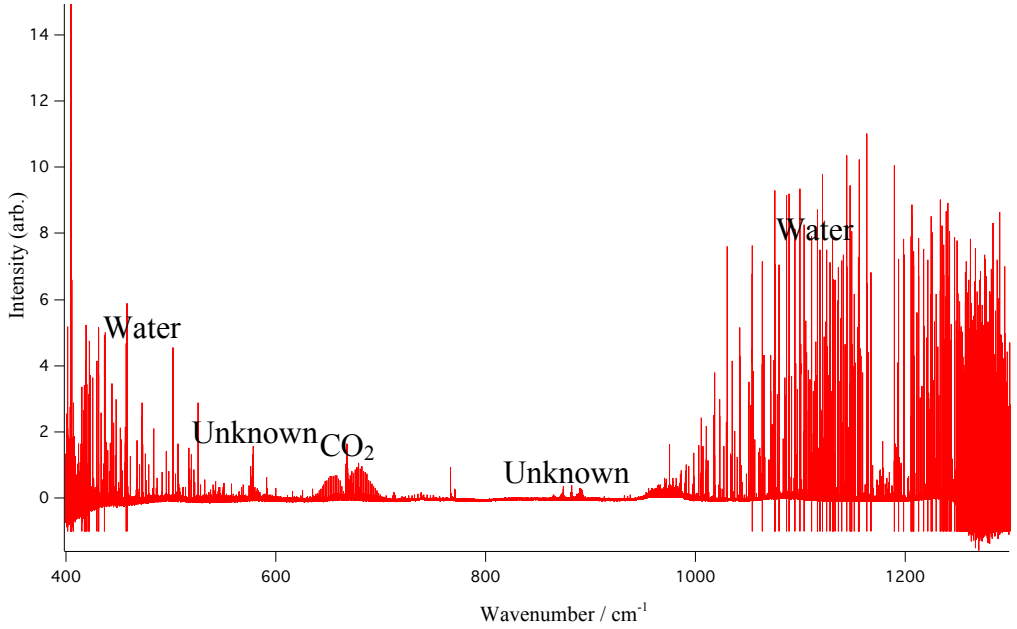

Figure 8.4 The result of the first high-resolution survey spectrum taken between 400 - 1200 cm^{-1}.

Figure 8.5 shows the expanded view of the high-resolution band observed at ~ 970 cm^{-1}.

It is near the vibrations shown in the low-resolution survey spectrum of Figure 8.2 and may belong to catechol. However, this unknown vibration at ~ 970 cm^{-1} is still too weak and too congested to be analyzed. Therefore, in order to increase the intensity of the band a new approach was taken.

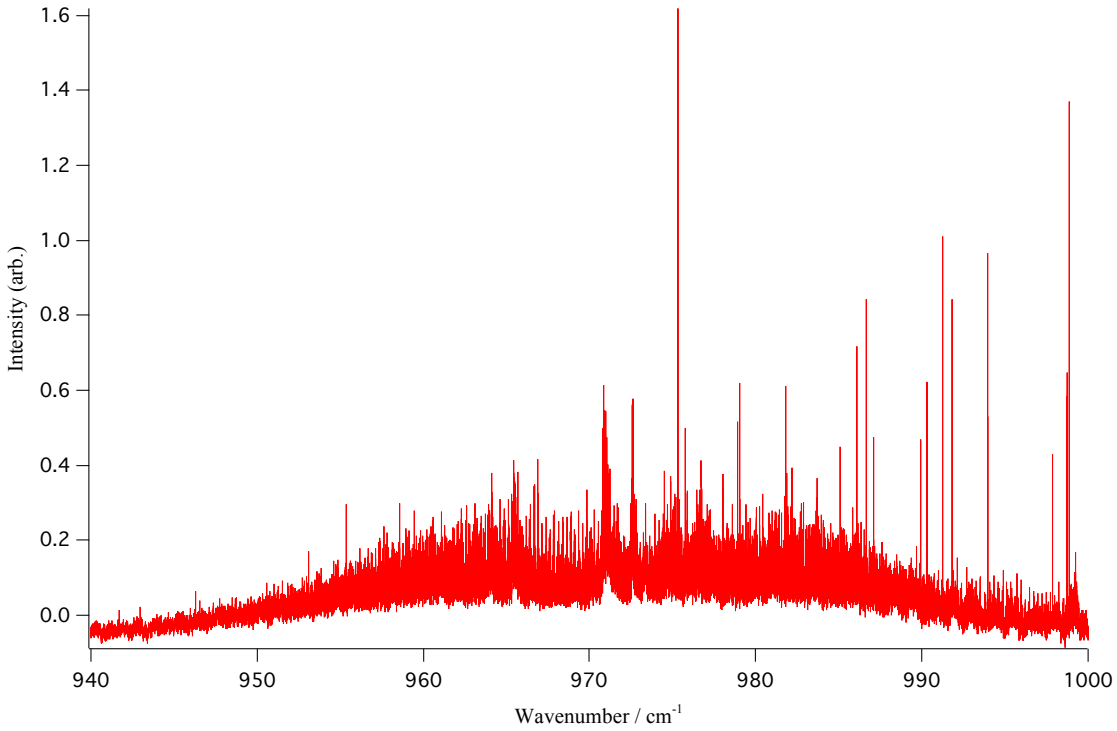

Figure 8.5 An expanded view of the first high-resolution band observed at 970 cm^{-1} is shown.

8.2.2 The second phase of the experiment

As mentioned, in the previous experiment the White cell was used and heated to about 60°C. However, the long length of the White cell may have prevented a uniform distribution of temperature throughout the cell. This means that we may have had colder

temperature regions within the cell. This may have led to the accumulation of the sample at the coldest spots. These cold spots also prevented getting a higher vapor pressure in the cell. In order to avoid condensation, a new approach that was successful with an imidozol [6] experiment was adapted for the second phase of the experiment.

In the wet lab, the same protective procedures as in phase one were taken but in the fume hood/glovebox a small amount of the sample was wrapped in aluminum foil to contain it. A 30 cm White cell with path length of 8.3 m (see Figure 8.6) was used instead of the 2 m long cell used previously.

A number of empty-cell background scans were taken at different temperatures. Due to the low vapor pressure of the sample heating the cell was necessary. This was done by wrapping a heating tape around the cell. The sample was heated to 100° C. In Figure 8.6 the crystalized grains formed on the surface of the cell can be seen. This confirmed that the sample was put to the gas phase.

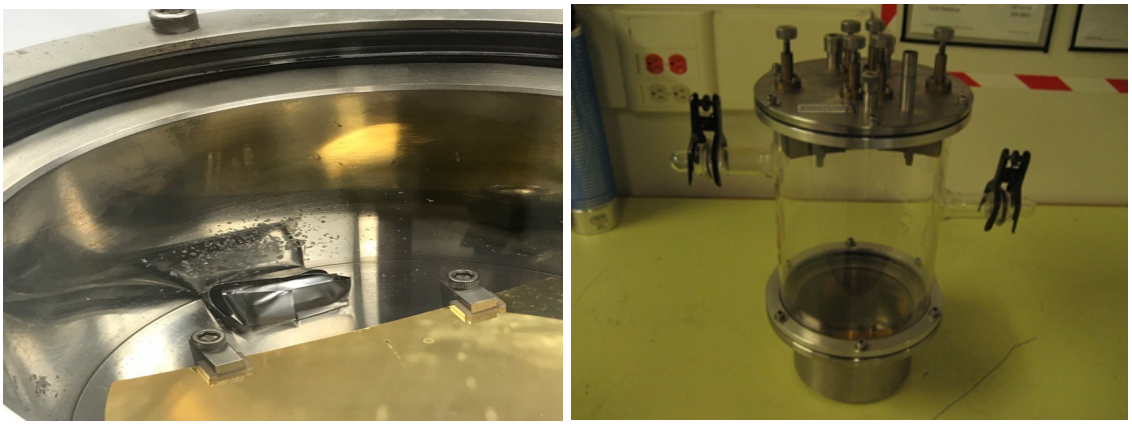

Figure 8.6 A picture of the sample wrapped in an aluminum foil (left) is shown and a picture of 30 cm White cell is also shown (right).

Figure 8.7 shows the second attempt to take the high-resolution Fourier transform spectrum of 1,2-dihydroxybenzene. The vibrational spectra seen in the first attempt were not observed in the second phase of the experiment.

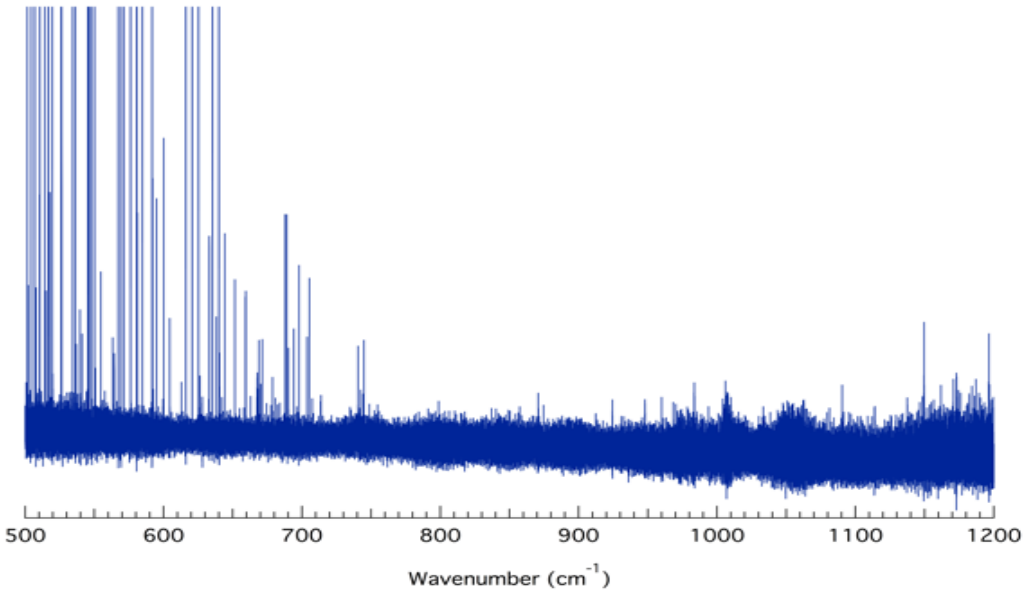

Figure 8.7 The result of the second high-resolution survey scan between 500-1200 cm^{-1}.

An improved White cell needs to be designed that encompasses heating capability which can be heated to 100° C with uniform temperature throughout the cell. Therefore, further experimental refinements need to be made in order to take high-resolution gas phase spectra of catechol in the future.

8.3 Concluding remarks

Attempts have been made to take the high-resolution Fourier transform spectrum of 1,2-dihydroxybenzene at the Canadian Light Source. In the first run of the experiments, the

~ 400 - 1200 cm^{-1} region was scanned based on the transitions observed in the low-resolution data. A weak band from an unidentified species was observed at ~ 970 cm^{-1}. In the second run of the experiments, the sample was wrapped in aluminum foil and the 30 cm cell was used instead of the 2 m long White cell. The sample was heated to 100° C. The crystalized grains on the surface of the cell showed that the molecule has undergone a phase transition from solid to gas. However, no transitions were observed during the experiments. This may confirm that the band obtained in the first experiment might have been of an unknown impurity. We had difficulty in getting vapor from the sample, which shows that the literature on the vapor pressure of catechol might be misleading. Also, it is possible that the low-resolution survey might be incorrect. Hence, retaking the low-resolution spectra, measuring the vapor pressure of catechol as a function of temperature and finding the optimal temperature and conditions for the experiment will be the next step toward accomplishment of a successful Light Source project in the future.

References

1. http://webbook.nist.gov/cgi/cbook.cgi?ID=C120809&Mask=80#IR-Spec

2. W. Caminati , S. D. Bernardo, J. Mol. Struc. **240**, 263 (1990).

3. C. M. Western, J. Quant. Spectrosc. Radiat. Transfer **186,** 221 (2017).

4. www.sigmaaldrich.com

5. https://pubchem.ncbi.nlm.nih.gov/compound/Catechol#section=Vapor-Density

6. S. Gruet, O. Pirali, M. Goubet, D. W. Tokaryk, P. Brechignac, J. Phys. Chem. A **120**, 95 (2016).

Chapter 9

Far infrared synchrotron-based spectroscopy of pyrrole

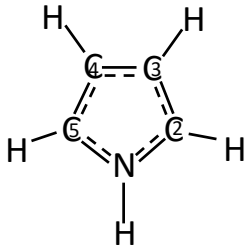

Figure 9.1 Schematic structure of the pyrrole molecule.

Pyrrole (C_4H_5N) is a heterocyclic aromatic organic molecule the structure of which is depicted in Figure 9.1. Its ten atoms are planar in equilibrium. The molecule exhibits C_{2v} symmetry, and it has 24 modes of vibration. Three modes of vibration of pyrrole, i.e., ν_9, ν_{24} and ν_{13} are studied in this thesis.

9.1 Modes of vibration of pyrrole

In Figure 9.2 the energy levels (in wavenumber units) of the vibrational modes of pyrrole below 1500 cm^{-1} are shown. These levels are grouped based on their symmetries [1]. The three modes of vibration I have studied are located at ν_9 ~ 881, ν_{24} ~ 865 and ν_{13} ~ 826 cm^{-1}. The ν_{10} level also lies nearby at ~ 861 cm^{-1}. All four levels are found in an interval of ~ 60 cm^{-1}. Since these states are close in energy, they might be susceptible to possible interactions. Therefore, considering the possible interactions among these levels and also

obtaining information about possible symmetry allowed transitions from nearby states to these levels is helpful for their analysis.

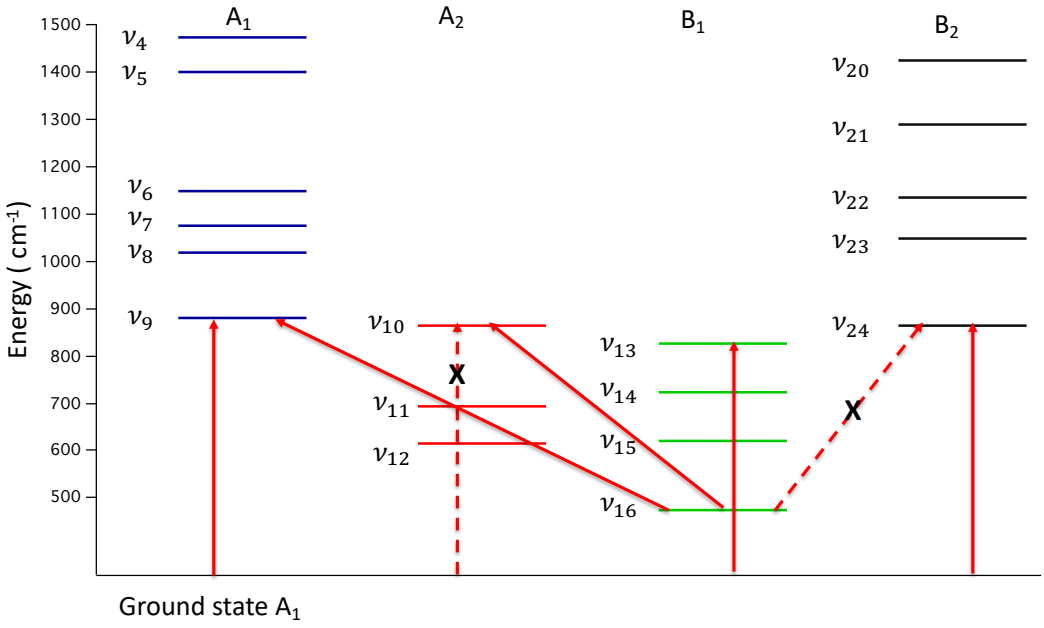

Figure 9.2 Vibrational levels of pyrrole grouped based on their symmetries. Selected allowed transitions are shown as solid lines and symmetry-forbidden transitions are given with dashed lines with a superimposed "X".

9.2 Possible transitions and interactions

In Table 9.1, the C_{2v} character table is defined in terms of the *a*, *b* and *c* axes of the principal reference frame such that *a* is chosen as the C_2 symmetry axis and *a*, *b* define the molecular plane.

Table 9.1 C_{2v} character table when *a* is chosen as the $\hat{C}_2$ symmetry axis.

C_{2v}	$\hat{E}$	$\hat{C}_2(a)$	$\hat{\sigma}_v(ab)$	$\hat{\sigma}_v(ac)$	linear functions, rotations
A_1	1	1	1	1	a
A_2	1	1	-1	-1	R_a
B_1	1	-1	-1	1	c , R_b
B_2	1	-1	1	-1	b , R_c

In Table 9.2, the multiplication of the A_1, A_2, B_1 and B_2 symmetries are given.

Table 9.2 Multiplication table of A_1, A_2, B_1 and B_2 symmetries.

$\otimes$	A_1	A_2	B_1	B_2
A_1	A_1	A_2	B_1	B_2
A_2	A_2	A_1	B_2	B_1
B_1	B_1	B_2	A_1	A_2
B_2	B_2	B_1	A_2	A_1

The symmetry of the ground state of pyrrole is A_1. The symmetries of the ν_9, ν_{13} and ν_{24} levels are A_1, B_1 and B_2 respectively. The types of transitions that can occur are determined according to $\Gamma(\upsilon)\otimes\Gamma(\upsilon')\supset\Gamma(\alpha)$ where $\Gamma(\upsilon)$ and $\Gamma(\upsilon')$ are the symmetries of the ground and excited states respectively and $\Gamma(\alpha)$ is the symmetry property of the translation where $\alpha = a$, b or c. Therefore, three types of symmetry-allowed transitions

originating from the ground state to these levels can be observed. These transitions are *a*-, *b*- and *c*-type since $A_1 \otimes A_1 = A_1$, $A_1 \otimes B_1 = B_1$ and $A_1 \otimes B_2 = B_2$ (see tables 9.1 and 9.2). The possible Coriolis interactions between the aforementioned levels can be determined [2] according to the $\Gamma(\upsilon) \otimes \Gamma(\upsilon') \supset \Gamma(R_\alpha)$ rule where $\Gamma(\upsilon)$ and $\Gamma(\upsilon')$ are the symmetries of the states involved and $\Gamma(R_\alpha)$ is the symmetry property of the rotation where $\alpha = a$, *b* or *c*. Therefore, three types of Coriolis interactions can be observed between the ν_9, ν_{13} and ν_{24} levels. The interaction between the ν_9 and ν_{24} levels are *c*-type since $A_1 \otimes B_2 = B_2$, while the ν_9 and ν_{24} levels interact with ν_{13} via *b*- and *a*-type coriolis interactions respectively since $A_1 \otimes B_1 = B_2$ and $B_2 \otimes B_1 = A_2$. It should be noted that ν_{13} is rather far from the other states and is not likely to perturb them. However, the ν_9 and ν_{24} levels (see Figure 9.2) are close and as mentioned above can be coupled with *c*-type Coriolis interactions. This is depicted in Figure 9.3 which shows how the motion of the nuclei of the ν_{24} mode are affected by the corresponding Coriolis force from the ν_9 state if we consider $\vec{\omega}$ pointing out of the page. Figure 9.3 shows the $\nu_9 \sim 881$ and $\nu_{24} \sim 865$ cm^{-1} vibrational modes of pyrrole and the blue arrows show the motion of their nuclei. These modes exhibit ring deformation; there exists in-plane C-H bending in ν_9 and the ν_{24} modes corresponds to C_2-H and N-H in-plane bending [3].



ν_9 ν_{24}

Figure 9.3 The ν_9 and ν_{24} vibrational modes of pyrrole.

As mentioned, there is also the ν_{10} level at ~ 864 cm^{-1} with A_2 symmetry which is close in energy to the other states. The transition from the ground state to this level is symmetry forbidden because $\Gamma(\upsilon)\otimes\Gamma(\upsilon')\not\supset\Gamma(\alpha)$. However, ν_{10} can interact with ν_9, ν_{24} and ν_{13} via *a*-, *b*- or *c*-type Coriolis interactions respectively since according to $\Gamma(\upsilon)\otimes\Gamma(\upsilon')\supset\Gamma(R_\alpha)$; $A_2\otimes A_1=A_2$, $A_2\otimes B_2=B_1$ and $A_2\otimes B_1=B_2$. Therefore, characterizing ν_{10} may prove helpful for the analysis of the ν_9 and ν_{24} states. Although the transition from the ground state to ν_{10} is symmetry forbidden, a symmetry-allowed transition can happen from the low-lying excited state ν_{16} ~ 474 cm^{-1} with B_1 symmetry to ν_{10} and ν_9. These transitions are of *b*- and *c*-type respectively since $B_1\otimes A_2 = B_2$, $B_1\otimes A_1 = B_1$ and are expected to be found at ~ 389 and 407 cm^{-1}. Therefore, by populating ν_{16}, which has already been characterized [4, 5], the ν_{10} and ν_9 states can be accessed. Note that the transition from ν_{16} to ν_{24} symmetry is forbidden.

9.3 Asymmetric top Hamiltonian

In Chapter 2, a simplified version of the asymmetric top Hamiltonian was discussed. The most general form of the rotational Hamiltonian for describing asymmetric top rotors involves the rigid rotor Hamiltonian plus two perturbing operators involving sums of powers of J^4 and J^6 with the related coefficients called quartic and sextic respectively [6].

$$H = H_r + H_d'^{(4)} + H_d''^{(6)} \tag{9.1}$$

$$H = \sum_\alpha B_\alpha J_\alpha^2 + \frac{\hbar^2}{4}\sum \tau_{\alpha\beta\gamma\delta} J_\alpha J_\beta J_\gamma J_\delta + \hbar^6 \sum \tau_{\alpha\beta\gamma\delta\varepsilon\eta} J_\alpha J_\beta J_\gamma J_\delta J_\varepsilon J_\eta \quad (\alpha,\beta,\gamma,\delta,\varepsilon,\eta = x,y,z)$$

where

$H_r = \sum_\alpha B_\alpha J_\alpha^2$ is the rigid rotor Hamiltonian with $B_\alpha = \frac{h}{4\pi c I_\alpha}$ being the rotational constants, $H_d'^{(4)} = \frac{\hbar^2}{4}\sum \tau_{\alpha\beta\gamma\delta} J_\alpha J_\beta J_\gamma J_\delta$ and $H_d''^{(6)} = \hbar^6 \sum \tau_{\alpha\beta\gamma\delta\varepsilon\eta} J_\alpha J_\beta J_\gamma J_\delta J_\varepsilon J_\eta$ being the perturbing Hamiltonians with distortion constants τ.

In the Hamiltonian there are 81 and 729 terms in the J^4 and J^6 sums respectively. In order to fit the experimental data properly, we need to remove the parameters that have indistinguishable effects in the model. Hence, a reduced form of the Hamiltonian is needed. A reduced Hamiltonian is the one that is obtained by a unitary transformation

$$\tilde{H} = U^{-1} H U \tag{9.2}$$

where $\tilde{H}$ is the transformed Hamiltonian and the unitary operator ($U^{-1} = U^\dagger$) is defined as $U = e^{iS}$ with S being Hermitian [7] ($S^\dagger = S$).

The eigenvalues of the original and the transformed Hamiltonians remain the same. In this Hamiltonian all the parameters that cannot be distinguished are removed to make it suitable for fitting of the experimental data. Two different methods that are used for the reduction are asymmetric (A) and symmetric (S) [6]. For molecules that are only slightly asymmetric, using the A-reduction might cause a problem. Hence, to prevent the possible divergence in the coefficients when A~B the S-reduction can be used. In a given vibrational state of an asymmetric top molecule, the reduced rotational Hamiltonian as proposed by Watson [8] is included in the Pgopher program [9]. It is used in both the ground and excited vibrational states for fitting to the observed transitions.

The A reduction form is [8]

$$H_{red}^{A} = AJ_x^2 + BJ_y^2 + CJ_z^2 + \Delta_J J^4 - \Delta_{Jk} J^2 J_z^2 - \Delta_k J_z^4 - \frac{1}{2}[\delta_J J^2 + \delta_k J_z^2, J_+^2 + J_-^2]_+ + \Phi_J J^6 + \Phi_{Jk} J^4 J_z^2 + \Phi_{kJ} J^2 J_z^4 + \Phi_k J^6 + \frac{1}{2}[\phi_J J^4 + \phi_{Jk} J^2 J_z^2 + \phi_k J_z^4, J_+^2 + J_-^2]_+ \quad (9.3)$$

and the S-reduction is as follows

$$H_{red}^{S} = AJ_x^2 + BJ_y^2 + CJ_z^2 - D_J J^4 - D_{Jk} J^2 J_z^2 - D_k J_z^4 + d_1 J^2 (J_+^2 + J_-^2) + d_2 (J_+^4 + J_-^4) + H_J J^6 + H_{Jk} J^4 J_z^2 + H_{kJ} J^2 J_z^4 + H_k J_k^6 + h_1 J^4 (J_+^2 + J_-^2) + h_2 J^2 (J_+^4 + J_-^4) + h_3 (J_+^6 + J_-^6) \quad (9.4)$$

In the above Hamiltonians the A, B and C are the usual rotational constants, the $(\Delta_J, \Delta_{Jk}, \Delta_k, \delta_J, \delta_k)$ and $(D_J, D_{Jk}, D_k, d_1, d_2)$ are quartic distortion constants and $(\Phi_J, \Phi_{Jk}, \Phi_{kJ}, \Phi_k, \phi_J, \phi_{Jk}, \phi_k)$ and $(H_J, H_{Jk}, H_{kJ}, H_k, h_1, h_2, h_3)$ are sextic distortion constants.

9.4 The correlation diagram of pyrrole

In Figure 9.4 the correlation diagram of pyrrole is depicted for J=0, 1, 2 and 3 rotational levels that are labeled as J_{KaKc}.

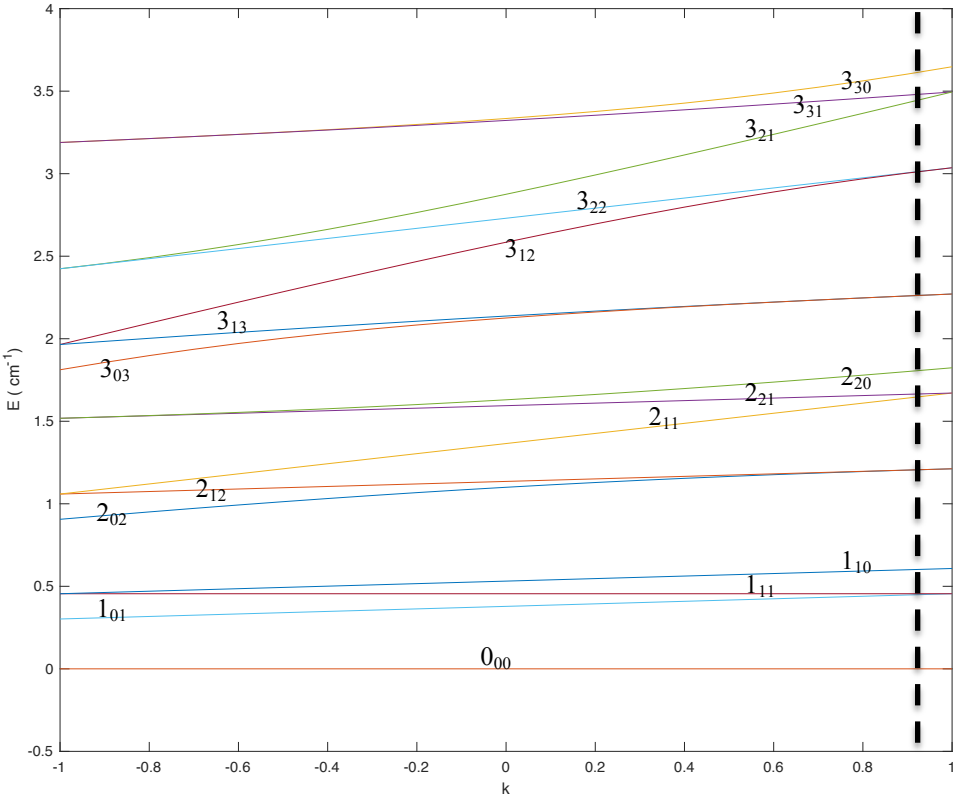

Figure 9.4 The correlation diagram of pyrrole for J=0, 1, 2 and 3 rotational levels labeled as J_{KaKc} with $\kappa = 0.9438$ identified as a vertical dotted line.

For the pyrrole molecule A≈B≈2C.The asymmetry parameter $\kappa = \frac{2B - A - C}{A - C}$ is ~ 0.9438 in the ground state, which indicates the molecule is near oblate. The dotted line in Figure 9.4 indicates the value of κ that applies to the ground state of pyrrole. As we will see the

value of κ is ~ 0.9486, 0.9331 and 0.8769 for the ν_9, ν_{13} and ν_{24} states respectively which shows the molecule is still near oblate when excited to these states. Note that, in the above diagram, as we go from right to left the symmetry of the molecule breaks and the levels with the same K_c start to split around $\kappa = 0.9438$ which means that they are not degenerate.

9.5 The spectral assignment process

A lower-state combination difference can be obtained from the spectrum if the difference between two rovibrational transitions from P and R branches that share the same upper state is calculated. These differences can then be used to determine lower state molecular constants. On the other hand, the ground state constants can be fixed to the values obtained in reference 4 because they were precisely determined. Eigenvalues can be calculated by diagonalizing the Hamiltonian for the ground state. Then lower state combination differences from the calculation can be formed and if they match the values obtained from the experiment, the transitions can be assigned and included in the fit. This method was used for data analysis.

9.6 Data analysis and results

In this section, the three vibrational bands of pyrrole at ν_9 ~ 881, ν_{24} ~ 865 and ν_{13} ~ 826 cm^{-1} that were previously taken at the CLS are studied and the results of the fitting will be provided. For taking the spectra, pyrrole with a sample pressure of 140 mTorr was

admitted to the White cell the path length of which was set to 28 m. A filter with a bandpass of 490-1190 cm^{-1} was used and 46 scans were taken and averaged to create the final interferogram that was transformed into the spectrum.

9.6.1 The ν_{13} state of pyrrole

Figure 9.5 shows the spectrum of the ν_{13} mode of pyrrole at ~ 826 cm^{-1}. The vertical axis shows the absorption, calculated as $\log_{10}(\frac{I}{I_0})$. This is a *c*-type band as is apparent from the strong congested Q branch. The Loomis-Wood plot of this band is depicted in Figure 9.6.

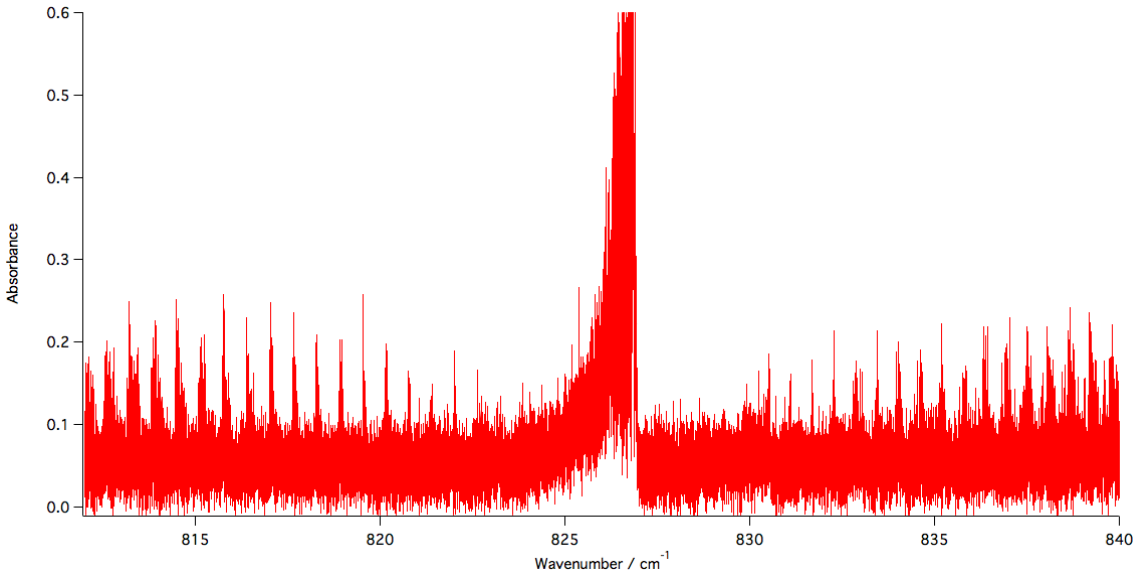

Figure 9.5 Absorption spectrum of the c-type ν_{13} fundamental of pyrrole.

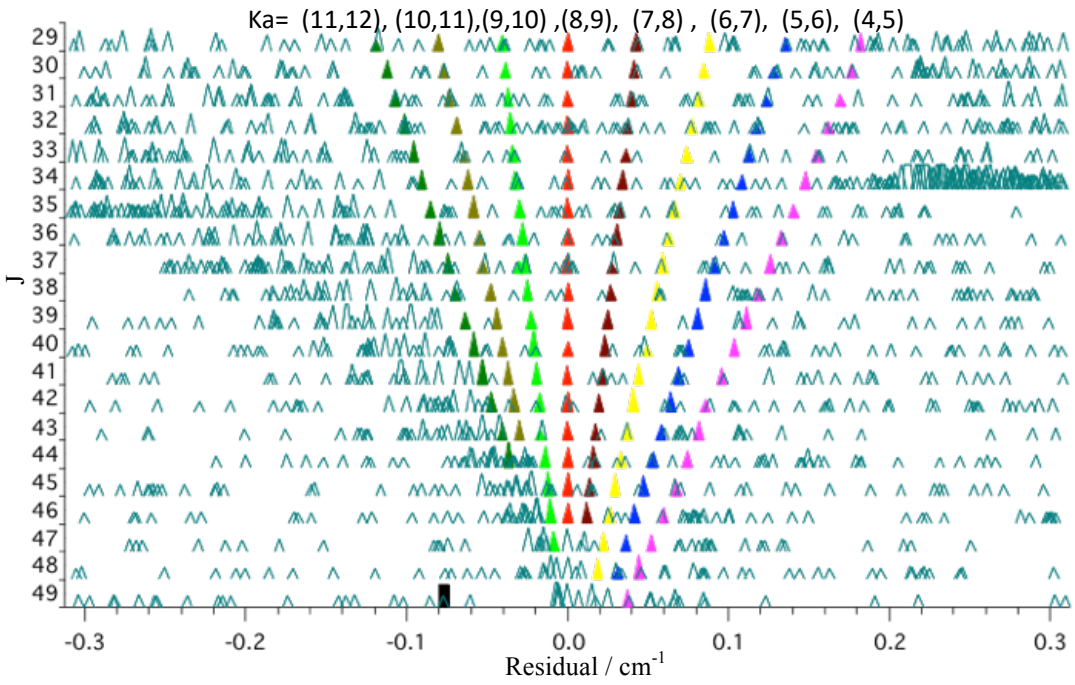

Figure 9.6 A Loomis-Wood plot of the P branch of the ν_9 vibrational mode of pyrrole.

When dealing with congested spectra, the Loomis-Wood plot serves as a useful tool. As can be seen in Figure 9.6 transitions which have the same K_a but different J form progressions that are grouped in vertical series. Note that K_a+K_c can be J or J+1, therefore for given values of J and K_c we can get two values for K_a that differ by 1 in the series. This is because of the near degeneracy of the levels J_{KaKc} and $J_{Ka+1\ Kc}$ in many instances resulting from the near-oblate structure of pyrrole.

In Figure 9.7, a portion of the *c*-type ν_{13} band in the P branch is selected. Four different clusters that belong to J′=19, J′=18, J′=17 and J′=16 of the *c*-type band of pyrrole in the P branch are expanded. The lower trace in the bottom panel is the spectrum calculated at room temperature from the constants obtained from the analysis and fitting.

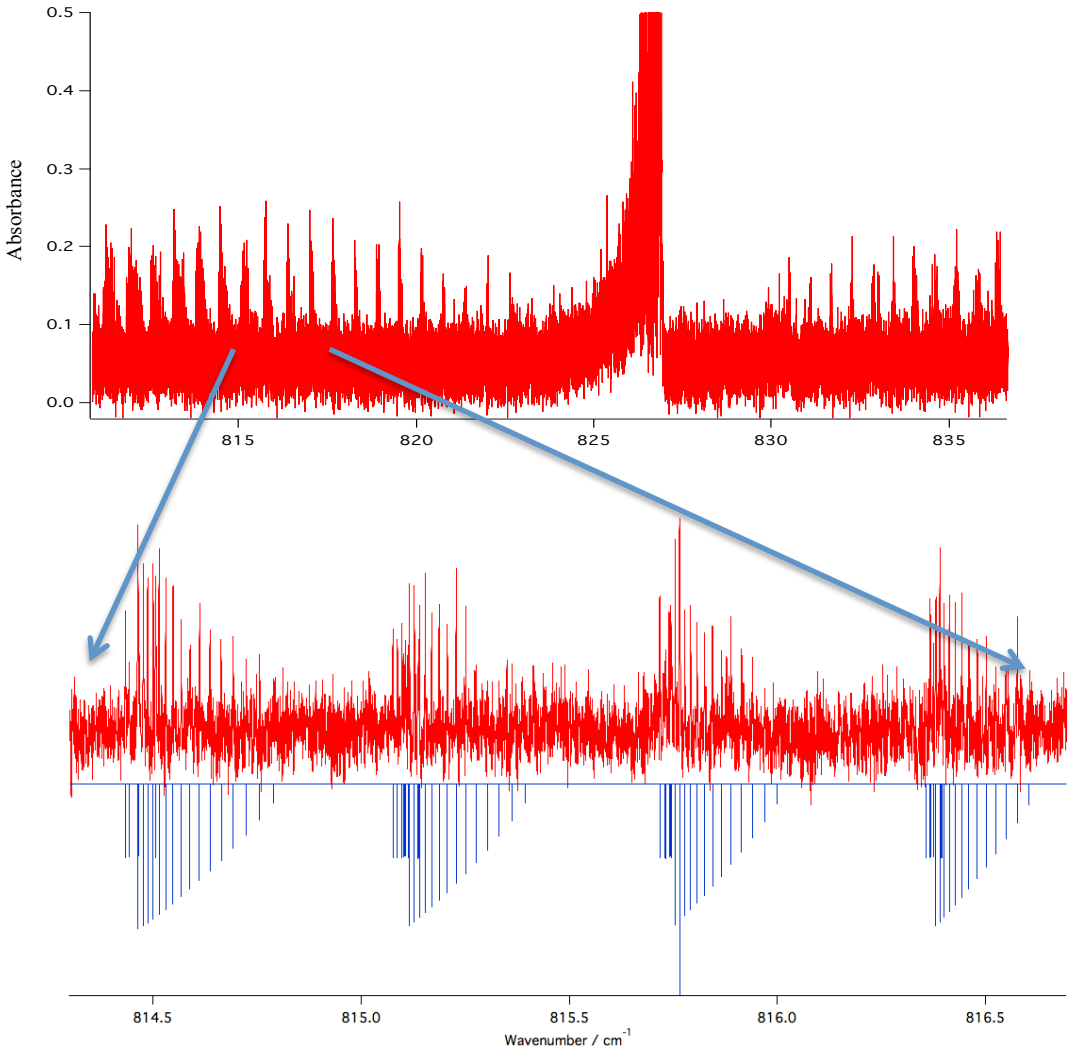

Figure 9.7 The expanded view of the high-resolution spectrum of pyrrole between ~ 814-816 cm^{-1} with the corresponding simulated spectra at the bottom.

A closer look at the rotational structure of the J′=19 cluster is shown in Figure 9.8. The quantum numbers of each transition are given as (J′, $K_{a'}$, $K_{c'}$)-(J″, $K_{a''}$, $K_{c''}$) in the detailed picture.

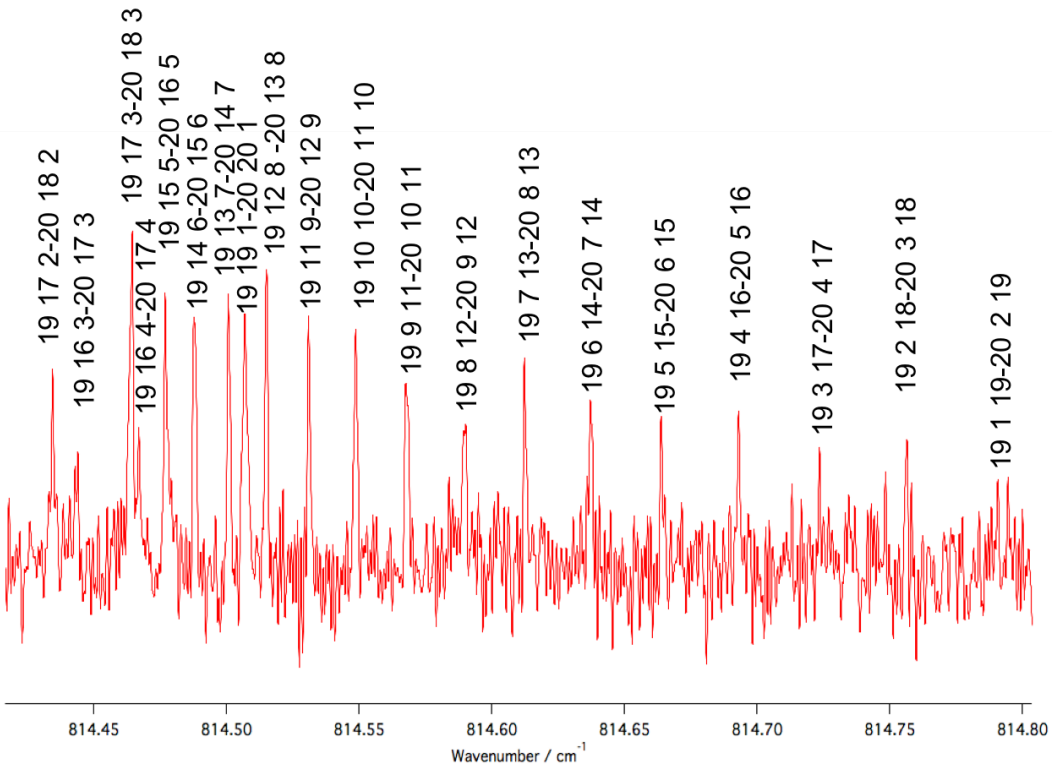

Figure 9.8 The P(20) cluster of the ν_{13} band of pyrrole: the quantum numbers of each transition are given as (J′, $K_{a'}$, $K_{c'}$)-(J″, $K_{a''}$, $K_{c''}$). For most features only the J =K_a+K_c-1 member of a degenerate pair is labeled.

Figure 9.9 shows a portion of the experimental and calculated spectrum of the Q branch of the ν_{13} band. As can be seen the transitions are badly overlapped and cannot be assigned.

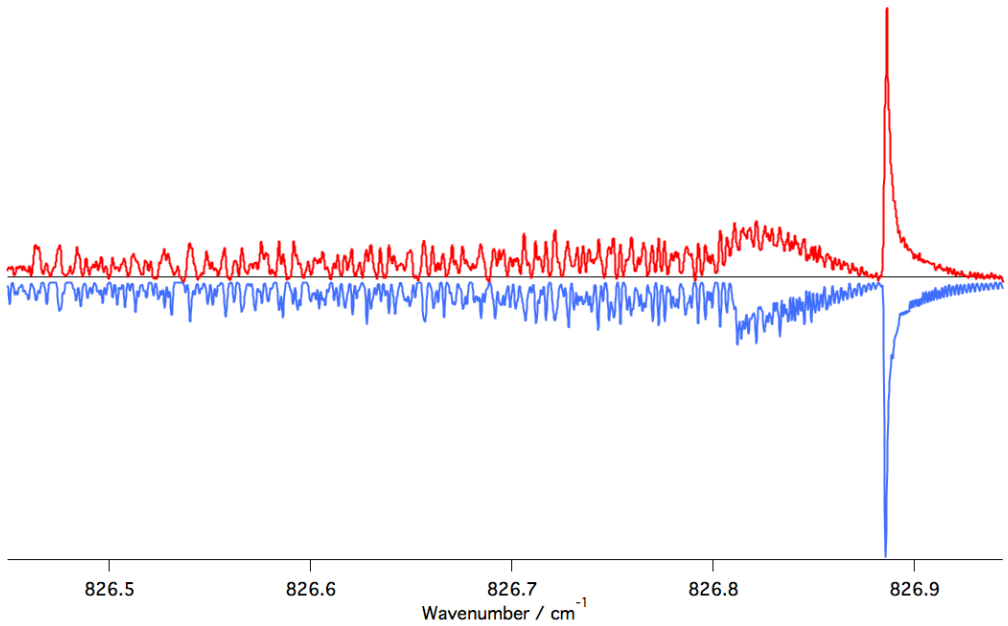

Figure 9.9 A portion of the Q branch of the ν_{13} band. The upper trace is the experimental spectrum and the lower trace is the calculated spectrum.

In Figure 9.10 the rotational structure of the ν_{13} band of pyrrole is depicted for $K_{a''}$=2,4,6,8,10 and all K_a values from top to bottom excluding the Q branch.

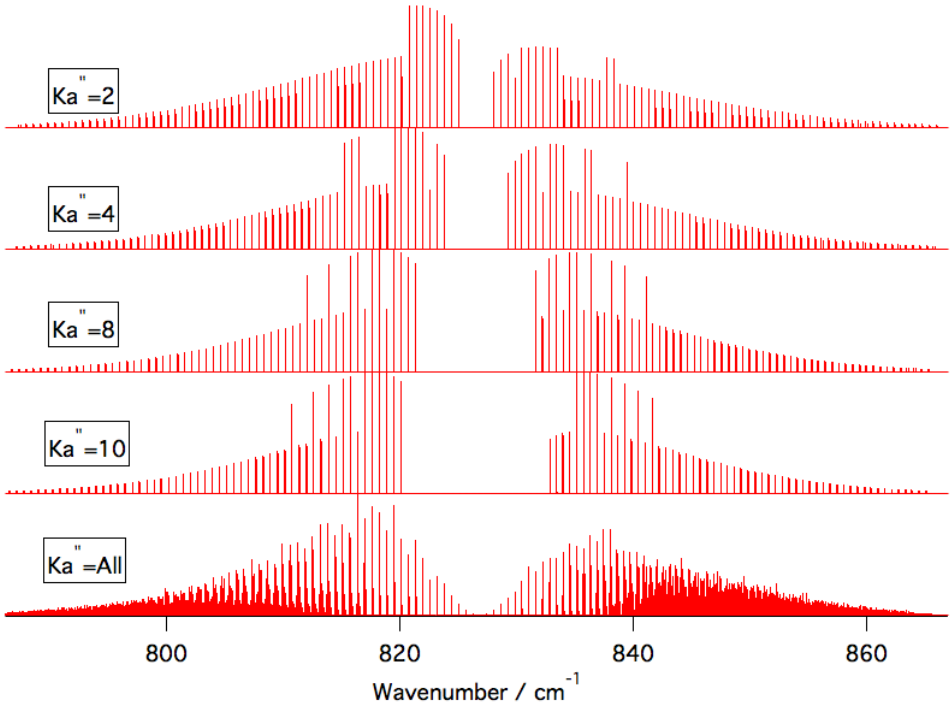

Figure 9.10 Simulated rotational structure of the ν_{13} band with selected K_a values excluding the Q branch.

The overview of the shape of the bottom picture with all the K_as included resembles the ν_{13} band.

In Figure 9.11, the low root mean square error of the fit for the ν_{13} band of pyrrole is shown which is of the order of ~ 0.00029 cm^{-1}. This value is comparable to the uncertainty in measurement of a single clear, unblended line of about ~ 0.0002 cm^{-1}. The molecular constants of this band are given in Table 9.3.

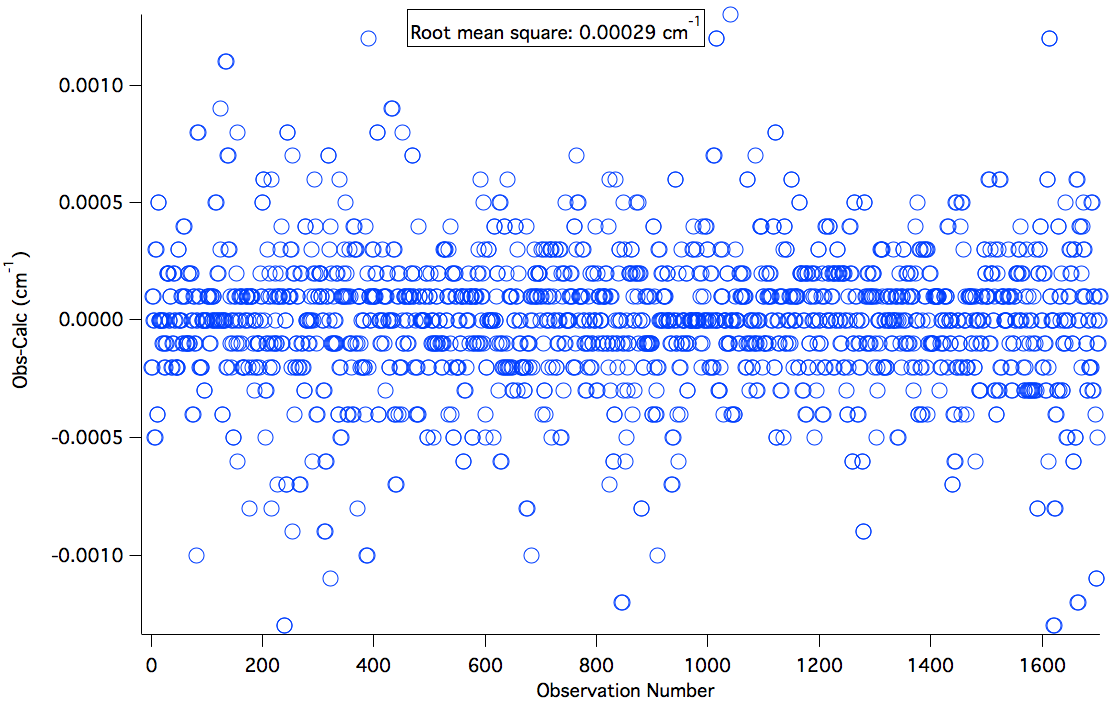

Figure 9.11 The difference between observed and calculated transitions shown as circles with the root mean square error of the fit for the ν_{13} band of pyrrole.

As can be seen from the extracted parameters for ν_{13} in Table 9.3, the A and B parameters are larger for the upper state than the ground state while the reverse is true for the C parameter. This indicates a smaller moment of inertia along the principal axis of *c* and larger moments of inertia along *a*- and *b*-axes compared to the ground state. In order to satisfy these conditions, the hydrogen atoms around the ring tend to move far apart from the *a*- and *b*-axes but at the same time become closer to the *c*-axis. This is consistent with the ν_{13} vibration being a ring-puckering mode in which the opposite ends bend downward and upward, hence the planar molecule takes the shape of a chair (see Figure

9.12) where the velocities of the front two and back two hydrogen atoms form the legs and back of the chair respectively.

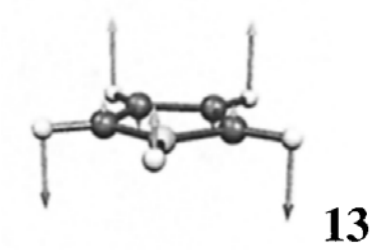

Figure 9.12 The ring puckering mode, ν_{13}, of pyrrole [1].

9.6.2 The ν_9 and ν_{24} states of pyrrole

Figure 9.13 shows the two vibrational bands of pyrrole, ν_{24} and ν_9 at ~ 864 and 881 cm^{-1} which correspond to *b*- and *a*-type transitions respectively. The two bands are blended and their analysis requires the identification of each transition in a way that it is clear that they belong to their corresponding bands. Therefore, constructing the Loomis-Wood plot of the bands is beneficial for classifying the transitions.

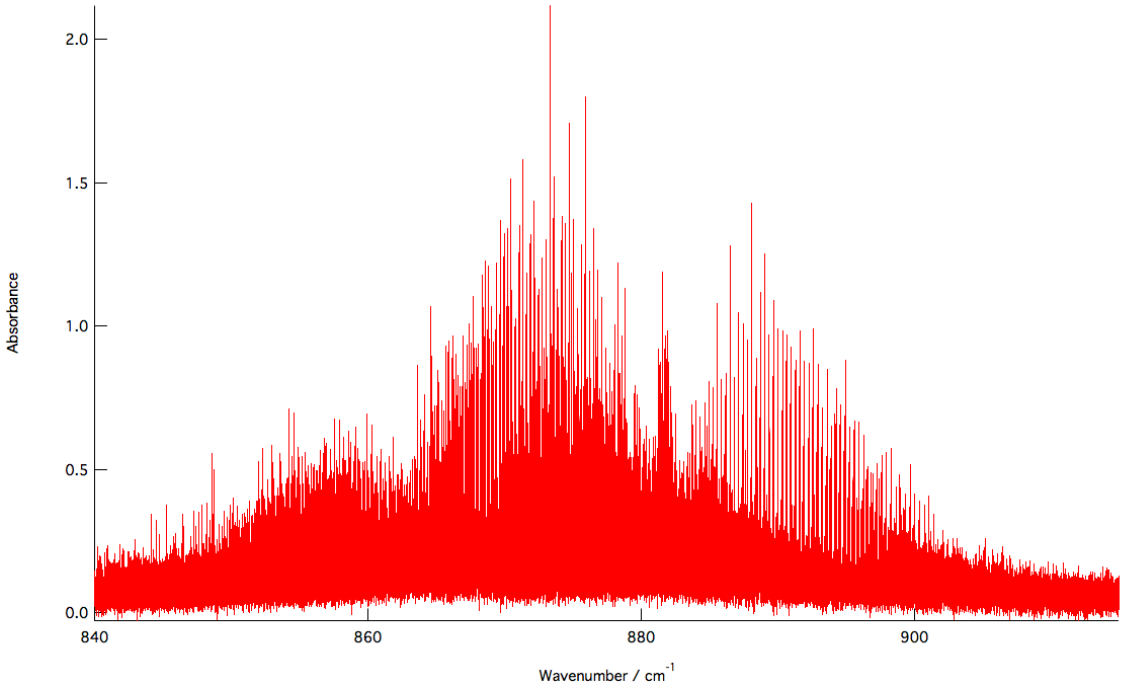

Figure 9.13 Two overlapping vibrational bands of pyrrole, ν_{24} and ν_9, at ~ 864 and 881 cm^{-1}.

In Figure 9.14 a Loomis-Wood plot of the P branch of the *a*-type ν_9 vibrational mode of pyrrole is depicted. Three vertical series with $K_{a''}$=(0,1), (1,2) and (2,3) can be observed in the picture. The series are smooth indicating that the band is not strongly affected by the nearby states.

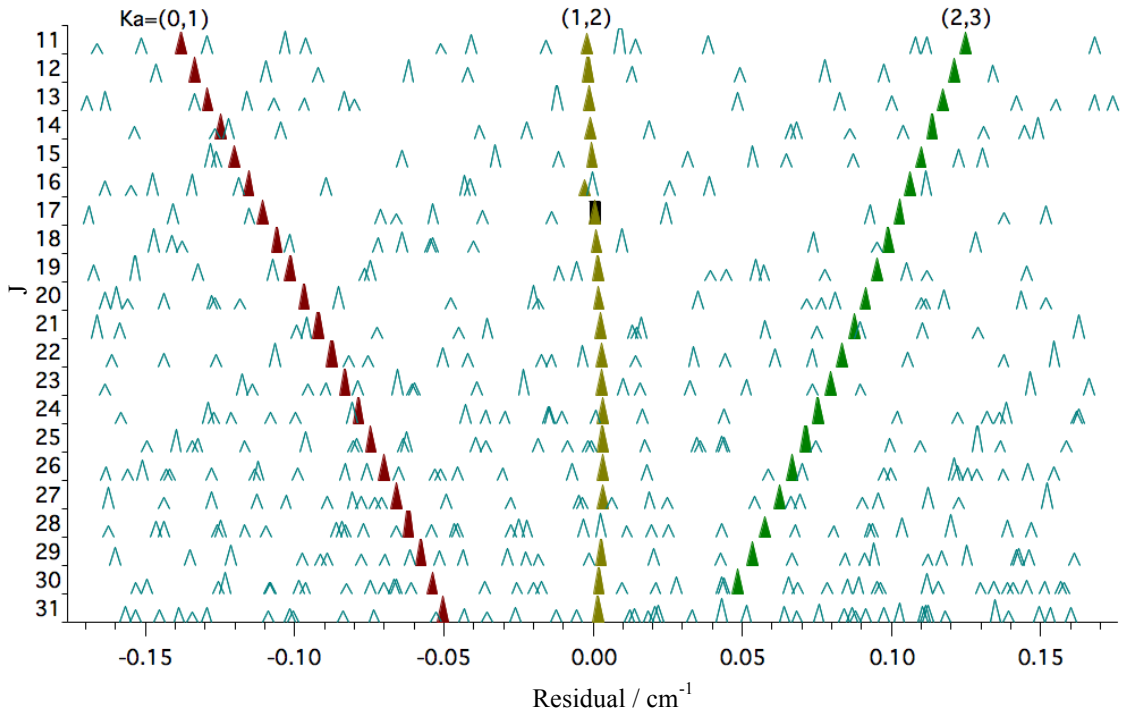

Figure 9.14 A Loomis-Wood plot of the P branch of the *a*-type ν_9 vibrational mode of pyrrole.

In Figure 9.15, the J progression of a cluster in the P branch of the ν_9 band of pyrrole in a span of ~ 0.7 cm^{-1} is depicted. The assignments of each transition in this detailed picture are given as (J′, $K_{a'}$, $K_{c'}$)-(J″, $K_{a''}$, $K_{c''}$). As can be seen, the cluster starts from J′=31 at ~ 871.60 cm^{-1} and reaches to J′=26 at ~ 871.60 cm^{-1} which can be considered as the head of the cluster. Then it reverses back to J′=19 at ~ 871.60 cm^{-1}.

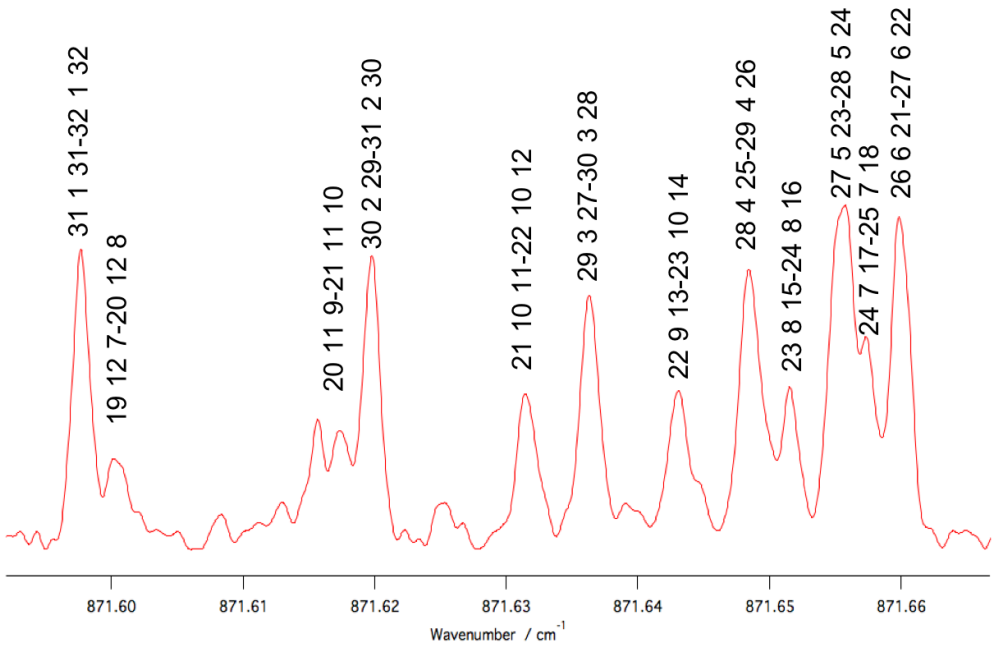

Figure 9.15 A portion of the rotational structure of a cluster in the P branch of the ν_9 band of pyrrole: the quantum numbers of each transition are given as (J′, $K_{a'}$, $K_{c'}$)-(J″, $K_{a''}$, $K_{c''}$). For most features only the J =K_a+K_c-1 member of a degenerate pair is labeled.

In Figure 9.16, the spectra of the ν_9 band of pyrrole are presented. The upper and lower traces show the experimental and simulated spectra respectively. The simulated spectrum resembles the experimental spectrum quite closely.

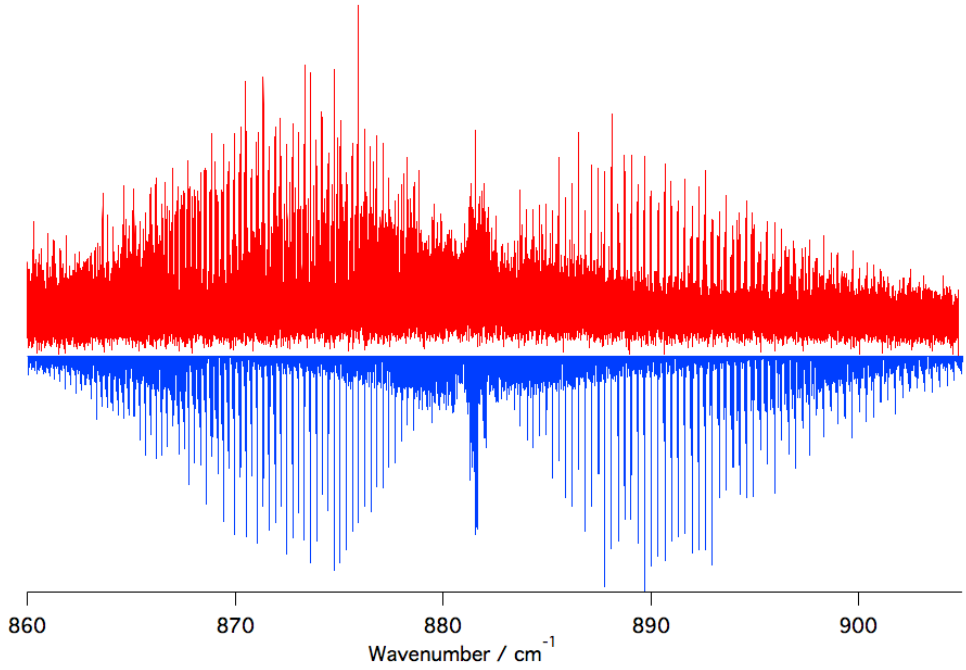

Figure 9.16 The upper and lower traces are the experimental and simulated spectra of the ν_9 band of pyrrole.

Figure 9.17 shows the low root mean square error of the fit, ~ 0.00029 cm^{-1}, for the ν_9 band of pyrrole indicating the fit is of good quality, since the rms is comparable to the measurement uncertainty.

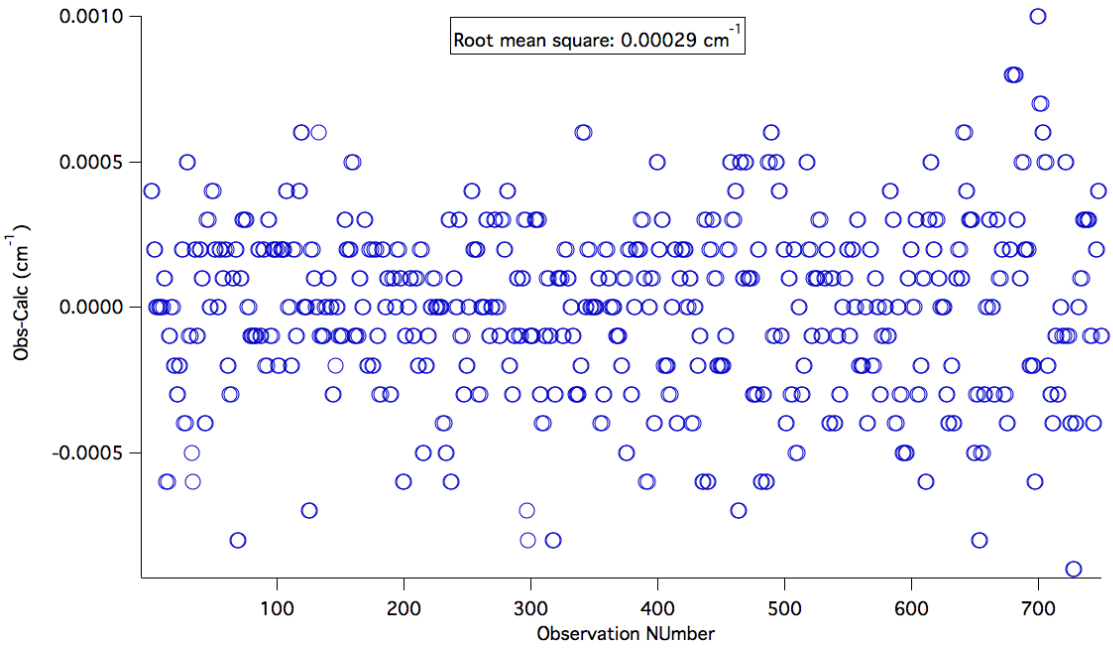

Figure 9.17 The difference between observed and calculated transitions shown as circles with the root mean square error of the fit for the ν_9 band of pyrrole.

Figure 9.18 shows the Loomis-Wood plot of the P branch of the ν_{24} state of pyrrole. Five vertical series with K_a''=(0,1), (1,2), (2,3), (3,4) and (4,5) are identified in the picture. As can be seen from the pattern, higher J lines in the series are slightly distorted and they do not form smooth lines as was observed for the ν_9 band. This deviation indicates that the band might be perturbed by the nearby state of ν_{10} at ~ 864 cm^{-1}.

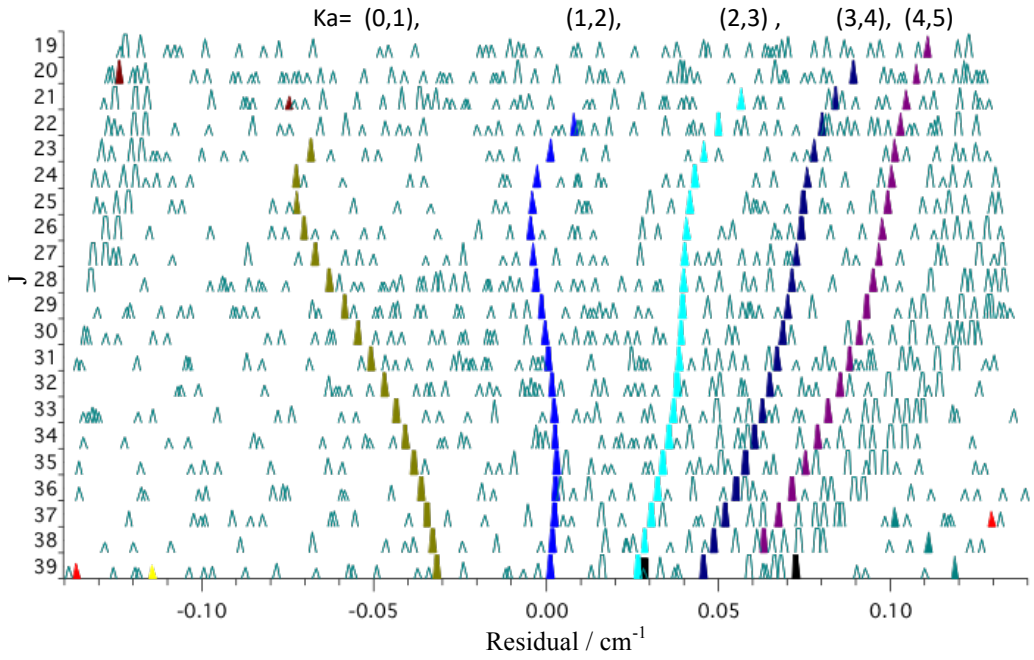

Figure 9.18 A Loomis-Wood plot of the P branch of the *b*-type ν_{24} vibrational mode of pyrrole.

In Figure 9.19 three different J progressions can be seen in a span of ~ 0.5 cm^{-1} with varying intensities which make the spectra highly blended. The quantum numbers of each transition in the progression are given as (J', $K_{a'}$, $K_{c'}$)-(J'', $K_{a''}$, $K_{c''}$). The J'=25 transition starts at ~ 856.6 cm^{-1} reaching to J'=18 at ~ 857.2 cm^{-1}. The second J progression starts with J'=22 at ~ 856.6 cm^{-1} and reaches J'=17 at ~ 856.9 cm^{-1}. The third J progression starts at J'=22 at ~ 856.95 cm^{-1} and reaches to J'=19 at ~ 857.1 cm^{-1}.

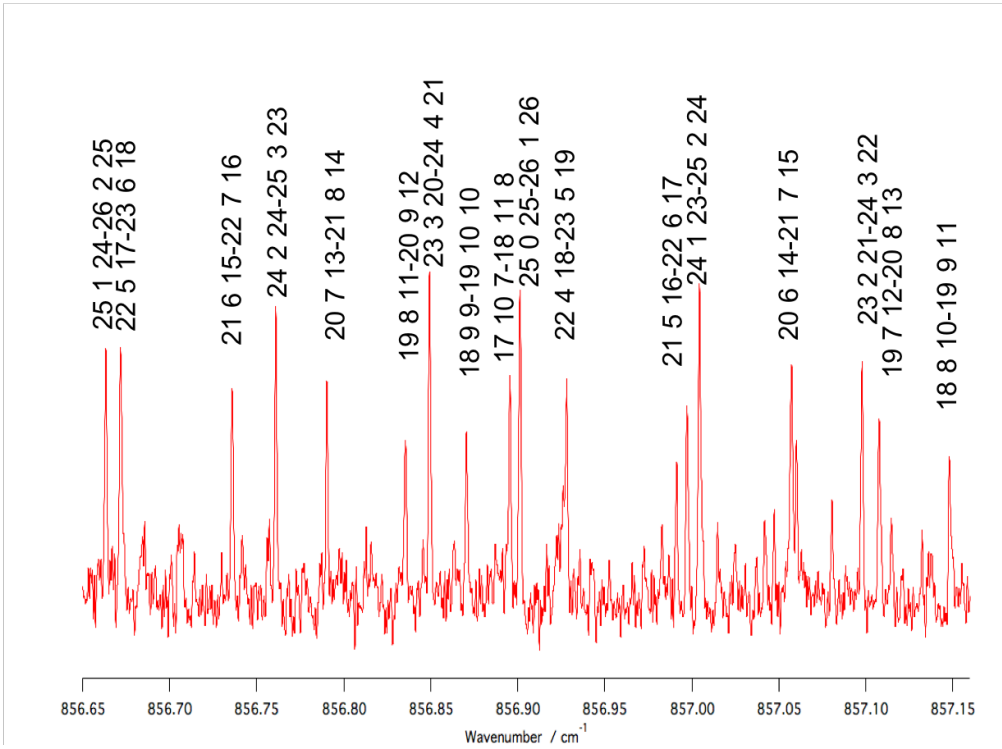

Figure 9.19 A portion of the rotational structure of a cluster in the P branch of the *b*-type ν_{24} band of pyrrole: the quantum numbers of each transition are given as (J′, $K_{a'}$, $K_{c'}$)-(J″, $K_{a''}$, $K_{c''}$).

In Figure 9.20, the upper and lower traces shown are the experimental and simulated spectra of the ν_{24} band of pyrrole. The general shape of the simulated spectrum resembles the experimental spectrum.

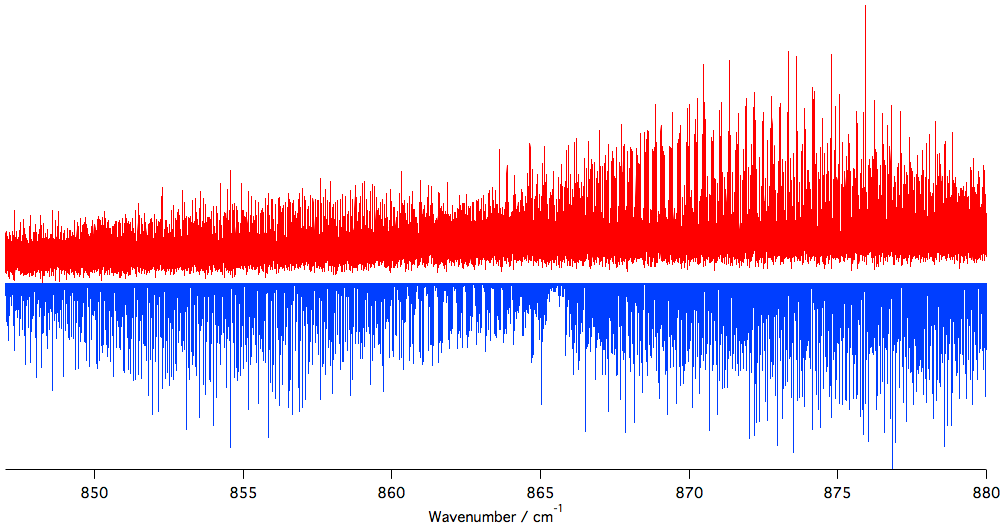

Figure 9.20 The upper and lower traces shown are the experimental and simulated spectra of the ν_{24} band of pyrrole.

In Figure 9.21, the root mean square error of the fit for the ν_{24} band of pyrrole is calculated to be ~ 0.00043 cm^{-1} which is 0.00014 cm^{-1} higher than that of the ν_9 band of pyrrole.

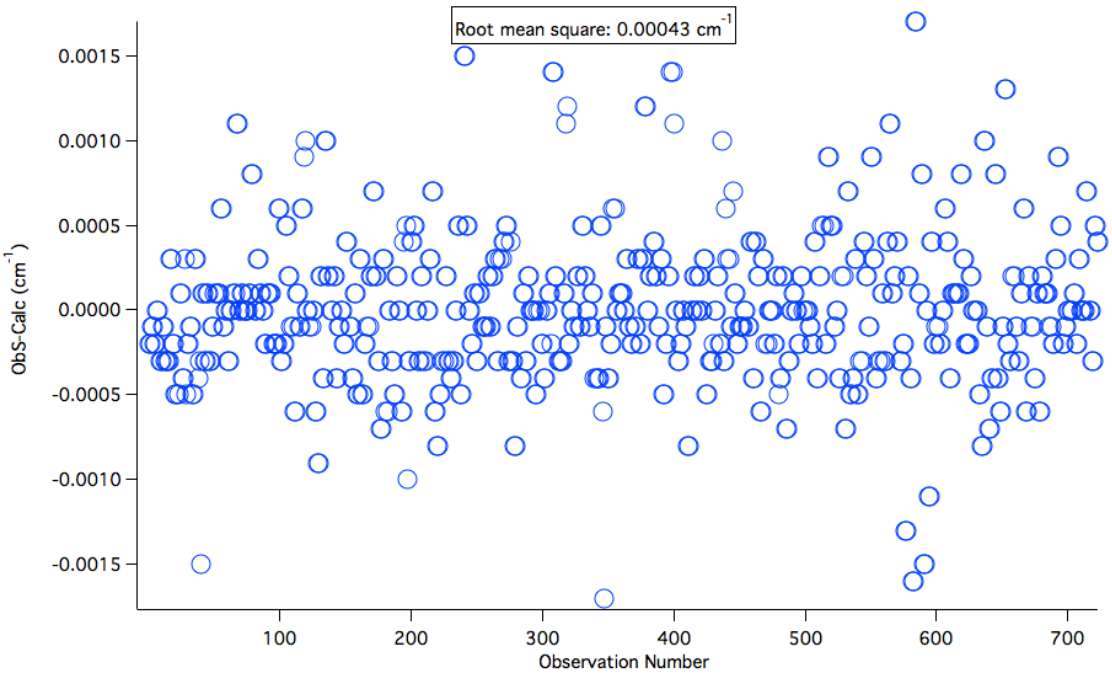

Figure 9.21 The difference between observed and calculated transitions shown as circles with the root mean square error of the fit for the ν_{24} band of pyrrole.

9.6.3 Molecular constants for three states of pyrrole

The molecular constants for four states of pyrrole are presented in Table 9.3. The ground state constants were fixed to those obtained in reference 4. The molecular constants for the ν_9 and ν_{13} states have been fully characterized from the fit. The A, B and C constants for the ν_{24} state are determined from the fit. However, even though the fit is reasonable the ν_{24} state is perturbed, likely by the nearby state of ν_{10} and therefore large values are obtained for the distortion constants of the ν_{24} state.

Table 9.3 Molecular constants (in cm^{-1}) for four states of pyrrole.

Constants	Ground state[a]	ν_9	ν_{13}	ν_{24}
ν	0	881.129907(57)	826.893380(23)	865.443181(74)
A	0.304565105	0.30524638(425)	0.30406723(30)	0.30775222(876)
B	0.300253145	0.30128703(401)	0.29894915(29)	0.29805878(923)
C	0.151174948	0.15146380(16)	0.15120167(17)	0.15029699(23)
$D_J \times 10^8$	3.365	2.4424(99)	2.932(26)	-280.868(2178)
$D_{Jk} \times 10^8$	9.315	-17.975(68)	10.03(13)	103.17(965)
$D_k \times 10^8$	-2.647	56.38(16)	-3.28(11)	1333.4(103)
$d_1 \times 10^8$	-2.048		-1.459(11)	192.911(1093)
$d_2 \times 10^9$	-8.71		-4.908(52)	530.43(418)
$H_{Jk} \times 10^{13}$	-4.76			
$H_{kJ} \times 10^{13}$	5.79			

[a] The ground state constants were fixed to those obtained in reference 4.

9.7 Inertial defect of analysed states of pyrrole

The quantity $\Delta = I_c - I_a - I_b$ is called the inertial defect and can be considered as the degree to which a molecule is planar. The inertial defects are calculated for the four analyzed states of pyrrole and are given in Table 9.4

Table 9.4 Inertial defects of four analysed states of pyrrole.

State	Inertial defect / amu Å^2
Ground	0.0161
ν_9	0.119
ν_{13}	-0.339
ν_{24}	0.8274

The small value of 0.0161 amu Å^2 for the inertial defect for the ground state of pyrrole shows that this molecule is planar. Although the ν_9 state is expected to exhibit in-plane motion, the value of 0.119 amu Å^2 for the inertial defect suggests that there might be some sort of out-of plane motion associated with this band or is an indication of interactions with other states. The relatively large value of Δ for the ν_{13} state is in agreement with out-of-plane motions. The ν_9 and ν_{13} modes have a different symmetry that may account for the positive and negative values of Δ for these states respectively. The ν_{24} state has the largest value of inertial defect among the states. This may result from the fact that ν_{24} is distorted by the unobserved ν_{10} state.

9.8 Conclusion

In this chapter, three new rotationally resolved vibrational bands of pyrrole were studied at $\nu_9 \sim 881$, $\nu_{24} \sim 865$ and $\nu_{13} \sim 826$ cm^{-1}. All the spectra were collected at the Canadian Light Source with an FTIR spectrometer. Three types of transitions, i.e., *a*-, *b*- and *c*-types were observed and analyzed. For the *c*-type band of ν_{13} at ~ 826 cm^{-1}, 1747 transitions were assigned and included in the fit. At ~ 826 cm^{-1}, the *b*-type band ν_9 was analyzed and 758 lines were assigned and included in the fit. There was an overlap between the ν_9 and ν_{24} bands which made the assignment a time consuming process. However, 729 lines in total were assigned and included in the fit of ν_{24} to extract the molecular constants. The band origins of the transitions were precisely determined and are in agreement with the experimental values reported in literature [1]. It should be mentioned that a *c*-type Coriolis coupling between the ν_9 and ν_{24} states was initially included in the fit and the value of $\xi^{c}_{9,24} = 0.004$ (see equation 2.69) was extracted. However, if this constant is omitted from the fit, the other parameters are not affected significantly. This confirms that the interaction between the ν_9 and ν_{24} states is very weak as indicated by the rms error ~ 0.00029 cm^{-1} of the fit for the ν_9 band of pyrrole. However, the ν_{24} state is perturbed, very likely by the unobserved ν_{10} state through a *b*-type Coriolis interaction. The ~ 100 to 430 cm^{-1} spectral region was surveyed at CLS in an attempt to access ν_{10} by populating the ν_{16} level but no transitions were observed. Note that at room temperature, the population of ν_{16} is low. Therefore, a much higher than normal pressure was applied to the cell to compensate for the low population of ν_{16}.

Although we were expecting a relative low-intensity transition from ν_{16} to ν_{10} compared to the analyzed bands, even taking a weak spectrum would have been helpful for analysis.

References

1. A. Mellouki, J. Lievin, M. Herman, J. Chem. Phys. **271**, 239 (2001).

2. I. M. Mills, Pure Appl. Chem. **11**, 325 (1966).

3. S. Y. Lee, B. H. Boo, J. Phys. Chem. **100**, 15073 (1996).

4. D. W. Tokaryk, J. Van Wijngaarden, Can. J. Phys. **87**, 443 (2009).

5. A. Mellouki, J. Vander Auwera, M. Herman, J. Mol. Spectrosc. **193**, 195 (1999).

6. W. Gordy, R. L. Cook, Microwave Molecular Spectra, 2nd ed., Toronto: John Wiley & Sons, Inc., (1984).

7. J. K. G. Watson, J. Chem. Phys. **46**, 1935 (1967).

8. J. K. G. Watson, J. Mol. Struc. **44**, 263 (1978).

9. C. M. Western, Pgopher, a program for simulating rotational, vibrational and electronic spectra, http://pgopher.chm.bris.ac.uk.

Chapter 10

Far-infrared synchrotron-based spectroscopy of furan

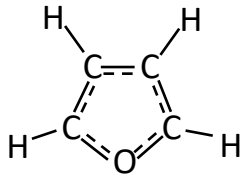

Figure 10.1 Schematic structure of the furan molecule.

The schematic structure of the furan molecule is depicted in Figure 10.1. Furan is a five-membered ring with the formula C_4H_4O. It is a nine-atom heterocyclic aromatic organic compound with 21 modes of vibration. In this thesis two overlapping vibrational bands of furan at ~ 870 and 873 cm^{-1} are studied.

10.1 Modes of vibration of furan

Figure 10.2 shows the band origins of the vibrational modes of furan. This molecule belongs to the C_{2V} point group and the vibrational states in the Figure are grouped according to their C_{2V} symmetries [1]. The vibrational levels ν_8 and ν_{21} are located at ~ 870 and 873 cm^{-1}. There is also the ν_9 state at ~ 864 cm^{-1} that is inaccessible from the ground state. Therefore, there are three levels in a narrow spectral span of ~ 10 cm^{-1}. In the next section, the possible interactions between these levels and new excitations from the ground and low-lying excited states to this triad will be discussed based on symmetry.

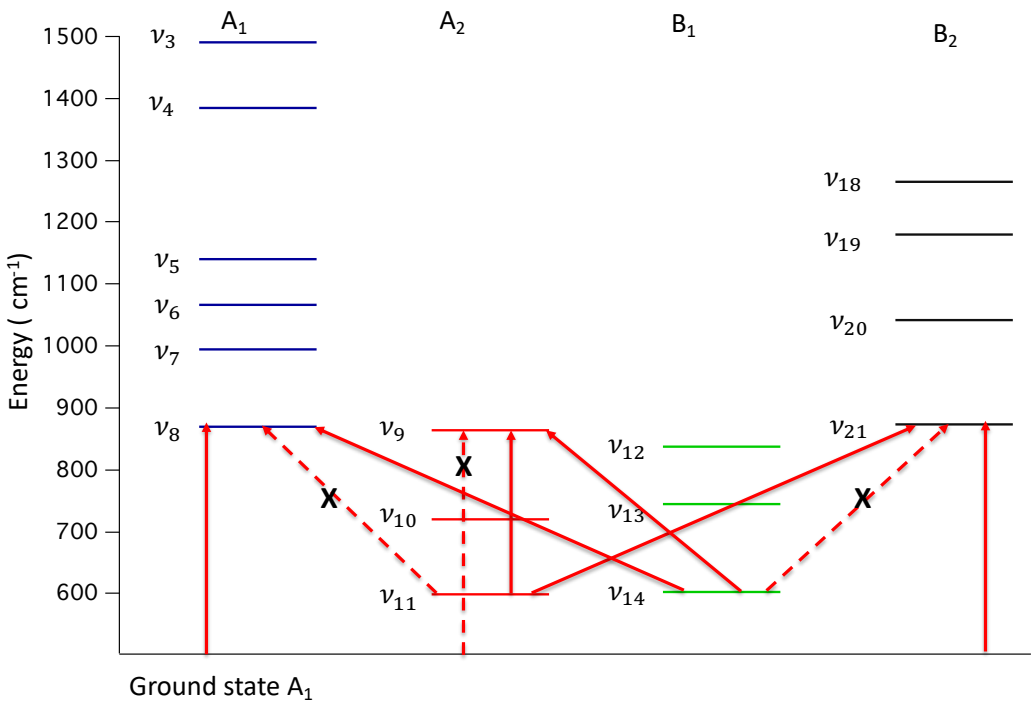

Figure 10.2 A vibrational energy level diagram of furan is shown where the levels are grouped by their symmetries. Selected allowed transitions are depicted as solid lines and symmetry forbidden transitions are drawn as dashed lines with a superimposed "X".

10.2 Possible transitions and interactions

As with pyrrole, the coordinate system that is attached to the molecule has the C_2 symmetry axis along the *a*-axis and the molecule is in the plane constructed by *a*- and *b*-axes. The ground state of this system has A_1 symmetry. The symmetries of the ν_8 and ν_{21} vibrational levels are A_1 and B_2. Therefore, transitions from the A_1 ground state to them are of *a*- and *b*-types because $A_1 \otimes A_1 = A_1$ and $A_1 \otimes B_2 = B_2$. These levels can interact with each other via a *c*-type Coriolis coupling since $A_1 \otimes B_2 = B_2$. There is also

the nearby ν_9 level which has A_2 symmetry and is inaccessible from the ground state since $A_1 \otimes A_2 = A_2$. This level can also interact with ν_8 and ν_{21} through Coriolis couplings of *a*- and *b*-types respectively, according to $A_1 \otimes A_2 = A_2$ and $B_2 \otimes A_2 = B_1$. Therefore, in order to fully characterize the ν_8 and ν_{21} states, accessing the ν_9 level is beneficial. There are two low-lying excited states in furan from which the ν_9 level may be accessed. They are the ν_{11} and ν_{14} with A_2 and B_1 symmetries and the transitions from them to the ν_9 level are of *a*- and *b*-type respectively. The ν_{11} and ν_{14} levels have previously been characterized [2] and are coupled via a *c*-type second order Coriolis interaction. At room temperature, the populations of the ν_{11} and ν_{14} levels are low. Therefore, by applying a much higher than normal pressure to the cell the low population of these levels may be compensated. Consequently, by increasing the pressure, four transitions originating from these states could potentially be observed. From ν_{11} to ν_9 and ν_{21}, *a*- and *b*-type transitions can occur respectively at ~ 264 and 273 cm^{-1}. Note that the transition from ν_8 to ν_{11} is symmetry forbidden. From ν_{14} to ν_9 and ν_8, *b*- and *c*-type transitions can occur at ~ 261 and 267 cm^{-1} respectively. There is also a symmetry-forbidden transition to ν_{21} from ν_{14}. Therefore, four transitions can be observed if the number of the molecules populated in ν_{11} and ν_{14} is sufficient. As I started the analysis of the ν_8 and ν_{21} states without the prior knowledge of the ν_9 state, new measurements at the Canadian Light Source were planned to access the ν_9 level from a vibrationally excited state of furan; however, no bands were found in ~ 100-400 cm^{-1} region.

10.3 The ν_8 and ν_{21} states of furan

Figure 10.3 shows the overview of the overlapping ν_8 and ν_{21} bands of furan at ~ 870 and 873 cm^{-1}. The asymmetry evident in the intensities of the R and P branches shows that the bands are overlapped. The rotational assignment of the bands was time consuming due to the dense rotational structure of intermingled *a*-and *b*-type bands.

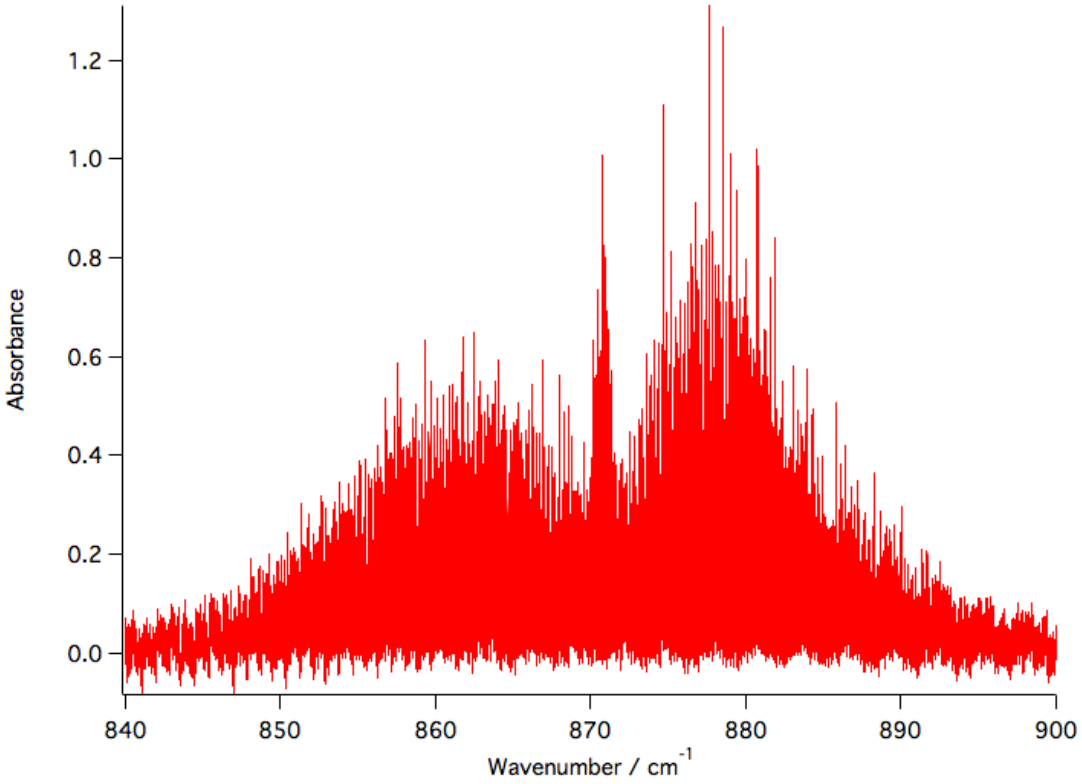

Figure 10.3 Two overlapping vibrational bands of furan, ν_8 and ν_{21}, at ~ 870 and 873 cm^{-1}.

10.3.1 Analysis of the ν_8 and ν_{21}states of furan

In Figure 10.4, a portion of the P branch of the ν_8 band of furan is shown. As can be seen, from the Loomis-Wood plot, the rovibrational transitions having the same K_a are grouped in series for K_a =0,1, K_a =1,2 and K_a =2,3. The series are distorted, likely due to interactions. The corresponding R branch for the K_a=0,1 series is also shown in Figure 10.5. As is evident from the Figure, these series are also distorted and perturbed. The higher J lines seem less perturbed and distorted than the lower J lines.

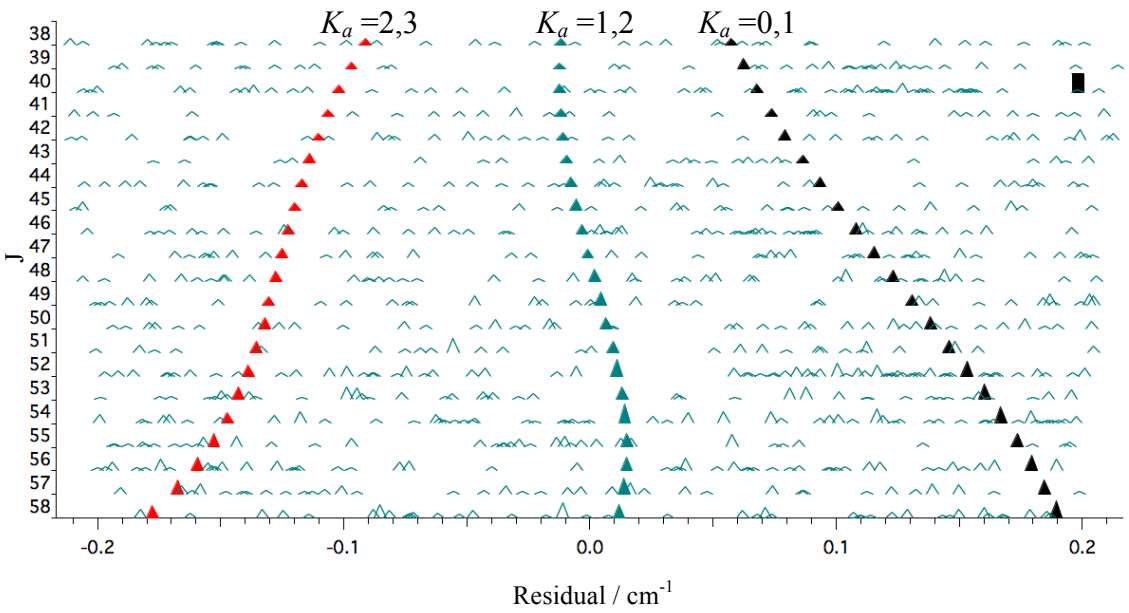

Figure 10.4 A Loomis-Wood plot of a portion of the P branch region of the *a*-type ν_8 band of furan is shown.

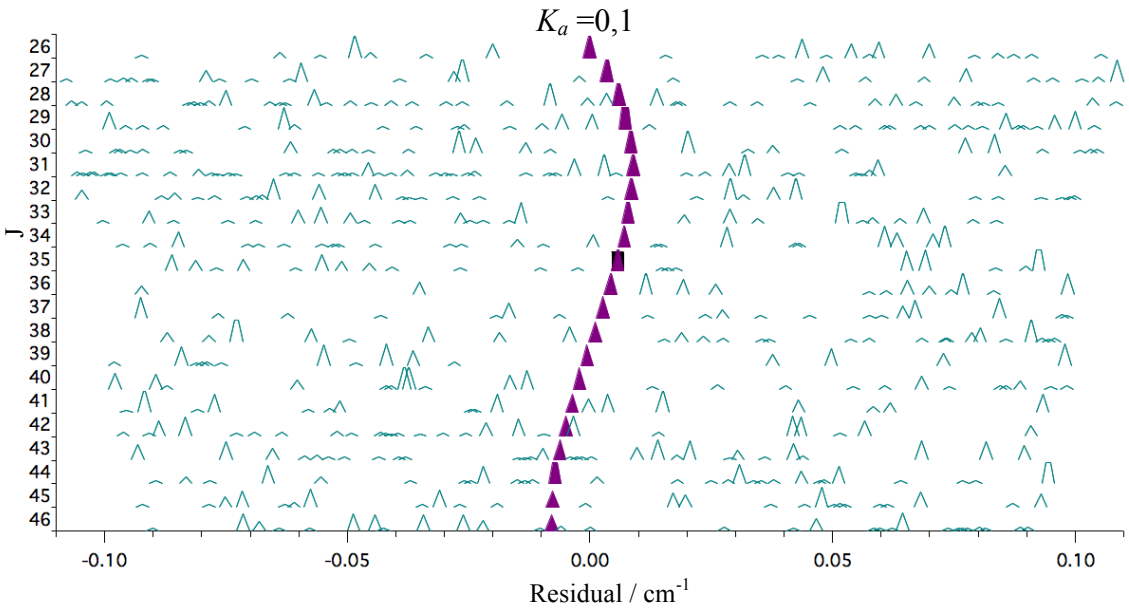

Figure 10.5 A Loomis-Wood plot of a portion of the R branch region of the *a*-type ν_8 band of furan is shown.

Figure 10.6 shows a portion of the P branch of the ν_{21} band of furan. As can be seen, the transitions with the same K_a are given in series for K_a =0,1, K_a =1,2 and K_a =2,3. The evident distortions in the series are due to the perturbations. A portion of the R branch region for K_a =0,1, K_a =1,2 and K_a =2,3 is also shown in the Loomis-Wood plot in Figure 10.7. These series are heavily perturbed.

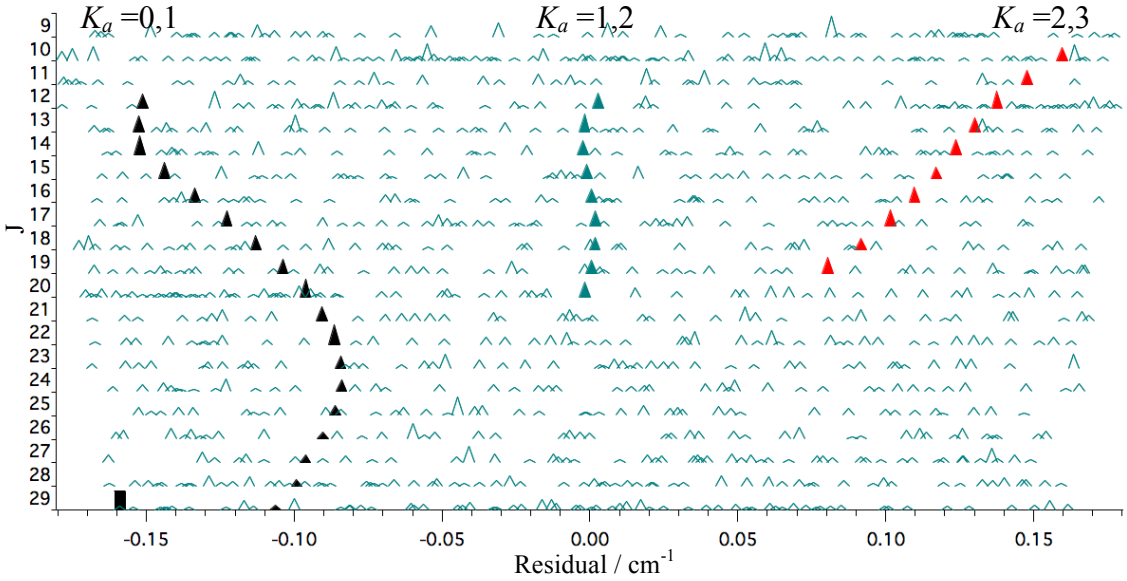

Figure 10.6 A Loomis-Wood plot of a portion of the P branch region of the *b*-type ν_{21} band of furan is shown.

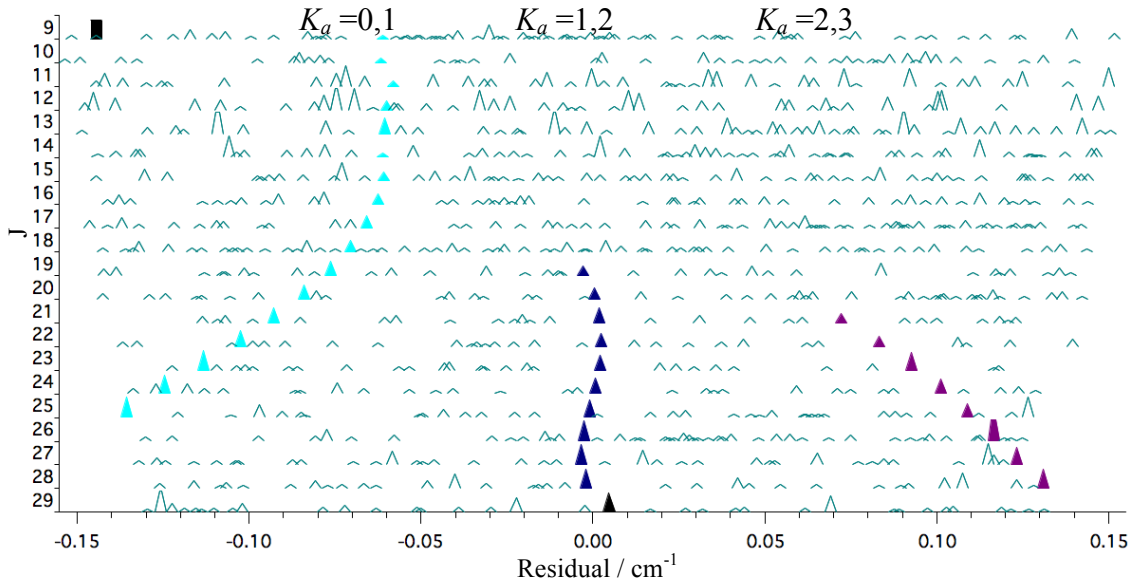

Figure 10.7 A Loomis-Wood plot of a portion of the R branch of the *b*-type ν_{21} band of furan is shown.

Note that the same procedure explained in section 9.5 was used for spectral analysis. Briefly speaking, the lower state combination differences from the calculation match the values obtained from the experiment and hence the transitions were assigned and included in the fit.

10.3.2 Results of the fitting for the ν_8 state of furan

Figure 10.8 shows the experimental and simulated spectra of the *a*-and *b*-type vibrational bands of furan, ν_8 and ν_{21}, at ~ 870 and ~ 873 cm^{-1}. Simulations were performed with

Pgopher [4] at room temperature using the asymmetric top Hamiltonian described in section 9.3.

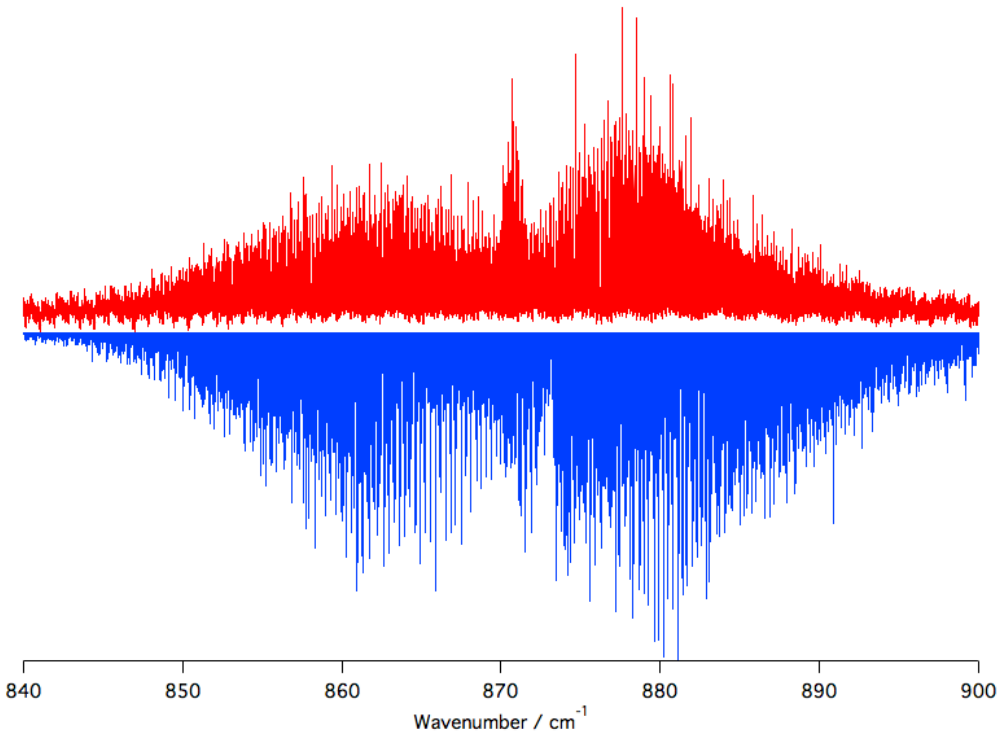

Figure 10.8 The upper and lower traces are the experimental and simulated spectra of the *a*-and *b*-type vibrational bands of furan, ν_8 and ν_{21}, at ~ 870 and ~ 873 cm^{-1}.

The results of the fitting for the ν_8 state of furan are given in Table 10.1. The ground states constants used during the fitting process of this molecule are taken from reference 3. The band is perturbed by the nearby ν_9 and also the ν_{21} states. In Figure 10.9, the difference between the observed and calculated data and the root mean square error of the fit for the ν_8 band of furan is shown which is of the order of ~ 0.0015 cm^{-1}, whereas the uncertainty of clearly measured, unblended lines is about ~ 0.0002 cm^{-1}. There is also a structure associated within the observed-calculated differences. This shows that the

model does not perfectly represent the observations. This is due to the severe perturbations in the system that should be included in the fit to adequately explain the data. In order to improve the results, the interactions with the other states need to be considered. This requires further experiments to access the ν_9 level in future work.

Table 10.1 Molecular constants (in cm^{-1}) for the ν_8 state of furan.

Constants	Ground state[a]	ν_8
ν	0	869.88666(34)
A	0.3151220975	0.3397121(237)
B	0.3084381338	0.2862276(191)
C	0.1558019455	0.15402223(54)
D_J	1.111682e-7	-2.294(5)e-5
D_{Jk}	-1.75584e-7	4.472(1)e-5
D_k	7.6175e-8	-2.188(1)e-5
d_1	-1.7487e-9	4.83(369)e-8
d_2	1.44e-9	2.5(34)e-8
H_{Jk}	-1.738e-13	
H_{kJ}	1.746e-13	

[a] The ground state constants were fixed to those obtained in reference 2.

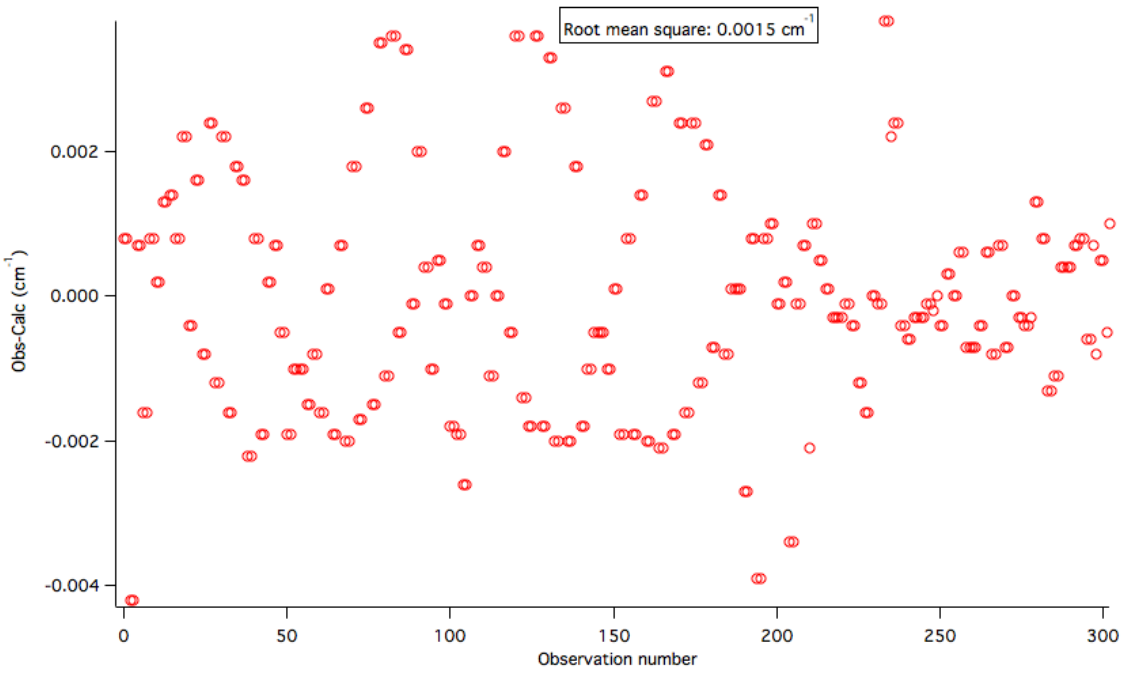

Figure 10.9 The difference between observed and calculated transitions shown as circles with the root mean square error of the fit for the ν_8 band of furan.

It should be mentioned that the molecular constants for the ν_{21} ~ 873 cm^{-1} transition were fixed to the ground state values to produce the simulated spectra of the overlapped ν_8 and ν_{21} vibrational bands.

10.4 The asymmetric parameter of furan

As can be seen from the molecular constants of furan presented in Table 10.1 the relation A≈B≈2C holds true for both the ground and excited (ν_8) states. The asymmetric parameter is found to be $\kappa = \frac{2B - A - C}{A - C}$ ~ 0.938 in the ground state. This indicates that

the molecule is a near oblate symmetric top. Upon the excitation to the ν_8 level, this parameter becomes ~ 0.923 which indicates that the molecule is still near oblate. Note that furan like pyrrole has a large κ value and shows it is a near-oblate rotator (see Figure 2.6 for the correlation diagram of furan).

10.5 Conclusion

In this chapter two fully overlapped vibrational bands of furan, ν_8 and ν_{21}, were studied. Two different transitions, *a*- and *b*-type, were associated with the bands. The ν_8 and ν_{21} levels are heavily perturbed by the Coriolis coupling between them and also the Coriolis interactions with the nearby ν_9 state. Attempts were made to access the ν_9 level in order to include the corresponding interactions ν_8 - ν_9 and ν_{21} - ν_9 but no transition to the ν_9 level was observed. However, the transitions were assigned and a global fit of the ν_8 and ν_{21} states was attempted. The *c*-type Coriolis interaction between them was also included. The result of the global fit showed a large error. This might be due to the exclusion of interactions with the nearby ν_9 state. However, the ν_8 band of furan was individually fitted and the molecular constants were extracted with the root mean square error of ~ 0.0015 cm^{-1}. Although the transitions for the ν_{21} were assigned, the molecular constants for this state were not reported because of severe perturbations. In order to fully characterize the ν_8 and ν_{21} bands of furan, the effects of the ν_9 interacting state should also be taken into account. Once this is done, the triad of states of ν_8, ν_{21} and ν_9 of furan will be fully established as a system.

References

1. A. Mellouki, J. Lievin, M. Herman. J. Chem.Phys. **271**, 239 (2001).

2. D. W. Tokaryk, S. D. Cullingan, B. E. Billinghurst, J. Van Wijngaarden, J. Mol. Spectrosc. **270**, 56 (2011).

3. A. Mellouki, J. V. Auwera, M. Herman, J. Mol. Spectrosc. **193**, 195 (1999).

4. C. M. Western, Pgopher, a program for simulating rotational, vibrational and electronic spectra, http://pgopher.chm.bris.ac.uk.

Chapter 11

Conclusions

The experiments described in this thesis were done at two different institutions: the University of New Brunswick (UNB), and the Canadian Light Source (CLS). At UNB, laser spectroscopy was used to obtain high and low-resolution spectra of small molecules. The Canadian Light Source (CLS) at the University of Saskatchewan was used to obtain high-resolution infrared spectra of medium-sized molecules.

In this thesis, six molecules have been studied in the gas phase. Three of them, i.e., RuF, RuCl and RuO, were ruthenium-bearing diatomic molecules and the rest catechol, pyrrole and furan, were examples of organic ring molecules.

The study of the three ruthenium-bearing diatomic molecules using high-resolution laser experiments informed us about extensive isotopic structure. For ruthenium monochloride and ruthenium monoxide, this was the first time that the isotopic structure has ever been observed. The isotopic structure due to ruthenium was almost fully resolved in ruthenium monofluoride and ruthenium monoxide. The data gathered for different isotopologues of ruthenium monoxide were exploited to establish T_e, the purely electronic energy of one excited state for this molecule. In ruthenium monochloride, the isotopic structure due to chlorine and ruthenium was also observed. Therefore, a mixture of ruthenium and chlorine isotopes was present in the spectra which added to the complexity of analysis but gave more information about the molecules.

In the study of ruthenium monofluoride and ruthenium monoxide, hyperfine structure was also observed. In ruthenium monofluoride, the hyperfine structure which stemmed from the fluorine nuclear spin was observed and analyzed. Some hyperfine structure due to the ^{101}Ru and ^{99}Ru isotopes was also observed in these molecules. In ruthenium monofluoride, the combined hyperfine effects of the two nuclear spins of the ruthenium and fluorine atoms made the analysis of hyperfine structure of the ^{101}Ru and ^{99}Ru isotopologues too complex. In ruthenium monoxide, however, hyperfine effects of the ^{101}Ru isotopologue were analyzed. This helped to confirm the electronic configuration as $\delta^3\sigma^1\pi^2$ for the ground state of this molecule. In ruthenium monochloride, no hyperfine structure was observed. Since the magnetic moment of chlorine is small, a higher signal to noise ratio and improved resolution can probably uncover some hyperfine structure in this molecule.

The first observation of the RuCl molecule was made during the course of this research. The study of the two halide molecules, RuF and RuCl, revealed similarities between them. For instance, the ground states of ruthenium monochloride and ruthenium monofluoride were determined theoretically to be $^4\Phi$. A previous experimental study on RuF showed the ground state was $^4\Phi$. My work on RuF and RuCl established that the ground states of these molecules were both $^4\Phi$. States of the same type might have the same electronic configuration. Since the ground state of RuF is $\delta^3\pi^3\sigma^1$ it is expected that RuCl will have the same configuration. Likewise similarities in electronic structure of excited states between RuF and RuCl may exist.

The current studies lead us to suggest further experiments with molecules with similar properties. Therefore, the next molecule in the halide series that can be made in the molecular beam is ruthenium monobromide. There is a good chance that many of the isotopologues of RuBr would be resolved. Also looking for the possibility of making ruthenium monoiodide is worthwhile. The moment of inertia of this molecule is the largest compared to the preceding molecules in the halide series. For instance, the rotational constant of RuI is approximately ~0.08 cm^{-1} which is about 3.5 times smaller than that of RuF. Therefore, the rotational lines may not be as easily resolvable as in RuF. However, the rotational lines will be about ~0.16 cm^{-1} apart and under the resolution of the experiments, i.e., 0.001 cm^{-1} it is still worth the attempt to make and study this molecule.

It should be mentioned that an attempt was made to make rhenium chloride by changing the metal from ruthenium to rhenium and using CCl_4 as a precursor. This ReCl molecule has never been observed. The 420 to 750 nm spectral region was scanned in a low-resolution survey but there was no indication the ReCl molecule was produced. Hence, for a future project, using BCl_3 as a precursor or some other chlorine-bearing precursor may be the next logical step toward making the molecule.

Apart from small molecules that I studied in the visible region, I also studied medium-sized ring molecules in the infrared region.

For the ring molecules, analogous bands of pyrrole and furan were studied. They had the same symmetries, basic motion and structure and were nearly in the same spectral region. In both cases, interactions were observed that perturb the molecular structure. In both of these molecules a nearby level with A_2 symmetry that was not observed might have influenced the structure of molecules. These studies extended the knowledge about the spectroscopy of furan and pyrrole and in future may help the detection of these molecules in outer space.

Finally, further experiments to observe the catechol molecule at the Canadian Light Source may be attempted. To put the catechol molecule into the gas phase and take the spectrum, a better understanding of the experimental conditions is required. This includes the study of the catechol vapor pressure as a function of temperature when the sample is heated. Due to the low vapor pressure of this molecule, heating the sample is required. Hence, a future project of measuring the vapor pressure while gradually heating the sample is suggested to find the optimal conditions for the experiment. Observation of the spectrum of catechol, if it proves successful, would provide the basis for the study of a large class of technologically important “ring-based-thiolated molecules”.

Appendix A

Observed and calculated frequencies (cm^{-1}) of the ^{102}RuF, ^{104}RuF, ^{100}RuF and ^{96}RuF isotopologues extracted from the multiple state fitting for the 0-0 [18.2] $^4\Gamma_{5.5} \rightarrow X^4\Phi_{4.5}$, [22.1] $^4\Delta_{3.5} \rightarrow X^4\Phi_{4.5}$ and [13.1] $^4\Delta_{3.5} \rightarrow X^4\Phi_{4.5}$ transitions.

The 0-0 band of the [18.2] $^4\Gamma_{5.5} \rightarrow X^4\Phi_{4.5}$ transition

Isotopologue	Branch	F'	F''	J''	Observed (cm^{-1})	Calculated (cm^{-1})	Obs-Cal (cm^{-1})
^{102}RuF	P	5	6	6.5	18250.3019	18250.3012	0.0007
	P	6	7	6.5	18250.3416	18250.3413	0.0002
	P	6	6	6.5	18250.3478	18250.3474	0.0004
	P	6	7	7.5	18249.7513	18249.7516	-0.0003
	P	7	8	7.5	18249.7847	18249.7857	-0.0009
	P	7	8	8.5	18249.2034	18249.2041	-0.0007
	P	8	9	8.5	18249.2327	18249.2338	-0.0011
	P	8	9	9.5	18248.6604	18248.6591	0.0013
	P	9	10	9.5	18248.6865	18248.6854	0.001
	P	9	10	10.5	18248.1166	18248.117	-0.0003
	P	10	11	10.5	18248.1403	18248.1406	-0.0003
	P	10	11	11.5	18247.5781	18247.5777	0.0004
	P	11	12	11.5	18247.5998	18247.5991	0.0007
	P	11	12	12.5	18247.0406	18247.0414	-0.0008
	P	12	13	12.5	18247.0606	18247.061	-0.0004
	P	12	13	13.5	18246.5099	18246.5082	0.0016
	P	13	14	13.5	18246.5275	18246.5263	0.0012
	P	13	14	14.5	18245.976	18245.9781	-0.0022
	P	14	15	14.5	18245.9923	18245.9949	-0.0026
	P	14	15	15.5	18245.4509	18245.4513	-0.0004
	P	15	16	15.5	18245.4669	18245.4669	0.0001
	P	15	16	16.5	18244.93	18244.9276	0.0024
	P	16	17	16.5	18244.9446	18244.9422	0.0024
	P	16	17	17.5	18244.4106	18244.4072	0.0034
	P	17	18	17.5	18244.4235	18244.4209	0.0026
	P	17	18	18.5	18243.8905	18243.8901	0.0004
	P	18	19	18.5	18243.9033	18243.9031	0.0003
	P	18	19	19.5	18243.3785	18243.3763	0.0021
	P	19	20	19.5	18243.3888	18243.3886	0.0002
	P	19	20	20.5	18242.8653	18242.866	-0.0006
	P	20	21	20.5	18242.8778	18242.8776	0.0002
	P	20	21	21.5	18242.3554	18242.359	-0.0036
	P	21	22	21.5	18242.3658	18242.3701	-0.0043
	P	21	22	22.5	18241.8527	18241.8554	-0.0028
	P	22	23	22.5	18241.8625	18241.866	-0.0035
	P	22	23	23.5	18241.3522	18241.3554	-0.0032
	P	23	24	23.5	18241.3627	18241.3655	-0.0028
	P	23	24	24.5	18240.8566	18240.8588	-0.0022

P	24	25	24.5	18240.8679	18240.8685	-0.0006
P	24	25	25.5	18240.3639	18240.3658	-0.0019
P	25	26	25.5	18240.3734	18240.3751	-0.0018
P	25	26	26.5	18239.8742	18239.8764	-0.0022
P	26	27	26.5	18239.883	18239.8854	-0.0024
P	26	27	27.5	18239.389	18239.3907	-0.0017
P	27	28	27.5	18239.3978	18239.3993	-0.0015
P	27	28	28.5	18238.9064	18238.9086	-0.0022
P	28	29	28.5	18238.915	18238.9169	-0.0019
P	28	29	29.5	18238.429	18238.4302	-0.0011
P	29	30	29.5	18238.4364	18238.4382	-0.0018
Q	15	15	15.5	18254.3835	18254.3811	0.0025
Q	16	16	15.5	18254.399	18254.3955	0.0035
Q	16	16	16.5	18254.4354	18254.4329	0.0025
Q	17	17	16.5	18254.4489	18254.4465	0.0025
Q	17	17	17.5	18254.49	18254.4878	0.0021
Q	18	18	17.5	18254.5023	18254.5007	0.0016
Q	18	18	18.5	18254.548	18254.546	0.002
Q	19	19	18.5	18254.5608	18254.5582	0.0026
Q	19	19	19.5	18254.6097	18254.6074	0.0023
Q	20	20	19.5	18254.621	18254.619	0.0021
Q	20	20	20.5	18254.6736	18254.6721	0.0016
Q	21	21	20.5	18254.6845	18254.6831	0.0015
Q	21	21	21.5	18254.742	18254.74	0.002
Q	22	22	21.5	18254.752	18254.7505	0.0015
Q	22	24	24.5	18254.8132	18254.8113	0.0019
Q	23	25	24.5	18254.8225	18254.8213	0.0012
Q	23	25	25.5	18254.8876	18254.8859	0.0017
Q	24	26	25.5	18254.8966	18254.8955	0.0011
Q	24	26	26.5	18254.965	18254.9639	0.0012
Q	25	27	26.5	18254.9744	18254.9731	0.0013
Q	25	27	27.5	18255.0461	18255.0452	0.0008
Q	26	28	27.5	18255.0555	18255.0541	0.0014
Q	26	28	28.5	18255.1311	18255.1301	0.001
Q	27	29	28.5	18255.14	18255.1386	0.0013
Q	27	29	29.5	18255.2193	18255.2183	0.0009
Q	28	30	29.5	18255.227	18255.2266	0.0004
Q	28	22	22.5	18255.3102	18255.3101	0.0001
Q	29	23	22.5	18255.3188	18255.3181	0.0007
Q	29	23	23.5	18255.406	18255.4054	0.0005

Q	30	24	23.5	18255.4132	18255.4131	0.0001
Q	31	31	30.5	18255.5118	18255.5118	0.0001
Q	30	30	30.5	18255.506	18255.5043	0.0017
Q	31	31	31.5	18255.6089	18255.6068	0.0022
Q	32	32	31.5	18255.6134	18255.614	-0.0006
Q	33	33	32.5	18255.7199	18255.7199	0
Q	32	32	32.5	18255.7132	18255.7129	0.0003
Q	34	34	33.5	18255.8293	18255.8295	-0.0002
Q	33	33	33.5	18255.8237	18255.8227	0.001
R	5	4	4.5	18257.1794	18257.1813	-0.0019
R	6	5	4.5	18257.2168	18257.219	-0.0022
R	5	5	4.5	18257.1715	18257.1728	-0.0013
R	6	5	5.5	18257.776	18257.7775	-0.0015
R	7	6	5.5	18257.8077	18257.8098	-0.0021
R	6	6	5.5	18257.7704	18257.7704	0
R	7	6	6.5	18258.3742	18258.3758	-0.0016
R	8	7	6.5	18258.4019	18258.4042	-0.0023
R	7	7	6.5	18258.3693	18258.3698	-0.0005
R	8	7	7.5	18258.9752	18258.9767	-0.0015
R	9	8	7.5	18259.0005	18259.0019	-0.0015
R	9	8	8.5	18259.5775	18259.5803	-0.0028
R	10	9	8.5	18259.6021	18259.603	-0.001
R	10	9	9.5	18260.1875	18260.1866	0.0009
R	11	10	9.5	18260.2081	18260.2073	0.0007
R	11	10	10.5	18260.7968	18260.7959	0.001
R	12	11	10.5	18260.8158	18260.8148	0.0009
R	12	11	11.5	18261.4089	18261.408	0.0009
R	13	12	11.5	18261.4265	18261.4255	0.001
R	13	12	12.5	18262.0231	18262.0231	0.0001
R	14	13	12.5	18262.0389	18262.0394	-0.0005
R	14	13	13.5	18262.6406	18262.6411	-0.0006
R	15	14	13.5	18262.6558	18262.6564	-0.0006
R	15	14	14.5	18263.2619	18263.2622	-0.0004
R	16	15	14.5	18263.2764	18263.2765	-0.0001
R	16	15	15.5	18263.8865	18263.8863	0.0002
R	17	16	15.5	18263.9009	18263.8998	0.0011
R	17	16	16.5	18264.5134	18264.5135	-0.0001
R	18	17	16.5	18264.5268	18264.5262	0.0006
R	18	17	17.5	18265.1444	18265.1437	0.0007
R	19	18	17.5	18265.1566	18265.1558	0.0008

	R	19	18	18.5	18265.7796	18265.7771	0.0025
	R	20	19	18.5	18265.7912	18265.7885	0.0026
	R	20	19	19.5	18266.4155	18266.4135	0.0019
	R	21	20	19.5	18266.4259	18266.4244	0.0014
	R	21	20	20.5	18267.0525	18267.0531	-0.0006
	R	22	21	20.5	18267.0639	18267.0635	0.0003
	R	22	21	21.5	18267.6947	18267.6959	-0.0012
	R	23	22	21.5	18267.7036	18267.7058	-0.0022
	R	23	22	22.5	18268.3404	18268.3418	-0.0014
	R	24	23	22.5	18268.3488	18268.3513	-0.0026
	R	24	23	23.5	18268.9889	18268.9909	-0.002
	R	25	24	23.5	18268.9986	18269.0001	-0.0015
	R	25	24	24.5	18269.6417	18269.6433	-0.0016
	R	26	25	24.5	18269.6498	18269.6521	-0.0023
	R	26	25	25.5	18270.2979	18270.2988	-0.001
	R	27	26	25.5	18270.3082	18270.3073	0.0008
	R	27	26	26.5	18270.958	18270.9577	0.0003
	R	28	27	26.5	18270.9649	18270.9659	-0.001
	R	28	27	27.5	18271.6184	18271.6199	-0.0015
	R	29	28	27.5	18271.6271	18271.6278	-0.0007
	R	29	28	28.5	18272.2847	18272.2854	-0.0007
	R	30	29	28.5	18272.2926	18272.293	-0.0004
	R	30	29	29.5	18272.9547	18272.9542	0.0004
	R	31	30	29.5	18272.9619	18272.9616	0.0003
	R	31	30	30.5	18273.627	18273.6264	0.0006
	R	32	31	30.5	18273.6342	18273.6336	0.0006
	R	33	32	31.5	18274.3081	18274.309	-0.0009
	R	32	31	31.5	18274.3017	18274.3021	-0.0004
	R	33	32	32.5	18274.9812	18274.9811	0.0001
	R	34	33	32.5	18274.9882	18274.9879	0.0004
	R	35	34	33.5	18275.672	18275.6702	0.0018
	R	34	33	33.5	18275.6663	18275.6637	0.0026
^{104}RuF	P	5	6	6.5	18250.2859	18250.2859	0
	P	6	7	6.5	18250.327	18250.3262	0.0008
	P	6	7	7.5	18249.7368	18249.7379	-0.0011
	P	7	8	7.5	18249.7708	18249.7722	-0.0015
	P	7	8	8.5	18249.1915	18249.1921	-0.0006
	P	8	9	8.5	18249.2189	18249.222	-0.0031
	P	8	9	9.5	18248.6504	18248.6488	0.0016
	P	9	10	9.5	18248.6756	18248.6753	0.0003

P	9	10	10.5	18248.1082	18248.1083	-0.0001
P	10	11	10.5	18248.1312	18248.132	-0.0008
P	10	11	11.5	18247.5723	18247.5706	0.0017
P	11	12	11.5	18247.5927	18247.5921	0.0005
P	12	13	12.5	18247.055	18247.0556	-0.0006
P	11	12	12.5	18247.0354	18247.0359	-0.0005
P	13	14	13.5	18246.5262	18246.5225	0.0037
P	12	13	13.5	18246.509	18246.5043	0.0047
P	14	15	14.5	18245.9923	18245.9927	-0.0003
P	13	14	14.5	18245.976	18245.9758	0.0002
P	15	16	15.5	18245.4669	18245.4662	0.0007
P	14	15	15.5	18245.4509	18245.4505	0.0004
P	16	17	16.5	18244.9446	18244.943	0.0016
P	15	16	16.5	18244.93	18244.9283	0.0017
P	17	18	17.5	18244.4236	18244.4233	0.0004
P	16	17	17.5	18244.4102	18244.4094	0.0008
P	18	19	18.5	18243.9031	18243.9069	-0.0038
P	17	18	18.5	18243.8902	18243.8938	-0.0037
P	19	20	19.5	18243.3938	18243.3939	0
P	18	19	19.5	18243.383	18243.3815	0.0015
P	20	21	20.5	18242.8853	18242.8843	0.001
P	19	20	20.5	18242.8737	18242.8726	0.0012
P	21	22	21.5	18242.3746	18242.3782	-0.0036
P	20	21	21.5	18242.3659	18242.367	-0.0011
P	22	23	22.5	18241.8729	18241.8755	-0.0027
P	21	22	22.5	18241.8625	18241.8649	-0.0024
P	23	24	23.5	18241.3735	18241.3764	-0.0029
P	22	23	23.5	18241.3627	18241.3662	-0.0035
P	24	25	24.5	18240.8795	18240.8808	-0.0013
P	23	24	24.5	18240.8679	18240.871	-0.0031
P	25	26	25.5	18240.3874	18240.3887	-0.0014
P	24	25	25.5	18240.3758	18240.3794	-0.0035
P	26	27	26.5	18239.899	18239.9003	-0.0013
P	25	26	26.5	18239.8893	18239.8913	-0.002
P	27	28	27.5	18239.415	18239.4155	-0.0005
P	26	27	27.5	18239.4061	18239.4068	-0.0007
P	28	29	28.5	18238.9338	18238.9343	-0.0005
P	27	28	28.5	18238.9248	18238.926	-0.0012
P	29	30	29.5	18238.4564	18238.4569	-0.0005
P	28	29	29.5	18238.4479	18238.4488	-0.0009
P	30	31	30.5	18237.982	18237.9832	-0.0012

P	29	30	30.5	18237.9746	18237.9754	-0.0008
P	31	32	31.5	18237.5122	18237.5133	-0.0011
P	30	31	31.5	18237.5049	18237.5058	-0.0009
Q	17	17	17.5	18254.4628	18254.4594	0.0034
Q	18	18	17.5	18254.4748	18254.4723	0.0025
Q	18	18	18.5	18254.5204	18254.5173	0.0031
Q	19	19	18.5	18254.5327	18254.5295	0.0031
Q	19	19	19.5	18254.5799	18254.5785	0.0014
Q	20	20	19.5	18254.5917	18254.5901	0.0016
Q	20	20	20.5	18254.6438	18254.6429	0.0009
Q	21	21	20.5	18254.6554	18254.6539	0.0015
Q	22	22	22.5	18254.783	18254.7815	0.0014
Q	23	23	22.5	18254.7936	18254.7916	0.002
Q	24	24	23.5	18254.8678	18254.8655	0.0023
Q	23	23	23.5	18254.8554	18254.8558	-0.0004
Q	25	25	25.5	18255.0158	18255.0145	0.0012
Q	26	26	25.5	18255.0258	18255.0235	0.0024
Q	26	26	26.5	18255.1006	18255.099	0.0016
Q	27	27	26.5	18255.109	18255.1076	0.0014
Q	27	27	27.5	18255.1878	18255.1869	0.0009
Q	28	28	27.5	18255.1964	18255.1952	0.0012
Q	28	28	28.5	18255.2791	18255.2783	0.0008
Q	29	29	28.5	18255.2871	18255.2864	0.0007
Q	29	29	29.5	18255.3741	18255.3733	0.0008
Q	30	30	29.5	18255.3816	18255.381	0.0006
Q	30	30	30.5	18255.4719	18255.4718	0.0002
Q	31	31	30.5	18255.4799	18255.4793	0.0006
Q	31	31	31.5	18255.574	18255.5738	0.0002
Q	32	32	31.5	18255.5823	18255.5811	0.0012
Q	32	32	32.5	18255.6802	18255.6795	0.0006
Q	33	33	32.5	18255.6868	18255.6866	0.0002
Q	33	33	33.5	18255.7893	18255.7889	0.0004
Q	34	34	33.5	18255.7961	18255.7957	0.0004
R	6	5	4.5	18257.1796	18257.1828	-0.0032
R	5	4	4.5	18257.1428	18257.1449	-0.0022
R	5	5	4.5	18257.1339	18257.1363	-0.0024
R	6	5	5.5	18257.7385	18257.7392	-0.0007
R	7	6	5.5	18257.7707	18257.7717	-0.001
R	6	6	5.5	18257.7315	18257.732	-0.0005

R	7	6	6.5	18258.3345	18258.3358	-0.0013
R	8	7	6.5	18258.3631	18258.3643	-0.0011
R	7	7	6.5	18258.329	18258.3296	-0.0006
R	8	7	7.5	18258.9339	18258.9348	-0.0009
R	9	8	7.5	18258.9587	18258.9602	-0.0015
R	9	8	8.5	18259.5354	18259.5365	-0.0011
R	10	9	8.5	18259.5584	18259.5594	-0.001
R	10	9	9.5	18260.1423	18260.141	0.0013
R	11	10	9.5	18260.1625	18260.1618	0.0007
R	11	10	10.5	18260.7499	18260.7483	0.0016
R	12	11	10.5	18260.7685	18260.7674	0.001
R	12	11	11.5	18261.3598	18261.3586	0.0012
R	13	12	11.5	18261.3774	18261.3762	0.0012
R	13	12	12.5	18261.9721	18261.9718	0.0003
R	14	13	12.5	18261.9884	18261.9882	0.0002
R	14	13	13.5	18262.588	18262.5879	0
R	15	14	13.5	18262.6037	18262.6033	0.0005
R	15	14	14.5	18263.2077	18263.2071	0.0006
R	16	15	14.5	18263.2223	18263.2215	0.0008
R	16	15	15.5	18263.83	18263.8293	0.0007
R	17	16	15.5	18263.844	18263.8428	0.0011
R	17	16	16.5	18264.4561	18264.4545	0.0016
R	18	17	16.5	18264.4679	18264.4673	0.0006
R	18	17	17.5	18265.0841	18265.0828	0.0013
R	19	18	17.5	18265.096	18265.0949	0.0011
R	20	19	19.5	18266.3507	18266.3487	0.002
R	21	20	19.5	18266.3619	18266.3597	0.0022
R	21	20	20.5	18266.9872	18266.9864	0.0008
R	22	21	20.5	18266.9984	18266.9968	0.0016
R	22	21	21.5	18267.6259	18267.6271	-0.0012
R	23	22	21.5	18267.6352	18267.6372	-0.002
R	23	22	22.5	18268.2697	18268.2711	-0.0014
R	24	23	22.5	18268.2795	18268.2807	-0.0012
R	24	23	23.5	18268.917	18268.9182	-0.0013
R	25	24	23.5	18268.9263	18268.9275	-0.0011
R	25	24	24.5	18269.5674	18269.5686	-0.0012
R	26	25	24.5	18269.5766	18269.5775	-0.0009
R	26	25	25.5	18270.2211	18270.2222	-0.0012
R	27	26	25.5	18270.2297	18270.2308	-0.0011
R	27	26	26.5	18270.8781	18270.8791	-0.001
R	28	27	26.5	18270.8867	18270.8874	-0.0006

	R	28	27	27.5	18271.5384	18271.5393	-0.0009
	R	29	28	27.5	18271.5466	18271.5472	-0.0006
	R	29	28	28.5	18272.2027	18272.2028	-0.0001
	R	30	29	28.5	18272.2101	18272.2105	-0.0003
	R	30	29	29.5	18272.87	18272.8696	0.0003
	R	31	30	29.5	18272.8774	18272.8771	0.0003
	R	31	30	30.5	18273.5404	18273.5398	0.0005
	R	32	31	30.5	18273.5471	18273.5471	0.0001
	R	33	32	31.5	18274.2209	18274.2205	0.0004
	R	32	31	31.5	18274.2136	18274.2135	0.0002
	R	34	33	32.5	18274.8981	18274.8973	0.0008
	R	33	32	32.5	18274.89	18274.8905	-0.0005
	R	35	34	33.5	18275.5786	18275.5777	0.0009
	R	34	33	33.5	18275.5717	18275.5711	0.0006
^{100}RuF	P	5	6	6.5	18250.3196	18250.3179	0.0017
	P	6	7	6.5	18250.3583	18250.3576	0.0007
	P	6	7	7.5	18249.7663	18249.7665	-0.0002
	P	7	8	7.5	18249.8	18249.8002	-0.0003
	P	9	8	8.5	18249.219	18249.2173	0.0017
	P	10	9	8.5	18249.2458	18249.2467	-0.0009
	P	8	9	9.5	18248.6731	18248.6708	0.0024
	P	9	10	9.5	18248.6985	18248.6967	0.0018
	P	7	10	10.5	18248.1301	18248.127	0.003
	P	8	11	10.5	18248.1489	18248.1503	-0.0014
	P	10	11	11.5	18247.5869	18247.5862	0.0006
	P	11	12	11.5	18247.6076	18247.6074	0.0002
	P	11	12	12.5	18247.0485	18247.0486	0
	P	12	13	12.5	18247.0669	18247.0679	-0.0009
	P	12	13	13.5	18246.5151	18246.514	0.0011
	P	13	14	13.5	18246.5318	18246.5318	-0.0001
	P	15	15	15.5	18245.4509	18245.4548	-0.0039
	P	14	16	15.5	18245.4669	18245.4701	-0.0033
	P	15	16	16.5	18244.9301	18244.9301	-0.0001
	P	16	17	16.5	18244.9446	18244.9445	0.0001
	P	16	17	17.5	18244.4102	18244.4089	0.0013
	P	17	18	17.5	18244.4234	18244.4225	0.001
	P	17	18	18.5	18243.8902	18243.8912	-0.001
	P	18	19	18.5	18243.9031	18243.9039	-0.0009
	P	18	19	19.5	18243.3775	18243.3769	0.0005
	P	19	20	19.5	18243.3893	18243.389	0.0002

	R	5	4	4.5	18257.2168	18257.2201	-0.0034
	R	6	5	4.5	18257.2553	18257.2567	-0.0014
	R	6	5	5.5	18257.8164	18257.818	-0.0016
	R	7	6	5.5	18257.8496	18257.8495	0.0001
	R	7	6	6.5	18258.4171	18258.4181	-0.001
	R	8	7	6.5	18258.4451	18258.4457	-0.0006
	R	8	7	7.5	18259.0198	18259.0208	-0.0011
	R	9	8	7.5	18259.0451	18259.0454	-0.0003
	R	9	8	8.5	18259.6251	18259.6262	-0.0012
	R	10	9	8.5	18259.6478	18259.6484	-0.0007
	R	10	9	9.5	18260.2359	18260.2345	0.0014
	R	11	10	9.5	18260.2563	18260.2547	0.0015
	R	11	10	10.5	18260.8475	18260.8456	0.0019
	R	12	11	10.5	18260.8662	18260.8642	0.002
	R	12	11	11.5	18261.4609	18261.4597	0.0012
	R	13	12	11.5	18261.4781	18261.4769	0.0012
	R	13	12	12.5	18262.0759	18262.0768	-0.0009
	R	14	13	12.5	18262.0924	18262.0928	-0.0004
	R	14	13	13.5	18262.6966	18262.697	-0.0004
	R	15	14	13.5	18262.7121	18262.7119	0.0002
	R	15	14	14.5	18263.3193	18263.3202	-0.0009
	R	16	15	14.5	18263.3348	18263.3342	0.0006
	R	16	15	15.5	18263.9454	18263.9465	-0.0011
	R	17	16	15.5	18263.9599	18263.9597	0.0002
	R	17	16	16.5	18264.5756	18264.576	-0.0003
	R	18	17	16.5	18264.5887	18264.5884	0.0002
	R	18	17	17.5	18265.2082	18265.2086	-0.0005
	R	19	18	17.5	18265.2204	18265.2204	0
	R	19	18	18.5	18265.8444	18265.8445	-0.0001
	R	20	19	18.5	18265.8575	18265.8557	0.0018
^{96}RuF	P	6	7	6.5	18250.394	18250.3984	-0.0044
	P	6	7	7.5	18249.8165	18249.8019	0.0146
	P	7	7	7.5	18249.8516	18249.845	0.0066
	P	8	9	8.5	18249.2883	18249.2801	0.0081
	P	10	11	10.5	18248.1937	18248.1765	0.0172
	R	5	5	4.5	18257.2914	18257.2908	0.0006
	R	5	4	4.5	18257.2973	18257.3031	-0.0058
	R	6	5	4.5	18257.3358	18257.3413	-0.0055

R	6	5	5.5	18257.9006	18257.9049	-0.0043
R	7	6	5.5	18257.9331	18257.9378	-0.0046
R	6	6	5.5	18257.8967	18257.8947	0.002
R	7	6	6.5	18258.5054	18258.5089	-0.0035
R	8	7	6.5	18258.5338	18258.5378	-0.0041
R	8	7	7.5	18259.1119	18259.1156	-0.0037
R	9	8	7.5	18259.1374	18259.1413	-0.0039
R	9	8	8.5	18259.7225	18259.7249	-0.0024
R	10	9	8.5	18259.745	18259.7481	-0.0031
R	10	9	9.5	18260.3364	18260.337	-0.0007
R	11	10	9.5	18260.3572	18260.3582	-0.001
R	11	10	10.5	18260.9515	18260.9521	-0.0006
R	12	11	10.5	18260.9707	18260.9715	-0.0008
R	12	11	11.5	18261.5697	18261.5701	-0.0004
R	13	12	11.5	18261.5878	18261.588	-0.0002
R	13	12	12.5	18262.1895	18262.191	-0.0015
R	14	13	12.5	18262.206	18262.2077	-0.0017
R	14	13	13.5	18262.8135	18262.815	-0.0015
R	15	14	13.5	18262.8292	18262.8306	-0.0014
R	15	14	14.5	18263.4418	18263.442	-0.0002
R	16	15	14.5	18263.4559	18263.4567	-0.0008
R	16	15	15.5	18264.0722	18264.0721	0
R	17	16	15.5	18264.0853	18264.0859	-0.0006
R	17	16	16.5	18264.7059	18264.7053	0.0006
R	18	17	16.5	18264.7184	18264.7184	0
R	18	17	17.5	18265.3422	18265.3416	0.0005
R	19	18	17.5	18265.3549	18265.354	0.0009
R	19	18	18.5	18265.9842	18265.9811	0.0031
R	20	19	18.5	18265.9954	18265.9928	0.0025
R	20	19	19.5	18266.6245	18266.6237	0.0008
R	21	20	19.5	18266.635	18266.6349	0.0001
R	21	20	20.5	18267.2701	18267.2695	0.0006
R	22	21	20.5	18267.2796	18267.2802	-0.0006
R	22	21	21.5	18267.9176	18267.9185	-0.0008
R	23	22	21.5	18267.9266	18267.9287	-0.0022
R	23	22	22.5	18268.5705	18268.5707	-0.0002
R	24	23	22.5	18268.5798	18268.5805	-0.0007
R	24	23	23.5	18269.2242	18269.2262	-0.002
R	25	24	23.5	18269.2315	18269.2356	-0.0041
R	25	24	24.5	18269.8851	18269.885	0.0002
R	26	25	24.5	18269.8934	18269.894	-0.0006

R	26	25	25.5	18270.547	18270.547	0
R	27	26	25.5	18270.556	18270.5558	0.0003
R	27	26	26.5	18271.2124	18271.2125	-0.0001
R	28	27	26.5	18271.2209	18271.2209	0
R	28	27	27.5	18271.8817	18271.8812	0.0004
R	29	28	27.5	18271.8897	18271.8894	0.0003
R	29	28	28.5	18272.554	18272.5534	0.0006
R	30	29	28.5	18272.5622	18272.5613	0.0009
R	30	29	29.5	18273.2303	18273.229	0.0012
R	31	30	29.5	18273.2381	18273.2366	0.0015
R	31	30	30.5	18273.9093	18273.9081	0.0012
R	32	31	30.5	18273.9163	18273.9155	0.0008
R	32	31	31.5	18274.5937	18274.5906	0.003
R	33	32	31.5	18274.5982	18274.5978	0.0004
R	34	33	32.5	18275.2779	18275.2837	-0.0057
R	33	32	32.5	18275.2779	18275.2767	0.0012
R	34	33	32.5	18275.2854	18275.2837	0.0017
R	35	34	33.5	18275.9684	18275.9731	-0.0047
R	34	33	33.5	18275.9684	18275.9664	0.0021

The [22.1] $^4\Delta_{3.5} \rightarrow X^4\Phi_{4.5}$ transition

Isotopologue	Branch	F'	F"	J"	Observed (cm^{-1})	Calculated (cm^{-1})	Obs-Cal (cm^{-1})
^{102}RuF	P	4	5	4.5	22155.4691	22155.4721	-0.003
	P	3	4	4.5	22155.4691	22155.4703	-0.0013
	P	5	6	5.5	22154.856	22154.8583	-0.0024
	P	4	5	5.5	22154.856	22154.8573	-0.0013
	P	6	7	6.5	22154.234	22154.236	-0.0019
	P	5	6	6.5	22154.234	22154.2352	-0.0012
	P	7	8	7.5	22153.6036	22153.605	-0.0015
	P	6	7	7.5	22153.6036	22153.6045	-0.0009
	P	8	9	8.5	22152.9645	22152.9657	-0.0012
	P	7	8	8.5	22152.9645	22152.9653	-0.0008
	P	9	10	9.5	22152.3178	22152.318	-0.0002
	P	8	9	9.5	22152.3178	22152.3177	0.0001
	P	10	11	10.5	22151.6626	22151.6622	0.0004
	P	9	10	10.5	22151.6626	22151.662	0.0006
	P	11	12	11.5	22150.9993	22150.9985	0.0008
	P	10	11	11.5	22150.9993	22150.9984	0.001
	P	12	13	12.5	22150.3265	22150.3272	-0.0007
	P	11	12	12.5	22150.3265	22150.3271	-0.0006
	P	13	14	13.5	22149.6455	22149.6484	-0.0028
	P	12	13	13.5	22149.6455	22149.6483	-0.0027
	P	14	15	14.5	22148.9611	22148.9624	-0.0013
	P	13	14	14.5	22148.9611	22148.9623	-0.0012
	P	15	16	15.5	22148.2689	22148.2695	-0.0006
	P	14	15	15.5	22148.2689	22148.2694	-0.0006
	P	16	17	16.5	22147.57	22147.57	0
	P	15	16	16.5	22147.57	22147.57	0
	P	17	18	17.5	22146.8643	22146.8643	0
	P	16	17	17.5	22146.8643	22146.8643	0
	P	18	19	18.5	22146.1546	22146.1527	0.0019
	P	17	18	18.5	22146.1546	22146.1527	0.002
	P	19	20	19.5	22145.4375	22145.4355	0.0019
	P	18	19	19.5	22145.4375	22145.4355	0.002
	P	20	21	20.5	22144.7166	22144.7132	0.0034
	P	19	20	20.5	22144.7166	22144.7132	0.0034
	P	21	22	21.5	22143.9903	22143.9862	0.004
	P	20	21	21.5	22143.9903	22143.9862	0.004
	P	22	23	22.5	22143.2595	22143.2549	0.0046
	P	21	22	22.5	22143.2595	22143.2549	0.0046

P	23	24	23.5	22142.5233	22142.5197	0.0036
P	22	23	23.5	22142.5233	22142.5197	0.0036
R	6	5	4.5	22161.1193	22161.1136	0.0057
R	5	4	4.5	22161.1193	22161.1153	0.0039
R	7	6	5.5	22161.6327	22161.6291	0.0035
R	6	5	5.5	22161.6327	22161.6304	0.0023
R	6	6	5.5	22161.6239	22161.6233	0.0006
R	8	7	6.5	22162.1386	22162.1361	0.0026
R	7	6	6.5	22162.1386	22162.137	0.0016
R	9	8	7.5	22162.6359	22162.6345	0.0014
R	8	7	7.5	22162.6359	22162.6353	0.0006
R	10	9	8.5	22163.1259	22163.1247	0.0012
R	9	8	8.5	22163.1259	22163.1253	0.0005
R	11	10	9.5	22163.609	22163.6068	0.0022
R	10	9	9.5	22163.609	22163.6073	0.0017
R	12	11	10.5	22164.0802	22164.081	-0.0009
R	11	10	10.5	22164.0802	22164.0815	-0.0013
R	13	12	11.5	22164.5463	22164.5476	-0.0014
R	12	11	11.5	22164.5463	22164.5481	-0.0018
R	14	13	12.5	22165.0048	22165.0069	-0.0021
R	13	12	12.5	22165.0048	22165.0072	-0.0025
R	15	14	13.5	22165.4598	22165.459	0.0008
R	14	13	13.5	22165.4598	22165.4593	0.0005
R	16	15	14.5	22165.9026	22165.9043	-0.0017
R	15	14	14.5	22165.9026	22165.9046	-0.002
R	17	16	15.5	22166.3412	22166.3432	-0.002
R	16	15	15.5	22166.3412	22166.3434	-0.0022
R	18	17	16.5	22166.775	22166.7758	-0.0008
R	17	16	16.5	22166.775	22166.7761	-0.0011
R	19	18	17.5	22167.2024	22167.2027	-0.0003
R	18	17	17.5	22167.2024	22167.2029	-0.0005
R	20	19	18.5	22167.6223	22167.6242	-0.0019
R	19	18	18.5	22167.6223	22167.6244	-0.0021
R	21	20	19.5	22168.0399	22168.0406	-0.0006
R	20	19	19.5	22168.0399	22168.0408	-0.0008
R	22	21	20.5	22168.4507	22168.4524	-0.0017
R	21	20	20.5	22168.4507	22168.4526	-0.0019
R	23	22	21.5	22168.8573	22168.86	-0.0027
R	22	21	21.5	22168.8573	22168.8602	-0.0029
R	24	23	22.5	22169.2595	22169.264	-0.0045

	R	23	22	22.5	22169.2595	22169.2641	-0.0046
^{104}RuF	P	4	5	4.5	22155.4375	22155.4406	-0.0032
	P	3	4	4.5	22155.4375	22155.4388	-0.0013
	P	5	6	5.5	22154.8258	22154.8282	-0.0023
	P	4	5	5.5	22154.8258	22154.827	-0.0012
	P	6	7	6.5	22154.2048	22154.207	-0.0022
	P	5	6	6.5	22154.2048	22154.2062	-0.0014
	P	7	8	7.5	22153.5754	22153.5771	-0.0018
	P	6	7	7.5	22153.5754	22153.5766	-0.0012
	P	8	9	8.5	22152.9377	22152.9388	-0.0011
	P	7	8	8.5	22152.9377	22152.9384	-0.0007
	P	9	10	9.5	22152.2918	22152.292	-0.0002
	P	8	9	9.5	22152.2918	22152.2917	0.0001
	P	10	11	10.5	22151.6367	22151.6371	-0.0004
	P	9	10	10.5	22151.6367	22151.6368	-0.0001
	P	11	12	11.5	22150.9751	22150.9741	0.001
	P	10	11	11.5	22150.9751	22150.9739	0.0012
	P	12	13	12.5	22150.302	22150.3034	-0.0014
	P	11	12	12.5	22150.302	22150.3033	-0.0013
	P	13	14	13.5	22149.6227	22149.6252	-0.0025
	P	12	13	13.5	22149.6227	22149.6251	-0.0024
	P	14	15	14.5	22148.9376	22148.9397	-0.0021
	P	13	14	14.5	22148.9376	22148.9396	-0.002
	P	15	16	15.5	22148.2465	22148.2473	-0.0008
	P	14	15	15.5	22148.2465	22148.2472	-0.0007
	P	16	17	16.5	22147.5475	22147.5482	-0.0007
	P	15	16	16.5	22147.5475	22147.5481	-0.0006
	P	17	18	17.5	22146.8433	22146.8428	0.0005
	P	16	17	17.5	22146.8433	22146.8428	0.0005
	P	18	19	18.5	22146.1323	22146.1315	0.0008
	P	17	18	18.5	22146.1323	22146.1314	0.0009
	P	19	20	19.5	22145.4167	22145.4146	0.0021
	P	18	19	19.5	22145.4167	22145.4146	0.0021
	P	20	21	20.5	22144.6956	22144.6925	0.0031
	P	19	20	20.5	22144.6956	22144.6925	0.0031
	P	21	22	21.5	22143.969	22143.9657	0.0033
	P	20	21	21.5	22143.969	22143.9657	0.0034
	P	22	23	22.5	22143.2383	22143.2346	0.0037
	P	21	22	22.5	22143.2383	22143.2345	0.0038
	P	23	24	23.5	22142.5031	22142.4996	0.0035

P	22	23	23.5	22142.5031	22142.4996	0.0035
R	6	5	4.5	22161.0693	22161.0635	0.0058
R	5	4	4.5	22161.0693	22161.0652	0.0041
R	7	6	5.5	22161.5811	22161.5766	0.0044
R	6	5	5.5	22161.5811	22161.5779	0.0032
R	8	7	6.5	22162.084	22162.081	0.003
R	7	6	6.5	22162.084	22162.082	0.002
R	9	8	7.5	22162.5792	22162.5769	0.0023
R	8	7	7.5	22162.5792	22162.5777	0.0015
R	10	9	8.5	22163.0659	22163.0644	0.0015
R	9	8	8.5	22163.0659	22163.0651	0.0009
R	11	10	9.5	22163.5448	22163.5438	0.001
R	10	9	9.5	22163.5448	22163.5443	0.0004
R	12	11	10.5	22164.0148	22164.0152	-0.0004
R	11	10	10.5	22164.0148	22164.0157	-0.0009
R	13	12	11.5	22164.4778	22164.4789	-0.0011
R	12	11	11.5	22164.4778	22164.4793	-0.0015
R	14	13	12.5	22164.9337	22164.9352	-0.0016
R	13	12	12.5	22164.9337	22164.9356	-0.0019
R	15	14	13.5	22165.3831	22165.3843	-0.0012
R	14	13	13.5	22165.3831	22165.3847	-0.0015
R	16	15	14.5	22165.8258	22165.8266	-0.0008
R	15	14	14.5	22165.8258	22165.8269	-0.0011
R	17	16	15.5	22166.2617	22166.2624	-0.0007
R	16	15	15.5	22166.2617	22166.2626	-0.0009
R	18	17	16.5	22166.6909	22166.6919	-0.001
R	17	16	16.5	22166.6909	22166.6921	-0.0012
R	19	18	17.5	22167.1159	22167.1156	0.0003
R	18	17	17.5	22167.1159	22167.1159	0.0001
R	20	19	18.5	22167.5334	22167.5339	-0.0005
R	19	18	18.5	22167.5334	22167.5341	-0.0007
R	21	20	19.5	22167.9472	22167.9472	0
R	20	19	19.5	22167.9472	22167.9474	-0.0002
R	22	21	20.5	22168.3548	22168.3558	-0.0011
R	21	20	20.5	22168.3548	22168.356	-0.0012
R	23	22	21.5	22168.7574	22168.7603	-0.003
R	22	21	21.5	22168.7574	22168.7605	-0.0031
R	24	23	22.5	22169.1565	22169.1611	-0.0047
R	23	22	22.5	22169.1565	22169.1613	-0.0048

^{100}RuF	P	4	5	4.5	22155.5038	22155.5056	-0.0018
	P	3	4	4.5	22155.5038	22155.5038	0
	P	5	6	5.5	22154.8895	22154.8904	-0.0009
	P	4	5	5.5	22154.8895	22154.8894	0.0001
	P	6	7	6.5	22154.2653	22154.2667	-0.0014
	P	5	6	6.5	22154.2653	22154.266	-0.0007
	P	7	8	7.5	22153.6332	22153.6345	-0.0013
	P	6	7	7.5	22153.6332	22153.6341	-0.0009
	P	8	9	8.5	22152.9943	22152.994	0.0002
	P	7	8	8.5	22152.9943	22152.9938	0.0005
	P	9	10	9.5	22152.3453	22152.3453	-0.0001
	P	8	9	9.5	22152.3453	22152.3452	0.0001
	P	10	11	10.5	22151.6892	22151.6886	0.0006
	P	9	10	10.5	22151.6892	22151.6885	0.0007
	P	11	12	11.5	22151.0261	22151.0241	0.002
	P	10	11	11.5	22151.0261	22151.0241	0.002
	P	12	13	12.5	22150.3552	22150.352	0.0032
	P	11	12	12.5	22150.3552	22150.352	0.0032
	P	13	14	13.5	22149.6696	22149.6726	-0.003
	P	12	13	13.5	22149.6696	22149.6726	-0.003
	P	14	15	14.5	22148.9828	22148.9861	-0.0033
	P	13	14	14.5	22148.9828	22148.9861	-0.0034
	P	15	16	15.5	22148.2912	22148.2928	-0.0016
	P	14	15	15.5	22148.2912	22148.2929	-0.0016
	P	16	17	16.5	22147.5933	22147.5931	0.0002
	P	15	16	16.5	22147.5933	22147.5931	0.0002
	P	17	18	17.5	22146.8865	22146.8872	-0.0006
	P	16	17	17.5	22146.8865	22146.8872	-0.0007
	P	18	19	18.5	22146.1773	22146.1755	0.0019
	P	19	18	18.5	22167.715	22167.7145	0.0005
	P	19	20	19.5	22145.4576	22145.4584	-0.0008
	P	18	19	19.5	22145.4576	22145.4584	-0.0009
	P	20	21	20.5	22144.7368	22144.7362	0.0005
	P	19	20	20.5	22144.7368	22144.7363	0.0005
	P	21	22	21.5	22144.0113	22144.0095	0.0018
	P	20	21	21.5	22144.0113	22144.0095	0.0017
	P	23	22	22.5	22169.364	22169.3662	-0.0022
	P	22	23	22.5	22143.2782	22143.2785	-0.0003
	P	21	22	23.5	22143.2782	22143.2786	-0.0004
	P	23	24	23.5	22142.5436	22142.5438	-0.0002

	R	8	7	6.5	22162.1957	22162.1931	0.0026
	R	7	6	6.5	22162.1957	22162.1945	0.0011
	R	9	8	7.5	22162.6965	22162.6941	0.0024
	R	8	7	7.5	22162.6965	22162.6952	0.0013
	R	10	9	8.5	22163.1888	22163.1868	0.0021
	R	9	8	8.5	22163.1888	22163.1878	0.0011
	R	11	10	9.5	22163.6727	22163.6715	0.0012
	R	10	9	9.5	22163.6727	22163.6723	0.0003
	R	12	11	10.5	22164.1482	22164.1484	-0.0001
	R	11	10	10.5	22164.1482	22164.1491	-0.0009
	R	13	12	11.5	22164.6163	22164.6177	-0.0014
	R	12	11	11.5	22164.6163	22164.6183	-0.002
	R	14	13	12.5	22165.0787	22165.0796	-0.0009
	R	13	12	12.5	22165.0787	22165.0802	-0.0015
	R	15	14	13.5	22165.5342	22165.5346	-0.0004
	R	14	13	13.5	22165.5342	22165.5351	-0.0009
	R	16	15	14.5	22165.9824	22165.9827	-0.0003
	R	15	14	14.5	22165.9824	22165.9832	-0.0007
	R	18	19	18.5	22146.1773	22146.1755	0.0019
	R	22	23	22.5	22143.2782	22143.2785	-0.0003
	R	22	23	23.5	22142.5436	22142.5439	-0.0003
	R	17	16	15.5	22166.4239	22166.4244	-0.0005
	R	16	15	15.5	22166.4239	22166.4248	-0.0009
	R	18	17	16.5	22166.8611	22166.86	0.0011
	R	17	16	16.5	22166.8611	22166.8604	0.0008
	R	18	17	17.5	22167.2907	22167.2901	0.0005
	R	20	19	18.5	22167.715	22167.7142	0.0008
	R	21	20	19.5	22168.1342	22168.1336	0.0006
	R	20	19	19.5	22168.1342	22168.1339	0.0003
	R	22	21	20.5	22168.5497	22168.5484	0.0013
	R	21	20	20.5	22168.5497	22168.5486	0.001
	R	23	22	21.5	22168.9595	22168.959	0.0005
	R	22	21	21.5	22168.9595	22168.9593	0.0002
	R	24	23	22.5	22169.364	22169.3659	-0.0019
	R	23	22	22.5	22169.364	22169.3662	-0.0022
^{96}RuF	P	4	5	4.5	22155.5722	22155.5763	-0.0041
	P	3	4	4.5	22155.5722	22155.5741	-0.0019
	P	5	6	5.5	22154.9552	22154.9582	-0.003
	P	4	5	5.5	22154.9552	22154.9569	-0.0017
	P	6	7	6.5	22154.3291	22154.3317	-0.0025

P	5	6	6.5	22154.3291	22154.3308	-0.0017
P	7	8	7.5	22153.6954	22153.6968	-0.0015
P	6	7	7.5	22153.6954	22153.6963	-0.0009
P	8	9	8.5	22153.0522	22153.0538	-0.0016
P	7	8	8.5	22153.0522	22153.0534	-0.0012
P	9	10	9.5	22152.4024	22152.4028	-0.0004
P	8	9	9.5	22152.4024	22152.4025	-0.0002
P	10	11	10.5	22151.7429	22151.7438	-0.0009
P	9	10	10.5	22151.7429	22151.7437	-0.0007
P	11	12	11.5	22151.0752	22151.0772	-0.002
P	10	11	11.5	22151.0752	22151.0771	-0.0019
P	13	14	13.5	22149.7221	22149.7219	0.0002
P	12	13	13.5	22149.7221	22149.7219	0.0002
P	14	15	14.5	22149.0311	22149.0337	-0.0025
P	13	14	14.5	22149.0311	22149.0336	-0.0025
P	15	16	15.5	22148.336	22148.3387	-0.0027
P	14	15	15.5	22148.336	22148.3387	-0.0027
P	16	17	16.5	22147.636	22147.6374	-0.0015
P	15	16	16.5	22147.636	22147.6374	-0.0015
P	17	18	17.5	22146.9284	22146.9301	-0.0017
P	16	17	17.5	22146.9284	22146.9301	-0.0017
P	18	19	18.5	22146.2143	22146.217	-0.0026
P	17	18	18.5	22146.2143	22146.217	-0.0027
P	22	23	22.5	22143.3173	22143.315	0.0023
P	21	22	22.5	22143.3173	22143.3151	0.0022
P	23	24	23.5	22142.5801	22142.5792	0.0009
P	22	23	23.5	22142.5801	22142.5793	0.0008
R	7	6	5.5	22161.8034	22161.7972	0.0062
R	6	5	5.5	22161.8034	22161.7993	0.0041
R	8	7	6.5	22162.3156	22162.3115	0.0041
R	7	6	6.5	22162.3156	22162.3131	0.0025
R	10	9	8.5	22163.3187	22163.3155	0.0032
R	9	8	8.5	22163.3187	22163.3166	0.0022
R	11	10	9.5	22163.8077	22163.8056	0.0021
R	10	9	9.5	22163.8077	22163.8065	0.0012
R	13	12	11.5	22164.7684	22164.763	0.0054
R	12	11	11.5	22164.7684	22164.7637	0.0047
R	14	13	12.5	22165.2335	22165.2309	0.0026
R	13	12	12.5	22165.2335	22165.2315	0.002
R	15	14	13.5	22165.6937	22165.6918	0.0019

R	14	13	13.5	22165.6937	22165.6923	0.0014
R	16	15	14.5	22166.1481	22166.1461	0.002
R	15	14	14.5	22166.1481	22166.1466	0.0015
R	17	16	15.5	22166.5937	22166.594	-0.0004
R	16	15	15.5	22166.5937	22166.5945	-0.0008
R	18	17	16.5	22167.0384	22167.036	0.0024
R	17	16	16.5	22167.0384	22167.0364	0.002
R	19	18	17.5	22167.4718	22167.4724	-0.0006
R	18	17	17.5	22167.4718	22167.4727	-0.001
R	20	19	18.5	22167.9001	22167.9034	-0.0033
R	19	18	18.5	22167.9001	22167.9038	-0.0036

The [13.1] $^4\Delta_{3.5} \rightarrow X^4\Phi_{4.5}$ transition

Isotopologue	Branch	F'	F''	J''	Observed (cm^{-1})	Calculated (cm^{-1})	Obs-Cal (cm^{-1})
^{102}RuF	P	4	4	4.5	13144.4989	13144.497	0.0019
	P	4	5	5.5	13143.8504	13143.852	-0.0017
	P	5	6	5.5	13143.8596	13143.8595	0.0001
	P	5	6	6.5	13143.2117	13143.2127	-0.0011
	P	6	7	6.5	13143.2197	13143.2188	0.0009
	P	7	8	8.5	13141.8934	13141.8969	-0.0036
	P	8	9	8.5	13141.8997	13141.9013	-0.0016
	P	8	9	9.5	13141.2161	13141.2207	-0.0046
	P	9	10	9.5	13141.2218	13141.2245	-0.0027
	P	11	12	11.5	13139.8385	13139.8347	0.0038
	P	12	13	12.5	13139.1238	13139.1218	0.002
	P	12	13	13.5	13138.3936	13138.3942	-0.0006
	P	13	14	13.5	13138.3936	13138.3967	-0.0031
	P	13	14	14.5	13137.6555	13137.6574	-0.0019
	P	14	15	14.5	13137.6555	13137.6597	-0.0042
	Q	9	9	9.5	13146.5533	13146.5503	0.003
	Q	10	10	9.5	13146.5556	13146.5533	0.0023
	Q	11	11	10.5	13146.4235	13146.4253	-0.0018
	Q	10	10	10.5	13146.4235	13146.4225	0.0009
	Q	12	12	11.5	13146.2821	13146.2851	-0.0029
	Q	11	11	11.5	13146.2821	13146.2826	-0.0004
	Q	13	13	12.5	13146.1306	13146.1327	-0.0021
	Q	12	12	12.5	13146.1306	13146.1304	0.0002
	Q	14	14	13.5	13145.9673	13145.9682	-0.0009
	Q	13	13	13.5	13145.9673	13145.9661	0.0012
	Q	15	15	14.5	13145.791	13145.7916	-0.0006
	Q	14	14	14.5	13145.791	13145.7896	0.0014
	Q	15	15	15.5	13145.601	13145.601	0
	Q	17	17	16.5	13145.3999	13145.402	-0.0021
	Q	16	16	16.5	13145.3999	13145.4002	-0.0003
	Q	18	18	17.5	13145.1866	13145.189	-0.0024
	Q	17	17	17.5	13145.1866	13145.1873	-0.0007
	Q	19	19	18.5	13144.9623	13144.9639	-0.0016
	Q	18	18	18.5	13144.9623	13144.9623	0
	Q	20	20	19.5	13144.7219	13144.7267	-0.0048
	Q	19	19	19.5	13144.7219	13144.7252	-0.0033

R	5	5	5	13150.087	13150.0843	0.0027
R	5	4	4	13150.0928	13150.0928	0
R	6	6	6	13150.5816	13150.5798	0.0018
R	6	5	5	13150.5883	13150.5869	0.0014
R	7	7	7	13151.0611	13151.0626	-0.0015
R	7	6	6	13151.0662	13151.0687	-0.0025
R	8	7	7	13151.0733	13151.0717	0.0016
R	8	7	7	13151.5382	13151.5383	-0.0001
R	9	8	8	13151.5438	13151.541	0.0028
R	9	9	9	13151.9918	13151.9909	0.001
R	9	8	8	13151.9972	13151.9956	0.0016
R	10	9	9	13152.0016	13151.9981	0.0035
R	10	9	9	13152.4436	13152.4406	0.0029
R	11	10	10	13152.4473	13152.443	0.0043
R	11	10	10	13152.8734	13152.8734	0
R	12	11	11	13152.8762	13152.8756	0.0006
R	12	11	11	13153.2928	13153.294	-0.0012
R	13	12	12	13153.2948	13153.296	-0.0012
R	13	12	12	13153.7018	13153.7023	-0.0005
R	14	13	13	13153.7018	13153.7042	-0.0024
R	18	17	17	13155.5626	13155.56	0.0026
R	19	18	18	13155.5626	13155.5615	0.0012
R	19	18	18	13155.8961	13155.8948	0.0013
R	20	19	19	13155.8961	13155.8962	-0.0001
R	20	19	19	13156.2206	13156.2174	0.0032
R	21	20	20	13156.2206	13156.2187	0.0019
R	21	20	20	13156.5287	13156.5277	0.001
R	22	21	21	13156.5287	13156.529	-0.0003
R	22	21	21	13156.8275	13156.8258	0.0017
R	23	22	22	13156.8275	13156.827	0.0005
R	23	22	22	13157.1133	13157.1117	0.0016
R	24	23	23	13157.1133	13157.1129	0.0004
R	24	23	23	13157.3876	13157.3853	0.0022
R	25	24	24	13157.3876	13157.3865	0.0011
R	25	24	24	13157.6483	13157.6468	0.0015
R	26	25	25	13157.6483	13157.6479	0.0004
R	26	25	25	13157.8974	13157.896	0.0014
R	27	26	26	13157.8974	13157.897	0.0003
R	27	26	26	13158.1326	13158.133	-0.0004
R	28	27	27	13158.1326	13158.134	-0.0014
R	28	27	27	13158.3565	13158.3578	-0.0013

	R	29	28	28	13158.3565	13158.3588	-0.0022
	R	29	28	28	13158.5707	13158.5704	0.0004
	R	30	29	29	13158.5707	13158.5713	-0.0006
	R	30	29	29	13158.7712	13158.7708	0.0004
	R	31	30	30	13158.7712	13158.7717	-0.0006
^{104}RuF	P	3	4	4.5	13144.4583	13144.4605	-0.0022
	P	4	5	5.5	13143.8333	13143.8362	-0.0029
	P	5	6	5.5	13143.8435	13143.8466	-0.0031
	P	5	6	6.5	13143.1976	13143.199	-0.0014
	P	6	7	6.5	13143.2049	13143.2074	-0.0025
	Q	8	8	8.5	13146.6435	13146.6413	0.0022
	Q	9	9	8.5	13146.6495	13146.6462	0.0033
	Q	9	9	9.5	13146.5264	13146.5258	0.0005
	Q	10	10	9.5	13146.5304	13146.5303	0.0001
	Q	10	10	10.5	13146.3963	13146.3982	-0.0019
	Q	11	11	10.5	13146.4005	13146.4022	-0.0017
	Q	12	12	11.5	13146.258	13146.2619	-0.0039
	Q	11	11	11.5	13146.258	13146.2583	-0.0002
	Q	13	13	12.5	13146.1068	13146.1096	-0.0027
	Q	12	12	12.5	13146.1068	13146.1062	0.0006
	Q	14	14	13.5	13145.9444	13145.9451	-0.0007
	Q	13	13	13.5	13145.9444	13145.9419	0.0024
	Q	15	15	14.5	13145.7672	13145.7684	-0.0012
	Q	14	14	14.5	13145.7672	13145.7655	0.0017
	Q	16	16	15.5	13145.5785	13145.5797	-0.0012
	Q	15	15	15.5	13145.5785	13145.5769	0.0016
	Q	17	17	16.5	13145.3776	13145.3788	-0.0012
	Q	16	16	16.5	13145.3776	13145.3762	0.0014
	Q	18	18	17.5	13145.1651	13145.1657	-0.0006
	Q	17	17	17.5	13145.1651	13145.1633	0.0018
	Q	19	19	18.5	13144.9416	13144.9406	0.001
	Q	18	18	18.5	13144.9416	13144.9383	0.0033
	Q	20	20	19.5	13144.7006	13144.7033	-0.0028
	Q	19	19	19.5	13144.7006	13144.7011	-0.0006
	R	5	4	4.5	13150.0574	13150.058	-0.0006
	R	6	5	4.5	13150.0692	13150.0639	0.0052
	R	5	5	4.5	13150.0515	13150.0493	0.0021
	R	6	5	5.5	13150.5521	13150.5505	0.0015

	R	7	6	5.5	13150.5613	13150.5558	0.0055
	R	6	6	5.5	13150.5443	13150.5433	0.001
	R	7	6	6.5	13151.0279	13151.0308	-0.0029
	R	8	7	6.5	13151.0347	13151.0355	-0.0009
	R	7	7	6.5	13151.024	13151.0246	-0.0006
	R	8	7	7.5	13151.4975	13151.4987	-0.0012
	R	9	8	7.5	13151.5036	13151.503	0.0005
	R	9	8	8.5	13151.9546	13151.9544	0.0002
	R	10	9	8.5	13151.9584	13151.9583	0.0001
	R	10	9	9.5	13152.4006	13152.3978	0.0027
	R	11	10	9.5	13152.4047	13152.4014	0.0033
	R	11	10	10.5	13152.8294	13152.829	0.0005
	R	12	11	10.5	13152.8328	13152.8323	0.0004
	R	13	12	11.5	13153.2495	13153.251	-0.0015
	R	12	11	11.5	13153.2495	13153.2479	0.0016
	R	14	13	12.5	13153.6529	13153.6574	-0.0046
	R	13	12	12.5	13153.6529	13153.6545	-0.0016
^{100}RuF	P	4	5	5.5	13143.8675	13143.8708	-0.0033
	P	5	6	5.5	13143.8781	13143.8799	-0.0018
	P	5	6	6.5	13143.2357	13143.2296	0.0061
	Q	8	8	8.5	13146.6975	13146.6936	0.0039
	Q	9	9	8.5	13146.7032	13146.6976	0.0056
	Q	9	9	9.5	13146.5798	13146.5775	0.0023
	Q	10	10	9.5	13146.5835	13146.5811	0.0025
	Q	10	10	10.5	13146.448	13146.4491	-0.0011
	Q	11	11	10.5	13146.4516	13146.4524	-0.0008
	Q	11	11	11.5	13146.3059	13146.3085	-0.0026
	Q	12	12	11.5	13146.3095	13146.3115	-0.0019
	Q	13	13	12.5	13146.156	13146.1583	-0.0024
	Q	12	12	12.5	13146.156	13146.1556	0.0004
	Q	14	14	13.5	13145.9914	13145.993	-0.0017
	Q	13	13	13.5	13145.9914	13145.9904	0.0009
	Q	15	15	14.5	13145.8152	13145.8155	-0.0003
	Q	14	14	14.5	13145.8152	13145.8131	0.0021
	Q	16	16	15.5	13145.6242	13145.6257	-0.0015
	Q	15	15	15.5	13145.6242	13145.6235	0.0007
	Q	17	17	16.5	13145.4235	13145.4238	-0.0003
	Q	16	16	16.5	13145.4235	13145.4217	0.0018
	Q	18	18	17.5	13145.2086	13145.2097	-0.0011

	Q	17	17	17.5	13145.2086	13145.2077	0.0009
	Q	19	19	18.5	13144.9838	13144.9834	0.0004
	Q	18	18	18.5	13144.9838	13144.9815	0.0022
	Q	20	20	19.5	13144.7435	13144.745	-0.0015
	Q	19	19	19.5	13144.7435	13144.7432	0.0003
	R	5	5	4.5	13150.1216	13150.1211	0.0005
	R	5	4	4.5	13150.129	13150.1319	-0.0029
	R	6	5	4.5	13150.1305	13150.136	-0.0056
	R	6	6	5.5	13150.6152	13150.6184	-0.0032
	R	7	5	5.5	13150.6271	13150.6273	-0.0003
	R	6	6	5.5	13150.6348	13150.6312	0.0036
	R	7	7	6.5	13151.1027	13151.1029	-0.0002
	R	8	6	6.5	13151.1073	13151.1105	-0.0032
	R	7	7	6.5	13151.1151	13151.114	0.0011
	R	8	8	7.5	13151.5761	13151.5747	0.0015
	R	9	7	7.5	13151.5805	13151.5813	-0.0009
	R	8	8	7.5	13151.5857	13151.5846	0.0011
	R	9	9	8.5	13152.0325	13152.0339	-0.0014
	R	10	8	8.5	13152.0406	13152.0398	0.0008
	R	9	9	8.5	13152.0455	13152.0428	0.0027
	R	10	9	9.5	13152.4859	13152.486	-0.0001
	R	11	10	9.5	13152.4908	13152.4888	0.0021
	R	11	10	10.5	13152.9206	13152.9198	0.0008
	R	12	11	10.5	13152.9254	13152.9224	0.003
	R	13	12	11.5	13153.3408	13153.3437	-0.0029
	R	12	11	11.5	13153.3408	13153.3413	-0.0005
	R	14	13	12.5	13153.7487	13153.7527	-0.004
	R	13	12	12.5	13153.7487	13153.7504	-0.0017
^{96}RuF	Q	11	11	10.5	13146.5056	13146.5069	-0.0013
	Q	10	10	10.5	13146.5056	13146.5042	0.0013
	Q	12	12	11.5	13146.3623	13146.365	-0.0027
	Q	11	11	11.5	13146.3623	13146.3626	-0.0003
	Q	13	13	12.5	13146.2078	13146.2109	-0.0031
	Q	12	12	12.5	13146.2078	13146.2086	-0.0009
	Q	14	14	13.5	13146.0431	13146.0445	-0.0014
	Q	13	13	13.5	13146.0431	13146.0424	0.0006
	Q	15	15	14.5	13145.8664	13145.8659	0.0006
	Q	14	14	14.5	13145.8664	13145.8639	0.0025
	Q	16	16	15.5	13145.6744	13145.675	-0.0006

Q	15	15	15.5	13145.6744	13145.6732	0.0012
Q	17	17	16.5	13145.4734	13145.472	0.0015
Q	16	16	16.5	13145.4734	13145.4703	0.0032
Q	18	18	17.5	13145.2558	13145.2567	-0.001
Q	17	17	17.5	13145.2558	13145.2551	0.0007
Q	19	19	18.5	13145.0285	13145.0293	-0.0008
Q	18	18	18.5	13145.0285	13145.0277	0.0008
Q	20	20	19.5	13144.7881	13144.7897	-0.0016
Q	19	19	19.5	13144.7881	13144.7882	-0.0001
R	6	5	5.5	13150.7071	13150.7098	-0.0027
R	7	6	5.5	13150.7156	13150.7125	0.0031
R	6	6	5.5	13150.702	13150.6996	0.0024
R	7	6	6.5	13151.1927	13151.1959	-0.0032
R	8	7	6.5	13151.198	13151.1984	-0.0004
R	7	7	6.5	13151.1883	13151.1871	0.0012
R	8	7	7.5	13151.6676	13151.6696	-0.002
R	9	8	7.5	13151.6741	13151.672	0.0021
R	8	8	7.5	13151.6592	13151.6619	-0.0028
R	9	8	8.5	13152.1339	13152.1309	0.003
R	10	9	8.5	13152.1339	13152.1331	0.0008
R	10	9	9.5	13152.5812	13152.5798	0.0013
R	11	10	9.5	13152.5838	13152.5819	0.0019
R	12	11	10.5	13153.0224	13153.0183	0.0041
R	13	12	11.5	13153.4386	13153.4424	-0.0038
R	12	11	11.5	13153.4386	13153.4406	-0.0019
R	14	13	12.5	13153.8525	13153.8541	-0.0016
R	13	12	12.5	13153.8525	13153.8524	0.0002

Appendix B

Observed and calculated frequencies (cm^{-1}) of the ^{101}RuF, ^{99}RuF and ^{98}RuF isotopologues extracted from the fit for the [22.1] $^4\Delta_{3.5} \rightarrow X^4\Phi_{4.5}$ transition.

Isotopolog	Branch	F'	F"	J"	Observed (cm^{-1})	Calculated (cm^{-1})	Obs-Cal (cm^{-1})
^{101}RuF	P	4	5	4.5	22155.482	22155.4845	-0.0026
	P	3	4	4.5	22155.482	22155.4828	-0.0009
	P	5	6	5.5	22154.8701	22154.87	0.0001
	P	4	5	5.5	22154.8701	22154.869	0.0011
	P	6	7	6.5	22154.2474	22154.2469	0.0005
	P	5	6	6.5	22154.2474	22154.2463	0.0011
	P	7	8	7.5	22153.6152	22153.6153	-0.0001
	P	6	7	7.5	22153.6152	22153.6149	0.0004
	P	8	9	8.5	22152.9738	22152.9753	-0.0015
	P	7	8	8.5	22152.9738	22152.975	-0.0012
	P	9	10	9.5	22152.3283	22152.3271	0.0012
	P	8	9	9.5	22152.3283	22152.3269	0.0014
	P	10	11	10.5	22151.6686	22151.6708	-0.0022
	P	9	10	10.5	22151.6686	22151.6706	-0.0021
	P	11	12	11.5	22151.009	22151.0066	0.0024
	P	10	11	11.5	22151.009	22151.0065	0.0025
	P	12	13	12.5	22150.3372	22150.3349	0.0023
	P	11	12	12.5	22150.3372	22150.3348	0.0024
	P	13	14	13.5	22149.6544	22149.6557	-0.0013
	P	12	13	13.5	22149.6544	22149.6556	-0.0013
	P	14	15	14.5	22148.9677	22148.9694	-0.0017
	P	13	14	14.5	22148.9677	22148.9694	-0.0017
	P	15	16	15.5	22148.2763	22148.2763	0
	P	14	15	15.5	22148.2763	22148.2763	0
	P	16	17	16.5	22147.5749	22147.5766	-0.0018
	P	15	16	16.5	22147.5749	22147.5766	-0.0018
	P	17	18	17.5	22146.8712	22146.8708	0.0004
	P	16	17	17.5	22146.8712	22146.8708	0.0004
	P	18	19	18.5	22146.1603	22146.1591	0.0012
	P	17	18	18.5	22146.1603	22146.1591	0.0012
	P	19	20	19.5	22145.4427	22145.4419	0.0008
	P	18	19	19.5	22145.4427	22145.442	0.0007
	P	20	21	20.5	22144.7196	22144.7197	-0.0001
	P	19	20	20.5	22144.7196	22144.7197	-0.0001
	P	21	22	21.5	22143.9935	22143.9928	0.0007
	P	20	21	21.5	22143.9935	22143.9928	0.0007
	P	22	23	22.5	22143.2607	22143.2617	-0.001
	P	21	22	22.5	22143.2607	22143.2617	-0.001
	P	23	24	23.5	22142.5269	22142.5267	0.0001
	P	22	23	23.5	22142.5269	22142.5268	0.0001

R	6	5	4.5	22161.1357	22161.1359	-0.0002
R	5	4	4.5	22161.1357	22161.1379	-0.0022
R	7	6	5.5	22161.6529	22161.6527	0.0002
R	6	5	5.5	22161.6529	22161.6542	-0.0012
R	6	6	5.5	22161.6491	22161.6466	0.0025
R	8	7	6.5	22162.1634	22162.1608	0.0026
R	7	6	6.5	22162.1634	22162.162	0.0015
R	9	8	7.5	22162.6613	22162.6605	0.0008
R	8	7	7.5	22162.6613	22162.6614	-0.0002
R	10	9	8.5	22163.1536	22163.1519	0.0016
R	9	8	8.5	22163.1536	22163.1527	0.0008
R	11	10	9.5	22163.6365	22163.6353	0.0012
R	10	9	9.5	22163.6365	22163.636	0.0005
R	12	11	10.5	22164.1107	22164.1109	-0.0002
R	11	10	10.5	22164.1107	22164.1114	-0.0007
R	13	12	11.5	22164.5782	22164.5788	-0.0006
R	12	11	11.5	22164.5782	22164.5793	-0.0011
R	14	13	12.5	22165.0373	22165.0393	-0.002
R	13	12	12.5	22165.0373	22165.0398	-0.0025
R	15	14	13.5	22165.4917	22165.4928	-0.0011
R	14	13	13.5	22165.4917	22165.4932	-0.0015
R	16	15	14.5	22165.9391	22165.9394	-0.0004
R	15	14	14.5	22165.9391	22165.9398	-0.0007
R	17	16	15.5	22166.379	22166.3796	-0.0007
R	16	15	15.5	22166.379	22166.3799	-0.001
R	18	17	16.5	22166.8138	22166.8136	0.0002
R	17	16	16.5	22166.8138	22166.8139	-0.0001
R	19	18	17.5	22167.2428	22167.2419	0.0009
R	18	17	17.5	22167.2428	22167.2421	0.0006
R	20	19	18.5	22167.665	22167.6646	0.0004
R	19	18	18.5	22167.665	22167.6649	0.0001
R	21	20	19.5	22168.085	22168.0824	0.0026
R	20	19	19.5	22168.085	22168.0826	0.0024
R	22	21	20.5	22168.4966	22168.4955	0.0011
R	21	20	20.5	22168.4966	22168.4958	0.0009
R	23	22	21.5	22168.905	22168.9045	0.0005
R	22	21	21.5	22168.905	22168.9047	0.0003
R	24	23	22.5	22169.3077	22169.3097	-0.0021
R	23	22	22.5	22169.3077	22169.3099	-0.0023

^{99}RuF	P	4	5	4.5	22155.482	22155.4845	-0.0026
	P	3	4	4.5	22155.482	22155.4828	-0.0009
	P	5	6	5.5	22154.8701	22154.87	0.0001
	P	4	5	5.5	22154.8701	22154.869	0.0011
	P	6	7	6.5	22154.2474	22154.2469	0.0005
	P	5	6	6.5	22154.2474	22154.2463	0.0011
	P	7	8	7.5	22153.6152	22153.6153	-0.0001
	P	6	7	7.5	22153.6152	22153.6149	0.0004
	P	8	9	8.5	22152.9738	22152.9753	-0.0015
	P	7	8	8.5	22152.9738	22152.975	-0.0012
	P	9	10	9.5	22152.3283	22152.3271	0.0012
	P	8	9	9.5	22152.3283	22152.3269	0.0014
	P	10	11	10.5	22151.6686	22151.6708	-0.0022
	P	9	10	10.5	22151.6686	22151.6706	-0.0021
	P	11	12	11.5	22151.009	22151.0066	0.0024
	P	10	11	11.5	22151.009	22151.0065	0.0025
	P	12	13	12.5	22150.3372	22150.3349	0.0023
	P	11	12	12.5	22150.3372	22150.3348	0.0024
	P	13	14	13.5	22149.6544	22149.6557	-0.0013
	P	12	13	13.5	22149.6544	22149.6556	-0.0013
	P	14	15	14.5	22148.9677	22148.9694	-0.0017
	P	13	14	14.5	22148.9677	22148.9694	-0.0017
	P	15	16	15.5	22148.2763	22148.2763	0
	P	14	15	15.5	22148.2763	22148.2763	0
	P	16	17	16.5	22147.5749	22147.5766	-0.0018
	P	15	16	16.5	22147.5749	22147.5766	-0.0018
	P	17	18	17.5	22146.8712	22146.8708	0.0004
	P	16	17	17.5	22146.8712	22146.8708	0.0004
	P	18	19	18.5	22146.1603	22146.1591	0.0012
	P	17	18	18.5	22146.1603	22146.1591	0.0012
	P	19	20	19.5	22145.4427	22145.4419	0.0008
	P	18	19	19.5	22145.4427	22145.442	0.0007
	P	20	21	20.5	22144.7196	22144.7197	-0.0001
	P	19	20	20.5	22144.7196	22144.7197	-0.0001
	P	21	22	21.5	22143.9935	22143.9928	0.0007
	P	20	21	21.5	22143.9935	22143.9928	0.0007
	P	22	23	22.5	22143.2607	22143.2617	-0.001
	P	21	22	22.5	22143.2607	22143.2617	-0.001
	P	23	24	23.5	22142.5269	22142.5267	0.0001
	P	22	23	23.5	22142.5269	22142.5268	0.0001

	R	6	5	4.5	22161.1357	22161.1359	-0.0002
	R	5	4	4.5	22161.1357	22161.1379	-0.0022
	R	7	6	5.5	22161.6529	22161.6527	0.0002
	R	6	5	5.5	22161.6529	22161.6542	-0.0012
	R	6	6	5.5	22161.6491	22161.6466	0.0025
	R	8	7	6.5	22162.1634	22162.1608	0.0026
	R	7	6	6.5	22162.1634	22162.162	0.0015
	R	9	8	7.5	22162.6613	22162.6605	0.0008
	R	8	7	7.5	22162.6613	22162.6614	-0.0002
	R	10	9	8.5	22163.1536	22163.1519	0.0016
	R	9	8	8.5	22163.1536	22163.1527	0.0008
	R	11	10	9.5	22163.6365	22163.6353	0.0012
	R	10	9	9.5	22163.6365	22163.636	0.0005
	R	12	11	10.5	22164.1107	22164.1109	-0.0002
	R	11	10	10.5	22164.1107	22164.1114	-0.0007
	R	13	12	11.5	22164.5782	22164.5788	-0.0006
	R	12	11	11.5	22164.5782	22164.5793	-0.0011
	R	14	13	12.5	22165.0373	22165.0393	-0.002
	R	13	12	12.5	22165.0373	22165.0398	-0.0025
	R	15	14	13.5	22165.4917	22165.4928	-0.0011
	R	14	13	13.5	22165.4917	22165.4932	-0.0015
	R	16	15	14.5	22165.9391	22165.9394	-0.0004
	R	15	14	14.5	22165.9391	22165.9398	-0.0007
	R	17	16	15.5	22166.379	22166.3796	-0.0007
	R	16	15	15.5	22166.379	22166.3799	-0.001
	R	18	17	16.5	22166.8138	22166.8136	0.0002
	R	17	16	16.5	22166.8138	22166.8139	-0.0001
	R	19	18	17.5	22167.2428	22167.2419	0.0009
	R	18	17	17.5	22167.2428	22167.2421	0.0006
	R	20	19	18.5	22167.665	22167.6646	0.0004
	R	19	18	18.5	22167.665	22167.6649	0.0001
	R	21	20	19.5	22168.085	22168.0824	0.0026
	R	20	19	19.5	22168.085	22168.0826	0.0024
	R	22	21	20.5	22168.4966	22168.4955	0.0011
	R	21	20	20.5	22168.4966	22168.4958	0.0009
	R	23	22	21.5	22168.905	22168.9045	0.0005
	R	22	21	21.5	22168.905	22168.9047	0.0003
	R	24	23	22.5	22169.3077	22169.3097	-0.0021
	R	23	22	22.5	22169.3077	22169.3099	-0.0023
^{98}RuF	P	4	5	4.5	22155.5366	22155.5404	-0.0038

P	3	4	4.5	22155.5366	22155.5385	-0.0019
P	5	6	5.5	22154.9225	22154.9236	-0.0011
P	4	5	5.5	22154.9225	22154.9224	0.0001
P	6	7	6.5	22154.2967	22154.2983	-0.0016
P	5	6	6.5	22154.2967	22154.2975	-0.0008
P	7	8	7.5	22153.6623	22153.6647	-0.0024
P	6	7	7.5	22153.6623	22153.6641	-0.0018
P	8	9	8.5	22153.0245	22153.0228	0.0017
P	7	8	8.5	22153.0245	22153.0223	0.0022
P	9	10	9.5	22152.3708	22152.3728	-0.0019
P	8	9	9.5	22152.3708	22152.3724	-0.0016
P	10	11	10.5	22151.7162	22151.7148	0.0014
P	9	10	10.5	22151.7162	22151.7146	0.0017
P	11	12	11.5	22151.0516	22151.0491	0.0025
P	10	11	11.5	22151.0516	22151.0489	0.0027
P	12	13	12.5	22150.3776	22150.3759	0.0017
P	11	12	12.5	22150.3776	22150.3758	0.0019
P	13	14	13.5	22149.6932	22149.6955	-0.0023
P	12	13	13.5	22149.6932	22149.6954	-0.0022
P	14	15	14.5	22149.0078	22149.008	-0.0002
P	13	14	14.5	22149.0078	22149.0079	-0.0001
P	15	16	15.5	22148.3133	22148.3138	-0.0005
P	14	15	15.5	22148.3133	22148.3137	-0.0004
P	16	17	16.5	22147.613	22147.6132	-0.0002
P	15	16	16.5	22147.613	22147.6132	-0.0002
P	17	18	17.5	22146.906	22146.9066	-0.0006
P	16	17	17.5	22146.906	22146.9065	-0.0005
P	18	19	18.5	22146.1945	22146.1941	0.0004
P	17	18	18.5	22146.1945	22146.1941	0.0004
P	19	20	19.5	22145.4773	22145.4763	0.001
P	18	19	19.5	22145.4773	22145.4763	0.001
P	20	21	20.5	22144.7555	22144.7535	0.002
P	19	20	20.5	22144.7555	22144.7535	0.002
P	21	22	21.5	22144.0266	22144.0262	0.0004
P	20	21	21.5	22144.0266	22144.0261	0.0004
P	22	23	22.5	22143.2926	22143.2946	-0.002
P	21	22	22.5	22143.2926	22143.2946	-0.002
P	23	24	23.5	22142.5591	22142.5594	-0.0003
P	22	23	23.5	22142.5591	22142.5594	-0.0003
R	6	5	4.5	22161.2253	22161.2216	0.0037

R	5	4	4.5	22161.2253	22161.2234	0.0019
R	7	6	5.5	22161.7442	22161.7419	0.0023
R	6	5	5.5	22161.7442	22161.7433	0.001
R	8	7	6.5	22162.2546	22162.2538	0.0008
R	7	6	6.5	22162.2546	22162.2548	-0.0002
R	9	8	7.5	22162.7598	22162.7573	0.0025
R	8	7	7.5	22162.7598	22162.7581	0.0017
R	10	9	8.5	22163.2537	22163.2527	0.001
R	9	8	8.5	22163.2537	22163.2533	0.0004
R	11	10	9.5	22163.7396	22163.7401	-0.0005
R	10	9	9.5	22163.7396	22163.7406	-0.0011
R	12	11	10.5	22164.2187	22164.2197	-0.001
R	11	10	10.5	22164.2187	22164.2202	-0.0015
R	13	12	11.5	22164.6909	22164.6918	-0.0009
R	12	11	11.5	22164.6909	22164.6922	-0.0013
R	14	13	12.5	22165.155	22165.1566	-0.0016
R	13	12	12.5	22165.155	22165.157	-0.0019
R	15	14	13.5	22165.6137	22165.6144	-0.0006
R	14	13	13.5	22165.6137	22165.6147	-0.001
R	16	15	14.5	22166.0647	22166.0654	-0.0007
R	15	14	14.5	22166.0647	22166.0657	-0.001
R	17	16	15.5	22166.5101	22166.51	0.0001
R	16	15	15.5	22166.5101	22166.5103	-0.0002
R	18	17	16.5	22166.9506	22166.9485	0.0021
R	17	16	16.5	22166.9506	22166.9488	0.0019
R	19	18	17.5	22167.3793	22167.3812	-0.0019
R	18	17	17.5	22167.3793	22167.3815	-0.0021
R	20	19	18.5	22167.8107	22167.8086	0.0021
R	19	18	18.5	22167.8107	22167.8088	0.0019
R	21	20	19.5	22168.2298	22168.2309	-0.0011
R	20	19	19.5	22168.2298	22168.2311	-0.0013
R	22	21	20.5	22168.6515	22168.6486	0.0029
R	21	20	20.5	22168.6515	22168.6488	0.0028
R	22	21	20.5	22168.6469	22168.6486	-0.0017
R	21	20	20.5	22168.6469	22168.6488	-0.0019

Appendix C

Observed and calculated frequencies (cm^{-1}) of the ^{102}RuF, ^{104}RuF and ^{100}RuF isotopologues extracted from the fit for the [18.2] $^4\Gamma_{4.5} \rightarrow X^4\Phi_{3.5}$ transition.

Isotopologue	Branch	F'	F''	J''	Observed (cm^{-1})	Calculated (cm^{-1})	Obs-Cal (cm^{-1})
^{102}RuF	P	5	6	6.5	18233.6698	18233.6678	0.002
	P	6	7	6.5	18233.6941	18233.6935	0.0005
	P	6	6	6.5	18233.7044	18233.7045	-0.0002
	P	6	7	7.5	18233.1217	18233.1205	0.0011
	P	7	8	7.5	18233.1409	18233.1422	-0.0014
	P	7	7	7.5	18233.1511	18233.1519	-0.0008
	P	7	8	8.5	18232.5741	18232.5762	-0.0021
	P	8	9	8.5	18232.5921	18232.5951	-0.0029
	P	8	9	9.5	18232.0319	18232.0352	-0.0033
	P	9	10	9.5	18232.0476	18232.0518	-0.0042
	P	10	11	10.5	18231.512	18231.5124	-0.0004
	P	9	10	10.5	18231.4982	18231.4975	0.0007
	P	10	11	11.5	18230.9648	18230.9633	0.0015
	P	12	13	12.5	18230.4456	18230.4449	0.0008
	P	11	12	12.5	18230.4347	18230.4326	0.0021
	P	13	14	13.5	18229.9175	18229.9167	0.0007
	P	12	13	13.5	18229.9083	18229.9055	0.0028
	P	14	15	14.5	18229.3891	18229.3923	-0.0033
	P	13	14	14.5	18229.3857	18229.3819	0.0038
	P	15	16	15.5	18228.8712	18228.8716	-0.0004
	P	14	15	15.5	18228.8628	18228.8619	0.0009
	Q	7	7	6.5	18237.4376	18237.4417	-0.0041
	Q	10	10	10.5	18237.5563	18237.557	-0.0007
	Q	11	11	10.5	18237.5696	18237.5699	-0.0003
	Q	11	11	11.5	18237.6006	18237.5996	0.0009
	Q	12	12	11.5	18237.612	18237.6114	0.0006
	Q	12	12	12.5	18237.6456	18237.6458	-0.0002
	Q	13	13	12.5	18237.6564	18237.6566	-0.0003
	Q	13	13	13.5	18237.6958	18237.6955	0.0003
	Q	14	14	13.5	18237.7055	18237.7056	-0.0001
	R	4	3	3.5	18239.9525	18239.9551	-0.0026
	R	5	4	3.5	18239.9821	18239.9798	0.0023
	R	4	4	3.5	18239.9344	18239.9355	-0.0012
	R	5	4	4.5	18240.55	18240.5506	-0.0005
	R	6	5	4.5	18240.5733	18240.5717	0.0016
	R	5	5	4.5	18240.5349	18240.535	-0.0002
	R	6	5	5.5	18241.1479	18241.1492	-0.0013
	R	7	6	5.5	18241.1679	18241.1676	0.0002

	R	6	6	5.5	18241.1382	18241.1363	0.0019
	R	7	6	6.5	18241.7499	18241.7511	-0.0012
	R	8	7	6.5	18241.767	18241.7674	-0.0004
	R	7	7	6.5	18241.7368	18241.7401	-0.0032
	R	9	8	7.5	18242.3725	18242.3711	0.0014
	R	8	7	7.5	18242.3561	18242.3564	-0.0003
	R	9	8	8.5	18242.9674	18242.9652	0.0022
	R	10	9	8.5	18242.9812	18242.9785	0.0027
	R	10	9	9.5	18243.5789	18243.5775	0.0014
	R	11	10	9.5	18243.5921	18243.5896	0.0024
	R	11	10	10.5	18244.195	18244.1934	0.0017
	R	12	11	10.5	18244.2053	18244.2045	0.0008
	R	12	11	11.5	18244.8155	18244.8128	0.0027
	R	13	12	11.5	18244.8258	18244.8232	0.0026
	R	14	13	12.5	18245.4462	18245.4455	0.0007
	R	13	12	12.5	18245.4356	18245.4358	-0.0003
	R	14	13	13.5	18246.0602	18246.0625	-0.0022
	R	15	14	13.5	18246.0698	18246.0715	-0.0017
	R	15	14	14.5	18246.6929	18246.6927	0.0002
	R	16	15	14.5	18246.7015	18246.7012	0.0003
	R	16	15	15.5	18247.3263	18247.3266	-0.0003
	R	17	16	15.5	18247.3347	18247.3346	0.0002
	R	17	16	16.5	18247.9619	18247.964	-0.0021
	R	18	17	16.5	18247.9705	18247.9716	-0.0011
	R	19	18	17.5	18248.6119	18248.6124	-0.0005
	R	18	17	17.5	18248.6052	18248.6052	0
	R	20	19	18.5	18249.2569	18249.2567	0.0001
	R	19	18	18.5	18249.2497	18249.2499	-0.0002
	R	21	20	19.5	18249.9053	18249.9048	0.0005
	R	20	19	19.5	18249.8975	18249.8983	-0.0008
	R	22	21	20.5	18250.556	18250.5565	-0.0005
	R	21	20	20.5	18250.5498	18250.5503	-0.0005
^{104}RuF	P	6	7	6.5	18233.694	18233.6938	0.0002
	P	5	6	6.5	18233.6708	18233.6676	0.0032
	P	7	8	7.5	18233.1453	18233.1465	-0.0011
	P	6	7	7.5	18233.1232	18233.1242	-0.001
	P	8	9	8.5	18232.6026	18232.6033	-0.0006
	P	7	8	8.5	18232.5843	18232.584	0.0003
	P	9	10	9.5	18232.064	18232.0641	-0.0002
	P	8	9	9.5	18232.0475	18232.0471	0.0004

P	10	11	10.5	18231.5273	18231.5289	-0.0017
P	9	10	10.5	18231.512	18231.5137	-0.0017
P	11	12	11.5	18230.9959	18230.9977	-0.0017
P	10	11	11.5	18230.9861	18230.9838	0.0023
P	11	12	12.5	18230.4553	18230.4576	-0.0023
P	12	13	12.5	18230.4696	18230.4702	-0.0006
P	13	14	13.5	18229.9459	18229.9467	-0.0008
P	12	13	13.5	18229.938	18229.935	0.0029
P	14	15	14.5	18229.4301	18229.4269	0.0032
P	13	14	14.5	18229.4147	18229.4161	-0.0014
P	15	16	15.5	18228.913	18228.911	0.002
P	14	15	15.5	18228.9002	18228.9009	-0.0007
R	5	4	3.5	18239.9431	18239.9447	-0.0015
R	4	3	3.5	18239.9155	18239.9179	-0.0023
R	6	5	4.5	18240.5332	18240.5337	-0.0006
R	5	4	4.5	18240.5096	18240.511	-0.0014
R	5	5	4.5	18240.4983	18240.499	-0.0008
R	7	6	5.5	18241.1252	18241.127	-0.0017
R	6	5	5.5	18241.1047	18241.1073	-0.0026
R	8	7	6.5	18241.7232	18241.7243	-0.0011
R	7	6	6.5	18241.7053	18241.7069	-0.0016
R	9	8	7.5	18242.3252	18242.3255	-0.0003
R	8	7	7.5	18242.3082	18242.31	-0.0018
R	10	9	8.5	18242.9335	18242.9307	0.0028
R	9	8	8.5	18242.9196	18242.9166	0.003
R	11	10	9.5	18243.5415	18243.5397	0.0017
R	10	9	9.5	18243.53	18243.5269	0.0031
R	12	11	10.5	18244.1549	18244.1526	0.0023
R	11	10	10.5	18244.1431	18244.1408	0.0023
R	13	12	11.5	18244.7725	18244.7693	0.0032
R	12	11	11.5	18244.7614	18244.7584	0.003
R	14	13	12.5	18245.3905	18245.3898	0.0007
R	13	12	12.5	18245.3808	18245.3797	0.0012
R	15	14	13.5	18246.014	18246.0142	-0.0001
R	14	13	13.5	18246.0045	18246.0046	-0.0002
R	16	15	14.5	18246.6427	18246.6423	0.0004
R	15	14	14.5	18246.6338	18246.6333	0.0004
R	17	16	15.5	18247.2742	18247.2742	0
R	16	15	15.5	18247.266	18247.2658	0.0002
R	18	17	16.5	18247.9075	18247.9099	-0.0024

	R	17	16	16.5	18247.8989	18247.9019	-0.003
	R	19	18	17.5	18248.5469	18248.5494	-0.0025
	R	18	17	17.5	18248.5402	18248.5418	-0.0016
	R	20	19	18.5	18249.1924	18249.1926	-0.0002
	R	19	18	18.5	18249.1859	18249.1854	0.0005
	R	21	20	19.5	18249.8401	18249.8396	0.0004
	R	20	19	19.5	18249.8325	18249.8328	-0.0003
	R	22	21	20.5	18250.4905	18250.4904	0.0001
	R	21	20	20.5	18250.4839	18250.4839	0
^{100}RuF	P	6	7	6.5	18233.7349	18233.7334	0.0014
	P	5	6	6.5	18233.7091	18233.7079	0.0012
	P	7	8	7.5	18233.1834	18233.1835	-0.0001
	P	6	7	7.5	18233.1617	18233.1618	-0.0002
	P	8	9	8.5	18232.6377	18232.6379	-0.0002
	P	7	8	8.5	18232.6191	18232.619	0
	P	9	10	9.5	18232.0974	18232.0965	0.001
	P	8	9	9.5	18232.0804	18232.0798	0.0006
	P	10	11	10.5	18231.5582	18231.5591	-0.0009
	P	9	10	10.5	18231.5418	18231.5441	-0.0023
	P	11	12	11.5	18231.0242	18231.0257	-0.0015
	P	10	11	11.5	18231.0137	18231.0121	0.0015
	P	12	13	12.5	18230.4976	18230.4964	0.0012
	P	11	12	12.5	18230.4849	18230.4839	0.001
	P	13	14	13.5	18229.9716	18229.971	0.0006
	P	12	13	13.5	18229.9599	18229.9595	0.0003
	P	14	15	14.5	18229.4486	18229.4496	-0.001
	P	13	14	14.5	18229.4359	18229.4389	-0.0031
	P	15	16	15.5	18228.9345	18228.9321	0.0024
	P	14	15	15.5	18228.9207	18228.9222	-0.0014
	R	5	4	3.5	18240.0236	18240.0224	0.0012
	R	4	3	3.5	18239.9956	18239.9946	0.001
	R	6	5	4.5	18240.6169	18240.6156	0.0013
	R	5	4	4.5	18240.5937	18240.5922	0.0015
	R	5	5	4.5	18240.5852	18240.5849	0.0003
	R	7	6	5.5	18241.2123	18241.2131	-0.0008
	R	6	5	5.5	18241.1937	18241.1929	0.0008
	R	8	7	6.5	18241.814	18241.8148	-0.0008
	R	7	6	6.5	18241.797	18241.797	-0.0001
	R	9	8	7.5	18242.4182	18242.4206	-0.0024

R	8	7	7.5	18242.4024	18242.4048	-0.0023
R	10	9	8.5	18243.032	18243.0304	0.0016
R	9	8	8.5	18243.0184	18243.0162	0.0022
R	11	10	9.5	18243.6432	18243.6443	-0.0012
R	10	9	9.5	18243.6318	18243.6313	0.0004
R	12	11	10.5	18244.2602	18244.2622	-0.002
R	11	10	10.5	18244.2504	18244.2502	0.0002
R	13	12	11.5	18244.883	18244.884	-0.001
R	12	11	11.5	18244.8714	18244.873	-0.0016
R	14	13	12.5	18245.5086	18245.5098	-0.0012
R	13	12	12.5	18245.4989	18245.4995	-0.0006
R	15	14	13.5	18246.1394	18246.1395	-0.0001
R	14	13	13.5	18246.1294	18246.1299	-0.0005
R	16	15	14.5	18246.7743	18246.7731	0.0012
R	15	14	14.5	18246.7659	18246.7641	0.0017
R	17	16	15.5	18247.4115	18247.4107	0.0008
R	16	15	15.5	18247.4016	18247.4022	-0.0006
R	18	17	16.5	18248.0525	18248.0521	0.0004
R	17	16	16.5	18248.0427	18248.0441	-0.0014
R	19	18	17.5	18248.6984	18248.6975	0.0009
R	18	17	17.5	18248.6866	18248.6899	-0.0033
R	20	19	18.5	18249.3474	18249.3468	0.0005
R	19	18	18.5	18249.339	18249.3396	-0.0006
R	21	20	19.5	18250.0013	18250	0.0013
R	20	19	19.5	18249.9936	18249.9932	0.0005
R	22	21	20.5	18250.6581	18250.6571	0.001
R	21	20	20.5	18250.6519	18250.6506	0.0013

Appendix D

Observed and calculated frequencies (cm^{-1}) of the ^{102}RuF, ^{104}RuF and ^{100}RuF isotopologues extracted from fit for the 1-1 band of the [18.2] $^4\Gamma_{5.5} \rightarrow X^4\Phi_{4.5}$ transition.

Isotopologue	Branch	F'	F''	J''	Observed (cm^{-1})	Calculated (cm^{-1})	Obs-Cal (cm^{-1})
^{102}RuF	P	5	6	6.5	18306.389	18306.389	0.0001
	P	6	7	6.5	18306.4302	18306.4279	0.0022
	P	6	7	7.5	18305.8495	18305.8465	0.003
	P	7	8	7.5	18305.8795	18305.8797	-0.0002
	P	7	8	8.5	18305.3043	18305.3068	-0.0024
	P	8	9	8.5	18305.3337	18305.3356	-0.0019
	P	8	9	9.5	18304.7697	18304.77	-0.0003
	P	9	10	9.5	18304.7943	18304.7956	-0.0013
	P	9	10	10.5	18304.233	18304.2365	-0.0035
	P	10	11	10.5	18304.2608	18304.2594	0.0014
	P	10	11	11.5	18303.7053	18303.7063	-0.001
	P	11	12	11.5	18303.7269	18303.7271	-0.0002
	P	11	12	12.5	18303.179	18303.1795	-0.0005
	P	12	13	12.5	18303.1974	18303.1986	-0.0012
	P	12	13	13.5	18302.6561	18302.6562	-0.0001
	P	13	14	13.5	18302.6744	18302.6738	0.0006
	P	13	14	14.5	18302.1363	18302.1365	-0.0002
	P	14	15	14.5	18302.1543	18302.1528	0.0015
	P	14	15	15.5	18301.621	18301.6203	0.0006
	P	15	16	15.5	18301.6353	18301.6355	-0.0003
	P	15	16	16.5	18301.1078	18301.1078	0
	P	16	17	16.5	18301.1224	18301.122	0.0003
	P	16	17	17.5	18300.5985	18300.5989	-0.0005
	P	17	18	17.5	18300.6131	18300.6123	0.0008
	P	17	18	18.5	18300.0963	18300.0937	0.0026
	P	18	19	18.5	18300.1114	18300.1064	0.0051
	P	18	19	19.5	18299.5895	18299.5922	-0.0027
	P	19	20	19.5	18299.6039	18299.6042	-0.0002
	P	19	20	20.5	18299.0932	18299.0945	-0.0013
	P	20	21	20.5	18299.1051	18299.1058	-0.0007
	P	20	21	21.5	18298.5977	18298.6004	-0.0028
	P	21	22	21.5	18298.6132	18298.6112	0.0019
	P	21	22	22.5	18298.1111	18298.1102	0.0009
	P	22	23	22.5	18298.1189	18298.1205	-0.0016
	Q	9	9	9.5	18310.2078	18310.2082	-0.0003
	Q	9	9	8.5	18310.199	18310.1984	0.0006
	Q	10	10	9.5	18310.2298	18310.2307	-0.0009
	Q	10	10	10.5	18310.2463	18310.2463	0
	Q	11	11	10.5	18310.2674	18310.2668	0.0006

Q	11	11	11.5	18310.2879	18310.2878	0.0001
Q	12	12	11.5	18310.3076	18310.3066	0.001
Q	12	12	12.5	18310.3341	18310.3328	0.0014
Q	13	13	12.5	18310.348	18310.3501	-0.0021
Q	13	13	13.5	18310.3791	18310.3811	-0.002
Q	14	14	13.5	18310.3977	18310.3972	0.0005
Q	14	14	14.5	18310.4333	18310.433	0.0004
Q	15	15	14.5	18310.4488	18310.448	0.0008
Q	15	15	15.5	18310.488	18310.4883	-0.0003
Q	16	16	15.5	18310.4994	18310.5024	-0.003
Q	16	16	16.5	18310.5494	18310.5472	0.0021
Q	5	5	5.5	18310.0861	18310.0867	-0.0006
Q	6	6	6.5	18310.1139	18310.1128	0.0011
Q	6	6	5.5	18310.1228	18310.1247	-0.0019
Q	7	7	7.5	18310.1424	18310.1415	0.0009
Q	7	7	6.5	18310.1437	18310.1452	-0.0015
Q	8	8	7.5	18310.1713	18310.1699	0.0015
Q	8	8	8.5	18310.1747	18310.1733	0.0014
Q	6	6	5.5	18310.0797	18310.0802	-0.0005
Q	17	17	17.5	18310.6092	18310.6096	-0.0005
Q	18	18	17.5	18310.6225	18310.6221	0.0004
Q	19	19	19.5	18310.747	18310.7452	0.0018
Q	20	20	19.5	18310.7568	18310.7565	0.0003
Q	19	19	18.5	18310.6873	18310.6875	-0.0002
Q	18	18	18.5	18310.6755	18310.6756	-0.0001
R	5	4	4.5	18313.2164	18313.2159	0.0004
R	6	5	4.5	18313.2519	18313.2526	-0.0007
R	5	5	4.5	18313.2099	18313.2081	0.0018
R	6	5	5.5	18313.8122	18313.8105	0.0017
R	7	6	5.5	18313.8442	18313.842	0.0022
R	6	6	5.5	18313.8028	18313.804	-0.0012
R	7	6	6.5	18314.4081	18314.4078	0.0004
R	8	7	6.5	18314.436	18314.4354	0.0006
R	8	7	7.5	18315.0079	18315.008	-0.0001
R	9	8	7.5	18315.033	18315.0326	0.0003
R	9	8	8.5	18315.6104	18315.6114	-0.001
R	10	9	8.5	18315.6328	18315.6336	-0.0007
R	10	9	9.5	18316.2167	18316.218	-0.0013
R	11	10	9.5	18316.2358	18316.2382	-0.0023
R	11	10	10.5	18316.8286	18316.8279	0.0008

	R	12	11	10.5	18316.8477	18316.8464	0.0014
	R	12	11	11.5	18317.4415	18317.4411	0.0004
	R	13	12	11.5	18317.4587	18317.4582	0.0005
	R	13	12	12.5	18318.0567	18318.0576	-0.0009
	R	14	13	12.5	18318.074	18318.0735	0.0004
	R	14	13	13.5	18318.6772	18318.6776	-0.0004
	R	15	14	13.5	18318.6909	18318.6924	-0.0016
^{104}RuF	P	8	9	8.5	18305.2352	18305.2377	-0.0024
	P	7	8	8.5	18305.2071	18305.2085	-0.0014
	P	9	10	9.5	18304.7022	18304.6997	0.0025
	P	8	9	9.5	18304.6725	18304.6738	-0.0014
	P	9	10	10.5	18304.1432	18304.1424	0.0008
	P	11	12	11.5	18303.6368	18303.6353	0.0016
	P	10	11	11.5	18303.6139	18303.6142	-0.0003
	P	12	13	12.5	18303.1058	18303.1086	-0.0028
	P	11	12	12.5	18303.088	18303.0894	-0.0013
	P	13	14	13.5	18302.5856	18302.5857	-0.0001
	P	12	13	13.5	18302.5708	18302.5679	0.0029
	P	14	15	14.5	18302.0659	18302.0664	-0.0004
	P	13	14	14.5	18302.0511	18302.0499	0.0013
	P	15	16	16.5	18301.0222	18301.0239	-0.0017
	P	16	17	16.5	18301.0384	18301.0383	0.0001
	P	16	17	17.5	18300.515	18300.5159	-0.001
	P	17	18	17.5	18300.5293	18300.5295	-0.0002
	P	18	19	18.5	18300.0257	18300.0241	0.0016
	P	17	18	18.5	18300.0158	18300.0113	0.0045
	P	18	19	19.5	18299.5081	18299.5099	-0.0019
	P	19	20	19.5	18299.5226	18299.522	0.0006
	P	20	21	20.5	18299.0229	18299.0233	-0.0004
	P	19	20	20.5	18299.0105	18299.0118	-0.0013
	P	22	23	22.5	18298.0344	18298.0356	-0.0012
	P	21	22	22.5	18298.026	18298.0252	0.0009
	R	5	4	4.5	18313.0935	18313.0944	-0.0009
	R	6	5	4.5	18313.1317	18313.1321	-0.0004
	R	5	5	4.5	18313.0886	18313.0888	-0.0002
	R	6	5	5.5	18313.6917	18313.6878	0.0039
	R	7	6	5.5	18313.7229	18313.7201	0.0028
	R	6	6	5.5	18313.6836	18313.6831	0.0005
	R	7	6	6.5	18314.2849	18314.2838	0.0011

	R	8	7	6.5	18314.3134	18314.3121	0.0013
	R	8	7	7.5	18314.8818	18314.8826	-0.0009
	R	9	8	7.5	18314.9077	18314.9078	-0.0001
	R	9	8	8.5	18315.4817	18315.4844	-0.0028
	R	10	9	8.5	18315.5055	18315.5071	-0.0017
	R	10	10	9.5	18316.0863	18316.0865	-0.0002
	R	11	10	9.5	18316.108	18316.1099	-0.0019
	R	11	10	10.5	18316.6969	18316.6972	-0.0003
	R	12	11	10.5	18316.7163	18316.7161	0.0003
	R	12	11	11.5	18317.3074	18317.3081	-0.0007
	R	13	12	11.5	18317.3248	18317.3256	-0.0007
	R	13	12	12.5	18317.9205	18317.9221	-0.0016
	R	14	13	12.5	18317.9386	18317.9383	0.0002
	R	15	14	13.5	18318.5551	18318.5542	0.0009
	R	14	13	13.5	18318.5417	18318.5391	0.0026
^{100}RuF	P	6	7	6.5	18306.5306	18306.5337	-0.0031
	P	5	6	6.5	18306.4941	18306.492	0.0021
	P	7	8	7.5	18305.9838	18305.9835	0.0003
	P	6	7	7.5	18305.946	18305.948	-0.002
	P	8	9	8.5	18305.4367	18305.4375	-0.0007
	P	7	8	8.5	18305.4053	18305.4066	-0.0013
	P	9	10	9.5	18304.8935	18304.8955	-0.002
	P	8	9	9.5	18304.8689	18304.8682	0.0007
	P	10	11	10.5	18304.3587	18304.3575	0.0012
	P	9	10	10.5	18304.3349	18304.333	0.0019
	P	11	12	11.5	18303.8233	18303.8234	-0.0001
	P	10	11	11.5	18303.8017	18303.8012	0.0004
	P	11	12	12.5	18303.2732	18303.2729	0.0003
	P	12	13	12.5	18303.2933	18303.2932	0.0001
	P	12	13	13.5	18302.7487	18302.7481	0.0005
	P	13	14	13.5	18302.7684	18302.7668	0.0015
	P	13	14	14.5	18302.2288	18302.227	0.0018
	P	14	15	14.5	18302.2445	18302.2443	0.0002
	P	15	16	16.5	18301.1968	18301.1959	0.0009
	P	16	17	16.5	18301.2117	18301.211	0.0007
	P	16	17	17.5	18300.6851	18300.686	-0.0009
	P	17	18	17.5	18300.7003	18300.7002	0.0001
	P	18	19	18.5	18300.1955	18300.1934	0.0021
	P	17	18	18.5	18300.1797	18300.18	-0.0002
	P	19	20	19.5	18299.6892	18299.6905	-0.0013

P	18	19	19.5	18299.6764	18299.6778	-0.0015
P	20	21	20.5	18299.189	18299.1917	-0.0027
P	19	20	20.5	18299.1765	18299.1796	-0.0032
P	21	22	21.5	18298.6991	18298.6969	0.0021
P	20	21	21.5	18298.6824	18298.6855	-0.0031
P	22	23	22.5	18298.2111	18298.2063	0.0049
P	21	22	22.5	18298.1933	18298.1953	-0.002
P	23	24	23.5	18297.7216	18297.7197	0.0019
P	22	23	23.5	18297.709	18297.7093	-0.0003
R	6	5	4.5	18313.3807	18313.3797	0.001
R	5	4	4.5	18313.3392	18313.3416	-0.0023
R	6	5	5.5	18313.9395	18313.938	0.0016
R	7	6	5.5	18313.9718	18313.9708	0.001
R	6	6	5.5	18313.9267	18313.9277	-0.001
R	7	6	6.5	18314.5389	18314.5371	0.0018
R	8	7	6.5	18314.5661	18314.566	0.0001
R	7	7	6.5	18314.5291	18314.5283	0.0008
R	8	7	7.5	18315.1389	18315.1392	-0.0003
R	9	8	7.5	18315.1646	18315.165	-0.0003
R	9	8	8.5	18315.7441	18315.7445	-0.0004
R	10	9	8.5	18315.7662	18315.7677	-0.0016
R	10	9	9.5	18316.353	18316.3531	0
R	11	10	9.5	18316.3751	18316.3742	0.0009
R	11	10	10.5	18316.9668	18316.9649	0.0019
R	12	11	10.5	18316.9843	18316.9844	-0.0001
R	12	11	11.5	18317.5799	18317.5802	-0.0003
R	13	12	11.5	18317.5948	18317.5982	-0.0033
R	14	13	12.5	18318.2177	18318.2156	0.0021
R	13	12	12.5	18318.1984	18318.199	-0.0006

Appendix E

Observed and calculated frequencies (cm^{-1}) of the $^{102}Ru^{35}Cl$, $^{104}Ru^{35}Cl$ and $^{100}Ru^{35}Cl$ isotopologues extracted from the multiple state fitting for the [17.5] $^4\Phi_{4.5} \rightarrow X^4\Phi_{4.5}$ and [19.6] $^4\Gamma_{5.5} \rightarrow X^4\Phi_{4.5}$ transitions.

The [17.5] $^4\Phi_{4.5} \rightarrow X^4\Phi_{4.5}$ transition

Isotopologue	Branch	J"	Observed (cm^{-1})	Calculated (cm^{-1})	Obs-Cal (cm^{-1})
$^{102}Ru^{35}Cl$	P	5.5	17551.7517	17551.7509	0.0008
	P	6.5	17551.4702	17551.4711	-0.0009
	P	7.5	17551.1857	17551.1866	-0.0009
	P	8.5	17550.8967	17550.8975	-0.0009
	P	9.5	17550.6038	17550.6039	-0.0001
	P	10.5	17550.3073	17550.3056	0.0017
	P	11.5	17550.0022	17550.0028	-0.0007
	P	12.5	17549.6962	17549.6955	0.0007
	P	13.5	17549.3836	17549.3835	0.0001
	P	15.5	17548.7436	17548.7459	-0.0023
	P	16.5	17548.4173	17548.4204	-0.0031
	P	17.5	17548.0877	17548.0902	-0.0025
	P	18.5	17547.7524	17547.7556	-0.0032
	P	19.5	17547.4165	17547.4164	0.0001
	P	20.5	17547.0726	17547.0727	-0.0001
	P	21.5	17546.7257	17546.7246	0.0012
	P	22.5	17546.37	17546.3719	-0.0019
	P	23.5	17546.0153	17546.0148	0.0005
	P	24.5	17545.6535	17545.6532	0.0003
	P	25.5	17545.2878	17545.2871	0.0007
	P	26.5	17544.9153	17544.9167	-0.0014
	Q	4.5	17553.1514	17553.1508	0.0006
	Q	5.5	17553.1238	17553.1254	-0.0016
	Q	6.5	17553.0954	17553.0954	-0.0001
	Q	7.5	17553.0627	17553.0608	0.0019
	Q	10.5	17552.9292	17552.9295	-0.0003
	Q	11.5	17552.8769	17552.8765	0.0004
	Q	12.5	17552.8199	17552.8189	0.001
	R	4.5	17554.5252	17554.5252	-0.0001
	R	5.5	17554.7507	17554.7498	0.0009
	R	6.5	17554.9696	17554.9697	-0.0001
	R	7.5	17555.1857	17555.1849	0.0007
	R	8.5	17555.3959	17555.3956	0.0003
	R	9.5	17555.6022	17555.6017	0.0006
	R	10.5	17555.8034	17555.8031	0.0003
	R	11.5	17556.0002	17556	0.0002

	R	12.5	17556.1929	17556.1922	0.0007
	R	13.5	17556.3801	17556.3799	0.0002
	R	14.5	17556.5625	17556.563	-0.0005
	R	15.5	17556.7419	17556.7414	0.0005
	R	16.5	17556.9147	17556.9153	-0.0006
	R	17.5	17557.0857	17557.0847	0.001
	R	18.5	17557.2509	17557.2494	0.0014
	R	19.5	17557.4097	17557.4096	0.0001
	R	20.5	17557.5672	17557.5653	0.0019
	R	21.5	17557.7185	17557.7164	0.0021
	R	22.5	17557.8634	17557.863	0.0004
	R	23.5	17558.0055	17558.005	0.0005
	R	24.5	17558.1428	17558.1426	0.0003
	R	25.5	17558.2759	17558.2756	0.0003
	R	26.5	17558.4046	17558.4041	0.0005
	R	27.5	17558.5265	17558.5281	-0.0017
$^{104}Ru^{35}Cl$	P	5.5	17551.7319	17551.7299	0.0019
	P	6.5	17551.4505	17551.4515	-0.0009
	P	7.5	17551.1691	17551.1684	0.0007
	P	8.5	17550.8803	17550.8808	-0.0006
	P	9.5	17550.5879	17550.5886	-0.0007
	P	10.5	17550.291	17550.2919	-0.0009
	P	11.5	17549.9902	17549.9906	-0.0004
	P	12.5	17549.6853	17549.6847	0.0006
	P	13.5	17549.3733	17549.3743	-0.001
	P	14.5	17549.0591	17549.0594	-0.0003
	P	15.5	17548.7438	17548.7399	0.0039
	P	16.5	17548.4173	17548.4158	0.0014
	P	17.5	17548.0876	17548.0872	0.0003
	P	18.5	17547.7524	17547.7541	-0.0017
	P	19.5	17547.4165	17547.4165	0
	P	20.5	17547.0726	17547.0744	-0.0018
	P	21.5	17546.7259	17546.7278	-0.0018
	R	4.5	17554.4901	17554.4905	-0.0004
	R	5.5	17554.7133	17554.7139	-0.0006
	R	6.5	17554.9327	17554.9328	-0.0001
	R	7.5	17555.1474	17555.147	0.0003
	R	8.5	17555.3567	17555.3567	0.0001
	R	9.5	17555.5626	17555.5617	0.0009

	R	10.5	17555.7625	17555.7622	0.0003
	R	11.5	17555.9577	17555.958	-0.0004
	R	12.5	17556.149	17556.1493	-0.0004
	R	13.5	17556.3349	17556.336	-0.0011
	R	14.5	17556.5172	17556.5182	-0.001
	R	15.5	17556.6959	17556.6957	0.0002
	R	16.5	17556.8697	17556.8687	0.001
	R	17.5	17557.037	17557.037	-0.0001
	R	18.5	17557.2012	17557.2009	0.0003
	R	19.5	17557.3609	17557.3601	0.0008
	R	20.5	17557.5152	17557.5148	0.0004
	R	21.5	17557.6659	17557.6649	0.001
	R	22.5	17557.8119	17557.8105	0.0014
	R	23.5	17557.9503	17557.9515	-0.0012
$^{100}Ru^{35}Cl$	P	5.5	17551.7741	17551.7743	-0.0002
	P	6.5	17551.4929	17551.4927	0.0002
	P	7.5	17551.2044	17551.2064	-0.002
	P	8.5	17550.9162	17550.9155	0.0007
	P	9.5	17550.6206	17550.62	0.0006
	P	10.5	17550.3212	17550.3199	0.0013
	P	11.5	17550.0156	17550.0152	0.0003
	P	12.5	17549.7074	17549.706	0.0014
	P	13.5	17549.3937	17549.3922	0.0015
	P	14.5	17549.0732	17549.074	-0.0007
	P	15.5	17548.7511	17548.7512	-0.0001
	P	16.5	17548.4173	17548.4241	-0.0068
	P	17.5	17548.0877	17548.0925	-0.0048
	P	18.5	17547.7523	17547.7566	-0.0043
	P	19.5	17547.4165	17547.4164	0.0001
	P	20.5	17547.0726	17547.0718	0.0007
	P	21.5	17546.7257	17546.7231	0.0027
	P	22.5	17546.37	17546.3701	-0.0001
	P	23.5	17546.0153	17546.013	0.0024
	P	24.5	17545.6537	17545.6517	0.002
	P	25.5	17545.2872	17545.2864	0.0008
	P	26.5	17544.9167	17544.9172	-0.0005
	R	4.5	17554.5621	17554.5629	-0.0008
	R	5.5	17554.7879	17554.7883	-0.0004
	R	6.5	17555.0099	17555.009	0.0009

R	7.5	17555.227	17555.2251	0.0019
R	8.5	17555.4374	17555.4365	0.0009
R	9.5	17555.6442	17555.6433	0.0009
R	10.5	17555.8448	17555.8456	-0.0007
R	11.5	17556.0448	17556.0432	0.0015
R	12.5	17556.2376	17556.2363	0.0013
R	13.5	17556.4263	17556.4249	0.0014
R	14.5	17556.6083	17556.609	-0.0007
R	15.5	17556.7885	17556.7886	-0.0001
R	16.5	17556.9637	17556.9637	-0.0001
R	17.5	17557.1342	17557.1345	-0.0003
R	18.5	17557.303	17557.3009	0.002
R	19.5	17557.4637	17557.463	0.0007
R	20.5	17557.6192	17557.6208	-0.0016
R	21.5	17557.7724	17557.7744	-0.002

The [19.6] $^4\Gamma_{5.5} \rightarrow X^4\Phi_{4.5}$ transition

Isotopologue	Branch	J"	Observed (cm^{-1})	Calculated (cm^{-1})	Obs-Cal (cm^{-1})
$^{102}Ru^{35}Cl$	P	8.5	19664.3002	19664.3038	-0.0036
	P	9.5	19664.0566	19664.0558	0.0008
	P	10.5	19663.8105	19663.8086	0.0019
	P	11.5	19663.561	19663.5621	-0.0012
	P	12.5	19663.3165	19663.3165	0.0001
	P	13.5	19663.072	19663.0716	0.0004
	P	14.5	19662.8287	19662.8275	0.0012
	P	15.5	19662.5839	19662.5842	-0.0003
	P	16.5	19662.3425	19662.3416	0.0008
	P	17.5	19662.1018	19662.0999	0.0019
	P	18.5	19661.8598	19661.8589	0.0009
	P	19.5	19661.6213	19661.6188	0.0025
	P	20.5	19661.3821	19661.3794	0.0027
	P	21.5	19661.143	19661.1408	0.0021
	P	22.5	19660.9055	19660.9031	0.0024
	P	23.5	19660.6647	19660.6661	-0.0014
	P	24.5	19660.4296	19660.43	-0.0003
	P	25.5	19660.1953	19660.1946	0.0007
	P	26.5	19659.9582	19659.9601	-0.0019
	R	4.5	19667.8559	19667.8563	-0.0004
	R	5.5	19668.1184	19668.1157	0.0026
	R	6.5	19668.3743	19668.3759	-0.0016
	R	7.5	19668.6328	19668.6369	-0.0041
	R	8.5	19668.8989	19668.8985	0.0003
	R	9.5	19669.1618	19669.161	0.0008
	R	10.5	19669.4247	19669.4241	0.0006
	R	11.5	19669.6884	19669.688	0.0003
	R	12.5	19669.9509	19669.9527	-0.0018
	R	13.5	19670.2179	19670.2181	-0.0002
	R	14.5	19670.4849	19670.4842	0.0007
	R	15.5	19670.7516	19670.7511	0.0005
	R	16.5	19671.0176	19671.0187	-0.0011
	R	17.5	19671.2872	19671.287	0.0001
	R	18.5	19671.5555	19671.5561	-0.0007
	R	19.5	19671.8248	19671.8259	-0.0011
	R	20.5	19672.0952	19672.0965	-0.0013
	R	21.5	19672.3666	19672.3678	-0.0012

	R	22.5	19672.638	19672.6398	-0.0017
	R	23.5	19672.9109	19672.9125	-0.0016
	R	24.5	19673.1838	19673.186	-0.0022
	R	25.5	19673.4614	19673.4602	0.0012
	R	26.5	19673.738	19673.7351	0.0029
	R	27.5	19674.012	19674.0107	0.0013
	R	28.5	19674.2875	19674.2871	0.0004
	R	29.5	19674.5639	19674.5642	-0.0004
	R	30.5	19674.8412	19674.842	-0.0008
	R	31.5	19675.1193	19675.1206	-0.0013
	R	32.5	19675.3984	19675.3999	-0.0015
	R	33.5	19675.6794	19675.6799	-0.0005
	R	34.5	19675.9611	19675.9606	0.0005
	R	35.5	19676.2426	19676.242	0.0006
	R	36.5	19676.5242	19676.5242	0.0001
	R	37.5	19676.8072	19676.807	0.0002
	R	38.5	19677.0909	19677.0906	0.0003
	R	39.5	19677.3753	19677.375	0.0003
$^{104}Ru^{35}Cl$	P	6.5	19664.8073	19664.8085	-0.0012
	P	7.5	19664.5634	19664.5601	0.0033
	P	8.5	19664.3131	19664.3125	0.0006
	P	9.5	19664.0644	19664.0657	-0.0013
	P	10.5	19663.8211	19663.8196	0.0014
	P	11.5	19663.5724	19663.5743	-0.0019
	P	12.5	19663.3298	19663.3298	0
	P	13.5	19663.0864	19663.086	0.0004
	P	14.5	19662.8415	19662.843	-0.0015
	P	15.5	19662.6006	19662.6008	-0.0003
	P	16.5	19662.3578	19662.3594	-0.0016
	P	17.5	19662.1177	19662.1187	-0.0011
	P	18.5	19661.8795	19661.8789	0.0006
	P	19.5	19661.6404	19661.6398	0.0006
	P	20.5	19661.403	19661.4015	0.0015
	P	21.5	19661.1653	19661.164	0.0013
	P	22.5	19660.9283	19660.9273	0.0011
	R	9.5	19669.146	19669.1454	0.0005
	R	10.5	19669.4093	19669.4072	0.0021
	R	11.5	19669.6693	19669.6698	-0.0004
	R	12.5	19669.9317	19669.933	-0.0014

	R	13.5	19670.1978	19670.197	0.0008
	R	14.5	19670.4608	19670.4617	-0.0009
	R	15.5	19670.7283	19670.7272	0.0011
	R	16.5	19670.9949	19670.9934	0.0015
	R	17.5	19671.2585	19671.2603	-0.0018
	R	18.5	19671.5257	19671.5279	-0.0022
	R	19.5	19671.7962	19671.7963	-0.0001
	R	20.5	19672.0645	19672.0654	-0.0009
	R	21.5	19672.3342	19672.3353	-0.0011
	R	22.5	19672.6046	19672.6058	-0.0013
	R	23.5	19672.8758	19672.8771	-0.0013
	R	24.5	19673.1477	19673.1491	-0.0014
	R	25.5	19673.4238	19673.4218	0.0019
	R	26.5	19673.6976	19673.6953	0.0023
	R	27.5	19673.9715	19673.9695	0.002
	R	28.5	19674.2465	19674.2444	0.002
	R	29.5	19674.5193	19674.5201	-0.0008
	R	30.5	19674.7958	19674.7965	-0.0007
	R	31.5	19675.0727	19675.0736	-0.0009
	R	32.5	19675.3505	19675.3514	-0.0008
	R	33.5	19675.63	19675.6299	0
	R	34.5	19675.9089	19675.9092	-0.0003
	R	35.5	19676.1895	19676.1892	0.0002
$^{100}Ru^{35}Cl$	P	7.5	19664.5445	19664.5487	-0.0041
	P	8.5	19664.3008	19664.2986	0.0022
	P	9.5	19664.0541	19664.0492	0.0049
	P	10.5	19663.8044	19663.8007	0.0037
	P	11.5	19663.5525	19663.5529	-0.0004
	P	12.5	19663.3038	19663.3059	-0.0021
	P	13.5	19663.0593	19663.0597	-0.0004
	P	14.5	19662.8148	19662.8143	0.0005
	P	15.5	19662.5701	19662.5697	0.0004
	P	16.5	19662.3279	19662.3259	0.002
	P	17.5	19662.0851	19662.0829	0.0021
	P	18.5	19661.8425	19661.8407	0.0018
	P	19.5	19661.6007	19661.5993	0.0013
	P	20.5	19661.361	19661.3588	0.0022
	P	21.5	19661.1224	19661.119	0.0033
	P	22.5	19660.8799	19660.8801	-0.0002
	P	23.5	19660.64	19660.642	-0.002

P	24.5	19660.4041	19660.4048	-0.0007
P	25.5	19660.1635	19660.1684	-0.0049
P	26.5	19659.9306	19659.9328	-0.0022
R	4.5	19667.866	19667.8698	-0.0038
R	5.5	19668.1339	19668.1305	0.0033
R	6.5	19668.3912	19668.392	-0.0009
R	7.5	19668.6561	19668.6543	0.0018
R	8.5	19668.9171	19668.9173	-0.0002
R	9.5	19669.1809	19669.181	-0.0001
R	10.5	19669.4443	19669.4455	-0.0012
R	11.5	19669.7107	19669.7107	0
R	12.5	19669.9748	19669.9767	-0.0018
R	13.5	19670.2423	19670.2433	-0.001
R	14.5	19670.5115	19670.5108	0.0008
R	15.5	19670.778	19670.7789	-0.0009
R	16.5	19671.0473	19671.0479	-0.0006
R	17.5	19671.3168	19671.3175	-0.0007
R	18.5	19671.5861	19671.5879	-0.0017
R	19.5	19671.8571	19671.859	-0.0019
R	20.5	19672.1292	19672.1309	-0.0017
R	21.5	19672.4015	19672.4035	-0.002
R	22.5	19672.674	19672.6768	-0.0029
R	23.5	19672.9499	19672.9509	-0.0009
R	24.5	19673.2251	19673.2257	-0.0006
R	25.5	19673.5003	19673.5012	-0.0009
R	26.5	19673.7805	19673.7775	0.003
R	27.5	19674.057	19674.0546	0.0024
R	28.5	19674.3341	19674.3323	0.0017
R	29.5	19674.611	19674.6109	0.0002
R	30.5	19674.89	19674.8901	-0.0001
R	31.5	19675.1698	19675.1701	-0.0003
R	32.5	19675.4516	19675.4509	0.0007
R	33.5	19675.7333	19675.7324	0.0009
R	34.5	19676.0165	19676.0146	0.0019
R	35.5	19676.2989	19676.2976	0.0012
R	36.5	19676.5826	19676.5814	0.0012
R	37.5	19676.8665	19676.8659	0.0006
R	38.5	19677.1501	19677.1512	-0.001
R	39.5	19677.4371	19677.4372	-0.0001
R	40.5	19677.7234	19677.724	-0.0006

R	41.5	19678.0104	19678.0115	-0.0012
R	42.5	19678.3009	19678.2998	0.0011
R	43.5	19678.589	19678.5889	0.0001
R	44.5	19678.8791	19678.8788	0.0003
R	45.5	19679.1698	19679.1694	0.0004
R	46.5	19679.4589	19679.4608	-0.0019
R	47.5	19679.7531	19679.753	0.0002

Appendix F

Observed and calculated frequencies (cm^{-1}) of the $^{102}Ru^{37}Cl$ isotopologue extracted from the multiple state fitting for the [17.5] $^4\Phi_{4.5} \rightarrow X^4\Phi_{4.5}$ and [19.6] $^4\Gamma_{5.5} \rightarrow X^4\Phi_{4.5}$ transitions.

The [17.5] $^4\Phi_{4.5} \rightarrow X^4\Phi_{4.5}$ transition

Isotopologue		J"	Observed (cm^{-1})	Calculated (cm^{-1})	Obs-Cal (cm^{-1})
$^{102}Ru^{37}Cl$	P	7.5	17550.9907	17550.9882	0.0025
	P	8.5	17550.7125	17550.7105	0.002
	P	9.5	17550.4291	17550.4284	0.0007
	P	10.5	17550.1433	17550.1419	0.0014
	P	11.5	17549.8472	17549.8511	-0.0039
	P	12.5	17549.5545	17549.5559	-0.0013
	P	13.5	17549.2569	17549.2563	0.0006
	P	14.5	17548.9518	17548.9523	-0.0005
	P	15.5	17548.6448	17548.6439	0.0009
	P	16.5	17548.3316	17548.3312	0.0005
	P	17.5	17548.0112	17548.014	-0.0028
	P	18.5	17547.6904	17547.6924	-0.002
	P	19.5	17547.3678	17547.3663	0.0015
	P	20.5	17547.0392	17547.0358	0.0034
	P	21.5	17546.7022	17546.7008	0.0013
	P	23.5	17546.0153	17546.0174	-0.0021
	Q	4.5	17552.8769	17552.8758	0.0012
	Q	5.5	17552.849	17552.8512	-0.0022
	Q	6.5	17552.8199	17552.8221	-0.0022
	Q	7.5	17552.7905	17552.7885	0.002
	R	5.5	17554.4113	17554.4117	-0.0004
	R	6.5	17554.6213	17554.6224	-0.0011
	R	7.5	17554.8275	17554.8284	-0.0009
	R	8.5	17555.0306	17555.0297	0.0008
	R	9.5	17555.227	17555.2264	0.0006

The [19.6] $^4\Gamma_{5.5} \rightarrow X^4\Phi_{4.5}$ transition

Isotopologue	Branch	J"	Observed (cm^{-1})	Calculated (cm^{-1})	Obs-Cal (cm^{-1})
$^{102}Ru^{37}Cl$	P	11.5	19663.5793	19663.5817	-0.0025
	P	12.5	19663.3436	19663.3456	-0.002
	P	13.5	19663.1124	19663.1105	0.0019
	P	14.5	19662.8792	19662.8766	0.0026
	P	15.5	19662.6461	19662.6439	0.0022
	P	16.5	19662.4136	19662.4124	0.0012
	P	17.5	19662.1809	19662.1823	-0.0013
	P	18.5	19661.9498	19661.9536	-0.0037
	P	22.5	19661.056	19661.055	0.001
	R	4.5	19667.7113	19667.7109	0.0004
	R	5.5	19667.9563	19667.959	-0.0028
	R	6.5	19668.2064	19668.2077	-0.0012
	R	7.5	19668.459	19668.4569	0.0021
	R	8.5	19668.7096	19668.7066	0.003
	R	9.5	19668.9546	19668.957	-0.0024
	R	10.5	19669.208	19669.2079	0
	R	11.5	19669.4593	19669.4595	-0.0003
	R	12.5	19669.714	19669.7118	0.0022
	R	13.5	19669.9682	19669.9648	0.0034
	R	14.5	19670.218	19670.2186	-0.0006
	R	15.5	19670.4699	19670.4731	-0.0032
	R	16.5	19670.7283	19670.7285	-0.0002
	R	25.5	19673.0792	19673.0759	0.0033
	R	26.5	19673.3419	19673.3435	-0.0016
	R	27.5	19673.6121	19673.6127	-0.0006
	R	28.5	19673.8831	19673.8837	-0.0007
	R	30.5	19674.429	19674.4315	-0.0026
	R	31.5	19674.7085	19674.7085	0
	R	32.5	19674.9914	19674.9877	0.0038
	R	33.5	19675.2679	19675.2692	-0.0013

Appendix G

Observed and calculated frequencies (cm^{-1}) for the ^{102}RuO, ^{104}RuO, ^{100}RuO, ^{99}RuO and ^{101}RuO isotopologues of 1-0 band of the [18.1] $4 \rightarrow X^5\Delta_4$ transition.

Isotopologue	Branch	J"	Observed (cm^{-1})	Calculated (cm^{-1})	Obs-Cal (cm^{-1})
^{102}RuO	P	9	18861.2426	18861.2418	0.0007
	P	8	18862.6158	18862.6177	-0.0019
	P	7	18863.9246	18863.9249	-0.0003
	P	6	18865.1636	18865.1632	0.0005
	P	10	18859.7974	18859.7972	0.0002
	P	12	18856.7016	18856.7016	0
	P	13	18855.051	18855.0507	0.0003
	P	14	18853.3293	18853.3312	-0.0019
	P	11	18858.2844	18858.2837	0.0007
	P	15	18851.545	18851.543	0.002
	P	5	18866.3337	18866.3327	0.0011
	Q	4	18870.4586	18870.4577	0.0009
	Q	5	18870.113	18870.1131	-0.0001
	Q	6	18869.7002	18869.6995	0.0007
	Q	7	18869.2174	18869.2171	0.0003
	Q	8	18868.6664	18868.6657	0.0007
	Q	9	18868.0469	18868.0455	0.0014
	Q	10	18867.3542	18867.3563	-0.0021
	Q	11	18866.5985	18866.5982	0.0003
	Q	13	18864.8734	18864.8755	-0.0021
	Q	12	18865.7708	18865.7713	-0.0006
	R	4	18874.2368	18874.2381	-0.0014
	R	5	18874.6483	18874.6495	-0.0011
	R	6	18874.9896	18874.9918	-0.0021
	R	7	18875.2657	18875.2651	0.0006
	R	8	18875.4684	18875.4693	-0.0009
	R	9	18875.6059	18875.6046	0.0013
	R	11	18875.6704	18875.668	0.0024
	R	12	18875.5974	18875.5962	0.0012
	R	13	18875.4566	18875.4553	0.0013
	R	14	18875.2466	18875.2453	0.0013
	R	15	18874.9658	18874.9663	-0.0006
	R	16	18874.6165	18874.6183	-0.0018
	R	17	18874.2002	18874.2012	-0.001
	R	18	18873.7145	18873.715	-0.0005
	R	19	18873.1596	18873.1598	-0.0002
	R	20	18872.5364	18872.5356	0.0008
	R	21	18871.8422	18871.8423	-0.0001

	R	22	18871.0803	18871.08	0.0004
^{104}RuO	P	5	18865.3577	18865.3593	-0.0015
	P	6	18864.1912	18864.1929	-0.0017
	P	7	18862.9545	18862.9578	-0.0033
	P	8	18861.6539	18861.6539	-0.0001
	P	9	18860.2808	18860.2814	-0.0006
	P	10	18858.8408	18858.8401	0.0007
	P	11	18857.331	18857.3302	0.0008
	P	12	18855.754	18855.7515	0.0025
	P	13	18854.1052	18854.1042	0.001
	P	15	18850.6018	18850.6034	-0.0017
	Q	4	18869.4732	18869.4726	0.0005
	Q	5	18869.1286	18869.1288	-0.0002
	Q	6	18868.7171	18868.7163	0.0007
	Q	7	18868.2372	18868.235	0.0022
	Q	8	18867.6878	18867.685	0.0027
	Q	9	18867.0662	18867.0662	0
	Q	10	18866.3794	18866.3787	0.0007
	Q	11	18865.6224	18865.6224	0
	Q	12	18864.7958	18864.7974	-0.0016
	Q	13	18863.9055	18863.9036	0.0019
	Q	14	18862.9389	18862.941	-0.0021
	Q	15	18861.9096	18861.9097	-0.0001
	R	4	18873.2424	18873.2422	0.0002
	R	5	18873.6525	18873.6523	0.0002
	R	6	18873.9942	18873.9936	0.0006
	R	7	18874.2665	18874.2661	0.0004
	R	8	18874.4696	18874.4698	-0.0003
	R	9	18874.6044	18874.6048	-0.0004
	R	10	18874.669	18874.6709	-0.0019
	R	11	18874.669	18874.6682	0.0008
	R	12	18874.5955	18874.5967	-0.0012
	R	13	18874.4561	18874.4564	-0.0003
	R	14	18874.247	18874.2473	-0.0003
	R	15	18873.9694	18873.9694	0
	R	16	18873.6234	18873.6226	0.0008
	R	17	18873.2064	18873.207	-0.0006
	R	18	18872.7239	18872.7225	0.0014

	R	19	18872.1689	18872.1692	-0.0003
	R	20	18871.5461	18871.5471	-0.001
	R	21	18870.857	18870.8561	0.0008
	R	22	18870.0962	18870.0963	-0.0001
^{100}RuO	P	5	18867.3459	18867.3436	0.0023
	P	6	18866.1714	18866.1709	0.0005
	P	7	18864.928	18864.9292	-0.0012
	P	8	18863.6167	18863.6185	-0.0018
	P	9	18862.2368	18862.2387	-0.002
	P	10	18860.791	18860.7899	0.001
	P	11	18859.2731	18859.2721	0.001
	P	12	18857.6848	18857.6854	-0.0005
	P	13	18856.0315	18856.0296	0.0019
	P	14	18854.3063	18854.3048	0.0015
	P	16	18850.6476	18850.6484	-0.0007
	Q	4	18871.478	18871.4798	-0.0019
	Q	5	18871.1333	18871.1343	-0.001
	Q	6	18870.7193	18870.7197	-0.0004
	Q	7	18870.2361	18870.2359	0.0002
	Q	8	18869.6835	18869.683	0.0004
	Q	9	18869.0619	18869.061	0.0009
	Q	10	18868.3708	18868.3699	0.0008
	Q	11	18867.6101	18867.6097	0.0004
	Q	13	18865.8802	18865.8819	-0.0017
	Q	15	18863.8756	18863.8776	-0.002
	R	5	18875.2701	18875.2705	-0.0004
	R	6	18875.6833	18875.683	0.0002
	R	7	18876.026	18876.0263	-0.0003
	R	8	18876.3014	18876.3004	0.001
	R	9	18876.5065	18876.5054	0.0011
	R	10	18876.6414	18876.6411	0.0003
	R	11	18876.7061	18876.7075	-0.0014
	R	12	18876.7061	18876.7048	0.0014
	R	13	18876.6321	18876.6327	-0.0006
	R	14	18876.4918	18876.4914	0.0003
	R	15	18876.2822	18876.2809	0.0014
	R	16	18876.0013	18876.001	0.0003
	R	17	18875.6511	18875.6518	-0.0007

	R	18	18875.2342	18875.2333	0.0009
	R	19	18874.744	18874.7454	-0.0014
	R	20	18874.187	18874.1882	-0.0011
	R	21	18873.5609	18873.5616	-0.0007
	R	22	18872.8674	18872.8656	0.0018
	R	23	18872.1003	18872.1002	0.0001
^{99}RuO	P	5	18867.8477	18867.8479	-0.0002
	P	6	18866.675	18866.6732	0.0018
	P	7	18865.4297	18865.4293	0.0004
	P	8	18864.1156	18864.1162	-0.0006
	P	9	18862.7311	18862.7339	-0.0028
	P	10	18861.2828	18861.2825	0.0003
	P	11	18859.7646	18859.7619	0.0027
	P	12	18858.1701	18858.1722	-0.0021
	P	13	18856.5125	18856.5134	-0.0009
	P	14	18854.7832	18854.7855	-0.0023
	P	15	18852.9873	18852.9884	-0.0011
	P	16	18851.1213	18851.1223	-0.0011
	Q	4	18871.9899	18871.9909	-0.001
	Q	5	18871.6455	18871.6447	0.0007
	Q	6	18871.2311	18871.2294	0.0017
	Q	7	18870.7443	18870.7448	-0.0005
	Q	9	18869.5678	18869.568	-0.0003
	Q	10	18868.8764	18868.8759	0.0006
	Q	11	18868.1159	18868.1145	0.0013
	Q	12	18867.2864	18867.284	0.0024
	Q	15	18864.3784	18864.3775	0.0009
	Q	16	18863.2714	18863.2705	0.0009
	Q	17	18862.0981	18862.0943	0.0038
	Q	18	18860.8517	18860.8491	0.0026
	Q	19	18859.5357	18859.5347	0.001
	Q	21	18856.6987	18856.699	-0.0003
	Q	22	18855.1765	18855.1776	-0.0011
	Q	23	18853.5868	18853.5872	-0.0004
	Q	24	18851.9266	18851.9279	-0.0013
	Q	25	18850.2005	18850.1996	0.001
	R	4	18875.7898	18875.7877	0.002
	R	5	18876.2013	18876.2009	0.0003

R	6	18876.5418	18876.5449	-0.0031
R	7	18876.8203	18876.8196	0.0007
R	8	18877.0243	18877.0251	-0.0008
R	9	18877.1594	18877.1614	-0.002
R	13	18877.0131	18877.0144	-0.0013
R	14	18876.8058	18876.8046	0.0012
R	16	18876.1762	18876.1776	-0.0014
R	17	18875.7592	18875.7604	-0.0011
R	18	18875.2703	18875.274	-0.0038
R	19	18874.7215	18874.7185	0.0029
R	20	18874.0964	18874.0939	0.0025
R	21	18873.3969	18873.4002	-0.0033
R	22	18872.6384	18872.6375	0.0009

Isotopologue	Branch	F'	F"	J"	Observed (cm^{-1})	Calculated (cm^{-1})	Obs-Cal (cm^{-1})
^{101}RuO	P	6.5	7.5	5	18866.871	18866.8713	-0.0002
	P	5.5	6.5	5	18866.8485	18866.8511	-0.0026
	P	4.5	5.5	5	18866.8327	18866.8335	-0.0007
	P	3.5	4.5	5	18866.8224	18866.8183	0.0042
	P	2.5	3.5	5	18866.8055	18866.8056	0
	P	1.5	2.5	5	18866.7918	18866.7953	-0.0035
	P	7.5	8.5	6	18865.6957	18865.6954	0.0003
	P	5.5	6.5	6	18865.6643	18865.6637	0.0006
	P	8.5	9.5	7	18864.4515	18864.4516	0
	P	7.5	8.5	7	18864.4359	18864.4373	-0.0013
	P	6.5	7.5	7	18864.4252	18864.4244	0.0008
	P	3.5	4.5	7	18864.3944	18864.3944	-0.0001
	P	4.5	5.5	7	18864.4027	18864.403	-0.0003
	P	9.5	10.5	8	18863.1395	18863.1394	0.0001
	P	8.5	9.5	8	18863.1261	18863.127	-0.0008
	P	7.5	8.5	8	18863.1152	18863.1157	-0.0005
	P	8.5	9.5	10	18860.2808	18860.2823	-0.0015
	P	12.5	13.5	11	18858.7907	18858.7915	-0.0008
	P	11.5	12.5	12	18857.1897	18857.189	0.0007
	P	14.5	15.5	13	18855.5486	18855.549	-0.0004
	P	14.5	15.5	13	18855.5488	18855.549	-0.0002
	P	11.5	12.5	14	18853.7986	18853.7994	-0.0008
	P	16.5	17.5	15	18852.0305	18852.0311	-0.0006
	P	12.5	13.5	15	18852.0074	18852.0076	-0.0002
	P	17.5	18.5	16	18850.1694	18850.1687	0.0006
	P	16.5	17.5	16	18850.1639	18850.1627	0.0012
	P	15.5	16.5	16	18850.1568	18850.1571	-0.0003
	P	14.5	15.5	16	18850.1527	18850.1517	0.001
	P	13.5	14.5	16	18850.1467	18850.1467	0
	P	12.5	13.5	16	18850.142	18850.1419	0
	Q	6.5	6.5	4	18871.0091	18871.0121	-0.003
	Q	5.5	5.5	4	18870.9843	18870.9829	0.0014
	Q	4.5	4.5	4	18870.9596	18870.9581	0.0015
	Q	3.5	3.5	4	18870.9403	18870.9378	0.0025
	Q	7.5	7.5	5	18870.6587	18870.6595	-0.0007
	Q	6.5	6.5	5	18870.6379	18870.6369	0.001
	Q	5.5	5.5	5	18870.6165	18870.6174	-0.0009
	Q	3.5	3.5	5	18870.5864	18870.5873	-0.0009
	Q	4.5	4.5	5	18870.6054	18870.6008	0.0046

Q	7.5	7.5	6	18870.2231	18870.2216	0.0015
Q	11.5	11.5	9	18868.5759	18868.5736	0.0023
Q	10.5	10.5	9	18868.5619	18868.562	-0.0001
Q	9.5	9.5	9	18868.5512	18868.5515	-0.0003
Q	8.5	8.5	9	18868.5416	18868.5419	-0.0003
Q	7.5	7.5	9	18868.5329	18868.5334	-0.0005
Q	6.5	6.5	9	18868.5256	18868.5259	-0.0003
Q	7.5	7.5	10	18867.8369	18867.8381	-0.0012
Q	11.5	11.5	10	18867.8704	18867.871	-0.0005
Q	10.5	10.5	10	18867.8614	18867.8615	-0.0001
Q	9.5	9.5	10	18867.852	18867.8529	-0.0008
Q	18.5	18.5	16	18862.2846	18862.2827	0.0019
Q	17.5	17.5	16	18862.2765	18862.2765	-0.0001
Q	24.5	24.5	23	18852.6113	18852.6106	0.0007
R	7.5	6.5	4	18874.7978	18874.8003	-0.0025
R	6.5	5.5	4	18874.7677	18874.7687	-0.0009
R	5.5	4.5	4	18874.7441	18874.742	0.002
R	4.5	3.5	4	18874.7214	18874.7204	0.001
R	3.5	2.5	4	18874.7018	18874.7038	-0.002
R	8.5	7.5	5	18875.2019	18875.204	-0.0021
R	7.5	6.5	5	18875.1795	18875.1799	-0.0004
R	6.5	5.5	5	18875.1576	18875.1591	-0.0016
R	9.5	8.5	6	18875.5411	18875.5411	0
R	8.5	7.5	6	18875.5226	18875.5218	0.0009
R	7.5	6.5	6	18875.5071	18875.5048	0.0023
R	6.5	5.5	6	18875.4899	18875.4901	-0.0003
R	10.5	9.5	7	18875.8161	18875.8107	0.0054
R	9.5	8.5	7	18875.7935	18875.7945	-0.001
R	8.5	7.5	7	18875.7797	18875.7802	-0.0005
R	6.5	5.5	7	18875.756	18875.7567	-0.0007
R	11.5	10.5	8	18876.0135	18876.0122	0.0013
R	10.5	9.5	8	18876.001	18875.9984	0.0026
R	6.5	5.5	8	18875.9566	18875.9568	-0.0002
R	7.5	6.5	8	18875.9672	18875.9652	0.002
R	12.5	11.5	9	18876.1474	18876.1454	0.002
R	11.5	10.5	9	18876.1339	18876.1333	0.0006
R	10.5	9.5	9	18876.1224	18876.1224	0
R	9.5	8.5	9	18876.1126	18876.1125	0.0001
R	8.5	7.5	10	18876.166	18876.1655	0.0005
R	9.5	8.5	10	18876.1706	18876.1727	-0.002

R	10.5	9.5	10	18876.1787	18876.1807	-0.002
R	12.5	11.5	10	18876.1968	18876.1993	-0.0026
R	9.5	8.5	11	18876.166	18876.1655	0.0005
R	10.5	9.5	11	18876.1706	18876.1721	-0.0015
R	15.5	14.5	12	18876.1339	18876.1332	0.0007
R	11.5	10.5	13	18875.9566	18875.9573	-0.0007
R	17.5	16.5	14	18875.7797	18875.7812	-0.0016
R	20.5	19.5	19	18873.6846	18873.6852	-0.0006
R	23.5	22.5	20	18873.0716	18873.0714	0.0002
R	22.5	21.5	20	18873.0662	18873.0665	-0.0003
R	21.5	20.5	20	18873.0618	18873.0618	0
R	19.5	18.5	20	18873.0532	18873.053	0.0002
R	18.5	17.5	20	18873.0488	18873.049	-0.0002

Appendix H

Observed and calculated frequencies (cm^{-1}) for the ν_{13} state of pyrrole.

P Branch

J'	Ka'	Kc'	J"	Ka"	Kc"	Observed (cm^{-1})	Calculated (cm^{-1})	Obs-Cal (cm^{-1})
3	3	1	4	4	1	824.4576	824.4579	-0.0003
3	3	0	4	4	0	824.4628	824.4626	0.0002
3	2	1	4	3	1	824.4708	824.4703	0.0005
3	0	3	4	1	3	824.4721	824.4718	0.0002
3	1	3	4	2	3	824.4721	824.4718	0.0002
3	2	2	4	3	2	824.4671	824.467	0.0001
3	1	2	4	2	2	824.4682	824.4677	0.0005
4	3	1	5	4	1	823.8589	823.8587	0.0002
4	1	3	5	2	3	823.8602	823.8599	0.0003
4	2	3	5	3	3	823.8602	823.8599	0.0003
4	3	2	5	4	2	823.8545	823.8548	-0.0004
4	4	1	5	5	1	823.8454	823.8452	0.0002
4	4	0	5	5	0	823.8501	823.8501	0.0001
4	0	4	5	1	4	823.8664	823.8663	0
4	1	4	5	2	4	823.8664	823.8663	0
5	5	0	6	6	0	823.2357	823.2357	0
5	4	2	6	5	2	823.2406	823.2409	-0.0003
5	3	2	6	4	2	823.2426	823.2428	-0.0002
5	1	4	6	2	4	823.2525	823.2525	-0.0001
5	2	4	6	3	4	823.2525	823.2525	-0.0001
5	0	5	6	1	5	823.261	823.2609	0.0002
5	1	5	6	2	5	823.261	823.2609	0.0002
6	2	4	7	3	4	822.6373	822.637	0.0003
6	3	4	7	4	4	822.6373	822.637	0.0003
6	1	5	7	2	5	822.6453	822.6453	0
6	2	5	7	3	5	822.6453	822.6453	0
6	0	6	7	1	6	822.6543	822.6555	-0.0012
6	1	6	7	2	6	822.6543	822.6555	-0.0012
6	6	1	7	7	1	822.6155	822.6157	-0.0001
6	6	0	7	7	0	822.6201	822.6196	0.0005
6	5	2	7	6	2	822.625	822.6252	-0.0003
6	4	2	7	5	2	822.6279	822.6276	0.0003
6	5	1	7	6	1	822.6287	822.6288	-0.0001
6	3	3	7	4	3	822.63	822.6306	-0.0006
6	4	3	7	5	3	822.63	822.6306	-0.0005
7	3	4	8	4	4	822.0197	822.0196	0.0001
7	4	4	8	5	4	822.0197	822.0196	0.0001
7	2	5	8	3	5	822.0278	822.0279	-0.0001

7	3	5	8	4	5	822.0278	822.0279	-0.0001
7	1	6	8	2	6	822.0375	822.0381	-0.0006
7	2	6	8	3	6	822.0375	822.0381	-0.0006
7	0	7	8	1	7	822.0498	822.0501	-0.0004
7	1	7	8	2	7	822.0498	822.0501	-0.0004
7	7	1	8	8	1	821.9994	821.9989	0.0006
7	7	0	8	8	0	822.0018	822.0019	0
7	6	2	8	7	2	822.0077	822.0078	-0.0001
7	6	1	8	7	1	822.0104	822.0107	-0.0002
7	5	2	8	6	2	822.0104	822.0105	-0.0001
7	4	3	8	5	3	822.0134	822.0133	0
7	5	3	8	6	3	822.0134	822.0132	0.0002
8	5	3	9	6	3	821.3942	821.3942	0
8	6	3	9	7	3	821.3942	821.394	0.0001
8	4	4	9	5	4	821.4004	821.4004	-0.0001
8	5	4	9	6	4	821.4004	821.4004	-0.0001
8	3	5	9	4	5	821.4088	821.4087	0.0001
8	4	5	9	5	5	821.4088	821.4087	0.0001
8	2	6	9	3	6	821.419	821.4189	0.0001
8	3	6	9	4	6	821.419	821.4189	0.0001
8	1	7	9	2	7	821.4311	821.4309	0.0002
8	2	7	9	3	7	821.4311	821.4309	0.0002
8	0	8	9	1	8	821.4448	821.4449	-0.0001
8	1	8	9	2	8	821.4448	821.4449	-0.0001
8	7	2	9	8	2	821.3889	821.3886	0.0004
8	7	1	9	8	1	821.3902	821.3904	-0.0002
8	6	2	9	7	2	821.3919	821.3914	0.0006
8	8	1	9	9	1	821.3801	821.3808	-0.0007
8	8	0	9	9	0	821.3824	821.3827	-0.0003
9	5	4	10	6	4	820.7793	820.7794	-0.0002
9	6	4	10	7	4	820.7793	820.7794	-0.0002
9	4	5	10	5	5	820.7876	820.7877	-0.0001
9	5	5	10	6	5	820.7876	820.7877	-0.0001
9	3	6	10	4	6	820.7981	820.7979	0.0002
9	4	6	10	5	6	820.7981	820.7979	0.0002
9	2	7	10	3	7	820.8099	820.8099	0
9	3	7	10	4	7	820.8099	820.8099	0
9	9	1	10	10	1	820.7618	820.7614	0.0004
9	9	0	10	10	0	820.7623	820.7623	0
9	8	2	10	9	2	820.7674	820.7677	-0.0003
9	8	1	10	9	1	820.7684	820.7681	0.0002

9	7	2	10	8	2	820.7697	820.77	-0.0003
9	7	3	10	8	3	820.7731	820.773	0.0001
9	6	3	10	7	3	820.7731	820.7732	-0.0001
9	1	8	10	2	8	820.8239	820.8239	0.0001
9	2	8	10	3	8	820.8239	820.8239	0.0001
9	0	9	10	1	9	820.8397	820.8397	0
9	1	9	10	2	9	820.8397	820.8397	0
10	6	4	11	7	4	820.1567	820.1566	0.0001
10	7	4	11	8	4	820.1567	820.1566	0.0001
10	5	5	11	6	5	820.165	820.1649	0.0001
10	6	5	11	7	5	820.165	820.1649	0.0001
10	4	6	11	5	6	820.1752	820.1751	0.0001
10	5	6	11	6	6	820.1752	820.1751	0.0001
10	3	7	11	4	7	820.1875	820.1871	0.0003
10	4	7	11	5	7	820.1875	820.1871	0.0003
10	2	8	11	3	8	820.201	820.201	0
10	3	8	11	4	8	820.201	820.201	0
10	2	9	11	3	9	820.2168	820.2168	-0.0001
10	1	9	11	2	9	820.2168	820.2168	-0.0001
10	0	10	11	1	10	820.2342	820.2345	-0.0003
10	1	10	11	2	10	820.2342	820.2345	-0.0003
10	10	0	11	11	0	820.1407	820.1408	-0.0001
10	10	1	11	11	1	820.1407	820.1409	-0.0002
10	9	1	11	10	1	820.1441	820.1439	0.0001
10	9	2	11	10	2	820.1451	820.1452	-0.0001
10	8	2	11	9	2	820.1463	820.1463	0
10	7	3	11	8	3	820.1503	820.1503	0
10	8	3	11	9	3	820.1503	820.1502	0.0002
11	7	4	12	8	4	819.5319	819.532	0
11	8	4	12	9	4	819.5319	819.532	0
11	6	5	12	7	5	819.5403	819.5403	0
11	7	5	12	8	5	819.5403	819.5403	0
11	5	6	12	6	6	819.5505	819.5505	0
11	6	6	12	7	6	819.5505	819.5505	0
11	4	7	12	5	7	819.5626	819.5625	0.0001
11	5	7	12	6	7	819.5626	819.5625	0.0001
11	3	8	12	4	8	819.5766	819.5764	0.0002
11	4	8	12	5	8	819.5766	819.5764	0.0002
11	2	9	12	3	9	819.5923	819.5922	0.0001
11	3	9	12	4	9	819.5923	819.5922	0.0001
11	2	10	12	3	10	819.6097	819.6099	-0.0002

11	1	10	12	2	10	819.6097	819.6099	-0.0002
11	1	11	12	2	11	819.6298	819.6294	0.0004
11	0	11	12	1	11	819.6298	819.6294	0.0004
11	8	3	12	9	3	819.5253	819.5254	-0.0001
11	9	3	12	10	3	819.5253	819.5255	-0.0002
11	11	0	12	12	0	819.5186	819.5183	0.0003
11	10	1	12	11	1	819.5186	819.5179	0.0007
11	11	1	12	12	1	819.5197	819.5191	0.0005
11	9	2	12	10	2	819.5203	819.5203	0
11	10	2	12	11	2	819.5216	819.5211	0.0005
12	7	5	13	8	5	818.9139	818.9139	0
12	8	5	13	9	5	818.9139	818.9139	0
12	6	6	13	7	6	818.9244	818.9241	0.0003
12	7	6	13	8	6	818.9244	818.9241	0.0003
12	5	7	13	6	7	818.9359	818.9362	-0.0002
12	6	7	13	7	7	818.9359	818.9362	-0.0002
12	4	8	13	5	8	818.95	818.9501	-0.0001
12	5	8	13	6	8	818.95	818.9501	-0.0001
12	3	9	13	4	9	818.9658	818.9658	0
12	4	9	13	5	9	818.9658	818.9658	0
12	2	10	13	3	10	818.9837	818.9835	0.0003
12	3	10	13	4	10	818.9837	818.9835	0.0003
12	1	11	13	2	11	819.0025	819.003	-0.0005
12	2	11	13	3	11	819.0025	819.003	-0.0005
12	8	4	13	9	4	818.9056	818.9054	0.0002
12	9	4	13	10	4	818.9056	818.9055	0.0001
12	9	3	13	10	3	818.8986	818.8984	0.0002
12	10	3	13	11	3	818.8986	818.8989	-0.0003
12	11	1	13	12	1	818.8904	818.8902	0.0002
12	10	2	13	11	2	818.8918	818.8919	-0.0001
12	12	0	13	13	0	818.8954	818.8949	0.0005
12	11	2	13	12	2	818.8953	818.8954	-0.0001
13	9	4	14	10	4	818.2771	818.277	0.0001
13	10	4	14	11	4	818.2771	818.2771	0.0001
13	8	5	14	9	5	818.2856	818.2856	0
13	9	5	14	10	5	818.2856	818.2856	0
13	7	6	14	8	6	818.2959	818.2959	0
13	8	6	14	9	6	818.2959	818.2959	0
13	6	7	14	7	7	818.308	818.308	0
13	7	7	14	8	7	818.308	818.308	0
13	5	8	14	6	8	818.3219	818.3219	0

13	6	8	14	7	8	818.3219	818.3219	0
13	4	9	14	5	9	818.3377	818.3376	0.0001
13	5	9	14	6	9	818.3377	818.3376	0.0001
13	4	10	14	5	10	818.3555	818.3552	0.0002
13	3	10	14	4	10	818.3555	818.3552	0.0002
13	2	11	14	3	11	818.3743	818.3747	-0.0005
13	3	11	14	4	11	818.3743	818.3747	-0.0005
13	2	12	14	3	12	818.3959	818.3961	-0.0002
13	1	12	14	2	12	818.3959	818.3961	-0.0002
13	1	13	14	2	13	818.4195	818.4194	0.0001
13	0	13	14	1	13	818.4195	818.4194	0.0001
13	12	1	14	13	1	818.2611	818.261	0.0002
13	11	2	14	12	2	818.2611	818.2612	-0.0001
13	13	0	14	14	0	818.2706	818.2706	0
13	11	3	14	12	3	818.2706	818.2706	0
13	10	3	14	11	3	818.2692	818.2693	-0.0001
13	13	1	14	14	1	818.2724	818.2724	0
13	12	2	14	13	2	818.2678	818.2683	-0.0005
13	10	3	14	11	3	818.2692	818.2693	-0.0001
14	9	5	15	10	5	817.6554	817.6555	-0.0001
14	10	5	15	11	5	817.6554	817.6555	-0.0001
14	8	6	15	9	6	817.666	817.6659	0.0001
14	9	6	15	10	6	817.666	817.6659	0.0001
14	7	7	15	8	7	817.678	817.678	0.0001
14	8	7	15	9	7	817.678	817.678	0.0001
14	6	8	15	7	8	817.6919	817.6919	0
14	7	8	15	8	8	817.6919	817.6919	0
14	5	9	15	6	9	817.7076	817.7077	-0.0001
14	6	9	15	7	9	817.7076	817.7077	-0.0001
14	5	10	15	6	10	817.7253	817.7253	0.0001
14	4	10	15	5	10	817.7253	817.7253	0.0001
14	3	11	15	4	11	817.7448	817.7447	0.0001
14	4	11	15	5	11	817.7448	817.7447	0.0001
14	3	12	15	4	12	817.7663	817.7661	0.0002
14	2	12	15	3	12	817.7663	817.7661	0.0002
14	0	14	15	1	14	817.8152	817.8145	0.0007
14	1	14	15	2	14	817.8152	817.8145	0.0007
14	1	13	15	2	13	817.7894	817.7893	0.0001
14	2	13	15	3	13	817.7894	817.7893	0.0001
14	12	2	15	13	2	817.6285	817.6283	0.0002
14	13	1	15	14	1	817.6302	817.6304	-0.0002

14	11	3	15	12	3	817.638	817.6379	0
14	13	2	15	14	2	817.6394	817.6398	-0.0004
14	12	3	15	13	3	817.6402	817.6405	-0.0002
14	14	1	15	15	1	817.647	817.6474	-0.0004
14	10	4	15	11	4	817.6464	817.6467	-0.0002
14	11	4	15	12	4	817.6464	817.6468	-0.0004
14	14	0	15	15	0	817.6459	817.6455	0.0004
15	9	6	16	10	6	817.0341	817.034	0.0001
15	10	6	16	11	6	817.0341	817.034	0.0001
15	8	7	16	9	7	817.0464	817.0462	0.0002
15	9	7	16	10	7	817.0464	817.0462	0.0002
15	7	8	16	8	8	817.0601	817.0601	0
15	8	8	16	9	8	817.0601	817.0601	0
15	6	9	16	7	9	817.0757	817.0759	-0.0002
15	7	9	16	8	9	817.0757	817.0759	-0.0002
15	5	10	16	6	10	817.0935	817.0935	0
15	6	10	16	7	10	817.0935	817.0935	0
15	4	11	16	5	11	817.1139	817.113	0.0009
15	5	11	16	6	11	817.1139	817.113	0.0009
15	3	12	16	4	12	817.1343	817.1343	0
15	4	12	16	5	12	817.1343	817.1343	0
15	2	13	16	3	13	817.1578	817.1575	0.0003
15	3	13	16	4	13	817.1578	817.1575	0.0003
15	1	14	16	2	14	817.1822	817.1826	-0.0004
15	2	14	16	3	14	817.1822	817.1826	-0.0004
15	0	15	16	1	15	817.209	817.2096	-0.0007
15	1	15	16	2	15	817.209	817.2096	-0.0007
15	10	5	16	11	5	817.0237	817.0235	0.0002
15	11	5	16	12	5	817.0237	817.0235	0.0001
15	13	2	16	14	2	816.9933	816.9932	0.0001
15	14	1	16	15	1	816.9983	816.9987	-0.0004
15	12	3	16	13	3	817.004	817.0042	-0.0002
15	11	4	16	12	4	817.0145	817.0144	0.0002
15	12	4	16	13	4	817.0145	817.0147	-0.0002
15	13	3	16	14	3	817.0084	817.0086	-0.0002
15	14	2	16	15	2	817.0095	817.0099	-0.0004
15	15	0	16	16	0	817.0203	817.0194	0.0008
15	15	1	16	16	1	817.0214	817.0214	0
16	10	6	17	11	6	816.4004	816.4004	0.0001
16	11	6	17	12	6	816.4004	816.4004	0.0001
16	9	7	17	10	7	816.4126	816.4126	0

16	10	7	17	11	7	816.4126	816.4126	0
16	8	8	17	9	8	816.4267	816.4266	0.0001
16	9	8	17	10	8	816.4267	816.4266	0.0001
16	7	9	17	8	9	816.4426	816.4424	0.0003
16	8	9	17	9	9	816.4426	816.4424	0.0003
16	6	10	17	7	10	816.46	816.46	0.0001
16	7	10	17	8	10	816.46	816.46	0.0001
16	6	11	17	7	11	816.4795	816.4794	0.0001
16	5	11	17	6	11	816.4795	816.4794	0.0001
16	5	12	17	6	12	816.5009	816.5007	0.0002
16	4	12	17	5	12	816.5009	816.5007	0.0002
16	3	13	17	4	13	816.5246	816.5239	0.0008
16	4	13	17	5	13	816.5246	816.5239	0.0008
16	2	14	17	3	14	816.5485	816.549	-0.0004
16	3	14	17	4	14	816.5485	816.549	-0.0004
16	1	15	17	2	15	816.5759	816.5759	0
16	2	15	17	3	15	816.5759	816.5759	0
16	15	1	17	16	1	816.3659	816.3659	0
16	13	3	17	14	3	816.3678	816.3679	-0.0001
16	14	3	17	15	3	816.3749	816.375	-0.0001
16	15	2	17	16	2	816.379	816.3787	0.0003
16	12	4	17	13	4	816.38	816.38	0
16	13	4	17	14	4	816.3807	816.3807	0
16	11	5	17	12	5	816.3898	816.3897	0.0001
16	12	5	17	13	5	816.3898	816.3897	0.0001
16	16	1	17	17	1	816.3944	816.3945	-0.0001
16	16	0	17	17	0	816.3923	816.3926	-0.0003
17	12	6	18	13	6	815.765	815.7648	0.0001
17	11	6	18	12	6	815.7649	815.7648	0.0001
17	11	7	18	12	7	815.7771	815.7772	-0.0001
17	10	7	18	11	7	815.7771	815.7772	-0.0001
17	10	8	18	11	8	815.7913	815.7913	0.0001
17	9	8	18	10	8	815.7913	815.7913	0.0001
17	9	9	18	10	9	815.807	815.807	0
17	8	9	18	9	9	815.807	815.807	0
17	8	10	18	9	10	815.8247	815.8246	0.0001
17	7	10	18	8	10	815.8247	815.8246	0.0001
17	7	11	18	8	11	815.8441	815.8441	0
17	6	11	18	7	11	815.8441	815.8441	0
17	5	12	18	6	12	815.8659	815.8654	0.0005
17	6	12	18	7	12	815.8659	815.8654	0.0005

17	4	13	18	5	13	815.8885	815.8885	0
17	5	13	18	6	13	815.8885	815.8885	0
17	3	14	18	4	14	815.9138	815.9135	0.0002
17	4	14	18	5	14	815.9138	815.9135	0.0002
17	13	5	18	14	5	815.754	815.754	0
17	12	5	18	13	5	815.754	815.754	0
17	13	4	18	14	4	815.7439	815.7436	0.0003
17	17	1	18	18	1	815.7665	815.7665	-0.0001
17	17	0	18	18	0	815.7648	815.7648	0
17	3	15	18	4	15	815.9399	815.9405	-0.0005
17	2	15	18	3	15	815.9399	815.9405	-0.0005
17	1	16	18	2	16	815.9694	815.9693	0.0001
17	2	16	18	3	16	815.9694	815.9693	0.0001
17	15	2	18	16	2	815.7172	815.7172	0
17	14	3	18	15	3	815.7291	815.7291	0.0001
17	16	1	18	17	1	815.7324	815.7324	0
17	15	3	18	16	3	815.7397	815.7398	-0.0001
18	10	8	19	11	8	815.1542	815.1541	0.0001
18	11	8	19	12	8	815.1542	815.1541	0.0001
18	9	9	19	10	9	815.1698	815.1699	-0.0002
18	10	9	19	11	9	815.1698	815.1699	-0.0002
18	8	10	19	9	10	815.1874	815.1876	-0.0002
18	9	10	19	10	10	815.1874	815.1876	-0.0002
18	8	11	19	9	11	815.207	815.207	0
18	7	11	19	8	11	815.207	815.207	0
18	7	12	19	8	12	815.2284	815.2282	0.0001
18	6	12	19	7	12	815.2284	815.2282	0.0001
18	5	13	19	6	13	815.2514	815.2514	0.0001
18	6	13	19	7	13	815.2514	815.2514	0.0001
18	16	2	19	17	2	815.0766	815.0766	0
18	15	3	19	16	3	815.0874	815.0876	-0.0002
18	17	1	19	18	1	815.0974	815.0982	-0.0008
18	12	6	19	13	6	815.1276	815.1275	0.0001
18	13	6	19	14	6	815.1276	815.1275	0.0001
18	11	7	19	12	7	815.1401	815.14	0.0001
18	12	7	19	13	7	815.1401	815.14	0.0001
18	18	1	19	19	1	815.1378	815.1377	0.0001
18	18	0	19	19	0	815.1359	815.1361	-0.0002
18	13	5	19	14	5	815.1163	815.1163	0
18	14	5	19	15	5	815.1163	815.1164	-0.0001
18	17	2	19	18	2	815.1125	815.1128	-0.0003

18	2	17	19	3	17	815.3628	815.3628	0
18	1	17	19	2	17	815.3628	815.3628	0
18	2	16	19	3	16	815.3319	815.3321	-0.0002
18	3	16	19	4	16	815.3319	815.3321	-0.0002
18	3	15	19	4	15	815.3031	815.3033	-0.0001
18	4	15	19	5	15	815.3031	815.3033	-0.0001
18	5	14	19	6	14	815.2762	815.2764	-0.0001
18	4	14	19	5	14	815.2762	815.2764	-0.0001
18	16	3	19	17	3	815.1027	815.1029	-0.0002
18	14	4	19	15	4	815.1053	815.1051	0.0002
18	15	4	19	16	4	815.1069	815.107	0
19	12	8	20	13	8	814.5151	814.5152	0
19	11	8	20	12	8	814.5151	814.5152	0
19	11	9	20	12	9	814.5311	814.5311	0
19	10	9	20	11	9	814.5311	814.5311	0
19	10	10	20	11	10	814.5488	814.5487	0.0001
19	9	10	20	10	10	814.5488	814.5487	0.0001
19	9	11	20	10	11	814.568	814.5681	-0.0001
19	8	11	20	9	11	814.568	814.5681	-0.0001
19	8	12	20	9	12	814.5897	814.5894	0.0004
19	7	12	20	8	12	814.5897	814.5894	0.0004
19	7	13	20	8	13	814.6126	814.6125	0.0001
19	6	13	20	7	13	814.6126	814.6125	0.0001
19	6	14	20	7	14	814.6374	814.6374	-0.0001
19	5	14	20	6	14	814.6374	814.6374	-0.0001
19	4	15	20	5	15	814.6642	814.6643	-0.0001
19	5	15	20	6	15	814.6642	814.6643	-0.0001
19	3	16	20	4	16	814.6932	814.693	0.0001
19	4	16	20	5	16	814.6932	814.693	0.0001
19	1	18	20	2	18	814.7568	814.7563	0.0005
19	2	18	20	3	18	814.7568	814.7563	0.0005
19	3	17	20	4	17	814.7243	814.7237	0.0006
19	2	17	20	3	17	814.7243	814.7237	0.0006
19	17	2	20	18	2	814.4345	814.4345	0
19	16	3	20	17	3	814.4431	814.4436	-0.0005
19	13	6	20	14	6	814.488	814.4883	-0.0003
19	14	6	20	15	6	814.488	814.4883	-0.0003
19	12	7	20	13	7	814.5009	814.501	-0.0001
19	13	7	20	14	7	814.5009	814.501	-0.0001
19	14	5	20	15	5	814.4771	814.4768	0.0003
19	15	5	20	16	5	814.4771	814.4769	0.0001

19	18	2	20	19	2	814.4784	814.4782	0.0002
19	16	4	20	17	4	814.4671	814.4673	-0.0002
19	17	3	20	18	3	814.4644	814.4645	-0.0001
19	15	4	20	16	4	814.4644	814.4643	0.0001
19	19	0	20	20	0	814.5071	814.5064	0.0006
19	19	1	20	20	1	814.5071	814.5078	-0.0008
20	11	10	21	12	10	813.9081	813.9081	0
20	10	10	21	11	10	813.9081	813.9081	0
20	10	11	21	11	11	813.9275	813.9275	0
20	9	11	21	10	11	813.9275	813.9275	0
20	9	12	21	10	12	813.9486	813.9487	-0.0001
20	8	12	21	9	12	813.9486	813.9487	-0.0001
20	8	13	21	9	13	813.9719	813.9718	0
20	7	13	21	8	13	813.9719	813.9718	0
20	7	14	21	8	14	813.9965	813.9967	-0.0002
20	6	14	21	7	14	813.9965	813.9967	-0.0002
20	5	16	21	6	16	814.0521	814.0522	-0.0001
20	4	16	21	5	16	814.0521	814.0522	-0.0001
20	4	17	21	5	17	814.083	814.0828	0.0002
20	3	17	21	4	17	814.083	814.0828	0.0002
20	12	9	21	13	9	813.8904	813.8904	0
20	11	9	21	12	9	813.8904	813.8904	0
20	13	8	21	14	8	813.8753	813.8745	0.0008
20	12	8	21	13	8	813.8753	813.8745	0.0008
20	14	7	21	15	7	813.8603	813.8601	0.0001
20	13	7	21	14	7	813.8603	813.8601	0.0001
20	15	6	21	16	6	813.847	813.8472	-0.0002
20	14	6	21	15	6	813.847	813.8472	-0.0002
20	6	15	21	7	15	814.0233	814.0235	-0.0002
20	5	15	21	6	15	814.0233	814.0235	-0.0002
20	2	18	21	3	18	814.1152	814.1154	-0.0002
20	3	18	21	4	18	814.1152	814.1154	-0.0002
20	1	19	21	2	19	814.1497	814.1498	-0.0001
20	2	19	21	3	19	814.1497	814.1498	-0.0001
20	18	2	21	19	2	813.7912	813.7911	0.0001
20	17	3	21	18	3	813.7971	813.7971	0
20	15	5	21	16	5	813.8354	813.8352	0.0002
20	16	5	21	17	5	813.8354	813.8355	-0.0001
20	19	2	21	20	2	813.8424	813.8425	-0.0001
20	20	1	21	21	1	813.8772	813.8771	0.0001
20	20	0	21	21	0	813.8751	813.8759	-0.0007

20	12	8	21	13	8	813.8745	813.8745	0.0001
20	13	8	21	14	8	813.8745	813.8745	0.0001
20	19	1	21	20	1	813.828	813.8279	0.0001
20	16	4	21	17	4	813.8213	813.8211	0.0002
20	18	3	21	19	3	813.825	813.8247	0.0003
20	17	4	21	18	4	813.8262	813.8258	0.0004
21	12	10	22	13	10	813.2658	813.2657	0.0002
21	11	10	22	12	10	813.2658	813.2657	0.0002
21	11	11	22	12	11	813.2852	813.2851	0
21	10	11	22	11	11	813.2852	813.2851	0
21	10	12	22	11	12	813.3065	813.3064	0.0001
21	9	12	22	10	12	813.3065	813.3064	0.0001
21	9	13	22	10	13	813.3292	813.3294	-0.0002
21	8	13	22	9	13	813.3292	813.3294	-0.0002
21	8	14	22	9	14	813.3542	813.3543	-0.0001
21	7	14	22	8	14	813.3542	813.3543	-0.0001
21	6	15	22	7	15	813.3809	813.3811	-0.0001
21	7	15	22	8	15	813.3809	813.3811	-0.0001
21	5	16	22	6	16	813.4098	813.4097	0.0001
21	6	16	22	7	16	813.4098	813.4097	0.0001
21	5	17	22	6	17	813.439	813.4403	-0.0013
21	4	17	22	5	17	813.439	813.4403	-0.0013
21	3	18	22	4	18	813.4727	813.4727	0
21	4	18	22	5	18	813.4727	813.4727	0
21	3	19	22	4	19	813.5064	813.5071	-0.0007
21	2	19	22	3	19	813.5064	813.5071	-0.0007
21	2	20	22	3	20	813.5443	813.5435	0.0008
21	1	20	22	2	20	813.5443	813.5435	0.0008
21	14	7	22	15	7	813.2175	813.2174	0.0001
21	15	7	22	16	7	813.2175	813.2174	0.0001
21	13	8	22	14	8	813.232	813.2319	0.0001
21	14	8	22	15	8	813.232	813.2319	0.0001
21	16	5	22	17	5	813.192	813.1917	0.0003
21	17	5	22	18	5	813.192	813.1922	-0.0002
21	17	4	22	18	4	813.1758	813.1754	0.0003
21	19	2	22	20	2	813.1473	813.1466	0.0007
21	18	3	22	19	3	813.1473	813.1482	-0.0009
21	12	9	22	13	9	813.2482	813.248	0.0002
21	13	9	22	14	9	813.2482	813.248	0.0002
21	21	1	22	22	1	813.245	813.2454	-0.0004
22	11	11	23	12	11	812.6408	812.641	-0.0002

22	12	11	23	13	11	812.6408	812.641	-0.0002
22	10	12	23	11	12	812.6621	812.6622	-0.0001
22	11	12	23	12	12	812.6621	812.6622	-0.0001
22	9	13	23	10	13	812.6854	812.6853	0.0001
22	10	13	23	11	13	812.6854	812.6853	0.0001
22	9	14	23	10	14	812.7099	812.7101	-0.0002
22	8	14	23	9	14	812.7099	812.7101	-0.0002
22	7	15	23	8	15	812.7362	812.7369	-0.0007
22	8	15	23	9	15	812.7362	812.7369	-0.0007
22	7	16	23	8	16	812.7656	812.7654	0.0002
22	6	16	23	7	16	812.7656	812.7654	0.0002
22	6	17	23	7	17	812.7958	812.7959	-0.0001
22	5	17	23	6	17	812.7958	812.7959	-0.0001
22	4	18	23	5	18	812.8282	812.8283	-0.0002
22	5	18	23	6	18	812.8282	812.8283	-0.0002
22	3	19	23	4	19	812.8624	812.8626	-0.0003
22	4	19	23	5	19	812.8624	812.8626	-0.0003
22	2	20	23	3	20	812.8993	812.8989	0.0004
22	3	20	23	4	20	812.8993	812.8989	0.0004
22	15	7	23	16	7	812.5729	812.5729	0
22	16	7	23	17	7	812.5729	812.5729	0
22	14	8	23	15	8	812.5876	812.5876	0
22	15	8	23	16	8	812.5876	812.5876	0
22	13	9	23	14	9	812.6037	812.6037	-0.0001
22	14	9	23	15	9	812.6037	812.6037	-0.0001
22	12	10	23	13	10	812.6215	812.6215	0
22	13	10	23	14	10	812.6215	812.6215	0
22	16	6	23	17	6	812.5595	812.5594	0.0001
22	17	6	23	18	6	812.5595	812.5595	0
22	17	5	23	18	5	812.5464	812.5461	0.0003
22	18	5	23	19	5	812.5464	812.5469	-0.0006
22	19	3	23	20	3	812.4973	812.4971	0.0002
22	18	4	23	19	4	812.5272	812.5272	0
22	20	2	23	21	2	812.5019	812.5013	0.0006
22	21	2	23	22	2	812.5684	812.5683	0.0001
22	20	3	23	21	3	812.5413	812.5409	0.0004
22	19	4	23	20	4	812.5375	812.5373	0.0002
22	19	4	23	20	4	812.5372	812.5373	-0.0001
23	12	11	24	13	11	811.9951	811.9951	-0.0001
23	13	11	24	14	11	811.9951	811.9951	-0.0001
23	11	12	24	12	12	812.0165	812.0164	0.0001

23	12	12	24	13	12	812.0165	812.0164	0.0001
23	11	13	24	12	13	812.0393	812.0394	-0.0001
23	10	13	24	11	13	812.0393	812.0394	-0.0001
23	10	14	24	11	14	812.0644	812.0642	0.0002
23	9	14	24	10	14	812.0644	812.0642	0.0002
23	8	15	24	9	15	812.0909	812.0909	0
23	9	15	24	10	15	812.0909	812.0909	0
23	7	16	24	8	16	812.1193	812.1194	-0.0001
23	8	16	24	9	16	812.1193	812.1194	-0.0001
23	6	17	24	7	17	812.1496	812.1499	-0.0002
23	7	17	24	8	17	812.1496	812.1499	-0.0002
23	6	18	24	7	18	812.1821	812.1822	-0.0001
23	5	18	24	6	18	812.1821	812.1822	-0.0001
23	18	6	24	19	6	811.913	811.9127	0.0003
23	17	6	24	18	6	811.913	811.9127	0.0003
23	16	7	24	17	7	811.9269	811.9266	0.0003
23	17	7	24	18	7	811.9269	811.9266	0.0003
23	15	8	24	16	8	811.9414	811.9415	0
23	16	8	24	17	8	811.9414	811.9415	0
23	14	9	24	15	9	811.9578	811.9577	0.0001
23	15	9	24	16	9	811.9578	811.9577	0.0001
23	21	2	24	22	2	811.8556	811.8553	0.0003
23	20	3	24	21	3	811.8435	811.844	-0.0004
23	19	4	24	20	4	811.8762	811.8762	0.0001
23	20	4	24	21	4	811.8904	811.8905	-0.0001
23	21	3	24	22	3	811.8976	811.8971	0.0004
23	18	5	24	19	5	811.898	811.8984	-0.0004
23	19	5	24	20	5	811.8996	811.8998	-0.0002
23	4	19	24	5	19	812.2166	812.2164	0.0002
23	5	19	24	6	19	812.2166	812.2164	0.0002
23	3	20	24	4	20	812.2522	812.2526	-0.0005
23	4	20	24	5	20	812.2522	812.2526	-0.0005
23	3	21	24	4	21	812.291	812.2908	0.0002
23	2	21	24	3	21	812.291	812.2908	0.0002
23	1	22	24	2	22	812.331	812.3309	0.0001
23	2	22	24	3	22	812.331	812.3309	0.0001
23	1	23	24	2	23	812.3728	812.373	-0.0002
23	0	23	24	1	23	812.3728	812.373	-0.0002
24	19	6	25	20	6	811.264	811.2641	-0.0001
24	18	6	25	19	6	811.264	811.264	0
24	18	7	25	19	7	811.2786	811.2784	0.0002

24	17	7	25	18	7	811.2786	811.2784	0.0002
24	17	8	25	18	8	811.2928	811.2935	-0.0008
24	16	8	25	17	8	811.2928	811.2935	-0.0008
24	16	9	25	17	9	811.3099	811.31	0
24	15	9	25	16	9	811.3099	811.31	0
24	15	10	25	16	10	811.3277	811.3279	-0.0002
24	14	10	25	15	10	811.3277	811.3279	-0.0002
24	13	12	25	14	12	811.3686	811.3687	-0.0001
24	12	12	25	13	12	811.3686	811.3687	-0.0001
24	11	13	25	12	13	811.3918	811.3918	0.0001
24	12	13	25	13	13	811.3918	811.3918	0.0001
24	11	14	25	12	14	811.4165	811.4166	-0.0001
24	10	14	25	11	14	811.4165	811.4166	-0.0001
24	10	15	25	11	15	811.4431	811.4432	-0.0001
24	9	15	25	10	15	811.4431	811.4432	-0.0001
24	9	16	25	10	16	811.4718	811.4717	0.0001
24	8	16	25	9	16	811.4718	811.4717	0.0001
24	7	17	25	8	17	811.502	811.5021	-0.0001
24	8	17	25	9	17	811.502	811.5021	-0.0001
24	6	18	25	7	18	811.5343	811.5343	-0.0001
24	7	18	25	8	18	811.5343	811.5343	-0.0001
24	5	19	25	6	19	811.5681	811.5685	-0.0004
24	6	19	25	7	19	811.5681	811.5685	-0.0004
24	4	20	25	5	20	811.605	811.6046	0.0004
24	5	20	25	6	20	811.605	811.6046	0.0004
24	21	3	25	22	3	811.1892	811.1891	0.0001
24	22	2	25	23	2	811.2088	811.2089	-0.0002
24	13	11	25	14	11	811.347	811.3475	-0.0004
24	14	11	25	15	11	811.347	811.3475	-0.0004
24	24	1	25	25	1	811.3447	811.345	-0.0003
24	24	0	25	25	0	811.3434	811.3444	-0.001
24	22	3	25	23	3	811.252	811.2522	-0.0002
24	20	5	25	21	5	811.2505	811.2506	-0.0002
24	19	5	25	20	5	811.2488	811.2485	0.0003
24	21	4	25	22	4	811.242	811.242	0
24	20	4	25	21	4	811.2226	811.2224	0.0003
25	19	7	26	20	7	810.6283	810.6283	0
25	18	7	26	19	7	810.6283	810.6283	0
25	17	9	26	18	9	810.6606	810.6604	0.0002
25	16	9	26	17	9	810.6606	810.6604	0.0002
25	16	10	26	17	10	810.6785	810.6785	0

25	15	10	26	16	10	810.6785	810.6785	0
25	15	11	26	16	11	810.6982	810.6981	0.0001
25	14	11	26	15	11	810.6982	810.6981	0.0001
25	13	12	26	14	12	810.7195	810.7194	0.0001
25	14	12	26	15	12	810.7195	810.7194	0.0001
25	13	13	26	14	13	810.7424	810.7424	0
25	12	13	26	13	13	810.7424	810.7424	0
25	11	14	26	12	14	810.7674	810.7672	0.0002
25	12	14	26	13	14	810.7674	810.7672	0.0002
25	10	15	26	11	15	810.7938	810.7938	0
25	11	15	26	12	15	810.7938	810.7938	0
25	9	16	26	10	16	810.8223	810.8223	0
25	10	16	26	11	16	810.8223	810.8223	0
25	9	17	26	10	17	810.8524	810.8526	-0.0001
25	8	17	26	9	17	810.8524	810.8526	-0.0001
25	7	18	26	8	18	810.884	810.8848	-0.0007
25	8	18	26	9	18	810.884	810.8848	-0.0007
25	7	19	26	8	19	810.9184	810.9188	-0.0005
25	6	19	26	7	19	810.9184	810.9188	-0.0005
25	6	20	26	7	20	810.9549	810.9549	0
25	5	20	26	6	20	810.9549	810.9549	0
25	4	21	26	5	21	810.9934	810.9928	0.0006
25	5	21	26	6	21	810.9934	810.9928	0.0006
25	18	8	26	19	8	810.6437	810.6438	-0.0001
25	17	8	26	18	8	810.6437	810.6438	-0.0001
25	24	2	26	25	2	810.6501	810.6501	0
25	22	4	26	23	4	810.5915	810.5918	-0.0004
25	20	5	26	21	5	810.5958	810.5964	-0.0006
25	21	5	26	22	5	810.5998	810.5996	0.0002
25	23	3	26	24	3	810.6061	810.6063	-0.0002
25	19	6	26	20	6	810.6132	810.6134	-0.0002
25	20	6	26	21	6	810.6132	810.6136	-0.0004
25	21	4	26	22	4	810.566	810.5656	0.0003
26	12	14	27	13	14	810.116	810.1161	-0.0001
26	13	14	27	14	14	810.116	810.1161	-0.0001
26	12	15	27	13	15	810.1427	810.1427	0
26	11	15	27	12	15	810.1427	810.1427	0
26	10	16	27	11	16	810.1711	810.1711	0
26	11	16	27	12	16	810.1711	810.1711	0
26	9	17	27	10	17	810.2012	810.2013	-0.0001
26	10	17	27	11	17	810.2012	810.2013	-0.0001

26	8	18	27	9	18	810.2336	810.2335	0.0002
26	9	18	27	10	18	810.2336	810.2335	0.0002
26	7	19	27	8	19	810.2672	810.2675	-0.0003
26	8	19	27	9	19	810.2672	810.2675	-0.0003
26	7	20	27	8	20	810.3033	810.3034	-0.0001
26	6	20	27	7	20	810.3033	810.3034	-0.0001
26	17	10	27	18	10	810.0273	810.0272	0
26	16	10	27	17	10	810.0273	810.0272	0
26	16	11	27	17	11	810.0469	810.047	0
26	15	11	27	16	11	810.0469	810.047	0
26	15	12	27	16	12	810.0683	810.0683	0
26	14	12	27	15	12	810.0683	810.0683	0
26	13	13	27	14	13	810.0916	810.0913	0.0003
26	14	13	27	15	13	810.0916	810.0913	0.0003
26	26	0	27	27	0	810.0736	810.0731	0.0004
26	26	1	27	27	1	810.0736	810.0735	0
26	25	2	27	26	2	810.009	810.009	0
26	18	9	27	19	9	810.009	810.0091	0
26	17	9	27	18	9	810.009	810.0091	0
26	25	1	27	26	1	810.0011	810.0008	0.0003
26	19	8	27	20	8	809.9922	809.9922	0
26	18	8	27	19	8	809.9922	809.9922	0
26	20	7	27	21	7	809.9764	809.9764	0
26	19	7	27	20	7	809.9764	809.9764	0
26	24	2	27	25	2	809.9156	809.9154	0.0002
26	24	3	27	25	3	809.9592	809.9593	-0.0001
26	20	6	27	21	6	809.9609	809.9608	0.0001
26	21	6	27	22	6	809.9609	809.9611	-0.0002
26	23	4	27	24	4	809.9404	809.9402	0.0002
26	21	5	27	22	5	809.9423	809.9419	0.0004
26	22	5	27	23	5	809.9465	809.9467	-0.0001
26	22	4	27	23	4	809.906	809.906	0
26	23	3	27	24	3	809.875	809.8749	0.0001
27	20	8	28	21	8	809.3389	809.3388	0
27	19	8	28	20	8	809.3389	809.3388	0
27	19	9	28	20	9	809.3563	809.3559	0.0004
27	18	9	28	19	9	809.3563	809.3559	0.0004
27	17	10	28	18	10	809.3743	809.3743	0
27	17	11	28	18	11	809.3944	809.3941	0.0003
27	16	11	28	17	11	809.3944	809.3941	0.0003
27	16	12	28	17	12	809.4155	809.4155	0

27	15	12	28	16	12	809.4155	809.4155	0
27	13	14	28	14	14	809.4631	809.4633	-0.0002
27	14	14	28	15	14	809.4631	809.4633	-0.0002
27	13	15	28	14	15	809.49	809.4899	0.0002
27	12	15	28	13	15	809.49	809.4899	0.0002
27	12	16	28	13	16	809.5182	809.5182	0
27	11	16	28	12	16	809.5182	809.5182	0
27	10	17	28	11	17	809.5482	809.5484	-0.0002
27	11	17	28	12	17	809.5482	809.5484	-0.0002
27	10	18	28	11	18	809.5812	809.5805	0.0007
27	9	18	28	10	18	809.5812	809.5805	0.0007
27	8	19	28	9	19	809.6144	809.6144	0
27	9	19	28	10	19	809.6144	809.6144	0
27	7	20	28	8	20	809.6514	809.6502	0.0012
27	8	20	28	9	20	809.6514	809.6502	0.0012
27	7	21	28	8	21	809.688	809.688	0
27	6	21	28	7	21	809.688	809.688	0
27	5	22	28	6	22	809.7274	809.7277	-0.0003
27	6	22	28	7	22	809.7274	809.7277	-0.0003
27	23	5	28	24	5	809.2915	809.2918	-0.0003
27	22	5	28	23	5	809.2853	809.285	0.0003
27	24	4	28	25	4	809.287	809.2872	-0.0002
27	21	7	28	22	7	809.3227	809.3226	0.0001
27	20	7	28	21	7	809.3227	809.3226	0.0001
27	25	3	28	26	3	809.3116	809.3114	0.0003
27	21	6	28	22	6	809.3063	809.3062	0.0001
27	22	6	28	23	6	809.3063	809.3067	-0.0004
27	4	23	28	5	23	809.7694	809.7694	0
27	5	23	28	6	23	809.7694	809.7694	0
27	3	24	28	4	24	809.813	809.8131	0
27	4	24	28	5	24	809.813	809.8131	0
27	3	25	28	4	25	809.8587	809.8587	-0.0001
27	2	25	28	3	25	809.8587	809.8587	-0.0001
27	15	13	28	16	13	809.4386	809.4385	0.0001
27	14	13	28	15	13	809.4386	809.4385	0.0001
27	27	1	28	28	1	809.4363	809.4365	-0.0002
27	27	0	28	28	0	809.4363	809.4362	0.0001
27	26	1	28	27	1	809.3599	809.36	-0.0002
27	26	2	28	27	2	809.367	809.3671	-0.0001
27	27	1	28	28	1	809.4362	809.4365	-0.0003
27	27	0	28	28	0	809.4362	809.4362	0

27	25	2	28	26	2	809.2686	809.2686	0
27	23	4	28	24	4	809.2435	809.2436	-0.0001
27	24	3	28	25	3	809.2161	809.2161	0
28	21	8	29	22	8	808.6838	808.6836	0.0002
28	20	8	29	21	8	808.6838	808.6836	0.0002
28	20	9	29	21	9	808.7009	808.701	-0.0001
28	19	9	29	20	9	808.7009	808.701	-0.0001
28	22	7	29	23	7	808.6669	808.667	-0.0001
28	21	7	29	22	7	808.6669	808.6669	0
28	27	1	29	28	1	808.7197	808.7184	0.0013
28	27	2	29	28	2	808.7243	808.7243	0
28	18	11	29	19	11	808.7391	808.7395	-0.0004
28	17	11	29	18	11	808.7391	808.7395	-0.0004
28	17	12	29	18	12	808.7609	808.7609	0
28	16	12	29	17	12	808.7609	808.7609	0
28	15	13	29	16	13	808.7836	808.784	-0.0004
28	16	13	29	17	13	808.7836	808.784	-0.0004
28	28	1	29	29	1	808.7986	808.7985	0.0001
28	28	0	29	29	0	808.7986	808.7983	0.0003
28	15	14	29	16	14	808.8088	808.8088	0
28	14	14	29	15	14	808.8088	808.8088	0
28	14	15	29	15	15	808.8354	808.8353	0
28	13	15	29	14	15	808.8354	808.8353	0
28	12	16	29	13	16	808.8636	808.8637	-0.0001
28	13	16	29	14	16	808.8636	808.8637	-0.0001
28	11	17	29	12	17	808.894	808.8938	0.0002
28	12	17	29	13	17	808.894	808.8938	0.0002
28	10	18	29	11	18	808.9259	808.9258	0.0001
28	11	18	29	12	18	808.9259	808.9258	0.0001
28	10	19	29	11	19	808.9597	808.9596	0.0001
28	9	19	29	10	19	808.9597	808.9596	0.0001
28	8	20	29	9	20	808.9956	808.9954	0.0002
28	9	20	29	10	20	808.9956	808.9954	0.0002
28	0	28	29	1	28	809.3528	809.3522	0.0006
28	1	28	29	2	28	809.3528	809.3522	0.0006
28	1	27	29	2	27	809.3004	809.3005	-0.0001
28	2	27	29	3	27	809.3004	809.3005	-0.0001
28	3	25	29	4	25	809.2031	809.2033	-0.0002
28	4	25	29	5	25	809.2031	809.2033	-0.0002
28	4	24	29	5	24	809.1577	809.1578	0
28	5	24	29	6	24	809.1577	809.1578	0

28	23	6	29	24	6	808.6503	808.6504	-0.0001
28	22	6	29	23	6	808.6503	808.6496	0.0007
28	25	3	29	26	3	808.5564	808.5565	-0.0001
28	24	4	29	25	4	808.5783	808.5784	-0.0001
28	23	5	29	24	5	808.6255	808.6255	0
28	26	2	29	27	2	808.6215	808.6216	-0.0001
28	24	5	29	25	5	808.6354	808.6352	0.0002
28	25	4	29	26	4	808.6332	808.6328	0.0004
28	26	3	29	27	3	808.6624	808.6626	-0.0002
29	3	26	30	4	26	808.5933	808.5936	-0.0003
29	4	26	30	5	26	808.5933	808.5936	-0.0003
29	6	24	30	7	24	808.5007	808.5007	0
29	5	24	30	6	24	808.5007	808.5007	0
29	3	27	30	4	27	808.6434	808.6431	0.0004
29	2	27	30	3	27	808.6434	808.6431	0.0004
29	2	28	30	3	28	808.6947	808.6946	0.0001
29	1	28	30	2	28	808.6947	808.6946	0.0001
29	1	29	30	2	29	808.7482	808.7482	-0.0001
29	0	29	30	1	29	808.7482	808.7482	-0.0001
29	18	12	30	19	12	808.1046	808.1047	-0.0001
29	17	12	30	18	12	808.1046	808.1047	-0.0001
29	17	13	30	18	13	808.128	808.1278	0.0002
29	16	13	30	17	13	808.128	808.1278	0.0002
29	15	14	30	16	14	808.1527	808.1526	0.0001
29	16	14	30	17	14	808.1527	808.1526	0.0001
29	29	1	30	30	1	808.1596	808.1597	-0.0001
29	29	0	30	30	0	808.1596	808.1595	0.0001
29	15	15	30	16	15	808.1793	808.1791	0.0002
29	14	15	30	15	15	808.1793	808.1791	0.0002
29	13	16	30	14	16	808.2075	808.2074	0.0001
29	14	16	30	15	16	808.2075	808.2074	0.0001
29	13	17	30	14	17	808.2375	808.2375	0
29	12	17	30	13	17	808.2375	808.2375	0
29	12	18	30	13	18	808.2698	808.2694	0.0004
29	11	18	30	12	18	808.2698	808.2694	0.0004
29	11	19	30	12	19	808.3029	808.3032	-0.0002
29	10	19	30	11	19	808.3029	808.3032	-0.0002
29	10	20	30	11	20	808.3396	808.3388	0.0008
29	9	20	30	10	20	808.3396	808.3388	0.0008
29	9	21	30	10	21	808.3759	808.3764	-0.0005
29	8	21	30	9	21	808.3759	808.3764	-0.0005

29	8	22	30	9	22	808.4159	808.4159	0
29	7	22	30	8	22	808.4159	808.4159	0
29	7	23	30	8	23	808.4573	808.4573	-0.0001
29	6	23	30	7	23	808.4573	808.4573	-0.0001
29	19	11	30	20	11	808.0832	808.0831	0.0001
29	18	11	30	19	11	808.0832	808.0831	0.0001
29	28	2	30	29	2	808.081	808.0807	0.0003
29	28	1	30	29	1	808.0752	808.0757	-0.0005
29	20	10	30	21	10	808.0635	808.0631	0.0004
29	19	10	30	20	10	808.0635	808.0631	0.0004
29	21	9	30	22	9	808.0442	808.0443	-0.0001
29	20	9	30	21	9	808.0442	808.0443	-0.0001
29	22	8	30	23	8	808.0266	808.0266	0
29	21	8	30	22	8	808.0266	808.0266	0
29	27	3	30	28	3	808.0129	808.013	-0.0001
29	23	7	30	24	7	808.0094	808.0094	0
29	22	7	30	23	7	808.0094	808.0093	0.0001
29	24	6	30	25	6	807.992	807.9921	-0.0001
29	23	6	30	24	6	807.9909	807.9909	0.0001
29	26	4	30	27	4	807.9772	807.9771	0.0001
29	25	5	30	26	5	807.9765	807.9767	-0.0002
29	27	2	30	28	2	807.9746	807.9745	0.0001
29	24	5	30	25	5	807.9633	807.9633	0
30	1	30	31	2	30	808.1445	808.1443	0.0001
30	0	30	31	1	30	808.1445	808.1443	0.0001
30	2	29	31	3	29	808.0885	808.0888	-0.0003
30	1	29	31	2	29	808.0885	808.0888	-0.0003
30	3	28	31	4	28	808.0356	808.0353	0.0003
30	2	28	31	3	28	808.0356	808.0353	0.0003
30	3	27	31	4	27	807.9845	807.9839	0.0006
30	4	27	31	5	27	807.9845	807.9839	0.0006
30	14	17	31	15	17	807.5795	807.5795	0
30	13	17	31	14	17	807.5795	807.5795	0
30	13	18	31	14	18	807.6115	807.6113	0.0001
30	12	18	31	13	18	807.6115	807.6113	0.0001
30	11	19	31	12	19	807.6451	807.645	0.0001
30	12	19	31	13	19	807.6451	807.645	0.0001
30	10	20	31	11	20	807.6804	807.6806	-0.0002
30	11	20	31	12	20	807.6804	807.6806	-0.0002
30	9	21	31	10	21	807.7186	807.7181	0.0005
30	10	21	31	11	21	807.7186	807.7181	0.0005

30	9	22	31	10	22	807.7577	807.7574	0.0002
30	8	22	31	9	22	807.7577	807.7574	0.0002
30	7	23	31	8	23	807.799	807.7988	0.0002
30	8	23	31	9	23	807.799	807.7988	0.0002
30	7	24	31	8	24	807.8418	807.842	-0.0003
30	6	24	31	7	24	807.8418	807.842	-0.0003
30	14	16	31	15	16	807.5494	807.5494	0
30	15	16	31	16	16	807.5494	807.5494	0
30	17	14	31	18	14	807.4948	807.4947	0.0002
30	16	14	31	17	14	807.4948	807.4947	0.0002
30	15	15	31	16	15	807.5207	807.5212	-0.0004
30	16	15	31	17	15	807.5207	807.5212	-0.0004
30	17	13	31	18	13	807.4701	807.4699	0.0002
30	18	13	31	19	13	807.4701	807.4699	0.0002
30	19	12	31	20	12	807.4465	807.4467	-0.0002
30	18	12	31	19	12	807.4465	807.4467	-0.0002
30	21	10	31	22	10	807.4048	807.4048	-0.0001
30	20	10	31	21	10	807.4048	807.4048	-0.0001
30	22	9	31	23	9	807.3859	807.3858	0.0001
30	21	9	31	22	9	807.3859	807.3858	0.0001
30	20	11	31	21	11	807.4252	807.425	0.0002
30	19	11	31	20	11	807.4252	807.425	0.0002
30	23	8	31	24	8	807.3677	807.3677	0
30	22	8	31	23	8	807.3677	807.3677	0
30	24	7	31	25	7	807.35	807.35	0.0001
30	23	7	31	24	7	807.35	807.3498	0.0002
30	25	5	31	26	5	807.2977	807.2982	-0.0005
30	27	4	31	28	4	807.3204	807.3203	0.0001
30	28	2	31	29	2	807.327	807.3271	0
30	25	6	31	26	6	807.3315	807.3319	-0.0003
30	24	6	31	25	6	807.3299	807.33	-0.0001
30	26	5	31	27	5	807.3163	807.3165	-0.0002
30	27	3	31	28	3	807.236	807.2359	0.0001
30	26	4	31	27	4	807.2411	807.2409	0.0002
30	29	2	31	30	2	807.4365	807.4363	0.0001
30	29	1	31	30	1	807.4322	807.4322	0
31	5	27	32	6	27	807.3234	807.3231	0.0003
31	4	27	32	5	27	807.3234	807.3231	0.0003
31	6	26	32	7	26	807.274	807.2739	0
31	5	26	32	6	26	807.274	807.2739	0
31	6	25	32	7	25	807.2267	807.2268	-0.0001

31	7	25	32	8	25	807.2267	807.2268	-0.0001
31	8	24	32	9	24	807.1812	807.1817	-0.0004
31	7	24	32	8	24	807.1812	807.1817	-0.0004
31	15	17	32	16	17	806.9199	806.9198	0.0001
31	14	17	32	15	17	806.9199	806.9198	0.0001
31	13	18	32	14	18	806.9514	806.9516	-0.0002
31	14	18	32	15	18	806.9514	806.9516	-0.0002
31	12	19	32	13	19	806.9856	806.9852	0.0004
31	13	19	32	14	19	806.9856	806.9852	0.0004
31	12	20	32	13	20	807.0206	807.0207	0
31	11	20	32	12	20	807.0206	807.0207	0
31	10	21	32	11	21	807.0583	807.058	0.0002
31	11	21	32	12	21	807.0583	807.058	0.0002
31	9	22	32	10	22	807.0978	807.0973	0.0004
31	10	22	32	11	22	807.0978	807.0973	0.0004
31	9	23	32	10	23	807.1385	807.1385	0
31	8	23	32	9	23	807.1385	807.1385	0
31	15	16	32	16	16	806.8899	806.8898	0.0001
31	16	16	32	17	16	806.8899	806.8898	0.0001
31	20	12	32	21	12	806.7872	806.787	0.0002
31	19	12	32	20	12	806.7872	806.787	0.0002
31	19	13	32	20	13	806.8101	806.8102	-0.0002
31	18	13	32	19	13	806.8101	806.8102	-0.0002
31	18	14	32	19	14	806.8353	806.8351	0.0002
31	17	14	32	18	14	806.8353	806.8351	0.0002
31	16	15	32	17	15	806.8616	806.8616	0
31	17	15	32	18	15	806.8616	806.8616	0
31	23	9	32	24	9	806.7258	806.7256	0.0003
31	22	9	32	23	9	806.7258	806.7256	0.0003
31	22	10	32	23	10	806.745	806.7448	0.0002
31	21	10	32	22	10	806.745	806.7448	0.0002
31	25	7	32	26	7	806.6886	806.6886	0
31	24	7	32	25	7	806.6886	806.6884	0.0002
31	29	3	32	30	3	806.7115	806.7115	0
31	24	8	32	25	8	806.7072	806.7071	0.0002
31	23	8	32	24	8	806.7072	806.707	0.0002
31	27	5	32	28	5	806.6548	806.6547	0.0002
31	28	4	32	29	4	806.6627	806.6624	0.0002
31	25	6	32	26	6	806.667	806.667	0
31	26	6	32	27	6	806.6697	806.6697	0
31	29	2	32	30	2	806.679	806.6793	-0.0003

31	26	5	32	27	5	806.6299	806.6301	-0.0002
31	2	29	32	3	29	807.428	807.4276	0.0004
31	3	29	32	4	29	807.428	807.4276	0.0004
31	1	30	32	2	30	807.4832	807.483	0.0002
31	2	30	32	3	30	807.4832	807.483	0.0002
32	5	28	33	6	28	806.7115	806.7116	-0.0001
32	4	28	33	5	28	806.7115	806.7116	-0.0001
32	6	27	33	7	27	806.6604	806.6606	-0.0002
32	5	27	33	6	27	806.6604	806.6606	-0.0002
32	7	26	33	8	26	806.6112	806.6116	-0.0004
32	6	26	33	7	26	806.6112	806.6116	-0.0004
32	18	15	33	19	15	806.1997	806.2003	-0.0006
32	17	15	33	18	15	806.1997	806.2003	-0.0006
32	17	16	33	18	16	806.2284	806.2285	-0.0001
32	16	16	33	17	16	806.2284	806.2285	-0.0001
32	16	17	33	17	17	806.259	806.2584	0.0005
32	15	17	33	16	17	806.259	806.2584	0.0005
32	14	18	33	15	18	806.2903	806.2902	0.0001
32	15	18	33	16	18	806.2903	806.2902	0.0001
32	13	19	33	14	19	806.3238	806.3237	0
32	14	19	33	15	19	806.3238	806.3237	0
32	11	22	33	12	22	806.4352	806.4355	-0.0004
32	10	22	33	11	22	806.4352	806.4355	-0.0004
32	11	21	33	12	21	806.3963	806.3964	-0.0001
32	12	21	33	13	21	806.3963	806.3964	-0.0001
32	13	20	33	14	20	806.3589	806.3591	-0.0002
32	12	20	33	13	20	806.3589	806.3591	-0.0002

R Branch

J'	Ka'	Kc'	J"	Ka"	Kc"	Observed (cm^{-1})	Calculated (cm^{-1})	Obs-Cal (cm^{-1})
5	5	1	4	4	1	829.909	829.9088	0.0002
6	5	1	5	4	1	830.4655	830.4653	0.0001
7	3	5	6	2	5	831.0992	831.0992	0.0001
7	2	5	6	1	5	831.0992	831.0992	0.0001
7	7	1	6	6	1	831.106	831.106	0
7	4	4	6	3	4	831.0908	831.0905	0.0003
7	3	4	6	2	4	831.0908	831.0905	0.0003
7	7	0	6	6	0	831.0866	831.0862	0.0003
7	5	2	6	4	2	831.0714	831.0719	-0.0005
7	6	1	6	5	1	831.0534	831.0536	-0.0002
8	4	5	7	3	5	831.6889	831.6892	-0.0003
8	3	5	7	2	5	831.6889	831.6892	-0.0003
8	7	2	7	6	2	831.6729	831.6728	0.0001
8	6	3	7	5	3	831.6729	831.6733	-0.0004
8	5	3	7	4	3	831.6729	831.6726	0.0003
8	5	4	7	4	4	831.6804	831.6804	0
8	4	4	7	3	4	831.6804	831.6804	0
8	8	0	7	7	0	831.6817	831.6819	-0.0002
9	9	0	8	8	0	832.2776	832.2773	0.0003
9	5	5	8	4	5	832.2776	832.2773	0.0002
9	4	5	8	3	5	832.2776	832.2773	0.0002
9	4	6	8	3	6	832.288	832.2879	0.0001
9	3	6	8	2	6	832.288	832.2879	0.0001
9	9	1	8	8	1	832.2989	832.2989	0.0001
9	3	7	8	2	7	832.3005	832.3002	0.0002
9	2	7	8	1	7	832.3005	832.3002	0.0002
9	2	8	8	1	8	832.3146	832.3144	0.0002
9	1	8	8	0	8	832.3146	832.3144	0.0002
9	6	4	8	5	4	832.2684	832.2684	0
9	5	4	8	4	4	832.2684	832.2683	0.0001
9	8	1	8	7	1	832.2255	832.2252	0.0003
9	7	2	8	6	2	832.2409	832.2408	0.0001
9	8	2	8	7	2	832.2621	832.2626	-0.0004
9	7	3	8	6	3	832.2609	832.2611	-0.0001
9	6	3	8	5	3	832.2601	832.2597	0.0003
10	5	6	9	4	6	832.874	832.8743	-0.0003
10	4	6	9	3	6	832.874	832.8743	-0.0003

10	4	7	9	3	7	832.8865	832.8867	-0.0002
10	3	7	9	2	7	832.8865	832.8867	-0.0002
10	10	1	9	9	1	832.8942	832.8938	0.0004
10	3	8	9	2	8	832.9001	832.9008	-0.0008
10	2	8	9	1	8	832.9001	832.9008	-0.0008
10	9	1	9	8	1	832.8088	832.8089	-0.0001
10	8	2	9	7	2	832.8206	832.8208	-0.0001
10	9	2	9	8	2	832.8508	832.8509	-0.0002
10	7	4	9	6	4	832.8543	832.8543	-0.0001
10	6	4	9	5	4	832.8543	832.8543	0
10	6	5	9	5	5	832.8637	832.8635	0.0001
10	5	5	9	4	5	832.8637	832.8635	0.0001
10	10	0	9	9	0	832.8714	832.8725	-0.001
10	7	3	9	6	3	832.8445	832.8445	0
10	8	3	9	7	3	832.8467	832.8469	-0.0002
10	1	9	9	0	9	832.917	832.9169	0.0001
10	2	9	9	1	9	832.917	832.9169	0.0001
11	7	5	10	6	5	833.4478	833.4478	0
11	6	5	10	5	5	833.4478	833.4478	0
11	6	6	10	5	6	833.4591	833.4587	0.0004
11	5	6	10	4	6	833.4591	833.4587	0.0004
11	5	7	10	4	7	833.4713	833.4712	0.0001
11	4	7	10	3	7	833.4713	833.4712	0.0001
11	10	1	10	9	1	833.3912	833.3914	-0.0003
11	9	2	10	8	2	833.3982	833.3978	0.0003
11	10	2	10	9	2	833.4382	833.438	0.0002
11	8	4	10	7	4	833.4382	833.4383	-0.0001
11	7	4	10	6	4	833.4382	833.4381	0
11	9	3	10	8	3	833.4307	833.4308	-0.0001
11	8	3	10	7	3	833.4268	833.4268	0
11	4	8	10	3	8	833.4852	833.4854	-0.0002
11	3	8	10	2	8	833.4852	833.4854	-0.0002
11	11	1	10	10	1	833.4877	833.4879	-0.0002
11	1	10	10	0	10	833.5192	833.5194	-0.0002
11	2	10	10	1	10	833.5192	833.5194	-0.0002
12	8	5	11	7	5	834.03	834.0301	-0.0001
12	7	5	11	6	5	834.03	834.0301	-0.0001
12	7	6	11	6	6	834.041	834.0412	-0.0002
12	6	6	11	5	6	834.041	834.0412	-0.0002
12	6	7	11	5	7	834.0542	834.0538	0.0004
12	5	7	11	4	7	834.0542	834.0538	0.0004

12	5	8	11	4	8	834.0679	834.0681	-0.0002
12	4	8	11	3	8	834.0679	834.0681	-0.0002
12	9	4	11	8	4	834.0201	834.0202	-0.0001
12	8	4	11	7	4	834.0201	834.0199	0.0002
12	10	2	11	9	2	833.9729	833.9723	0.0006
12	11	1	11	10	1	833.9729	833.973	-0.0002
12	10	3	11	9	3	834.0126	834.0128	-0.0002
12	9	3	11	8	3	834.0065	834.0064	0.0001
12	11	2	11	10	2	834.0236	834.0237	-0.0002
12	12	1	11	11	1	834.0811	834.081	0.0001
12	4	9	11	3	9	834.0843	834.0842	0.0001
12	3	9	11	2	9	834.0843	834.0842	0.0001
12	2	10	11	1	10	834.102	834.1022	-0.0002
12	3	10	11	2	10	834.102	834.1022	-0.0002
12	2	11	11	1	11	834.1217	834.1219	-0.0003
12	1	11	11	0	11	834.1217	834.1219	-0.0003
13	8	6	12	7	6	834.6221	834.6218	0.0003
13	7	6	12	6	6	834.6221	834.6218	0.0003
13	7	7	12	6	7	834.6345	834.6345	0
13	6	7	12	5	7	834.6345	834.6345	0
13	6	8	12	5	8	834.6489	834.649	0
13	5	8	12	4	8	834.6489	834.649	0
13	13	0	12	12	0	834.656	834.6561	0
13	5	9	12	4	9	834.6651	834.6651	0
13	4	9	12	3	9	834.6651	834.6651	0
13	13	1	12	12	1	834.6728	834.6732	-0.0005
13	3	10	12	2	10	834.6835	834.6831	0.0004
13	4	10	12	3	10	834.6835	834.6831	0.0004
13	9	5	12	8	5	834.6104	834.6104	0
13	8	5	12	7	5	834.6104	834.6104	0
13	12	2	12	11	2	834.6084	834.6083	0.0001
13	11	2	12	10	2	834.5443	834.5444	-0.0001
13	11	3	12	10	3	834.5932	834.593	0.0002
13	9	4	12	8	4	834.5998	834.5996	0.0002
13	10	4	12	9	4	834.5998	834.6001	-0.0003
13	12	1	12	11	1	834.5539	834.554	-0.0001
13	2	11	12	1	11	834.7034	834.7029	0.0005
13	3	11	12	2	11	834.7034	834.7029	0.0005
13	1	12	12	0	12	834.7239	834.7245	-0.0006
13	2	12	12	1	12	834.7239	834.7245	-0.0006
14	9	6	13	8	6	835.2003	835.2004	-0.0001

14	8	6	13	7	6	835.2003	835.2004	-0.0001
14	8	7	13	7	7	835.2135	835.2134	0.0001
14	7	7	13	6	7	835.2135	835.2134	0.0001
14	7	8	13	6	8	835.2279	835.2279	0.0001
14	6	8	13	5	8	835.2279	835.2279	0.0001
14	3	11	13	2	11	835.2819	835.2819	-0.0001
14	4	11	13	3	11	835.2819	835.2819	-0.0001
14	6	9	13	5	9	835.2443	835.2441	0.0002
14	5	9	13	4	9	835.2443	835.2441	0.0002
14	14	0	13	13	0	835.2497	835.2495	0.0003
14	5	10	13	4	10	835.262	835.2621	-0.0001
14	4	10	13	3	10	835.262	835.2621	-0.0001
14	14	1	13	13	1	835.2653	835.2646	0.0006
14	13	1	13	12	1	835.1347	835.1346	0
14	11	3	13	10	3	835.157	835.1569	0.0001
14	10	5	13	9	5	835.1888	835.1887	0.0001
14	9	5	13	8	5	835.1888	835.1887	0.0002
14	13	2	13	12	2	835.1918	835.1918	-0.0001
14	12	3	13	11	3	835.1719	835.1714	0.0005
14	10	4	13	9	4	835.1774	835.1771	0.0003
14	11	4	13	10	4	835.1774	835.1779	-0.0005
14	12	2	13	11	2	835.114	835.1144	-0.0004
14	3	12	13	2	12	835.3035	835.3036	-0.0002
14	2	12	13	1	12	835.3035	835.3036	-0.0002
14	1	13	13	0	13	835.3272	835.3272	0
14	2	13	13	1	13	835.3272	835.3272	0
15	9	7	14	8	7	835.7901	835.7903	-0.0002
15	8	7	14	7	7	835.7901	835.7903	-0.0002
15	8	8	14	7	8	835.8049	835.8049	0
15	7	8	14	6	8	835.8049	835.8049	0
15	7	9	14	6	9	835.8211	835.8212	-0.0001
15	6	9	14	5	9	835.8211	835.8212	-0.0001
15	3	12	14	2	12	835.8809	835.8808	0.0001
15	4	12	14	3	12	835.8809	835.8808	0.0001
15	11	5	14	10	5	835.765	835.765	0.0001
15	10	5	14	9	5	835.765	835.7649	0.0001
15	10	6	14	9	6	835.7764	835.7771	-0.0006
15	9	6	14	8	6	835.7764	835.7771	-0.0006
15	12	3	14	11	3	835.7271	835.7273	-0.0003
15	11	4	14	10	4	835.7523	835.7522	0.0001
15	12	4	14	11	4	835.7533	835.7536	-0.0003

15	13	3	14	12	3	835.7481	835.7481	0
15	14	1	14	13	1	835.715	835.7151	-0.0002
15	13	2	14	12	2	835.6827	835.6826	0.0001
15	6	10	14	5	10	835.8393	835.8393	0
15	5	10	14	4	10	835.8393	835.8393	0
15	15	0	14	14	0	835.8423	835.842	0.0002
15	15	1	14	14	1	835.855	835.8551	-0.0001
15	4	11	14	3	11	835.8592	835.8591	0.0001
15	5	11	14	4	11	835.8592	835.8591	0.0001
15	3	13	14	2	13	835.9045	835.9044	0.0001
15	2	13	14	1	13	835.9045	835.9044	0.0001
15	1	14	14	0	14	835.9294	835.9299	-0.0005
15	2	14	14	1	14	835.9294	835.9299	-0.0005
16	10	7	15	9	7	836.3651	836.3652	-0.0001
16	9	7	15	8	7	836.3651	836.3652	-0.0001
16	9	8	15	8	8	836.38	836.38	0
16	8	8	15	7	8	836.38	836.38	0
16	8	9	15	7	9	836.3963	836.3964	-0.0001
16	7	9	15	6	9	836.3963	836.3964	-0.0001
16	7	10	15	6	10	836.4147	836.4146	0.0002
16	6	10	15	5	10	836.4147	836.4146	0.0002
16	4	13	15	3	13	836.4794	836.4798	-0.0004
16	3	13	15	2	13	836.4794	836.4798	-0.0004
16	16	1	15	15	1	836.4454	836.4448	0.0006
16	4	12	15	3	12	836.456	836.4562	-0.0002
16	5	12	15	4	12	836.456	836.4562	-0.0002
16	6	11	15	5	11	836.434	836.4345	-0.0005
16	5	11	15	4	11	836.434	836.4345	-0.0005
16	11	6	15	10	6	836.3519	836.3517	0.0001
16	10	6	15	9	6	836.3519	836.3517	0.0001
16	15	2	15	14	2	836.356	836.3558	0.0002
16	12	5	15	11	5	836.3393	836.3392	0.0001
16	11	5	15	10	5	836.3393	836.3391	0.0001
16	13	3	15	12	3	836.2947	836.2944	0.0003
16	15	1	15	14	1	836.2962	836.2957	0.0005
16	14	3	15	13	3	836.3233	836.3231	0.0001
16	12	4	15	11	4	836.3251	836.325	0.0001
16	13	4	15	12	4	836.3275	836.3273	0.0002
16	14	2	15	13	2	836.2489	836.2493	-0.0004
17	13	4	16	12	4	836.8962	836.8953	0.0009
17	12	6	16	11	6	836.9244	836.9244	0

17	11	6	16	10	6	836.9244	836.9244	0
17	11	7	16	10	7	836.9378	836.9382	-0.0004
17	10	7	16	9	7	836.9378	836.9382	-0.0004
17	10	8	16	9	8	836.9533	836.9532	0
17	9	8	16	8	8	836.9533	836.9532	0
17	9	9	16	8	9	836.9698	836.9698	0
17	8	9	16	7	9	836.9698	836.9698	0
17	8	10	16	7	10	836.9891	836.988	0.0011
17	7	10	16	6	10	836.9891	836.988	0.0011
17	7	11	16	6	11	837.0077	837.0079	-0.0002
17	6	11	16	5	11	837.0077	837.0079	-0.0002
17	6	12	16	5	12	837.0304	837.0297	0.0007
17	5	12	16	4	12	837.0304	837.0297	0.0007
17	5	13	16	4	13	837.0535	837.0533	0.0003
17	4	13	16	3	13	837.0535	837.0533	0.0003
17	13	5	16	12	5	836.9113	836.9113	-0.0001
17	12	5	16	11	5	836.9113	836.9112	0.0001
17	17	1	16	16	1	837.0334	837.0336	-0.0002
17	17	0	16	16	0	837.0243	837.0243	0
17	15	2	16	14	2	836.8147	836.8148	-0.0001
17	16	1	16	15	1	836.8768	836.8766	0.0002
17	14	3	16	13	3	836.8589	836.8581	0.0008
17	16	2	16	15	2	836.9358	836.9364	-0.0006
17	14	4	16	13	4	836.8988	836.8989	-0.0001
17	15	3	16	14	3	836.8967	836.8966	0
17	13	4	16	12	4	836.8954	836.8953	0.0001
18	13	6	17	12	6	837.4947	837.4951	-0.0004
18	12	6	17	11	6	837.4947	837.4951	-0.0004
18	12	7	17	11	7	837.5093	837.5093	0.0001
18	11	7	17	10	7	837.5093	837.5093	0.0001
18	11	8	17	10	8	837.5247	837.5245	0.0002
18	10	8	17	9	8	837.5247	837.5245	0.0002
18	10	9	17	9	9	837.5414	837.5412	0.0002
18	9	9	17	8	9	837.5414	837.5412	0.0002
18	9	10	17	8	10	837.5596	837.5595	0.0001
18	8	10	17	7	10	837.5596	837.5595	0.0001
18	7	11	17	6	11	837.5795	837.5795	0
18	8	11	17	7	11	837.5795	837.5795	0
18	7	12	17	6	12	837.601	837.6013	-0.0003
18	6	12	17	5	12	837.601	837.6013	-0.0003
18	5	13	17	4	13	837.6241	837.6249	-0.0009

18	6	13	17	5	13	837.6241	837.6249	-0.0009
18	5	14	17	4	14	837.6498	837.6504	-0.0006
18	4	14	17	3	14	837.6498	837.6504	-0.0006
18	3	15	17	2	15	837.6778	837.6777	0.0001
18	4	15	17	3	15	837.6778	837.6777	0.0001
18	2	16	17	1	16	837.7076	837.707	0.0007
18	3	16	17	2	16	837.7076	837.707	0.0007
18	14	5	17	13	5	837.4814	837.4814	0
18	13	5	17	12	5	837.4814	837.4811	0.0003
18	16	2	17	15	2	837.3798	837.3793	0.0004
18	15	3	17	14	3	837.4172	837.4183	-0.0011
18	17	1	17	16	1	837.4581	837.4579	0.0002
18	14	4	17	13	4	837.4628	837.4629	-0.0001
18	16	3	17	15	3	837.4686	837.4687	-0.0001
18	15	4	17	14	4	837.4686	837.4685	0.0001
19	12	8	18	11	8	838.094	838.0938	0.0002
19	11	8	18	10	8	838.094	838.0938	0.0002
19	11	9	18	10	9	838.1107	838.1107	-0.0001
19	10	9	18	9	9	838.1107	838.1107	-0.0001
19	10	10	18	9	10	838.1293	838.1291	0.0002
19	9	10	18	8	10	838.1293	838.1291	0.0002
19	9	11	18	8	11	838.1492	838.1492	0
19	8	11	18	7	11	838.1492	838.1492	0
19	8	12	18	7	12	838.1706	838.171	-0.0004
19	7	12	18	6	12	838.1706	838.171	-0.0004
19	7	13	18	6	13	838.1948	838.1947	0.0001
19	6	13	18	5	13	838.1948	838.1947	0.0001
19	6	14	18	5	14	838.2201	838.2201	-0.0001
19	5	14	18	4	14	838.2201	838.2201	-0.0001
19	4	15	18	3	15	838.2465	838.2475	-0.001
19	13	7	18	12	7	838.0784	838.0783	0
19	12	7	18	11	7	838.0784	838.0783	0
19	14	6	18	13	6	838.0637	838.0637	0
19	13	6	18	12	6	838.0637	838.0637	0
19	15	5	18	14	5	838.0489	838.0493	-0.0004
19	14	5	18	13	5	838.0489	838.0488	0.0001
19	17	2	18	16	2	837.9431	837.9432	-0.0001
19	16	3	18	15	3	837.9756	837.9753	0.0003
19	15	4	18	14	4	838.0278	838.0277	0.0001
19	16	4	18	15	4	838.0359	838.036	-0.0001
19	18	1	18	17	1	838.0393	838.0396	-0.0002

19	17	3	18	16	3	838.0393	838.0395	-0.0001
19	3	16	18	2	16	838.2763	838.2767	-0.0004
19	4	16	18	3	16	838.2763	838.2767	-0.0004
19	2	17	18	1	17	838.3083	838.3079	0.0004
19	3	17	18	2	17	838.3083	838.3079	0.0004
19	2	18	18	1	18	838.3413	838.341	0.0003
19	1	18	18	0	18	838.3413	838.341	0.0003
20	11	10	19	10	10	838.6966	838.6969	-0.0002
20	10	10	19	9	10	838.6966	838.6969	-0.0002
20	10	11	19	9	11	838.7171	838.717	0.0001
20	9	11	19	8	11	838.7171	838.717	0.0001
20	9	12	19	8	12	838.7389	838.7389	0
20	8	12	19	7	12	838.7389	838.7389	0
20	8	13	19	7	13	838.7621	838.7626	-0.0005
20	7	13	19	6	13	838.7621	838.7626	-0.0005
20	7	14	19	6	14	838.7884	838.7881	0.0003
20	6	14	19	5	14	838.7884	838.7881	0.0003
20	5	15	19	4	15	838.815	838.8154	-0.0004
20	6	15	19	5	15	838.815	838.8154	-0.0004
20	4	16	19	3	16	838.8451	838.8446	0.0005
20	5	16	19	4	16	838.8451	838.8446	0.0005
20	4	17	19	3	17	838.8758	838.8758	0
20	3	17	19	2	17	838.8758	838.8758	0
20	13	8	19	12	8	838.6613	838.6612	0
20	12	8	19	11	8	838.6613	838.6612	0
20	15	6	19	14	6	838.6303	838.6303	0
20	14	6	19	13	6	838.6303	838.6302	0
20	12	9	19	11	9	838.678	838.6783	-0.0003
20	11	9	19	10	9	838.678	838.6783	-0.0003
20	14	7	19	13	7	838.6455	838.6454	0.0001
20	13	7	19	12	7	838.6455	838.6454	0.0001
20	18	2	19	17	2	838.5066	838.5067	-0.0001
20	17	3	19	16	3	838.5295	838.5293	0.0003
20	16	5	19	15	5	838.6143	838.6151	-0.0008
20	15	5	19	14	5	838.6143	838.6143	-0.0001
20	19	2	19	18	2	838.6736	838.6735	0.0001
20	19	1	19	18	1	838.6215	838.6214	0.0001
20	18	3	19	17	3	838.6091	838.609	0.0001
20	17	4	19	16	4	838.6016	838.6015	0.0001
20	16	4	19	15	4	838.5894	838.5896	-0.0002
21	12	10	20	11	10	839.2629	839.2627	0.0002

21	11	10	20	10	10	839.2629	839.2627	0.0002
21	11	11	20	10	11	839.2829	839.283	0
21	10	11	20	9	11	839.2829	839.283	0
21	10	12	20	9	12	839.3047	839.3049	-0.0002
21	9	12	20	8	12	839.3047	839.3049	-0.0002
21	8	13	20	7	13	839.3284	839.3286	-0.0002
21	9	13	20	8	13	839.3284	839.3286	-0.0002
21	8	14	20	7	14	839.3544	839.3541	0.0003
21	7	14	20	6	14	839.3544	839.3541	0.0003
21	15	7	20	14	7	839.2104	839.2105	-0.0001
21	14	7	20	13	7	839.2104	839.2105	0
21	14	8	20	13	8	839.2265	839.2267	-0.0002
21	13	8	20	12	8	839.2265	839.2267	-0.0002
21	13	9	20	12	9	839.244	839.244	0
21	12	9	20	11	9	839.244	839.244	0
21	5	16	20	4	16	839.4105	839.4107	-0.0002
21	6	16	20	5	16	839.4105	839.4107	-0.0002
21	17	4	20	16	4	839.1478	839.1482	-0.0004
21	19	3	20	18	3	839.1777	839.1774	0.0004
21	17	5	20	16	5	839.1777	839.1787	-0.001
21	16	5	20	15	5	839.1777	839.1775	0.0002
21	18	4	20	17	4	839.1642	839.1651	-0.001
21	17	4	20	16	4	839.1494	839.1482	0.0012
21	18	4	20	17	4	839.165	839.1651	-0.0002
22	12	11	21	11	11	839.847	839.847	0
22	11	11	21	10	11	839.847	839.847	0
22	10	12	21	9	12	839.8685	839.869	-0.0006
22	11	12	21	10	12	839.8685	839.869	-0.0006
22	9	13	21	8	13	839.8919	839.8928	-0.0009
22	10	13	21	9	13	839.8919	839.8928	-0.0009
22	9	14	21	8	14	839.9188	839.9183	0.0005
22	8	14	21	7	14	839.9188	839.9183	0.0005
22	7	15	21	6	15	839.9457	839.9457	0.0001
22	8	15	21	7	15	839.9457	839.9457	0.0001
22	6	16	21	5	16	839.9748	839.9749	-0.0001
22	7	16	21	6	16	839.9748	839.9749	-0.0001
22	5	17	21	4	17	840.0062	840.006	0.0002
22	6	17	21	5	17	840.0062	840.006	0.0002
22	4	18	21	3	18	840.0391	840.039	0.0001
22	5	18	21	4	18	840.0391	840.039	0.0001
22	14	9	21	13	9	839.8076	839.8077	-0.0001

22	13	9	21	12	9	839.8076	839.8077	-0.0001
22	15	8	21	14	8	839.7903	839.7902	0.0001
22	14	8	21	13	8	839.7903	839.7902	0.0001
22	16	7	21	15	7	839.7737	839.7735	0.0001
22	15	7	21	14	7	839.7737	839.7735	0.0002
22	17	6	21	16	6	839.7573	839.7571	0.0002
22	16	6	21	15	6	839.7573	839.7571	0.0002
22	19	4	21	18	4	839.727	839.7269	0.0001
22	17	5	21	16	5	839.7381	839.7383	-0.0002
22	18	5	21	17	5	839.7401	839.7402	-0.0001
22	20	3	21	19	3	839.7448	839.7447	0.0001
22	21	1	21	20	1	839.7845	839.785	-0.0005
22	18	4	21	17	4	839.7031	839.7035	-0.0003
22	19	3	21	18	3	839.6294	839.6295	-0.0002
22	20	2	21	19	2	839.6337	839.6337	0
22	13	10	21	12	10	839.8266	839.8266	0
22	12	10	21	11	10	839.8266	839.8266	0
22	21	2	21	20	2	839.8279	839.828	-0.0001
22	22	1	21	21	1	839.9643	839.964	0.0003
22	22	0	21	21	0	839.961	839.9608	0.0003
22	3	19	21	2	19	840.0742	840.0739	0.0003
22	4	19	21	3	19	840.0742	840.0739	0.0003
23	21	2	22	20	2	840.1979	840.1978	0.0001
23	19	4	22	18	4	840.2549	840.2551	-0.0002
23	17	7	22	16	7	840.3344	840.3345	-0.0002
23	16	7	22	15	7	840.3344	840.3345	-0.0002
23	16	8	22	15	8	840.3516	840.3516	0
23	15	8	22	14	8	840.3516	840.3516	0
23	15	9	22	14	9	840.3693	840.3695	-0.0002
23	14	9	22	13	9	840.3693	840.3695	-0.0002
23	14	10	22	13	10	840.3887	840.3886	0.0001
23	13	10	22	12	10	840.3887	840.3886	0.0001
23	13	11	22	12	11	840.4092	840.4091	0
23	12	11	22	11	11	840.4092	840.4091	0
23	12	12	22	11	12	840.4312	840.4313	0
23	11	12	22	10	12	840.4312	840.4313	0
23	10	13	22	9	13	840.4552	840.4551	0.0001
23	11	13	22	10	13	840.4552	840.4551	0.0001
23	9	14	22	8	14	840.4805	840.4806	-0.0001
23	10	14	22	9	14	840.4805	840.4806	-0.0001
23	9	15	22	8	15	840.508	840.508	0

23	8	15	22	7	15	840.508	840.508	0
23	22	2	22	21	2	840.4045	840.4042	0.0003
23	7	16	22	6	16	840.5372	840.5372	0
23	8	16	22	7	16	840.5372	840.5372	0
23	23	0	22	22	0	840.5448	840.5447	0.0001
23	23	1	22	22	1	840.5473	840.5472	0
23	5	18	22	4	18	840.6014	840.6013	0.0001
23	6	18	22	5	18	840.6014	840.6013	0.0001
23	7	17	22	6	17	840.5678	840.5683	-0.0005
23	6	17	22	5	17	840.5678	840.5683	-0.0005
23	18	6	22	17	6	840.3174	840.3174	0
23	17	6	22	16	6	840.3174	840.3173	0.0002
23	21	3	22	20	3	840.3111	840.3112	-0.0001
23	20	4	22	19	4	840.2871	840.287	0.0001
23	18	5	22	17	5	840.2966	840.2966	0
23	19	5	22	18	5	840.2993	840.2995	-0.0002
24	18	7	23	17	7	840.8936	840.8935	0.0001
24	17	7	23	16	7	840.8936	840.8935	0.0001
24	17	8	23	16	8	840.9114	840.9112	0.0003
24	16	8	23	15	8	840.9114	840.9112	0.0003
24	16	9	23	15	9	840.9294	840.9294	0
24	15	9	23	14	9	840.9294	840.9294	0
24	14	11	23	13	11	840.9693	840.9694	-0.0001
24	13	11	23	12	11	840.9693	840.9694	-0.0001
24	13	12	23	12	12	840.9918	840.9916	0.0002
24	12	12	23	11	12	840.9918	840.9916	0.0002
24	11	13	23	10	13	841.0155	841.0155	0.0001
24	12	13	23	11	13	841.0155	841.0155	0.0001
24	11	14	23	10	14	841.041	841.0411	-0.0001
24	10	14	23	9	14	841.041	841.0411	-0.0001
24	10	15	23	9	15	841.0686	841.0685	0.0002
24	9	15	23	8	15	841.0686	841.0685	0.0002
24	23	2	23	22	2	840.9796	840.9798	-0.0002
24	15	10	23	14	10	840.9488	840.9487	0.0001
24	14	10	23	13	10	840.9488	840.9487	0.0001
24	23	1	23	22	1	840.9468	840.9466	0.0001
24	19	5	23	18	5	840.8521	840.8524	-0.0003
24	20	5	23	19	5	840.8565	840.8566	-0.0001
24	21	4	23	20	4	840.8451	840.8453	-0.0002
24	19	6	23	18	6	840.8757	840.8755	0.0002
24	18	6	23	17	6	840.8757	840.8753	0.0004

24	22	3	23	21	3	840.8768	840.8768	0
24	8	16	23	7	16	841.0976	841.0977	0
24	9	16	23	8	16	841.0976	841.0977	0
24	24	1	23	23	1	841.13	841.1296	0.0005
24	8	17	23	7	17	841.1283	841.1287	-0.0004
24	7	17	23	6	17	841.1283	841.1287	-0.0004
24	7	18	23	6	18	841.162	841.1617	0.0003
24	6	18	23	5	18	841.162	841.1617	0.0003
24	5	19	23	4	19	841.1964	841.1966	-0.0002
24	6	19	23	5	19	841.1964	841.1966	-0.0002
24	4	20	23	3	20	841.233	841.2334	-0.0004
24	5	20	23	4	20	841.233	841.2334	-0.0004
24	4	21	23	3	21	841.2725	841.2722	0.0003
24	3	21	23	2	21	841.2725	841.2722	0.0003
24	2	22	23	1	22	841.313	841.3129	0.0001
24	3	22	23	2	22	841.313	841.3129	0.0001
24	1	23	23	0	23	841.356	841.3557	0.0003
24	2	23	23	1	23	841.356	841.3557	0.0003
25	22	3	24	21	3	841.2674	841.2674	0
25	23	2	24	22	2	841.3288	841.3286	0.0003
25	21	4	24	20	4	841.347	841.3472	-0.0002
25	20	6	24	19	6	841.4312	841.4315	-0.0004
25	19	6	24	18	6	841.4312	841.4311	0
25	23	3	24	22	3	841.4416	841.4417	-0.0001
25	19	7	24	18	7	841.4506	841.4504	0.0002
25	18	7	24	17	7	841.4506	841.4504	0.0002
25	18	8	24	17	8	841.4686	841.4687	-0.0001
25	17	8	24	16	8	841.4686	841.4687	-0.0001
25	17	9	24	16	9	841.4872	841.4873	-0.0001
25	16	9	24	15	9	841.4872	841.4873	-0.0001
25	16	10	24	15	10	841.5067	841.5069	-0.0001
25	15	10	24	14	10	841.5067	841.5069	-0.0001
25	14	12	24	13	12	841.5502	841.5501	0.0001
25	13	12	24	12	12	841.5502	841.5501	0.0001
25	13	13	24	12	13	841.5741	841.574	0.0001
25	12	13	24	11	13	841.5741	841.574	0.0001
25	11	14	24	10	14	841.5998	841.5997	0.0001
25	12	14	24	11	14	841.5998	841.5997	0.0001
25	11	15	24	10	15	841.6272	841.6271	0.0001
25	10	15	24	9	15	841.6272	841.6271	0.0001
25	10	16	24	9	16	841.6564	841.6563	0.0001

25	9	16	24	8	16	841.6564	841.6563	0.0001
25	24	2	24	23	2	841.5543	841.5546	-0.0003
25	24	1	24	23	1	841.5261	841.5262	-0.0001
25	15	11	24	14	11	841.5275	841.5277	-0.0002
25	14	11	24	13	11	841.5275	841.5277	-0.0002
25	8	17	24	7	17	841.6874	841.6874	0
25	9	17	24	8	17	841.6874	841.6874	0
25	7	18	24	6	18	841.7202	841.7203	-0.0001
25	8	18	24	7	18	841.7202	841.7203	-0.0001
25	6	19	24	5	19	841.7553	841.7551	0.0001
25	7	19	24	6	19	841.7553	841.7551	0.0001
25	25	1	24	24	1	841.7109	841.7109	0
25	25	0	24	24	0	841.7094	841.7093	0
25	5	20	24	4	20	841.792	841.7919	0.0001
25	6	20	24	5	20	841.792	841.7919	0.0001
25	4	21	24	3	21	841.831	841.8306	0.0004
25	5	21	24	4	21	841.831	841.8306	0.0004
25	3	23	24	2	23	841.9146	841.914	0.0005
25	2	23	24	1	23	841.9146	841.914	0.0005
26	23	3	25	22	3	841.8115	841.8116	-0.0002
26	19	8	25	18	8	842.0242	842.0242	0
26	18	8	25	17	8	842.0242	842.0242	0
26	18	9	25	17	9	842.0432	842.0432	-0.0001
26	17	9	25	16	9	842.0432	842.0432	-0.0001
26	17	10	25	16	10	842.0631	842.0631	0
26	16	10	25	15	10	842.0631	842.0631	0
26	16	11	25	15	11	842.0835	842.0842	-0.0007
26	15	11	25	14	11	842.0835	842.0842	-0.0007
26	15	12	25	14	12	842.1063	842.1067	-0.0004
26	14	12	25	13	12	842.1063	842.1067	-0.0004
26	14	13	25	13	13	842.1301	842.1307	-0.0006
26	13	13	25	12	13	842.1301	842.1307	-0.0006
26	12	14	25	11	14	842.1569	842.1564	0.0005
26	13	14	25	12	14	842.1569	842.1564	0.0005
26	11	15	25	10	15	842.1837	842.1839	-0.0002
26	12	15	25	11	15	842.1837	842.1839	-0.0002
26	10	16	25	9	16	842.2131	842.2131	0
26	11	16	25	10	16	842.2131	842.2131	0
26	9	17	25	8	17	842.244	842.2441	-0.0001
26	10	17	25	9	17	842.244	842.2441	-0.0001
26	21	6	25	20	6	841.9851	841.9853	-0.0002

26	20	6	25	19	6	841.9851	841.9847	0.0004
26	24	2	25	23	2	841.8951	841.8955	-0.0004
26	21	5	25	20	5	841.9554	841.9556	-0.0002
26	23	4	25	22	4	841.9578	841.9576	0.0003
26	22	5	25	21	5	841.9645	841.9645	0
26	20	7	25	19	7	842.0053	842.0052	0
26	19	7	25	18	7	842.0053	842.0052	0.0001
26	24	3	25	23	3	842.0059	842.0059	0
26	25	1	25	24	1	842.1043	842.1047	-0.0004
26	25	2	25	24	2	842.1286	842.1287	-0.0002
26	6	20	25	5	20	842.3483	842.3486	-0.0002
26	7	20	25	6	20	842.3483	842.3486	-0.0002
26	26	1	25	25	1	842.2913	842.2913	0.0001
26	26	0	25	25	0	842.2901	842.29	0.0001
26	7	19	25	6	19	842.3119	842.3118	0.0001
26	8	19	25	7	19	842.3119	842.3118	0.0001
26	8	18	25	7	18	842.277	842.277	-0.0001
26	9	18	25	8	18	842.277	842.277	-0.0001
26	5	21	25	4	21	842.3873	842.3872	0.0001
26	6	21	25	5	21	842.3873	842.3872	0.0001
26	4	22	25	3	22	842.4277	842.4279	-0.0002
26	5	22	25	4	22	842.4277	842.4279	-0.0002
27	24	3	26	23	3	842.3559	842.3557	0.0001
27	23	4	26	22	4	842.4241	842.4241	0
27	22	5	26	21	5	842.5028	842.5028	0.0001
27	24	4	26	23	4	842.511	842.5116	-0.0006
27	23	5	26	22	5	842.5154	842.5153	0
27	21	6	26	20	6	842.5359	842.536	-0.0001
27	22	6	26	21	6	842.5369	842.5369	0
27	21	7	26	20	7	842.5579	842.558	0
27	20	7	26	19	7	842.5579	842.5579	0
27	25	3	26	24	3	842.5693	842.5695	-0.0003
27	19	9	26	18	9	842.5969	842.5972	-0.0003
27	18	9	26	17	9	842.5969	842.5972	-0.0003
27	18	10	26	17	10	842.6173	842.6174	-0.0001
27	17	10	26	16	10	842.6173	842.6174	-0.0001
27	17	11	26	16	11	842.6388	842.6387	0.0001
27	16	11	26	15	11	842.6388	842.6387	0.0001
27	20	8	26	19	8	842.5777	842.5777	0
27	19	8	26	18	8	842.5777	842.5777	0
27	14	13	26	13	13	842.6858	842.6855	0.0003

27	15	13	26	14	13	842.6858	842.6855	0.0003
27	13	14	26	12	14	842.7115	842.7113	0.0002
27	14	14	26	13	14	842.7115	842.7113	0.0002
27	16	12	26	15	12	842.6615	842.6614	0.0001
27	15	12	26	14	12	842.6615	842.6614	0.0001
27	13	15	26	12	15	842.7389	842.7388	0.0001
27	12	15	26	11	15	842.7389	842.7388	0.0001
27	11	16	26	10	16	842.7686	842.768	0.0006
27	12	16	26	11	16	842.7686	842.768	0.0006
27	11	17	26	10	17	842.7989	842.799	-0.0001
27	10	17	26	9	17	842.7989	842.799	-0.0001
27	26	1	26	25	1	842.6823	842.682	0.0003
27	26	2	26	25	2	842.7023	842.7021	0.0002
27	9	18	26	8	18	842.8321	842.8319	0.0002
27	10	18	26	9	18	842.8321	842.8319	0.0002
27	8	19	26	7	19	842.8667	842.8667	0
27	9	19	26	8	19	842.8667	842.8667	0
27	7	21	26	6	21	842.9417	842.942	-0.0003
27	6	21	26	5	21	842.9417	842.942	-0.0003
27	6	22	26	5	22	842.9821	842.9825	-0.0004
27	5	22	26	4	22	842.9821	842.9825	-0.0004
28	25	3	27	24	3	842.9001	842.9	0.0001
28	24	4	27	23	4	842.9576	842.9573	0.0003
28	22	7	27	21	7	843.1088	843.1086	0.0002
28	21	7	27	20	7	843.1088	843.1085	0.0003
28	21	8	27	20	8	843.1288	843.1291	-0.0003
28	20	8	27	19	8	843.1288	843.1291	-0.0003
28	20	9	27	19	9	843.1498	843.1492	0.0006
28	19	9	27	18	9	843.1498	843.1492	0.0006
28	19	10	27	18	10	843.1696	843.1698	-0.0002
28	18	10	27	17	10	843.1696	843.1698	-0.0002
28	18	11	27	17	11	843.1915	843.1914	0.0001
28	17	11	27	16	11	843.1915	843.1914	0.0001
28	17	12	27	16	12	843.2143	843.2142	0.0001
28	16	12	27	15	12	843.2143	843.2142	0.0001
28	16	13	27	15	13	843.2384	843.2384	0
28	15	13	27	14	13	843.2384	843.2384	0
28	14	15	27	13	15	843.2918	843.2918	0
28	13	15	27	12	15	843.2918	843.2918	0
28	12	16	27	11	16	843.321	843.3211	0
28	13	16	27	12	16	843.321	843.3211	0

28	15	14	27	14	14	843.2644	843.2643	0.0001
28	14	14	27	13	14	843.2644	843.2643	0.0001
28	27	1	27	26	1	843.2584	843.2581	0.0003
28	27	2	27	26	2	843.2746	843.2748	-0.0001
28	11	17	27	10	17	843.3522	843.3521	0.0001
28	12	17	27	11	17	843.3522	843.3521	0.0001
28	11	18	27	10	18	843.3847	843.385	-0.0002
28	10	18	27	9	18	843.3847	843.385	-0.0002
28	9	19	27	8	19	843.4194	843.4197	-0.0003
28	10	19	27	9	19	843.4194	843.4197	-0.0003
28	6	23	27	5	23	843.5776	843.5779	-0.0003
28	5	23	27	4	23	843.5776	843.5779	-0.0003
28	5	24	27	4	24	843.6221	843.6224	-0.0003
28	4	24	27	3	24	843.6221	843.6224	-0.0003
28	3	25	27	2	25	843.6686	843.6689	-0.0003
28	4	25	27	3	25	843.6686	843.6689	-0.0003
28	7	22	27	6	22	843.5354	843.5354	0
28	6	22	27	5	22	843.5354	843.5354	0
28	8	21	27	7	21	843.4946	843.4949	-0.0003
28	7	21	27	6	21	843.4946	843.4949	-0.0003
28	28	1	27	27	1	843.4489	843.449	-0.0001
28	28	0	27	27	0	843.448	843.4483	-0.0003
28	25	4	27	24	4	843.0645	843.0646	-0.0001
28	24	5	27	23	5	843.0645	843.0641	0.0003
28	23	5	27	22	5	843.0465	843.0467	-0.0003
29	21	9	28	20	9	843.6991	843.6992	-0.0001
29	20	9	28	19	9	843.6991	843.6992	-0.0001
29	20	10	28	19	10	843.7203	843.7202	0.0001
29	19	10	28	18	10	843.7203	843.7202	0.0001
29	19	11	28	18	11	843.7421	843.7421	0
29	18	11	28	17	11	843.7421	843.7421	0
29	18	12	28	17	12	843.7653	843.7651	0.0002
29	17	12	28	16	12	843.7653	843.7651	0.0002
29	17	13	28	16	13	843.7897	843.7895	0.0002
29	16	13	28	15	13	843.7897	843.7895	0.0002
29	16	14	28	15	14	843.8158	843.8154	0.0003
29	15	14	28	14	14	843.8158	843.8154	0.0003
29	15	15	28	14	15	843.843	843.843	0
29	14	15	28	13	15	843.843	843.843	0
29	28	2	28	27	2	843.847	843.8467	0.0004
29	27	3	28	26	3	843.6952	843.6952	0

29	22	8	28	21	8	843.6787	843.6785	0.0002
29	21	8	28	20	8	843.6787	843.6785	0.0002
29	23	7	28	22	7	843.6568	843.6571	-0.0002
29	22	7	28	21	7	843.6568	843.6569	-0.0001
29	24	5	28	23	5	843.5871	843.5872	-0.0002
29	27	2	28	26	2	843.6022	843.602	0.0001
29	25	5	28	24	5	843.6112	843.611	0.0003
29	26	4	28	25	4	843.6164	843.6164	0
29	23	6	28	22	6	843.6316	843.6314	0.0001
29	24	6	28	23	6	843.6334	843.6335	-0.0001
29	25	4	28	24	4	843.4876	843.4875	0.0001
29	26	3	28	25	3	843.4445	843.4448	-0.0003
29	12	17	28	11	17	843.9025	843.9033	-0.0008
29	13	17	28	12	17	843.9025	843.9033	-0.0008
29	12	18	28	11	18	843.9363	843.9362	0.0002
29	11	18	28	10	18	843.9363	843.9362	0.0002
29	11	19	28	10	19	843.9712	843.9709	0.0003
29	10	19	28	9	19	843.9712	843.9709	0.0003
29	9	20	28	8	20	844.0079	844.0075	0.0004
29	10	20	28	9	20	844.0079	844.0075	0.0004
29	7	22	28	6	22	844.0864	844.0864	0
29	8	22	28	7	22	844.0864	844.0864	0
29	13	16	28	12	16	843.8721	843.8723	-0.0002
29	14	16	28	13	16	843.8721	843.8723	-0.0002
29	3	26	28	2	26	844.2684	844.2681	0.0004
29	4	26	28	3	26	844.2684	844.2681	0.0004
29	4	25	28	3	25	844.2195	844.2196	-0.0001
29	5	25	28	4	25	844.2195	844.2196	-0.0001
29	2	27	28	1	27	844.3187	844.3186	0
29	3	27	28	2	27	844.3187	844.3186	0
29	6	24	28	5	24	844.1727	844.1732	-0.0005
29	5	24	28	4	24	844.1727	844.1732	-0.0005
30	13	18	29	12	18	844.4858	844.4856	0.0002
30	12	18	29	11	18	844.4858	844.4856	0.0002
30	11	19	29	10	19	844.5202	844.5202	-0.0001
30	12	19	29	11	19	844.5202	844.5202	-0.0001
30	10	20	29	9	20	844.5565	844.5568	-0.0003
30	11	20	29	10	20	844.5565	844.5568	-0.0003
30	9	21	29	8	21	844.5958	844.5952	0.0006
30	10	21	29	9	21	844.5958	844.5952	0.0006
30	30	1	29	29	1	844.6021	844.6027	-0.0006

30	30	0	29	29	0	844.6021	844.6023	-0.0002
30	13	17	29	12	17	844.4539	844.4527	0.0012
30	14	17	29	13	17	844.4539	844.4527	0.0012
30	20	11	29	19	11	844.291	844.2909	0.0001
30	19	11	29	18	11	844.291	844.2909	0.0001
30	19	12	29	18	12	844.3142	844.3141	0
30	18	12	29	17	12	844.3142	844.3141	0
30	18	13	29	17	13	844.3386	844.3387	0
30	17	13	29	16	13	844.3386	844.3387	0
30	17	14	29	16	14	844.3634	844.3647	-0.0013
30	16	14	29	15	14	844.3634	844.3647	-0.0013
30	15	15	29	14	15	844.3915	844.3923	-0.0008
30	16	15	29	15	15	844.3915	844.3923	-0.0008
30	15	16	29	14	16	844.4213	844.4217	-0.0004
30	14	16	29	13	16	844.4213	844.4217	-0.0004
30	21	10	29	20	10	844.2684	844.2687	-0.0003
30	20	10	29	19	10	844.2684	844.2687	-0.0003
30	28	3	29	27	3	844.257	844.2573	-0.0003
30	22	9	29	21	9	844.2473	844.2473	0.0001
30	21	9	29	20	9	844.2473	844.2473	0.0001
30	24	7	29	23	7	844.2034	844.2034	0
30	23	7	29	22	7	844.2034	844.2032	0.0002
30	23	8	29	22	8	844.2256	844.2259	-0.0003
30	22	8	29	21	8	844.2256	844.2259	-0.0003
30	25	6	29	24	6	844.1783	844.1784	-0.0001
30	24	6	29	23	6	844.176	844.1754	0.0005
31	19	13	30	18	13	844.886	844.886	0
31	18	13	30	17	13	844.886	844.886	0
31	17	14	30	16	14	844.9122	844.9121	0.0001
31	18	14	30	17	14	844.9122	844.9121	0.0001
31	16	15	30	15	15	844.9401	844.9398	0.0003
31	17	15	30	16	15	844.9401	844.9398	0.0003
31	15	16	30	14	16	844.9694	844.9692	0.0002
31	16	16	30	15	16	844.9694	844.9692	0.0002
31	14	17	30	13	17	845.0002	845.0003	-0.0001
31	15	17	30	14	17	845.0002	845.0003	-0.0001
31	13	18	30	12	18	845.0325	845.0331	-0.0006
31	14	18	30	13	18	845.0325	845.0331	-0.0006
31	12	19	30	11	19	845.068	845.0677	0.0003
31	13	19	30	12	19	845.068	845.0677	0.0003
31	24	8	30	23	8	844.7707	844.7712	-0.0005

31	23	8	30	22	8	844.7707	844.7711	-0.0005
31	23	9	30	22	9	844.7939	844.7933	0.0006
31	22	9	30	21	9	844.7939	844.7933	0.0006
31	22	10	30	21	10	844.814	844.8153	-0.0012
31	21	10	30	20	10	844.814	844.8153	-0.0012
31	21	11	30	20	11	844.8377	844.8378	0
31	20	11	30	19	11	844.8377	844.8378	0
31	20	12	30	19	12	844.8616	844.8612	0.0004
31	19	12	30	18	12	844.8616	844.8612	0.0004
31	31	1	30	30	1	845.1781	845.178	0.0001
31	31	0	30	30	0	845.1781	845.1777	0.0004
32	26	7	31	25	7	845.2893	845.2895	-0.0002
32	25	7	31	24	7	845.2893	845.2891	0.0002
32	28	5	31	27	5	845.2412	845.2407	0.0005
32	3	30	31	2	30	846.1224	846.1223	0.0001
32	2	30	31	1	30	846.1224	846.1223	0.0001
32	2	31	31	1	31	846.1798	846.1809	-0.0011
32	1	31	31	0	31	846.1798	846.1809	-0.0011
33	24	10	32	23	10	845.9028	845.9025	0.0003
33	23	10	32	22	10	845.9028	845.9025	0.0003
33	23	11	32	22	11	845.9258	845.9258	0.0001
33	22	11	32	21	11	845.9258	845.9258	0.0001
33	22	12	32	21	12	845.9497	845.9498	-0.0001
33	21	12	32	20	12	845.9497	845.9498	-0.0001
33	21	13	32	20	13	845.9747	845.9749	-0.0003
33	20	13	32	19	13	845.9747	845.9749	-0.0003
33	20	14	32	19	14	846.0014	846.0014	0
33	19	14	32	18	14	846.0014	846.0014	0
33	18	15	32	17	15	846.0291	846.0293	-0.0002
33	19	15	32	18	15	846.0291	846.0293	-0.0002
33	17	16	32	16	16	846.0585	846.0587	-0.0002
33	18	16	32	17	16	846.0585	846.0587	-0.0002
33	16	17	32	15	17	846.0904	846.0898	0.0005
33	17	17	32	16	17	846.0904	846.0898	0.0005
33	15	18	32	14	18	846.1224	846.1227	-0.0003
33	16	18	32	15	18	846.1224	846.1227	-0.0003
33	32	2	32	31	2	846.1258	846.1258	0
33	32	1	32	31	1	846.1196	846.12	-0.0004
33	13	20	32	12	20	846.1936	846.1937	-0.0001
33	14	20	32	13	20	846.1936	846.1937	-0.0001
33	14	19	32	13	19	846.1573	846.1573	0

33	15	19	32	14	19	846.1573	846.1573	0
33	13	21	32	12	21	846.2321	846.232	0.0001
33	12	21	32	11	21	846.2321	846.232	0.0001
34	31	3	33	30	3	846.1869	846.1874	-0.0005

Appendix I

Observed and calculated frequencies (cm^{-1}) for the ν_9 state of pyrrole.

P Branch

J'	Ka'	Kc'	J"	Ka"	Kc"	Observed (cm^{-1})	Calculated (cm^{-1})	Obs-Cal (cm^{-1})
9	4	5	10	4	6	876.8083	876.8087	-0.0004
9	5	5	10	5	6	876.8083	876.8087	-0.0004
10	5	5	11	5	6	876.221	876.2211	-0.0001
10	6	5	11	6	6	876.221	876.2211	-0.0001
10	3	8	11	3	9	877.106	877.1062	-0.0003
10	2	8	11	2	9	877.106	877.1062	-0.0003
11	5	6	12	5	7	875.9312	875.9315	-0.0003
11	6	6	12	6	7	875.9312	875.9315	-0.0003
11	2	9	12	2	10	876.813	876.8132	-0.0002
11	3	9	12	3	10	876.813	876.8132	-0.0002
11	2	10	12	2	11	877.1046	877.1046	0
11	1	10	12	1	11	877.1046	877.1046	0
12	6	6	13	6	7	875.3473	875.3474	0
12	7	6	13	7	7	875.3473	875.3474	0
12	2	10	13	2	11	876.5205	876.5207	-0.0002
12	3	10	13	3	11	876.5205	876.5207	-0.0002
12	2	11	13	2	12	876.8112	876.811	0.0002
12	1	11	13	1	12	876.8112	876.811	0.0002
12	1	12	13	1	13	877.1001	877.1	0.0001
12	0	12	13	0	13	877.1001	877.1	0.0001
13	5	8	14	5	9	875.354	875.354	-0.0001
13	6	8	14	6	9	875.354	875.354	-0.0001
13	7	6	14	7	7	874.7645	874.7649	-0.0004
13	8	6	14	8	7	874.7645	874.7649	-0.0004
13	8	5	14	8	6	874.468	874.4685	-0.0005
13	9	5	14	9	6	874.468	874.4685	-0.0006
13	2	11	14	2	12	876.2288	876.2288	0
13	3	11	14	3	12	876.2288	876.2288	0
13	2	12	14	2	13	876.5177	876.5179	-0.0002
13	1	12	14	1	13	876.5177	876.5179	-0.0002
13	1	13	14	1	14	876.8057	876.8056	0
13	0	13	14	0	14	876.8057	876.8056	0
14	4	11	15	4	12	875.6483	875.6483	0
14	3	11	15	3	12	875.6483	875.6483	0
14	7	7	15	7	8	874.4792	874.4793	-0.0001
14	8	7	15	8	8	874.4792	874.4793	-0.0001
14	9	5	15	9	6	873.8869	873.8876	-0.0008
14	10	5	15	10	6	873.8869	873.8876	-0.0008

14	2	12	15	2	13	875.9376	875.9374	0.0001
14	3	12	15	3	13	875.9376	875.9374	0.0001
14	2	13	15	2	14	876.2255	876.2253	0.0002
14	1	13	15	1	14	876.2255	876.2253	0.0002
14	1	14	15	1	15	876.5122	876.5119	0.0003
14	0	14	15	0	15	876.5122	876.5119	0.0003
15	4	12	16	4	13	875.3581	875.3587	-0.0006
15	3	12	16	3	13	875.3581	875.3587	-0.0006
15	2	14	16	2	15	875.9334	875.9334	0
15	1	14	16	1	15	875.9334	875.9334	0
15	0	15	16	0	16	876.2189	876.2187	0.0002
15	1	15	16	1	16	876.2189	876.2187	0.0002
16	1	15	17	1	16	875.6421	875.642	0.0002
16	2	15	17	2	16	875.6421	875.642	0.0002
16	3	13	17	3	14	875.0696	875.0698	-0.0002
16	4	13	17	4	14	875.0696	875.0698	-0.0002
16	4	12	17	4	13	874.7816	874.7817	-0.0001
16	5	12	17	5	13	874.7816	874.7817	-0.0001
16	5	11	17	5	12	874.4926	874.4923	0.0003
16	6	11	17	6	12	874.4926	874.4923	0.0003
16	7	9	17	7	10	873.9102	873.9099	0.0002
16	8	9	17	8	10	873.9102	873.9099	0.0002
16	9	7	17	9	8	873.3231	873.3228	0.0003
16	10	7	17	10	8	873.3231	873.3228	0.0003
16	11	5	17	11	6	872.7301	872.7308	-0.0007
16	12	5	17	12	6	872.7301	872.7309	-0.0008
16	0	16	17	0	17	875.9259	875.926	-0.0001
16	1	16	17	1	17	875.9259	875.926	-0.0001
17	1	17	18	1	18	875.6343	875.6339	0.0004
17	0	17	18	0	18	875.6343	875.6339	0.0004
17	2	16	18	2	17	875.3513	875.3512	0.0001
17	1	16	18	1	17	875.3513	875.3512	0.0001
17	3	15	18	3	16	875.0667	875.067	-0.0003
17	2	15	18	2	16	875.0667	875.067	-0.0003
17	5	13	18	5	14	874.4942	874.4945	-0.0004
17	4	13	18	4	14	874.4942	874.4945	-0.0004
17	7	11	18	7	12	873.9169	873.9168	0.0001
17	6	11	18	6	12	873.9169	873.9168	0.0001
17	8	9	18	8	10	873.3342	873.3343	-0.0001
17	9	9	18	9	10	873.3342	873.3343	-0.0001
17	10	7	18	10	8	872.7469	872.7471	-0.0001

17	11	7	18	11	8	872.7469	872.7471	-0.0001
17	10	7	18	10	8	872.7469	872.7471	-0.0001
17	11	7	18	11	8	872.7469	872.7471	-0.0001
17	11	6	18	11	7	872.4508	872.4517	-0.0008
17	12	6	18	12	7	872.4508	872.4517	-0.0008
18	1	18	19	1	19	875.3423	875.3423	0
18	0	18	19	0	19	875.3423	875.3423	0
18	2	17	19	2	18	875.0607	875.0609	-0.0002
18	1	17	19	1	18	875.0607	875.0609	-0.0002
18	6	13	19	6	14	873.9206	873.9209	-0.0003
18	5	13	19	5	14	873.9206	873.9209	-0.0003
18	7	12	19	7	13	873.6328	873.6326	0.0003
18	6	12	19	6	13	873.6328	873.6326	0.0003
18	8	10	19	8	11	873.0522	873.0522	-0.0001
18	9	10	19	9	11	873.0522	873.0522	-0.0001
18	10	9	19	10	10	872.7606	872.7603	0.0003
18	9	9	19	9	10	872.7606	872.7603	0.0003
18	10	8	19	10	9	872.4673	872.4672	0.0001
18	11	8	19	11	9	872.4673	872.4672	0.0001
18	11	7	19	11	8	872.1728	872.1729	-0.0002
18	12	7	19	12	8	872.1728	872.1729	-0.0002
18	11	7	19	11	8	872.1726	872.1729	-0.0004
18	12	7	19	12	8	872.1726	872.1729	-0.0004
19	1	19	20	1	20	875.0513	875.0513	0
19	0	19	20	0	20	875.0513	875.0513	0
19	1	18	20	1	19	874.7717	874.7712	0.0005
19	2	18	20	2	19	874.7717	874.7712	0.0005
19	2	17	20	2	18	874.4897	874.4896	0.0001
19	3	17	20	3	18	874.4897	874.4896	0.0001
19	3	16	20	3	17	874.2067	874.2065	0.0002
19	4	16	20	4	17	874.2067	874.2065	0.0002
19	4	15	20	4	16	873.9218	873.922	-0.0002
19	5	15	20	5	16	873.9218	873.922	-0.0002
19	7	12	20	7	13	873.0604	873.0605	-0.0001
19	8	12	20	8	13	873.0604	873.0605	-0.0001
19	10	10	20	10	11	872.4798	872.48	-0.0001
19	9	10	20	9	11	872.4798	872.48	-0.0001
19	11	8	20	11	9	871.895	871.8948	0.0002
19	12	8	20	12	9	871.895	871.8948	0.0002
19	12	7	20	12	8	871.6007	871.6004	0.0002
19	13	7	20	13	8	871.6007	871.6004	0.0002

20	0	20	21	0	21	874.761	874.7608	0.0002
20	1	20	21	1	21	874.761	874.7608	0.0002
20	2	19	21	2	20	874.4822	874.482	0.0002
20	1	19	21	1	20	874.4822	874.482	0.0002
20	3	18	21	3	19	874.2017	874.2017	0
20	2	18	21	2	19	874.2017	874.2017	0
20	5	16	21	5	17	873.6366	873.6367	-0.0001
20	4	16	21	4	17	873.6366	873.6367	-0.0001
20	6	15	21	6	16	873.3522	873.352	0.0002
20	5	15	21	5	16	873.3522	873.352	0.0002
20	9	12	21	9	13	872.4902	872.4901	0.0001
20	8	12	21	8	13	872.4902	872.4901	0.0001
20	10	11	21	10	12	872.2008	872.2003	0.0006
20	9	11	21	9	12	872.2008	872.2003	0.0006
20	11	10	21	11	11	871.9093	871.9093	0
20	10	10	21	10	11	871.9093	871.9093	0
20	12	9	21	12	10	871.6169	871.6172	-0.0003
20	11	9	21	11	10	871.6169	871.6172	-0.0003
20	12	8	21	12	9	871.3245	871.3239	0.0005
20	13	8	21	13	9	871.3245	871.3239	0.0005
21	0	21	22	0	22	874.471	874.4708	0.0002
21	1	21	22	1	22	874.471	874.4708	0.0002
21	2	20	22	2	21	874.1938	874.1934	0.0004
21	1	20	22	1	21	874.1938	874.1934	0.0004
21	2	19	22	2	20	873.9147	873.9145	0.0002
21	3	19	22	3	20	873.9147	873.9145	0.0002
21	3	18	22	3	19	873.634	873.6339	0
21	4	18	22	4	19	873.634	873.6339	0
21	9	13	22	9	14	872.2102	872.2099	0.0002
21	8	13	22	8	14	872.2102	872.2099	0.0002
21	10	12	22	10	13	871.9211	871.9212	-0.0001
21	9	12	22	9	13	871.9211	871.9212	-0.0001
21	13	9	22	13	10	871.0483	871.048	0.0003
21	12	9	22	12	10	871.0483	871.048	0.0003
21	13	8	22	13	9	870.755	870.7547	0.0002
21	14	8	22	14	9	870.755	870.7547	0.0002
22	0	22	23	0	23	874.1813	874.1813	0
22	1	22	23	1	23	874.1813	874.1813	0
22	2	21	23	2	22	873.9055	873.9054	0.0001
22	1	21	23	1	22	873.9055	873.9054	0.0001
22	2	20	23	2	21	873.6277	873.6278	0

22	3	20	23	3	21	873.6277	873.6278	0
22	4	19	23	4	20	873.3489	873.3485	0.0004
22	3	19	23	3	20	873.3489	873.3485	0.0004
22	4	18	23	4	19	873.0681	873.0678	0.0003
22	5	18	23	5	19	873.0681	873.0678	0.0003
22	5	17	23	5	18	872.7851	872.7855	-0.0004
22	6	17	23	6	18	872.7851	872.7855	-0.0004
22	7	16	23	7	17	872.5015	872.5018	-0.0003
22	6	16	23	6	17	872.5015	872.5018	-0.0003
22	7	15	23	7	16	872.2168	872.2168	0
22	8	15	23	8	16	872.2168	872.2168	0
22	10	13	23	10	14	871.643	871.6428	0.0002
22	9	13	23	9	14	871.643	871.6428	0.0002
22	12	11	23	12	12	871.0641	871.0639	0.0002
22	11	11	23	11	12	871.0641	871.0639	0.0002
22	13	10	23	13	11	870.7732	870.7728	0.0004
22	12	10	23	12	11	870.7732	870.7728	0.0004
22	14	8	23	14	9	870.1873	870.1871	0.0001
22	15	8	23	15	9	870.1873	870.1871	0.0001
23	0	23	24	0	24	873.8925	873.8923	0.0002
23	1	23	24	1	24	873.8925	873.8923	0.0002
23	2	22	24	2	23	873.6176	873.6178	-0.0003
23	1	22	24	1	23	873.6176	873.6178	-0.0003
23	2	21	24	2	22	873.3419	873.3416	0.0003
23	3	21	24	3	22	873.3419	873.3416	0.0003
23	3	20	24	3	21	873.0638	873.0637	0.0001
23	4	20	24	4	21	873.0638	873.0637	0.0001
23	4	19	24	4	20	872.7841	872.7842	-0.0001
23	5	19	24	5	20	872.7841	872.7842	-0.0001
23	5	18	24	5	19	872.5031	872.5032	-0.0001
23	6	18	24	6	19	872.5031	872.5032	-0.0001
23	6	17	24	6	18	872.2208	872.2207	0.0001
23	7	17	24	7	18	872.2208	872.2207	0.0001
23	8	15	24	8	16	871.6517	871.6516	0.0001
23	9	15	24	9	16	871.6517	871.6516	0.0001
23	10	14	24	10	15	871.3652	871.3651	0.0002
23	9	14	24	9	15	871.3652	871.3651	0.0002
23	10	13	24	10	14	871.0773	871.0773	0
23	11	13	24	11	14	871.0773	871.0773	0
23	11	12	24	11	13	870.7888	870.7883	0.0005
23	12	12	24	12	13	870.7888	870.7883	0.0005

23	13	11	24	13	12	870.4982	870.4981	0.0001
23	12	11	24	12	12	870.4982	870.4981	0.0001
23	16	7	24	16	8	869.3261	869.3265	-0.0004
23	17	7	24	17	8	869.3261	869.3265	-0.0004
24	0	24	25	0	25	873.6041	873.6039	0.0002
24	1	24	25	1	25	873.6041	873.6039	0.0002
24	1	23	25	1	24	873.3309	873.3308	0
24	2	23	25	2	24	873.3309	873.3308	0
24	2	22	25	2	23	873.0561	873.056	0.0001
24	3	22	25	3	23	873.0561	873.056	0.0001
24	4	21	25	4	22	872.7792	872.7795	-0.0003
24	3	21	25	3	22	872.7792	872.7795	-0.0003
24	8	17	25	8	18	871.6576	871.6575	0
24	7	17	25	7	18	871.6576	871.6575	0
24	9	16	25	9	17	871.3733	871.3734	-0.0002
24	8	16	25	8	17	871.3733	871.3734	-0.0002
24	9	15	25	9	16	871.0875	871.088	-0.0004
24	10	15	25	10	16	871.0875	871.088	-0.0004
24	11	14	25	11	15	870.8014	870.8013	0.0002
24	10	14	25	10	15	870.8014	870.8013	0.0002
24	11	13	25	11	14	870.5134	870.5133	0.0001
24	12	13	25	12	14	870.5134	870.5133	0.0001
24	13	12	25	13	13	870.224	870.2242	-0.0001
24	12	12	25	12	13	870.224	870.2242	-0.0001
24	16	9	25	16	10	869.3502	869.3501	0.0001
24	15	9	25	15	10	869.3502	869.3501	0.0001
25	0	25	26	0	26	873.3159	873.3159	0
25	1	25	26	1	26	873.3159	873.3159	0
25	1	24	26	1	25	873.0441	873.0444	-0.0003
25	2	24	26	2	25	873.0441	873.0444	-0.0003
25	2	23	26	2	24	872.7711	872.771	0.0001
25	3	23	26	3	24	872.7711	872.771	0.0001
25	4	22	26	4	23	872.4958	872.4958	0
25	3	22	26	3	23	872.4958	872.4958	0
25	5	21	26	5	22	872.2189	872.219	0
25	4	21	26	4	22	872.2189	872.219	0
25	6	20	26	6	21	871.9404	871.9405	-0.0001
25	5	20	26	5	21	871.9404	871.9405	-0.0001
25	9	16	26	9	17	870.8114	870.8116	-0.0002
25	10	16	26	10	17	870.8114	870.8116	-0.0002
25	11	14	26	11	15	870.2394	870.239	0.0005

25	12	14	26	12	15	870.2394	870.239	0.0005
26	0	26	27	0	27	873.0283	873.0284	-0.0002
26	1	26	27	1	27	873.0283	873.0284	-0.0002
26	2	25	27	2	26	872.7587	872.7584	0.0003
26	1	25	27	1	26	872.7587	872.7584	0.0003
26	2	24	27	2	25	872.4867	872.4865	0.0002
26	3	24	27	3	25	872.4867	872.4865	0.0002
26	3	23	27	3	24	872.2128	872.2127	0
26	4	23	27	4	24	872.2128	872.2127	0
26	5	22	27	5	23	871.937	871.9372	-0.0002
26	4	22	27	4	23	871.937	871.9372	-0.0002
26	5	21	27	5	22	871.6602	871.66	0.0001
26	6	21	27	6	22	871.6602	871.66	0.0001
26	7	19	27	7	20	871.1007	871.1009	-0.0001
26	8	19	27	8	20	871.1007	871.1009	-0.0001
26	9	18	27	9	19	870.8189	870.819	-0.0002
26	8	18	27	8	19	870.8189	870.819	-0.0002
26	10	17	27	10	18	870.5355	870.5358	-0.0003
26	9	17	27	9	18	870.5355	870.5358	-0.0003
26	11	16	27	11	17	870.2511	870.2512	-0.0001
26	10	16	27	10	17	870.2511	870.2512	-0.0001
26	12	15	27	12	16	869.9655	869.9654	0.0002
26	11	15	27	11	16	869.9655	869.9654	0.0002
26	12	14	27	12	15	869.6784	869.6783	0.0001
26	13	14	27	13	15	869.6784	869.6783	0.0001
26	14	13	27	14	14	869.3902	869.39	0.0002
26	13	13	27	13	14	869.3902	869.39	0.0002
27	1	27	28	1	28	872.7414	872.7414	-0.0001
27	0	27	28	0	28	872.7414	872.7414	-0.0001
27	2	26	28	2	27	872.4731	872.473	0.0001
27	1	26	28	1	27	872.4731	872.473	0.0001
27	3	25	28	3	26	872.2026	872.2026	0
27	2	25	28	2	26	872.2026	872.2026	0
27	3	24	28	3	25	871.9303	871.9302	0.0001
27	4	24	28	4	25	871.9303	871.9302	0.0001
27	4	23	28	4	24	871.6555	871.6561	-0.0006
27	5	23	28	5	24	871.6555	871.6561	-0.0006
27	5	22	28	5	23	871.3802	871.3802	0
27	6	22	28	6	23	871.3802	871.3802	0
27	7	21	28	7	22	871.102	871.1026	-0.0006
27	6	21	28	6	22	871.102	871.1026	-0.0006

27	8	19	28	8	20	870.543	870.5428	0.0002
27	9	19	28	9	20	870.543	870.5428	0.0002
27	10	17	28	10	18	869.9771	869.9772	-0.0002
27	11	17	28	11	18	869.9771	869.9772	-0.0002
28	0	28	29	0	29	872.4547	872.4549	-0.0003
28	1	28	29	1	29	872.4547	872.4549	-0.0003
28	2	26	29	2	27	871.9192	871.9191	0
28	3	26	29	3	27	871.9192	871.9191	0
28	4	25	29	4	26	871.6486	871.6483	0.0003
28	3	25	29	3	26	871.6486	871.6483	0.0003
28	4	24	29	4	25	871.3753	871.3755	-0.0003
28	5	24	29	5	25	871.3753	871.3755	-0.0003
28	5	23	29	5	24	871.1007	871.101	-0.0002
28	6	23	29	6	24	871.1007	871.101	-0.0002
28	8	21	29	8	22	870.5465	870.5468	-0.0003
28	7	21	29	7	22	870.5465	870.5468	-0.0003
28	10	19	29	10	20	869.9859	869.9863	-0.0005
28	9	19	29	9	20	869.9859	869.9863	-0.0005
28	11	17	29	11	18	869.4198	869.4202	-0.0004
28	12	17	29	12	18	869.4198	869.4202	-0.0004
29	1	29	30	1	30	872.1686	872.1689	-0.0003
29	0	29	30	0	30	872.1686	872.1689	-0.0003
29	2	28	30	2	29	871.9038	871.9036	0.0001
29	1	28	30	1	29	871.9038	871.9036	0.0001
29	2	27	30	2	28	871.6365	871.6363	0.0002
29	3	27	30	3	28	871.6365	871.6363	0.0002
29	3	26	30	3	27	871.3667	871.3669	-0.0002
29	4	26	30	4	27	871.3667	871.3669	-0.0002
29	5	25	30	5	26	871.0955	871.0955	0
29	4	25	30	4	26	871.0955	871.0955	0
29	5	24	30	5	25	870.8223	870.8224	-0.0001
29	6	24	30	6	25	870.8223	870.8224	-0.0001
30	1	30	31	1	31	871.8829	871.8833	-0.0003
30	0	30	31	0	31	871.8829	871.8833	-0.0003
30	1	29	31	1	30	871.6197	871.6197	0
30	2	29	31	2	30	871.6197	871.6197	0
30	3	28	31	3	29	871.3542	871.3539	0.0003
30	2	28	31	2	29	871.3542	871.3539	0.0003
30	3	27	31	3	28	871.0861	871.086	0.0001
30	4	27	31	4	28	871.0861	871.086	0.0001
30	4	26	31	4	27	870.816	870.8162	-0.0002

30	5	26	31	5	27	870.816	870.8162	-0.0002
30	5	25	31	5	26	870.5437	870.5443	-0.0006
30	6	25	31	6	26	870.5437	870.5443	-0.0006
31	1	31	32	1	32	871.5976	871.5981	-0.0005
31	0	31	32	0	32	871.5976	871.5981	-0.0005
31	2	30	32	2	31	871.3364	871.3362	0.0002
31	1	30	32	1	31	871.3364	871.3362	0.0002
31	3	29	32	3	30	871.0722	871.0721	0.0002
31	2	29	32	2	30	871.0722	871.0721	0.0002
31	4	28	32	4	29	870.8059	870.8057	0.0001
31	3	28	32	3	29	870.8059	870.8057	0.0001
31	4	27	32	4	28	870.537	870.5373	-0.0003
31	5	27	32	5	28	870.537	870.5373	-0.0003
31	6	26	32	6	27	870.2666	870.267	-0.0004
31	5	26	32	5	27	870.2666	870.267	-0.0004
31	6	25	32	6	26	869.9944	869.9947	-0.0003
31	7	25	32	7	26	869.9944	869.9947	-0.0003
32	1	32	33	1	33	871.313	871.3134	-0.0004
32	0	32	33	0	33	871.313	871.3134	-0.0004
32	1	31	33	1	32	871.0534	871.0532	0.0001
32	2	31	33	2	32	871.0534	871.0532	0.0001
32	2	30	33	2	31	870.791	870.7907	0.0003
32	3	30	33	3	31	870.791	870.7907	0.0003
32	3	29	33	3	30	870.5261	870.526	0.0001
32	4	29	33	4	30	870.5261	870.526	0.0001
32	5	28	33	5	29	870.2593	870.2591	0.0002
32	4	28	33	4	29	870.2593	870.2591	0.0002
32	6	27	33	6	28	869.9902	869.9902	0
32	5	27	33	5	28	869.9902	869.9902	0
33	1	33	34	1	34	871.0287	871.0291	-0.0004
33	0	33	34	0	34	871.0287	871.0291	-0.0004
33	2	32	34	2	33	870.771	870.7707	0.0003
33	1	32	34	1	33	870.771	870.7707	0.0003
33	2	31	34	2	32	870.5104	870.5099	0.0005
33	3	31	34	3	32	870.5104	870.5099	0.0005
33	3	30	34	3	31	870.2472	870.2468	0.0004
33	4	30	34	4	31	870.2472	870.2468	0.0004
33	5	29	34	5	30	869.9816	869.9814	0.0002
33	4	29	34	4	30	869.9816	869.9814	0.0002
34	1	34	35	1	35	870.7446	870.7452	-0.0006
34	0	34	35	0	35	870.7446	870.7452	-0.0006

34	1	33	35	1	34	870.4891	870.4886	0.0005
34	2	33	35	2	34	870.4891	870.4886	0.0005
34	3	32	35	3	33	870.2302	870.2296	0.0006
34	2	32	35	2	33	870.2302	870.2296	0.0006
34	4	31	35	4	32	869.9686	869.9681	0.0005
34	3	31	35	3	32	869.9686	869.9681	0.0005
34	4	30	35	4	31	869.7045	869.7043	0.0001
34	5	30	35	5	31	869.7045	869.7043	0.0001
34	5	29	35	5	30	869.4383	869.4384	-0.0001
34	6	29	35	6	30	869.4383	869.4384	-0.0001
35	0	35	36	0	36	870.461	870.4617	-0.0007
35	1	35	36	1	36	870.461	870.4617	-0.0007
35	1	34	36	1	35	870.2076	870.207	0.0005
35	2	34	36	2	35	870.2076	870.207	0.0005
35	4	31	36	4	32	869.4281	869.4278	0.0003
35	5	31	36	5	32	869.4281	869.4278	0.0003
36	1	36	37	1	37	870.178	870.1786	-0.0006
36	0	36	37	0	37	870.178	870.1786	-0.0006
37	1	37	38	1	38	869.8956	869.8959	-0.0003
37	0	37	38	0	38	869.8956	869.8959	-0.0003
38	1	38	39	1	39	869.6135	869.6136	-0.0001
38	0	38	39	0	39	869.6135	869.6136	-0.0001
39	0	39	40	0	40	869.3317	869.3316	0.0001
39	1	39	40	1	40	869.3317	869.3316	0.0001

R Branch

J'	Ka'	Kc'	J"	Ka"	Kc"	Observed (cm^{-1})	Calculated (cm^{-1})	Obs-Cal (cm^{-1})
11	5	6	10	5	5	886.2119	886.2121	-0.0001
11	6	6	10	6	5	886.2119	886.2121	-0.0001
12	6	6	11	6	5	886.837	886.8374	-0.0004
12	7	6	11	7	5	886.837	886.8374	-0.0004
13	7	7	12	7	6	887.1545	887.1546	-0.0001
13	6	7	12	6	6	887.1545	887.1546	-0.0001
13	8	6	12	8	5	887.4645	887.4645	-0.0001
13	7	6	12	7	5	887.4645	887.4645	-0.0001
13	10	3	12	10	2	888.4365	888.4359	0.0006
13	11	2	12	11	1	888.7574	888.7577	-0.0002
13	5	8	12	5	7	886.8434	886.8436	-0.0003
13	6	8	12	6	7	886.8434	886.8436	-0.0003
14	6	8	13	6	7	887.4721	887.4723	-0.0002
14	7	8	13	7	7	887.4721	887.4723	-0.0002
14	8	7	13	8	6	887.7836	887.7833	0.0004
14	7	7	13	7	6	887.7836	887.7833	0.0004
14	9	6	13	9	5	888.0931	888.0933	-0.0002
14	8	6	13	8	5	888.0931	888.0933	-0.0002
14	2	12	13	2	11	886.2177	886.2173	0.0004
14	3	12	13	3	11	886.2177	886.2173	0.0004
14	1	14	13	1	13	885.5823	885.5822	0.0001
14	0	14	13	0	13	885.5823	885.5822	0.0001
15	6	10	14	6	9	887.4776	887.4777	-0.0001
15	5	10	14	5	9	887.4776	887.4777	-0.0001
15	6	9	14	6	8	887.791	887.7907	0.0002
15	7	9	14	7	8	887.791	887.7907	0.0002
15	7	8	14	7	7	888.1033	888.1027	0.0006
15	8	8	14	8	7	888.1033	888.1027	0.0006
15	9	7	14	9	6	888.4136	888.4136	-0.0001
15	8	7	14	8	6	888.4136	888.4136	-0.0001
15	10	6	14	10	5	888.7239	888.7239	0
15	9	6	14	9	5	888.7239	888.7239	0
15	1	14	14	1	13	886.2131	886.2131	0
15	2	14	14	2	13	886.2131	886.2131	0
16	2	15	15	2	14	886.5266	886.5263	0.0003
16	1	15	15	1	14	886.5266	886.5263	0.0003
16	4	13	15	4	12	887.1635	887.1636	-0.0001
16	3	13	15	3	12	887.1635	887.1636	-0.0001

16	7	9	15	7	8	888.4221	888.4227	-0.0007
16	8	9	15	8	8	888.4221	888.4227	-0.0007
16	10	7	15	10	6	889.0455	889.0457	-0.0001
16	9	7	15	9	6	889.0455	889.0457	-0.0001
16	0	16	15	0	15	886.2055	886.2056	-0.0001
16	1	16	15	1	15	886.2055	886.2056	-0.0001
17	0	17	16	0	16	886.5182	886.5181	0.0001
17	1	17	16	1	16	886.5182	886.5181	0.0001
17	2	15	16	2	14	887.1606	887.1607	-0.0001
17	3	15	16	3	14	887.1606	887.1607	-0.0001
17	8	9	16	8	8	889.0566	889.0564	0.0003
17	9	9	16	9	8	889.0566	889.0564	0.0003
17	8	10	16	8	9	888.7435	888.7434	0.0001
17	7	10	16	7	9	888.7435	888.7434	0.0001
17	2	16	16	2	15	886.8401	886.8401	0
17	1	16	16	1	15	886.8401	886.8401	0
18	2	17	17	2	16	887.1545	887.1545	0
18	1	17	17	1	16	887.1545	887.1545	0
18	3	16	17	3	15	887.4766	887.4763	0.0003
18	2	16	17	2	15	887.4766	887.4763	0.0003
18	3	15	17	3	14	887.7965	887.7967	-0.0002
18	4	15	17	4	14	887.7965	887.7967	-0.0002
18	5	14	17	5	13	888.1156	888.1156	-0.0001
18	4	14	17	4	13	888.1156	888.1156	-0.0001
18	6	13	17	6	12	888.4333	888.4333	0
18	5	13	17	5	12	888.4333	888.4333	0
18	9	9	17	9	8	889.6914	889.6916	-0.0002
18	10	9	17	10	8	889.6914	889.6916	-0.0002
18	0	18	17	0	17	886.8314	886.8311	0.0003
18	1	18	17	1	17	886.8314	886.8311	0.0003
18	11	7	17	11	6	890.3148	890.3148	0
18	12	7	17	12	6	890.3148	890.3148	0
19	1	19	18	1	18	887.145	887.1447	0.0003
19	0	19	18	0	18	887.145	887.1447	0.0003
19	2	18	18	2	17	887.4696	887.4694	0.0002
19	1	18	18	1	17	887.4696	887.4694	0.0002
19	3	17	18	3	16	887.7926	887.7925	0.0002
19	2	17	18	2	16	887.7926	887.7925	0.0002
19	5	15	18	5	14	888.4344	888.4342	0.0001
19	4	15	18	4	14	888.4344	888.4342	0.0001
19	13	7	18	13	6	890.9516	890.9519	-0.0002

19	12	7	18	12	6	890.9516	890.9519	-0.0002
19	10	9	18	10	8	890.3284	890.3284	0
19	11	9	18	11	8	890.3284	890.3284	0
20	1	20	19	1	19	887.459	887.4588	0.0002
20	0	20	19	0	19	887.459	887.4588	0.0002
20	2	19	19	2	18	887.785	887.7848	0.0002
20	1	19	19	1	18	887.785	887.7848	0.0002
20	2	18	19	2	17	888.1096	888.1092	0.0004
20	3	18	19	3	17	888.1096	888.1092	0.0004
20	9	12	19	9	11	890.0256	890.0253	0.0002
20	8	12	19	8	11	890.0256	890.0253	0.0002
20	13	8	19	13	7	891.2791	891.279	0.0002
20	12	8	19	12	7	891.2791	891.279	0.0002
20	13	7	19	13	6	891.5902	891.5906	-0.0005
20	14	7	19	14	6	891.5902	891.5906	-0.0005
21	0	21	20	0	20	887.7736	887.7734	0.0002
21	1	21	20	1	20	887.7736	887.7734	0.0002
21	1	20	20	1	19	888.101	888.1008	0.0002
21	2	20	20	2	19	888.101	888.1008	0.0002
21	3	19	20	3	18	888.4267	888.4265	0.0002
21	2	19	20	2	18	888.4267	888.4265	0.0002
21	3	18	20	3	17	888.7503	888.7506	-0.0003
21	4	18	20	4	17	888.7503	888.7506	-0.0003
21	5	17	20	5	16	889.0734	889.0732	0.0002
21	4	17	20	4	16	889.0734	889.0732	0.0002
21	8	14	20	8	13	890.0325	890.0325	0.0001
21	7	14	20	7	13	890.0325	890.0325	0.0001
21	10	12	20	10	11	890.6656	890.6655	0.0001
21	9	12	20	9	11	890.6656	890.6655	0.0001
21	11	11	20	11	10	890.9806	890.9803	0.0003
21	10	11	20	10	10	890.9806	890.9803	0.0003
21	12	10	20	12	9	891.2941	891.294	0
21	11	10	20	11	9	891.2941	891.294	0
21	12	9	20	12	8	891.6067	891.6069	-0.0002
21	13	9	20	13	8	891.6067	891.6069	-0.0002
21	14	7	20	14	6	892.2312	892.2311	0.0001
21	15	7	20	15	6	892.2312	892.2311	0.0001
21	9	13	20	9	12	890.3499	890.3496	0.0003
21	8	13	20	8	12	890.3499	890.3496	0.0003
22	1	22	21	1	21	888.0885	888.0885	0
22	0	22	21	0	21	888.0885	888.0885	0

22	2	21	21	2	20	888.4172	888.4173	0
22	1	21	21	1	20	888.4172	888.4173	0
22	3	20	21	3	19	888.7443	888.7443	0
22	2	20	21	2	19	888.7443	888.7443	0
22	3	19	21	3	18	889.0702	889.0697	0.0005
22	4	19	21	4	18	889.0702	889.0697	0.0005
22	5	18	21	5	17	889.3939	889.3936	0.0003
22	4	18	21	4	17	889.3939	889.3936	0.0003
22	6	16	21	6	15	890.0365	890.0368	-0.0003
22	7	16	21	7	15	890.0365	890.0368	-0.0003
22	10	13	21	10	12	890.9916	890.9914	0.0001
22	9	13	21	9	12	890.9916	890.9914	0.0001
22	12	10	21	12	9	891.9361	891.9356	0.0005
22	13	10	21	13	9	891.9361	891.9356	0.0005
22	13	9	21	13	8	892.2488	892.2485	0.0003
22	14	9	21	14	8	892.2488	892.2485	0.0003
22	14	8	21	14	7	892.561	892.5608	0.0002
22	15	8	21	15	7	892.561	892.5608	0.0002
23	1	23	22	1	22	888.4041	888.4041	0
23	0	23	22	0	22	888.4041	888.4041	0
23	2	22	22	2	21	888.7344	888.7343	0.0001
23	1	22	22	1	21	888.7344	888.7343	0.0001
23	2	21	22	2	20	889.0629	889.0627	0.0002
23	3	21	22	3	20	889.0629	889.0627	0.0002
23	4	20	22	4	19	889.3895	889.3894	0
23	3	20	22	3	19	889.3895	889.3894	0
23	4	19	22	4	18	889.7143	889.7146	-0.0003
23	5	19	22	5	18	889.7143	889.7146	-0.0003
23	8	16	22	8	15	890.6809	890.6808	0.0001
23	7	16	22	7	15	890.6809	890.6808	0.0001
23	9	15	22	9	14	891.0001	891.0001	0
23	8	15	22	8	14	891.0001	891.0001	0
23	10	14	22	10	13	891.3184	891.318	0.0004
23	9	14	22	9	13	891.3184	891.318	0.0004
23	11	13	22	11	12	891.6348	891.6348	0
23	10	13	22	10	12	891.6348	891.6348	0
23	11	12	22	11	11	891.9506	891.9504	0.0002
23	12	12	22	12	11	891.9506	891.9504	0.0002
23	12	11	22	12	10	892.2652	892.265	0.0001
23	13	11	22	13	10	892.2652	892.265	0.0001
23	14	9	22	14	8	892.8922	892.8916	0.0006

23	15	9	22	15	8	892.8922	892.8916	0.0006
23	15	8	22	15	7	893.2041	893.2042	-0.0001
23	16	8	22	16	7	893.2041	893.2042	-0.0001
24	1	24	23	1	23	888.7201	888.7202	-0.0001
24	0	24	23	0	23	888.7201	888.7202	-0.0001
24	2	23	23	2	22	889.0518	889.0518	-0.0001
24	1	23	23	1	22	889.0518	889.0518	-0.0001
24	3	22	23	3	21	889.3817	889.3817	0.0001
24	2	22	23	2	21	889.3817	889.3817	0.0001
24	4	21	23	4	20	889.7096	889.7097	-0.0001
24	3	21	23	3	20	889.7096	889.7097	-0.0001
24	8	17	23	8	16	891.0055	891.0059	-0.0004
24	7	17	23	7	16	891.0055	891.0059	-0.0004
24	8	16	23	8	15	891.3261	891.3263	-0.0001
24	9	16	23	9	15	891.3261	891.3263	-0.0001
24	10	15	23	10	14	891.645	891.6453	-0.0003
24	9	15	23	9	14	891.645	891.6453	-0.0003
24	10	14	23	10	13	891.9632	891.9631	0.0001
24	11	14	23	11	13	891.9632	891.9631	0.0001
24	12	13	23	12	12	892.28	892.2797	0.0004
24	11	13	23	11	12	892.28	892.2797	0.0004
24	5	19	23	5	18	890.3606	890.3609	-0.0003
24	6	19	23	6	18	890.3606	890.3609	-0.0003
24	12	12	23	12	11	892.5955	892.5952	0.0003
24	13	12	23	13	11	892.5955	892.5952	0.0003
24	13	11	23	13	10	892.9103	892.9097	0.0007
24	14	11	23	14	10	892.9103	892.9097	0.0007
24	15	9	23	15	8	893.5367	893.5364	0.0003
24	16	9	23	16	8	893.5367	893.5364	0.0003
24	16	8	23	16	7	893.8491	893.8492	-0.0001
24	17	8	23	17	7	893.8491	893.8492	-0.0001
25	0	25	24	0	24	889.0368	889.0368	0
25	1	25	24	1	24	889.0368	889.0368	0
25	2	24	24	2	23	889.3698	889.3699	-0.0001
25	1	24	24	1	23	889.3698	889.3699	-0.0001
25	3	23	24	3	22	889.7014	889.7011	0.0002
25	2	23	24	2	22	889.7014	889.7011	0.0002
25	4	22	24	4	21	890.0306	890.0306	0
25	3	22	24	3	21	890.0306	890.0306	0
25	6	20	24	6	19	890.6841	890.6843	-0.0002
25	5	20	24	5	19	890.6841	890.6843	-0.0002

25	7	19	24	7	18	891.0082	891.0087	-0.0005
25	6	19	24	6	18	891.0082	891.0087	-0.0005
25	9	16	24	9	15	891.9732	891.9732	0
25	10	16	24	10	15	891.9732	891.9732	0
25	5	21	24	5	20	890.3584	890.3582	0.0002
25	4	21	24	4	20	890.3584	890.3582	0.0002
25	12	14	24	12	13	892.6096	892.6096	0.0001
25	11	14	24	11	13	892.6096	892.6096	0.0001
25	13	12	24	13	11	893.2419	893.2413	0.0005
25	14	12	24	14	11	893.2419	893.2413	0.0005
25	14	11	24	14	10	893.5561	893.5558	0.0003
25	15	11	24	15	10	893.5561	893.5558	0.0003
26	0	26	25	0	25	889.3537	889.3538	-0.0001
26	1	26	25	1	25	889.3537	889.3538	-0.0001
26	1	25	25	1	24	889.6887	889.6885	0.0002
26	2	25	25	2	24	889.6887	889.6885	0.0002
26	3	24	25	3	23	890.0213	890.0211	0.0001
26	2	24	25	2	23	890.0213	890.0211	0.0001
26	5	22	25	5	21	890.6809	890.681	-0.0001
26	4	22	25	4	21	890.6809	890.681	-0.0001
26	9	18	25	9	17	891.9802	891.9806	-0.0004
26	8	18	25	8	17	891.9802	891.9806	-0.0004
26	10	17	25	10	16	892.3012	892.3018	-0.0005
26	9	17	25	9	16	892.3012	892.3018	-0.0005
26	4	23	25	4	22	890.3521	890.3519	0.0001
26	3	23	25	3	22	890.3521	890.3519	0.0001
26	10	16	25	10	15	892.6218	892.6216	0.0002
26	11	16	25	11	15	892.6218	892.6216	0.0002
26	12	14	25	12	13	893.2574	893.2575	-0.0001
26	13	14	25	13	13	893.2574	893.2575	-0.0001
27	1	27	26	1	26	889.6711	889.6713	-0.0002
27	0	27	26	0	26	889.6711	889.6713	-0.0002
27	1	26	26	1	25	890.0075	890.0075	0
27	2	26	26	2	25	890.0075	890.0075	0
27	3	24	26	3	23	890.6741	890.6739	0.0002
27	4	24	26	4	23	890.6741	890.6739	0.0002
27	4	23	26	4	22	891.0043	891.0042	0
27	5	23	26	5	22	891.0043	891.0042	0
27	6	22	26	6	21	891.3326	891.3328	-0.0002
27	5	22	26	5	21	891.3326	891.3328	-0.0002
27	7	20	26	7	19	891.9848	891.985	-0.0002

27	8	20	26	8	19	891.9848	891.985	-0.0002
27	2	25	26	2	24	890.3414	890.3417	-0.0003
27	3	25	26	3	24	890.3414	890.3417	-0.0003
27	9	18	26	9	17	892.6308	892.631	-0.0002
27	10	18	26	10	17	892.6308	892.631	-0.0002
27	11	17	26	11	16	892.9516	892.9518	-0.0002
27	10	17	26	10	16	892.9516	892.9518	-0.0002
27	12	15	26	12	14	893.5896	893.5897	-0.0001
27	13	15	26	13	14	893.5896	893.5897	-0.0001
28	0	28	27	0	27	889.9895	889.9893	0.0002
28	1	28	27	1	27	889.9895	889.9893	0.0002
28	2	26	27	2	25	890.6627	890.6627	0
28	3	26	27	3	25	890.6627	890.6627	0
28	3	25	27	3	24	890.9964	890.9964	0
28	4	25	27	4	24	890.9964	890.9964	0
28	4	24	27	4	23	891.3279	891.3281	-0.0003
28	5	24	27	5	23	891.3279	891.3281	-0.0003
28	8	21	27	8	20	892.3122	892.3126	-0.0005
28	7	21	27	7	20	892.3122	892.3126	-0.0005
28	2	27	27	2	26	890.3274	890.3271	0.0003
28	1	27	27	1	26	890.3274	890.3271	0.0003
28	10	19	27	10	18	892.9605	892.9609	-0.0004
28	9	19	27	9	18	892.9605	892.9609	-0.0004
28	11	17	27	11	16	893.603	893.6033	-0.0004
28	12	17	27	12	16	893.603	893.6033	-0.0004
29	2	28	28	2	27	890.6471	890.6471	-0.0001
29	1	28	28	1	27	890.6471	890.6471	-0.0001
29	2	27	28	2	26	890.9843	890.9843	0
29	3	27	28	3	26	890.9843	890.9843	0
29	3	26	28	3	25	891.3195	891.3194	0
29	4	26	28	4	25	891.3195	891.3194	0
29	5	25	28	5	24	891.6527	891.6526	0.0001
29	4	25	28	4	24	891.6527	891.6526	0.0001
29	1	29	28	1	28	890.3075	890.3078	-0.0003
29	0	29	28	0	28	890.3075	890.3078	-0.0003
30	1	30	29	1	29	890.626	890.6266	-0.0006
30	0	30	29	0	29	890.626	890.6266	-0.0006
30	1	29	29	1	28	890.9675	890.9676	-0.0001
30	2	29	29	2	28	890.9675	890.9676	-0.0001
30	3	28	29	3	27	891.3067	891.3064	0.0003
30	2	28	29	2	27	891.3067	891.3064	0.0003

30	3	27	29	3	26	891.6433	891.643	0.0003
30	4	27	29	4	26	891.6433	891.643	0.0003
30	4	26	29	4	25	891.9773	891.9776	-0.0003
30	5	26	29	5	25	891.9773	891.9776	-0.0003
30	5	25	29	5	24	892.3094	892.3102	-0.0008
30	6	25	29	6	24	892.3094	892.3102	-0.0008
30	8	22	29	8	21	893.2966	893.297	-0.0004
30	9	22	29	9	21	893.2966	893.297	-0.0004
31	0	31	30	0	30	890.9455	890.9459	-0.0005
31	1	31	30	1	30	890.9455	890.9459	-0.0005
31	1	30	30	1	29	891.2887	891.2886	0.0001
31	2	30	30	2	29	891.2887	891.2886	0.0001
31	3	29	30	3	28	891.6292	891.629	0.0002
31	2	29	30	2	28	891.6292	891.629	0.0002
31	3	28	30	3	27	891.9671	891.9671	0
31	4	28	30	4	27	891.9671	891.9671	0
31	5	27	30	5	26	892.3029	892.3031	-0.0003
31	4	27	30	4	26	892.3029	892.3031	-0.0003
31	6	26	30	6	25	892.6369	892.6371	-0.0002
31	5	26	30	5	25	892.6369	892.6371	-0.0002
31	6	25	30	6	24	892.9689	892.9691	-0.0003
31	7	25	30	7	24	892.9689	892.9691	-0.0003
32	1	32	31	1	31	891.2651	891.2656	-0.0006
32	0	32	31	0	31	891.2651	891.2656	-0.0006
32	1	31	31	1	30	891.6102	891.6101	0.0001
32	2	31	31	2	30	891.6102	891.6101	0.0001
32	2	30	31	2	29	891.9524	891.9521	0.0003
32	3	30	31	3	29	891.9524	891.9521	0.0003
32	3	29	31	3	28	892.292	892.2918	0.0003
32	4	29	31	4	28	892.292	892.2918	0.0003
32	4	28	31	4	27	892.6295	892.6293	0.0002
32	5	28	31	5	27	892.6295	892.6293	0.0002
32	5	27	31	5	26	892.9646	892.9646	-0.0001
32	6	27	31	6	26	892.9646	892.9646	-0.0001
32	6	26	31	6	25	893.2981	893.298	0
32	7	26	31	7	25	893.2981	893.298	0
33	1	33	32	1	32	891.5852	891.5858	-0.0005
33	0	33	32	0	32	891.5852	891.5858	-0.0005
33	2	32	32	2	31	891.9322	891.9319	0.0003
33	1	32	32	1	31	891.9322	891.9319	0.0003
33	3	31	32	3	30	892.2763	892.2756	0.0006

33	2	31	32	2	30	892.2763	892.2756	0.0006
33	4	30	32	4	29	892.6175	892.6169	0.0005
33	3	30	32	3	29	892.6175	892.6169	0.0005
33	4	29	32	4	28	892.9557	892.9559	-0.0003
33	5	29	32	5	28	892.9557	892.9559	-0.0003
33	5	28	32	5	27	893.2919	893.2928	-0.0009
33	6	28	32	6	27	893.2919	893.2928	-0.0009
34	0	34	33	0	33	891.9057	891.9063	-0.0006
34	1	34	33	1	33	891.9057	891.9063	-0.0006
34	1	33	33	1	32	892.2545	892.2543	0.0002
34	2	33	33	2	32	892.2545	892.2543	0.0002
34	3	32	33	3	31	892.6005	892.5997	0.0008
34	2	32	33	2	31	892.6005	892.5997	0.0008
34	3	31	33	3	30	892.9431	892.9426	0.0005
34	4	31	33	4	30	892.9431	892.9426	0.0005
34	4	30	33	4	29	893.2828	893.2832	-0.0004
34	5	30	33	5	29	893.2828	893.2832	-0.0004
34	5	29	33	5	28	893.6217	893.6215	0.0002
34	6	29	33	6	28	893.6217	893.6215	0.0002
35	1	35	34	1	34	892.2268	892.2272	-0.0004
35	0	35	34	0	34	892.2268	892.2272	-0.0004
35	1	34	34	1	33	892.5778	892.577	0.0008
35	2	34	34	2	33	892.5778	892.577	0.0008
36	0	36	35	0	35	892.5481	892.5485	-0.0004
36	1	36	35	1	35	892.5481	892.5485	-0.0004
36	1	35	35	1	34	892.9012	892.9002	0.001
36	2	35	35	2	34	892.9012	892.9002	0.001
37	1	37	36	1	36	892.8696	892.8701	-0.0006
37	0	37	36	0	36	892.8696	892.8701	-0.0006
38	1	38	37	1	37	893.1921	893.1921	0
38	0	38	37	0	37	893.1921	893.1921	0
39	1	39	38	1	38	893.5148	893.5145	0.0003
39	0	39	38	0	38	893.5148	893.5145	0.0003
40	1	40	39	1	39	893.8376	893.8372	0.0004
40	0	40	39	0	39	893.8376	893.8372	0.0004

Appendix J

Observed and calculated frequencies (cm^{-1}) for the ν_{24} state of pyrrole.

P Branch

J'	Ka'	Kc'	J"	Ka"	Kc"	Observed (cm^{-1})	Calculated (cm^{-1})	Obs-Cal (cm^{-1})
8	6	2	9	7	3	860.73	860.7302	-0.0002
9	4	6	10	3	7	861.3529	861.3526	0.0002
9	3	6	10	4	7	861.3529	861.3526	0.0002
10	3	8	11	2	9	861.3248	861.3251	-0.0003
10	2	8	11	3	9	861.3248	861.3251	-0.0003
10	4	7	11	3	8	861.0422	861.0422	0
10	3	7	11	4	8	861.0422	861.0422	0
10	5	6	11	4	7	860.7577	860.7563	0.0014
10	4	6	11	5	7	860.7577	860.7563	0.0014
10	6	5	11	5	6	860.4684	860.4672	0.0011
10	5	5	11	6	6	860.4684	860.4672	0.0012
10	7	3	11	8	4	859.8648	859.8653	-0.0006
10	8	3	11	7	4	859.8807	859.8823	-0.0017
11	2	10	12	1	11	861.2877	861.2877	0.0001
11	1	10	12	2	11	861.2877	861.2877	0.0001
11	3	9	12	2	10	861.0097	861.0102	-0.0005
11	2	9	12	3	10	861.0097	861.0102	-0.0005
11	4	8	12	3	9	860.73	860.73	0.0001
11	3	8	12	4	9	860.73	860.73	0.0001
11	5	7	12	4	8	860.447	860.4469	0.0001
11	4	7	12	5	8	860.447	860.4469	0.0001
11	6	6	12	5	7	860.1611	860.1608	0.0002
11	5	6	12	6	7	860.1611	860.1608	0.0002
12	1	12	13	0	13	861.2401	861.2405	-0.0004
12	0	12	13	1	13	861.2401	861.2405	-0.0004
12	2	11	13	1	12	860.9683	860.9683	0
12	1	11	13	2	12	860.9683	860.9683	0
12	3	10	13	2	11	860.6935	860.6935	0
12	2	10	13	3	11	860.6935	860.6935	0
12	4	9	13	3	10	860.4158	860.416	-0.0003
12	3	9	13	4	10	860.4158	860.416	-0.0003
12	5	8	13	4	9	860.1363	860.1358	0.0005
12	4	8	13	5	9	860.1363	860.1358	0.0005
12	6	7	13	5	8	859.8531	859.8526	0.0005
12	5	7	13	6	8	859.8531	859.8526	0.0005
12	7	6	13	6	7	859.5675	859.5663	0.0012
12	6	6	13	7	7	859.5675	859.5663	0.0012
12	12	0	13	13	1	857.7553	857.7542	0.001

12	12	1	13	13	0	857.691	857.6903	0.0006
13	1	13	14	0	14	860.9167	860.9168	0
13	0	13	14	1	14	860.9167	860.9168	0
13	1	12	14	2	13	860.6469	860.6472	-0.0004
13	2	12	14	1	13	860.6469	860.6472	-0.0004
13	3	11	14	2	12	860.3748	860.3751	-0.0003
13	2	11	14	3	12	860.3748	860.3751	-0.0003
13	4	10	14	3	11	860.1002	860.1003	-0.0001
13	3	10	14	4	11	860.1002	860.1003	-0.0001
13	5	9	14	4	10	859.8224	859.8228	-0.0004
13	4	9	14	5	10	859.8224	859.8228	-0.0004
13	7	7	14	6	8	859.2594	859.2592	0.0003
13	6	7	14	7	8	859.2594	859.2592	0.0003
13	6	8	14	5	9	859.5427	859.5425	0.0003
13	5	8	14	6	9	859.5427	859.5425	0.0003
13	9	4	14	10	5	858.3861	858.385	0.0011
13	11	2	14	12	3	857.6507	857.65	0.0007
13	13	1	14	14	0	857.0897	857.0902	-0.0005
14	0	14	15	1	15	860.5911	860.5914	-0.0002
14	1	14	15	0	15	860.5911	860.5914	-0.0002
14	1	13	15	2	14	860.3246	860.3245	0.0002
14	2	13	15	1	14	860.3246	860.3245	0.0002
14	3	12	15	2	13	860.0552	860.055	0.0002
14	2	12	15	3	13	860.0552	860.055	0.0002
14	4	11	15	3	12	859.7826	859.7829	-0.0004
14	3	11	15	4	12	859.7826	859.7829	-0.0004
14	7	8	15	6	9	858.9508	858.9501	0.0006
14	6	8	15	7	9	858.9508	858.9501	0.0006
14	6	9	15	5	10	859.2306	859.2305	0
14	5	9	15	6	10	859.2306	859.2305	0
14	5	10	15	4	11	859.5079	859.5081	-0.0002
14	4	10	15	5	11	859.5079	859.5081	-0.0002
14	8	7	15	7	8	858.6672	858.6668	0.0004
14	7	7	15	8	8	858.6672	858.6668	0.0004
14	9	6	15	8	7	858.3816	858.3802	0.0014
14	8	6	15	9	7	858.3816	858.3802	0.0014
14	14	0	15	15	1	856.5246	856.5241	0.0005
15	1	15	16	0	16	860.2641	860.2642	-0.0002
15	0	15	16	1	16	860.2641	860.2642	-0.0002
15	1	14	16	2	15	859.9999	860	-0.0001
15	2	14	16	1	15	859.9999	860	-0.0001

15	3	13	16	2	14	859.7333	859.7332	0.0001
15	2	13	16	3	14	859.7333	859.7332	0.0001
15	5	11	16	4	12	859.1918	859.1917	0.0001
15	4	11	16	5	12	859.1918	859.1917	0.0001
15	4	12	16	3	13	859.464	859.4638	0.0003
15	3	12	16	4	13	859.464	859.4638	0.0003
15	7	9	16	6	10	858.6394	858.6392	0.0002
15	6	9	16	7	10	858.6394	858.6392	0.0002
15	9	7	16	8	8	858.0755	858.0754	0.0002
15	8	7	16	9	8	858.0755	858.0754	0.0002
15	10	6	16	9	7	857.7886	857.7889	-0.0003
15	9	6	16	10	7	857.7886	857.7888	-0.0002
16	1	16	17	0	17	859.9354	859.9354	0
16	0	16	17	1	17	859.9354	859.9354	0
16	1	15	17	2	16	859.6737	859.6738	-0.0001
16	2	15	17	1	16	859.6737	859.6738	-0.0001
16	5	12	17	4	13	858.8731	858.8735	-0.0004
16	4	12	17	5	13	858.8731	858.8735	-0.0004
16	2	14	17	3	15	859.4096	859.4096	-0.0001
16	3	14	17	2	15	859.4096	859.4096	-0.0001
16	6	11	17	5	12	858.6017	858.6014	0.0003
16	5	11	17	6	12	858.6017	858.6014	0.0003
16	7	10	17	6	11	858.3262	858.3265	-0.0003
16	6	10	17	7	11	858.3262	858.3265	-0.0003
16	8	9	17	7	10	858.0489	858.0488	0
16	7	9	17	8	10	858.0489	858.0488	0
16	9	8	17	8	9	857.7685	857.7683	0.0002
16	8	8	17	9	9	857.7685	857.7683	0.0002
16	10	7	17	9	8	857.4853	857.485	0.0004
16	9	7	17	10	8	857.4853	857.485	0.0004
17	0	17	18	1	18	859.6049	859.6049	0
17	1	17	18	0	18	859.6049	859.6049	0
17	4	14	18	3	15	858.8203	858.8203	-0.0001
17	3	14	18	4	15	858.8203	858.8203	-0.0001
17	3	15	18	2	16	859.0845	859.0844	0.0001
17	2	15	18	3	16	859.0845	859.0844	0.0001
17	1	16	18	2	17	859.3457	859.3459	-0.0002
17	2	16	18	1	17	859.3457	859.3459	-0.0002
17	5	13	18	4	14	858.5531	858.5536	-0.0005
17	4	13	18	5	14	858.5531	858.5536	-0.0005
17	6	12	18	5	13	858.2841	858.2842	-0.0001

17	5	12	18	6	13	858.2841	858.2842	-0.0001
17	8	10	18	7	11	857.7368	857.737	-0.0002
17	7	10	18	8	11	857.7368	857.737	-0.0002
17	9	9	18	8	10	857.4591	857.4592	-0.0001
17	8	9	18	9	10	857.4591	857.4592	-0.0001
17	10	8	18	9	9	857.1788	857.1787	0
17	9	8	18	10	9	857.1788	857.1787	0
17	11	7	18	10	8	856.8956	856.8955	0.0001
17	10	7	18	11	8	856.8956	856.8955	0.0001
18	2	17	19	1	18	859.0163	859.0163	0
18	1	17	19	2	18	859.0163	859.0163	0
18	0	18	19	1	19	859.2726	859.2727	-0.0001
18	1	18	19	0	19	859.2726	859.2727	-0.0001
18	3	16	19	2	17	858.7575	858.7575	0
18	2	16	19	3	17	858.7575	858.7575	0
18	4	15	19	3	16	858.4959	858.4961	-0.0002
18	3	15	19	4	16	858.4959	858.4961	-0.0002
18	5	14	19	4	15	858.2318	858.232	-0.0002
18	4	14	19	5	15	858.2318	858.232	-0.0002
18	6	13	19	5	14	857.9652	857.9652	0
18	5	13	19	6	14	857.9652	857.9652	0
18	7	12	19	6	13	857.6953	857.6956	-0.0003
18	6	12	19	7	13	857.6953	857.6956	-0.0003
18	8	11	19	7	12	857.4232	857.4233	-0.0001
18	7	11	19	8	12	857.4232	857.4233	-0.0001
18	9	10	19	8	11	857.1482	857.1482	0
18	8	10	19	9	11	857.1482	857.1482	0
18	10	9	19	9	10	856.8704	856.8703	0
18	9	9	19	10	10	856.8704	856.8703	0
18	12	7	19	11	8	856.3062	856.3069	-0.0007
18	11	7	19	12	8	856.3062	856.3069	-0.0007
19	1	19	20	0	20	858.9387	858.9388	-0.0002
19	0	19	20	1	20	858.9387	858.9388	-0.0002
19	2	18	20	1	19	858.6852	858.685	0.0002
19	1	18	20	2	19	858.6852	858.685	0.0002
19	2	17	20	3	18	858.429	858.4289	0.0002
19	3	17	20	2	18	858.429	858.4289	0.0002
19	3	16	20	4	17	858.1693	858.1701	-0.0008
19	4	16	20	3	17	858.1693	858.1701	-0.0008
19	5	15	20	4	16	857.9082	857.9087	-0.0005
19	4	15	20	5	16	857.9082	857.9087	-0.0005

19	5	14	20	6	15	857.6444	857.6445	-0.0001
19	6	14	20	5	15	857.6444	857.6445	-0.0001
19	7	13	20	6	14	857.3771	857.3775	-0.0004
19	6	13	20	7	14	857.3771	857.3775	-0.0004
19	8	12	20	7	13	857.1076	857.1077	-0.0002
19	7	12	20	8	13	857.1076	857.1077	-0.0002
19	9	11	20	8	12	856.8353	856.8351	0.0002
19	8	11	20	9	12	856.8353	856.8351	0.0002
19	10	10	20	9	11	856.5603	856.5598	0.0005
19	9	10	20	10	11	856.5603	856.5598	0.0005
19	11	9	20	10	10	856.2827	856.2819	0.0007
19	10	9	20	11	10	856.2827	856.2819	0.0007
19	12	8	20	11	9	856.0024	856.0015	0.0009
19	11	8	20	12	9	856.0024	856.0015	0.0009
20	0	20	21	1	21	858.6032	858.6033	-0.0001
20	1	20	21	0	21	858.6032	858.6033	-0.0001
20	2	19	21	1	20	858.3522	858.3521	0
20	1	19	21	2	20	858.3522	858.3521	0
20	3	18	21	2	19	858.0986	858.0986	0
20	2	18	21	3	19	858.0986	858.0986	0
20	4	17	21	3	18	857.8422	857.8425	-0.0003
20	3	17	21	4	18	857.8422	857.8425	-0.0003
20	4	16	21	5	17	857.5835	857.5837	-0.0002
20	5	16	21	4	17	857.5835	857.5837	-0.0002
20	6	15	21	5	16	857.3223	857.3221	0.0002
20	5	15	21	6	16	857.3223	857.3221	0.0002
20	6	14	21	7	15	857.0572	857.0576	-0.0004
20	7	14	21	6	15	857.0572	857.0576	-0.0004
20	8	13	21	7	14	856.7903	856.7903	0
20	7	13	21	8	14	856.7903	856.7903	0
20	9	12	21	8	13	856.5211	856.5202	0.0009
20	8	12	21	9	13	856.5211	856.5202	0.0009
20	10	11	21	9	12	856.2469	856.2473	-0.0004
20	9	11	21	10	12	856.2469	856.2473	-0.0004
20	11	10	21	10	11	855.9713	855.9717	-0.0004
20	10	10	21	11	11	855.9713	855.9717	-0.0004
20	13	8	21	12	9	855.4149	855.4132	0.0017
20	12	8	21	13	9	855.4149	855.4132	0.0017
21	1	21	22	0	22	858.2661	858.2661	0
21	0	21	22	1	22	858.2661	858.2661	0
21	1	20	22	2	21	858.0178	858.0176	0.0002

21	2	20	22	1	21	858.0178	858.0176	0.0002
21	3	19	22	2	20	857.7667	857.7667	0
21	2	19	22	3	20	857.7667	857.7667	0
21	4	18	22	3	19	857.5131	857.5132	-0.0001
21	3	18	22	4	19	857.5131	857.5132	-0.0001
21	4	17	22	5	18	857.2563	857.257	-0.0006
21	5	17	22	4	18	857.2563	857.257	-0.0006
21	6	16	22	5	17	856.9973	856.9979	-0.0007
21	5	16	22	6	17	856.9973	856.9979	-0.0007
21	7	15	22	6	16	856.7359	856.736	-0.0001
21	6	15	22	7	16	856.7359	856.736	-0.0001
21	8	14	22	7	15	856.4716	856.4711	0.0005
21	7	14	22	8	15	856.4716	856.4711	0.0005
21	9	13	22	8	14	856.2028	856.2033	-0.0005
21	8	13	22	9	14	856.2028	856.2033	-0.0005
21	11	11	22	10	12	855.6577	855.6593	-0.0016
21	10	11	22	11	12	855.6577	855.6593	-0.0016
21	12	10	22	11	11	855.3841	855.3833	0.0008
21	11	10	22	12	11	855.3841	855.3833	0.0008
22	0	22	23	1	23	857.9277	857.9273	0.0003
22	1	22	23	0	23	857.9277	857.9273	0.0003
22	2	21	23	1	22	857.6817	857.6813	0.0003
22	1	21	23	2	22	857.6817	857.6813	0.0003
22	2	20	23	3	21	857.4331	857.4331	0
22	3	20	23	2	21	857.4331	857.4331	0
22	4	19	23	3	20	857.182	857.1822	-0.0002
22	3	19	23	4	20	857.182	857.1822	-0.0002
22	5	18	23	4	19	856.9283	856.9286	-0.0003
22	4	18	23	5	19	856.9283	856.9286	-0.0003
22	6	17	23	5	18	856.6719	856.6721	-0.0002
22	5	17	23	6	18	856.6719	856.6721	-0.0002
22	6	16	23	7	17	856.4126	856.4126	0
22	7	16	23	6	17	856.4126	856.4126	0
22	8	15	23	7	16	856.1505	856.15	0.0004
22	7	15	23	8	16	856.1505	856.15	0.0004
22	10	13	23	9	14	855.6158	855.616	-0.0003
22	9	13	23	10	14	855.6158	855.616	-0.0003
22	11	12	23	10	13	855.3447	855.3447	0
22	10	12	23	11	13	855.3447	855.3447	0
23	1	23	24	0	24	857.587	857.5869	0.0001
23	0	23	24	1	24	857.587	857.5869	0.0001

23	2	22	24	1	23	857.3438	857.3435	0.0004
23	1	22	24	2	23	857.3438	857.3435	0.0004
23	3	21	24	2	22	857.0981	857.0978	0.0002
23	2	21	24	3	22	857.0981	857.0978	0.0002
23	4	20	24	3	21	856.8494	856.8496	-0.0002
23	3	20	24	4	21	856.8494	856.8496	-0.0002
23	4	19	24	5	20	856.5982	856.5985	-0.0004
23	5	19	24	4	20	856.5982	856.5985	-0.0004
23	6	18	24	5	19	856.3441	856.3445	-0.0004
23	5	18	24	6	19	856.3441	856.3445	-0.0004
23	7	16	24	8	17	855.8276	855.8272	0.0004
23	8	16	24	7	17	855.8276	855.8272	0.0004
23	9	15	24	8	16	855.5625	855.5638	-0.0013
23	8	15	24	9	16	855.5625	855.5638	-0.0013
23	10	14	24	9	15	855.2963	855.2974	-0.0011
23	9	14	24	10	15	855.2963	855.2974	-0.0011
24	1	24	25	0	25	857.2451	857.2448	0.0003
24	0	24	25	1	25	857.2451	857.2448	0.0003
24	2	23	25	1	24	857.0042	857.004	0.0002
24	1	23	25	2	24	857.0042	857.004	0.0002
24	2	22	25	3	23	856.761	856.761	0
24	3	22	25	2	23	856.761	856.761	0
24	3	21	25	4	22	856.5151	856.5153	-0.0002
24	4	21	25	3	22	856.5151	856.5153	-0.0002
24	5	20	25	4	21	856.2663	856.2668	-0.0005
24	4	20	25	5	21	856.2663	856.2668	-0.0005
24	6	19	25	5	20	856.0151	856.0153	-0.0001
24	5	19	25	6	20	856.0151	856.0153	-0.0001
24	7	18	25	6	19	855.7616	855.7605	0.0011
24	6	18	25	7	19	855.7616	855.7605	0.0011
25	1	25	26	0	26	856.9012	856.9011	0
25	0	25	26	1	26	856.9012	856.9011	0
25	2	24	26	1	25	856.6633	856.6629	0.0004
25	1	24	26	2	25	856.6633	856.6629	0.0004
25	2	23	26	3	24	856.4223	856.4225	-0.0001
25	3	23	26	2	24	856.4223	856.4225	-0.0001
25	3	22	26	4	23	856.1791	856.1794	-0.0003
25	4	22	26	3	23	856.1791	856.1794	-0.0003
25	4	21	26	5	22	855.9332	855.9335	-0.0003
25	5	21	26	4	22	855.9332	855.9335	-0.0003
25	6	20	26	5	21	855.6846	855.6843	0.0002

25	5	20	26	6	21	855.6846	855.6843	0.0002
26	1	26	27	0	27	856.5561	856.5559	0.0002
26	0	26	27	1	27	856.5561	856.5559	0.0002
26	1	25	27	2	26	856.3204	856.3202	0.0002
26	2	25	27	1	26	856.3204	856.3202	0.0002
26	3	24	27	2	25	856.0826	856.0824	0.0002
26	2	24	27	3	25	856.0826	856.0824	0.0002
26	4	23	27	3	24	855.8416	855.8419	-0.0003
26	3	23	27	4	24	855.8416	855.8419	-0.0003
26	5	22	27	4	23	855.5982	855.5985	-0.0002
26	4	22	27	5	23	855.5982	855.5985	-0.0002
26	5	21	27	6	22	855.3503	855.3517	-0.0015
26	6	21	27	5	22	855.3503	855.3517	-0.0015
27	1	27	28	0	28	856.2094	856.2091	0.0003
27	0	27	28	1	28	856.2094	856.2091	0.0003
27	1	26	28	2	27	855.9763	855.9759	0.0003
27	2	26	28	1	27	855.9763	855.9759	0.0003
27	3	25	28	2	26	855.7408	855.7407	0.0001
27	2	25	28	3	26	855.7408	855.7407	0.0001
27	4	24	28	3	25	855.5024	855.5028	-0.0004
27	3	24	28	4	25	855.5024	855.5028	-0.0004
27	4	23	28	5	24	855.2616	855.2618	-0.0002
27	5	23	28	4	24	855.2616	855.2618	-0.0002
27	6	22	28	5	23	855.018	855.0174	0.0006
27	5	22	28	6	23	855.018	855.0174	0.0006
28	1	28	29	0	29	855.8607	855.8607	0.0001
28	0	28	29	1	29	855.8607	855.8607	0.0001
28	1	27	29	2	28	855.6305	855.6301	0.0004
28	2	27	29	1	28	855.6305	855.6301	0.0004
28	3	26	29	2	27	855.3975	855.3974	0.0001
28	2	26	29	3	27	855.3975	855.3974	0.0001
28	4	25	29	3	26	855.1618	855.1621	-0.0002
28	3	25	29	4	26	855.1618	855.1621	-0.0002
28	4	24	29	5	25	854.9232	854.9236	-0.0004
28	5	24	29	4	25	854.9232	854.9236	-0.0004
28	10	19	29	9	20	853.6728	853.6736	-0.0008
28	9	19	29	10	20	853.6728	853.6736	-0.0008
29	1	29	30	0	30	855.5109	855.5107	0.0002
29	0	29	30	1	30	855.5109	855.5107	0.0002
29	2	28	30	1	29	855.2831	855.2827	0.0004
29	1	28	30	2	29	855.2831	855.2827	0.0004

29	3	27	30	2	28	855.0527	855.0526	0
29	2	27	30	3	28	855.0527	855.0526	0
30	0	30	31	1	31	855.1591	855.1592	-0.0001
30	1	30	31	0	31	855.1591	855.1592	-0.0001
30	1	29	31	2	30	854.9341	854.9337	0.0004
30	2	29	31	1	30	854.9341	854.9337	0.0004
30	2	28	31	3	29	854.7063	854.7062	0.0001
30	3	28	31	2	29	854.7063	854.7062	0.0001
30	5	26	31	4	27	854.2431	854.2423	0.0008
30	4	26	31	5	27	854.2431	854.2423	0.0008
31	2	29	32	3	30	854.3584	854.3583	0.0001
31	3	29	32	2	30	854.3584	854.3583	0.0001
31	4	28	32	3	29	854.1304	854.1305	-0.0002
31	3	28	32	4	29	854.1304	854.1305	-0.0002
31	5	26	32	6	27	853.6634	853.6639	-0.0005
31	6	26	32	5	27	853.6634	853.6639	-0.0005
32	1	32	33	0	33	854.4518	854.4517	0.0001
32	0	32	33	1	33	854.4518	854.4517	0.0001
32	2	31	33	1	32	854.2316	854.2313	0.0003
32	1	31	33	2	32	854.2316	854.2313	0.0003
32	4	29	33	3	30	853.7836	853.7836	0
32	3	29	33	4	30	853.7836	853.7836	0
32	4	28	33	5	29	853.5557	853.5547	0.001
32	5	28	33	4	29	853.5557	853.5547	0.001
33	0	33	34	1	34	854.0956	854.0957	-0.0002
33	1	33	34	0	34	854.0956	854.0957	-0.0002
33	1	32	34	2	33	853.878	853.8778	0.0002
33	2	32	34	1	33	853.878	853.8778	0.0002
33	3	31	34	2	32	853.6579	853.6579	0
33	2	31	34	3	32	853.6579	853.6579	0
33	4	30	34	3	31	853.4347	853.4351	-0.0004
33	3	30	34	4	31	853.4347	853.4351	-0.0004
33	4	29	34	5	30	853.2094	853.2085	0.0008
33	5	29	34	4	30	853.2094	853.2085	0.0008
34	3	32	35	2	33	853.3054	853.3055	-0.0001
34	2	32	35	3	33	853.3054	853.3055	-0.0001
34	5	30	35	4	31	852.8621	852.8609	0.0013
34	4	30	35	5	31	852.8621	852.8609	0.0013
35	0	35	36	1	36	853.3787	853.3794	-0.0007
35	1	35	36	0	36	853.3787	853.3794	-0.0007
35	2	33	36	3	34	852.9512	852.9516	-0.0004

35	3	33	36	2	34	852.9512	852.9516	-0.0004
35	1	34	36	2	35	853.1663	853.1664	-0.0001
35	2	34	36	1	35	853.1663	853.1664	-0.0001
36	0	36	37	1	37	853.0184	853.019	-0.0006
36	1	36	37	0	37	853.0184	853.019	-0.0006
36	1	35	37	2	36	852.8083	852.8085	-0.0002
36	2	35	37	1	36	852.8083	852.8085	-0.0002

R Branch

J'	Ka'	Kc'	J"	Ka"	Kc"	Observed (cm^{-1})	Calculated (cm^{-1})	Obs-Cal (cm^{-1})
6	6	0	5	5	1	869.2365	869.237	-0.0005
7	2	6	6	1	5	867.99	867.9902	-0.0002
7	1	6	6	2	5	867.99	867.9902	-0.0002
7	2	5	6	3	4	868.3069	868.3069	0
7	3	5	6	2	4	868.3069	868.3069	0
7	6	2	6	5	1	869.297	869.2967	0.0003
8	2	7	7	1	6	868.2823	868.2825	-0.0002
8	1	7	7	2	6	868.2823	868.2825	-0.0002
8	3	5	7	4	4	868.9181	868.9182	-0.0002
8	5	3	7	6	2	869.5312	869.5327	-0.0015
8	4	5	7	3	4	868.9181	868.9182	-0.0002
9	1	9	8	0	8	868.2482	868.2483	-0.0001
9	2	8	8	1	7	868.5729	868.573	-0.0001
9	0	9	8	1	8	868.2482	868.2483	-0.0001
9	1	8	8	2	7	868.5729	868.573	-0.0001
9	2	7	8	3	6	868.8953	868.895	0.0003
9	3	7	8	2	6	868.8953	868.895	0.0003
9	3	6	8	4	5	869.2138	869.2142	-0.0004
9	4	5	8	5	4	869.53	869.5303	-0.0003
9	4	6	8	3	5	869.2138	869.2142	-0.0004
9	5	5	8	4	4	869.53	869.5304	-0.0004
10	1	10	9	0	9	868.5341	868.5344	-0.0003
10	2	9	9	1	8	868.8615	868.8618	-0.0003
10	0	10	9	1	9	868.5341	868.5344	-0.0003
10	1	9	9	2	8	868.8615	868.8618	-0.0003
10	3	8	9	2	7	869.1866	869.1865	0.0001
10	2	8	9	3	7	869.1866	869.1865	0.0001
10	3	7	9	4	6	869.5087	869.5084	0.0003
10	4	7	9	3	6	869.5087	869.5084	0.0003
11	1	11	10	0	10	868.8186	868.8188	-0.0003
11	2	10	10	1	9	869.1483	869.1488	-0.0005
11	0	11	10	1	10	868.8186	868.8188	-0.0003
11	3	9	10	2	8	869.4757	869.4762	-0.0005
11	1	10	10	2	9	869.1483	869.1488	-0.0005
11	2	9	10	3	8	869.4757	869.4762	-0.0005
11	3	8	10	4	7	869.8009	869.8008	0.0001
11	4	7	10	5	6	870.1232	870.1226	0.0006
11	5	6	10	6	5	870.4425	870.4414	0.0011

11	4	8	10	3	7	869.8009	869.8008	0.0001
11	5	7	10	4	6	870.1232	870.1226	0.0006
11	6	6	10	5	5	870.4425	870.4414	0.0011
12	2	11	11	1	10	869.434	869.4341	-0.0001
12	3	10	11	2	9	869.7638	869.7641	-0.0003
12	0	12	11	1	11	869.101	869.1015	-0.0005
12	1	11	11	2	10	869.434	869.4341	-0.0001
12	2	10	11	3	9	869.7638	869.7641	-0.0003
12	4	9	11	3	8	870.0916	870.0914	0.0001
12	3	9	11	4	8	870.0916	870.0914	0.0001
12	4	8	11	5	7	870.4161	870.416	0.0001
12	5	7	11	6	6	870.7384	870.7377	0.0008
12	5	8	11	4	7	870.4161	870.416	0.0001
12	6	7	11	5	6	870.7384	870.7377	0.0008
12	12	0	11	11	1	872.9379	872.9389	-0.001
13	1	13	12	0	12	869.3822	869.3824	-0.0002
13	3	11	12	2	10	870.0505	870.0504	0.0001
13	4	10	12	3	9	870.3804	870.3804	0
13	5	9	12	4	8	870.7078	870.7076	0.0001
13	0	13	12	1	12	869.3822	869.3824	-0.0002
13	2	11	12	3	10	870.0505	870.0504	0.0001
13	3	10	12	4	9	870.3804	870.3804	0
13	4	9	12	5	8	870.7078	870.7076	0.0001
13	6	7	12	7	6	871.3542	871.3537	0.0005
13	7	6	12	8	5	871.6733	871.6724	0.001
13	7	7	12	6	6	871.3542	871.3537	0.0005
13	1	12	12	2	11	869.7181	869.7177	0.0004
13	8	6	12	7	5	871.6733	871.6724	0.0009
13	2	12	12	1	11	869.7181	869.7177	0.0004
14	1	14	13	0	13	869.6617	869.6617	0.0001
14	2	13	13	1	12	869.9995	869.9996	-0.0001
14	3	12	13	2	11	870.3345	870.3349	-0.0003
14	4	11	13	3	10	870.6675	870.6676	0
14	5	10	13	4	9	870.9973	870.9975	-0.0002
14	6	9	13	5	8	871.3245	871.3247	-0.0002
14	0	14	13	1	13	869.6617	869.6617	0.0001
14	1	13	13	2	12	869.9995	869.9996	-0.0001
14	2	12	13	3	11	870.3345	870.3349	-0.0003
14	3	11	13	4	10	870.6675	870.6676	0
14	4	10	13	5	9	870.9973	870.9975	-0.0002
14	5	9	13	6	8	871.3245	871.3247	-0.0002

14	7	7	13	8	6	871.9717	871.9707	0.001
14	8	7	13	7	6	871.9717	871.9707	0.001
14	14	1	13	13	0	874.0824	874.082	0.0004
15	1	15	14	0	14	869.9389	869.9392	-0.0003
15	2	14	14	1	13	870.2797	870.2797	0
15	3	13	14	2	12	870.6176	870.6177	0
15	4	12	14	3	11	870.953	870.953	0
15	5	11	14	4	10	871.2853	871.2857	-0.0003
15	7	9	14	6	8	871.9424	871.9427	-0.0004
15	8	8	14	7	7	872.2675	872.2671	0.0004
15	0	15	14	1	14	869.9389	869.9392	-0.0003
15	1	14	14	2	13	870.2797	870.2797	0
15	2	13	14	3	12	870.6176	870.6177	0
15	3	12	14	4	11	870.953	870.953	0
15	4	11	14	5	10	871.2853	871.2857	-0.0003
15	6	9	14	7	8	871.9424	871.9427	-0.0004
15	9	7	14	8	6	872.5895	872.5888	0.0007
15	7	8	14	8	7	872.2675	872.2671	0.0004
15	8	7	14	9	6	872.5895	872.5888	0.0007
15	9	6	14	10	5	872.9082	872.9077	0.0005
15	10	6	14	9	5	872.9082	872.9078	0.0004
16	1	16	15	0	15	870.2149	870.215	-0.0001
16	2	15	15	1	14	870.5583	870.5581	0.0001
16	3	14	15	2	13	870.8988	870.8988	0.0001
16	4	13	15	3	12	871.2366	871.2368	-0.0002
16	5	12	15	4	11	871.572	871.5721	-0.0001
16	6	11	15	5	10	871.9038	871.9047	-0.0009
16	7	10	15	6	9	872.2343	872.2345	-0.0002
16	8	9	15	7	8	872.5618	872.5616	0.0002
16	9	8	15	8	7	872.8861	872.886	0
16	0	16	15	1	15	870.2149	870.215	-0.0001
16	10	7	15	9	6	873.2082	873.2078	0.0003
16	1	15	15	2	14	870.5583	870.5581	0.0001
16	2	14	15	3	13	870.8988	870.8988	0.0001
16	3	13	15	4	12	871.2366	871.2368	-0.0002
16	4	12	15	5	11	871.572	871.5721	-0.0001
16	5	11	15	6	10	871.9038	871.9047	-0.0009
16	6	10	15	7	9	872.2343	872.2345	-0.0002
16	7	9	15	8	8	872.5618	872.5616	0.0002
16	8	8	15	9	7	872.8861	872.886	0
16	9	7	15	10	6	873.2082	873.2078	0.0003

17	1	17	16	0	16	870.4891	870.4891	0
17	2	16	16	1	15	870.8351	870.8349	0.0003
17	3	15	16	2	14	871.1779	871.1781	-0.0002
17	4	14	16	3	13	871.5181	871.5188	-0.0006
17	5	13	16	4	12	871.8562	871.8568	-0.0006
17	6	12	16	5	11	872.192	872.192	0
17	7	11	16	6	10	872.5243	872.5245	-0.0002
17	8	10	16	7	9	872.854	872.8542	-0.0003
17	9	9	16	8	8	873.1813	873.1813	0
17	10	8	16	9	7	873.5058	873.5058	0
17	0	17	16	1	16	870.4891	870.4891	0
17	1	16	16	2	15	870.8351	870.8349	0.0003
17	2	15	16	3	14	871.1779	871.1781	-0.0002
17	3	14	16	4	13	871.5181	871.5188	-0.0006
17	4	13	16	5	12	871.8562	871.8568	-0.0006
17	5	12	16	6	11	872.192	872.192	0
17	6	11	16	7	10	872.5243	872.5245	-0.0002
17	7	10	16	8	9	872.854	872.8542	-0.0003
17	8	9	16	9	8	873.1813	873.1813	0
17	9	8	16	10	7	873.5058	873.5058	0
18	1	18	17	0	17	870.7615	870.7615	0
18	2	17	17	1	16	871.11	871.1099	0.0001
18	3	16	17	2	15	871.4557	871.4558	-0.0001
18	4	15	17	3	14	871.799	871.7991	-0.0001
18	5	14	17	4	13	872.1393	872.1397	-0.0004
18	6	13	17	5	12	872.477	872.4776	-0.0005
18	7	12	17	6	11	872.8122	872.8126	-0.0005
18	9	10	17	8	9	873.4744	873.4746	-0.0003
18	10	9	17	9	8	873.8015	873.8016	-0.0001
18	11	8	17	10	7	874.1255	874.1262	-0.0008
18	0	18	17	1	17	870.7615	870.7615	0
18	1	17	17	2	16	871.11	871.1099	0.0001
18	2	16	17	3	15	871.4557	871.4558	-0.0001
18	3	15	17	4	14	871.799	871.7991	-0.0001
18	4	14	17	5	13	872.1393	872.1397	-0.0004
18	5	13	17	6	12	872.477	872.4776	-0.0005
18	6	12	17	7	11	872.8122	872.8126	-0.0005
18	8	10	17	9	9	873.4744	873.4746	-0.0003
18	9	9	17	10	8	873.8015	873.8016	-0.0001
18	10	8	17	11	7	874.1255	874.1262	-0.0008
19	1	19	18	0	18	871.0324	871.0323	0.0001

19	2	18	18	1	17	871.3834	871.3832	0.0002
19	3	17	18	2	16	871.7318	871.7318	0
19	4	16	18	3	15	872.0777	872.0777	0
19	5	15	18	4	14	872.4204	872.4209	-0.0005
19	6	14	18	5	13	872.7608	872.7614	-0.0006
19	7	13	18	6	12	873.0988	873.099	-0.0003
19	8	12	18	7	11	873.4336	873.4339	-0.0003
19	9	11	18	8	10	873.7662	873.766	0.0002
19	10	10	18	9	9	874.0952	874.0955	-0.0003
19	0	19	18	1	18	871.0324	871.0323	0.0001
19	1	18	18	2	17	871.3834	871.3832	0.0002
19	2	17	18	3	16	871.7318	871.7318	0
19	3	16	18	4	15	872.0777	872.0777	0
19	4	15	18	5	14	872.4204	872.4209	-0.0005
19	5	14	18	6	13	872.7608	872.7614	-0.0006
19	6	13	18	7	12	873.0988	873.099	-0.0003
19	7	12	18	8	11	873.4336	873.4339	-0.0003
19	8	11	18	9	10	873.7662	873.766	0.0002
19	9	10	18	10	9	874.0952	874.0955	-0.0003
20	1	20	19	0	19	871.302	871.3013	0.0006
20	2	19	19	1	18	871.6555	871.6549	0.0006
20	3	18	19	2	17	872.0063	872.0061	0.0002
20	4	17	19	3	16	872.3542	872.3546	-0.0004
20	5	16	19	4	15	872.6998	872.7005	-0.0007
20	6	15	19	5	14	873.044	873.0435	0.0005
20	7	14	19	6	13	873.3833	873.3836	-0.0003
20	8	13	19	7	12	873.7211	873.7209	0.0001
20	9	12	19	8	11	874.0559	874.0554	0.0005
20	0	20	19	1	19	871.302	871.3013	0.0006
20	1	19	19	2	18	871.6555	871.6549	0.0006
20	2	18	19	3	17	872.0063	872.0061	0.0002
20	3	17	19	4	16	872.3542	872.3546	-0.0004
20	4	16	19	5	15	872.6998	872.7005	-0.0007
20	5	15	19	6	14	873.044	873.0435	0.0005
20	6	14	19	7	13	873.3833	873.3836	-0.0003
20	7	13	19	8	12	873.7211	873.7209	0.0001
20	8	12	19	9	11	874.0559	874.0554	0.0005
21	1	21	20	0	20	871.5688	871.5687	0.0001
21	2	20	20	1	19	871.9251	871.9249	0.0002
21	3	19	20	2	18	872.2785	872.2787	-0.0001
21	4	18	20	3	17	872.6296	872.6299	-0.0003

21	5	17	20	4	16	872.978	872.9783	-0.0003
21	6	16	20	5	15	873.3231	873.3238	-0.0008
21	7	15	20	6	14	873.6663	873.6665	-0.0002
21	8	14	20	7	13	874.0065	874.0062	0.0003
21	0	21	20	1	20	871.5688	871.5687	0.0001
21	1	20	20	2	19	871.9251	871.9249	0.0002
21	2	19	20	3	18	872.2785	872.2787	-0.0001
21	3	18	20	4	17	872.6296	872.6299	-0.0003
21	4	17	20	5	16	872.978	872.9783	-0.0003
21	5	16	20	6	15	873.3231	873.3238	-0.0008
21	6	15	20	7	14	873.6663	873.6665	-0.0002
21	7	14	20	8	13	874.0065	874.0062	0.0003
22	1	22	21	0	21	871.8345	871.8345	0
22	2	21	21	1	20	872.1932	872.1932	-0.0001
22	3	20	21	2	19	872.5495	872.5496	-0.0001
22	4	19	21	3	18	872.9028	872.9034	-0.0006
22	5	18	21	4	17	873.2538	873.2544	-0.0006
22	6	17	21	5	16	873.604	873.6025	0.0015
22	7	16	21	6	15	873.9478	873.9475	0.0003
22	0	22	21	1	21	871.8345	871.8345	0
22	1	21	21	2	20	872.1932	872.1932	-0.0001
22	2	20	21	3	19	872.5495	872.5496	-0.0001
22	3	19	21	4	18	872.9028	872.9034	-0.0006
22	4	18	21	5	17	873.2538	873.2544	-0.0006
22	5	17	21	6	16	873.604	873.6025	0.0015
22	6	16	21	7	15	873.9478	873.9475	0.0003
22	7	15	21	8	14	874.2905	874.2896	0.0009
22	8	15	21	7	14	874.2905	874.2896	0.0009
23	1	23	22	0	22	872.0988	872.0986	0.0002
23	2	22	22	1	21	872.4602	872.4599	0.0003
23	3	21	22	2	20	872.819	872.8189	0
23	4	20	22	3	19	873.175	873.1753	-0.0003
23	5	19	22	4	18	873.5283	873.5289	-0.0005
23	0	23	22	1	22	872.0988	872.0986	0.0002
23	1	22	22	2	21	872.4602	872.4599	0.0003
23	2	21	22	3	20	872.819	872.8189	0
23	3	20	22	4	19	873.175	873.1753	-0.0003
23	4	19	22	5	18	873.5283	873.5289	-0.0005
23	6	17	22	7	16	874.2273	874.2268	0.0005
23	7	17	22	6	16	874.2273	874.2268	0.0005
24	1	24	23	0	23	872.3613	872.3611	0.0001

24	2	23	23	1	22	872.7253	872.725	0.0003
24	3	22	23	2	21	873.0866	873.0866	0
24	4	21	23	3	20	873.4452	873.4456	-0.0004
24	5	20	23	4	19	873.8015	873.8016	-0.0001
24	0	24	23	1	23	872.3613	872.3611	0.0001
24	1	23	23	2	22	872.7253	872.725	0.0003
24	2	22	23	3	21	873.0866	873.0866	0
24	3	21	23	4	20	873.4452	873.4456	-0.0004
24	4	20	23	5	19	873.8015	873.8016	-0.0001
25	1	25	24	0	24	872.6222	872.622	0.0002
25	2	24	24	1	23	872.9888	872.9884	0.0004
25	3	23	24	2	22	873.3522	873.3526	-0.0005
25	4	22	24	3	21	873.7139	873.7142	-0.0003
25	5	21	24	4	20	874.0725	874.0727	-0.0003
25	0	25	24	1	24	872.6222	872.622	0.0002
25	1	24	24	2	23	872.9888	872.9884	0.0004
25	2	23	24	3	22	873.3522	873.3526	-0.0005
25	3	22	24	4	21	873.7139	873.7142	-0.0003
25	4	21	24	5	20	874.0725	874.0727	-0.0003
25	5	20	24	6	19	874.4282	874.4281	0.0001
25	6	20	24	5	19	874.4282	874.4281	0.0001
26	1	26	25	0	25	872.8815	872.8813	0.0002
26	2	25	25	1	24	873.251	873.2503	0.0007
26	3	24	25	2	23	873.6175	873.617	0.0005
26	4	23	25	3	22	873.9809	873.9811	-0.0003
26	0	26	25	1	25	872.8815	872.8813	0.0002
26	1	25	25	2	24	873.251	873.2503	0.0007
26	2	24	25	3	23	873.6175	873.617	0.0005
26	3	23	25	4	22	873.9809	873.9811	-0.0003
26	5	21	25	6	20	874.7005	874.6999	0.0006
26	4	22	25	5	21	874.3421	874.3422	-0.0001
26	6	21	25	5	20	874.7005	874.6999	0.0006
26	5	22	25	4	21	874.3421	874.3422	-0.0001
27	1	27	26	0	26	873.1391	873.139	0.0002
27	2	26	26	1	25	873.511	873.5105	0.0005
27	3	25	26	2	24	873.8797	873.8798	-0.0001
27	0	27	26	1	26	873.1391	873.139	0.0002
27	1	26	26	2	25	873.511	873.5105	0.0005
27	2	25	26	3	24	873.8797	873.8798	-0.0001
27	4	23	26	5	22	874.6099	874.61	-0.0001
27	3	24	26	4	23	874.2462	874.2465	-0.0002

27	7	20	26	8	19	875.6796	875.6791	0.0005
27	5	23	26	4	22	874.6099	874.61	-0.0001
27	4	24	26	3	23	874.2462	874.2465	-0.0002
27	8	20	26	7	19	875.6796	875.6791	0.0005
28	1	28	27	0	27	873.3953	873.3951	0.0002
28	2	27	27	1	26	873.7693	873.7691	0.0001
28	3	26	27	2	25	874.141	874.141	-0.0001
28	0	28	27	1	27	873.3953	873.3951	0.0002
28	1	27	27	2	26	873.7693	873.7691	0.0001
28	2	26	27	3	25	874.141	874.141	-0.0001
28	3	25	27	4	24	874.5099	874.5102	-0.0003
28	4	24	27	5	23	874.8761	874.8762	-0.0001
28	4	25	27	3	24	874.5099	874.5102	-0.0003
28	5	24	27	4	23	874.8761	874.8762	-0.0001
29	1	29	28	0	28	873.6496	873.6496	0
29	2	28	28	1	27	874.0265	874.0262	0.0004
29	0	29	28	1	28	873.6496	873.6496	0
29	1	28	28	2	27	874.0265	874.0262	0.0004
29	3	26	28	4	25	874.7718	874.7724	-0.0006
29	4	25	28	5	24	875.141	875.1407	0.0002
29	2	27	28	3	26	874.4006	874.4007	0
29	4	26	28	3	25	874.7718	874.7724	-0.0006
29	5	25	28	4	24	875.141	875.1407	0.0002
29	3	27	28	2	26	874.4006	874.4007	0
30	1	30	29	0	29	873.9028	873.9026	0.0002
30	0	30	29	1	29	873.9028	873.9026	0.0002
30	2	28	29	3	27	874.6588	874.6587	0.0001
30	1	29	29	2	28	874.282	874.2817	0.0003
30	3	27	29	4	26	875.0328	875.0329	-0.0002
30	3	28	29	2	27	874.6588	874.6587	0.0001
30	2	29	29	1	28	874.282	874.2817	0.0003
30	4	27	29	3	26	875.0328	875.0329	-0.0002
31	1	30	30	2	29	874.5358	874.5357	0.0002
31	2	29	30	3	28	874.9153	874.9152	0.0001
31	3	28	30	4	27	875.2919	875.2919	-0.0001
31	4	27	30	5	26	875.6657	875.665	0.0007
31	2	30	30	1	29	874.5358	874.5357	0.0002
31	3	29	30	2	28	874.9153	874.9152	0.0001
31	4	28	30	3	27	875.2919	875.2919	-0.0001
31	5	27	30	4	26	875.6657	875.665	0.0007
32	1	31	31	2	30	874.7883	874.7881	0.0002

32	2	30	31	3	29	875.1702	875.1702	0.0001
32	0	32	31	1	31	874.4039	874.404	0
32	3	29	31	4	28	875.5494	875.5493	0
32	2	31	31	1	30	874.7883	874.7881	0.0002
32	3	30	31	2	29	875.1702	875.1702	0.0001
32	1	32	31	0	31	874.4039	874.404	0
32	4	29	31	3	28	875.5494	875.5493	0
33	0	33	32	1	32	874.6521	874.6524	-0.0003
33	2	31	32	3	30	875.4234	875.4236	-0.0002
33	1	32	32	2	31	875.0393	875.039	0.0003
33	1	33	32	0	32	874.6521	874.6524	-0.0003
33	3	31	32	2	30	875.4234	875.4236	-0.0002
33	2	32	32	1	31	875.0393	875.039	0.0003
34	0	34	33	1	33	874.899	874.8994	-0.0004
34	1	33	33	2	32	875.2885	875.2884	0.0001
34	2	32	33	3	31	875.6755	875.6756	0
34	1	34	33	0	33	874.899	874.8994	-0.0004
34	2	33	33	1	32	875.2885	875.2884	0.0001
34	3	32	33	2	31	875.6755	875.6756	0
35	1	35	34	0	34	875.1443	875.1448	-0.0006
35	0	35	34	1	34	875.1443	875.1448	-0.0006
35	1	34	34	2	33	875.5364	875.5364	0
35	2	34	34	1	33	875.5364	875.5364	0
36	1	35	35	2	34	875.7826	875.7829	-0.0003
36	2	35	35	1	34	875.7826	875.7829	-0.0003

Appendix K

Observed and calculated frequencies (cm^{-1}) for the ν_8 state of furan.

P Branch

J'	Ka'	Kc'	J"	Ka"	Kc"	Observed (cm^{-1})	Calculated (cm^{-1})	Obs-Cal (cm^{-1})
10	3	8	11	3	9	865.5444	865.544	0.0004
10	2	8	11	2	9	865.5444	865.544	0.0004
11	3	9	12	3	10	865.2085	865.2081	0.0004
11	2	9	12	2	10	865.2085	865.2081	0.0004
11	2	10	12	2	11	865.4843	865.4836	0.0007
11	1	10	12	1	11	865.4843	865.4836	0.0007
11	1	11	12	1	12	865.7663	865.7669	-0.0006
11	0	11	12	0	12	865.7663	865.7669	-0.0006
12	5	8	13	5	9	864.3358	864.3361	-0.0003
12	4	9	13	4	10	864.607	864.6062	0.0008
12	3	9	13	3	10	864.607	864.6062	0.0008
12	1	12	13	1	13	865.4151	865.4143	0.0008
12	0	12	13	0	13	865.4151	865.4143	0.0008
13	5	9	14	5	10	864.0269	864.0272	-0.0003
13	4	9	14	4	10	864.0269	864.0271	-0.0003
13	3	11	14	3	12	864.5293	864.528	0.0013
13	2	11	14	2	12	864.5293	864.528	0.0013
13	2	12	14	2	13	864.7837	864.7849	-0.0011
13	1	12	14	1	13	864.7837	864.7849	-0.0011
14	1	14	15	1	15	864.6975	864.6989	-0.0013
14	0	14	15	0	15	864.6975	864.6989	-0.0013
15	4	11	16	6	10	856.5441	856.5475	-0.0034
15	5	11	16	7	10	856.5441	856.5475	-0.0034
15	6	10	16	6	11	863.1896	863.1904	-0.0008
15	5	10	16	5	11	863.1896	863.1904	-0.0008
15	5	11	16	5	12	863.4053	863.4061	-0.0007
15	4	11	16	4	12	863.4053	863.4061	-0.0007
15	1	15	16	1	16	864.3358	864.3362	-0.0004
15	0	15	16	0	16	864.3358	864.3362	-0.0004
16	4	13	17	4	14	863.2859	863.2852	0.0007
16	3	13	17	3	14	863.2859	863.2852	0.0007
16	0	16	17	0	17	863.9702	863.9702	0
16	1	16	17	1	17	863.9702	863.9702	0
17	10	8	18	12	7	856.7941	856.7962	-0.0021
18	6	13	19	6	14	862.3352	862.3355	-0.0004
18	5	13	19	5	14	862.3352	862.3355	-0.0004
19	4	16	20	4	17	862.2753	862.276	-0.0007
19	3	16	20	3	17	862.2753	862.276	-0.0007

20	5	16	21	5	17	861.8418	861.8412	0.0006
20	4	16	21	4	17	861.8418	861.8412	0.0006
20	4	17	21	4	18	861.9356	861.9363	-0.0007
20	3	17	21	3	18	861.9356	861.9363	-0.0007
22	0	22	23	0	23	861.7083	861.708	0.0003
22	1	22	23	1	23	861.7083	861.708	0.0003
23	1	23	24	1	24	861.3185	861.3203	-0.0018
23	0	23	24	0	24	861.3185	861.3203	-0.0018
24	0	24	25	0	25	860.9297	860.9297	-0.0001
24	1	24	25	1	25	860.9297	860.9297	-0.0001
25	2	24	26	2	25	860.3341	860.3351	-0.001
25	1	24	26	1	25	860.3341	860.3351	-0.001
25	1	25	26	1	26	860.5369	860.5363	0.0005
25	0	25	26	0	26	860.5369	860.5363	0.0005
26	2	25	27	2	26	859.9475	859.9455	0.002
26	1	25	27	1	26	859.9475	859.9455	0.002
26	1	26	27	1	27	860.1406	860.1402	0.0004
26	0	26	27	0	27	860.1406	860.1402	0.0004
26	5	21	27	5	22	860.0944	860.0956	-0.0012
26	6	21	27	6	22	860.0944	860.0956	-0.0012
27	2	26	28	2	27	859.5565	859.5531	0.0034
27	1	26	28	1	27	859.5565	859.5531	0.0034
27	1	27	28	1	28	859.7412	859.7413	-0.0001
27	0	27	28	0	28	859.7412	859.7413	-0.0001
27	4	23	28	4	24	859.6301	859.6305	-0.0004
27	5	23	28	5	24	859.6301	859.6305	-0.0004
27	8	20	28	8	21	860.36	860.3616	-0.0016
27	7	20	28	7	21	860.36	860.3616	-0.0016
27	12	16	28	12	17	861.7055	861.7054	0
27	11	16	28	11	17	861.7055	861.7054	0
28	2	27	29	2	28	859.1617	859.1582	0.0036
28	1	27	29	1	28	859.1617	859.1582	0.0036
28	1	28	29	1	29	859.3392	859.3398	-0.0005
28	0	28	29	0	29	859.3392	859.3398	-0.0005
29	2	28	30	2	29	858.7641	858.7606	0.0035
29	1	28	30	1	29	858.7641	858.7606	0.0035
29	1	29	30	1	30	858.9346	858.9357	-0.0011
29	0	29	30	0	30	858.9346	858.9357	-0.0011
29	2	27	30	2	28	858.7228	858.7232	-0.0003
29	3	27	30	3	28	858.7228	858.7232	-0.0003
30	1	29	31	1	30	858.3632	858.3606	0.0026

30	2	29	31	2	30	858.3632	858.3606	0.0026
30	1	30	31	1	31	858.5277	858.5292	-0.0015
30	0	30	31	0	31	858.5277	858.5292	-0.0015
30	6	24	31	6	25	859.4094	859.4096	-0.0001
30	7	24	31	7	25	859.4094	859.4096	-0.0001
31	1	30	32	1	31	857.9598	857.9581	0.0018
31	2	30	32	2	31	857.9598	857.9581	0.0018
31	1	31	32	1	32	858.1185	858.1202	-0.0017
31	0	31	32	0	32	858.1185	858.1202	-0.0017
31	8	23	32	8	24	860.3389	860.3389	0
31	9	23	32	9	24	860.3389	860.3389	0
31	13	19	32	13	20	863.0638	863.0632	0.0006
31	12	19	32	12	20	863.0638	863.0632	0.0006
32	1	31	33	1	32	857.5539	857.5532	0.0007
32	2	31	33	2	32	857.5539	857.5532	0.0007
32	1	32	33	1	33	857.7069	857.7089	-0.002
32	0	32	33	0	33	857.7069	857.7089	-0.002
32	3	30	33	3	31	857.5691	857.5687	0.0005
32	2	30	33	2	31	857.5691	857.5687	0.0005
33	1	32	34	1	33	857.1462	857.146	0.0001
33	2	32	34	2	33	857.1462	857.146	0.0001
33	1	33	34	1	34	857.2935	857.2954	-0.0019
33	0	33	34	0	34	857.2935	857.2954	-0.0019
33	6	28	34	6	29	858.194	858.1939	0.0001
33	5	28	34	5	29	858.194	858.1939	0.0001
34	2	33	35	2	34	856.7358	856.7366	-0.0008
34	1	33	35	1	34	856.7358	856.7366	-0.0008
34	1	34	35	1	35	856.8781	856.8797	-0.0016
34	0	34	35	0	35	856.8781	856.8797	-0.0016
34	2	32	35	2	33	856.7896	856.7889	0.0007
34	3	32	35	3	33	856.7896	856.7889	0.0007
35	2	34	36	2	35	856.324	856.3249	-0.001
35	1	34	36	1	35	856.324	856.3249	-0.001
35	1	35	36	1	36	856.4604	856.4619	-0.0015
35	0	35	36	0	36	856.4604	856.4619	-0.0015
35	4	32	36	4	33	856.6554	856.6555	-0.0001
35	3	32	36	3	33	856.6554	856.6555	-0.0001
35	4	31	36	4	32	857.0845	857.0835	0.001
35	5	31	36	5	32	857.0845	857.0835	0.001
36	2	35	37	2	36	855.9094	855.9112	-0.0019
36	1	35	37	1	36	855.9094	855.9112	-0.0019

36	1	36	37	1	37	856.0411	856.0421	-0.001
36	0	36	37	0	37	856.0411	856.0421	-0.001
37	1	36	38	1	37	855.4962	855.4955	0.0007
37	2	36	38	2	37	855.4962	855.4955	0.0007
37	1	37	38	1	38	855.62	855.6205	-0.0005
37	0	37	38	0	38	855.62	855.6205	-0.0005
37	7	30	38	7	31	858.9538	858.9541	-0.0003
37	8	30	38	8	31	858.9538	858.9541	-0.0003
38	1	37	39	1	38	855.076	855.0779	-0.0019
38	2	37	39	2	38	855.076	855.0779	-0.0019
38	1	38	39	1	39	855.1972	855.1971	0.0002
38	0	38	39	0	39	855.1972	855.1971	0.0002
39	1	38	40	1	39	854.6562	854.6584	-0.0022
39	2	38	40	2	39	854.6562	854.6584	-0.0022
39	0	39	40	0	40	854.7727	854.7719	0.0008
39	1	39	40	1	40	854.7727	854.7719	0.0008
40	1	40	41	1	41	854.3468	854.3452	0.0016
40	0	40	41	0	41	854.3468	854.3452	0.0016
41	1	40	42	1	41	853.8126	853.8143	-0.0016
41	2	40	42	2	41	853.8126	853.8143	-0.0016
41	0	41	42	0	42	853.9188	853.917	0.0018
41	1	41	42	1	42	853.9188	853.917	0.0018
42	2	41	43	2	42	853.3886	853.3898	-0.0012
42	1	41	43	1	42	853.3886	853.3898	-0.0012
42	1	42	43	1	43	853.4897	853.4874	0.0022
42	0	42	43	0	43	853.4897	853.4874	0.0022
43	2	42	44	2	43	852.9631	852.9638	-0.0008
43	1	42	44	1	43	852.9631	852.9638	-0.0008
43	0	43	44	0	44	853.059	853.0566	0.0024
43	1	43	44	1	44	853.059	853.0566	0.0024
44	1	43	45	1	44	852.5361	852.5365	-0.0004
44	2	43	45	2	44	852.5361	852.5365	-0.0004
44	0	44	45	0	45	852.6262	852.6246	0.0016
44	1	44	45	1	45	852.6262	852.6246	0.0016
45	2	44	46	2	45	852.1087	852.1079	0.0008
45	1	44	46	1	45	852.1087	852.1079	0.0008
45	0	45	46	0	46	852.1938	852.1916	0.0022
45	1	45	46	1	46	852.1938	852.1916	0.0022
45	7	39	46	7	40	856.5246	856.5244	0.0002
45	6	39	46	6	40	856.5246	856.5244	0.0002
46	1	45	47	1	46	851.6795	851.6782	0.0013

46	2	45	47	2	46	851.6795	851.6782	0.0013
46	1	46	47	1	47	851.7591	851.7577	0.0014
46	0	46	47	0	47	851.7591	851.7577	0.0014
47	1	46	48	1	47	851.2482	851.2474	0.0008
47	2	46	48	2	47	851.2482	851.2474	0.0008
47	0	47	48	0	48	851.3231	851.3229	0.0002
47	1	47	48	1	48	851.3231	851.3229	0.0002
48	1	47	49	1	48	850.8164	850.8156	0.0007
48	2	47	49	2	48	850.8164	850.8156	0.0007
48	0	48	49	0	49	850.8859	850.8875	-0.0016
48	1	48	49	1	49	850.8859	850.8875	-0.0016
49	1	48	50	1	49	850.3839	850.3831	0.0008
49	2	48	50	2	49	850.3839	850.3831	0.0008
49	0	49	50	0	50	850.4474	850.4516	-0.0042
49	1	49	50	1	50	850.4474	850.4516	-0.0042

R Branch

J'	Ka'	Kc'	J"	Ka"	Kc"	Observed (cm^{-1})	Calculated (cm^{-1})	Obs-Cal (cm^{-1})
13	7	6	12	7	5	876.1398	876.1377	0.0022
15	6	10	14	6	9	876.2795	876.2799	-0.0004
15	5	10	14	5	9	876.2795	876.2799	-0.0004
16	4	13	15	4	12	875.7502	875.7504	-0.0003
16	3	13	15	3	12	875.7502	875.7504	-0.0003
16	2	15	15	2	14	874.9312	874.9312	-0.0001
16	1	15	15	1	14	874.9312	874.9312	-0.0001
16	1	16	15	1	15	874.5641	874.5646	-0.0004
16	0	16	15	0	15	874.5641	874.5646	-0.0004
15	4	11	16	6	10	856.5441	856.5475	-0.0034
15	5	11	16	7	10	856.5441	856.5475	-0.0034
17	3	15	16	3	14	875.6008	875.6011	-0.0003
17	2	15	16	2	14	875.6008	875.6011	-0.0003
18	4	15	17	4	14	876.3279	876.3255	0.0024
18	3	15	17	3	14	876.3279	876.3255	0.0024
17	10	8	18	12	7	856.7941	856.7962	-0.0021
19	3	17	18	3	16	876.1398	876.1361	0.0038
19	2	17	18	2	16	876.1398	876.1361	0.0038
19	1	18	18	1	17	875.7005	875.7011	-0.0006
19	2	18	18	2	17	875.7005	875.7011	-0.0006
20	3	18	19	3	17	876.3997	876.3997	-0.0001
20	2	18	19	2	17	876.3997	876.3997	-0.0001
22	1	21	21	1	20	876.4413	876.4439	-0.0026
22	2	21	21	2	20	876.4413	876.4439	-0.0026
23	1	23	22	1	22	876.2744	876.2763	-0.0019
23	0	23	22	0	22	876.2744	876.2763	-0.0019
24	1	24	23	1	23	876.5087	876.5087	0
24	0	24	23	0	23	876.5087	876.5087	0
25	0	25	24	0	24	876.739	876.7384	0.0007
25	1	25	24	1	24	876.739	876.7384	0.0007
25	2	24	24	2	23	877.1596	877.1607	-0.0011
25	1	24	24	1	23	877.1596	877.1607	-0.0011
26	1	26	25	1	25	876.9656	876.9652	0.0004
26	0	26	25	0	25	876.9656	876.9652	0.0004
26	2	25	25	2	24	877.396	877.394	0.002
26	1	25	25	1	24	877.396	877.394	0.002

27	0	27	26	0	26	877.1893	877.1893	0
27	1	27	26	1	26	877.1893	877.1893	0
27	2	26	26	2	25	877.6283	877.6247	0.0036
27	1	26	26	1	25	877.6283	877.6247	0.0036
28	1	28	27	1	27	877.4103	877.4108	-0.0005
28	0	28	27	0	27	877.4103	877.4108	-0.0005
28	2	27	27	2	26	877.8563	877.8527	0.0036
28	1	27	27	1	26	877.8563	877.8527	0.0036
29	0	29	28	0	28	877.6283	877.6297	-0.0014
29	1	29	28	1	28	877.6283	877.6297	-0.0014
29	2	28	28	2	27	878.0814	878.0781	0.0033
29	1	28	28	1	27	878.0814	878.0781	0.0033
30	0	30	29	0	29	877.8443	877.8461	-0.0018
30	1	30	29	1	29	877.8443	877.8461	-0.0018
30	2	29	29	2	28	878.3035	878.3009	0.0026
30	1	29	29	1	28	878.3035	878.3009	0.0026
31	1	31	30	1	30	878.0583	878.06	-0.0018
31	0	31	30	0	30	878.0583	878.06	-0.0018
31	1	30	30	1	29	878.5231	878.5214	0.0018
31	2	30	30	2	29	878.5231	878.5214	0.0018
32	0	32	31	0	31	878.2697	878.2717	-0.002
32	1	32	31	1	31	878.2697	878.2717	-0.002
33	0	33	32	0	32	878.479	878.481	-0.002
33	1	33	32	1	32	878.479	878.481	-0.002
34	1	33	33	1	32	879.1679	879.1684	-0.0005
34	2	33	33	2	32	879.1679	879.1684	-0.0005
35	0	35	34	0	34	878.8915	878.8933	-0.0018
35	1	35	34	1	34	878.8915	878.8933	-0.0018
35	2	34	34	2	33	879.3787	879.3796	-0.001
35	1	34	34	1	33	879.3787	879.3796	-0.001
36	0	36	35	0	35	879.0953	879.0963	-0.001
36	1	36	35	1	35	879.0953	879.0963	-0.001
36	1	35	35	1	34	879.5869	879.5888	-0.0019
36	2	35	35	2	34	879.5869	879.5888	-0.0019
37	1	37	36	1	36	879.297	879.2975	-0.0005
37	0	37	36	0	36	879.297	879.2975	-0.0005
37	2	36	36	2	35	879.7939	879.7958	-0.0019
37	1	36	36	1	35	879.7939	879.7958	-0.0019
38	0	38	37	0	37	879.497	879.4969	0.0001
38	1	38	37	1	37	879.497	879.4969	0.0001
38	1	37	37	1	36	879.999	880.0009	-0.002

38	2	37	37	2	36	879.999	880.0009	-0.002
39	0	39	38	0	38	879.6952	879.6945	0.0008
39	1	39	38	1	38	879.6952	879.6945	0.0008
39	1	38	38	1	37	880.2021	880.2042	-0.0021
39	2	38	38	2	37	880.2021	880.2042	-0.0021
40	0	40	39	0	39	879.8919	879.8905	0.0014
40	1	40	39	1	39	879.8919	879.8905	0.0014
40	1	39	39	1	38	880.4038	880.4057	-0.0019
40	2	39	39	2	38	880.4038	880.4057	-0.0019
41	1	41	40	1	40	880.0878	880.085	0.0027
41	0	41	40	0	40	880.0878	880.085	0.0027
41	2	40	40	2	39	880.6039	880.6055	-0.0016
41	1	40	40	1	39	880.6039	880.6055	-0.0016
42	1	42	41	1	41	880.2812	880.2782	0.0031
42	0	42	41	0	41	880.2812	880.2782	0.0031
42	1	41	41	1	40	880.8025	880.8037	-0.0012
42	2	41	41	2	40	880.8025	880.8037	-0.0012
43	1	43	42	1	42	880.4724	880.47	0.0024
43	0	43	42	0	42	880.4724	880.47	0.0024
43	1	42	42	1	41	880.9996	881.0004	-0.0007
43	2	42	42	2	41	880.9996	881.0004	-0.0007
44	1	44	43	1	43	880.6631	880.6607	0.0024
44	0	44	43	0	43	880.6631	880.6607	0.0024
44	1	43	43	1	42	881.1949	881.1957	-0.0008
44	2	43	43	2	42	881.1949	881.1957	-0.0008
45	0	45	44	0	44	880.8523	880.8503	0.0021
45	1	45	44	1	44	880.8523	880.8503	0.0021
45	1	44	44	1	43	881.3898	881.3897	0.0001
45	2	44	44	2	43	881.3898	881.3897	0.0001
46	1	46	45	1	45	881.0403	881.0389	0.0014
46	0	46	45	0	45	881.0403	881.0389	0.0014
46	2	45	45	2	44	881.5833	881.5825	0.0008
46	1	45	45	1	44	881.5833	881.5825	0.0008
47	0	47	46	0	46	881.2269	881.2268	0.0001
47	1	47	46	1	46	881.2269	881.2268	0.0001
47	2	46	46	2	45	881.7751	881.7742	0.0008
47	1	46	46	1	45	881.7751	881.7742	0.0008
48	0	48	47	0	47	881.4112	881.4139	-0.0027
48	1	48	47	1	47	881.4112	881.4139	-0.0027
48	2	47	47	2	46	881.966	881.965	0.001
48	1	47	47	1	46	881.966	881.965	0.001

49	1	49	48	1	48	881.5966	881.6005	-0.0039
49	0	49	48	0	48	881.5966	881.6005	-0.0039
49	2	48	48	2	47	882.1548	882.1549	-0.0001
49	1	48	48	1	47	882.1548	882.1549	-0.0001

Appendix L

Assigned observed frequencies (cm^{-1}) for the ν_{21} state of furan.

P Branch

J'	Ka'	Kc'	J"	Ka"	Kc"	Observed (cm^{-1})
5	0	5	6	1	6	867.9033
5	1	5	6	0	6	867.9033
6	0	6	7	1	7	867.5709
6	1	6	7	0	7	867.5709
7	0	7	8	1	8	867.2343
7	1	7	8	0	8	867.2343
8	0	8	9	1	9	866.8941
8	1	8	9	0	9	866.8941
9	3	6	10	4	7	865.7686
9	4	6	10	3	7	865.7686
9	2	7	10	3	8	866.0363
9	3	7	10	2	8	866.0363
9	2	8	10	1	9	866.2975
9	1	8	10	2	9	866.2975
9	1	9	10	0	10	866.5503
9	0	9	10	1	10	866.5503
10	3	7	11	4	8	865.4412
10	4	7	11	3	8	865.4412
10	2	8	11	3	9	865.7024
10	3	8	11	2	9	865.7024
10	2	9	11	1	10	865.9565
10	1	9	11	2	10	865.9565
10	0	10	11	1	11	866.2029
10	1	10	11	0	11	866.2029
11	4	8	12	3	9	865.1107
11	3	8	12	4	9	865.1107
11	3	9	12	2	10	865.3653
11	2	9	12	3	10	865.3653
11	0	11	12	1	12	865.852
11	1	11	12	0	12	865.852
12	3	9	13	4	10	864.7767
12	4	9	13	3	10	864.7767
12	2	10	13	3	11	865.0248
12	3	10	13	2	11	865.0248
12	2	11	13	1	12	865.2655
12	1	11	13	2	12	865.2655
12	1	12	13	0	13	865.4978
12	0	12	13	1	13	865.4978

13	3	10	14	4	11	864.4398
13	4	10	14	3	11	864.4398
13	2	11	14	3	12	864.6815
13	3	11	14	2	12	864.6815
13	1	12	14	2	13	864.9156
13	2	12	14	1	13	864.9156
14	3	11	15	4	12	864.1001
14	4	11	15	3	12	864.1001
14	2	12	15	3	13	864.3358
14	3	12	15	2	13	864.3358
14	1	13	15	2	14	864.5633
14	2	13	15	1	14	864.5633
15	3	12	16	4	13	863.7584
15	4	12	16	3	13	863.7584
15	2	13	16	3	14	863.9882
15	3	13	16	2	14	863.9882
15	2	14	16	1	15	864.2097
15	1	14	16	2	15	864.2097
16	3	13	17	4	14	863.4153
16	4	13	17	3	14	863.4153
16	2	14	17	3	15	863.6398
16	3	14	17	2	15	863.6398
17	3	14	18	4	15	863.0717
17	4	14	18	3	15	863.0717
17	2	15	18	3	16	863.2923
17	3	15	18	2	16	863.2923
17	1	16	18	2	17	863.505
17	2	16	18	1	17	863.505
18	3	15	19	4	16	862.7299
18	4	15	19	3	16	862.7299
18	3	16	19	2	17	862.9446
18	2	16	19	3	17	862.9446

R Branch

J'	Ka'	Kc'	J''	Ka''	Kc''	Observed (cm^{-1})
4	0	4	3	1	3	871.3482
4	1	4	3	0	3	871.3482
5	1	5	4	0	4	871.6429
5	0	5	4	1	4	871.6429
6	0	6	5	1	5	871.9334
6	1	6	5	0	5	871.9334
7	0	7	6	1	6	872.2202
7	1	7	6	0	6	872.2202
8	1	8	7	0	7	872.5035
8	0	8	7	1	7	872.5035
9	0	9	8	1	8	872.7828
9	1	9	8	0	8	872.7828
9	2	8	8	1	7	873.1526
9	1	8	8	2	7	873.1526
9	2	7	8	3	6	873.5163
9	3	7	8	2	6	873.5163
9	3	6	8	4	5	873.8723
9	4	6	8	3	5	873.8723
10	1	10	9	0	9	873.0583
10	0	10	9	1	9	873.0583
10	1	9	9	2	8	873.4356
10	2	9	9	1	8	873.4356
10	3	8	9	2	7	873.8054
10	2	8	9	3	7	873.8054
10	3	7	9	4	6	874.1682
10	4	7	9	3	6	874.1682
11	2	10	10	1	9	873.7149
11	1	10	10	2	9	873.7149
11	2	9	10	3	8	874.0913
11	3	9	10	2	8	874.0913
11	4	8	10	3	7	874.4605
11	3	8	10	4	7	874.4605
12	1	12	11	0	11	873.5996
12	0	12	11	1	11	873.5996
12	1	11	11	2	10	873.991
12	2	11	11	1	10	873.991
12	2	10	11	3	9	874.374
12	3	10	11	2	9	874.374

12	4	9	11	3	8	874.7497
12	3	9	11	4	8	874.7497
13	2	12	12	1	11	874.2642
13	1	12	12	2	11	874.2642
13	3	11	12	2	10	874.6543
13	2	11	12	3	10	874.6543
13	3	10	12	4	9	875.0357
13	4	10	12	3	9	875.0357
14	3	11	13	4	10	875.3192
14	4	11	13	3	10	875.3192
15	3	13	14	2	12	875.2068
15	2	13	14	3	12	875.2068
15	3	12	14	4	11	875.6008
15	4	12	14	3	11	875.6008
16	1	15	15	2	14	875.0739
16	2	15	15	1	14	875.0739
16	3	14	15	2	13	875.4814
16	2	14	15	3	13	875.4814
16	3	13	15	4	12	875.8805
16	4	13	15	3	12	875.8805
17	1	16	16	2	15	875.3461
17	2	16	16	1	15	875.3461
17	3	15	16	2	14	875.7571
17	2	15	16	3	14	875.7571
17	3	14	16	4	13	876.1601
17	4	14	16	3	13	876.1601
18	3	16	17	2	15	876.0346
18	2	16	17	3	15	876.0346
18	3	15	17	4	14	876.4413
18	4	15	17	3	14	876.4413

Curriculum Vitae (CV)

Candidate's full name: Hanif Zarringhalam

Universities attended: B.Sc. (Physics), Razi University, 2005

M.Sc. (Physics), University of Guilan, 2008

Ph.D. (Physics), University of New Brunswick, 2021

Conference presentations: "Laser-Induced Fluorescence Spectroscopy of Two Ruthenium-Bearing Molecules: RuF and RuCl." H. Zarringhalam, A. G. Adam, C. Linton, and D. W. Tokaryk, 72nd International Symposium on Molecular Spectroscopy, University of Illinois, Champaign-Urbana, June 2017.

"Studying Medium-Sized Molecules in the Far-Infrared Spectral Region with the Canadian Light Source." H. Zarringhalam and D. Tokaryk. CAP Congress, Dalhousie University, June 2018.